WORLDWIDE EMERGENCE OF DRUG RESISTANT FUNGI: FROM BASIC TO CLINIC

EDITED BY: Weihua Pan, Keke Huo, Ying-Chun Xu, David S. Perlin and Macit Ilkit

PUBLISHED IN: Frontiers in Microbiology

frontiers Research Topics

frontiers

ISSN 1664-8714
ISBN 978-2-88971-608-1
DOI 10.3389/978-2-88971-608-1

About Frontiers

Frontiers is more than just an open-access publisher of scholarly articles: it is a pioneering approach to the world of academia, radically improving the way scholarly research is managed. The grand vision of Frontiers is a world where all people have an equal opportunity to seek, share and generate knowledge. Frontiers provides immediate and permanent online open access to all its publications, but this alone is not enough to realize our grand goals.

Frontiers Journal Series

The Frontiers Journal Series is a multi-tier and interdisciplinary set of open-access, online journals, promising a paradigm shift from the current review, selection and dissemination processes in academic publishing. All Frontiers journals are driven by researchers for researchers; therefore, they constitute a service to the scholarly community. At the same time, the Frontiers Journal Series operates on a revolutionary invention, the tiered publishing system, initially addressing specific communities of scholars, and gradually climbing up to broader public understanding, thus serving the interests of the lay society, too.

Dedication to Quality

Each Frontiers article is a landmark of the highest quality, thanks to genuinely collaborative interactions between authors and review editors, who include some of the world's best academicians. Research must be certified by peers before entering a stream of knowledge that may eventually reach the public - and shape society; therefore, Frontiers only applies the most rigorous and unbiased reviews.
Frontiers revolutionizes research publishing by freely delivering the most outstanding research, evaluated with no bias from both the academic and social point of view. By applying the most advanced information technologies, Frontiers is catapulting scholarly publishing into a new generation.

What are Frontiers Research Topics?

Frontiers Research Topics are very popular trademarks of the Frontiers Journals Series: they are collections of at least ten articles, all centered on a particular subject. With their unique mix of varied contributions from Original Research to Review Articles, Frontiers Research Topics unify the most influential researchers, the latest key findings and historical advances in a hot research area! Find out more on how to host your own Frontiers Research Topic or contribute to one as an author by contacting the Frontiers Editorial Office: frontiersin.org/about/contact

WORLDWIDE EMERGENCE OF DRUG RESISTANT FUNGI: FROM BASIC TO CLINIC

Topic Editors:
Weihua Pan, Shanghai Changzheng Hospital, China
Keke Huo, Fudan University, China
Ying-Chun Xu, Peking Union Medical College Hospital (CAMS), China
David S. Perlin, Hackensack Meridian Health, United States
Macit Ilkit, Çukurova University, Turkey

Citation: Pan, W., Huo, K., Xu, Y.-C., Perlin, D. S., Ilkit, M., eds. (2021). Worldwide Emergence of Drug Resistant Fungi: From Basic to Clinic. Lausanne: Frontiers Media SA. doi: 10.3389/978-2-88971-608-1

Table of Contents

06 ***Amphotericin B Specifically Induces the Two-Component System LnrJK: Development of a Novel Whole-Cell Biosensor for the Detection of Amphotericin-Like Polyenes***
Ainhoa Revilla-Guarinos, Franziska Dürr, Philipp F. Popp, Maximilian Döring and Thorsten Mascher

22 ***Synthetic Naphthofuranquinone Derivatives Are Effective in Eliminating Drug-Resistant* Candida albicans *in Hyphal, Biofilm, and Intracellular Forms: An Application for Skin-Infection Treatment***
Jia-You Fang, Kai-Wei Tang, Sien-Hung Yang, Ahmed Alalaiwe, Yu-Ching Yang, Chih-Hua Tseng and Shih-Chun Yang

35 ***SWL-1 Reverses Fluconazole Resistance in* Candida albicans *by Regulating the Glycolytic Pathway***
Xiao-Ning Li, Lu-Mei Zhang, Yuan-Yuan Wang, Yi Zhang, Ze-Hua Jin, Jun Li, Rui-Rui Wang and Wei-Lie Xiao

45 ***Synergistic Effect of Pyrvinium Pamoate and Azoles Against* Aspergillus fumigatus in vitro *and* in vivo**
Yi Sun, Lujuan Gao, Youwen Zhang, Ji Yang and Tongxiang Zeng

53 ***The Multi-Fungicide Resistance Status of* Aspergillus fumigatus *Populations in Arable Soils and the Wider European Environment***
Bart Fraaije, Sarah Atkins, Steve Hanley, Andy Macdonald and John Lucas

70 ***Prevalence and Antifungal Susceptibility of* Candida parapsilosis *Species Complex in Eastern China: A 15-Year Retrospective Study by ECIFIG***
Jian Guo, Min Zhang, Dan Qiao, Hui Shen, Lili Wang, Dongjiang Wang, Li Li, Yun Liu, Huaiwei Lu, Chun Wang, Hui Ding, Shuping Zhou, Wanqing Zhou, Yingjue Wei, Haomin Zhang, Wei Xi, Yi Zheng, Yueling Wang, Rong Tang, Lingbing Zeng, Heping Xu and Wenjuan Wu

80 ***A High Rate of Recurrent Vulvovaginal Candidiasis and Therapeutic Failure of Azole Derivatives Among Iranian Women***
Amir Arastehfar, Melika Laal Kargar, Shahla Roudbar Mohammadi, Maryam Roudbary, Nayereh Ghods, Ladan Haghighi, Farnaz Daneshnia, Mahin Tavakoli, Jalal Jafarzadeh, Mohammad Taghi Hedayati, Huiwei Wang, Wenjie Fang, Agostinho Carvalho, Macit Ilkit, David S. Perlin and Cornelia Lass-Flörl

89 **ALS3 *Expression as an Indicator for* Candida albicans *Biofilm Formation and Drug Resistance***
Keke Deng, Wei Jiang, Yanyu Jiang, Qi Deng, Jinzhong Cao, Wenjie Yang and Xuequn Zhao

99 ***Antifungal Activity of Minocycline and Azoles Against Fluconazole-Resistant* Candida *Species***
Jingwen Tan, Shaojie Jiang, Lihua Tan, Haiyan Shi, Lianjuan Yang, Yi Sun and Xiuli Wang

105 ***Effects of Hsp90 Inhibitor Ganetespib on Inhibition of Azole-Resistant* Candida albicans**
Rui Yuan, Jie Tu, Chunquan Sheng, Xi Chen and Na Liu

114 *Antifungal Combination of Ethyl Acetate Extract of* **Poincianella pluviosa** *(DC.) L. P. Queiros Stem Bark With Amphotericin B in* **Cryptococcus neoformans**
Gabriella Maria Andriani, Ana Elisa Belotto Morguette, Laís Fernanda Almeida Spoladori, Patrícia Morais Lopes Pereira, Weslei Roberto Correia Cabral, Bruna Terci Fernandes, Eliandro Reis Tavares, Ricardo Sérgio Almeida, Cesar Armando Contreras Lancheros, Celso Vataru Nakamura, João Carlos Palazzo Mello, Lucy Megumi Yamauchi and Sueli Fumie Yamada-Ogatta

129 *A Novel Diagnostic Method for Invasive Fungal Disease Using the Factor G Alpha Subunit From* **Limulus polyphemus**
Fang Cui, Peng Luo, Yao Bai and Jiangping Meng

136 *Mechanism of Growth Regulation of Yeast Involving Hydrogen Sulfide From* **S-Propargyl-Cysteine** *Catalyzed by Cystathionine-γ-Lyase*
Zhongkai Gu, Yufan Sun, Feizhen Wu and Xiaomo Wu

149 *Continual Decline in Azole Susceptibility Rates in* **Candida tropicalis** *Over a 9-Year Period in China*
Yao Wang, Xin Fan, He Wang, Timothy Kudinha, Ya-Ning Mei, Fang Ni, Yu-Hong Pan, Lan-Mei Gao, Hui Xu, Hai-Shen Kong, Qing Yang, Wei-Ping Wang, Hai-Yan Xi, Yan-Ping Luo, Li-Yan Ye, Meng Xiao and China Hospital Invasive Fungal Surveillance Net (CHIF-NET) Study Group

159 *A Comparative Transcriptome Between Anti-drug Sensitive and Resistant* **Candida auris** *in China*
Wenkai Zhou, Xiuzhen Li, Yiqing Lin, Wei Yan, Shuling Jiang, Xiaotian Huang, Xinglong Yang, Dan Qiao and Na Li

172 *A 20-Year Antifungal Susceptibility Surveillance (From 1999 to 2019) for* **Aspergillus** *spp. and Proposed Epidemiological Cutoff Values for* **Aspergillus fumigatus** *and* **Aspergillus flavus***: A Study in a Tertiary Hospital in China*
Xinyu Yang, Wei Chen, Tianyu Liang, JingWen Tan, Weixia Liu, Yi Sun, Qian Wang, Hui Xu, Lijuan Li, Yabin Zhou, Qiqi Wang, Zhe Wan, Yinggai Song, Ruoyu Li and Wei Liu

183 *The Elevated Endogenous Reactive Oxygen Species Contribute to the Sensitivity of the Amphotericin B-Resistant Isolate of* **Aspergillus flavus** *to Triazoles and Echinocandins*
Tianyu Liang, Wei Chen, Xinyu Yang, Qiqi Wang, Zhe Wan, Ruoyu Li and Wei Liu

193 **In vitro** *Antifungal Susceptibility Profiles of* **Cryptococcus neoformans** *var.* **grubii** *and* **Cryptococcus gattii** *Clinical Isolates in Guangxi, Southern China*
Najwa Al-Odaini, Xiu-ying Li, Bing-kun Li, Xing-chun Chen, Chun-yang Huang, Chun-ying Lv, Kai-su Pan, Dong-yan Zheng, Yan-qing Zheng, Wan-qing Liao and Cun-wei Cao

201 *Antifungal Activity and Potential Mechanism of 6,7, 4′-O-Triacetylscutellarein Combined With Fluconazole Against Drug-Resistant* **C. albicans**
Liu-Yan Su, Guang-Hui Ni, Yi-Chuan Liao, Liu-Qing Su, Jun Li, Jia-Sheng Li, Gao-Xiong Rao and Rui-Rui Wang

211 ***Preliminary Study on Antifungal Mechanism of Aqueous Extract of* Cnidium monnieri *Against* Trichophyton rubrum**
Cao Yanyun, Tang Ying, Kong Wei, Fang Hua, Zhu Haijun, Zheng Ping, Xu Shunming and Wan Jian

221 ***Transcription Factors of CAT1, EFG1, and BCR1 Are Effective in Persister Cells of* Candida albicans*-Associated HIV-Positive and Chemotherapy Patients***
Elham Aboualigalehdari, Maryam Tahmasebi Birgani, Mahnaz Fatahinia and Mehran Hosseinzadeh

234 ***Evaluation of Droplet Digital PCR Assay for the Diagnosis of Candidemia in Blood Samples***
Biao Chen, Yingguang Xie, Ning Zhang, Wenqiang Li, Chen Liu, Dongmei Li, Shaodong Bian, Yufeng Jiang, Zhiya Yang, Renzhe Li, Yahui Feng, Xiaojie Zhang and Dongmei Shi

241 ***Effects of 3% Boric Acid Solution on Cutaneous* Candida albicans *Infection and Microecological Flora Mice***
Qing Liu, Zhao Liu, Changlin Zhang, Yanyan Xu, Xiaojing Li and Hongqi Gao

252 ***Contribution of NADPH-cytochrome P450 Reductase to Azole Resistance in* Fusarium oxysporum**
Dan He, Zeqing Feng, Song Gao, Yunyun Wei, Shuaishuai Han and Li Wang

frontiers in Microbiology

ORIGINAL RESEARCH
published: 21 August 2020
doi: 10.3389/fmicb.2020.02022

Amphotericin B Specifically Induces the Two-Component System LnrJK: Development of a Novel Whole-Cell Biosensor for the Detection of Amphotericin-Like Polyenes

*Ainhoa Revilla-Guarinos†, Franziska Dürr†, Philipp F. Popp, Maximilian Döring and Thorsten Mascher**

Department of General Microbiology, Institut für Mikrobiologie, Technische Universität Dresden, Dresden, Germany

OPEN ACCESS

Edited by:
Macit Ilkit,
Çukurova University, Turkey

Reviewed by:
Slawomir Milewski,
Gdańsk University of Technology, Poland
Aylin Döğen,
Mersin University, Turkey

***Correspondence:**
Thorsten Mascher
thorsten.mascher@tu-dresden.de

† These authors have contributed equally to this work and share first authorship

Specialty section:
This article was submitted to Antimicrobials, Resistance and Chemotherapy, a section of the journal Frontiers in Microbiology

Received: *22 May 2020*
Accepted: *30 July 2020*
Published: *21 August 2020*

Citation:
Revilla-Guarinos A, Dürr F, Popp PF, Döring M and Mascher T (2020) Amphotericin B Specifically Induces the Two-Component System LnrJK: Development of a Novel Whole-Cell Biosensor for the Detection of Amphotericin-Like Polyenes. Front. Microbiol. 11:2022. doi: 10.3389/fmicb.2020.02022

The rise of drug-resistant fungal pathogens urges for the development of new tools for the discovery of novel antifungal compounds. Polyene antibiotics are potent agents against fungal infections in humans and animals. They inhibit the growth of fungal cells by binding to sterols in the cytoplasmic membrane that subsequently causes pore formation and eventually results in cell death. Many polyenes are produced by Streptomycetes and released into the soil environment, where they can then target fungal hyphae. While not antibacterial, these compounds could nevertheless be also perceived by bacteria sharing the same habitat and serve as signaling molecules. We therefore addressed the question of how polyenes such as amphotericin B are perceived by the soil bacterium, *Bacillus subtilis*. Global transcriptional profiling identified a very narrow and specific response, primarily resulting in strong upregulation of the *lnrLMN* operon, encoding an ABC transporter previously associated with linearmycin resistance. Its strong and specific induction prompted a detailed analysis of the *lnrL* promoter element and its regulation. We demonstrate that the amphotericin response strictly depends on the two-component system LnrJK and that the target of LnrK-dependent gene regulation, the *lnrLMN operon,* negatively affects LnrJK-dependent signal transduction. Based on this knowledge, we developed a novel whole-cell biosensor, based on a P_{lnrL}-*lux* fusion reporter construct in a *lnrLMN* deletion mutant background. This highly sensitive and dynamic biosensor is ready to be applied for the discovery or characterization of novel amphotericin-like polyenes, hopefully helping to increase the repertoire of antimycotic and antiparasitic polyenes available to treat human and animal infections.

Keywords: amphotericin, antifungal polyenes, drug discovery, fungal infections, nystatin, stress response, two-component system, whole-cell biosensor

INTRODUCTION

Fungal infections are a major threat to human health: close to one billion patients suffer annually from various types of mycotic diseases, such as mild skin and nail infections. When associated with immunodeficiency disorders, such fungal infections can lead to severe medical complications and in serious cases have fatal consequences (Bongomin et al., 2017). The treatment of fungal infections is difficult: only few compound classes have been approved for antifungal therapy, and even their application is restricted due to issues with regard to their toxicity, or fungistatic versus fungicidal action (Aldholmi et al., 2019). This generates a major threat for the rise of antifungal-resistant fungal pathogens (Revie et al., 2018; Geddes-McAlister and Shapiro, 2019). Thus, there is a clear need for identifying new compounds for antifungal treatment (Almeida et al., 2019).

Natural polyenes are a primary choice for the treatment of fungal infections. Hence, the identification of novel polyenes or their modification poses an ideal approach to develop novel potent antifungal drugs (Rochette et al., 2003; Zotchev, 2003; Madden et al., 2014). As their name indicates, polyenes are poly unsaturated (at least three alternating double bonds), cyclic or linear organic compounds (**Figure 1**). They are classified by the number of conjugated double bonds as trienes, tetraenes, pentaenes, etc., and include a variety of chemical structures with different biological activities (Madden et al., 2014).

Cyclic polyenes belonging to the macrolide family, such as amphotericin B, candicidin, nystatin, and natamycin (**Figure 1**), contain a large macrolactone ring and have received considerable attention since many of them are used in human as well as animal therapy (Hamilton-Miller, 1973; Rochette et al., 2003; Zotchev, 2003). The polyene macrolide amphotericin B, produced by *Streptomyces nodosus* ATCC14899, is among the most commonly applied antifungal therapies (Caffrey et al., 2001; Cereghetti and Carreira, 2006). Amphotericin B forms trans-membrane channels in sterol-containing membranes. Its affinity (and hence activity) is higher toward ergosterol (characteristic for fungal membranes) than toward cholesterol (present in mammalian membranes) (Baginski et al., 2005). Due to this selectivity, amphotericin B is the most important antibiotic for the treatment of life-threatening systemic mycotic infections in humans (Torrado et al., 2008). Amphotericin B, alone or in combination with other drugs, is the only well-stablished therapy to treat primary amebic meningoencephalitis (PAM) caused by the free-living ameba *Naegleria fowleri* (Grace et al., 2015). In addition, it is also used for the treatment of visceral leishmaniasis (VL) caused by protozoan parasites of the genus *Leishmania* (Chattopadhyay and Jafurulla, 2011). Unfortunately, treatment of these, often fatal, systemic infections usually requires high dosages of amphotericin B, resulting in adverse side reactions in the human body such as nephrotoxicity, shaking chills, fever and anemia (Gallis et al., 1990; Zotchev, 2003; Antillón et al., 2016). Consequently, new amphotericin-like polyenes with less severe side effects for humans and stronger antimycotic and antiparasitic activities are highly sought after as alternatives to the conventional treatments (Tevyashova et al., 2013; Antillón et al., 2016).

Research efforts suggest three different directions: a) the creation of new derivatives from existing polyenes like amphotericin B (Power et al., 2008; Debnath et al., 2012; Tevyashova et al., 2013); b) new formulations for drug delivery aimed at decreased toxicity (Hamill, 2013; Palma et al., 2018); and c) the identification of new linear or cyclic polyenes from natural producers (Cai et al., 2007; Stodulkova et al., 2011; Vartak et al., 2014; Wang et al., 2017; Yao et al., 2018). The latter strategy can be accomplished by harnessing the metabolic diversity of Streptomycetes, which are known to produce a vast variety of natural products including many natural polyenes (Baltz, 2008; Madden et al., 2014). In order to efficiently identify these natural compounds, bacterial whole-cell biosensors have proven to be powerful screening tools (Wolf and Mascher, 2016).

Whole-cell biosensors consist of modified bacterial reporter strains, in which an antibiotic- specific promoter is transcriptionally fused to a reporter gene/operon. The selected promoters should be tightly switched off in the absence of the inducer but activated in a dose response manner in its presence, at concentrations well below the minimal inhibitory concentration (MIC) of the biosensor strain (Wolf and Mascher, 2016). The promoter selectivity can either be determined by the antibiotic target (e.g., inhibition of a specific essential cellular process) or by its chemical nature (Hutter et al., 2004; Urban et al., 2007). The Gram-positive model organism *Bacillus subtilis* has been widely used for developing whole-cell biosensors due to its GRAS status, wide availability of known antibiotic-inducible promoters and its ease of genetic manipulations (Hutter et al., 2004; Urban et al., 2007; Czarny et al., 2014).

In the soil microbiome where *B. subtilis* and *Streptomyces* spp. coexist, *B. subtilis* is exposed to the diversity of *Streptomyces*-produced antibiotics at fluctuating concentrations. Beyond the inhibitory action of antibiotics and the corresponding stress responses against them, hormesis has also been observed, which describes a concentration-dependent transcription modulation of antibiotics independent of the antimicrobial activity. Antibiotics with stimulatory effects at subinhibitory concentrations are proposed to act as cell-signaling molecules involved in modulating the interactions within microbial populations (Yim et al., 2007). In this work, we explore such natural soil-microbiome interactions and the effect of the presence of bioactive microbial metabolites. This allowed us to identify new biosensor candidates for expanding the tools for screening novel antibiotics, such as antifungals. Challenging *B. subtilis* with the antifungal amphotericin B resulted in the induction of the *lnrLMN* operon encoding an ABC transporter that is regulated by the LnrJK two-component signaling system (TCS). We characterized the *lnrL* promoter and the signal transduction mediated by the LnrJK TCS to develop a whole-cell biosensor specific for amphotericin-like polyenes in *B. subtilis*. We removed the negative regulatory constrains exerted by the LnrLMN transporter on LnrJK-dependent

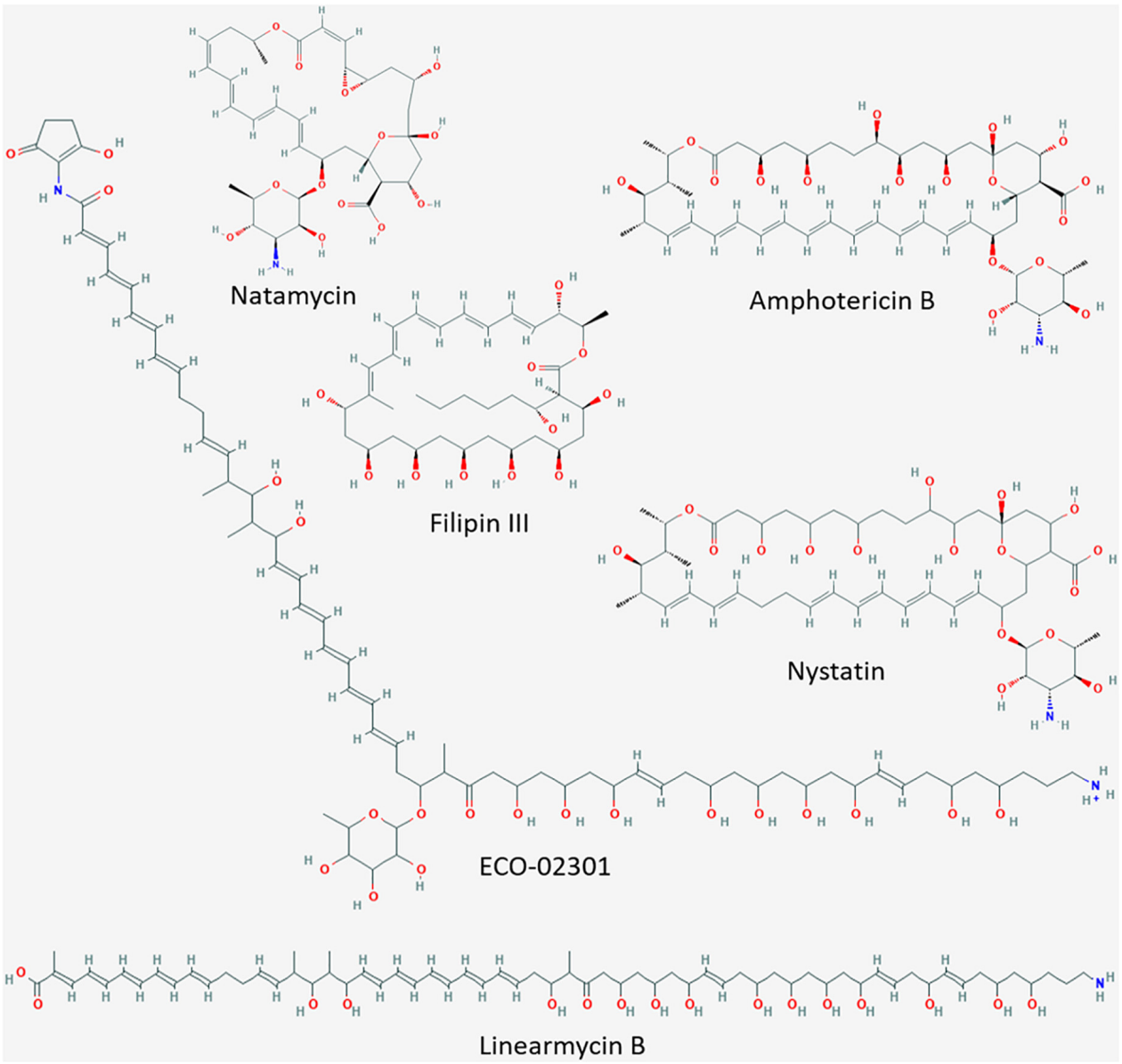

FIGURE 1 | Cyclic and linear polyenes. Molecular structure images downloaded from National Center for Biotechnology Information, PubChem Database (accessed on Apr. 20, 2020) (Kim et al., 2015). Amphotericin B, CID = 5280965 (https://pubchem.ncbi.nlm.nih.gov/compound/5280965#section~=~2D-Structure); nystatin, CID = 6433272 (https://pubchem.ncbi.nlm.nih.gov/compound/6433272#section~=~2D-Structure); ECO-02301, CID = 90658124 (https://pubchem.ncbi.nlm.nih.gov/compound/90658124#section = 2D-Structure); filipin III, CID = 6433194 (https://pubchem.ncbi.nlm.nih.gov/compound/6433194#section = 2D-Structure); natamycin, CID = 5284447 (https://pubchem.ncbi.nlm.nih.gov/compound/5284447#section = 2D-Structure); linearmycin B, CID = 10328913 (https://pubchem.ncbi.nlm.nih.gov/compound/10328913#section = 2D-Structure).

signaling to implement a biosensor with optimized promoter readout and enhanced dynamics. We demonstrate the robustness and sensitivity of our novel biosensor with different samples. Our data highlights the potential of exploring bacterial perception of harmless bioactive molecules present in their natural niches and it indicates that this cell-based biosensor could be very useful for identifying new amphotericin-like polyene antibiotics with possible therapeutic applications.

MATERIALS AND METHODS

Bacterial Strains, Plasmids and Growth Conditions

Table 1 lists the strains used in this study. *Escherichia coli* DH10β was used as an intermediate host for cloning. *B. subtilis* and *E. coli* cells were routinely grown in Luria-Bertani medium (LB-Medium (Luria/Miller), Carl Roth

TABLE 1 | Bacterial strains used in this study.

Strain	Description[a]	Source or references
Escherichia coli DH10β	F$^-$ *mcrA* Δ(*mrr-hsdRMS-mcrBC*) Φ80d*lacZ*Δ*M15* Δ*lacX74 endA1 recA1 deoR* Δ(*ara,leu*)7697 *araD139 galU galK nupG rpsL* λ$^-$	Laboratory stock
Streptomyces nodosus ATCC14899	–	DSMZ – German Collection of Microorganisms and Cell Cultures
Streptomyces noursei	–	Laboratory stock
Bacillus subtilis		
W168	Wild type; *trpC2*	Laboratory stock
TMB1151	W168 Δ*lialH*	Radeck et al., 2016
TMB3822	W168 pBS3C*lux*-P$_{lialI}$	Popp et al., 2017
TMB4173 (P$_{lnrL\,127}$)	W168 *sacA*:*cm*^{r} P$_{lnrL}$ (127)- *luxABCDE*	This study
TMB4220 (P$_{lnrL\,468}$)	W168 *sacA*:*cm*^{r} P$_{lnrL}$ (468)- *luxABCDE*	This study
TMB4221 (P$_{lnrL\,383}$)	W168 *sacA*:*cm*^{r} P$_{lnrL}$ (383)- *luxABCDE*	This study
TMB4222 (P$_{lnrL\,308}$)	W168 *sacA*:*cm*^{r} P$_{lnrL}$ (308)- *luxABCDE*	This study
TMB4223 (P$_{lnrL\,231}$)	W168 *sacA*:*cm*^{r} P$_{lnrL}$ (231)- *luxABCDE*	This study
TMB4237	W168 *lnrLMN*:*kan*^{r}	This study
TMB4238	W168 *lnrJK*:*kan*^{r}	This study
TMB4241	W168 Δ*lialH lnrLMN*:*kan*^{r}	This study
TMB5408 (P$_{lnrL\,147}$)	W168 *sacA*:*cm*^{r} P$_{lnrL}$ (147)- *luxABCDE*	This study
MB5422	W168 *lnrJK*:*kan*^{r}, *sacA*:*cm*^{r} P$_{lnrL\,231}$-*luxABCDE*	This study
TMB5423	W168 *lnrLMN*:*kan*^{r}, *sacA*:*cm*^{r} P$_{lnrL\,231}$-*luxABCDE*	This study
TMB5473 (P$_{lnrL\,191}$)	W168 *sacA*:*cm*^{r} P*lnrL* (191<-)- *luxABCDE*	This study
TMB5578	W168 Δ*lnrLMN*, clean deletion	This study
TMB5600	W168 Δ*lnrLMN sacA*:*cm*^{r} P$_{lnrL\,231}$-*luxABCDE*	This study
TMB5771	W168 *yhblJ-yhcABC*:*kan*^{r}	This study
TMB5772	W168 *mdtRP*:*mls*^{r}	This study
TMB5779	W168 *sacA*:*cm*^{r} P$_{yhbI}$ *luxABCDE*	This study
TMB5780	W168 *sacA*:*cm*^{r} P$_{mdtR}$ *luxABCDE*	This study

[a] *cm*^{r}, *chloramphenicol resistance; kan*^{r}, *kanamycin resistance; mls*^{r}, *macrolide-lincosamide-streptogramine resistance.*

GmbH + Co., KG, Karlsruhe, Germany) at 37°C with agitation. 1.5% (w/v) agar (Agar-Agar Kobe I, Carl Roth GmbH + Co., KG, Karlsruhe, Germany) was added to prepare the corresponding solid media. *Streptomyces* spp. were grown in MYM medium supplemented with trace elements [0.4% (w/v) maltose, 0.4% (w/v) yeast extract, 1% (w/v) malt extract, trace elements: 0.004% (w/v) $ZnCl_2$, 0.02% (w/v) $FeCl_3 \times 6H_2O$, 0.001% (w/v) $CuCl_2 \times 2H_2O$, 0.001% (w/v) $MnCl_2 \times 4H_2O$, 0.001% (w/v) $Na_2B_4O_7 \times 10H_2O$, 0.001% (w/v) $(NH_4)_6Mo_7O_{24} \times 4H_2O$ (w/v)] and for solid medium 2% (w/v) agar was added. *Streptomyces* spp. strains were either incubated at 28°C or at room temperature. All bacterial strains were stored at −80°C in their corresponding growth media supplemented with 20% (v/v) glycerol (Carl Roth GmbH + Co., KG, Karlsruhe, Germany). Ampicillin (Carl Roth GmbH + Co., KG, Karslruhe, Germany) 100 μg ml^{-1} was added to *E. coli* when required. Chloramphenicol (Sigma-Aldrich, Merck KGaA, Darmstadt, Germany) 5 μg ml^{-1}, kanamycin (VWR International GmbH, Darmstadt, Germany) 10 μg ml^{-1} or erythromycin (Sigma-Aldrich, Merck KGaA, Darmstadt, Germany) 1 μg ml^{-1} and lincomycin (Sigma-Aldrich, Merck KGaA, Darmstadt, Germany) 25 μg ml^{-1} (MLS resistance) were added to *B. subtilis* when required.

Cloning Procedures

Construction of Transcriptional Promoter-*luxABCDE* Fusions

All vectors and plasmids used in this study are listed in **Table 2**; all oligonucleotides used in this study are listed in **Supplementary Table S1**. Ectopic integrations of the different promoter-*luxABCDE* fusion fragments into the *B. subtilis sacA* locus were constructed based on the vector pBS3C-*lux* (Radeck et al., 2013). Promoter fragments were generated by PCR from genomic DNA with specific primers (**Supplementary Table S1**) designed according to the BioBrick cloning standard (Radeck et al., 2013). For the P$_{lnrL468}$ promoter, primers TM5098 and TM5695 were used; for all 5′ end truncations, the reverse primer TM5695 was used in combination with the corresponding forward primers; for the 191 bps length 3′ end truncation, the forward primer TM5789 was used in combination with TM6014 (**Supplementary Table S1**). For the confirmation of the RNA seq results, two additional promoter-*luxABCDE* fusions - P$_{yhbI}$ and P$_{mdtR}$ - were constructed using the primer pairs TM6334/6335 and TM6336/6337. After transformation into *E. coli* DH10β, ampicillin resistant colonies were examined by PCR with primers TM2262/2263, the inserts were verified by DNA sequencing and the resulting pBS3C-derived plasmids (**Table 2**) were linearized with *Sca*I and used to transform *B. subtilis*. Correct integration

TABLE 2 | Vectors and plasmids used in this study.

Name	Description (primers used for cloning/antibiotic resistances[a])	Source or references
Vectors		
pBS3Clux	*pAH328* derivative; *amp*^{r}, *cm*^{r}, *sacA*'…'*sacA*, *luxABCDE*	Laboratory stock
pMAD	*erm*^{r}, ori(pE194-Ts), MCS-$P_{clpB-bgaB}$, ori(pBR322), *bla*^{r}	Arnaud et al., 2004
pDG647	*pSB119*, *erm*^{r}	Guérout-Fleury et al., 1995
pDG783	*pSB118*, *kan*^{r}	Guérout-Fleury et al., 1995
Plasmids		
pBS3C-P_{lnrL}(468)-*lux*	TM5098/TM5695; *cm*^{r}, *amp*^{r}	This study
pBS3C-P_{lnrL}(383)-*lux*	TM5787/TM5695; *cm*^{r}, *amp*^{r}	This study
pBS3C-P_{lnrL}(308)-*lux*	TM5788/TM5695; *cm*^{r}, *amp*^{r}	This study
pBS3C-P_{lnrL}(231)-*lux*	TM5789/TM5695; *cm*^{r}, *amp*^{r}	This study
pBS3C-P_{lnrL}(147)-*lux*	TM5855/TM5695; *cm*^{r}, *amp*^{r}	This study
pBS3C-P_{lnrL}(127)-*lux*	TM5694/TM5695; *cm*^{r}, *amp*^{r}	This study
pBS3C-P_{lnrL}(191<-)-*lux*	TM5789/TM6014; *cm*^{r}, *amp*^{r}	This study
pBS3C-P_{yhbI}-*lux*	TM6334/TM6335; *cm*^{r}, *amp*^{r}	This study
pBS3C-P_{mdtR}-*lux*	TM6336/TM6337; *cm*^{r}, *amp*^{r}	This study

[a] *cm*^{r}, *chloramphenicol resistance, amp*^{r}, *ampicillin resistance, erm*^{r}, *erythromycin resistance, kan*^{r}, *kanamycin resistance, bla*^{r}, *β-lactam resistance.*

into the *sacA* locus was checked by amplification of an *up*- and *down*- PCR fragment with primers TM2505/2506 and TM5955/5956 or TM2507/2508, respectively. In each case, two independent positive clones were selected as reporter strains.

Construction of Allelic Replacement Mutant Strains

Mutant strains lacking either *lnrJK* or *lnrLMN* (strains TMB4238 and TMB4237, respectively, **Table 1**) were generated by allelic replacement mutagenesis in *B. subtilis* W168 using long flanking homology (LFH)-PCR (Mascher et al., 2003). The genes were replaced by a kanamycin (*kan*) resistance cassette. The procedure was performed as described previously (Staroń et al., 2011). The same procedure was applied to construct the two *B. subtilis* W168 mutant strains *yhbIJ-yhcABC:kan* (TMB5771) and *mdtRP:mls* (TMB5772). Primer pairs used for amplification of the *kanamycin* and *mls* cassettes, up- and down-fragments, and primers used to check the allelic replacements are listed in **Supplementary Table S1**.

The reporter strains TMB5422 and TMB5423 (lacking *lnrJK* or *lnrLMN*, respectively) containing the $P_{lnrL231}$-*luxABCDE* operon were created by transformation of TMB4238 and TMB4237 with pBS3C-P_{lnrL}(231)-*lux* (**Tables 1**, **2**).

Development of the Whole-Cell Biosensor

The *B. subtilis* Δ*lnrLMN* $P_{lnrL231}$ whole-cell-biosensor (TMB5600, **Table 1**) was created by deleting the ABC-transporter *lnrLMN* and the subsequent introduction of the already created plasmid pBS3C-P_{lnrL}(231)-*lux*. At first, two 1000 bp fragments up- and down of the *lnrLMN* operon were joined *in silico* (*lnrLMN*updo) and synthesized as gBlock by Integrated DNA Technologies (IDT, Coralville, IA, United States). The gBlock was solubilized according to manufacturer's instructions and amplified using the primer pair TM6094/95. Afterward, the PCR product and the vector pMAD were digested with the restriction enzymes *Eco*RI and *Bam*HI (New England Biolabs, Ipswich, Massachusetts, United States) and ligated using the T4 DNA polymerase (New England Biolabs, Ipswich, MA, United States). The ligation mix was directly used for the transformation of *B. subtilis* W168 [see protocol for *B. subtilis* transformation (Harwood and Cutting, 1990)]. The pMAD based deletion was carried out as described in Arnaud et al. (2004). In brief, the *B. subtilis* transformants were selected on macrolide-lincosamide-streptogramines (MLS) LB agar plates that also contained X-gal at 30°C. Afterward, one blue colony was picked to inoculate an MLS-LB day culture. After an incubation of 2 h at 30°C, the temperature was shifted to 42°C for 6 h to induce an integration of the plasmid into the genome. The culture was plated again on MLS – X-gal LB agar plates and incubated at 45°C overnight. The successful integration of pMAD-*lnrLMNupdo* into the genome was checked by PCR using the primer pairs TM253/6026 and TM254/6027. Subsequently, positive clones were inoculated into an LB day culture without selection and incubated at 30°C for 6 h, then the temperature was shifted to 42°C again for 3h and finally the culture was plated on X-gal LB plates without selection and incubated at 42°C overnight. Positive clones, which did not show any β-galactosidase activity but MLS sensitivity, were examined by PCR with the primer pair TM6028/29 and successful deletion of *lnrLMN* was verified by subsequent sequencing (TM6028/6029/5694). Afterward, the strain W168 Δ*lnrLMN* (TMB5578, **Table 1**) was transformed with pBS3C-P_{lnrL}(231)-*lux* to create the biosensor strain TMB5600.

Reagents

The Amphotericin B solution (product code L0009) was purchased from Biowest (VWR International GmbH, Darmstadt, Germany). Filipin III (from *Streptomyces filipinensis*, product code F4767), natamycin (product code 32417), and sodium deoxycholate (product code D6750) were purchased from Sigma-Aldrich (Merck KGaA, Darmstadt, Germany). Nystatin (product code 15340029) was purchased from Gibco (Thermo Fisher Scientific, Waltham, Massachusetts, United States). Ethanol (product code 9065.4) and methanol (CP43.3) were purchased from Carl Roth (GmbH + Co., KG, Karslruhe, Germany).

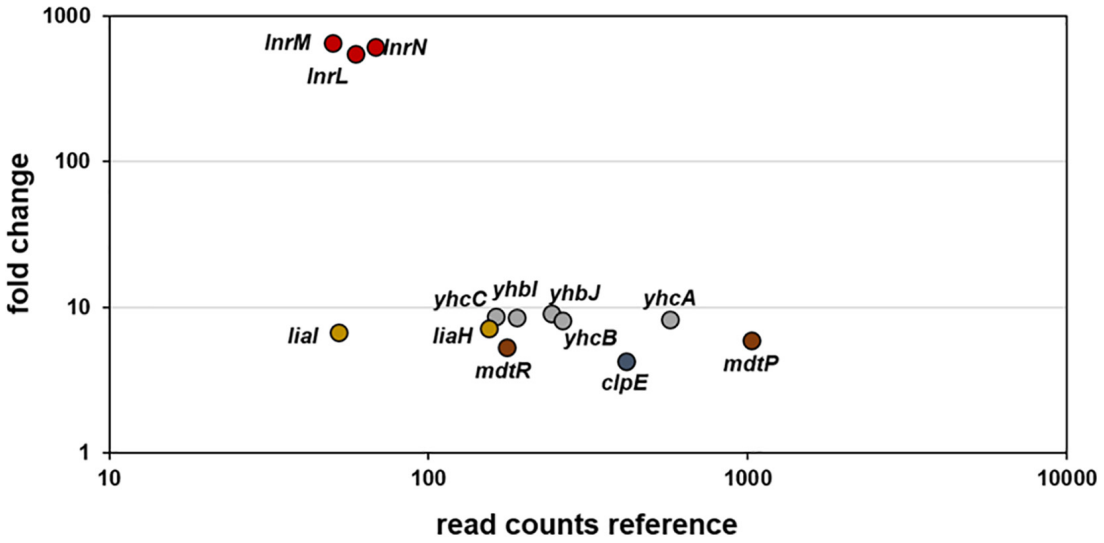

FIGURE 2 | RNA-sequencing (RNA-seq) profile of *B. subtilis* upon amphotericin B treatment. Visualization of altered gene expression in *B. subtilis* upon 10 μg ml^{-1} amphotericin B exposure after 10 min, compared to non-induced control samples. Fold change of elevated RNA-seq counts are plotted over read counts in the reference condition. Same colored dots highlight genes encoded within an operon. For further details, see **Table 3**.

TABLE 3 | RNA-seq results.

Gene(s)[1]	log2 fold change, *p*-value[2]	Regulators[3]	Products/function[3]
*lnr**LMN***	**9.33**, $5{\cdot}10^{-210}$	SigG/F, LnrK	ABC transporter, resistance against linearmycin
*yhb**IJ**-yhc**ABC***	**3.17**, $4{\cdot}10^{-16}$	–	Putative efflux system
*lia**IH***	**2.83**, $6{\cdot}10^{-4}$	LiaRS	Phage shock protein, resistance against cell wall antibiotics
*mdt**RP***	**2.55**, $3{\cdot}10^{-38}$	–	Multidrug-efflux system
clpE	**2.08**, $4{\cdot}10^{-6}$	CtsR	ATPase subunit of ClpEP protease

Differential gene expression between samples exposed to 10 μg ml^{-1} amphotericin B compared to non-induced conditions. Genes were considered that showed a log2 fold change greater than 2 and a p-value smaller than 0.05. No genes were significantly down regulated upon amphotericin B treatment. [1]All genes with fold-induction ≥ 2 fold are indicated in bold. [2]For each operon, the highest value is listed. [3](Putative) regulators and the function of the gene products are adapted from SubtiWiki (Zhu and Stülke, 2017).

Preparation of *Streptomyces* spp. Subnatants

Streptomyces spp. subnatants were prepared by transferring *Streptomyces* spp. spore material into 20 ml liquid MYM medium in round culture dishes (ref. 633180; Greiner Bio-One International GmbH, Kremsmünster, Austria) and incubated at room temperature for 2–3 weeks. Afterward, the liquid MYM medium underneath the *Streptomyces* spp. cultures was transferred to a centrifugation tube and remaining cell particles were removed by centrifugation and sterile filtration (0.2 μm; Filtropur S 0.2, ref. 83.1826.001; Sarstedt AG & Co., KG, Nümbrecht, Germany). The resulting *Streptomyces* spp. subnatants were stored at 4°C until further use.

Sensitivity Assays and Promoter Induction Assays in Liquid Medium

All the experiments were performed in Luria-Bertani medium. Overnight cultures of the strains under study were prepared with antibiotic selection when required. The day cultures (10 ml) were inoculated 1:1000 with overnight cultures and incubated at 37°C (220 rpm) without antibiotic selection until an OD_{600} of around 0.2 was reached. Then, the cell suspensions were diluted to an OD_{600} of 0.01, they were distributed into a 96-well plate (80 μl per well) and incubated at 37°C (continuous middle shacking) in the Synergy™ NeoAlpha B plate reader (BioTek®, Winooski, VT, United States). After one hour of incubation, 20 μl of the substances under study (at 5 times the desired final concentration) were added to the wells and incubation at 37°C with continuous middle shaking was continued for further 18 h. For the sensitivity assays, the cells were plated in transparent 96-wells plates (ref. 83.3924, Sarstedt AG & Co., KG, Nümbrecht, Germany) and OD_{600} was measured every 5 min to monitor the growth rate. For the promoter induction assays, the cells were plated in black 96-wells plates (ref. 655097, Greiner Bio-One International GmbH, Kremsmünster, Austria) and besides OD_{600}, luminesce was monitored every 5 min for at least 18 h.

In the case of amphotericin B whose composition includes sodium deoxycholate to improve solubility (in a ratio 250 μg/ml: 205 μg/ml, amphotericin B: sodium deoxycholate), a control sensitivity assay was performed with equivalent concentrations of pure deoxycholate. While some toxicity could be observed with the highest concentration of sodium deoxycholate (**Supplementary Figure S1A**), no promoter induction was detected (**Supplementary Figure S1B**) confirming the specific activation of P_{lnrL} by amphotericin B. In the case of filipin III and natamycin, control assays with the corresponding solvents, ethanol and methanol, respectively, performed with equivalent

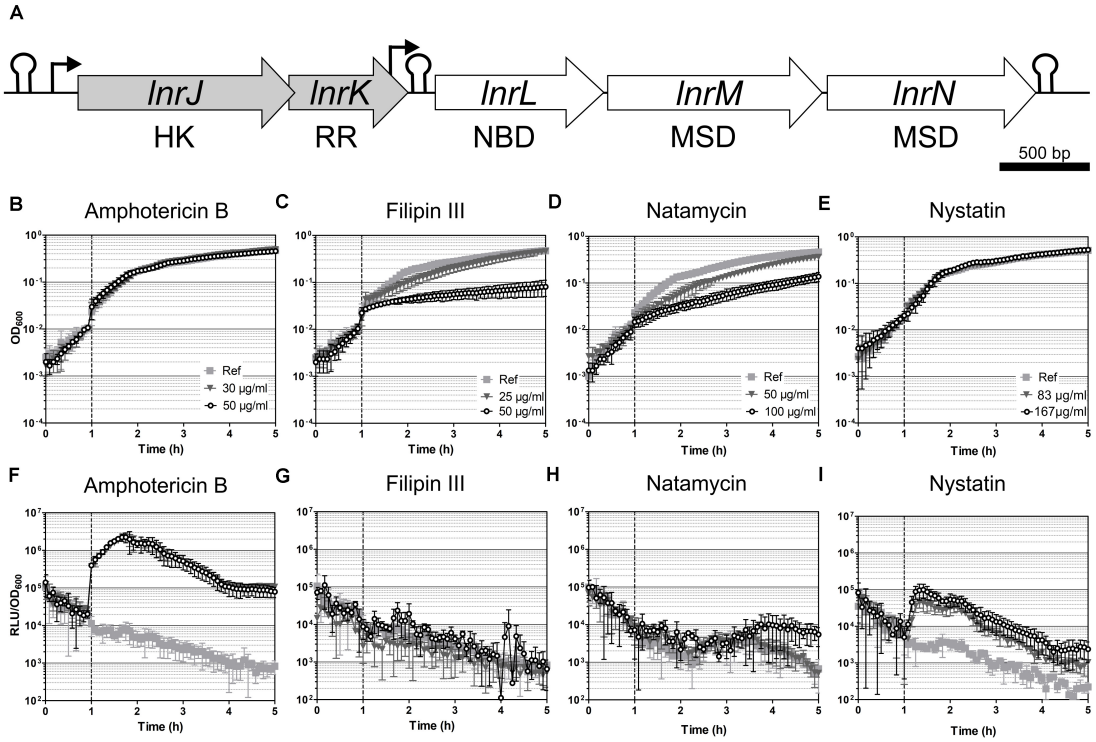

FIGURE 3 | Induction spectrum of the LnrJKLMN system in *B. subtilis*. **(A)** Genetic organization of the *lnrJKLMN* operon (formerly known as *yfiJKLMN*) (Yamamoto et al., 1996). The genes *lnrJ* and *lnrK* (block gray arrows) encode for a two-component system; the genes *lnrL*, *lnrM* and *lnrN* (block white arrows) encode for an ABC transporter. Genes drawn to scale. Rho-independent transcriptional terminators are indicated by hairpins; promoters are indicated by black bent arrows; HK, histidine kinase; RR, response regulator; NBD, nucleotide binding domain; MSD, membrane spanning domain. **(B–I)** Induction of the $P_{lnrL468}$ promoter by macrolide polyenes in liquid media. Effect of antibiotic exposure on growth is indicated as OD_{600} **(B–E)**, and promoter induction as relative luminescence units by OD_{600} **(F–I)**. The time of antibiotic addition is indicated with a vertical dashed line. The antibiotic concentrations used are indicated in the upper panel graphs. The results presented from **(B)** to **(I)** correspond to strain TMB4220. The experiments were performed at least in triplicate with two independent clones. Means and standard deviations are depicted.

concentrations showed that the *B. subtilis* growth impairment was due to the solvent toxicity (**Supplementary Figures S1C–F**).

In the experiments with *Streptomyces sp.* subnatants, at concentrations ranging from 20% to 1.25%, addition of the suspensions caused a color change of the LB medium thus affecting the absorbance values. OD_{600} values were corrected by the mean blank values obtained from the different subnatants concentrations in LB medium without the inoculation with *B. subtilis*. In the case of the induction with pure compounds, the same correction was applied when necessary, otherwise the OD_{600} values were corrected by the mean blank values of LB medium prior to inoculation with cells. Afterward, the absolute luminescence values were divided by these corrected OD_{600} values resulting in relative luminescence units by OD_{600} (RLU/OD_{600}).

Spot-on-lawn Assay

The overnight and day cultures of the *B. subtilis* reporter strains were prepared in LB liquid medium as described above. In the case of the induction with *Streptomyces* spp. secreted natural products, *Streptomyces* spp. spore suspensions were spotted onto MYM agar plates and incubated for 3 days at room temperature or 28°C. Next, day cultures of the biosensor strain TMB5600 were incubated at 37°C (220 rpm) until an OD_{600} of around 0.4–0.7 was reached. Then, the cell suspensions were diluted to an OD_{600} of 0.01 in 10 ml of LB-soft (0.75%) agar, homogenized by shortly vortexing, and poured on top of the pre-grown *Streptomyces* spp. plates. In the case of induction with pure compounds, after a drying period of at least 10 min, the biosensor lawn was inoculated with 20 µl of macrolide polyene stock solutions [amphotericin B, 250 µg ml^{-1}; nystatin, 3.33 mg ml^{-1}, equivalent to 10^4 U ml^{-1} (Lightbown et al., 1963)] on top of the agar. Subsequently, another drying period was conducted to allow the antibiotics to be completely absorbed into the agar. Afterward, all plates were incubated upside down overnight at 37°C. The luminescence output was measured with a FluorChem™ SP from Alpha Innotech with an exposition time of 2 min at a high-medium intensity.

RNA Sample Preparation and Sequencing

RNA-seq experiments were performed in triplicates with *B. subtilis* WT (BaSysBio) (Anagnostopoulos and Spizizen, 1961; Nicolas et al., 2012) in LB medium (Sigma L3522). Day

cultures were inoculated from overnight cultures and grown until mid-exponential phase (OD_{600} approx. 0.4) at 37°C. Subsequently, a second day culture of 200 ml LB (Sigma L3522) was started with an OD_{600} = 0.1. Once this second day culture reached OD_{600} = 0.5, cells were split into 25 ml aliquots and either exposed to 10 μg ml^{-1} amphotericin B (final concentration) or remained untreated for 10 min. Even the highest amphotericin B concentration tested did not lead to a growth impairment (**Supplementary Figure S2A**). Therefore, a concentration of 10 μg ml^{-1} was selected ensuring full P_{lnrL} induction (**Supplementary Figure S2C**) and allowing a margin for potential expression of less sensitive amphotericin B responding genes, while preventing a big dilution of the RNA samples relative to the control samples. After treatment, cells were transferred to 50 ml falcons and growth was immediately stopped in an ice water bath followed by centrifugation at 8000 rpm at 4°C for 3 min. The supernatants were discarded, and the resulting pellets were stored at −80°C. RNA isolation was performed with a phenol-chloroform extraction method as previously described (Popp et al., 2020). The cDNA library was prepared using the NEB Ultra RNA directional prep kit for Illumina and sequencing was performed on an Illumina HiSeq3000 system. Sequencing reads were mapped to the BaSysBio 168 strain (NC_000964.3) using Bowtie2 (Langmead and Salzberg, 2012). The software program featureCounts of the Subread package (Liao et al., 2014) was applied to generate counts for known genes. Differentially expressed genes were identified using the R/Bioconductor package DESeq2 (Love et al., 2014). The raw and processed RNA sequencing data obtained in this study has been deposited at the NCBIs Gene Expression Omnibus (Edgar et al., 2002) and is accessible via the GEO accession number GSE148903.

RESULTS AND DISCUSSION

Identification of the Amphotericin B Stimulon of *B. subtilis* by Transcriptome Profiling

Streptomyces spp. are common soil bacteria, where they produce antibiotics targeting fungi and bacteria (Baltz, 2008). However, at concentrations below inhibitory levels, antibiotics might also function as signaling molecules (Yim et al., 2007). As *B. subtilis* is also a soil inhabitant and competing for the same ecological niche, we aimed at identifying cellular processes activated in *B. subtilis* upon exposure to *Streptomyces*-produced bioactive molecules potentially present in the same habitat. We selected amphotericin B since it has only weak inhibitory activity toward bacteria and primarily targets fungal cells. We challenged *B. subtilis* wild type with a sublethal concentration of amphotericin B and compared the global RNA transcriptional profile with non-induced samples (for details see Materials and Methods).

RNA-sequencing (RNA-seq) experiments were performed with *B. subtilis* treated with 10 μg ml^{-1} amphotericin B and gene expression profiles between treated and non-treated samples were compared 10 min post induction (see methods for details). Upon exposure to amphotericin B, only 13 genes were differentially expressed (**Figure 2** and **Table 3**). Most prominent was the upregulation of the *lnrLMN* operon, an ABC transporter driven by the P_{lnrL} promoter and part of the LnrJK TCS regulon (Yamamoto et al., 1996). Previously, this system has been identified as resistance determinant against linearmycins (Stubbendieck and Straight, 2015). Additionally, moderate induction of the LiaRS TCS controlled genes *liaIH* was observed. This system is a specific marker for cell envelope stress and responds to interference with the lipid II cycle of cell wall biosynthesis (Mascher et al., 2004; Wolf et al., 2010). Further, amphotericin B treatment caused moderate induction of the *mdtRP* operon encoding a regulator and a multidrug efflux transporter involved in mediating resistance against several antibiotics (Kim et al., 2009). Induction of *clpE*, the ATPase subunit of the ClpE-ClpP protease, suggests a moderate general physiological impact upon amphotericin B exposure in *B. subtilis*. This protease controls the stability and activity of central transcriptional regulators, thereby influencing developmental decisions and stress-responses (Frees et al., 2007). Also, the *yhbIJ-yhcABC* operon showed moderate induction, however, so far only little is known about these genes and linking a physiological impact to amphotericin B response will require further investigations.

In order to verify the RNA-seq data for the induced operons, we next constructed promoter-*luxABCDE* fusions that were inserted into the *sacA* locus of the *B. subtilis* wild type strain W168, resulting in strains P_{liaI} (TMB3822), P_{yhbI} (TMB5779), P_{mdtR} (TMB5780) and $P_{lnrL468}$ (TMB4220) (**Table 1**). We tested their activation but failed to observe amphotericin B-dependent induction for P_{liaI}, P_{yhbI} and P_{mdtR} (data not shown). In addition, single mutants lacking the *liaIH* operon, the *yhbIJ-yhcABC* operon, the *mdtRP* operon and double mutants of *liaIH* combined with *lnrLMN* (strains TMB1151, TMB5771, TMB5772 and TMB4241, **Table 1**), showed no phenotype when challenged with amphotericin B (data not shown). However, we observed a strong, dose-dependent induction of $P_{lnrL468}$ in response to amphotericin B (**Figure 3F** and **Supplementary Figure S2**). The global response of *B. subtilis* to amphotericin B treatment therefore does not mount a specific resistance and mainly affects the expression of the *lnrLMN* operon alone, which showed an induction of over 500-fold (**Figure 2** and **Table 3**).

Furthermore, own unpublished results comparing the amphotericin B induced transcriptome with that of nine other non-polyene antibiotics indicates that the transcriptome pattern for amphotericin B is indeed unique. With the exception of *liaIH* operon, which is more strongly induced by bacitracin and vancomycin, the induction of the eleven remaining genes, and particularly the induction of the *LnrLMN* operon, is specifically triggered by amphotericin B exposure (Zhang et al. personal communication). This highly specific cellular response of *B. subtilis* upon amphotericin B exposure without having any effect on growth and the strong induction of the *lnr* operon motivated us to further characterize this system to develop a whole-cell biosensor.

Induction Spectrum of the *lnr* System in *B. subtilis*

The *lnrJKLMN* locus of *B. subtilis* W168 (*BSU08290-BSU08330,* formerly *yfiJKLMN*) encodes a TCS, LnrJK, and an ABC transporter, LnrLMN (**Figure 3A**; Yamamoto et al., 1996). TCSs consist of a membrane-anchored histidine kinase (HK) and a cytoplasmic response regulator (RR). Upon stimulus perception, the HK autophosphorylates at a histidine residue. Subsequently, the high energy phosphate group is specifically transferred to an aspartyl residue in the cognate RR leading to its activation. As a consequence, the activated RRs usually mediate the cellular output, often by acting as transcriptional activators/repressors (Stock et al., 2000). In *B. subtilis* NCIB3610, the TCS LnrJK regulates the expression of the LnrLMN transporter, which confers resistance to linearmycins: long linear polyene antibiotics (**Figure 1**) with antifungal and antibacterial activity, isolated from *Streptomyces* sp. no. 30 (Sakuda et al., 1996; Stubbendieck and Straight, 2015). A reporter strain, P_{yfiLMN}-*lacZ* was activated by linearmycins and ECO-02301 and weakly induced by the non-lytic amphotericin B and nystatin, while it was not induced by the lytic lipopeptide daptomycin (Stubbendieck and Straight, 2017). The authors concluded that the signaling leading to promoter activation was specific for linearmycins, and hence renamed the system to *lnrJKLMN* for linearmycin sensing and response (Stubbendieck and Straight, 2015, 2017).

We next studied the response of the $P_{lnrL468}$-lux reporter strain in liquid medium to the commercially available cyclic polyenes filipin III, natamycin, and nystatin (**Figure 1**). Filipin III and natamycin did not activate $P_{lnrL468}$ (**Figures 3G,H**), but we observed a weak induction of $P_{lnrL468}$ by nystatin (**Figure 3I**), a compound structurally related to amphotericin B (**Figure 1**). Our results supported the previously reported weak induction of the *lnrL* promoter after spotting nystatin and amphotericin B on top of *B. subtilis* P_{yfiLMN}-*lacZ* colonies (Stubbendieck and Straight, 2017). We next aimed at determining the minimal polyene-responsive *lnrL* promoter, in order to develop the P_{lnrL} promoter into a whole-cell biosensor.

Optimization of the *lnrL* Promoter to Develop a Whole-Cell Biosensor

Toward this goal, we progressively truncated the *lnrL* promoter fragment, starting at the 5′-position from $P_{lnrL468}$ to a final promoter length of 127 base pairs, and generated corresponding transcriptional *luxABCDE* reporter fusions (**Table 1**). All of the promoter constructs ended at the identical 3′-end as the previous fragment, that is, −16 base pairs relative to the GTG start codon of *lnrL* (**Figure 4A**). In case of the 3′-truncation, the promoter extended from the 5′-end of $P_{lnrL231}$ until - 57 base pairs relative to the *lnrL* start codon (**Figure 4A**). The promoter fusions were integrated into the *sacA* locus in *B. subtilis* W168 wild type and the promoter activity of the resulting reporter strains (**Table 1**) was determined by a quantitative luminescence assay after induction with 4 μg ml^{-1} of amphotericin B, since this concentration was sufficient to generate full $P_{lnrL468}$ induction (**Supplementary Figure S2C**).

The progressively 5′-end truncated *lnrL* promoters $P_{lnrL383}$, $P_{lnrL308}$ and $P_{lnrL231}$ showed activities comparable to $P_{lnrL468}$ after amphotericin B addition (**Figure 4A** gray bars). While $P_{lnrL147}$ showed an almost negligible decreased promoter activity, a further truncation of 20 nucleotides in $P_{lnrL127}$ led to a complete loss of inducible promoter activity. The 3′-truncation $P_{lnrL191}$ starting at the 5′ end of $P_{lnrL231}$ until - 57 base pairs relative to the *lnrL* start codon also led to a complete loss of promoter activity after amphotericin B addition (**Figure 4A**). We therefore proceeded our characterization with $P_{lnrL231}$, thereby ensuring the coverage/inclusion of all potential regulatory elements of the promoter and optimal promoter activity (**Figure 4A**).

Characterization of the LnrJKLMN System Regulation: Boosting Output to Background Ratio

The LnrLMN ABC transporter was reported to confer resistance to linearmycins but not to be required for signaling the presence of the linearmycins to the TCS LnrJK (Stubbendieck and Straight, 2015, 2017). Since P_{lnrL} is strongly induced by amphotericin B and weakly by nystatin (**Figure 3**), we next investigated if the LnrJKLMN system mediates amphotericin B and/or nystatin resistance. For that goal, two mutant strains (TMB4238 and TMB4237, **Table 1**) were constructed that eliminated either *lnrJK*, encoding the TCS, or *lnrLMN*, encoding the ABC transporter. These strains were then subjected to sensitivity assays in liquid medium with increasing serial dilutions of amphotericin B (from 4 to 64 μg ml^{-1}) and nystatin (from 42 to 333 μg ml^{-1}). No difference was observed for both strains compared to the wild type strain (data not shown), indicating that the LnrJKLMN system does not mediate any resistance to these two polyenes.

While LnrLMN is not involved in mediating amphotericin B or nystatin resistance, we still wondered if this ABC transporter might nevertheless be involved in sensing these polyene compounds. This idea was inspired by the analogous Bce-like modules involved in antimicrobial peptide resistance in Firmicutes (named after the prototypical BceRSAB system of *B. subtilis*), which consist of an ABC transporter (BceAB) that senses and signals the presence of the antimicrobial peptide bacitracin to its associated TCS (BceRS). BceR, in turn, strongly induces *bceAB* expression to ultimately mediate high-level bacitracin resistance (Ohki et al., 2003; Rietkötter et al., 2008; Fritz et al., 2015). Consequently, we next investigated if the transporter LnrLMN is required for amphotericin B and nystatin perception and signaling to the TCS LnrJK. We therefore deleted *lnrJK* and *lnrLMN* in the $P_{lnrL231}$-*lux* reporter strain, resulting in strains TMB5422 and TMB5423, respectively. These strains were subjected to induction assays with amphotericin B (4 μg ml^{-1}) and nystatin (167 μg ml^{-1}). While the absence of the TCS LnrJK completely abolished promoter induction, as expected, the absence of the ABC transporter LnrLMN led to a higher $P_{lnrL231}$ activity compared to the wild type (**Figure 4B**): we observed a six-fold increased induction in response to amphotericin B and a 36-fold increased induction in response to nystatin in the *lnrLMN* mutant strain, relative to the corresponding wild type strain. This result demonstrates that the LnrLMN transporter

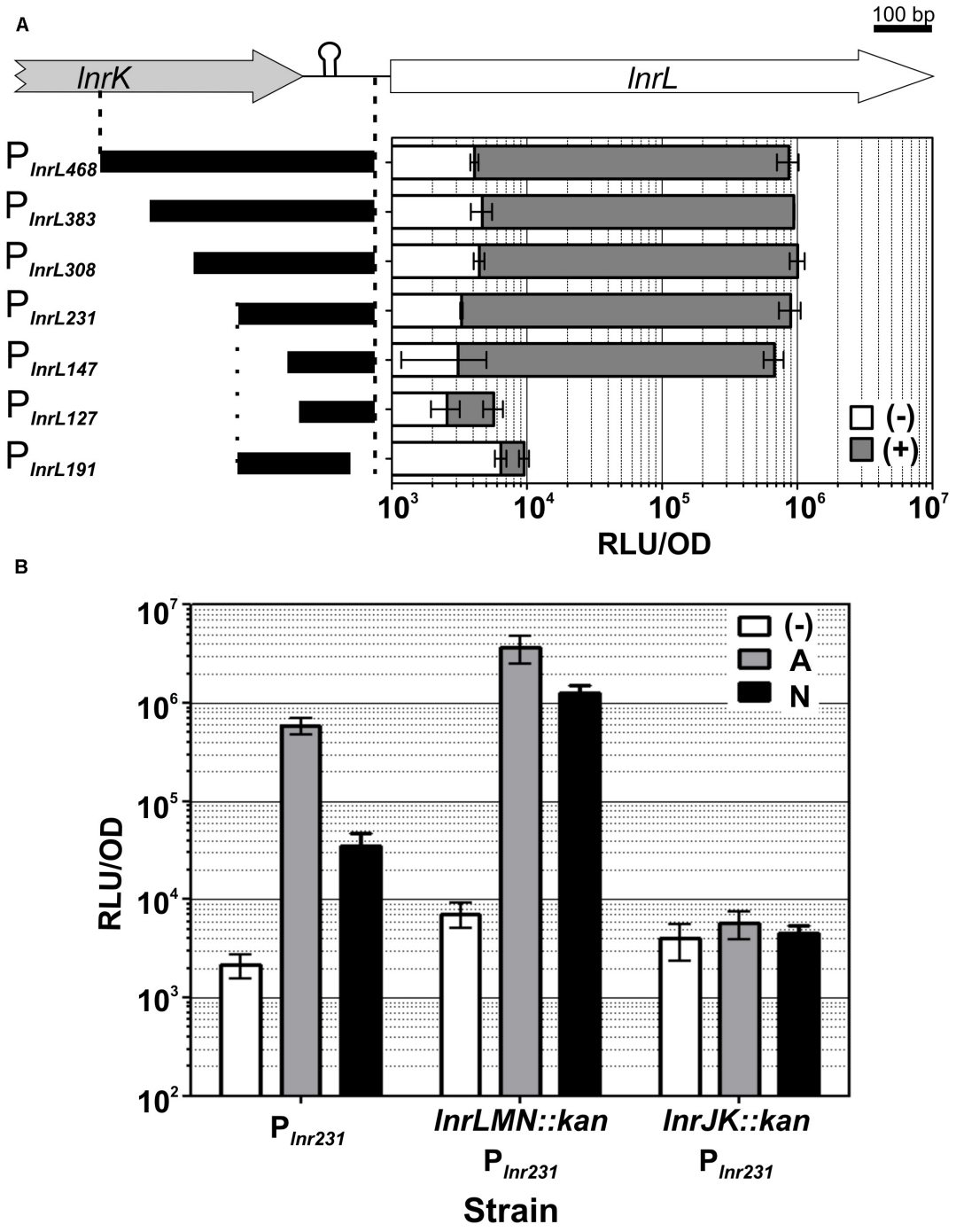

FIGURE 4 | LnrJKLMN system characterization. **(A)** Identification of the minimal *lnrL* promoter fragment. The genetic region containing the P_{lnrL} promoter, the promoter truncations constructs and their functional analysis are presented. The genes *lnrK* (block gray arrow) and *lnrL* (block white arrow) are depicted; the length of the initial $P_{lnrL468}$ promoter is indicated by vertical dashed lines. The vertical dotted line indicates the beginning of the 3' promoter truncation. Rho-independent transcriptional terminator between *lnrK* and *lnrL* is indicated by a hairpin. Schematics of P_{lnrL} promoter truncations are drawn as black bars on the left side. Genes and promoter fragments drawn to scale. Promoter activities one hour after induction with 4 μg ml^{-1} of amphotericin B (gray bars) relative to the activities of the uninduced promoters at the same time point (white bars), are presented in the right graph as relative luminescence units by OD_{600}. **(B)** Mechanism of sensing. The activity of $P_{lnrL231}$ in response to amphotericin B and nystatin was determined in a wild type background (strain TMB4223), in a mutant eliminated in the *lnrLMN* transporter (strain TMB5423) and in a mutant eliminated in the *lnrJK* TCS (strain TMB5422). The promoter activity at one-hour post induction with amphotericin B 4 μg ml^{-1} (gray) and nystatin 167 μg ml^{-1} (black) is presented relative to the uninduced state (white), as relative luminescence units by OD_{600}. The chosen concentrations of the compounds correspond to the maximum promoter induction, as indicated by the data shown in Fig. 5. The experiments were performed in quadruplicate with two independent clones; means and standard deviations are depicted.

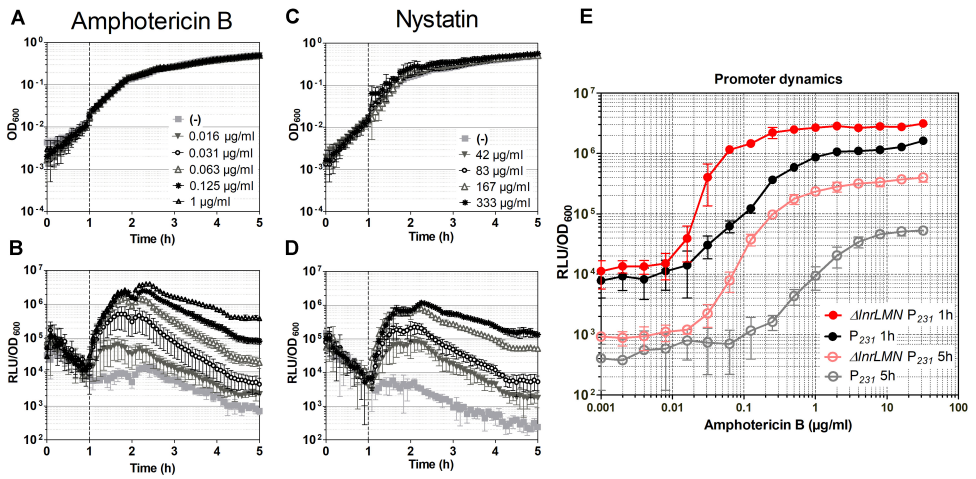

FIGURE 5 | Characterization of the Δ*lnrLMN* $P_{lnrL231}$-*lux* (TMB5600) whole-cell biosensor. **(A–D)** Induction of the Δ*lnrLMN* $P_{lnrL231}$ (TMB5600) by amphotericin B and nystatin in liquid media. The effect of antibiotic exposure on growth is indicated as OD_{600} **(A)** and **(C)**; the promoter induction is presented as relative luminescence units by OD_{600} **(B)** and **(D)**. The time of antibiotic addition is indicated with a vertical black dashed line. The antibiotic concentrations used are indicated in the upper panels. **(E)** Effect of deletion of *lnrLMN* genes on $P_{lnrL231}$ promoter dynamics. The amphotericin B-concentration dependent promoter induction when the LnrLMN transporter is present (P_{231}, strain TMB4223) or absent (Δ*lnrLMN* P_{231}, strain TMB5600) on the cell is presented. The values correspond to promoter activities one and five hours after induction with serial dilutions of amphotericin B. The symbols color code is indicated in the graph. The experiments were performed at least in triplicate with two independent clones. Means and standard deviations are depicted.

is not involved in polyene sensing, in line with a postulated repressory function of LnrLMN on LnrJK-dependent signaling (Stubbendieck and Straight, 2017), the molecular nature of which remains to be uncovered.

Development and Validation of a Whole-Cell Biosensor Based on the *lnrL* Promoter

Taken together, our results show that (i) the *lnrLMN* operon is the only regulatory target of LnrK and (ii) that LnrLMN exerts an inhibitory effect on LnrJK signaling. For the final whole-cell biosensor strain, an *lnrLMN* clean deletion (strain TMB5578, **Table 1**) was therefore combined with the $P_{lnrL231}$-*lux* construct into strain TMB5600 (Δ*lnrLMN* $P_{lnrL231}$-*lux*, **Table 1**) to (i) decrease the metabolic burden of *lnrLMN* expression upon P_{lnrL} induction, and (ii) optimize biosensor sensitivity and dynamics. Its performance as a polyene whole-cell biosensor was subsequently comprehensively analyzed.

We characterized the robustness of the Δ*lnrLMN* $P_{lnrL231}$ whole-cell biosensor by checking its induction in liquid and in plate-based assays. For the induction assays in liquid, the cells were challenged with amphotericin B and nystatin in exponential phase, and growth and luminescence readouts were monitored over time. The activation on solid medium was determined by spot-on-lawn assays: a lawn of the *B. subtilis* biosensor in soft agar was challenged with 20 µl of stock solutions of the macrolide polyenes and the luminescence output was determined after 24 h. In liquid conditions, the biosensor showed an over 100-fold induction in the presence of both compounds (**Figures 5B,D**). The dynamic range of $P_{lnrL231}$ in a Δ*lnrLMN* background is over 10-fold higher than that observed in the wild type and particularly pronounced for nystatin (compare **Figure 3I** with **Figure 5D**). The final biosensor also demonstrated its sensitivity in solid media, where Δ*lnrLMN* $P_{lnrL231}$ produced a significantly stronger luminescence output for amphotericin B and a weaker but detectable luminescence output for nystatin (**Figure 6A**).

We next determined the dose-response kinetics by challenging our biosensor (TMB5600) – and the isogenic wild type predecessor strain (TMB4223) – with serial dilutions (from 0.001 to 32 µg ml^{-1}) of amphotericin B. Our results highlight that removing *lnrLMN* improves the promoter performance with regard to both sensitivity and dynamic range (**Figure 5E**). $P_{lnrL231}$ in the wild type background has a gradual increase in promoter induction (**Figure 5E**, black line), highlighting its potential to resolve a more linear dose-response to the inducing agent. However, the Δ*lnrLMN* $P_{lnrL231}$ reporter strain has a sigmoidal response with a sharper off-on activation resulting in higher sensitivity (**Figure 5E**, red line). For example, at one hour post-induction an amphotericin B concentration of 1 µg ml^{-1} was required to detect a reporter activity of 10^6 RLU/OD_{600} with $P_{lnrL231}$ in a wild type background, however, an almost 16-fold lower concentration of 0.063 µg ml^{-1} was enough to induce the same luminescence output with strain Δ*lnrLMN* $P_{lnrL231}$. The same difference in dynamic range is maintained at 5 h post induction (**Figure 5E**), but there is a significant decrease in background signal, relative to the background signal at 1-h post induction, for both strains.

Overall, our reporter strains therefore show a low background signal, and a highly dynamic, dose-dependent response that covers more than two orders of magnitude in range, which makes both TMB4223 (wild type) and TMB5600 (Δ*lnrLMN*) superbly performing whole-cell biosensors (**Figures 3**, **5**). While this

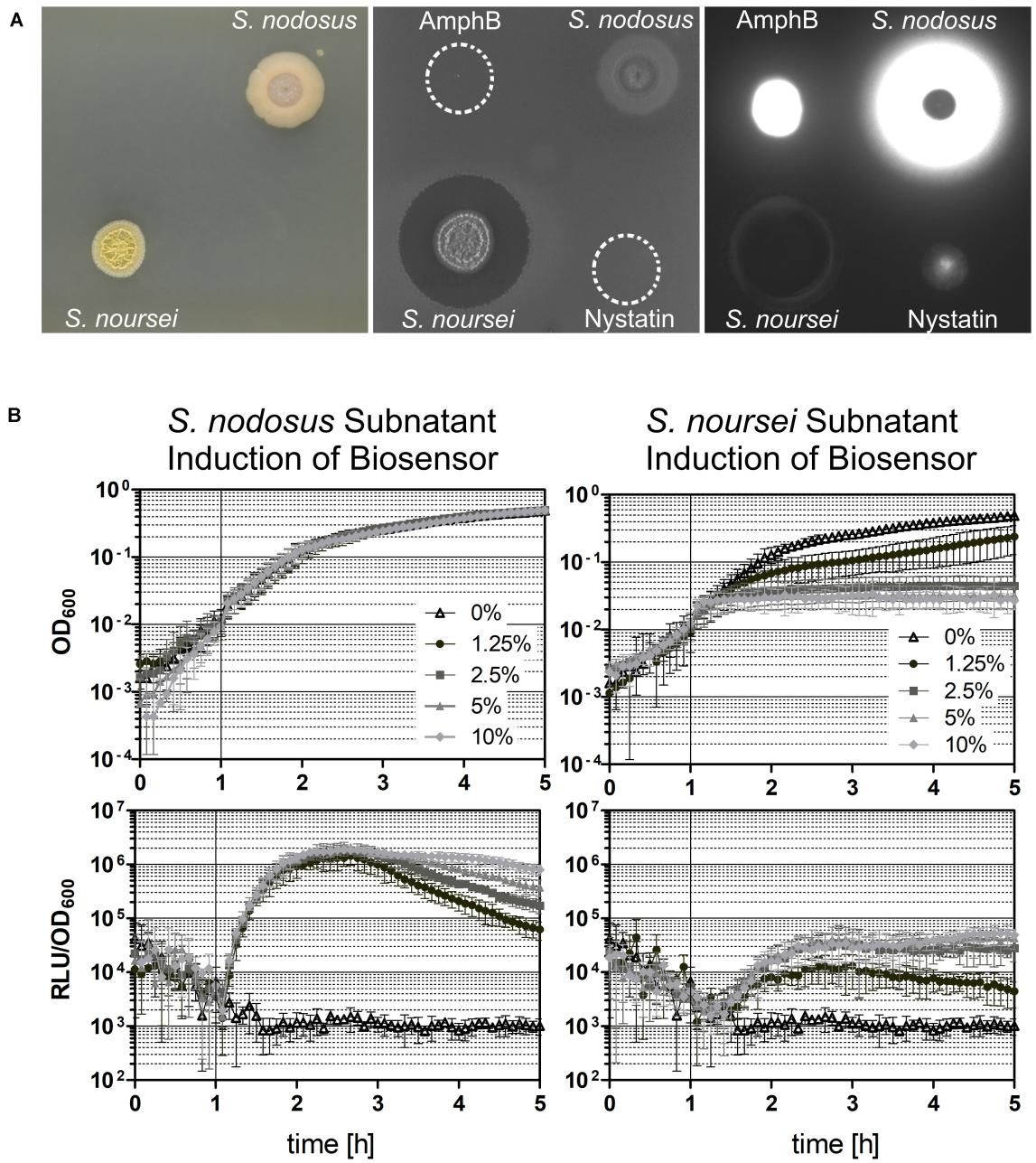

FIGURE 6 | Induction of the Δ*lnrLMN* $P_{lnrL231}$-*lux* (TMB5600) biosensor with *Streptomyces* spp. subnatants. The biosensor was tested for its robustness by analyzing its ability to detect polyenes in a complex mixture of different produced compounds by the two *Streptomyces* species *S. nodosus* and *S. noursei,* which are known producers of amphotericin B and nystatin, respectively. **(A)** Spot-on-lawn in solid medium. Both *Streptomyces* spp. strains were grown on solid medium for 4 days at 28°C (left picture), before they were overlaid with the biosensor strain (middle picture) and the produced luminescence signal was detected (right picture). In addition, 20 μl of amphotericin B (AmphB) and nystatin stock solutions were spotted on top of the overlay as controls. **(B)** Induction in liquid medium. The Δ*lnrLMN* $P_{lnrL231}$-*lux* biosensor was also analyzed in liquid conditions by inducing exponentially growing cells with different concentrations of the subnatants produced by the two *Streptomyces* species. The top panels illustrate the growth of the biosensor strain (indicated as OD_{600}) and the bottom panels show the induction with the subnatants produced by *S. nodosus* (left) and *S. noursei* (right) (as relative luminescence units by OD_{600}). The graphs depict the behavior of the biosensor over the course of five hours as means and standard deviations of three independent experiments.

quantitative output with pure compounds is impressive, whole-cell biosensors are usually applied in a more qualitative setting to screen either raw culture extracts or potential producing strains directly. We therefore wanted to also demonstrate the potential of our biosensor by screening the producers of amphotericin B and nystatin, *S. nodosus* ATCC14899 and *S. noursei* (Caffrey et al., 2001; Fjaervik and Zotchev, 2005), for their ability to induce the Δ*lnrLMN* $P_{lnrL231}$ biosensor. The results (**Figure 6**)

show no zone of inhibition – in agreement with the preference for macrolide polyenes for fungal membranes – but a bright luminescence halo around the *S. nodosus* colony, comparable in intensity to the amphotericin B halo (**Figure 6A**). On the other hand, *S. noursei* created a zone of inhibition for *B. subtilis*, while there is only a very slight luminescence halo detectable at the very rim of the inhibition zone (**Figure 6A**). This observation fits the weak luminescence signal observed for the pure compound, nystatin (**Figure 6A**). These results could be corroborated in liquid: *S. nodosus* and *S. noursei* were grown on top of liquid medium and the harvested subnatant was used to induce exponentially growing *B. subtilis* TMB5600 biosensor cells (**Figure 6B**). The *S. nodosus* subnatant induced the biosensor equally strong as amphotericin B (**Figure 5**) and had no effect on growth, while the *S. noursei* subnatant heavily impaired growth and therefore no luminescence signal could be detected. Since no interference of pure nystatin with the growth of *B. subtilis* was observed (**Figures 5C**, **6A**), the observed growth impairment in the presence of *S. noursei* is most likely due to the production of another antibacterial compound by this *Streptomyces* species (Abou-Zeid and El-Sherbini, 1974; Wu et al., 2009).

Investigation of the Whole-Cell Biosensor Specificity

The Δ*lnrLMN* $P_{lnrL231}$ biosensor is activated by amphotericin B and nystatin (**Figure 5**) and it was described that a reporter strain, P_{yfiLMN}-*lacZ,* in *B. subtilis* NCIB3610, was activated by linearmycins and ECO-02301 (Stubbendieck and Straight, 2017). Interestingly, natamycin and filipin III fail to induce the most sensitive biosensor TMB5600 in liquid and in solid (data not shown), suggesting that the absence of promoter induction is due to a lack of recognition by the LnrJ histidine kinase rather than a poor sensitivity of the detection/reporter system. Furthermore, a control study testing the response of Δ*lnrLMN* $P_{lnrL231}$ biosensor to a collection of 13 non-polyene antibiotics (**Supplementary Figure S3**) of different chemical natures (**Supplementary Figure S4**), also showed no induction of the most sensitive TMB5600 biosensor, further supporting the specific recognition of some polyene compounds by the LnrJ histidine kinase.

Linearmycins and ECO-02301 are linear polyenes (**Figure 1**), while amphotericin B and nystatin are macrolide polyenes (**Figure 1**), all of which are produced by *Streptomyces* species (Sakuda et al., 1996; Caffrey et al., 2001; Fjaervik and Zotchev, 2005; McAlpine et al., 2005). According to the polyene classification (Hamilton-Miller, 1973; Madden et al., 2014), linearmycins and ECO-02301 are both pentaenes (Sakuda et al., 1996; McAlpine et al., 2005); amphotericin B is an heptaene and the structurally related nystatin is a tetraene that has been called a "degenerated heptaene" since it has one double bond reduced (a saturated bond) that separates a diene and a tetraene region in the chromophore (Kotler-Brajtburg et al., 1979; **Figure 1**). Linearmycins and ECO-02301 lyse *B. subtilis* cells, whereas amphotericin B and nystatin do not (Stubbendieck and Straight, 2017). The activity of linearmycins on *B. subtilis* cells is due to cytoplasmic membrane depolarization (Stubbendieck et al., 2018). Our experimental results [following established protocols described in te Winkel et al. (2016)] showed that amphotericin B at a concentration of 10 $\mu g\ ml^{-1}$ and nystatin at 83 $\mu g\ ml^{-1}$ do not depolarize the *B. subtilis* cytoplasmic membrane (data not shown). These results rule out that membrane depolarization is the stimulus for the activation of LnrJK TCS.

Interestingly, in 1979 Kotler-Brajtburg et al. classified fourteen polyene antibiotics and six semisynthetic derivatives in two groups with different mechanism of action on mouse erythrocytes and *Saccharomyces cerevisiae* (Kotler-Brajtburg et al., 1979). For Group I antibiotics, hemolysis or cell death and K^+ leakage were caused at the same concentrations of added polyene, while for Group II antibiotics, K^+ ion leakage was caused at low polyene concentrations and hemolysis or cell death at high polyene concentrations. Within this classification by differential mode of action on eukaryotic cells, natamycin and filipin belong to Group I whereas amphotericin B and nystatin belong to Group II. This classification was later supported by the work of Akiyama et al. concerning the concentration of polyenes required to inhibit the colony formation of Chinese hamster V79 or *Saccharomyces cerevisiae* cells (Akiyama et al., 1980). Considering our results, showing no induction of P_{lnrL} by natamycin and filipin III (Group I), and the induction by amphotericin B and nystatin (Group II) (**Figure 3**), and previous studies showing the activation of the promoter by the linear polyenes linearmycins and ECO-02301 (Stubbendieck and Straight, 2017), we propose that *B. subtilis* Δ*lnrLMN* $P_{lnrL231}$ is a biosensor specific for such large linearmycin-like and amphotericin-like (Group II) polyenes. The full spectrum of LnrJ-sensed polyenes, as well as the potential similarities these linear and cyclic polyenes share, for example regarding mechanism of action over eukaryotic cells, will be the focus of future investigations.

CONCLUSION

Our results show that challenging *B. subtilis* with bioactive molecules that are not antibacterial but might occur in the same soil microbiome habitat, could indeed be a very promising strategy to identify new biosensor candidates for expanding the toolbox to screen for novel antibiotics, including antifungal polyenes. In this work, we investigated *B. subtilis* perception *of* and response *to* the bioactive, antifungal secondary metabolite amphotericin B, which is produced by *Streptomyces* spp. While this compound does not inhibit *B. subtilis*, it strongly and specifically induces the *lnrLMN* operon in a LnrJK-dependent manner. The LnrLMN ABC transporter has a physiological relevance by mediating linearmycin resistance in *B. subtilis* (Stubbendieck and Straight, 2015). However, besides sensing damage-inducing linearmycins and ECO-02301 (Stubbendieck and Straight, 2017), LnrJK TCS has a wider (but specific) sensitivity for non-damaging polyenes such as amphotericin B and nystatin. Using *B. subtilis* molecular tools, we created

Δ*lnrLMN* $P_{lnrL231}$ (TMB5600), a sensitive reporter strain based on the P_{lnrL} target promoter of the antibiotic-responsive LnrJK two-component signaling system, with a direct application in identification and discovery of antifungal-drugs. The biosensor dynamics was characterized, and it was subsequently applied to identify known *Streptomyces* spp. producers of natural polyenes. We have shown that the $P_{lnrL231}$ promoter is switched off in the absence of its inducers and responds in a dynamic, dose-dependent manner to increasing concentrations of them, providing an over 100-fold induction over background activity. The new biosensor is very sensitive and has proven to be robust working under different experimental conditions and responding to pure compounds as well as inducing compounds in complex samples such as *Streptomyces* subnatants. The Δ*lnrLMN* $P_{lnrL231}$ (TMB5600) biosensor is ready to serve the discovery of novel polyenes with potential application in human medicine.

DATA AVAILABILITY STATEMENT

The raw data supporting the conclusions of this article will be made available by the authors, without undue reservation, to any qualified researcher. The raw and processed RNA sequencing data obtained in this study has been deposited at the NCBIs Gene Expression Omnibus (Edgar et al., 2002) and is accessible via the GEO accession number GSE148903.

AUTHOR CONTRIBUTIONS

AR-G, FD, PP, and TM conceived the study. AR-G wrote the manuscript with the help of FD and PP, under the supervision of TM. AR-G, FD, and PP planned the experiments. AR-G, FD, PP, and MD carried out all the experiments with *B. subtilis* and analyzed the data; the experiments with the *Streptomyces* strains were carried out by FD. All authors read the article and agreed on the final manuscript.

FUNDING

This research was funded by SMWK Saxony (TG70 grant BACMOT 100315856 to AR-G) "Entwicklung biokompatibler bakterieller Mikromotoren zum Transport von biomedizinisch relevanten Nanoobjekten," and by a grant from the Deutsche Forschungsgemeinschaft (MA2837/3 to TM) in the framework of the priority program SPP1617 Phenotypic heterogeneity and sociobiology of bacterial populations. FD thanks the TU Dresden Graduate Academy for a partial Ph.D. scholarship. Open Access Funding by the Publication Fund of the TU Dresden.

ACKNOWLEDGMENTS

We thank the Becker and Goesmann labs for RNA-sequencing and data processing. In particular, we thank Doreen Meier for RNA sample preparation and Raphael Müller for setting up the RNA-seq data analysis pipeline.

SUPPLEMENTARY MATERIAL

The Supplementary Material for this article can be found online at: https://www.frontiersin.org/articles/10.3389/fmicb.2020.02022/full#supplementary-material

FIGURE S1 | Control assays with the $P_{lnrL468}$ promoter (strain TMB4220).

FIGURE S2 | Amphotericin B dose response with $P_{lnrL468}$ promoter (strain TMB4220).

FIGURE S3 | Control study testing the response of Δ*lnrLMN* $P_{lnrL231}$ biosensor to a collection of 13 non-polyene antibiotics (strain TMB5600).

FIGURE S4 | Molecular structures of the non-polyene antibiotics used in the control study presented in **Supplementary Figure S3**.

TABLE S1 | Oligonucleotides used in this study.

REFERENCES

Abou-Zeid, A. A., and El-Sherbini, S. H. (1974). Fermentative production of cycloheximide by *Streptomyces griseus* and *Streptomyces noursei*. *J. Appl. Chem. Biotechnol.* 24, 283–291. doi: 10.1002/jctb.2720240413

Akiyama, S., Tabuki, T., Kaneko, M., Komiyama, S., and Kuwano, M. (1980). Classification of polyene antibiotics according to their synergistic effect in combination with bleomycin A2 or fusidic acid. *Antimicrob. Agents Chemother.* 18, 226–230. doi: 10.1128/aac.18.2.226

Aldholmi, M., Marchand, P., Ourliac-Garnier, I., Le Pape, P., and Ganesan, A. (2019). A decade of antifungal leads from natural products: 2010-2019. *Pharmaceuticals* 12:182. doi: 10.3390/ph12040182

Almeida, F., Rodrigues, M. L., and Coelho, C. (2019). The still underestimated problem of fungal diseases worldwide. *Front. Microbiol.* 10:214. doi: 10.3389/fmicb.2019.00214

Anagnostopoulos, C., and Spizizen, J. (1961). Requirements for Transformation in *Bacillus Subtilis*. *J. Bacteriol.* 81, 741–746.

Antillón, A., de Vries, A. H., Espinosa-Caballero, M., Falcón-González, J. M., Flores Romero, D., González-Damián, J., et al. (2016). An Amphotericin B derivative equally potent to amphotericin B and with increased safety. *PLoS One* 11:e0162171. doi: 10.1371/journal.pone.0162171

Arnaud, M., Chastanet, A., and Débarbouillé, M. (2004). New vector for efficient allelic replacement in naturally nontransformable, low-GC-content, gram-positive bacteria. *Appl. Environ. Microbiol.* 70, 6887–6891. doi: 10.1128/aem.70.11.6887-6891.2004

Baginski, M., Sternal, K., Czub, J., and Borowski, E. (2005). Molecular modelling of membrane activity of amphotericin B, a polyene macrolide antifungal antibiotic. *Acta Biochim. Pol.* 52, 655–658. doi: 10.18388/abp.2005_3426

Baltz, R. H. (2008). Renaissance in antibacterial discovery from actinomycetes. *Curr. Opin. Pharmacol.* 8, 557–563. doi: 10.1016/j.coph.2008.04.008

Bongomin, F., Gago, S., Oladele, R. O., and Denning, D. W. (2017). Global and multi-national prevalence of fungal diseases-estimate precision. *J. Fungi* 3:57. doi: 10.3390/jof3040057

Caffrey, P., Lynch, S., Flood, E., Finnan, S., and Oliynyk, M. (2001). Amphotericin biosynthesis in *Streptomyces nodosus*: deductions from analysis of polyketide synthase and late genes. *Chem. Biol.* 8, 713–723. doi: 10.1016/s1074-5521(01)00046-1

Cai, P., Kong, F., Fink, P., Ruppen, M. E., Williamson, R. T., and Keiko, T. (2007). Polyene antibiotics from *Streptomyces mediocidicus*. *J. Nat. Prod.* 70, 215–219. doi: 10.1021/np060542f

Cereghetti, D. M., and Carreira, E. M. (2006). Amphotericin B: 50 years of chemistry and biochemistry. *Synthesis* 6, 914–942.

Chattopadhyay, A., and Jafurulla, M. (2011). A novel mechanism for an old drug: Amphotericin B in the treatment of visceral leishmaniasis. *Biochem. Biophys. Res. Commun.* 416, 7–12. doi: 10.1016/j.bbrc.2011.11.023

Czarny, T. L., Perri, A. L., French, S., and Brown, E. D. (2014). Discovery of novel cell wall-active compounds using PywaC, a sensitive reporter of cell wall stress, in the model gram-positive bacterium *Bacillus subtilis*. *Antimicrob. Agents Chemother.* 58, 3261–3269. doi: 10.1128/Aac.02352-14

Debnath, A., Tunac, J. B., Galindo-Gomez, S., Silva-Olivares, A., Shibayama, M., and McKerrow, J. H. (2012). Corifungin, a new drug lead against *Naegleria*, identified from a high-throughput screen. *Antimicrob. Agents Chemother.* 56, 5450–5457. doi: 10.1128/AAC.00643-12

Edgar, R., Domrachev, M., and Lash, A. E. (2002). Gene Expression Omnibus: NCBI gene expression and hybridization array data repository. *Nucleic Acids Res.* 30, 207–210. doi: 10.1093/nar/30.1.207

Fjaervik, E., and Zotchev, S. B. (2005). Biosynthesis of the polyene macrolide antibiotic nystatin in *Streptomyces noursei*. *Appl. Microbiol. Biotechnol.* 67, 436–443. doi: 10.1007/s00253-004-1802-4

Frees, D., Savijoki, K., Varmanen, P., and Ingmer, H. (2007). Clp ATPases and ClpP proteolytic complexes regulate vital biological processes in low GC, Gram-positive bacteria. *Mol. Microbiol.* 63, 1285–1295. doi: 10.1111/j.1365-2958.2007.05598.x

Fritz, G., Dintner, S., Treichel, N. S., Radeck, J., Gerland, U., Mascher, T., et al. (2015). A new way of sensing: need-based activation of antibiotic resistance by a flux-sensing mechanism. *mBio* 6:e00975-15. doi: 10.1128/mBio.00975-15

Gallis, H. A., Drew, R. H., and Pickard, W. W. (1990). Amphotericin B: 30 years of clinical experience. *Rev. Infect. Dis.* 12, 308–329. doi: 10.1093/clinids/12.2.308

Geddes-McAlister, J., and Shapiro, R. S. (2019). New pathogens, new tricks: emerging, drug-resistant fungal pathogens and future prospects for antifungal therapeutics. *Ann. N. Y. Acad. Sci.* 1435, 57–78. doi: 10.1111/nyas.13739

Grace, E., Asbill, S., and Virga, K. (2015). *Naegleria fowleri*: pathogenesis, diagnosis, and treatment options. *Antimicrob. Agents Chemother.* 59, 6677–6681. doi: 10.1128/aac.01293-15

Guérout-Fleury, A. M., Shazand, K., Frandsen, N., and Stragier, P. (1995). Antibiotic-resistance cassettes for *Bacillus subtilis*. *Gene* 167, 335–336. doi: 10.1016/0378-1119(95)00652-4

Hamill, R. J. (2013). Amphotericin B formulations: a comparative review of efficacy and toxicity. *Drugs* 73, 919–934. doi: 10.1007/s40265-013-0069-4

Hamilton-Miller, J. M. (1973). Chemistry and biology of the polyene macrolide antibiotics. *Bacteriol. Rev.* 37, 166–196. doi: 10.1128/mmbr.37.3.166-196.1973

Harwood, C. R., and Cutting, S. M. (1990). *Molecular Biological Methods for Bacillus*. Chichester: Wiley.

Hutter, B., Fischer, C., Jacobi, A., Schaab, C., and Loferer, H. (2004). Panel of *Bacillus subtilis* reporter strains indicative of various modes of action. *Antimicrob. Agents Chemother.* 48, 2588–2594. doi: 10.1128/AAC.48.7.2588-2594.2004

Kim, J. Y., Inaoka, T., Hirooka, K., Matsuoka, H., Murata, M., Ohki, R., et al. (2009). Identification and characterization of a novel multidrug resistance operon, *mdtRP* (*yusOP*), of *Bacillus subtilis*. *J. Bacteriol.* 191, 3273–3281. doi: 10.1128/JB.00151-09

Kim, S., Thiessen, P. A., Bolton, E. E., Chen, J., Fu, G., Gindulyte, A., et al. (2015). PubChem substance and compound databases. *Nucleic Acids Res.* 44, D1202–D1213. doi: 10.1093/nar/gkv951

Kotler-Brajtburg, J., Medoff, G., Kobayashi, G. S., Boggs, S., Schlessinger, D., Pandey, R. C., et al. (1979). Classification of polyene antibiotics according to chemical structure and biological effects. *Antimicrob. Agents Chemother.* 15, 716–722. doi: 10.1128/aac.15.5.716

Langmead, B., and Salzberg, S. L. (2012). Fast gapped-read alignment with Bowtie 2. *Nat. Methods* 9, 357–359. doi: 10.1038/nmeth.1923

Liao, Y., Smyth, G. K., and Shi, W. (2014). featureCounts: an efficient general purpose program for assigning sequence reads to genomic features. *Bioinformatics* 30, 923–930. doi: 10.1093/bioinformatics/btt656

Lightbown, J. W., Kogut, M., and Uemura, K. (1963). The international standard for Nystatin. *Bull. World Health Organ.* 29, 87–94.

Love, M. I., Huber, W., and Anders, S. (2014). Moderated estimation of fold change and dispersion for RNA-seq data with DESeq2. *Genome Biol.* 15:550.

Madden, K. S., Mosa, F. A., and Whiting, A. (2014). Non-isoprenoid polyene natural products–structures and synthetic strategies. *Org. Biomol. Chem.* 12, 7877–7899. doi: 10.1039/c4ob01337a

Mascher, T., Margulis, N. G., Wang, T., Ye, R. W., and Helmann, J. D. (2003). Cell wall stress responses in *Bacillus subtilis*: the regulatory network of the bacitracin stimulon. *Mol. Microbiol.* 50, 1591–1604. doi: 10.1046/j.1365-2958.2003.03786.x

Mascher, T., Zimmer, S. L., Smith, T. A., and Helmann, J. D. (2004). Antibiotic-inducible promoter regulated by the cell envelope stress-sensing two-component system LiaRS of *Bacillus subtilis*. *Antimicrob. Agents Chemother.* 48, 2888–2896. doi: 10.1128/AAC.48.8.2888-2896.2004

McAlpine, J. B., Bachmann, B. O., Piraee, M., Tremblay, S., Alarco, A. M., Zazopoulos, E., et al. (2005). Microbial genomics as a guide to drug discovery and structural elucidation: ECO-02301, a novel antifungal agent, as an example. *J. Nat. Prod.* 68, 493–496. doi: 10.1021/np0401664

Nicolas, P., Mäder, U., Dervyn, E., Rochat, T., Leduc, A., Pigeonneau, N., et al. (2012). Condition-dependent transcriptome reveals high-level regulatory architecture in *Bacillus subtilis*. *Science* 335, 1103–1106.

Ohki, R., Giyanto, Tateno, K., Masuyama, W., Moriya, S., Kobayashi, K., et al. (2003). The BceRS two-component regulatory system induces expression of the bacitracin transporter, BceAB, in *Bacillus subtilis*. *Mol. Microbiol.* 49, 1135–1144. doi: 10.1046/j.1365-2958.2003.03653.x

Palma, E., Pasqua, A., Gagliardi, A., Britti, D., Fresta, M., and Cosco, D. (2018). Antileishmanial activity of Amphotericin B-loaded-PLGA nanoparticles: an overview. *Materials* 11:1167. doi: 10.3390/ma11071167

Popp, P. F., Benjdia, A., Strahl, H., Berteau, O., and Mascher, T. (2020). The Epipeptide YydF intrinsically triggers the cell envelope stress response of *Bacillus subtilis* and causes severe membrane perturbations. *Front. Microbiol.* 11:151. doi: 10.3389/fmicb.2020.00151

Popp, P. F., Dotzler, M., Radeck, J., Bartels, J., and Mascher, T. (2017). The *Bacillus* BioBrick Box 2.0: expanding the genetic toolbox for the standardized work with *Bacillus subtilis*. *Sci. Rep.* 7:15058. doi: 10.1038/s41598-017-15107-z

Power, P., Dunne, T., Murphy, B., Nic Lochlainn, L., Rai, D., Borissow, C., et al. (2008). Engineered Synthesis of 7-Oxo- and 15-Deoxy-15-Oxo-Amphotericins: insights into Structure-Activity Relationships in Polyene Antibiotics. *Chem. Biol.* 15, 78–86. doi: 10.1016/j.chembiol.2007.11.008

Radeck, J., Gebhard, S., Orchard, P. S., Kirchner, M., Bauer, S., Mascher, T., et al. (2016). Anatomy of the bacitracin resistance network in *Bacillus subtilis*. *Mol. Microbiol.* 100, 607–620. doi: 10.1111/mmi.13336

Radeck, J., Kraft, K., Bartels, J., Cikovic, T., Dürr, F., Emenegger, J., et al. (2013). The Bacillus BioBrick Box: generation and evaluation of essential genetic building blocks for standardized work with *Bacillus subtilis*. *J. Biol. Eng.* 7:29. doi: 10.1186/1754-1611-7-29

Revie, N. M., Iyer, K. R., Robbins, N., and Cowen, L. E. (2018). Antifungal drug resistance: evolution, mechanisms and impact. *Curr. Opin. Microbiol.* 45, 70–76. doi: 10.1016/j.mib.2018.02.005

Rietkötter, E., Hoyer, D., and Mascher, T. (2008). Bacitracin sensing in *Bacillus subtilis*. *Mol. Microbiol.* 68, 768–785. doi: 10.1111/j.1365-2958.2008.06194.x

Rochette, F., Engelen, M., and Vanden Bossche, H. (2003). Antifungal agents of use in animal health–practical applications. *J. Vet. Pharmacol. Ther.* 26, 31–53. doi: 10.1046/j.1365-2885.2003.00457.x

Sakuda, S., Guce-Bigol, U., Itoh, M., Nishimura, T., and Yamada, Y. (1996). Novel linear polyene antibiotics: linearmycins. *J. Chem. Soc. Perkin Trans.* 1, 2315–2319. doi: 10.1039/p19960002315

Staroń, A., Finkeisen, D. E., and Mascher, T. (2011). Peptide antibiotic sensing and detoxification modules of *Bacillus subtilis*. *Antimicrob. Agents Chemother.* 55, 515–525. doi: 10.1128/AAC.00352-10

Stock, A. M., Robinson, V. L., and Goudreau, P. N. (2000). Two-component signal transduction. *Annu. Rev. Biochem.* 69, 183–215. doi: 10.1146/annurev.biochem.69.1.183

Stodulkova, E., Kuzma, M., Hench, I. B., Cerny, J., Kralova, J., Novak, P., et al. (2011). New polyene macrolide family produced by submerged culture of *Streptomyces durmitorensis*. *J. Antibiot.* 64, 717–722. doi: 10.1038/ja.2011.81

Stubbendieck, R. M., Brock, D. J., Pellois, J. P., Gill, J. J., and Straight, P. D. (2018). Linearmycins are lytic membrane-targeting antibiotics. *J. Antibiot.* 71, 372–381. doi: 10.1038/s41429-017-0005-z

Stubbendieck, R. M., and Straight, P. D. (2015). Escape from lethal bacterial competition through coupled activation of antibiotic resistance and a mobilized subpopulation. *PLoS Genet.* 11:e1005722. doi: 10.1371/journal.pgen.1005722

Stubbendieck, R. M., and Straight, P. D. (2017). Linearmycins activate a two-component signaling system involved in bacterial competition and biofilm morphology. *J. Bacteriol.* 199:e00186-17. doi: 10.1128/JB.00186-17

te Winkel, J. D., Gray, D. A., Seistrup, K. H., Hamoen, L. W., and Strahl, H. (2016). Analysis of antimicrobial-triggered membrane depolarization using voltage sensitive dyes. *Front. Cell Dev. Biol.* 4:29. doi: 10.3389/fcell.2016.00029

Tevyashova, A. N., Olsufyeva, E. N., Solovieva, S. E., Printsevskaya, S. S., Reznikova, M. I., Trenin, A. S., et al. (2013). Structure-antifungal activity relationships of polyene antibiotics of the amphotericin B group. *Antimicrob. Agents Chemother.* 57, 3815–3822. doi: 10.1128/AAC.00270-13

Torrado, J. J., Espada, R., Ballesteros, M. P., and Torrado-Santiago, S. (2008). Amphotericin B formulations and drug targeting. *J. Pharm. Sci.* 97, 2405–2425. doi: 10.1002/jps.21179

Urban, A., Eckermann, S., Fast, B., Metzger, S., Gehling, M., Ziegelbauer, K., et al. (2007). Novel whole-cell antibiotic biosensors for compound discovery. *Appl. Environ. Microbiol.* 73, 6436–6443. doi: 10.1128/AEM.00586-07

Vartak, A., Mutalik, V., Parab, R. R., Shanbhag, P., Bhave, S., Mishra, P. D., et al. (2014). Isolation of a new broad spectrum antifungal polyene from *Streptomyces* sp. MTCC 5680. *Lett. Appl. Microbiol.* 58, 591–596. doi: 10.1111/lam.12229

Wang, W., Song, T., Chai, W., Chen, L., Chen, L., Lian, X.-Y., et al. (2017). Rare Polyene-polyol Macrolides from Mangrove-derived *Streptomyces* sp. ZQ4BG. *Sci. Rep.* 7:1703. doi: 10.1038/s41598-017-01912-z

Wolf, D., Kalamorz, F., Wecke, T., Juszczak, A., Mader, U., Homuth, G., et al. (2010). In-depth profiling of the LiaR response of *Bacillus subtilis*. *J. Bacteriol.* 192, 4680–4693. doi: 10.1128/JB.00543-10

Wolf, D., and Mascher, T. (2016). The applied side of antimicrobial peptide-inducible promoters from Firmicutes bacteria: expression systems and whole-cell biosensors. *Appl. Microbiol. Biotechnol.* 100, 4817–4829. doi: 10.1007/s00253-016-7519-3

Wu, X., Huang, H., Chen, G., Sun, Q., Peng, J., Zhu, J., et al. (2009). A novel antibiotic produced by *Streptomyces noursei* Da07210. *Antonie Van Leeuwenhoek* 96, 109–112. doi: 10.1007/s10482-009-9333-8

Yamamoto, H., Uchiyama, S., and Sekiguchi, J. (1996). The *Bacillus subtilis* chromosome region near 78 degrees contains the genes encoding a new two-component system, three ABC transporters and a lipase. *Gene* 181, 147–151. doi: 10.1016/s0378-1119(96)00495-7

Yao, T., Liu, Z., Li, T., Zhang, H., Liu, J., Li, H., et al. (2018). Characterization of the biosynthetic gene cluster of the polyene macrolide antibiotic reedsmycins from a marine-derived *Streptomyces* strain. *Microb. Cell Fact.* 17:98. doi: 10.1186/s12934-018-0943-6

Yim, G., Wang, H. H., and Davies, J. (2007). Antibiotics as signalling molecules. *Philos. Trans. R. Soc. Lond. B Biol. Sci.* 362, 1195–1200. doi: 10.1098/rstb.2007.2044

Zhu, B., and Stülke, J. (2017). SubtiWiki in 2018: from genes and proteins to functional network annotation of the model organism *Bacillus subtilis*. *Nucleic Acids Res.* 46, D743–D748. doi: 10.1093/nar/gkx908

Zotchev, S. B. (2003). Polyene macrolide antibiotics and their applications in human therapy. *Curr. Med. Chem.* 10, 211–223. doi: 10.2174/0929867033368448

Conflict of Interest: The authors declare that the research was conducted in the absence of any commercial or financial relationships that could be construed as a potential conflict of interest.

frontiers in Microbiology

ORIGINAL RESEARCH
published: 26 August 2020
doi: 10.3389/fmicb.2020.02053

Synthetic Naphthofuranquinone Derivatives Are Effective in Eliminating Drug-Resistant *Candida albicans* in Hyphal, Biofilm, and Intracellular Forms: An Application for Skin-Infection Treatment

Jia-You Fang[1,2,3], Kai-Wei Tang[4], Sien-Hung Yang[5,6], Ahmed Alalaiwe[7], Yu-Ching Yang[1], Chih-Hua Tseng[4,8,9,10,11] and Shih-Chun Yang[12]**

[1] Pharmaceutics Laboratory, Graduate Institute of Natural Products, Chang Gung University, Taoyuan City, Taiwan, [2] Research Center for Food and Cosmetic Safety, Research Center for Chinese Herbal Medicine, Chang Gung University of Science and Technology, Taoyuan City, Taiwan, [3] Department of Anesthesiology, Chang Gung Memorial Hospital, Taoyuan City, Taiwan, [4] School of Pharmacy, College of Pharmacy, Kaohsiung Medical University, Kaohsiung, Taiwan, [5] School of Traditional Chinese Medicine, Chang Gung University, Taoyuan City, Taiwan, [6] Department of Traditional Chinese Medicine, Chang Gung Memorial Hospital, Taoyuan City, Taiwan, [7] Department of Pharmaceutics, College of Pharmacy, Prince Sattam Bin Abdulaziz University, Al Kharj, Saudi Arabia, [8] Department of Fragrance and Cosmetic Science, College of Pharmacy, Kaohsiung Medical University, Kaohsiung, Taiwan, [9] Drug Development and Value Creation Research Center, Kaohsiung Medical University, Kaohsiung, Taiwan, [10] Department of Medical Research, Kaohsiung Medical University Hospital, Kaohsiung, Taiwan, [11] Department of Pharmacy, Kaohsiung Municipal Ta-Tung Hospital, Kaohsiung, Taiwan, [12] Department of Cosmetic Science, Providence University, Taichung, Taiwan

OPEN ACCESS

Edited by:
Macit Ilkit,
Çukurova University, Turkey

Reviewed by:
Rajendra Prasad,
Jawaharlal Nehru University, India
István Pócsi,
University of Debrecen, Hungary

***Correspondence:**
Chih-Hua Tseng
chihhua@.kmu.edu.tw
Shih-Chun Yang
yangsc@pu.edu.tw

Specialty section:
This article was submitted to Antimicrobials, Resistance and Chemotherapy, a section of the journal Frontiers in Microbiology

Received: *14 May 2020*
Accepted: *05 August 2020*
Published: *26 August 2020*

Citation:
Fang J-Y, Tang K-W, Yang S-H, Alalaiwe A, Yang Y-C, Tseng C-H and Yang S-C (2020) Synthetic Naphthofuranquinone Derivatives Are Effective in Eliminating Drug-Resistant Candida albicans in Hyphal, Biofilm, and Intracellular Forms: An Application for Skin-Infection Treatment. Front. Microbiol. 11:2053. doi: 10.3389/fmicb.2020.02053

Candida albicans is the most common cause of fungal infection. The emergence of drug resistance leads to the need for novel antifungal agents. We aimed to design naphthofuranquinone analogs to treat drug-resistant *C. albicans* for topical application on cutaneous candidiasis. The time-killing response, agar diffusion, and live/dead assay of the antifungal activity were estimated against 5-fluorocytosine (5-FC)- or fluconazole-resistant strains. A total of 14 naphthofuranquinones were compared for their antifungal potency. The lead compounds with hydroxyimino (TCH-1140) or *O*-acetyl oxime (TCH-1142) moieties were the most active agents identified, showing a minimum inhibitory concentration (MIC) of 1.5 and 1.2 μM, respectively. Both compounds were superior to 5-FC and fluconazole for killing planktonic fungi. Naphthofuranquinones efficiently diminished the microbes inside and outside the biofilm. TCH-1140 and TCH-1142 were delivered into *C. albicans*-infected keratinocytes to eradicate intracellular fungi. The compounds did not reduce the *C. albicans* burden inside the macrophages, but the naphthofuranquinones promoted the transition of fungi from the virulent hypha form to the yeast form. In the *in vivo* skin mycosis mouse model, topically applied 5-FC and TCH-1140 reduced the *C. albicans* load from 1.5×10^6 to 5.4×10^5 and 1.4×10^5 CFU, respectively. The infected abscess diameter was significantly

decreased by TCH-1140 (3-4 mm) as compared to the control (8 mm). The disintegrated skin-barrier function induced by the fungi was recovered to the baseline by the compound. The data support the potential of TCH-1140 as a topical agent for treating drug-resistant *C. albicans* infection without causing skin irritation.

Keywords: *C. albicans*, skin, drug resistance, naphthofuranquinone, biofilm, hypha

INTRODUCTION

Pathogenic fungi have caused a huge threat to global health. The epidemiological data reveal that superficial fungi infection affects 25% of the worldwide population (Ghannoum et al., 2013). *Candida albicans* is the most frequent cause of fungal infection. It is estimated as the third most common infection in United States hospitals (Romo et al., 2017). As an opportunistic pathogen, *C. albicans* can accumulate in oral, vaginal, gastric, and cutaneous surfaces. Candidiasis is one of the most widespread classes of superficial fungal infection (Kühbacher et al., 2017). Cutaneous mycosis is also caused by the other dermatophytes, including *Microsporum*, *Epidermophyton*, and *Trichophyton* (Martinez-Rossi et al., 2017). In recent years, the increasing use of antifungal drugs for cutaneous mycosis treatment has led to the development of drug-resistant *C. albicans* (Larsen et al., 2018). This situation advocates the urgent need for novel antifungal agents.

There are only four classes of USFDA-approved antifungal drugs to treat candidiasis, including the structures of flucytosines, azoles, echinocandins, and polyenes. Naphthofuranquinones are a quinine subclass possessing some bioactivities such as antimicrobial, anti-inflammatory, and antitumor potencies (Tsang et al., 2018). Previous studies (Gershon and Shanks, 1975; Nagata et al., 1998; Neto et al., 2014; Rejiniemon et al., 2014; Hassan et al., 2016; Xie et al., 2016) demonstrated that naphthofuranquinones showed the capability to eradicate *Candida* species. We prepared a series of naphthofuranquinone derivatives, which displayed anti-inflammatory and anticancer activities (Tseng et al., 2009; Chien et al., 2010; Tsai et al., 2014). Recently we found that some of the compounds with a naphthofuranquinone backbone were antibacterial agents against methicillin-resistant *Staphylococcus aureus* (MRSA) (Yang et al., 2017). There are far fewer antifungal drugs than antibacterial drugs available in clinics. Because the incidence of dermatophytoses remains so high, there is still a need for efficient topical antifungal therapy. To address the necessity of novel antifungals, we have screened naphthofuranquinones developed in our lab to treat the *C. albicans* strains ATCC90029 and ATCC10231. ATCC90029 is resistant to 5-fluorocytosine (5-FC) while ATCC10231 is resistant to most of the antifungals, including fluconazole. ATCC90029 also can be regarded as the susceptible strain since it is only resistant to 5-FC but sensitive to most of the antifungal drugs. The emergence of resistance to antifungal drugs is usually due to the formation of biofilm, host cell residence, and filamentation, which increase the virulence of *C. albicans* (Monika et al., 2017). The ability of the naphthofuranquinone analogs to kill these difficult-to-treat *C. albicans* was also evaluated in this study.

The intracellular fungi killing was examined by employing keratinocytes and macrophages as the host cells infected by *C. albicans*. To explore the fungicidal mechanism of the compounds, morphological observation, total DNA, RNA, protein, and hypha-related genes were assessed to determine the mode of action on *C. albicans*. Finally, we compared the antifungal activity between the compound and 5-FC in the *in vivo* skin mycosis mouse model. Here, we demonstrated that topical delivery of the angular naphthofuranquinone with the hydroxyimino group (TCH-1140) remarkably mitigated abscess and the associated *C. albicans* burden.

MATERIALS AND METHODS

Synthesis of Naphthofuranquinones

We synthesized 14 naphthofuranquinone-related compounds as shown in**Supplementary Table S1**. The protocols for synthesizing TCH-1139 and TCH-1199 were described in our previous investigation (Tseng et al., 2010). The synthetic protocols for the other compounds were shown in another study (Yang et al., 2019). The structures of all compounds were confirmed by ^{1}H NMR, ^{13}C NMR, and electrospray ionization mass spectrometry as exhibited previously.

Fungal Strains

The strains of *C. albicans* employed in this work were ATCC90029 and ATCC10231 obtained from the Food Industry Research and Development Institute (Hsinchu, Taiwan). Both species were drug-resistant isolates.

Minimum Inhibitory Concentration (MIC) and Minimum Fungicidal Concentration (MFC)

The antifungal activity of naphthofuranquinones was first estimated by MIC and MFC. A two-fold broth-dilution method was used to determine MIC as described previously (Chou et al., 2019). The treatment duration of the compounds to *C. albicans* was 16 h. MFC was detected as the lowest compound concentration for killing ≥99.9% of the fungi. The detailed procedures were represented in the previous study (Chou et al., 2019).

Time-Response Fungus Eradication

The eradication of *C. albicans* by naphthofuranquinones during a 48-h period was evaluated in 96-well plates. The compounds at 2.9-11.6 μM were inoculated with test microbes (OD_{600} = 0.01) and incubated for 48 h at 37°C. The absorbance of each well was

detected at 600 nm to determine the growth of *C. albicans* in a real-time mode.

Inhibition Zone in Agar Diffusion Assay

This assay was performed by plating *C. albicans* (OD_{600} = 0.7) on the agar plate. Naphthofuranquinones at 0.7-2.9 μM (10 μl) were loaded onto the plate. After incubating for 12 h at 37°C, the clear zone diameter without fungi was calculated.

Live/Dead Fungi Detection

The viability and death of *C. albicans* by treatment of naphthofuranquinones were monitored by Live/Dead BacLight® kit. *C. albicans* was grown to OD_{600} = 0.1, and then treated with the compounds at 23.5-93.8 μM for 4 h. The strains stained by SYTO9 and propidium iodide (PI) were analyzed by fluorescence microscopy and flow cytometry. The detailed procedures were described earlier (Chou et al., 2019).

Fungal Survival in Biofilm

The biofilm was established in a Cellview® dish by incubating the microbes (OD_{600} = 0.1) in 1% glucose at 37°C for 24 h. The compounds at 11.6 μM were then incorporated into the biofilm for 24 h. The recovered *C. albicans* inside and outside the biofilm was loaded in an agar plate for 24 h to calculate CFU.

Cytotoxicity of Keratinocytes and Macrophages

The vulture method for keratinocytes (HaCaT) was described in detail in our previous study (Lin et al., 2018). THP-1 cells were differentiated into macrophages by stimulation with 100 ng/ml phorbol myristate acetate for 36 h, followed by overnight incubation in fresh medium. Both 3-(4,5-dimethylthiazol-2-yl)-2,5-diphenyltetrazodium bromide (MTT) and CCK-8 assays were utilized to recognize cytotoxicity. The number of HaCaT and macrophages used in this experiment was 2×10^4 and 1×10^5 cells/well, respectively. The MTT assay was reported previously (Lin et al., 2018). The experimental procedures of CCK-8 were carried out based on the manufacturer's protocol (BioTools, Taipei, Taiwan).

Apoptosis

Analysis of Annexin V-fluorescein isothiocyanate (FITC) and PI cell staining was performed after 24 h of incubation of HaCaT or *C. albicans* in DMEM at 37°C and 5% CO_2. The naphthofuranquinones dosed at 93.8 and 22.5 μM was used to treat HaCaT and *C. albicans*, respectively. After incubation, the cells were detached, washed with cold PBS, and treated with Annexin V-FITC and PI as suggested by the manufacturer (R&D Systems). The cells incubated with DMEM were employed as the control.

Intracellular Fungus Eradication

Keratinocytes and macrophages differentiated from THP-1 were used as the host cells to estimate killing by naphthofuranquinones (11.7 μM). The fungal survival inside the host cells was appraised by colony-forming unit (CFU) counting and observed by confocal microscopy. DAPI and anti-*C. albicans* antibody/Alexa Fluor® 488 goat anti-mouse IgG was utilized to stain the host cell nucleus and the fungi, respectively. The detailed processes were shown in the previous work (Alalaiwe et al., 2018).

Morphological Visualization

Candida albicans morphology after treatment by naphthofuranquinones was monitored by scanning electron microscopy (SEM). The microbes at OD_{600} = 0.1 were treated with compounds at 11.7 μM for 24 h. The detailed processes of morphological observation were described earlier (Yang et al., 2016).

Total Amounts of DNA, RNA, and Protein in Fungi

Candida albicans was grown to OD_{600} = 0.3. The compounds at 11.7 μM were incorporated with *C. albicans* suspension at 37°C for 4 h. The quantification of the total DNA, RNA, and protein in the fungi was performed using a Tools Bacterial and Fungal DNA Extraction kit, EasyPrep Total RNA kit (BioTools, Taipei, Taiwan), and Bio-Rad protein assay kit, respectively.

Determination of Hypha-Related Genes

We employed real-time reverse transcription-polymerase chain reaction (RT-PCR) to analyze *efg1*, *ume6*, and *hgc1* in *C. albicans* after treatment of the compounds (11.7 μM). The RNA extraction and cDNA synthesis were conducted as described before (Yang et al., 2016). The cDNA was the template for RT-PCR amplification using gene-specific primers.

Animals

Eight-week-old male Balb/c mice were used in the *in vivo* experiments. All protocols were performed in strict accordance with the recommendations set forth in the Guidelines for the Institutional Animal Care and Use Committee of Chang Gung University.

In vivo Antifungal Activity of Naphthofuranquinones

All mice were prepared by shaving the dorsal fur. The mice were intradermally injected with 100 μl of the 5×10^6 CFU ATCC10231 strain. The topically applied lead compound or 5-FC (2.9 mM) with a volume of 0.1 ml was administered onto the infection region every 24 h for 7 days. The skin-surface appearance was visualized by phenotypic and microscopic images after 7 days. The infected area was excised for homogenization. Fungus CFU in the infected site was estimated. TEWL was evaluated by Tewameter from 0 to 7 days post-injection.

Histopathology

The mouse skin specimen was immersed in 10% formaldehyde and embedded in paraffin. The specimen was cut into a 5-μm thickness for hematoxylin and eosin (H&E) staining. We also examined immunoglobulin (Ig)G, interferon (IFN)-γ, interleukin (IL)-17, and Ly6G in the skin by immunohistochemistry (IHC). The skin sections were incubated

with the related antibodies for 1 h, then incubated with biotinylated donkey anti-goat IgG for 20 min. The slices were visualized by optical microscopy.

In vivo Skin Irritation

The vehicle with naphthofuranquinones or 5-FC (2.9 mM) was topically applied on the back of the mice for 5 days. The vehicle was replaced by a new one each day. The skin was examined for its microscopic appearance, transepidermal water loss (TEWL), erythema (a*), skin-surface pH, and H&E-stained histology.

Statistical Analysis

The data shown in this study presented the mean and standard deviation (S.D.). The significant difference between the various groups was checked by the Kruskal–Wallis test. The *post hoc* test for examining the individual difference was Dunn's test. The significance was demonstrated as * for $p < 0.05$, ** for $p < 0.01$, and *** for $p < 0.001$.

RESULTS

Screening of Antifungal Activity of Naphthofuranquinones

We designed naphthofuranquinones conjugated with imine moiety with angular or linear structures to test the antifungal effect. As a first step to screen the activity, we sought to identify the MFC against ATCC90029 (**Table 1**). Four analogs (TCH-1140, TCH-1142, TCH-2958, and TCH-5261) showed the MFC of <300 μM against 5-FC-resistant microbes. The structures of the four compounds are illustrated in **Figure 1A**. A negligible fungus inhibition was observed for the other analogs (MFC > 1,000 μM). The four derivatives were selected to further compare the MIC and MFC against ATCC90029 and ATCC10231 with 5-FC and fluconazole (**Table 1**). ATCC90029 was found to be susceptible to fluconazole but resistant to 5-FC. A contrary result was shown for ATCC10231. The MFC for fluconazole was 510-fold higher than the MIC against ATCC90029, indicating a fungistatic activity. ATCC90029 was most sensitive to TCH-1142, followed by TCH-1140. The MFC of both compounds against ATCC90029 was much less than against the positive controls. TCH-2958 and TCH-5261 were less effective than TCH-1140 and TCH-1142. TCH-1140 and TCH-1142 exhibited MFC of 2.9 and 2.4 μM against ATCC10231, respectively. Both compounds were found to be about 110- and 1,500-fold stronger than 5-FC and fluconazole, respectively.

TABLE 1 | The MIC and MFC of naphthofuranquinones and the positive control against drug-resistant *C. albicans*.

	ATCC90029		ATCC10231	
	MIC (μM)	MFC (μM) 9683.2	MIC (μM) 37.8	MFC (μM)
5-Fluorocytosine	4841.6	9683.2	37.8	302.6
Fluconazole	4.0	2040.7	4081.4	4081.4
TCH-1140	1.5	2.9	2.9	2.9
TCH-1142	1.2	2.4	2.4	2.4
TCH-2958	134.1	268.2	268.2	268.2
TCH-5261	122.7	245.4	122.7	122.7

MIC, minimum inhibitory concentration; MFC, minimum fungicidal concentration. Each value represents the 3 replicates.

Naphthofuranquinones Eradicate Planktonic *C. albicans*

TCH-1140 and TCH-1142 were the most promising naphthofuranquinones against drug-resistant *C. albicans*. The time-killing study offers information regarding the extent and rate of antifungal activity (**Figure 1B**). In the 5-FC-resistant microbes, 5-FC showed less fungal growth inhibition than the other agents tested. 5-FC demonstrated a sigmoidal response curve against planktonic ATCC90029. The positive controls inhibited ATCC90029 development in a concentration-dependent manner. The killing curve displayed that TCH-1140 and TCH-1142 completely inhibited ATCC90029 growth over a prolonged period (48 h). We observed a greater inhibition by TCH-1140 than TCH-1142 at 2.9 μM, the dose near the MFC of both compounds. However, a significant growth of *C. albicans* was observed after a 30-h treatment of both compounds at 2.9 μM. The time-killing curve showed that ATCC10231 was more resistant to the antifungal agents tested here than ATCC90029. ATCC10231 growth suppression was comparable between TCH-1140 and TCH-1142. The antifungal potency was estimated based on an agar diffusion assay (**Figure 1C**). 5-FC and fluconazole had a similar effect on the inhibition zone of both *C. albicans* strains. The zone diameter treated by different concentrations of the positive controls was comparable. There was a threefold increase of the inhibition diameter with naphthofuranquinone treatment compared with the positive controls. The inhibition diameter increased following the increase of the naphthofuranquinone dose, although this difference was not large.

We used live/dead staining with SYTO9 and PI to visualize the antifungal activity (**Figure 1D**). SYTO9 (green) stains the live microbes, whereas PI (red) penetrates the dead cells with a damaged membrane. The control group showed a diffuse distribution of live *C. albicans*. In the case of ATCC90029, SYTO9 was not decreased by 5-FC and fluconazole at 23.5 μM compared to the control. Naphthofuranquinone intervention led to a reduction of live ATCC90029 (green signal). On the other hand, 5-FC at 23.5 μM significantly decreased the fluconazole-resistant strain (ATCC10231), whereas fluconazole could not. A further decrease of the live ATCC10231 burden (green signal) was observed for naphthofuranquinones than 5-FC. The live/dead images of *C. albicans* treated with higher doses (46.9 and 93.8 μM) showed some SYTO9 reduction by the positive controls (**Supplementary Figure S1**). The green signal was nearly absent in the naphthofuranquinone-treated groups with higher concentrations. Though the live fungi were significantly restrained by the lead compounds, the PI signal was scanty. This suggests that the compounds eradicated fungi with limited membrane damage. A more precise reflection of live-cell detection is provided by flow-cytometry-based counting

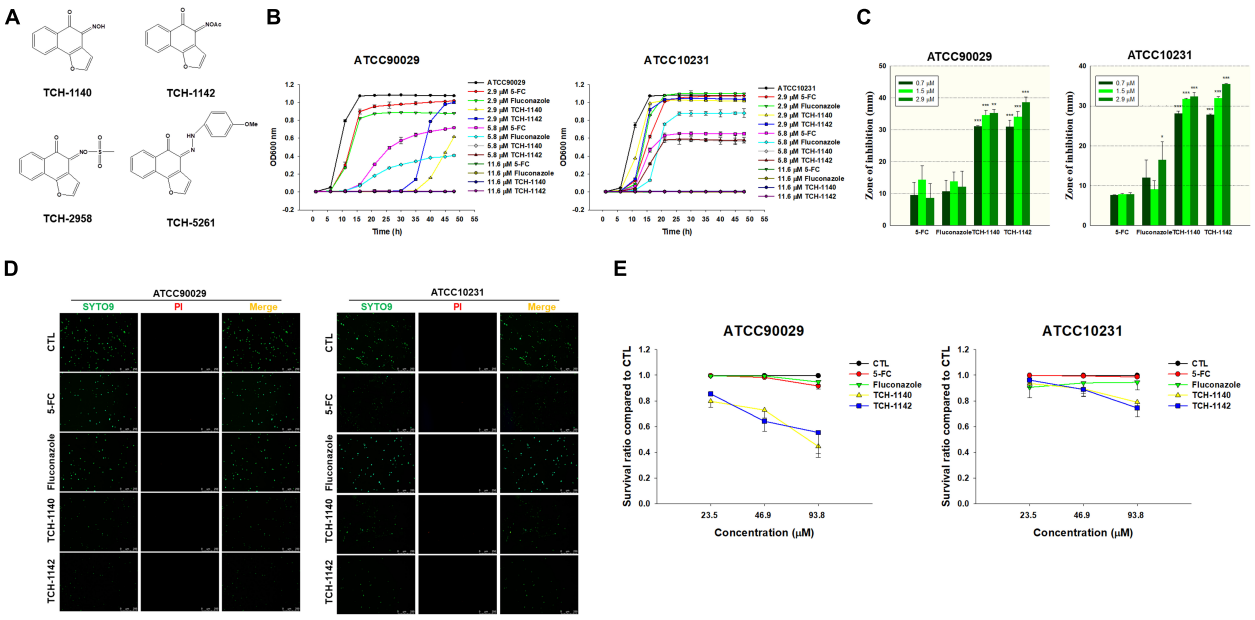

FIGURE 1 | Determination of the antifungal activity of naphthofuranquinone derivatives against planktonic drug-resistant *C. albicans*: **(A)** the chemical structures of naphthofuranquinones; **(B)** time-killing curves of 5-FC, fluconazole, and naphthofuranquinones; **(C)** zone of inhibition measured from agar diffusion assay; **(D)** the planktonic live/dead *C. albicans* strains treated by the agents at 23.5 μM viewed under fluorescence microscopy; and **(E)** the survival rate of *C. albicans* measured by flow cytometry according to **Supplementary Figure S2**. All data are presented as the mean of three experiments ±SD. $^{***}p < 0.001$, $^{**}p < 0.01$, $^{*}p < 0.05$.

(**Figure 1E**). No fungus eradication was found in the control group (non-treatment). 5-FC and fluconazole (23.5-93.8 μM) diminished < 10% of *C. albicans* of both ATCC90029 and ATCC10231. On the other hand, naphthofuranquinones revealed a greater reduction of fungus viability compared to the positive controls. The lead compounds demonstrated a dose-dependent biocidal activity. TCH-1140 and TCH-1142 were equipotent. The lead compounds at 93.8 μM reduced the ATCC90029 and ATCC10231 viability by about 50 and 25%, respectively. The representative profiles of flow cytometry are depicted in **Supplementary Figure S2**.

Naphthofuranquinones Eradicate Biofilm and Intracellular *C. albicans*

Biofilm and intracellular residence are virulence mechanisms assisting *C. albicans* to resist antifungal drugs. We quantified the *C. albicans* amount inside and outside the biofilm after antifungal treatment (**Figure 2A**). The counting of the colony-forming unit (CFU) was log-transformed. 5-FC did not inhibit ATCC90029 viability inside and outside the biofilm. Fluconazole diminished CFU outside the biofilm by a 1.5 log reduction, but no inhibition was detected inside the biofilm. Both CFU inside and outside the ATCC90029 biofilm was significantly reduced by both lead compounds at a comparable level. In the case of ATCC10231, fluconazole diminished the number of live fungi inside the biofilm by about 12%. Both naphthofuranquinones inhibited fungus burden inside biofilm by about 50%. The positive controls and naphthofuranquinones lessened ATCC10231 CFU outside the biofilm by about 1 and 2 logs, respectively.

Keratinocytes are the main cells participating in the cutaneous immune response. Macrophages are the immune cells playing the major reservoirs for intracellular *C. albicans*. We employed both cells to examine the effect of lead compounds on intracellular fungus killing. First, the dose-dependent cytotoxicity against HaCaT (keratinocytes) and THP-1 (macrophages) was assessed using MTT and cell counting kit-8 (CCK-8) assays. The control in this experiment was the cells treated with DMSO vehicle (100% survival). The positive control drugs and TCH-1140 did not exhibit cytotoxicity against both cells (viability > 80%) in the MTT assay (**Figure 2B**). The same result was found in the CCK-8 assay (**Supplementary Figure S3**). The viability was reduced to 60-80% by TCH-1142, indicating a mild cytotoxicity. To elucidate if the treatment of TCH-1140 and TCH-1142 was associated with HaCaT cell death through apoptosis, the cultured keratinocytes were analyzed by flow cytometry after staining with FITC-labeled Annexin V and PI. Annexin V exhibits a high affinity to phosphatidylserine after its externalization from inner to the outer plasma membrane of apoptotic cells, while PI is a membrane-impermeant dye staining DNA. No significant increase in Annexin V and PI binding on the HaCaT surface was visualized after 24 h of compound treatment compared to the control cells (**Supplementary Figures S4A,B**), indicating no keratinocyte apoptosis occurred by naphthofuranquinone treatment at a high dose (93.8 μM).

The staining of Annexin V and PI was also performed for *C. albicans*. The results of ATCC90029 and ATCC10231 treated with TCH1140 show that the dot plots to lower right (LR) area is increased by this compound (**Supplementary Figures S4C,D**), manifesting an early apoptosis. The dot plots were also

increased in the upper left (UL) area by TCH1140 intervention, indicating the late apoptosis. A similar result was observed for TCH1142 (**Supplementary Figures S4E,F**). These results demonstrated that the lead compounds caused both early and late apoptosis for killing *C. albicans*. We then evaluated whether the compounds could kill intracellular *C. albicans* in HaCaT or THP-1. The infected cells were treated by the compounds for 4 h after unphagocytosed fungus removal. All agents tested significantly reduced ATCC90029 in keratinocytes (**Figure 2C**). Fluconazole and naphthofuranquinones exhibited a 1-log greater anti-ATCC90029 effect than 5-FC. The effect among fluconazole, TCH-1140, and TCH-1142 was comparable. In the case of ATCC10231, naphthofuranquinones demonstrated a greater capability to kill fungi than fluconazole. None of the agents revealed a significant *C. albicans* CFU reduction in the macrophages (**Figure 2D**).

Encouraged by these findings, we visualized the morphology of *C. albicans* in the host cells after treatment with lead compounds (**Figure 3**). The infected cells were exposed to fluorescently labeled *C. albicans* (green) and DAPI (blue) for monitoring by confocal microscopy. The images indicated that both fungal strains in HaCaT or THP-1 showed significant hyphae. Some fungi were present outside the host cells, suggesting a possible escape from the cells during a 4-h

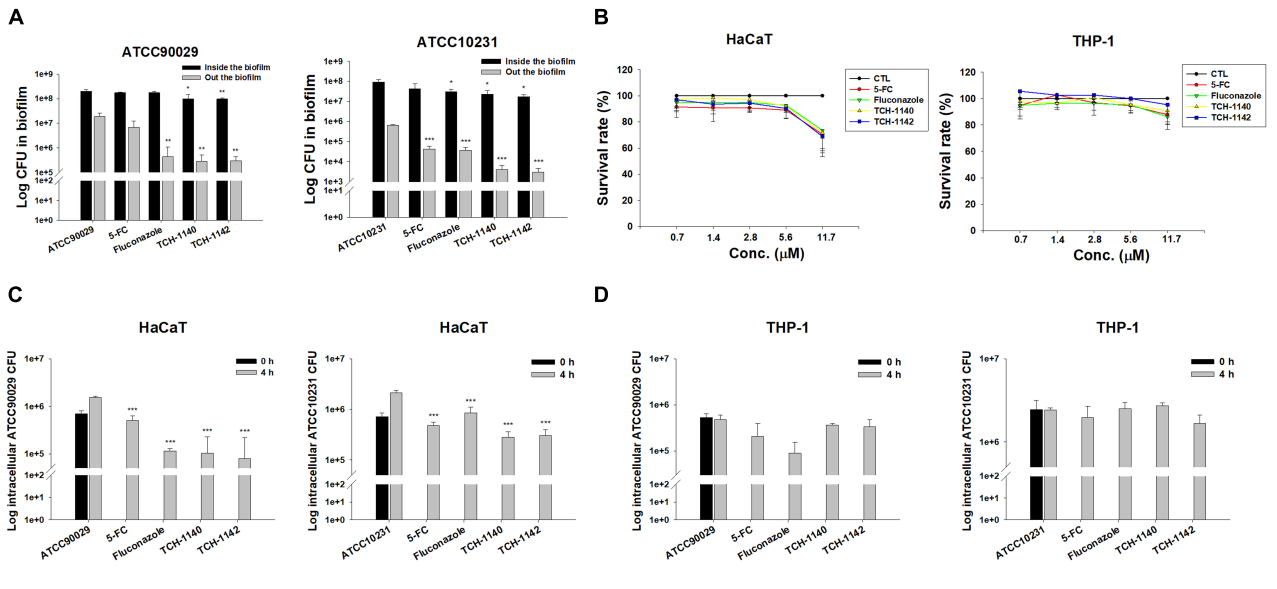

FIGURE 2 | Determination of antifungal activity of naphthofuranquinone derivatives against biofilm and intracellular drug-resistant *C. albicans*: **(A)** *C. albicans* CFU outside and inside the biofilm; **(B)** the survival rate of keratinocytes and macrophages treated by 5-FC, fluconazole, and naphthofuranquinones measured by MTT assay; **(C)** the intracellular *C. albicans* CFU inside keratinocytes after treatment of 5-FC, fluconazole, and naphthofuranquinones; and **(D)** the intracellular *C. albicans* CFU inside macrophages after treatment of 5-FC, fluconazole, and naphthofuranquinones. All data are presented as the mean of three experiments ±SD (biological triplicate). ***$p < 0.001$, **$p < 0.01$.

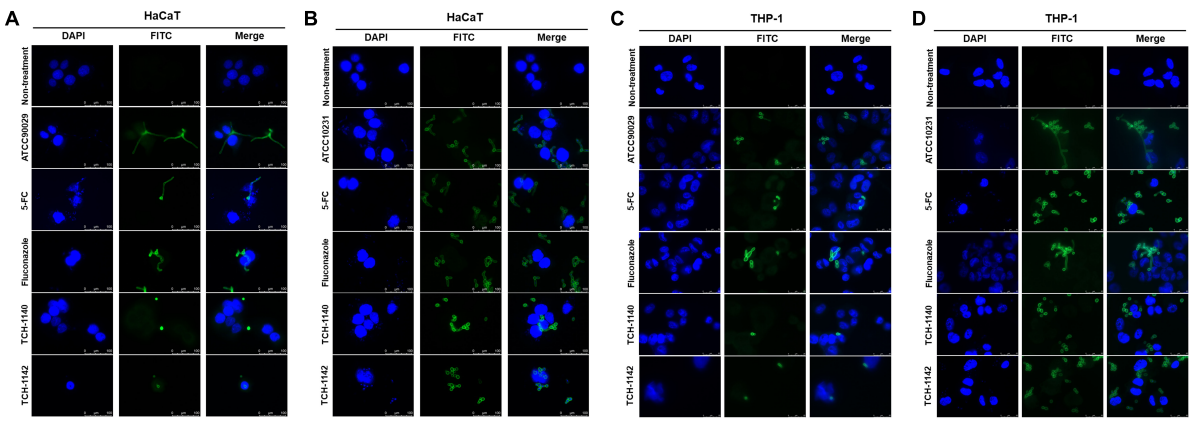

FIGURE 3 | The confocal microscopic images of *C. albicans* (green) in the host cells (blue) after treatment of 5-FC, fluconazole, and naphthofuranquinones: **(A)** ATCC90029-infected keratinocytes; **(B)** ATCC10231-infected keratinocytes; **(C)** ATCC90029-infected macrophages; and **(D)** ATCC10231-infected macrophages.

incubation. These filamentous hyphae in keratinocytes were unaffected by 5-FC and fluconazole (**Figures 3A,B**). On the other hand, the hypha filament could be shortened or transferred into pseudohypha form by 5-FC and fluconazole in macrophages (**Figures 3C,D**). The inhibited fungal filamentation was observed in naphthofuranquinone-treated keratinocytes. The filamentous fungi could change into unicellular yeast or pseudohypha form after lead compound intervention in macrophages. The large field view of ATCC10231 infected in HaCaT and THP-1 under confocal microscopy is shown in **Supplementary Figures S5A,B,** respectively.

Elucidation of Possible Antifungal Mechanisms of Naphthofuranquinones

Antifungal mechanisms of the lead compounds were investigated. We began this study by SEM (**Figure 4A**). ATCC10231 in dense biofilm form was observed to show both yeast and hypha morphologies. The hypha form was absent with treatment of the positive controls and naphthofuranquinones. The fungal shape and surface remained intact after 5-FC intervention. Fluconazole and naphthofuranquinones generated a morphological alteration on the fungal surface, demonstrating the membrane destabilization. The wrinkled and rough surfaces with cavities indicated a phenotype of dead microbes. The size of some *C. albicans* decreased when exposed to TCH-1140 and TCH-1142, which was indicative of fungal death. Next, we quantified the total DNA, RNA, and protein in 5-FC- and TCH-1140-treated ATCC10231 (**Figures 4B–D**). TCH-1142 was not used in the following experiments because of its higher toxicity toward mammalian cells than TCH-1140. The DNA load in *C. albicans* was reduced by 87 and 90% in the 5-FC and TCH-1140 groups, respectively. The RNA and protein analyses also indicated a depressed amount after treatment of 5-FC and TCH-1140. The reduction between 5-FC and hydroxyimino-conjugated naphthofuranquinone was comparable.

To explore the role of TCH-1140 on hypha suppression, the expression of hypha-related genes *efg1*, *ume6*, and *hgc1* at the transcriptional level was measured (**Figure 4E**). TCH-1140 reduced *efg1* expression as compared to the control although the statistical significance was not achieved. Surprisingly, 5-FC elevated *efg1* by eightfold. The gene *ume6* was found to be significantly downregulated by 5-FC and TCH-1140. The same result was observed in *hgc1*, with TCH-1140 showing greater inhibition.

TCH-1140 Mitigates *C. albicans* Burden *In vivo*

A mouse model of skin mycosis induced by ATCC10231 was used to rate the efficacy of TCH-1140 *in vivo*. After induction of cutaneous candidiasis, the nidus showed pustule, edema, and inflammation of the skin with an abscess diameter of about 8 mm (**Figure 5A**). 5-FC treatment restricted the abscess diameter to 5-6 mm. The severity of the lesion was further decreased in the TCH-1140-treated animals with the diameter of 3-4 mm, indicating a significant wound healing. The same tendency was

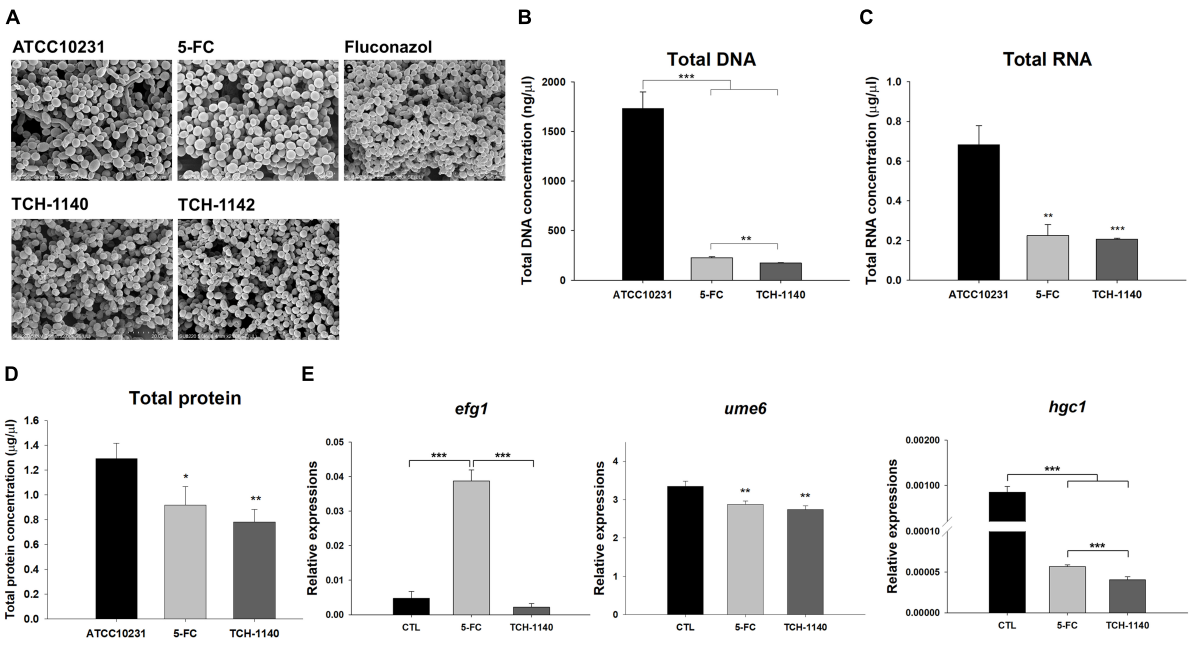

FIGURE 4 | Antifungal mechanisms of naphthofuranquinones: **(A)** morphological changes of ATCC10231 viewed under TEM; **(B)** total DNA amount in ATCC10231; **(C)** total RNA amount in ATCC10231; **(D)** total protein amount in ATCC10231; and **(E)** the expression of hypha-related genes *efg1*, *ume6*, and *hgc1*. All data are presented as the mean of three experiments ±SD. ***$p < 0.001$, **$p < 0.01$, *$p < 0.05$.

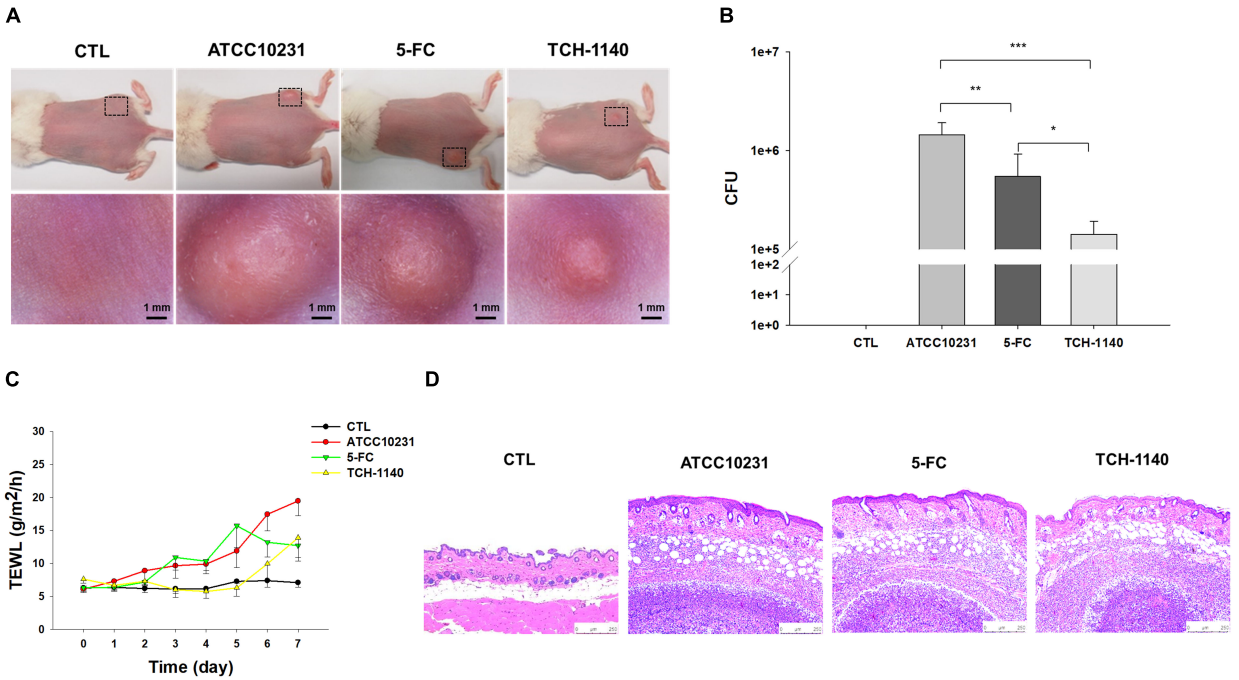

FIGURE 5 | *In vivo* topical application of TCH-1140 against ATCC10231: **(A)** the skin surface of ATCC10231-infected mice after treatment of 5-FC or TCH-1140 viewed under phenotypic and microscopic images; **(B)** ATCC10231 CFU in mouse skin after treatment of 5-FC or TCH-1140; **(C)** TEWL of ATCC10231-infected mice after treatment of 5-FC or TCH-1140; and **(D)** histological observation of ATCC10231-infected mouse skin biopsy stained by H&E. All data are presented as the mean of six experiments ±SD. ***$p < 0.001$, **$p < 0.01$, *$p < 0.05$.

found in the fungal count (**Figure 5B**). TCH-1140 achieved a 1-log CFU reduction as compared to the infection group without treatment. TEWL was detected daily to evaluate skin-barrier function (**Figure 5C**). *C. albicans* infection produced cutaneous inflammation to disintegrate the barrier feature for increasing TEWL. 5-FC reduced this elevation from day 6. The baseline TEWL remained up to day 5 by TCH-1140; however, some barrier disruption was observed after day 6. A histopathological assay of the abscess of ATCC10231-infected skin showed a large *C. albicans* burden under the subcutis (**Figure 5D**). Some fungi invaded to the dermis and subcutis. Inflammatory cell infiltration was also visualized in the viable skin. The animals receiving 5-FC displayed an improvement in the fungal load and immune cell accumulation. A further mitigation of the fungal burden and infiltration was detected after TCH-1140 administration.

Some proinflammatory mediators expressed in the skin were observed by IHC. The IgG expression was higher in the infected abscess and dermis compared with the healthy skin (**Supplementary Figure S6A**). The IgG upregulation by infection could be improved by 5-FC and TCH-1140. The level of IFN-γ in the dermis and around the abscess after ATCC10231 injection was higher than in the control animal (**Supplementary Figure S6B**). No significant IFN-γ reduction was observed by 5-FC treatment. TCH-1140 significantly downregulated IFN-γ in cutaneous tissue compared to the infected animal, whereas the expression in the margin of abscess seemed to increase. IL-17 was extensively distributed in the abscess and subcutaneous region of ATCC10231-infected animals (**Supplementary Figure S6C**). This distribution was not diminished by antifungal agent application. The neutrophil infiltration in the skin was observed by Ly6G staining (**Supplementary Figure S6D**). Some focal neutrophils in the dermis were seen after *C. albicans* injection. This focal accumulation was still detected after 5-FC treatment. The focal Ly6G was minimal in the TCH-1140-treated dermis.

TCH-1140 Elicits a Negligible Skin Irritation

5-FC or TCH-1140 was topically applied on healthy mouse skin to check the possibility of inducing irritation. No visible redness, scaling, or edema was observed on the cutaneous surface treated with the compounds as compared to vehicle control for 5 days (**Figure 6A**). No disrupted barrier function (TEWL), erythema (a*), or skin surface pH was changed after administration of the compounds (**Figures 6B–D**). TEWL was increased from 6 to 8 g/m^2/h at day 1 for all groups. This could be due to the capability of the aqueous vehicle to hydrate the stratum corneum. The 5-FC and TCH-1140 groups exhibited cutaneous histology similar to the vehicle control (**Figure 6E**).

DISCUSSION

Candida albicans is a primary fungus responsible for skin and mucous infection. Drug-resistant fungus strains present an

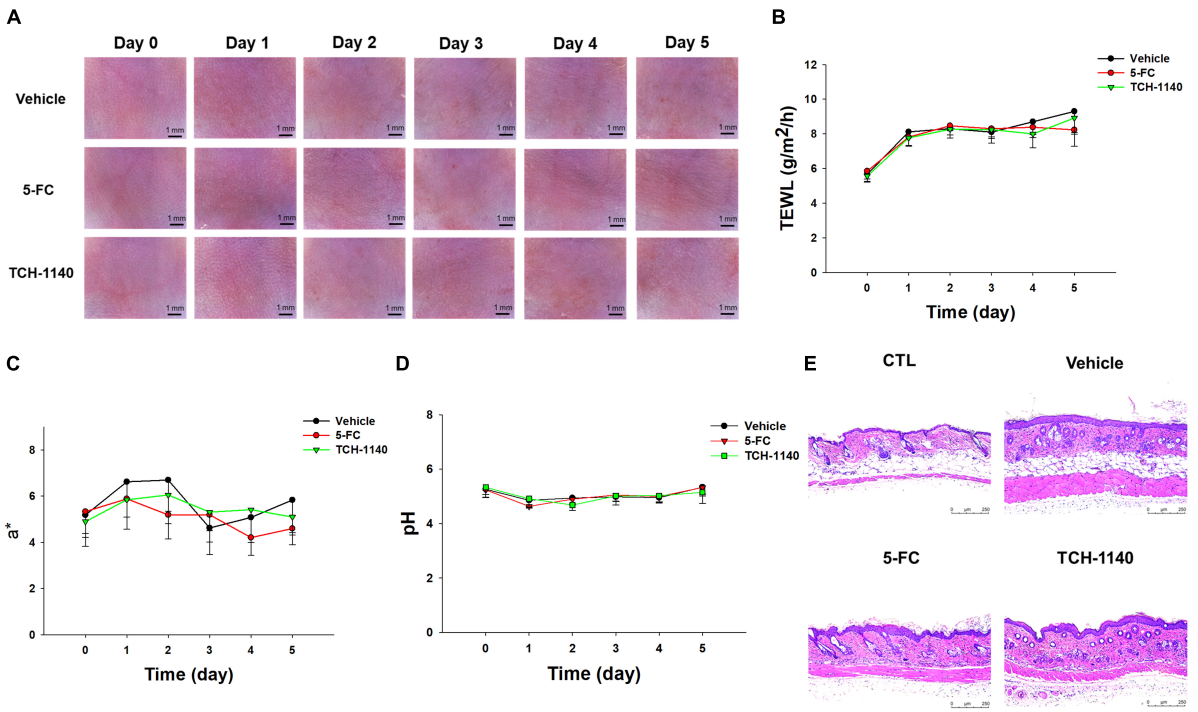

FIGURE 6 | Skin tolerance examination of mouse skin by a 5-day treatment of topically applied TCH-1140: **(A)** the skin surface of mice viewed under handheld digital magnifier; **(B)** TEWL of mouse skin after treatment of 5-FC or TCH-1140; **(C)** erythema (a*) of mouse skin after treatment of 5-FC or TCH-1140; **(D)** pH of mouse skin after treatment of 5-FC or TCH-1140; and **(E)** histological observation of mouse skin biopsy stained by H&E. All data are presented as the mean of six experiments ±SD.

important clinical concern. As a result, novel agents are urgently needed to resolve the problem of resistance. In this study, thorough analyses were conducted to evaluate the capability of *C. albicans* eradication by naphthofuranquinones prepared in our lab. We found that TCH-1140 and TCH-1142 were effective in killing drug-resistant *C. albicans* either in planktonic form or in the highly virulent forms (hypha, biofilm, and host cell residence). The *in vivo* effect of the lead compound in the cutaneous candidiasis mouse model together with acceptable safety reinforce the potential as a candidate in the development of an antifungal agent.

After screening the antifungal activity of naphthofuranquinones by MFC, the angular-structured compounds substituted by hydroxyimino (TCH-1140) and *O*-acetyl oxime (TCH-1142) moieties at the 4-position showed the greatest potency. All others had negligible activity. The linear naphthofuranquinone structures totally lost the antifungal activity. The conjugation of the hydrazino group at 4-position also eliminated the activity. We selected TCH-1140 and TCH-1142 for further comparison with 5-FC and fluconazole. The MIC of TCH-1140 and TCH-1142 against ATCC90029 was 1.5 μM (0.32 μg/ml) and 1.2 μM (0.31 μg/ml), respectively. These values were greatly lower than the other naphthoquinone derivatives reported earlier such as 2-methyl-5-hydroxynaphtho[2,3-*b*]furan-4,9-dione (2-8 μg/ml), phenanthrenequinone (60 μg/ml), 2-[iodomethyl]-2,3-dihydronaphtho[2,3-*b*]furan-4,9-dione (12 μg/ml), and plumbagin (8 μg/ml) (Nagata et al., 1998; Neto et al., 2014; Rejiniemon et al., 2014; Hassan et al., 2016), although the *C. albicans* strains used were different among the different studies. This suggested the potent antifungal activity of the naphthofuranquinones developed in this work. Clinical use of 5-FC and fluconazole is limited due to toxicity concerns and resistance emergence. 5-FC is a nucleoside analog impairing DNA and protein synthesis. Its side effects are bone-marrow suppression, diarrhea, and skin rash (Meletiadis et al., 2008). Fluconazole is the agent most commonly used to treat *Candida* infection. The overuse of fluconazole has developed a significant incidence of resistance, resulting in therapeutic failure (Reis de Sá et al., 2017). It is appreciated that *C. albicans* is considered resistant at the MIC ≥ 210 μM (Ghannoum and Rice, 1999). We recognized that ATCC10231 was resistant to fluconazole, while ATCC90029 was sensitive to this drug. A contrary tendency was found for 5-FC. An agent is regarded as fungicidal and fungistatic when the MFC/MIC ratio is less or higher than 4, respectively (Ganan et al., 2019). Our results demonstrated that naphthofuranquinones were fungicidal. An ideal biocidal agent should kill the microbes quickly to avoid the opportunity for resistance development (Ng et al., 2017). Our time-killing curve showed a rapid fungicidal effect with the use of TCH-1140 and TCH-1142.

The naphthofuranquinones evoked fungal wall and/or membrane disturbance based on SEM, indicating the occurrence of compromised membrane integrity. However,

this damage could be regarded as mild since PI could not permeate into the cytoplasm as observed in the live/dead assay. Naphthofuranquinone intervention interfered with the total DNA, RNA, and protein synthesis in the fungi. The lead compounds might penetrate the membrane into the fungal cytoplasm, producing killing by DNA replication inhibition but not the direct membrane disintegration. Drug efflux is an important resistance mechanism, especially for fluconazole resistance (Berkov and Lockhart, 2017). The superior eradication of the drug-resistant *C. albicans* by naphthofuranquinones compared to that by fluconazole could be due to the inhibition of the efflux pump regulated by some genes such as *mdr1*. The mechanisms of *C. albicans* death elicited by the lead compounds are still not completely understood. It should also be noticeable that the *C. albicans* growth was elevated after a 30-h treatment of lead compounds at 2.9 μM in the time-response test. The strains might gain resistance toward the compounds after a long-term intervention. Further study is needed to explore the details.

Candida species are difficult to treat as they invade host cells. This is a manifestation of drug resistance. More than 60% of the antimicrobials failed to manage intracellular microbes (Murali et al., 2018). Both keratinocytes and macrophages are the host cells that are invaded by topical fungi infecting the skin (Lopez et al., 2014). Although macrophages are the innate immune systems for eliminating *C. albicans*, most of the fungi survive inside the macrophages with only a portion of the population being killed (Diez-Orejas and Fernández-Arenas, 2008). Here, we demonstrated that TCH-1140 could enter the keratinocytes to kill *C. albicans* without affecting host-cell viability. This intracellular elimination by naphthofuranquinones was better than 5-FC and fluconazole. The lead compounds did not arrest *C. albicans* growth in the macrophages. Rather, they drove the fungal transition from the pathologic hypha to the pseudohypha or yeast. The naphthofuranquinones can be anti-virulence agents. Engulfment of yeast *C. albicans* by keratinocytes and macrophages induces the production of hypha, which exerts a virulent action (Kano et al., 2003; Arnaud et al., 2009). The hyphal formation allows the puncture of the macrophage membrane, leading to the escape of *C. albicans* from the cells (Wartenberg et al., 2014). This was the reason why we saw some microbes outside the infected macrophages. The naphthofuranquinones maintained the fungi in the yeast or pseudohypha type, which was beneficial to preserving the function of macrophages for eliminating fungi.

The development of resistance to antifungal drugs often occurs in filamentous fungi. *efg1*, *ume6*, and *hgc1* are transcription regulators associated with hypha formation. The transcription factor *efg1* functions to promote filamentous growth (Park et al., 2020). *ume6* is a downstream target of hypha-growth signaling (Zeidler et al., 2009). This key regulator functions downstream of *efg1* and upstream of *hgc1*. The experimental data demonstrated that TCH-1140 suppressed the transcription of these genes. The upregulation of *efg1* by 5-FC was surprising. *efg1* appears to be an upstream regulator in the network of filamentation. Besides the involvement of the hypha form, *efg1* also acts as the regulator of cell wall proteins, adhesion, aspartic protease, and antifungal resistance (Gow et al., 2012). 5-FC stimuli might cause *efg1* upregulation in response to the environmental change because of the complex role of this gene in adapting morphogenetic transition.

Both morphogenesis and biofilm are the important virulences of drug-resistant *C. albicans*. Hyphal elements are the main structures embedded in mature *C. albicans* biofilm (Vavala et al., 2013). The biofilm presents a permeation barrier to antifungal drugs and phagocytes (Roscetto et al., 2018). 5-FC and fluconazole are less sensitive to treat biofilm-associated invasion. The evidence shows that the drug concentration needed to eradicate biofilm fungi is 5-8 times greater than that needed to eradicate planktonic fungi (Mathé and Van Dijck, 2013). The antifungal agents with the ability to diminish biofilm microbes are promising for reducing colonization on the skin and in the mucus (Rejiniemon et al., 2014). We demonstrated that the synthetic naphthofuranquinones showed their activity against *C. albicans* inside the mature biofilm. Although a statistically significant CFU reduction was obtained, this killing by the compounds was still limited. The high cell density inside the biofilm has markedly lowered susceptibility to all drugs (Mathé and Van Dijck, 2013). The dispersed *C. albicans* from biofilm displays increased virulence, filamentation, and drug resistance, which are responsible for invasive infection (Wall et al., 2019). The naphthofuranquinones were fungicidal not only against *C. albicans* inside the biofilm but also against the microbes dispersed from the biofilm. The dispersal inhibition by TCH-1140 and TCH-1142 was superior to that in the positive controls.

The emergence of *C. albicans* strains resistant to current agents has contributed to an increase in the skin infection reported in humans. Our results manifested that TCH-1140 was superior to 5-FC for ameliorating drug-resistant *C. albicans*-induced infection and inflammation. TCH-1140 also recovered skin-barrier capacity disrupted by fungi. *C. albicans* infection is a result of a coordinated battle with host cells. The recognition of *C. albicans* by skin cells and innate immune cells induces the production of proinflammatory mediators. A previous study (Zhang et al., 2018) proved that *C. albicans* infection induced candidiasis with IL-17 and IFN-γ expression. Th17 cells are vital in the defense against fungal infection (Engelhardt and Grimbacher, 2012). IL-17 overexpression by Th17 cells can cause inflammation. IL-17 clears *C. albicans* through neutrophil recruitment for killing the pathogens by releasing antimicrobial peptides or phagocytosis (Kashem and Kaplan, 2016). The phagocytosis is an early line of defense for clearing fungi. The skin infected with ATCC10231 and topically treated with TCH-1140 showed a reduction of the fungal burden and focal neutrophil accumulation. We hypothesized that the inhibition of fungal colonization by TCH-1140 in the early infection stage attenuated the host immune response and inflammation. IgG reveals an important role in the immunity via raising fungal phagocytosis (Munawara et al., 2017). We also showed a significant reduction of IgG distribution in the skin and abscess regions infected by ATCC10231.

IFN-γ is chiefly secreted by keratinocytes to play a key role in the defense against *C. albicans* (Shiraki et al., 2008). TCH-1140 suppressed IFN-γ in the dermis, suggesting inflammation mitigation. However, IFN-γ expression increased around the

fungus-induced abscess by TCH-1140. This could be because the increase of IgG by macrophages in the presence of *C. albicans* results in the decrease of IFN-γ, the Th1-related response (Munawara et al., 2017). Gow et al. (2012) also demonstrated that fungal hypha fails to evoke the Th1 immune response. The assessment of toxicity is principal in the development of new therapeutic drugs for clinical use. We were inspired by the skin irritation test to confirm that topical TCH-1140 was toxic toward drug-resistant fungi but tolerable to the skin.

CONCLUSION

After screening a series of naphthofuranquinones, TCH-1140 and TCH-1142 were proven to be the most potent for eradicating drug-resistant *C. albicans*. Both compounds were active against yeast, filamentous, and biofilm *C. albicans* strains that were resistant to 5-FC or fluconazole. The lead compounds could deliver into the host cells, leading to a marked clearance of intracellular fungi. The resistant fungus infection and the associated inflammation in the skin were mitigated by TCH-1140. Our findings suggested that TCH-1140 could be a candidate for the treatment of skin mycosis. There is room for further structural modification in naphthofuranquinones for lead optimization of the potentiating activity. Naphthofuranquinone analogs do warrant further investigation as a topical agent for treating fungus-infected skin lesions.

DATA AVAILABILITY STATEMENT

The raw data supporting the conclusions of this article will be made available by the authors, without undue reservation, to any qualified researcher.

ETHICS STATEMENT

The animal study was reviewed and approved by Institutional Animal Care and Use Committee of Chang Gung University.

AUTHOR CONTRIBUTIONS

J-YF initiated the study and drafted the manuscript. K-WT involved in the design of all experiments. S-HY, S-CY, and Y-CY carried out the experiments. AA analyzed data and wrote the manuscript. S-CY supervised the entire project. C-HT reviewed critically and approved the final manuscript. All authors read and approved the final manuscript.

FUNDING

The authors are grateful for the financial support from Ministry of Science and Technology of Taiwan (MOST-107-2320-B-182-016-MY3), Chang Gung Memorial Hospital (CMRD1F0231-3), and Kaohsiung Medical University (KMU-TC108A03-2 and KMU-TC108 A03-10).

ACKNOWLEDGMENTS

We thank the Center for Research Resources and Development at Kaohsiung Medical University for the instrumentation and equipment support.

SUPPLEMENTARY MATERIAL

The Supplementary Material for this article can be found online at: https://www.frontiersin.org/articles/10.3389/fmicb.2020.02053/full#supplementary-material

FIGURE S1 | The planktonic live/dead *C. albicans* strains treated by the agents at 46.9 or 93.8 μM viewed under fluorescence microscopy: **(A)** ATCC90029 treated by 5-FC, fluconazole, and naphthofuranquinones at 46.9 μM. **(B)** ATCC10231 treated by 5-FC, fluconazole, and naphthofuranquinones at 46.9 μM. **(C)** ATCC90029 treated by 5-FC, fluconazole, and naphthofuranquinones at 93.8 μM. **(D)** ATCC10231 treated by 5-FC, fluconazole, and naphthofuranquinones at 93.8 μM.

FIGURE S2 | The flow cytometry of *C. albicans* viability treated by 5-FC, fluconazole, and naphthofuranquinones : **(A)** ATCC90029; and **(B)** ATCC10231. FL1 (*x*-axis) represents SYTO9 staining. FL3 (*y*-axis) represents PI staining.

FIGURE S3 | The survival rate of keratinocytes and macrophages treated by 5-FC, fluconazole, and naphthofuranquinones measured by CCK-8 assay: **(A)** keratinocytes; and **(B)** macrophages. All data are presented as the mean of three experiments ±S.D.

FIGURE S4 | The flow cytometry of keratinocytes and *C. albicans* stained by Annexin V and PI to detect the early or late apoptosis: **(A)** keratinocytes treated with TCH-1140 at 93.8 μM; **(B)** keratinocytes treated with TCH-1142 at 93.8 μM; **(C)** ATCC90029 treated with TCH-1140 at 23.5 μM; **(D)** ATCC10231 treated with TCH-1140 at 23.5 μM; **(E)** ATCC90029 treated with TCH-1142 at 23.5 μM; and **(F)** ATCC10231 treated with TCH-1142 at 23.5 μM. All data are presented as the mean of three experiments ±S.D. LL, lower left; LR, lower right; UL, upper left; UR, upper right.

FIGURE S5 | The large field view of confocal microscopic images of ATCC10231 after treatment of 5-FC, fluconazole, and naphthofuranquinones: **(A)** ATCC10231-infected keratinocytes; and **(B)** ATCC10231-infected macrophages.

FIGURE S6 | The IHC staining of ATCC10231-infected mouse skin after treatment of 5-FC or TCH-1140: **(A)** IgG; **(B)** IFN-γ; **(C)** IL-17, and **(D)** Ly6G.

REFERENCES

Alalaiwe, A., Wang, P. W., Lu, P. L., Chen, Y. P., Fang, J. Y., and Yang, S. C. (2018). Synergistic anti-MRSA activity of cationic nanostructured lipid carriers in combination with oxacillin for cutaneous application. *Front. Microbiol.* 9:1493. doi: 10.3389/fmicb.2018.01493

Arnaud, M. B., Costanzo, M. C., Shah, P., Skrzypek, M. S., and Sherlock, G. (2009). Gene ontology and the annotation of pathogen genomes: the case of *Candida albicans*. *Trends Microbiol.* 17, 295–303. doi: 10.1016/j.tim.2009.04.007

Berkov, E. L., and Lockhart, S. R. (2017). Fluconazole resistance in *Candida* species: a current perspective. *Infect. Drug Resist.* 10, 237–245. doi: 10.2147/idr.s118892

Chien, C. M., Lin, K. L., Su, J. C., Chuang, P. W., Tseng, C. H., Chen, Y. L., et al. (2010). Naphtho[1,2-*b*]furan-4,5-dione induces apoptosis of oral squamous cell carcinoma: involvement of EGF receptor/PI3K/Akt signaling pathway. *Eur. J. Pharmacol.* 636, 52–58. doi: 10.1016/j.ejphar.2010.03.030

Chou, W. L., Lee, T. H., Huang, T. H., Wang, P. W., Chen, Y. P., Chen, C. C., et al. (2019). Coenzyme Q0 from *Antrodia cinnamomea* exhibits drug-resistant bacteria eradication and keratinocyte inflammation mitigation to ameliorate infected atopic dermatitis in mouse. *Front. Pharmacol.* 10:1445. doi: 10.3389/fmicb.2018.01445

Diez-Orejas, R., and Fernández-Arenas, E. (2008). *Candida albicans*-macrophage interactions: genomic and proteomic insights. *Future Microbiol.* 3, 661–681. doi: 10.2217/17460913.3.6.661

Engelhardt, K. R., and Grimbacher, B. (2012). Mendelian traits causing susceptibility to mucocutaneous fungal infections in human subjects. *J. Allergy Clin. Immunol.* 129, 294–305. doi: 10.1016/j.jaci.2011.12.966

Ganan, M., Lorentzen, S. B., Agger, J. W., Heyward, C. A., Bakke, O., Knutsen, S. H., et al. (2019). Antifungal activity of well-defined chito-oligosaccharide preparations against medically relevant yeasts. *PLoS One* 14:e0210208. doi: 10.1371/journal.pone.0210208

Gershon, H., and Shanks, L. (1975). Fungitoxicity of 1,4-naphthoquinones to *Candida albicans* and *Trichophyton mentagrophytes*. *Can. J. Microbiol.* 21, 1317–1321. doi: 10.1139/m75-198

Ghannoum, M., Isham, N., Verma, A., Plaum, S., Fleischer, A., and Hardas, B. (2013). In vitro antifungal activity of naftifine hydrochloride against dermatophytes. *Antimicrob. Agents Chemother.* 57, 4369–4372. doi: 10.1128/aac.01084-13

Ghannoum, M. A., and Rice, L. B. (1999). Antifungal agents: mode of action, mechanisms of resistance, and correlation of these mechanisms with bacterial resistance. *Clin. Microbiol. Rev.* 12, 501–517. doi: 10.1128/cmr.12.4.501

Gow, N. A. R., van de Veerdonk, F. L., Brown, A. J. P., and Netea, M. G. (2012). *Candida albicans* morphogenesis and host defense: discriminating invasion from colonization. *Nat. Rev. Microbiol.* 10, 112–122. doi: 10.1038/nrmicro2711

Hassan, S. T. S., Berchová-Bímová, K., and Petráš, J. (2016). Plumbagin, a plant-derived compound, exhibits antifungal combinatory effect with amphotericin B against *Candida albicans* clinical isolates and anti-hepatitis C virus activity. *Phytother. Res.* 30, 1487–1492. doi: 10.1002/ptr.5650

Kano, R., Hasegawa, A., Watanabe, S., Sato, H., and Nakamura, Y. (2003). *Candida albicans* induced interleukin 8 production by human keratinocytes. *J. Dermatol. Sci.* 31, 233–235. doi: 10.1016/s0923-1811(03)00043-4

Kashem, S. W., and Kaplan, D. H. (2016). Skin immunity to *Candida albicans*. *Trends Immunol.* 37, 440–450. doi: 10.1016/j.it.2016.04.007

Kühbacher, A., Burger-Kentischer, A., and Rupp, S. (2017). Interaction of *Candida* species with the skin. *Microorganisms* 5:32. doi: 10.3390/microorganisms5020032

Larsen, B., Petrovic, M., and De Seta, F. (2018). Boric acid and commercial organoboron products as inhibitors of drug-resistant *Candida albicans*. *Mycopathologia* 183, 349–357. doi: 10.1007/s11046-017-0209-6

Lin, Z. C., Hsieh, P. W., Hwang, T. L., Chen, C. Y., Sung, C. T., and Fang, J. Y. (2018). Topical application of anthranilate derivatives ameliorates psoriatic inflammation in a mouse model by inhibiting keratinocyte-derived chemokine expression and neutrophil infiltration. *FASEB J.* 32, 6783–6795. doi: 10.1096/fj.201800354

Lopez, C. M., Wallich, R., Riesbeck, K., Skerka, C., and Zipfel, P. F. (2014). *Candida albicans* uses the surface gpm1 to attach to human endothelial cells and to keratinocytes via the adhesive protein vitronectin. *PLoS One* 9:e90796. doi: 10.1371/journal.pone.090796

Martinez-Rossi, N. M., Peres, N. T., and Rossi, A. (2017). Pathogenesis of dermatophytosis: sensing the host tissue. *Mycopathologia* 182, 215–227. doi: 10.1007/s11046-016-0057-9

Mathé, L., and Van Dijck, P. (2013). Recent insights into *Candida albicans* biofilm resistance mechsnisms. *Curr. Genet.* 59, 251–264. doi: 10.1007/s00294-013-0400-3

Meletiadis, J., Chanock, S., and Walsh, T. J. (2008). Defining targets for investigating the pharmacogenomics of adverse drug reactions to antifungal agents. *Pharmacogenomics* 9, 561–584. doi: 10.2217/14622416.9.5.561

Monika, S., Małgorzata, B., and Zbigniew, O. (2017). Contribution of aspartic proteases in *Candida* virulence. Protease inhibitors against *Candida* infections. *Curr. Protein Pept. Sci.* 18, 1050–1062.

Munawara, U., Small, A. G., Quach, A., Gorgani, N. N., Abbott, C. A., and Ferrante, A. (2017). Cytokines regulate complement receptor immunoglobulin expression and phagocytosis of *Candida albicans* in human macrophages: a control point in anti-microbial immunity. *Sci. Rep.* 7:4050.

Murali, S., Aparna, V., Suresh, M. K., Biswas, R., Jayakumar, R., and Sathianarayanan, S. (2018). Amphotericin B loaded sulfonated chitosan nanoparticles for targeting macrophages to treat intracellular *Candida glabrata* infections. *Int. J. Biol. Macromol.* 110, 133–139. doi: 10.1016/j.ijbiomac.2018.01.028

Nagata, K., Hirai, K. I., Koyama, J., Wada, Y., and Tamura, T. (1998). Antimicrobial activity of novel furanonaphthoquinone analogs. *Antimicrib. Agents Chemother.* 42, 700–702. doi: 10.1128/aac.42.3.700

Neto, J. B. A., da Silva, C. R., Neta, M. A. S., Campos, R. S., Siebra, J. T., Silva, R. A. C., et al. (2014). Antifungal activity of naphthoquinoidal compounds in vitro against fluconazole-resistant strains of different *Candida* species: a special emphasis on mechanisms of action on *Candida tropicalis*. *PLoS One* 9:e93698. doi: 10.1371/journal.pone.093698

Ng, S. M. S., Teo, S. W., Yong, Y. E., Ng, F. M., Lau, Q. Y., Jureen, R., et al. (2017). Preliminary investigations into developing all-*D* omiganan for treating mupirocin-resistant MRSA skin infections. *Chem. Biol. Drug Res.* 90, 1155–1160. doi: 10.1111/cbdd.13035

Park, Y. N., Conway, K., Pujol, C., Daniels, K. J., and Soll, D. R. (2020). EFG1 mutations, phenotypic switching, and colonization by clinical a/α strains of *Candida albicans*. *mSphere* 5:e0795-19.

Reis de Sá, L. F., Toledo, F. T., Gonçalves, A. C., Sousa, B. A., dos Santos, A. A., Brasil, P. F., et al. (2017). Synthetic organotellurium compounds sensitize drug-resistant *Candida albicans* clinical isolates to fluconazole. *Antimicrob. Agents Chemother.* 61:e001231-16.

Rejiniemon, T. S., Arasu, M. V., Duraipandiyan, V., Ponmurugan, K., Al-Dhabi, N. A., Arokiyaraj, S., et al. (2014). In-vitro antimicrobial, antibiofilm, cytotoxic, antifeedant and larvicidal properties of novel quinine isolated from *Aegle marmelos* (Linn.) Correa. *Ann. Clin. Microbiol. Antimicrob.* 13:48.

Romo, J. A., Pierce, C. G., Chaturvedi, A. K., Lazzell, A. L., McHardy, S. F., Saville, S. P., et al. (2017). Development of anti-virulence approaches for candidiasis via a novel series of small-molecule inhibitors of *Candida albicans* filamentation. *mBio* 8:e01991-17.

Roscetto, E., Contursi, P., Vollaro, A., Fusco, S., Notomista, E., and Catania, M. R. (2018). Antifungal and anti-biofilm activity of the first cryptic antimicrobial peptide from an archaeal protein against *Candida* spp. Clinical isolates. *Sci. Rep.* 8:17570.

Shiraki, Y., Ishibashi, Y., Hiruma, M., Nishikawa, A., and Ikeda, S. (2008). *Candida albicans* abrogates the expression of interferon-γ-inducible protein-10 in human keratinocytes. *FEMS Immunol. Med. Microbiol.* 54, 122–128. doi: 10.1111/j.1574-695x.2008.00457.x

Tsai, P. C., Chu, C. L., Fu, Y. S., Tseng, C. H., Chen, Y. L., Chang, L. S., et al. (2014). Naphtho[1,2-*b*]furan-4,5-dione inhibits MDA-MB-231 cell migration and invasion by suppressing Src-mediated signaling pathways. *Mol. Cell. Biochem.* 387, 101–111. doi: 10.1007/s11010-013-1875-4

Tsang, N. Y., Chik, W. I., Sze, L. P., Wang, M. Z., Tsang, S. W., and Zhang, H. J. (2018). The use of naphthoquinones and furano-naphthoquinones as antiinvasive agents. *Curr. Med. Chem.* 25, 5007–5056. doi: 10.2174/0929867324666171006131927

Tseng, C. H., Chen, Y. L., Yang, S. H., Peng, S. I., Cheng, C. M., Han, C. H., et al. (2010). Synthesis and antiproliferative evaluation of certain iminonaphtho[2,3-*b*]furan derivatives. *Bioorg. Med. Chem.* 18, 5172–5182. doi: 10.1016/j.bmc.2010.05.062

Tseng, C. H., Lin, C. S., Shih, P. K., Tsao, L. T., Wang, J. P., Cheng, C. M., et al. (2009). Furo[3',2':3,4]naphtha[1,2-*d*]imidazole derivatives as potential inhibitors of inflammatory factors in sepsis. *Bioorg. Med. Chem.* 17, 6773–6779. doi: 10.1016/j.bmc.2009.07.054

Vavala, E., Colone, M., Passariello, C., Celestino, I., Toccacieli, L., Stringaro, A., et al. (2013). Characterization of biofilms in drug-sensitive and drug-resistant strains of *Candida albicans*. *J. Chemother.* 25, 87–95. doi: 10.1179/1973947812y.0000000047

Wall, G., Montelongo-Jauregui, D., Bonifacio, B. V., Lopez-Ribot, J. L., and Uppuluri, P. (2019). *Candida albicans* biofilm growth and dispersal: contributions to pathogenesis. *Curr. Opin. Microbiol.* 52, 1–6. doi: 10.1016/j.mib.2019.04.001

Wartenberg, A., Linde, J., Martin, R., Schreiner, M., Horn, F., Jacobsen, I. D., et al. (2014). Microevolution of *Candida albicans* in macrophages restores filamentation in a nonfilamentous mutant. *PLoS Genet.* 10:e1004824. doi: 10.1371/journal.pone.1004824

Xie, F., Chang, W., Zhang, M., Li, Y., Li, W., Shi, H., et al. (2016). Quinone derivatives isolated from the endolichenic fungus *Phialocephala fortinii* are Mdr1 modulators that combat azole resistance in *Candida albicans*. *Sci. Rep.* 6:33687.

Yang, S. C., Aljuffali, I. A., Sung, C. T., Lin, C. F., and Fang, J. Y. (2016). Antimicrobial activity of topically-applied soyaethyl morpholinium ethosulfate micelles against *Staphylococcus* species. *Nanomedicine* 11, 657–671. doi: 10.2217/nnm.15.217

Yang, S. C., Tang, K. W., Lin, C. H., Alalaiwe, A., Tseng, C. H., and Fang, J. Y. (2019). Discovery of furanoquinone derivatives as a novel class of DNA polymerase and gyrase inhibitors for MRSA eradication in cutaneous infection. *Front. Microbiol.* 10:1197. doi: 10.3389/fmicb.2018.1197

Yang, S. C., Yen, F. L., Wang, P. W., Aljuffali, I. A., Weng, Y. H., Tseng, C. H., et al. (2017). Naphtho[1,2-*b*]furan-4,5-dione is a potent anti-MRSA agent against planktonic, biofilm, and intracellular bacteria. *Future Microbiol.* 12, 1059–1073. doi: 10.2217/fmb-2017-0044

Zeidler, U., Lettner, T., Lassnig, C., Muller, M., Lajko, R., Hintner, H., et al. (2009). UME6 is a crucial downstream target of other transcriptional regulators of true hyphal development in *Candida albicans*. *FEMS Yeast Res.* 9, 126–142. doi: 10.1111/j.1567-1364.2008.00459.x

Zhang, X., Li, T., Chen, X., Wang, S., and Liu, Z. (2018). Nystatin enhances the immune response against *Candida albicans* and protects the ultrastucture of the vaginal epithelium in a rat model of vulvovaginal candidiasis. *BMC Microbiol.* 18:166. doi: 10.1186/s12866-018-1316-3

Conflict of Interest: The authors declare that the research was conducted in the absence of any commercial or financial relationships that could be construed as a potential conflict of interest.

frontiers in Microbiology

ORIGINAL RESEARCH
published: 16 October 2020
doi: 10.3389/fmicb.2020.572608

SWL-1 Reverses Fluconazole Resistance in *Candida albicans* by Regulating the Glycolytic Pathway

Xiao-Ning Li[1,2†], Lu-Mei Zhang[1,2†], Yuan-Yuan Wang[3], Yi Zhang[1,2], Ze-Hua Jin[1,2], Jun Li[1,2], Rui-Rui Wang[1,2]* and Wei-Lie Xiao[4]**

[1]School of Chinese Materia Medica, Yunnan University of Chinese Medicine, Kunming, China, [2]Engineering Laboratory for National Health Theory and Product of Yunnan Province, Yunnan University of Chinese Medicine, Kunming, China, [3]College of Oceanology, Harbin Institute of Technology (Weihai), Weihai, China, [4]Key Laboratory of Medicinal Chemistry for Natural Resource, Ministry of Education and Yunnan Province, School of Chemical Science and Technology, Yunnan University, Kunming, China

OPEN ACCESS

Edited by:
Weihua Pan,
Shanghai Changzheng Hospital, China

Reviewed by:
Malcolm Whiteway,
Concordia University, Canada
Ashutosh Singh,
University of Lucknow, India

***Correspondence:**
Rui-Rui Wang
wangrryucm@126.com
Yuan-Yuan Wang
wangyuanyuan@hitwh.edu.cn
Wei-Lie Xiao
xiaoweilie@ynu.edu.cn

†These authors have contributed equally to this work

Specialty section:
This article was submitted to Antimicrobials, Resistance and Chemotherapy, a section of the journal Frontiers in Microbiology

Received: 15 June 2020
Accepted: 17 September 2020
Published: 16 October 2020

Citation:
Li X-N, Zhang L-M, Wang Y-Y, Zhang Y, Jin Z-H, Li J, Wang R-R and Xiao W-L (2020) SWL-1 Reverses Fluconazole Resistance in Candida albicans by Regulating the Glycolytic Pathway. Front. Microbiol. 11:572608. doi: 10.3389/fmicb.2020.572608

Candida albicans is a ubiquitous clinical fungal pathogen. Prolonged use of the first-line antifungal agent fluconazole (FLC) has intensified fungal resistance and limited its effectiveness for the treatment of fungal infections. The combined administration of drugs has been extensively studied and applied. SWL-1 is a lignin compound derived from the Traditional Chinese Medicine *Schisandra chinensis*. In this study, we show that SWL-1 reverses resistance to fluconazole in *C. albicans* when delivered in combination, with a sharp decrease in the IC_{50} of fluconazole from >200 to 3.74 ± 0.25 μg/ml, and also reverses the fluconazole resistance of *C. albicans in vitro*, with IC_{50} from >200 to 5.3 ± 0.3 μg/ml. Moreover, killing kinetics curves confirmed the synergistic effects of fluconazole and SWL-1. Intriguingly, when SWL-1 was administered in combination with fluconazole in a mouse model of systemic infection, the mortality of mice was markedly decreased and fungal colonization of the kidney and lung was reduced. Further mechanistic studies showed that SWL-1 significantly decreased intracellular adenosine 5'-triphosphate (ATP) levels and inhibited the function of the efflux pump responsible for fluconazole resistance of *C. albicans*. Proteomic analysis of the effects of SWL-1 on *C. albicans* showed that several enzymes were downregulated in the glycolytic pathway. We speculate that SWL-1 significantly decreased intracellular ATP levels by hindering the glycolysis, and the function of the efflux pump responsible for fluconazole resistance of *C. albicans* was inhibited, resulting in restoration of fluconazole sensitivity in FLC-resistant *C. albicans*. This study clarified the effects and mechanism of SWL-1 on *C. albicans in vitro* and *in vivo*, providing a novel approach to overcoming fungal resistance.

Keywords: *Candida albicans*, SWL-1, glycolysis, resistant, natural compounds, combination

INTRODUCTION

Candida albicans is an important opportunistic etiological commensal organism in humans. Generally, it resides asymptomatically in the digestive and vaginal mucosae in humans and causes only superficial infection in some people (Gow and Yadav, 2017). However, candidiasis infections are a common clinical infection in immunocompromized individuals (Pappas et al., 2018).

Moreover, prolonged and widespread use of antifungal drugs, especially the first-line antifungal azoles drugs, has contributed to serious resistance, which has become an obstacle to the treatment of fungal infections worldwide (Alexander and Perfect, 1997; Prasad et al., 2019). However, the currently available agents are limited, and the development of new antifungal drug is slow and costly. Thus, new therapeutic drugs and antifungal methods are urgently required.

Efflux pump-mediated resistance is the most ubiquitous pathway among the variety of molecular mechanisms underlying fungal resistance (Kontoyiannis, 2000; Gong et al., 2019). The efflux protein mainly comprises two different types proteins. One is the ATP-binding cassette (ABC) superfamily, mainly consisting of the Candida drug resistance 1 (*CDR1*) and Candida drug resistance 2 (*CDR2*) genes encoding the Cdr1 and Cdr2 proteins, respectively. The other is the major facilitator superfamily (MFS) including multidrug resistance 1 (*MDR1*), which encodes the Mdr1 protein. The function of ABC proteins is dependent on ATP (Prasad et al., 2019). *C. albicans* has the capacity to decrease intracellular accumulation of harmful agents through the action of ABC family efflux pumps in an ATP-dependent manner. Glycolysis plays a critical role as a carbon and energy source in producing ATP for *C. albicans* (Sandai et al., 2016).

We hope to find compounds from traditional medicinal plants that have antifungal or combined antifungal effects. In this study, we showed that SWL-1 is a lignin compound derived from the Traditional Chinese Medicine *Schisandra chinensis*. *Schisandra* genus species are medicinally important and commonly used in Traditional Chinese Medicine due to their diverse beneficial bioactivities. Recently, with the isolation of specific types of natural products, such as biphenyl clooctene lignans and schinortriterpenoids, secondary metabolites from this genus have attracted widespread attention from chemists and biologists (Gao et al., 2013; Liang et al., 2013; Shi et al., 2015). In this study, we aimed to discover antifungal small molecules from traditional medicinal plants by screening a small natural product library for compounds with antifungal activity using an antifungal assay. As a result, the polymethoxy biphenyl clooctene lignan (+)-Gomisin K3 (designated SWL-1; **Figure 1A**) isolated from the Traditional Chinese Medicine *Schisandra neglecta* (Gao et al., 2013), exerts synergistic antifungal effects when administered in combination with fluconazole (FLC) both *in vitro* and *in vivo*. Moreover, SWL-1 reversed the FLC resistance of *C. albicans* by hindering the glycolytic process to reduce the production of ATP. Thus, we showed that the glycolytic pathway was also related to drug resistance in *C. albicans*.

MATERIALS AND METHODS

Chemical, Strains, and Culture Conditions

SWL-1 was isolated from the Traditional Chinese Medicine *S. chinensis* as described previously (Ikeya et al., 1980). SWL-1 solution (50 mg/ml) was prepared in DMSO (dimethyl sulfoxide). DCFH-DA (2',7'-dichlorofluorescin diacetate), the fluorescent probe JC-1 (5,5',6,6'-tetrachloro-1,1',3,3'-tetraethylbenzimidazolocarbocyanine iodide), Enhanced ATP Assay Kits and BCA protein assay kits were purchased from Beyotime Biotechnology (Shanghai, China). FLC was obtained from Helioeast company (Nanchang, China), and dissolved in DMSO at (50 mg/ml). BBR (berberine) was obtained from Jinke Pharmaceutical Co., Ltd. (Yunnan, China).

The standard *C. albicans* strain ATCC10231 was donated by Xue Bai of the Kunming Institute of Botany, Chinese Academy of Sciences. The clinically FLC-sensitive *C. albicans* strain 4574# and FLC-resistant *C. albicans* strains 23#, 187#, 3816# were donated by Professor Yu-Ye Li of the First Affiliated Hospital of Kunming Medical University of China. The FLC-sensitive *C. albicans* strain SC5314 was purchased from Yunnan Denglou Technology Co., Ltd. ATCC10231 was treated successively with

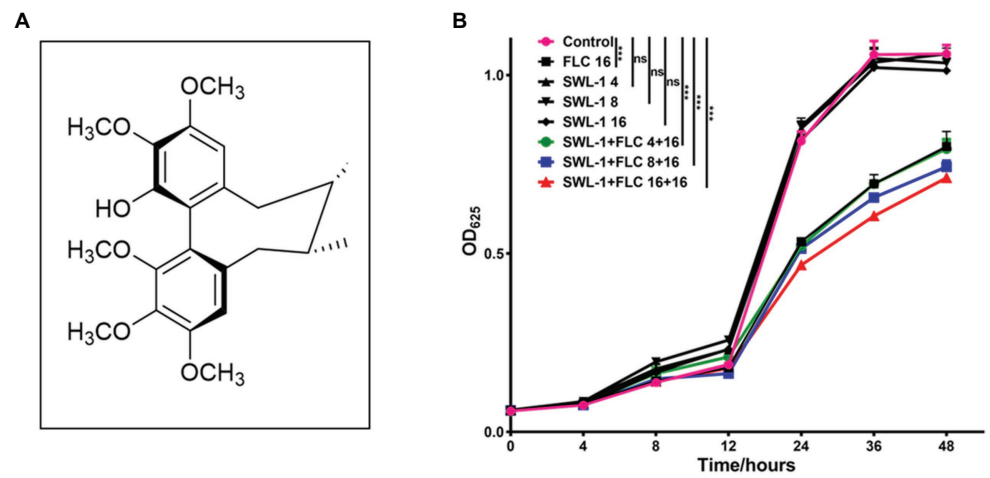

FIGURE 1 | Time-course of killing of SWL-1 and FLC against FLC-resistant *C. albicans* 23#. **(A)** Chemical structure of SWL-1, which is derived from the Traditional Chinese Medicine *Schisandra chinensis*. **(B)** *C. albicans* 23# was treated with SWL-1 or SWL-1 plus FLC at different concentrations. Each group was compared with the control group. ***$p < 0.001$

FLC to obtain the FLC-resistant *C. albicans* strain (designated FLC-resistant ATCC10231). Strain 23# was treated successively with SWL-1 to obtain the FLC-sensitive strain (designated SWL-1 treated 23#). Both strains were cultured in liquid YEPD medium (1% yeast extract, 2% peptone, 2% glucose) overnight at 30°C with constant shaking (150 rpm) before use in experiments.

Antifungal Susceptibility Testing

The IC_{50} of SWL-1 alone and in combination with fluconazole against *C. albicans* was determined using the microdilution method (Alexander et al., 2017). Briefly, 100 μl YEPD medium was added to each well of a 96-well flat-bottomed microtiter plate before adding fluconazole and SWL-1 (final concentration 200–0.064 μg/ml in 5-fold serial dilutions). The suspension of *C. albicans* was then added to wells at a density of 10^5 CFU/ml; the negative control contained only YEPD medium and no drugs were added in the positive control. The final volume in each well was 200 μl. Subsequently, the plates were cultured at 37°C for 24 h. Fungal growth was then determined by measurement of the optical density (OD) at 625 nm using a multi-function microplate reader. The inhibition ratio of drugs was calculated as follows:

$$\text{Inhibition ratio} = 100 - (A - C)/(B - C) \times 100\%$$

where A, B, and C represent the OD of positive control wells, drug-containing wells, and negative control wells, respectively. The IC_{50} was calculated using GraphPad Prism 7.0 software.

To assess the effect of the interaction between SWL-1 and fluconazole, the fractional inhibitory concentration index (FICI) was calculated according to the formula FICI = FIC_{FLC} + FIC_{SWL-1}. FICI ≤ 0.5 indicates a synergistic effect, 0.5 < FICI < 4.0 indicates no interaction, and FICI ≥ 4.0 indicates an antagonistic effect (Odds, 2003).

Antifungal Kinetics Assay

To investigate the dynamic inhibitory effect of SWL-1 on *C. albicans*, time-course curves of fungal killing were plotted by measuring the OD of different groups treated with varying concentrations of SWL-1 and FLC. The overnight cultures of *C. albicans* strains were diluted with YEPD medium to 1×10^5 CFU/ml and exposed to SWL-1 (4, 8, 16 μg/ml), FLC (16 μg/ml) and a combination of SWL-1 (4, 8, 16 μg/ml) with FLC (16 μg/ml); no drug was added to the control group. The cells were then incubated at 37°C with constant shaking (150 rpm) and 100-μl samples were collected from each well after 0, 4, 8, 12, 24, 36, and 48 h to measure the OD at 625 nm. Each sample was analyzed in triplicate in three independent experiments.

Efflux Pump Assay

The effect of SWL-1 on the function of efflux pump was determined using rhodamine 6G (R6G), a fluorochrome substrate of the efflux pump (Bhattacharya et al., 2016). Briefly, approximately 1×10^7 CFU/ml overnight cultures of *C. albicans* were collected after being washed three times with phosphate-buffered saline (PBS). *C. albicans* was then resuspended in PBS and cultured for 1 h in the absence of glucose at 37°C with constant shaking (150 rpm). The culture was then divided into two groups treated with and without SWL-1. These two groups were then subdivided into two more groups (four groups overall) and incubated in the presence and absence of 5% glucose to evaluate the effect of SWL-1 on the ATP-dependent and ATP-independent transporters. R6G was then added to each group at a final concentration of 10 μM and incubated for 2 h at 37°C with constant shaking (150 rpm). The absorption of R6G was terminated by placing each group on ice. Cells were pelleted and washed with ice-cold PBS to remove exogenous dye. The fungi were then resuspended in PBS before samples were removed from each group and centrifuged at 9,000 rpm for 5 min. Supernatants were collected and fluorescence was measured at an excitation wavelength 488 nm and emission wavelength 525 nm using a multi-function microplate reader.

Measurement of Reactive Oxygen Species Production

Reactive oxygen species (ROS) generation was assayed using a DCFH-DA (2',7'-dichlorofluorescin diacetate) staining (Song et al., 2019). In brief, overnight cultures of *C. albicans* were collected, washed three times with PBS buffer, and adjusted to 1×10^7 CFU/ml in PBS buffer. The fluorescent probe was added at a final concentration of 10 μg/ml and the cells were incubated at 37°C for 30 min in the dark. The cells were then collected and washed with PBS buffer before the fluorescence intensity was measured at an excitation wavelength of 488 nm and an emission wavelength of 525 nm using a multifunctional plate reader.

Measurement of Intracellular ATP Production

Briefly, *C. albicans* were cultured overnight at 37°C and adjusted to 1×10^6 CFU/ml in YEPD medium. Cells were then collected and washed with ice-cold PBS. The intracellular ATP production was then measured using ATP assay kits (Beyotime Institute of Biotechnology, Haimen, China) according to the manufacturer's instructions (Silao et al., 2019). ATP levels in cells were calculated with reference to the standard curve, and normalized using the protein content of each sample. The results were expressed as nmol/mg protein.

In vivo Antifungal Activity Evaluation Using a Murine Model of Systemic Fungal Infection

The antifungal activity of SWL-1 *in vivo* was evaluated in a murine model of systemic infection. All animals were maintained and treated in accordance with the guidelines approved by the Animal Care and Use Committee of China.

The infection model was established in male and female (1:1) BALB/C mice (aged 6–8 weeks; weighing 18–22 g). BALB/C mice were injected with cyclophosphamide *via* the intraperitoneal route (1 mg/10 g body weight) to induce immunodeficiency model before the experiment. Subsequently, the mice were randomly assigned to the following experimental groups: control (without *C. albicans*), FLC, SWL-1 (15 mg/ml), SWL-1 (30 mg/ml),

SWL-1 (15 mg/ml) + FLC, SWL-1 (30 mg/ml) + FLC, BBR + FLC (positive control). BBR combined with FLC was reported to show good antifungal activity in mice systemically infected with *C. albicans* (Quan, 2006).

Mice were infected with FLC-resistant *C. albicans* suspension 10^5 CFU/body *via* the lateral tail vein. The experimental treatments were dosed intragastrically by weight starting 2 h after model establishment. As a control, the mice in the vehicle group received only carboxymethylcellulose sodium (CMC-Na) without being infected with *C. albicans*. During successive treatments over 10 days, the general condition (activity, hair condition, weight and survival) of mice was observed and recorded. Finally, the mice were sacrificed by cervical dislocation after anesthesia, and the kidney and lung were collected and weighed before immersion in 10% buffered-neutral formalin for 24 h. Next, the fungal colonization and morphology of tissues in the different groups were evaluated following hematoxylin and eosin (H&E) and periodic acid-Schiff (PAS) staining (Kong et al., 2018; Swidergall et al., 2019).

Determination of Mitochondrial Membrane Potential

To study the effect of SWL-1 treatment on fungal mitochondria, we measured changes in the mitochondrial membrane potential, which is a sensitive indicator of mitochondrial function and reflects the integrity of mitochondrial function (Zhang et al., 2016; Zheng et al., 2018). In brief, *C. albicans* was cultured overnight and washed twice with PBS. Cells (1×10^7 CFU/ml) were then co-incubated with fluorescent probe JC-1 at a final concentration of 10 g/ml in the dark for 10 min. Subsequently, the cells were washed twice with PBS and resuspended in PBS buffer. The red fluorescence of the resuspended suspension was measured at an excitation wavelength of 550 nm and an emission wavelength of 600 nm with the full-wavelength multifunctional enzyme marker. The green fluorescence was measured at an excitation wavelength of 485 nm and an emission wavelength of 535 nm. The membrane potential was determined by calculating the ratio of red to green FI.

Proteomics Analysis of *Candida albicans*

To understand the molecular mechanism by which SWL-1 reversed fluconazole resistance in *C. albicans*, we performed an iTRAQ-based proteomics analysis to identify differential protein expression between resistant strains and SWL-1 treated resistant strains.

Expression of Drug Resistance Genes

To evaluate the mechanism by which SWL-1 reverses fluconazole resistance, the expression of the resistance genes *CDR1*, *CDR2*, *MDR1*, and *ERG11* was initially analyzed through qRT-PCR. Resistant strains of fungi and SWL-1 treated strains were ground into powder under liquid nitrogen, and RNA was extracted using TRIzol (Invitrogen, Carlsbad, CA, United States) according to the manufacturer's instructions. The RNA was converted to cDNA using a reverse transcription reagent kit (Thermo Scientific) and the expression levels of resistance genes were assessed by real-time PCR (Thermo Scientific). Relative gene expression was calculated using the $2^{-(\Delta\Delta Ct)}$ method (Li et al., 2019). Primers for the real-time PCR analysis were designed using Primer Premier 5 and synthesized in Sangon Biotech. Primer sequences are listed in **Table 1**.

TABLE 1 | Primers used in this study.

Genes	Primer sequences (5'-3')
CDR1	F: GGTGCTGCCATGTTCTTTGC
	R: AGGCATCAGCTGAAGGACGA
CDR2	F: AAGAGAAGCTCCATCGAGAACATTCAG
	R: CTGTCGGTTCAGCATTGGCATATAATC
ERG11	F: ATTGGAGACGTGATGCTGCT
	R: ATCACCACGTTCTCTTCTCAGT
MDR1	F: GTGCTGCTACTACTGCTTCTGGTG
	R: AACACTGATGCAATGACTGATCTGAAC

**ERG11, 14α-demethylase gene; CDR1, Candida drug resistance 1 gene; CDR2, Candida drug resistance 2 gene; MDR1, multidrug resistance 1 gene.*

Statistical Analysis

All experiments were performed in triplicate independently. All statistical analyses were performed with GraphPad Prism 7. Data were presented as the mean ± SD of triplicate experiments and differences between groups were evaluated by ANOVA. $p < 0.05$ was considered to indicate statistical significance.

RESULTS

The Antifungal Effects of SWL-1 on *Candida albicans*

We determined the antifungal effects of SWL-1 on *C. albicans* strains, including the standard strain (ATCC10231 and SC5314), a clinically sensitive strain ($4574^{\#}$), clinical FLC-resistant strains ($23^{\#}$, $187^{\#}$, and $3816^{\#}$) and an induced FLC-resistant strain (FLC-resistant ATCC10231). As shown in **Table 2**, no antifungal effects on the *C. albicans* standard and clinically sensitive strains (ATCC10231, SC5314, and $4574^{\#}$) were observed following treatment with SWL-1 alone. No interaction between SWL-1 combined with FLC was observed on the *C. albicans* standard and clinically sensitive strains, with FICIs ranging from 0.93 to 3.23. Interestingly, SWL-1 and FLC individually also had no significant inhibitory effect on the growth of FLC-resistant strains, while SWL-1 combined with FLC exhibited potent antifungal activity against FLC-resistant strains, with IC50s of 3.74–28.28 μg/ml, and FICIs of 0.13–0.38, indicating a strong synergistic effect.

Kinetics of Antifungal Activity

In the antifungal kinetic assay, strong antifungal activity of SWL-1 combined with FLC was observed after treatment for 12 h (**Figure 1**). The results revealed that SWL-1 administered alone had no antifungal effect at 4, 8, 16 μg/ml, while FLC showed a minor effect on FLC-resistant strains $23^{\#}$ at 16 μg/ml. In contrast, when delivered in combination with FLC at 16 μg/ml, SWL-1 exerted dose-dependent antifungal effects when administered at 4, 8, and 16 μg/ml.

TABLE 2 | The antifungal activity of SWL-1 and fluconazole (FLC) alone and in combination in *Candida albicans* and the reversal of FLC-resistance in *C. albicans in vitro*.

Strains		IC_{50} (μg/ml)			FICI
		FLC	SWL-1	FLC + SWL-1	
Standard	ATCC 10231	5.06	98.92	15.78	3.23
Sensitive	SC5314	5.12 ± 1.69	94.47 ± 1.28	13.67 ± 0.41	2.81
Clinically sensitive	4574#	0.50 ± 0.00	91.41 ± 1.68	0.46 ± 0.13	0.93
Clinically resistant	187# (FLC-resistant)	>200	90.89 ± 0.15	28.28 ± 22.17	0.38
	3816# (FLC-resistant)	>200	94.51 ± 1.33	15.05 ± 3.95	0.20
Resistant	FLC-resistant ATCC 10231	>200	92.17 ± 2.01	24.45 ± 10.35	0.33
Clinically resistant	FLC-resistant 23#	>200	89.28	3.74	0.13
	SWL-1 treated 23#	5.30	—	—	—

After successive treatment with SWL-1, the fluconazole sensitivity of resistant strains was determined (**Table 2**). The IC_{50} of FLC against treatment strains reached 5.30 μg/ml, indicating that SWL-1 reverses FLC-resistance in *C. albicans*.

In vivo Antifungal Activity Evaluation Using a Murine Model of Systemic Fungal Infection

To determine the effect of SWL-1 *in vivo*, we established a mouse model of systemic infection. After treatment with SWL-1 alone and combination with fluconazole, the survival rate and weight of mice were recorded daily. Our study showed that SWL-1 affected the survival and condition of mice. The survival rate in the model group infected with *C. albicans* was very low at less than 10%. In the SWL-1 + FLC group, the survival rate was significantly increased to more than 65% compared with that in the model group and the group treated with FLC alone (**Figure 2A**), indicating that SWL-1 combined with FLC increases the survival of *C. albicans*-infected mice *in vivo*.

The weight of mice reflects the general health of the mouse. As shown in the **Figure 2B**, there was no difference in weight of the mice in the control group between first and last day of the experimental period. The weight of the mice in the model group decreased sharply after infection with FLC-resistant strains. In contrast, the weight changes in the groups treated with low and high-dose SWL-1 combined with FLC were much slower compared with the changes observed in the FLC group and the BBR + FLC positive control group.

To better clarify effects of SWL-1 *in vivo*, we conducted histopathological and morphological studies of the kidney and lung of model mice. Paraffin-embedded sections of kidney and lung were stained with H&E and PAS. As shown in **Figure 2C**, there were high levels of fungal colonization in the kidney of the model group, with *C. albicans* and hyphae visible in the sections. In addition, numerous fungal cells were detected in the kidneys of mice treated with SWL-1 or FLC alone. Pathological bleeding within and from the renal tubule was observed in all the groups treated with FLC or SWL-1 alone and in the infection only group. In contrast, the kidneys of mice treated with SWL-1 + FLC or BBR + FLC (positive control) were significantly protected against the effects of fungal infection and exhibited normal morphology. Moreover, the kidneys of the model infection group and the groups treated with SWL-1 or FLC alone exhibited marked infiltration by inflammatory cells. These results demonstrated that combination therapy alleviated fungal infection. Neither hyphae nor yeast were found in the lung tissues of any of the groups. However, marked changes were observed in the morphology of the lung tissues in the model group and the groups treated with SWL-1 or FLC alone. As shown in **Figure 2C**, alveolar septa were thickened, with increased numbers of inflammatory cells. However, lung tissues in the SWL-1 + FLC and BBR + FLC groups were normal compared with those in the control group. Overall, these findings indicated that SWL-1 combined with FLC resulted in significant improvements in tissue pathology and that SWL-1 and FLC exert synergistic effects in the treatment of fungal infections *in vivo*.

Expression of Drug Resistance Genes

The expression levels of FLC-resistance genes are shown in **Figure 3**. There were no differences in the expression levels of FLC-resistance genes between the FLC-resistant and SWL-1 treated strains.

SWL-1 Decreases Efflux Pump Function

To investigate the effects of SWL-1 on the efflux pump of *C. albicans*, we compared the efflux activity of the FLC-resistant *C. albicans* 23# and SWL-1-treated strains in R6G assays. As shown in **Figure 4A**, efflux of the SWL-1-treated strains was decreased significantly compared with that of the FLC-resistant, indicating that SWL-1 reverses fluconazole resistance by inhibiting the function of the efflux pump.

SWL-1 Decreases the ATP Content of Cells

To determine the effects of SWL-1 treatment on mitochondrial function, we measured the intracellular ATP content using ATP assay kits. As shown in **Figure 4B**, the ATP level in the SWL-1-treated strains was markedly decreased compared to that in the FLC-resistant strains.

SWL-1 Affects the Function of Mitochondria

The production of ROS in the SWL-1 strains was obviously increased compared to that in the FLC-resistant strains 23#

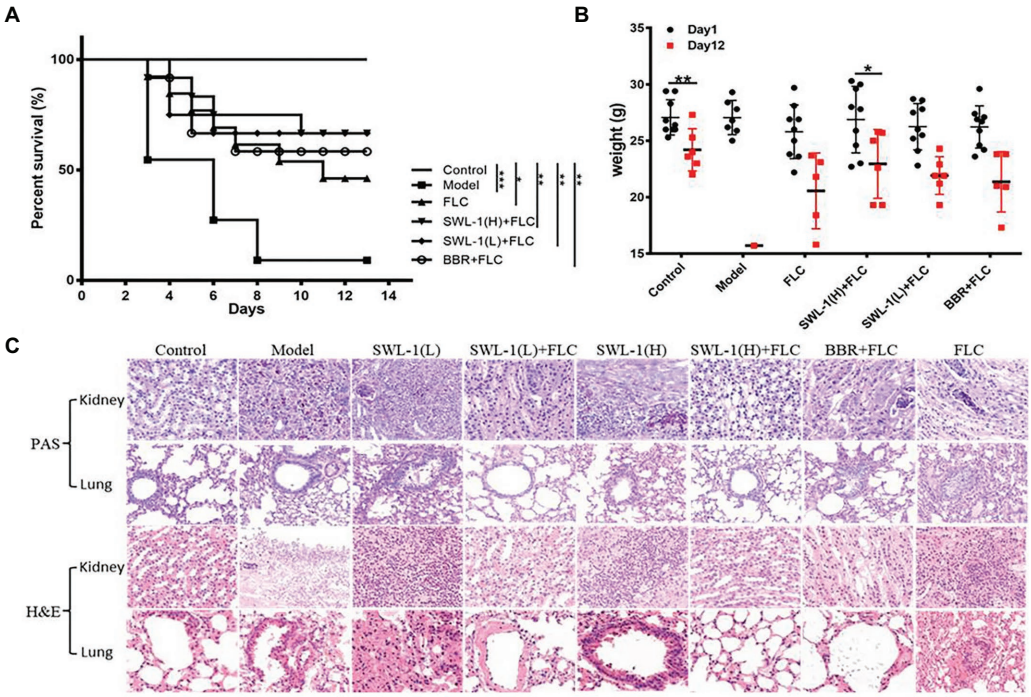

FIGURE 2 | Effects of SWL-1 on fungal infection. Mice were infected with FLC-resistant *C. albicans* 23# by intravenous injection (tail vein), and then treated with CMC-Na (control), FLC, SWL-1 combined with FLC, BBR combined with FLC in the model group. The condition of mice was monitored and the survival rate was calculated daily. **(A)** The weight of infected mice was recorded daily to reflect the antifungal activity of SWL-1. **(B)** Survival curves of mice infected with *C. albicans*. **(C)** Representative PAS- and H&E-stained sections of the kidney and lung from mice in the various groups 12 days after treatment. Results showed that the weight of mice in the combination therapy groups increased compared with that of mice in the model group. Each group was compared with the model group. SWL-1(H) represents the SWL-1 dose of 30 mg/ml, SWL-1(L) represents the SWL-1 dose of 15 mg/ml. $^{*}p < 0.05$, $^{**}p < 0.01$, $^{***}p < 0.001$.

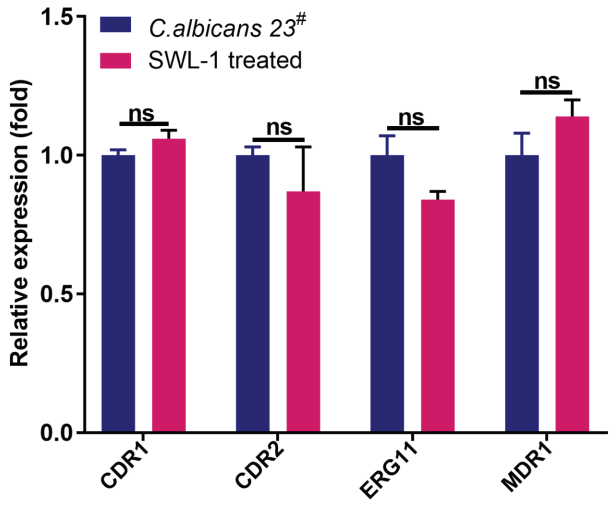

FIGURE 3 | The effect of SWL-1 on resistance-related gene expression in *C. albicans*. Expression of four genes (*CDR1*, *CDR2*, *ERG11*, and *MDR1*) was detected by RT-PCR. ns, not significant.

(**Figure 5A**), indicating that SWL-1-treated strains increase endogenous ROS production, which may be related to mitochondrial function (**Figure 5B**).

SWL-1 Changes the Expression of Glucose Metabolism-Related Proteins

Proteomics analysis of *C. albicans* 23# and the SWL-1 treated strains revealed 605 differentially expressed proteins (307 upregulated and 298 downregulated) in the SWL-1treated stains compared with the *C. albicans* 23# strains (**Figure 6A**). As shown in **Figures 6B,C**, hierarchical cluster analysis revealed that these differentially expressed proteins were mainly involved in metabolism, especially glucose metabolism. Phosphoglucose isomerase, aldolase, phosphoglycerate kinase, phosphoglycerate mutase, and pyruvate kinase, which are involved in the glycolysis pathway, were all downregulated, indicating repression of glycolysis (**Figure 7**).

DISCUSSION

The widespread and prolonged use of antifungals results not only in the development of tolerance toward the drug in use, but also in the development of collateral resistance to other drugs and to a variety of unrelated compounds (Prasad and Rawal, 2014). We aimed to identify compounds derived from traditional medicinal plants that exert good or synergistic effects on resistant fungi. In this study, we found that SWL-1, which is derived from *S. chinensis*, exerts synergistic antifungal effects when combined with fluconazole by inhibiting efflux pump function.

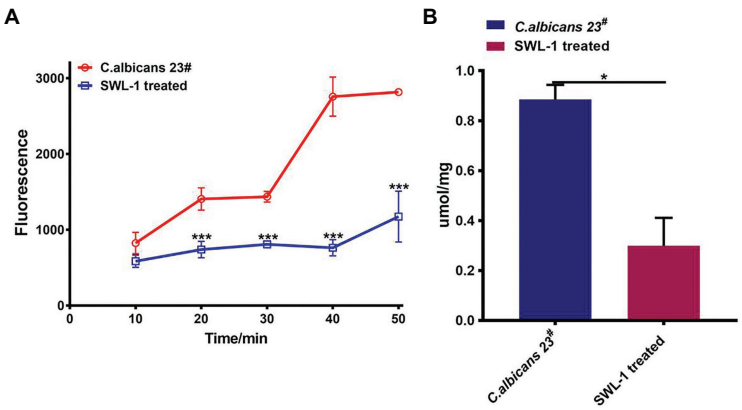

FIGURE 4 | SWL-1 affected the pump activity of *C. albicans*. **(A)** Glucose-induced R6G efflux in FLC-resistant *C. albicans* 23# and SWL-1-treated 23#. **(B)** The intracellular ATP levels in FLC-resistant *C. albicans* 23# and SWL-1-treated 23#. $^{*}p < 0.05$, $^{***}p < 0.001$.

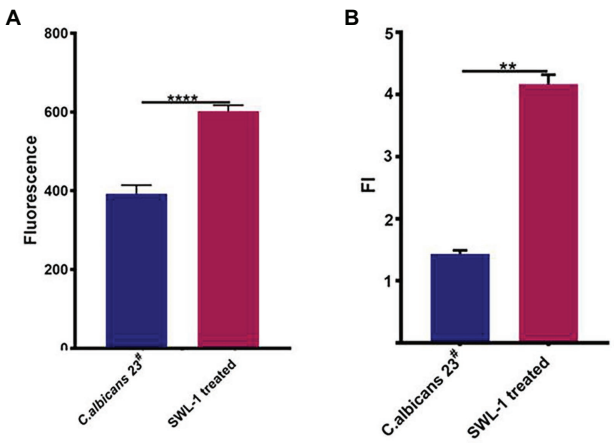

FIGURE 5 | The effects of SWL-1 on the function of mitochondria. **(A)** Intracellular reactive oxygen species (ROS) production of FLC-resistant *C. albicans* 23# strains and SWL-1 treatment 23#. **(B)** Mitochondrial membrane potential of *C. albicans* 23#. Data represent the mean ± SD. $^{**}p < 0.01$, $^{****}p < 0.0001$.

Reduced intracellular accumulation of drugs is a common mechanism of resistance in *Candida* cells, clinical azole-resistant isolates of *C. albicans* display transcriptional activation of genes encoding ABC (*CDR1*, *CDR2*) or MFS (*MDR1*) proteins. Invariably, resistant *Candida* cells, which show enhanced expression of efflux pump-encoding genes, also show a simultaneous increase in the efflux of drugs (Cannon et al., 2009; Redhu et al., 2016). Our results show that SWL-1 significantly reduced efflux pump activity without affecting the expression of the *MDR1*, *CDR1*, and *CDR2*, indicating that SWL-1 affects the efflux pump function in a gene expression-independent manner. The important characteristic feature of ABC drug transporters is that they utilize the energy generated by ATP hydrolysis to transport a variety of substrates across the plasma membrane (Prasad et al., 2006). In this study, we showed that SWL-1 inhibited the function of the ATP-dependent-efflux pump in the presence of glucose. Furthermore, the intracellular ATP content of SWL-1 treated stains was markedly decreased compared with that in *C. albicans* strains. We speculated that SWL-1 inhibits efflux pump function by inhibiting ATP synthesis.

Carbohydrates are the primary and preferred source of metabolic carbon for most organisms, and are used for energy and biomolecule production. In eukaryotic cells, glycolysis is a common initial glycometabolism pathway (Icard et al., 2018). Most sugars are converted to glucose 6-phosphate or fructose 6-phosphate before entering the glycolytic pathway. Glycolysis is then responsible for converting these hexose phosphates into the key metabolite pyruvate, while also producing ATP and NADH. Then, cells employ two major strategies for energy production: fermentation (without oxygen) and respiration (with oxygen). Fermentation produces lactic acid, while respiration produces additional ATP *via* the tricarboxylic acid (TCA) cycle and oxidative phosphorylation. As a central metabolic pathway, glycolysis is strictly regulated and although ATP is relatively low, glycolysis provides ATP more rapidly than the TCA cycle in mitochondria. The opportunistic human fungal pathogen *C. albicans* is a facultative aerobe and thus, metabolizes carbon sources in response to oxygen availability similar to that of a typical eukaryotic cell (Askew et al., 2009). Our proteomics data showed significant downregulation of the expression of genes related to the glycolytic pathway of drug-resistant *C. albicans* after SWL-1 treatment, thus reducing the activity of the glycolytic pathway. Since efflux pump activity is higher in resistant *C. albicans* than that in sensitive strains, ATP is more important for resistant strains to maintain the function of efflux pump. Taking these results into consideration, we propose the following hypothesis to explain the phenomenon observed in FLC-resistant strains: SWL-1 disrupts glucose metabolism, thus reducing ATP production. The energy available to the efflux pump is therefore decreased, leading to a reduction in efflux function. As a result, *C. albicans* resistance to FLC is reversed (**Figure 8**). Efflux pump activity is low in sensitive strains, and less ATP is used for efflux function; therefore, no similar phenomenon

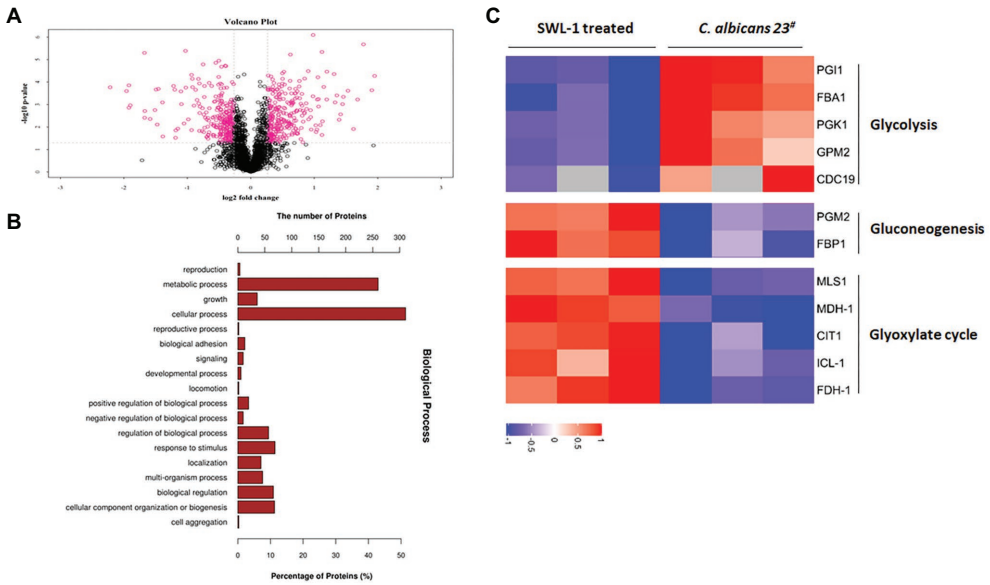

FIGURE 6 | Proteins related to *C. albicans* metabolic routes identified by proteomics analysis. **(A)** Volcano map of *C. albicans* and SWL-1treated 23#. **(B)** Hierarchical clustering analyses of proteins that were up- or downregulated in *C. albicans* and SWL-1 treated 23#. **(C)** Proteins related to metabolism identified in GO analysis.

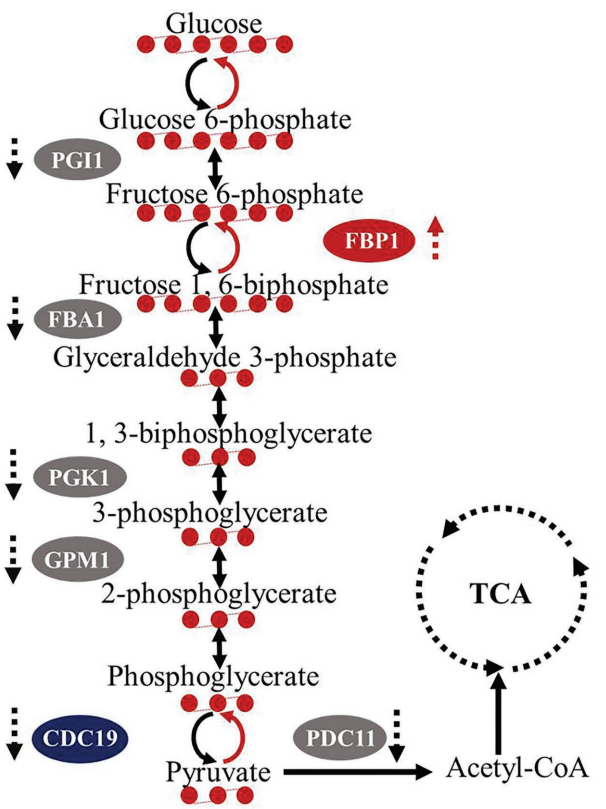

FIGURE 7 | Impacts of SWL-1 treatment on glycolysis. SWL-1 inhibits some key enzymes in the glycolytic pathway, resulting in downregulation of the pathway. In contrast, some enzymes in the gluconeogenic pathway are upregulated.

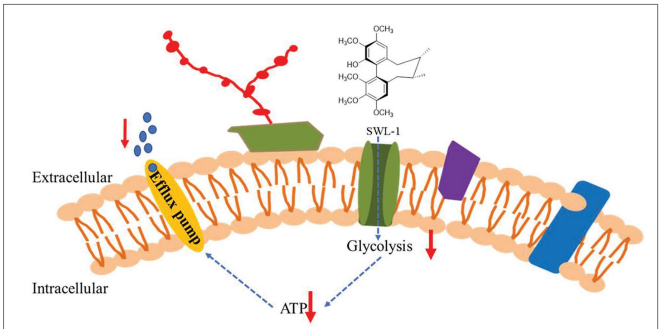

FIGURE 8 | The proposed mechanisms by which SWL-1 reverses drug resistance in *C. albicans*. The glycometabolism of *C. albicans* is changed by decreasing glycolysis but increasing gluconeogenesis, resulting in a decrease in ATP levels. The efflux pump-mediated removal of FLC from cell is blocked. The resistance to FLC is reversed and the antifungal effects of FLC are restored.

was observed in the sensitive strains (**Table 2**). The results of the present study indicate that the glycolytic pathway plays an important role in drug resistance in *C. albicans*.

Macrophage-based defense is crucial for host survival in invasive candidiasis as demonstrated by the fact that ablation of kidney macrophage numbers leads to fatal *C. albicans* infection in the mouse model. As a successful pathogen, *C. albicans* has evolved mechanisms to evade macrophage-based immunity (Lionakis et al., 2013). Glucose metabolism plays a central role in immune cell function. Following recognition of microbial ligands, macrophages upregulate glucose uptake and its anaerobic catabolism instead of relying on the TCA cycle and mitochondrial oxidative phosphorylation (OXPHOS; use of glycolysis coupled to lactic acid fermentation in normoxic conditions, i.e., aerobic glycolysis).

Thus, cells obtained the required energy required to boost antimicrobial mechanisms and cytokine production. This behavior resembles the so-called Warburg effect observed in cancer cells, in which aerobic glycolysis is the main source of energy (Pearce and Pearce, 2013; Pellon et al., 2020). When macrophages are challenged with *C. albicans*, *C. albicans* rapidly consumes glucose, causing macrophage death (Tucey et al., 2018). Our *in vivo* histopathological data showed that SWL-1 + FLC treated mice had less inflammatory cell infiltration of the kidney and significant improvements in the kidney and lung lesions were observed. Thus, we speculate that SWL-1 also regulates antifungal immunity by inhibiting the glycolytic pathway.

In this study, we preliminarily elucidated the mechanism of action of SWL-1 on fluconazole-resistant *C. albicans*. More importantly, the combination of SWL-1 with fluconazole was shown to reverse *C. albicans* resistance to fluconazole *in vitro* and *in vivo*. Furthermore, proteomics analysis showed that SWL-1 hinders the glycolysis process in *C. albicans*. We speculate that SWL-1 may reverse drug resistance in *C. albicans* by reducing the activity of the glycolytic pathway. Our findings highlight new strategies for the treatment and reversal of fungal resistance and are of great significance for the treatment of *C. albicans* infection, although the underlying molecular mechanism remains to be fully elucidated.

DATA AVAILABILITY STATEMENT

The datasets presented in this study can be found in online repositories. The names of the repository/repositories and accession number(s) can be found in the article/**Supplementary Material**.

ETHICS STATEMENT

The animal study was reviewed and approved by Animal Experiment Ethics Review Committee of Yunnan University of Traditional Chinese Medicine.

AUTHOR CONTRIBUTIONS

R-RW, Y-YW, and W-LX designed the experiments. X-NL, L-MZ, YZ, Z-HJ, and JL performed the experiments and interpreted the data. X-NL, L-MZ, and R-RW wrote the manuscript. All authors contributed to the article and approved the submitted version.

FUNDING

This work was financially supported by the National Natural Science Foundation of China (81660737, 81422046, and 21762048), Applied Basic Research Foundation of Yunnan Province (2017FF117-003, 2015FB205-023, 2018FY001, and 2018FA048), the Program for Changjiang Scholars and Innovative Research Team in University (IRT_17R94), and the Project of Innovative Research Team of Yunnan Province to W-LX.

ACKNOWLEDGMENTS

We are especially grateful to Professor Yu-Ye Li of the First Affiliated Hospital of Kunming Medical University and Xue Bai of the Kunming Institute of Botany, Chinese Academy of Sciences for sharing *C. albicans* strains with us and for the many helpful conversations regarding this work.

SUPPLEMENTARY MATERIAL

The Supplementary Material for this article can be found online at: https://www.frontiersin.org/articles/10.3389/fmicb.2020.572608/full#supplementary-material

The mass-spectrum data of *Candida albicans* proteomics were deposited in ProteomeXchange with the primary accession code PXD019736.

REFERENCES

Alexander, B. D., and Perfect, J. R. (1997). Antifungal resistance trends towards the year 2000. Implications for therapy and new approaches. *Drugs* 54, 657–678. doi: 10.2165/00003495-199754050-00002

Alexander, B. D., Procop, G. W., Dufresne, P., Fuller, J., Ghannoum, M. A., Hanson, K. E., et al. (2017). "Clinical and Laboratory Standards Institute (CLSI). Reference Method for Broth Dilution Antifungal Susceptibility Testing of Yeasts. *4th edn*. CLSI standard M27". (Wayne, PA, United States: Clinical and Laboratory Standards Institute).

Askew, C., Sellam, A., Epp, E., Hogues, H., Mullick, A., Nantel, A., et al. (2009). Transcriptional regulation of carbohydrate metabolism in the human pathogen *Candida albicans*. *PLoS Pathog.* 5:e1000612. doi: 10.1371/journal.ppat.1000612

Bhattacharya, S., Sobel, J., and White, T. (2016). A combination fluorescence assay demonstrates increased efflux pump activity as a resistance mechanism in azole-resistant vaginal *Candida albicans* isolates. *Antimicrob. Agents Chemother.* 60, 5858–5866. doi: 10.1128/AAC.01252-16

Cannon, R. D., Lamping, E., Holmes, A. R., Niimi, K., Baret, P. V., Keniya, M. V., et al. (2009). Efflux-mediated antifungal drug resistance. *Clin. Microbiol. Rev.* 22, 291–321. doi: 10.1128/CMR.00051-08

Gao, X. -M., Wang, R. -R., Niu, D. -Y., Meng, C. -Y., Yang, L. -M., Zheng, Y. -T., et al. (2013). Bioactive dibenzocyclooctadiene lignans from the stems of Schisandra neglecta. *J. Nat. Prod.* 76, 1052–1057. doi: 10.1021/np400070x

Gong, Y., Liu, W., Huang, X., Hao, L., Li, Y., and Sun, S. (2019). Antifungal activity and potential mechanism of N-butylphthalide alone and in combination with fluconazole against *Candida albicans*. *Front. Microbiol.* 10:1461. doi: 10.3389/fmicb.2019.01461

Gow, N. A. R., and Yadav, B. (2017). Microbe profile: *Candida albicans*: a shape-changing, opportunistic pathogenic fungus of humans. *Microbiology* 163, 1145–1147. doi: 10.1099/mic.0.000499

Icard, P., Shulman, S., Farhat, D., Steyaert, J. -M., Alifano, M., and Lincet, H. (2018). How the Warburg effect supports aggressiveness and drug resistance of cancer cells? *Drug Resist. Updat.* 38, 1–11. doi: 10.1016/j.drup.2018.03.001

Ikeya, Y., Taguchi, H., and Yosioka, I. (1980). The constituents of Schizandra chinensis BAILL. VII. The structures of three new lignans, (−)-Gomisin K_1 and (+)-Gomisins K_2 and K_3. *Chem. Pharm. Bull.* 28, 2422–2427. doi: 10.1248/cpb.28.2422

Kong, X., Leng, D., Liang, G., Zheng, H., Wang, Q., Shen, Y., et al. (2018). Paeoniflorin augments systemic *Candida albicans* infection through inhibiting Th1 and Th17 cell expression in a mouse model. *Int. Immunopharmacol.* 60, 76–83. doi: 10.1016/j.intimp.2018.03.001

Kontoyiannis, D. P. (2000). Efflux-mediated resistance to fluconazole could be modulated by sterol homeostasis in *Saccharomyces cerevisiae*. *J. Antimicrob. Chemother.* 46, 199–203. doi: 10.1093/jac/46.2.199

Li, W., Liu, J., Shi, C., Zhao, Y., Meng, L., Wu, F., et al. (2019). FLO8 deletion leads to azole resistance by upregulating CDR1 and CDR2 in *Candida albicans*. *Res. Microbiol.* 170, 272–279. doi: 10.1016/j.resmic.2019.08.005

Liang, C. -Q., Hu, J., Luo, R. -H., Shi, Y. -M., Shang, S. -Z., Gao, Z. -H., et al. (2013). Six new lignans from the leaves and stems of Schisandra sphenanthera. *Fitoterapia* 86, 171–177. doi: 10.1016/j.fitote.2013.03.008

Lionakis, M. S., Swamydas, M., Fischer, B. G., Plantinga, T. S., Johnson, M. D., Jaeger, M., et al. (2013). CX3CR1-dependent renal macrophage survival promotes *Candida* control and host survival. *J. Clin. Invest.* 123, 5035–5051. doi: 10.1172/JCI71307

Odds, F. C. (2003). Synergy, antagonism, and what the chequerboard puts between them. *J. Antimicrob. Chemother.* 52:1. doi: 10.1093/jac/dkg301

Pappas, P. G., Lionakis, M. S., Arendrup, M. C., Ostrosky-Zeichner, L., and Kullberg, B. J. (2018). Invasive candidiasis. *Nat. Rev. Dis. Primers* 4:18026. doi: 10.1038/nrdp.2018.26

Pearce, E. L., and Pearce, E. J. (2013). Metabolic pathways in immune cell activation and quiescence. *Immunity* 38, 633–643. doi: 10.1016/j.immuni.2013.04.005

Pellon, A., Nasab, S. D. S., and Moyes, D. L. (2020). New insights in *Candida albicans* innate immunity at the mucosa: toxins, epithelium, metabolism, and beyond. *Front. Cell. Infect. Microbiol.* 10:81. doi: 10.3389/fcimb.2020.00081

Prasad, R., Gaur, N. A., Gaur, M., and Komath, S. S. (2006). Efflux pumps in drug resistance of *Candida*. *Infect. Disord. Drug Targets* 6, 69–83. doi: 10.2174/187152606784112164

Prasad, R., Nair, R., and Banerjee, A. (2019). Multidrug transporters of *Candida* species in clinical azole resistance. *Fungal Genet. Biol.* 132:103252. doi: 10.1016/j.fgb.2019.103252

Prasad, R., and Rawal, M. K. (2014). Efflux pump proteins in antifungal resistance. *Front. Pharmacol.* 5:202. doi: 10.3389/fphar.2014.00202

Quan, H. (2006). "Synergism of fluconazole and berberine against clinical isolates of *Candida albicans* resistant to fluconazole." The Second Military Medical University.

Redhu, A. K., Shah, A. H., and Prasad, R. (2016). MFS transporters of *Candida* species and their role in clinical drug resistance. *FEMS Yeast Res.* 16:fow043. doi: 10.1093/femsyr/fow043

Sandai, D., Tabana, Y. M., Ouweini, A. E., and Ayodeji, I. O. (2016). Resistance of *Candida albicans* biofilms to drugs and the host immune system. *J. Microbiol.* 9:e37385. doi: 10.5812/jjm.37385

Shi, Y. -M., Xiao, W. -L., Pu, J. -X., and Sun, H. -D. (2015). Triterpenoids from the *Schisandraceae* family: an update. *Nat. Prod. Rep.* 32, 367–410. doi: 10.1039/C4NP00117F

Silao, F., Ward, M., Ryman, K., Wallström, A., Brindefalk, B., Udekwu, K., et al. (2019). Mitochondrial proline catabolism activates Ras1/cAMP/PKA-induced filamentation in *Candida albicans*. *PLoS Genet.* 15:e1007976. doi: 10.1371/journal.pgen.1007976

Song, Y., Li, S., Zhao, Y., Zhang, Y., Lv, Y., Jiang, Y., et al. (2019). ADH1 promotes *Candida albicans* pathogenicity by stimulating oxidative phosphorylation. *Int. J. Med. Microbiol.* 309:151330. doi: 10.1016/j.ijmm.2019.151330

Swidergall, M., Khalaji, M., Solis, N., Moyes, D., Drummond, R., Hube, B., et al. (2019). Candidalysin is required for neutrophil recruitment and virulence during systemic *Candida albicans* infection. *J. Infect. Dis.* 220, 1477–1488. doi: 10.1093/infdis/jiz322

Tucey, T. M., Verma, J., Harrison, P. F., Snelgrove, S. L., Lo, T. L., Scherer, A. K., et al. (2018). Glucose homeostasis is important for immune cell viability during Candida challenge and host survival of systemic fungal infection. *Cell Metab.* 27, 988.e1007–1006.e1007. doi: 10.1016/j.cmet.2018.03.019

Zhang, B., Yu, Q., Wang, Y., Xiao, C., Li, J., Huo, D., et al. (2016). The *Candida albicans* fimbrin Sac6 regulates oxidative stress response (OSR) and morphogenesis at the transcriptional level. *Biochim. Biophys. Acta* 1863, 2255–2266. doi: 10.1016/j.bbamcr.2016.06.002

Zheng, S., Chang, W., Zhang, M., Shi, H., and Lou, H. (2018). Chiloscyphenol A derived from Chinese liverworts exerts fungicidal action by eliciting both mitochondrial dysfunction and plasma membrane destruction. *Sci. Rep.* 8:326. doi: 10.1038/s41598-017-18717-9

Conflict of Interest: The authors declare that the research was conducted in the absence of any commercial or financial relationships that could be construed as a potential conflict of interest.

frontiers in Microbiology

ORIGINAL RESEARCH
published: 03 November 2020
doi: 10.3389/fmicb.2020.579362

Synergistic Effect of Pyrvinium Pamoate and Azoles Against *Aspergillus fumigatus in vitro* and *in vivo*

Yi Sun[1], Lujuan Gao[2,3], Youwen Zhang[4], Ji Yang[2,3] and Tongxiang Zeng[1]*

[1] Department of Dermatology, Jingzhou Central Hospital, The Second Clinical Medical College, Yangtze University, Jingzhou, China, [2] Department of Dermatology, Zhongshan Hospital Fudan University, Shanghai, China, [3] Department of Dermatology, Zhongshan Hospital Fudan University, Xiamen, China, [4] Department of Clinical Medicine, Yangtze University, Jingzhou, China

The effects of pyrvinium pamoate alone and in combination with azoles [itraconazole (ITC), posaconazole (POS), and voriconazole (VRC)] were evaluated against *Aspergillus fumigatus* both *in vitro* and *in vivo*. A total of 18 clinical strains of *A. fumigatus* were studied, including azole-resistant isolates harboring the combination of punctual mutation and a tandem repeat sequence in the Cyp51A gene (AFR1 with TR34/L98H and AFR2 with TR46/Y121F/T289A). The *in vitro* results revealed that pyrvinium individually exhibited minimal inhibitory concentration (MIC) of 2 μg/ml against AFR1 but was ineffective against other tested strains (MIC > 32 μg/ml). Nevertheless, the synergistic effects of pyrvinium with ITC, VRC, or POS were observed in 15 [83.3%, fractional inhibitory concentration index (FICI) 0.125–0.375], 11 (61.1%, FICI 0.258–0.281), and 16 (88.9%, FICI 0.039–0.281) strains, respectively, demonstrating the potential of pyrvinium in reversion of ITC and POS resistance of both AFR1 (FICI 0.275, 0.281) and AFR2 (FICI 0.125, 0.039). The effective MIC ranges in synergistic combinations were 0.25–8 μg/ml for pyrvinium, 0.125–4 μg/ml for ITC, and 0.125 μg/ml for both VRC and POS, demonstrating 4- to 32-fold reduction in MICs of azoles and up to 64-fold reduction in MICs of pyrvinium, respectively. There was no antagonism. The effect of pyrvinium–azole combinations *in vivo* was evaluated by survival assay and fungal burden determination in the *Galleria mellonella* model infected with AF293, AFR1, and AFR2. Pyrvinium alone significantly prolonged the survival of larvae infected with AF293 ($P < 0.01$) and AFR1 ($P < 0.0001$) and significantly decreased the tissue fungal burden of larvae infected with AFR1 ($P < 0.0001$). Pyrvinium combined with azoles significantly improved larvae survival ($P < 0.0001$) and decreased larvae tissue fungal burden in all three isolates ($P < 0.0001$). Notably, despite AFR2 infection was resistant to VRC or pyrvinium alone, pyrvinium combined with VRC significantly prolonged survival of both AFR1 and AFR2 infected larvae ($P < 0.0001$). In summary, the preliminary results indicated that the combination with pyrvinium and azoles had the potential to overcome azole resistance issues of *A. fumigatus* and could be a promising option for anti-*Aspergillus* treatment.

Keywords: pyrvinium, *Aspergillus fumigatus*, synergy, fungi, antifungal, resistance, azole

OPEN ACCESS

Edited by:
Weihua Pan,
Shanghai Changzheng Hospital, China

Reviewed by:
Ruoyu Li,
Peking University First Hospital, China
Florent Morio,
Centre Hospitalier Universitaire (CHU) de Nantes, France

****Correspondence:***
Lujuan Gao
gao_lujuan@163.com

Specialty section:
This article was submitted to Antimicrobials, Resistance and Chemotherapy, a section of the journal Frontiers in Microbiology

Received: *02 July 2020*
Accepted: *07 October 2020*
Published: *03 November 2020*

Citation:
Sun Y, Gao L, Zhang Y, Yang J and Zeng T (2020) Synergistic Effect of Pyrvinium Pamoate and Azoles Against Aspergillus fumigatus in vitro and in vivo. Front. Microbiol. 11:579362. doi: 10.3389/fmicb.2020.579362

INTRODUCTION

Invasive aspergillosis (IA) remains a frequent and lethal disease in high-risk immunocompromised individuals (Kontoyiannis and Bodey, 2002). The most frequent causative pathogen of IA is *Aspergillus fumigatus*. Antifungal drugs are limited to treatment options. Azoles are the mainstay of treatment and prevention of IA (Patterson et al., 2016). Nevertheless, azole resistance, especially in *A. fumigatus*, has increased alarmingly and is responsible for the high mortality rate of IA (van der Linden et al., 2011; Verweij et al., 2016; Perez-Cantero et al., 2020). Alternative therapeutic options include amphotericin B and echinocandins. However, limited efficacy or potential toxicity have restricted their use in IA. In addition, clinically significant amphotericin B resistance in *Aspergillus* spp. has been increasingly reported (Sterling and Merz, 1998; Arabatzis et al., 2011; Ozkaya-Parlakay et al., 2016). Therefore, drug repositioning in combination therapy might be a promising option.

Pyrvinium pamoate (PP), a quinoline-derived cyanine dye, was approved as an antihelmintic agent by Food and Drug Administration in 1955. PP is used to treat parasitic infections in humans (Beck et al., 1959; Wagner, 1963). Interestingly, PP has also been demonstrated to strongly inhibit the growth of fluconazole-resistant *Candida albicans* and potentiate the antifungal effect of fluconazole (Chen et al., 2015). In our previous study, PP was shown to exhibit antifungal activity alone [minimal inhibitory concentration (MIC) 2 μg/ml] and synergize with azoles against *Exophiala dermatitidis* both *in vitro* (Gao et al., 2018) and *in vivo* (Sun et al., 2020). Therefore, we speculate that PP might also exert some antifungal effect and positive interactions with conventional antifungals against *A. fumigatus*. Herein, the antifungal efficacy of PP alone and in combination with triazoles against *A. fumigatus* were investigated both *in vitro* and *in vivo*.

MATERIALS AND METHODS

Fungal Strains, Antifungals, and Chemical Agents

Eighteen clinical *A. fumigatus* isolates were studied, including two isolates with the combination of punctual mutation and a tandem repeat sequence of the Cyp51A gene (TR46/Y121F/T289A and TR34/L98H). *Aspergillus flavus* (ATCC 204304) and *Candida parapsilosis* (ATCC 22019) were included for quality control. Morphologic and molecular identification of all isolates were performed via microscopy observation and sequencing of β-tubulin, calmodulin, and the internal transcribed spacer ribosomal DNA (Glass and Donaldson, 1995; Hong et al., 2005; Samson and Varga, 2009).

All four drugs, including PP, itraconazole (ITC), voriconazole (VRC), and posaconazole (POS), were purchased from Selleck Chemicals, Houston, TX, United States. Stock solutions were prepared by dissolving the drugs in dimethyl sulfoxide to achieve stock solutions of 3,200 μ g/ml.

In vitro Effect of Pyrvinium Pamoate Alone and Combined With Azoles Against *A. fumigatus*

The effects of PP alone and PP–azoles interactions against *A. fumigatus* were evaluated via the microdilution chequerboard technique, adapted from broth microdilution method M38-A2 (Clinical and Laboratory Standards Institute, 2008). Fungal cultures were grown on Sabouraud dextrose agar (SDA) for 7 days. Conidia were then harvested and suspended in sterile distilled water containing 0.03% Triton. The conidia suspension was diluted to a concentration of 1–5 $\times$ 10^6 spores/ml and subsequently diluted in Roswell Park Memorial Institute 1640 medium to approximately 1–5 $\times$ 10^4 spores/ml. Twofold serial dilutions of tested agents were prepared from stock solutions with Roswell Park Memorial Institute 1640 medium, according to M38-A2. The working concentration ranges were 0.06–32 μg/ml for PP and 0.03–16 μg/ml for azoles. As described, a 100-μl prepared conidia suspension was inoculated in each cell of the 96-well plate. Subsequently, the horizontal direction was inoculated with 50 μl of serial diluted PP, whereas the vertical direction was inoculated with another 50 μl of serially diluted azoles. The results were evaluated after incubation at 35°C for 48 h. The MICs were defined as the lowest concentration achieving complete inhibition of growth (Clinical and Laboratory Standards Institute, 2008). The interaction of drug combination was classified according to the fractional inhibitory concentration index (FICI). The FICI was calculated by the formula: FICI = (Ac/Aa) + (Bc/Ba), where Ac and Bc are the MICs of antifungals in combination, and Aa and Ba are the MICs of antifungals A and B alone, respectively, (Tobudic et al., 2010). A FICI of $\leq$0.5 indicates synergy, a FICI of $>$0.5 to $\leq$4 is classified as no interaction (indifference), whereas a FICI of $>$4 suggests antagonism (Odds, 2003). All tests were performed in triplicate.

In vivo Efficacy of Pyrvinium Pamoate Alone and in Combination With Azoles in *Galleria mellonella*

The *in vivo* antifungal activity of PP alone and in combination with azoles against *A. fumigatus* infections was evaluated by *G. mellonella* survival assay as described previously (Maurer et al., 2015). Groups of 20 sixth instar larvae (∼300 mg, Sichuan, China) were maintained in the dark at room temperature before experiments. Fungal cultures of AF293, AFR1, and AFR2 were grown on SDA at 37°C for 72 h. Conidia were then harvested by gentle scraping of colony surfaces with sterile plastic loops, washed twice, and adjusted to 1 $\times$ 10^8 spores/ml in sterile saline. For evaluation of the *in vivo* effects of PP alone and combined with azoles, the following intervention groups were included: PP group, ITC group, POS group, VRC group, PP with ITC group, PP with POS group, and PP with VRC group. Groups of larvae injected with 10-μl sterile saline or conidia suspension, and untouched larvae were served as control groups. Conidia suspension and therapeutic and control solutions were injected into the larvae via the last right proleg using a Hamilton syringe

(25 gauge, 50 μl). Larvae were infected with fungal suspension 2 h before introducing therapeutic agents (0.5 μg per agent). All groups of larvae were incubated at 30°C in the dark. For survival studies, the death of larvae was monitored by visual inspection of the color (brown-dark/brown) every 24 h for a duration of 5 days. For tissue burden studies, three larvae from each group were selected without discrimination every 24 h for 4 days. Subsequently, selected larvae were suspended in 1 ml of saline-ampicillin and homogenized gently for a few seconds. The mix was 1,000-fold diluted with phosphate-buffered saline buffer, and 100 μl of the dilutions was inoculated on the SDA. The colonies were counted after incubation at 37°C for 24 h. The experiment was repeated triplicate using larvae from different batches.

Statistical Analysis

Data were presented as mean ± SEM. Graph Pad Prism 7 was used for graphs and statistical analyses. The survival curves were analyzed by the Kaplan–Meier method. Tissue fungal burden was analyzed by analysis of variance. Differences were considered significant when $P < 0.05$.

RESULTS

In vitro Effect of Pyrvinium Pamoate Alone and Combined With Azoles Against *A. fumigatus*

As shown in **Table 1**, the MIC ranges of PP alone were 2 μg/ml against AFR1 and >32 μg/ml against the other strains. The MIC ranges of azoles against azole-sensitive *A. fumigatus* were 1 μg/ml for ITC, 0.5 μg/ml for VRC, and 0.5–1 μg/ml for POS. The MIC ranges of azoles were >16 μg/ml for ITC, 4 μg/ml for VRC and POS against AFR1 (TR_{34}/L98H), and >16 μg/ml for VRC, 4 μg/ml for ITC and POS against AFR2 (TR_{46}/Y121F/T 289A).

When PP was combined with ITC, VRC, or POS, synergism was observed in 15 (83.3%, FICI 0.125–0.375), 11 (61.1%, FICI 0.258–0.281), and 16 (88.9%, FICI 0.039–0.281) strains of *A. fumigatus* (**Table 1**). Although AFR1 and AFR2 showed resistance to azoles, PP combined with ITC or POS showed favorable synergism against both strains. The effective MIC ranges of PP and ITC in synergistic combinations decreased to 1–8 and 0.125–0.25 μg/ml against azole-sensitive strains and 0.5–4 and 0.25–4 μg/ml against azole-resistant strains, respectively, (**Table 1**). In synergistic PP–POS combination, the MIC ranges of PP and POS against *A. fumigatus* decreased to 0.25–1 and 0.125 μg/ml, respectively. The effective working ranges of PP and VRC in synergistic combinations against *A. fumigatus* were 0.5–2 and 0.125 μg/ml, respectively, (**Table 1**). There was no antagonism observed in all combinations.

In vivo Efficacy of Pyrvinium Pamoate Alone and in Combination With Azoles Against *A. fumigatus*

For AF293-infected groups, the survival rates of larvae treated with PP, VRC, ITC, POS, PP with VRC, PP with ITC, and PP with POS were 3.3, 33.3, 30, 30, 55, 43, and 60%, respectively. Treatment with PP alone, azoles alone, and PP combined with azoles all significantly increased the survival rate of larvae ($P < 0.01$ for PP group, and $P < 0.0001$ for other

TABLE 1 | MICs and FICIs results with the combinations of PP and azoles.

Strains	MIC[a] (μg/ml) for						
	Agent alone				Combination[b]		
	PP	ITC	VRC	POS	PP/ITC	PP/VRC	PP/POS
AF293	>32	1	0.5	1	0.5/1 (1.008, I)	0.25/0.5 (1.003, I)	1/0.125 (0.141, S)
AF001	>32	1	0.5	0.5	2/0.25 (0.281, S)	0.5/0.25 (0.508, I)	0.5/0.25 (0.508, I)
AF002	>32	1	0.5	1	2/0.25 (0.281, S)	0.5/0.125 (0.258, S)	0.25/0.125 (0.129, S)
AF003	>32	1	0.5	1	0.25/1 (1.003, I)	1/0.125 (0.266, S)	1/0.125 (0.141, S)
AF004	>32	1	0.5	1	8/0.25 (0.375, S)	2/0.125 (0.281, S)	0.5/0.125 (0.132, S)
AF005	>32	1	0.5	1	8/0.125 (0.25, S)	0.5/0.5 (1.008, I)	0.5/0.125 (0.132, S)
AF006	>32	1	0.5	1	2/0.125 (0.156, S)	1/0.125 (0.266, S)	0.5/0.125 (0.132, S)
AF007	>32	1	0.5	1	0.5/1 (1.008, I)	1/0.125 (0.266, S)	0.5/0.125 (0.132, S)
AF008	>32	1	0.5	1	4/0.125 (0.188, S)	0.5/0.125 (0.258, S)	1/0.125 (0.141, S)
AF009	>32	1	0.5	1	4/0.25 (0.313, S)	0.5/0.25 (0.508, I)	0.25/0.125 (0.129, S)
AF010	>32	1	0.5	1	1/0.25 (0.266, S)	0.5/0.125 (0.258, S)	0.5/0.125 (0.132, S)
AF011	>32	1	0.5	1	2/0.25 (0.281, S)	0.5/0.5 (1.008, I)	0.5/0.125 (0.132, S)
AF012	>32	1	0.5	1	1/0.25 (0.266, S)	0.5/0.125 (0.258, S)	1/0.125 (0.141, S)
AF013	>32	1	0.5	1	2/0.25 (0.281, S)	0.5/0.25 (0.508, I)	0.25/0.125 (0.129, S)
AF014	>32	1	0.5	1	4/0.25 (0.313, S)	1/0.125 (0.266, S)	0.5/0.5 (0.508, I)
AF015	>32	1	0.5	1	4/0.25 (0.313, S)	0.5/0.25 (0.508, I)	0.5/0.125 (0.132, S)
AFR1	2	>16	4	4	0.5/4 (0.275, S)	0.5/2 (0.75, I)	0.5/0.125 (0.281, S)
AFR2	>32	4	>16	4	4/0.25 (0.125, S)	16/16 (0.75, I)	0.5/0.125 (0.039, S)

[a] *MIC is the concentration resulting in 100% growth inhibition.*

[b] *FICI results are shown in parentheses. S, synergy (FICI of ≤0.5); I, no interaction (indifference; 0.5 < FICI ≤ 4). For FICI calculations, concentrations of 64 and 32 μg/ml were used when MICs were >32 and >16 μg/ml, respectively.*

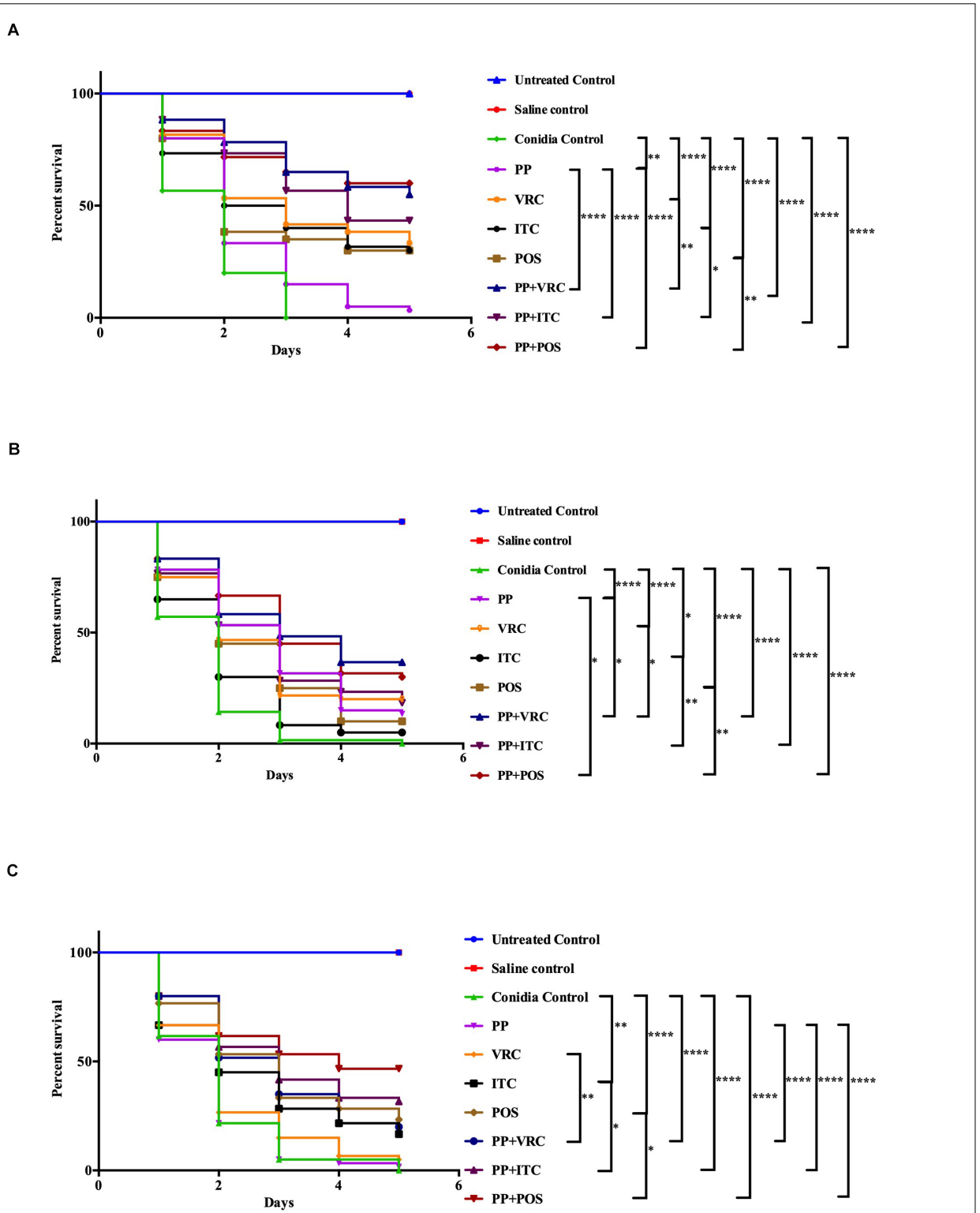

FIGURE 1 | Survival curve of *A. fumigatus*-infected larvae with different interventions. **(A)** *G. mellonella* infected with AF293. Treatment with PP alone, azoles alone, or combined with PP all significantly improved larvae survival. Combination of PP with azoles acted synergistically against AF293 infection. **(B)** *G. mellonella* infected with AFR1. Treatment with PP alone, azoles alone, or combined with PP all significantly increased larvae survival. Combination of PP with azoles acted synergistically against AFR1 infection. **(C)** *G. mellonella* infected with AFR2. Larvae survival rates were significantly improved in groups treated with ITC alone, POS alone, and PP–azoles combinations. Larvae survival rates in the combination groups were significantly improved compared with azoles or PP alone groups (***$P < 0.0001$; **$P < 0.01$; and *$P < 0.05$).

groups; **Figure 1A**). The combination of PP with azoles acted synergistically against AF293 infection, compared with azoles alone or PP alone ($P < 0.05$).

Regarding AFR1 infection, the survival rates of larvae treated with PP, VRC, ITC, POS, PP with VRC, PP with ITC, and PP with POS were 13.3, 20, 5, 10, 36.7, 18.3, and 30%, respectively. PP alone, azoles alone, and azoles combined with PP all significantly improved the survival of larvae infected with AFR1 ($P < 0.05$ for ITC group, and $P < 0.0001$ for other groups; **Figure 1B**). The combination of PP with azoles acted synergistically against AFR1 infection, compared with the azoles alone group ($P < 0.05$). In addition, the survival of larvae in groups treated PP with VRC or POS was significantly higher than the PP alone group ($P < 0.05$).

With respect to AFR2 infection, the survival rates of larvae treated with PP, VRC, ITC, POS, PP with VRC, PP with ITC, and PP with POS were 1.7, 5, 16.7, 23.3, 20, 31.7, and 46.7%, respectively. AFR2 infections showed resistance to neither VRC nor PP treatment alone. Nevertheless, POS alone, ITC alone, and PP–azoles combinations all significantly increased the survival rate of AFR2-infected larvae ($P < 0.01$ for ITC group, and $P < 0.0001$ for other groups; **Figure 1C**). In addition, combination groups exhibited a significantly higher survival rate than azoles or PP treatment alone groups ($P < 0.05$).

Fungal Burden Determination

Over the time of infection, increasing colony-forming unit (CFU) counting in larvae was observed (**Figure 2**). For larvae infected with AF293 (**Figure 2A**), the fungal burden of the PP alone group was comparable with the control group. The fungal burden in all azole groups was significantly lower than the PP group and control group ($P < 0.0001$). There was no significant difference between POS and VRC groups, whereas both groups exhibited significantly lower CFU counting than the ITC group ($P < 0.001$ for POS group versus ITC group, $P < 0.0001$ for VRC group versus ITC group). All combination groups exhibited significantly lower CFUs compared with the control group, azole alone group, and PP alone group ($P < 0.0001$).

As for larvae infected with AFR1 (**Figure 2B**), all intervention groups significantly decreased CFU number compared with the control group ($P < 0.01$ for the ITC group and $P < 0.0001$ for other groups). All combination groups exhibited significantly lower fungal burden than the azole alone and PP alone groups ($P < 0.0001$). The VRC group, POS group, and PP group exhibited comparable CFU counting, whereas the ITC group exhibited significantly higher CFU numbers compared with these three groups. Similarly, ITC combined with the PP group exhibited significantly higher fungal burden than PP combined with the POS or VRC group ($P < 0.0001$).

As for larvae infected with AFR2 (**Figure 2C**), the fungal burden of the PP group, ITC group, and VRC group were all comparable with the control group. There was no significant difference between the PP and azoles groups. However, the POS group significantly decreased CFU number compared with the ITC group ($P < 0.001$), VRC group ($P < 0.05$), and control group ($P < 0.0001$). All combination groups exhibited significantly lower CFUs compared with the control group, azole alone group, and PP alone group ($P < 0.0001$).

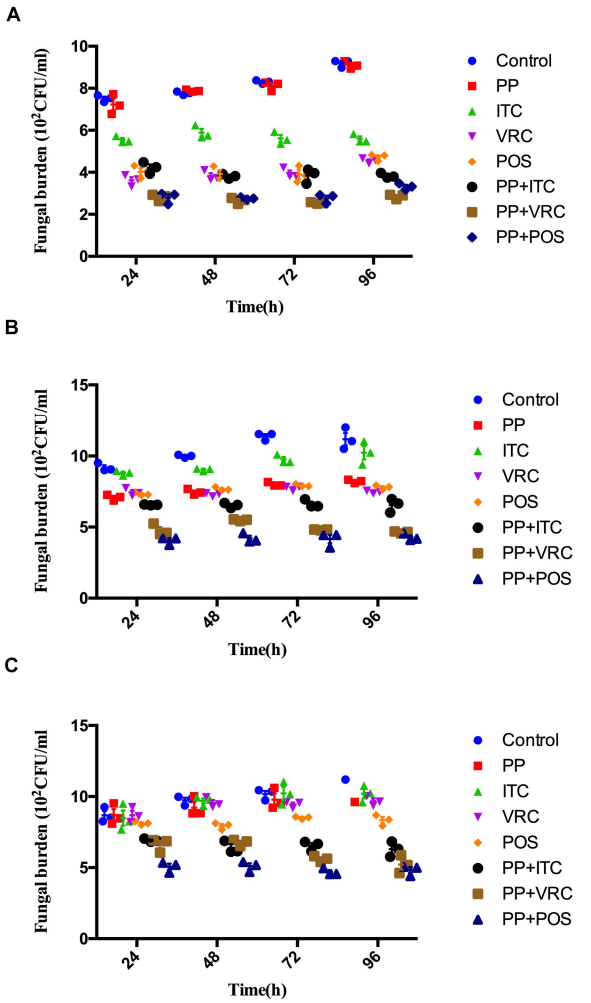

FIGURE 2 | Effect of drug combinations on fungal burdens of larvae infected with *A. fumigatus*. **(A)** Larvae infected with AF293. All azole alone groups and combination groups exhibited significantly lower CFUs compared with control group ($P < 0.0001$). Groups treated with azoles in combination with PP exhibited significant ($P < 0.0001$) lower fungal burden than azole alone and PP alone group. **(B)** Larvae infected with AFR1. All groups exhibited significantly lower CFUs compared with control group ($P < 0.01$ for ITC group and <0.0001 for other groups). All combination groups exhibited significantly ($P < 0.0001$) lower fungal burden than azole alone and PP alone group. **(C)** Larvae infected with AFR2. POS group and all combination groups exhibited significantly lower CFUs compared with control group ($P < 0.0001$). All combination groups exhibited significant ($P < 0.0001$) lower fungal burden than azole alone and PP alone group.

DISCUSSION

Aspergillus infections have been increasingly recognized as a global health challenge. Due to the occurrence of azole-resistant strains worldwide and limited antifungal options, the therapy of IA has been proved to be difficult (Chen et al., 2020).

Combination therapies, which can expand the antifungal spectrum, improve therapeutic efficacy, and reduce adverse effects, could be a promising treatment option.

In the present study, PP was evaluated alone and combined with azoles against *A. fumigatus*. Although PP alone showed limited antifungal efficacy against most isolates tested *in vitro*, PP exhibited MIC of 2 μg/ml against azole-resistant strain AFR1. Accordingly, PP alone significantly improved the survival rate of larvae infected with AFR1 ($P < 0.0001$) and AF293 ($P < 0.01$), demonstrating the anti-*Aspergillus* effect of PP alone both *in vitro* and *in vivo*. Synergism between PP and ITC, VRC, or POS was observed in 15 (83.3%), 11 (61.1%), and 16 (88.9%) isolates *in vitro*. It was notable that PP potentiated the antifungal activity of both POS and ITC against AFR1 and AFR2. A fourfold and 16-fold reduction of ITC MICs against AFR1 and AFR2, respectively, and up to a 32-fold reduction of POS MICs against both AFR1 and AFR2 were observed, as shown in **Table 1**. Similarly, synergistic activity between PP and azoles resulted in up to an eightfold reduction of the MICs of azoles in azole-sensitive strains. The *in vitro* data were further confirmed *in vivo* because antifungal treatment with azoles and PP significantly improved larvae survival ($P < 0.0001$). Notably, despite AFR2 infection was resistant to VRC or PP alone and *in vitro* combination of PP-VRC showed inactive against both AFR1 and AFR2, PP combined with VRC significantly increased the survival of both AFR1 and AFR2 infected larvae ($P < 0.0001$). All azoles–PP combinations showed a significantly positive effect on larvae survival in comparison with the corresponding azole applied alone ($P < 0.05$). In accordance with *in vitro* susceptibility assay and *in vivo* survival assays, PP treatment alone significantly decreased CFU counting of larvae infected with AFR1. PP combined with azoles significantly decreased tissue fungal burden in larvae compared with PP alone and azole alone groups.

To date, mechanisms of azoles resistance in *A. fumigatus* are not fully characterized. The most investigated molecular mechanisms can be classified into the following two categories, namely *cyp51*-mediated resistance, including Cyp51 protein alterations and overexpression of the target enzyme, and non-*cyp51*-mediated resistance, including upregulation of efflux pump systems, fungal stress response, antifungal enzymatic degradation, biofilm formation, and alternative pathways activated to overcome the efficacy of antifungals (Wei et al., 2015; Hagiwara et al., 2016; Chen et al., 2020; Perez-Cantero et al., 2020). In these cases, azole resistance caused by a mutation in the Cyp51A gene combined with tandem repeats of the gene promoter region, e.g., TR_{34}/L98H and TR_{46}/Y121F/T289A, which leads to significant cyp51A overexpression, challenges the current understanding of the development of azole resistance in *A. fumigatus* (Mellado et al., 2007; van der Linden et al., 2013).

The TR_{34}/L98H and TR_{46}/Y121F/T289A were first reported in Netherlands in 1998 (Snelders et al., 2008) and 2009 (van der Linden et al., 2013), respectively. Up to date, isolates harboring these two mechanisms were found to be the major route for resistance cases and spread worldwide (Meis et al., 2016). It was estimated that 82–89% of azole-resistant cases in Netherlands were due to TR34/L98H and TR46/Y121F/T289A (Verweij et al., 2016), whereas this was the case in 64% of cases in Belgium (Vermeulen et al., 2015) and 87% of cases in Turkey (Ozmerdiven et al., 2015). Clinically, the role of azoles in aspergillosis caused by azole-resistant strains is very limited (Meis et al., 2016). Therefore, it is exciting to find that PP was able to reverse ITC and POS resistance of AFR1 and AFR2 *in vitro* and synergize with VRC, ITC, or POS *in vivo* against both AFR1 and AFR2. In addition, it is noteworthy that PP alone showed moderate antifungal effect against AFR1 both *in vitro* and *in vivo* but was inactive against AFR2 and other isolates tested. We suspected that non-*cyp51*-mediated factors might have played a critical role in the antifungal effect of PP against AFR1.

Previously, PP has been demonstrated to strongly inhibit the growth of the fluconazole-resistant i(5L) strain of *C. albicans*, which contains double copies of the left arm of chromosome 5 (Selmecki et al., 2006; Chen et al., 2015), and enhances the antifungal efficacy of fluconazole, demonstrating the efficacy of PP toward aneuploidy-based azole resistance. Acquisition of aneuploidy has been documented in pathogenic fungi *C. albicans*, *Saccharomyces cerevisiae*, and *Cryptococcus neoformans* (Todd et al., 2017). Specific environmental conditions, such as antifungal stress and fungal interactions with the host, might result in aneuploidy, which has been associated with drug resistance of fungi (Todd et al., 2017). Although the role of the aneuploid genome has not been described in *A. fumigatus* up to date, we suspected that ploidy changes might have occurred in *A. fumigatus*. In-depth studies are needed to investigate the probability of aneuploidy in *A. fumigatus,* especially AFR1 strain, and the possible role of aneuploidy in the anti-*Aspergillus* effect of PP. Furthermore, previous studies revealed that PP exhibited anticancer effects via mitochondrial respiration inhibition and CK1α activation, affecting multiple important biological processes and signaling pathways, such as Akt and Wnt-β-catenin-dependent pathways, autophagy, and energy (Momtazi-Borojeni et al., 2017). Therefore, we suspected that PP might also have some effect on critical fungal biological processes, such as stress response, biofilm formation, and drug efflux pump, as demonstrated in *E. dermatitidis* (Sun et al., 2020). However, further investigations are needed to elucidate the underlying mechanism.

In conclusion, the preliminary results indicated that PP could overcome azole resistance issues of *A. fumigatus* and might be a promising therapeutic strategy for anti-*Aspergillus* treatment. However, the limitation of the present study is the sample size of resistant strains of *A. fumigatus* studied. More isolates of resistant strains involving different phenotypes and genotypes are needed in the future study to help establish a comprehensive profile of the effect of PP alone and in combination with azoles against *A. fumigatus*.

DATA AVAILABILITY STATEMENT

The raw data supporting the conclusions of this article will be made available by the authors, without undue reservation.

ETHICS STATEMENT

Written informed consent was obtained from the individual(s) for the publication of any potentially identifiable images or data included in this article.

AUTHOR CONTRIBUTIONS

LG and YS conceived and designed the study. YZ and YS performed all the experiments. LG analyzed the data and wrote the manuscript. JY and TZ provided general guidance and revised the manuscript. All authors contributed to the article and approved the submitted version.

FUNDING

This work was supported by grant WJ2018H178 from Hubei Province Health and Family Planning Scientific Research Project and grant 2019CFB567 from the Natural Science Foundation of Hubei Province.

REFERENCES

Arabatzis, M., Kambouris, M., Kyprianou, M., Chrysaki, A., Foustoukou, M., Kanellopoulou, M., et al. (2011). Polyphasic identification and susceptibility to seven antifungals of 102 *Aspergillus* isolates recovered from immunocompromised hosts in Greece. *Antimicrob. Agents Chemother.* 55, 3025–3030. doi: 10.1128/AAC.01491-10

Beck, J. W., Saavedra, D., Antell, G. J., and Tejeiro, B. (1959). The treatment of pinworm infections in humans (enterobiasis) with pyrvinium chloride and pyrvinium pamoate. *Am. J. Trop. Med. Hyg.* 8, 349–352.

Chen, G., Mulla, W. A., Kucharavy, A., Tsai, H. J., Rubinstein, B., Conkright, J., et al. (2015). Targeting the adaptability of heterogeneous aneuploids. *Cell* 160, 771–784. doi: 10.1016/j.cell.2015.01.026

Chen, P., Liu, J., Zeng, M., and Sang, H. (2020). Exploring the molecular mechanism of azole resistance in *Aspergillus fumigatus*. *J. Mycol. Med.* 30:100915. doi: 10.1016/j.mycmed.2019.100915

Clinical and Laboratory Standards Institute (2008). *Reference Method for Broth Dilution Antifungal Susceptibility Testing of Filamentous Fungi; Approved Standard-2nd ed. CLSI Document M38-A2*. Wayne, PA: CLSI.

Gao, L., Sun, Y., He, C., Zeng, T., and Li, M. (2018). Synergy between pyrvinium pamoate and azoles against exophiala dermatitidis. *Antimicrob. Agents Chemother.* 62, e2361–e2317. doi: 10.1128/AAC.02361-17

Glass, N. L., and Donaldson, G. C. (1995). Development of primer sets designed for use with the PCR to amplify conserved genes from filamentous ascomycetes. *Appl. Environ. Microbiol.* 61, 1323–1330.

Hagiwara, D., Watanabe, A., Kamei, K., and Goldman, G. H. (2016). Epidemiological and genomic landscape of azole resistance mechanisms in *Aspergillus* fungi. *Front. Microbiol.* 7:1382. doi: 10.3389/fmicb.2016.01382

Hong, S. B., Go, S. J., Shin, H. D., Frisvad, J. C., and Samson, R. A. (2005). Polyphasic taxonomy of *Aspergillus fumigatus* and related species. *Mycologia* 97, 1316–1329. doi: 10.3852/mycologia.97.6.1316

Kontoyiannis, D. P., and Bodey, G. P. (2002). Invasive aspergillosis in 2002: an update. *Eur. J. Clin. Microbiol. Infect. Dis.* 21, 161–172. doi: 10.1007/s10096-002-0699-z

Maurer, E., Browne, N., Surlis, C., Jukic, E., Moser, P., Kavanagh, K., et al. (2015). Galleria mellonella as a host model to study Aspergillus terreus virulence and amphotericin B resistance. *Virulence* 6, 591–598. doi: 10.1080/21505594.2015.1045183

Meis, J. F., Chowdhary, A., Rhodes, J. L., Fisher, M. C., and Verweij, P. E. (2016). Clinical implications of globally emerging azole resistance in *Aspergillus fumigatus*. *Philos. Trans. R. Soc. Lond. B Biol. Sci.* 371:20150460. doi: 10.1098/rstb.2015.0460

Mellado, E., Garcia-Effron, G., Alcazar-Fuoli, L., Melchers, W. J., Verweij, P. E., Cuenca-Estrella, M., et al. (2007). A new *Aspergillus fumigatus* resistance mechanism conferring in vitro cross-resistance to azole antifungals involves a combination of cyp51A alterations. *Antimicrob. Agents Chemother.* 51, 1897–1904. doi: 10.1128/AAC.01092-06

Momtazi-Borojeni, A. A., Abdollahi, E., Ghasemi, F., Caraglia, M., and Sahebkar, A. (2017). The novel role of pyrvinium in cancer therapy. *J. Cell. Physiol.* 233, 2871–2881. doi: 10.1002/jcp.26006

Odds, F. C. (2003). Synergy, antagonism, and what the chequerboard puts between them. *J. Antimicrob. Chemother.* 52:1. doi: 10.1093/jac/dkg301

Ozkaya-Parlakay, A., Ozer-Bekmez, B., Kara, A., Kuskonmaz, B., Akcoren, Z., Arikan-Dagli, S., et al. (2016). An important finding of systemic *Aspergillosis*: skin involvement and amphotericin B resistance in an adolescent. *Pediatr. Neonatol.* 57, 343–346. doi: 10.1016/j.pedneo.2013.09.010

Ozmerdiven, G. E., Ak, S., Ener, B., Agca, H., Cilo, B. D., Tunca, B., et al. (2015). First determination of azole resistance in *Aspergillus fumigatus* strains carrying the TR34/L98H mutations in Turkey. *J. Infect. Chemother.* 21, 581–586. doi: 10.1016/j.jiac.2015.04.012

Patterson, T. F., Thompson, G. R. III, Denning, D. W., Fishman, J. A., Hadley, S., Herbrecht, R., et al. (2016). Practice guidelines for the diagnosis and management of aspergillosis: 2016 update by the infectious diseases Society of America. *Clin. Infect. Dis.* 63, e1–e60. doi: 10.1093/cid/ciw326

Perez-Cantero, A., Lopez-Fernandez, L., Guarro, J., and Capilla, J. (2020). Azole resistance mechanisms in *Aspergillus*: update and recent advances. *Int. J. Antimicrob. Agents* 55:105807. doi: 10.1016/j.ijantimicag.2019.09.011

Samson, R. A., and Varga, J. (2009). What is a species in *Aspergillus*? *Med. Mycol.* 47(Suppl. 1), S13–S20. doi: 10.1080/13693780802354011

Selmecki, A., Forche, A., and Berman, J. (2006). Aneuploidy and isochromosome formation in drug-resistant *Candida albicans*. *Science* 313, 367–370. doi: 10.1126/science.1128242

Snelders, E., van der Lee, H. A., Kuijpers, J., Rijs, A. J., Varga, J., Samson, R. A., et al. (2008). Emergence of azole resistance in Aspergillus fumigatus and spread of a single resistance mechanism. *PLoS Med.* 5:e219. doi: 10.1371/journal.pmed.0050219

Sterling, T. R., and Merz, W. G. (1998). Resistance to amphotericin B: emerging clinical and microbiological patterns. *Drug Resist. Updat.* 1, 161–165.

Sun, Y., Gao, L., Yuan, M., Yuan, L., Yang, J., and Zeng, T. (2020). In vitro and in vivo Study of Antifungal Effect of Pyrvinium Pamoate Alone and in Combination With Azoles Against Exophiala dermatitidis. *Front. Cell. Infect. Microbiol.* 10:576975. doi: 10.3389/fcimb.2020.576975

Tobudic, S., Kratzer, C., Lassnigg, A., Graninger, W., and Presterl, E. (2010). In vitro activity of antifungal combinations against *Candida albicans* biofilms. *J. Antimicrob. Chemother.* 65, 271–274. doi: 10.1093/jac/dkp429

Todd, R. T., Forche, A., and Selmecki, A. (2017). Ploidy variation in fungi: polyploidy, aneuploidy, and genome evolution. *Microbiol. Spectr.* 5:FUNK-0051-2016. doi: 10.1128/microbiolspec.FUNK-0051-2016

van der Linden, J. W., Camps, S. M., Kampinga, G. A., Arends, J. P., Debets-Ossenkopp, Y. J., Haas, P. J., et al. (2013). Aspergillosis due to voriconazole highly resistant *Aspergillus fumigatus* and recovery of genetically related resistant isolates from domiciles. *Clin. Infect. Dis.* 57, 513–520. doi: 10.1093/cid/cit320

van der Linden, J. W., Snelders, E., Kampinga, G. A., Rijnders, B. J., Mattsson, E., Debets-Ossenkopp, Y. J., et al. (2011). Clinical implications of azole resistance in *Aspergillus fumigatus*, The Netherlands, 2007-2009. *Emerg. Infect. Dis.* 17, 1846–1854. doi: 10.3201/eid1710.110226

Vermeulen, E., Maertens, J., De Bel, A., Nulens, E., Boelens, J., Surmont, I., et al. (2015). Nationwide surveillance of azole resistance in *Aspergillus*

diseases. *Antimicrob. Agents Chemother.* 59, 4569–4576. doi: 10.1128/AAC.00233-15

Verweij, P. E., Chowdhary, A., Melchers, W. J., and Meis, J. F. (2016). Azole resistance in *Aspergillus fumigatus*: can we retain the clinical use of mold-active antifungal azoles? *Clin. Infect. Dis.* 62, 362–368. doi: 10.1093/cid/civ885

Wagner, E. D. (1963). Pyrvinium pamoate in the treatment of strongyloidiasis. *Am. J. Trop. Med. Hyg.* 12, 60–61.

Wei, X., Zhang, Y., and Lu, L. (2015). The molecular mechanism of azole resistance in *Aspergillus fumigatus*: from bedside to bench and back. *J. Microbiol.* 53, 91–99. doi: 10.1007/s12275-015-5014-7

Conflict of Interest: The authors declare that the research was conducted in the absence of any commercial or financial relationships that could be construed as a potential conflict of interest.

frontiers in Microbiology

ORIGINAL RESEARCH
published: 15 December 2020
doi: 10.3389/fmicb.2020.599233

The Multi-Fungicide Resistance Status of *Aspergillus fumigatus* Populations in Arable Soils and the Wider European Environment

Bart Fraaije[1,2]*, *Sarah Atkins*[2], *Steve Hanley*[2], *Andy Macdonald*[2] and *John Lucas*[2]

[1] NIAB, Cambridge, United Kingdom, [2] Rothamsted Research, Harpenden, United Kingdom

The evolution and spread of pan-azole resistance alleles in clinical and environmental isolates of *Aspergillus fumigatus* is a global human health concern. The identification of hotspots for azole resistance development in the wider environment can inform optimal measures to counteract further spread by minimizing exposure to azole fungicides and reducing inoculum build-up and pathogen dispersal. We investigated the fungicide sensitivity status of soil populations sampled from arable crops and the wider environment and compared these with urban airborne populations. Low levels of azole resistance were observed for isolates carrying the CYP51A variant F46Y/M172V/E427K, all belonging to a cluster of related cell surface protein (CSP) types which included t07, t08, t13, t15, t19, and t02B, a new allele. High levels of resistance were found in soil isolates carrying CYP51A variants TR_{34}/L98H and TR_{46}/Y121F/T289A, all belonging to CSP types t01, t02, t04B, or t11. TR_{46}/Y121F/M172V/T289A/G448S (CSP t01) and TR_{46}/Y121F/T289A/S363P/I364V/G448S (CSP t01), a new haplotype associated with high levels of resistance, were isolated from Dutch urban air samples, indicating azole resistance evolution is ongoing. Based on low numbers of pan-azole resistant isolates and lack of new genotypes in soils of fungicide-treated commercial and experimental wheat crops, we consider arable crop production as a coldspot for azole resistance development, in contrast to previously reported flower bulb waste heaps. This study also shows that, in addition to azole resistance, several lineages of *A. fumigatus* carrying TR-based CYP51A variants have also developed acquired resistance to methyl benzimidazole carbamate, quinone outside inhibitor and succinate dehydrogenase (Sdh) inhibitor fungicides through target-site alterations in the corresponding fungicide target proteins; beta-tubulin (F200Y), cytochrome *b* (G143A), and Sdh subunit B (H270Y and H270R), respectively. Molecular typing showed that several multi-fungicide resistant strains found in agricultural soils in this study were clonal as identical isolates have been found earlier in the environment and/or in patients. Further research on the spread of different fungicide-resistant alleles from the wider environment to patients and *vice versa* can inform optimal practices to tackle the further spread of antifungal resistance in *A. fumigatus* populations and to safeguard the efficacy of azoles for future treatment of invasive aspergillosis.

Keywords: *Aspergillus fumigatus*, antifungal resistance, azoles, MBC fungicides, QoI fungicides, SDHI fungicides, environment

OPEN ACCESS

Edited by:
Ying-Chun Xu,
Peking Union Medical College Hospital (CAMS), China

Reviewed by:
Hamid Badali,
The University of Texas Health Science Center at San Antonio, United States
Jochem B. Buil,
Radboud University Nijmegen Medical Centre, Netherlands
Shallu Kathuria,
National Centre for Disease Control (NCDC), India

***Correspondence:**
Bart Fraaije
bart.fraaije@niab.com

Specialty section:
This article was submitted to Antimicrobials, Resistance and Chemotherapy, a section of the journal Frontiers in Microbiology

Received: *26 August 2020*
Accepted: *23 November 2020*
Published: *15 December 2020*

Citation:
Fraaije B, Atkins S, Hanley S, Macdonald A and Lucas J (2020) The Multi-Fungicide Resistance Status of Aspergillus fumigatus Populations in Arable Soils and the Wider European Environment. Front. Microbiol. 11:599233. doi: 10.3389/fmicb.2020.599233

INTRODUCTION

Aspergillus fumigatus is a mold commonly found on plant debris and in soil. It is also an opportunistic human pathogen causing allergic symptoms and life-threatening invasive infections. The incidence of invasive aspergillosis (IA) has been increasing in recent years largely due to increased numbers of immunocompromised individuals in the population unable to fight off infection. Treatment of IA is difficult as there are few effective antifungal drugs without toxic side-effects. Azoles are among the most widely used antifungals due to their efficacy and low toxicity. However, resistance to azoles has occurred in clinical isolates of *A. fumigatus* and is becoming more common, with potentially serious consequences for the treatment of invasive infections.

The first cases of azole resistance in *A. fumigatus* were reported in clinical strains from the USA isolated during the late 1980's (Denning et al., 1997). Recent studies have shown that resistance to medical azoles in both clinical and environmental isolates has increased in Europe and elsewhere since the late 1990's (Snelders et al., 2008; Howard et al., 2009). Azoles inhibit the enzyme sterol 14α-demethylase (CYP51), a key step in the synthesis of sterols essential for the integrity of cell membranes. *Aspergillus fumigatus* has two CYP51 proteins, CYP51A and CYP51B. Many different resistant strains, mostly with CYP51A alterations, have been isolated from patients undergoing azole therapy (Howard et al., 2009). Other resistance mechanisms have also been found, including increased expression of *CYP51* (Camps et al., 2012a,b; Buied et al., 2013) and efflux pump encoding genes (Fraczek et al., 2013; Meneau et al., 2016), accumulation of ergosterol precursors (Hagiwara et al., 2018; Rybak et al., 2019), and reduced intracellular retention of azoles (Wei et al., 2017).

Highly azole-resistant isolates have been found in the Netherlands in azole-naïve patients since 2007 (Van der Linden et al., 2011). These clinical strains and the majority of azole-resistant environmental isolates that have been characterized belong to two unique genotypes based on a combination of CYP51A alterations and promoter tandem repeat (TR) inserts of 34 or 46 bp. Clinical isolates carrying simultaneously CYP51A alterations TR_{34} and amino acid substitution L98H (TR_{34}/L98H) have been found in Europe since 1998 (Snelders et al., 2008; Lazzarini et al., 2016), whereas the first TR_{46}/Y121F/T289A isolate was reported from North America in 2008 (Wiederhold et al., 2016). These genotypes, which are now spread worldwide Verweij et al., 2016), are also highly resistant to several azole fungicides commonly used to preserve materials (e.g., wood, paints, and fabrics) and to prevent fungal diseases in animals, birds and plants. Subsequently, concerns have been raised about an environmental route of resistance selection through an unintended exposure of *A. fumigatus* as a non-target pathogen to azole fungicides in agricultural settings (Verweij et al., 2009; Berger et al., 2017; Hollomon, 2017). Detailed information on the origin and further spread of pan-azole resistant strains in the wider environment is therefore urgently needed (Chowdhary and Meis, 2018). This will enable thorough assessment of the extent of risk as predicted by Gisi (2014), and implementation of strategies to slow down and/or prevent future spread of azole resistance.

Flower bulb waste, green waste and wood chippings have recently been reported as "hotspots" for azole resistance development in the Netherlands (Schoustra et al., 2019). A hotspot is defined as a habitat that supports the growth and reproduction of *A. fumigatus* for relatively long periods of time in the presence of azole residues at concentrations that can select for resistant strains. This aim of this study is to investigate if fungicide applications on arable crops, particularly cereals, can be regarded as a hotspot for azole resistance development. Large amounts of fungicides are used to control diseases in cereals, including several triazoles that have been shown to have similar CYP51 binding modes and high levels of cross-resistance to medical azoles (Snelders et al., 2012). As such, living in agricultural areas was suggested to increase the risk of inhaling azole-resistant isolates (Rocchi et al., 2014). However, due to a low competitive ability of *A. fumigatus* to grow on straw in comparison with other saprophytic fungi, the low residue levels and short periods of bioavailability of azoles in soils after foliar spray applications, the risk of azole resistance development is estimated to be low (Gisi, 2014). Previous studies carried out with a limited number of samples and isolates suggest pan-azole resistance can be detected at low frequencies (2–3%) in UK cereal fields (Bromley et al., 2014; Tsitsopoulou et al., 2018).

Having access to the long-term Park Grass (permanent grassland since 1856, no fungicides), as well as Broadbalk (continuous winter wheat since 1843) and two experiments examining the effects of repeatedly incorporating straw of continuous wheat crops at Rothamsted and Woburn with plots that have been sprayed with foliar fungicides or left untreated (Macdonald et al., 2018, enabled us to investigate if cereal foliar fungicide applications can select for resistance in *A. fumigatus* populations. For comparison, we also isolated and characterized *A. fumigatus* strains from air samples and soils of arable crops sampled at different locations in Europe using cell surface protein (CSP) sequence analysis (Klaassen et al., 2009) and microsatellite typing based on short tandem repeats (STR*Af*) (De Valk et al., 2005). The majority of strains were not only tested for sensitivity to several clinical and agricultural azoles but also to fungicides with different modes of action, including methyl benzimidazole carbamate (MBC), quinone outside inhibitor (QoI) and succinate dehydrogenase inhibitor (SDHI) fungicides, targeting beta-tubulin, cytochrome *b* and succinate dehydrogenase (Sdh) subunits B, C, and D, respectively. These fungicides are all commonly used to control diseases in arable crops and horticulture. An improved understanding of resistance development to different classes of fungicides in the environment can provide more information on the emergence and origin of novel resistant genotypes, and where and under which circumstances, selection is likely to occur in environmental and/or clinical settings.

MATERIALS AND METHODS

Sampling of Soils

Soil from Park Grass and some sections of Broadbalk have never been exposed to azole fungicides. Soils from other sections of Broadbalk have been annually exposed to single or multiple azole

treatments since 1979. The amounts and identity of azoles used in seed treatments and foliar sprays reflect commercial practices and are recorded each year in the Results of the Classical and other Long-term Field Experiments available via the electronic Rothamsted Archive (http://www.era.rothamsted.ac.uk/eradoc/book). During 2012–2015, prothioconazole was used in seed treatments and three azoles were applied in foliar sprays that were applied as part of a three-spray based disease management programme using mixtures of fungicides belonging to different mode of actions. Epoxiconazole, nine out of 12 applications, was most often used, followed by tebuconazole and prothioconazole, which were used three times together in a spray application. For this study, we sampled soil from plot 3d (permanent pasture, receiving no fertilizers or chalk inputs) on Park Grass and from strips 2.2 (farmyard manure), 3 (no fertilizers), and 8 (144 kg N, 90 kg K, and 12 kg Mg per hectare) on sections 1 (with spring and summer fungicide treatments) and 6 (no fungicide treatments) under continuous winter wheat on Broadbalk (Macdonald et al., 2018). Soils were sampled to a depth of 5 cm using a 3 cm diameter auger at three sampling points, separated five meters apart, in July 2015. Samples of air-dried topsoil (0–23 cm) collected in August 2016 were also available from three replicated plots without straw incorporation (straw removed) and from three replicated plots in which fungicide-exposed straw was incorporated at four times the annual straw yield on the Long-term Amounts of Straw Experiments at Rothamsted and Woburn (Macdonald et al., 2018). These experiments examined the effects of long-term straw incorporation on soil properties and yields of continuous wheat grown on contrasting soils at Rothamsted and Woburn (silty clay loam v sandy loam). They began in 1987 and were stopped after 30 years (Powlson et al., 2011). The azole fungicides used in these experiments, as part of mixtures with other fungicides belonging to different modes of action, during 2013–2016 are listed in **Table 1**. The wheat seeds grown on these experiments were also treated with prothioconazole before drilling. Topsoil to a depth of 5 cm was also sampled from 15 commercial wheat fields in Germany (locations Burscheid, Vechta, Göttingen, Dormagen, and Ergolding), France (Tierce, Obenheim, Grisolles, Lignon, and Reims), and the UK (Kent, Suffolk, Somerset, Norfolk, and Herefordshire). In addition, topsoils representing arable crops, woodland, and grass verges were also sampled from 14 other locations in five countries across Europe (**Table 2**). Each topsoil sample contained three subsamples, each collected at three different sampling points separated at least 5 m apart.

TABLE 1 | The long-term amounts of straw experiments at Rothamsted and Woburn.

Location/foliar azole exposure	Straw incorporation/plot numbers	Frequency pan-azole resistant strains per plot[a]
Rothamsted farm	Nil (straw removed)	
Epoxiconazole (2013, 2014, 2015, 2016)	1	0/7
Prochloraz (2014, 2016)	8	1/18
Prothioconazole (2013, 2015, 2016)	12	0/10
Tebuconazole (2013, 2014, 2015, 2016)	Four times amount of straw	
	3	1/16
	5	0/14
	9	0/19
Woburn farm	Nil (straw removed)	
Epoxiconazole (2013, 2014, 2015, 2016)	19	1/6
Prochloraz (2015)	21	0/8
Prothioconazole (2014, 2015, 2016)	28	1/10
Tebuconazole (2014, 2015, 2016)	Four times amount of straw	
	20	0/5
	23	0/4
	27	0/5

Foliar exposure to azoles and the frequency of pan-azole resistant A. fumigatus isolates in soils sampled in 2016.

[a] *Pan-azole resistant (R) strains have elevated MIC levels for voriconazole (>1.0 μg/ml), imazalil (>2.5 μg/ml), and tebuconazole (>3.0 μg/ml).*

Sampling of Airborne *A. fumigatus* Strains

Airborne spores were captured on untreated or fungicide amended Sabouraud dextrose (SD) agar (Oxoid Ltd, Basingstoke, UK) containing penicillin (100 U/ml) and streptomycin (100 μg/ml) using mobile spin air samplers (IUL, Spain). Each time, 5,000 L of air was sampled during rotating of SD agar plates at 1 rpm for 50 min. Fungicide amended agar plates contained carbendazim (10 μg/ml), pyraclostrobin (10 μg/ml) or tebuconazole (5 μg/ml). Colonies of *A. fumigatus* were recovered from the plates after two days incubation at 48°C.

Isolation of *A. fumigatus* Strains and Inoculum Preparation

To isolate strains belonging to the *A. fumigatus* complex, 2 g aliquots of soil samples were added to 8 ml of phosphate buffered saline amended with 0.1 % (v/v) Tween 20. After 2 h incubation at 37°C with shaking (150 rpm), the supernatant after sedimentation was plated out on SD agar amended with penicillin (100 U/ml) and streptomycin (100 μg/ml). Colonies of *A. fumigatus* were recovered from the plates after 2 days incubation at 48°C. No or low numbers up to 10 colony forming units per g soil were usually detected. After subculturing single colonies in tissue culture flasks with 12 ml SD agar for seven days at 37°C, spores were harvested through shaking with 5 mm glass beads after addition of 3 ml of saline. Final spore suspensions were directly used for storage in 50 % (v/v) glycerol at −80°C, DNA extractions or for fungicide sensitivity testing using spiral plating.

Fungicide Sensitivity Testing Using Spiral Plating

Spore suspensions containing ∼10^6 spores/ml in sterile distilled water were used in the microprocessor controlled Autoplate

TABLE 2 | Soil samples from different geographical regions sampled in 2015 and the frequency of pan-azole resistant *A. fumigatus* strains.

Sample	Location	Soil description	Number of pan-azole resistant strains[a]
SS1	Penzesgyör, Hungary	Wheat field	0/10
SS2	Vönock, Hungary	Sunflower field	0/10
SS3	Vönock, Hungary	Woodland	0/10
SS4	Kenyeri, Hungary	Corn field	0/14
SS5	Kemmelbach, Austria	Grass verge at petrol station	0/12
SS6	Hunderdorf, Germany	Grass verge at petrol station	0/10
SS7	Hösbach, Germany	Ploughed cereal field	0/16
SS8	Waremme, Belgium	Sugar beet field	1/10
SS9	Adinkerke, Belgium	Sugar beet field	0/10
SS10	Afferden, The Netherlands	Corn field	1/12
SS11	Beekbergen, The Netherlands	Forest	0/10
SS12	Boxtel, The Netherlands	Forest	0/10
SS13	Boxtel, The Netherlands	Harrowed sugar beet field	0/10
SS14	Boxtel, The Netherlands	Corn field	0/10

[a] *Pan-azole resistant (R) strains have elevated MIC levels for voriconazole (>1.0 μg/ml), imazalil (>2.5 μg/ml) and tebuconazole (>3.0 μg/ml).*

Spiral Plating System AP5000 (Advanced Biosystems) according to the manufacturer's instructions. This method has been used for antimicrobial susceptibility testing of fastidious bacteria and fungi (Förster et al., 2004; Pong et al., 2010). The test fungicides, solutions made in DMSO, were placed in a sample cup of the spiral plater and automatically plated at exponentially decreasing concentrations achieving. Depending on the molecular weight of the compounds, an up to a 200-fold fungicide dilution gradient on SD agar was achieved using 15 cm plates. The concentration ranges (μg/ml) for the different fungicides were: boscalid (0.1–18.469), carbendazim (0.1–11.464), imazalil (0.25–43.153), itraconazole (0.025–6.113 or 0.1–22.324), pyraclostrobin (0.1–20.120), tebuconazole (0.1–17.349), terbinafine (0.01–1.7), and voriconazole (0.1–19.120). The different concentration ranges were chosen to distinguish sensitive wild-type (wt) isolates without known resistance mechanisms with those of insensitive isolates harboring resistance mechanism in one assay. Isolates were streaked on these spiral SD agar plates (8 per plate) from the outside to the center using cotton swaps and incubated at 37°C in the dark. After 24 h incubation, the fungal growth of each isolate on the spiral plate was visually assessed and the MIC value determined using the Spiral Gradient Endpoint (SGE) software.

DNA Extractions

After harvesting spores from one-week cultures in tissue culture flasks, 1.5 ml of spore suspensions was transferred into a 2 ml tube and centrifuged for 2 min at 13,200 rpm. After removing the supernatant, DNA was extracted according to the MasterPure Yeast DNA Purification kit (Lucigen Corporation) with the inclusion of an extra bead-beating step which involved the addition of glass beads (0.425–0.600 mm) and the use of the Genie 2 Vortex (Scientific Industries) at full power for 2 min. This step was carried out after the lysis step just before adding the MPC Protein Precipitation Reagent.

PCR Amplification and Sequencing

All PCR reactions were carried out using the Easy A cloning Enzyme kit (Agilent Technologies, UK). Typical reactions of 40 μl contained 4.0 μl Easy A cloning buffer (10 x stock), 0.8 μl dNTPs (10 mM stock), 30.4 μl PCR grade water, 0.2 μl of each of primer (100 μM primer stocks) (**Supplementary Table 1**), 0.4 μl Easy A cloning enzyme, and 4.0 μl genomic DNA (40 ng total). PCR cycling started with an initial denaturation of 95°C for 2 min, followed by 40 cycles of denaturation (10 s at 95°C), annealing (20 s at annealing temperature) and extension (depending on amplicon size 1 or 2 min at 72°C), and a final extension (8 or 9 min at 72°C) and hold step at 4°C. All primers and corresponding annealing temperatures are shown in **Supplementary Table 1**. PCR products were visualized by agarose gel electrophoresis to confirm the expected PCR amplicon size, and subsequently sent to MWG Eurofins (UK) for purification and sequencing using the primers used in PCR or with additional primers when needed (**Supplementary Table 1**). Primers used in this study were either reported before or designed based on published *A. fumigatus* sequences for CYP51A (Genbank Accession JX283445), CYP51B (AF338660), beta tubulin (NC_007200; region 70221-71948), cytochrome *b* (JQ346808), and succinate dehydrogenase subunit B (NC_007194.1; region 2654821-2655836), C (NC_007198.1; region 2501949-2502752), and D (NC_007198.1; region 4215045-4215968) covering all regions of the fungicide target encoding genes where mutations affecting inhibitor binding have been reported (Mair et al., 2016). Sequences were analyzed and aligned using Geneious software version 10.0 (Biomatters, New Zealand).

Short Tandem Repeat and Cell Surface Protein Typing

Isolates of *A. fumigatus* with different levels of azole sensitivity were further characterized using microsatellite genotyping based on a panel of nine short tandem repeat markers (STR*Af* 2A, 2B, 2C, 3A, 3B, 3C, 4A, 4B, and 4C) according to the method previously described and validated (De Valk et al., 2005; De Groot and Meis, 2019). In addition, the cell surface protein (CSP) (XM_749624.1) encoding gene of *A. fumigatus* was also partially sequenced from selected strains (Balajee et al., 2007). CSP typing of strains was carried out according to the nomenclature proposed by Klaassen et al. (2009),

which is based on the tandem repeat region, in which up to 10 different 12-bp repeat sequences have been found in different copy numbers, and the flanking regions. After manual alignment of sequences, a phylogenetic tree for the different CSP sequences encountered in this study was constructed using the Geneious Tree Builder software (Biomatters, New Zealand) based on the Tamura-Nei distance model and the Neighbor-Joining method.

RESULTS

Isolation and Fungicide Sensitivity Testing of *A. fumigatus* Isolates From the Broadbalk and Park Grass Long-Term Experiments

A total of 180 *A. fumigatus* strains were isolated from soils taken from selected plots on the Broadbalk Wheat Experiment, at Rothamsted (Harpenden, Hertfordshire, UK) (Macdonald et al., 2018). Soils were sampled from plots receiving three different fertilizer/manure treatments [plots 2.2 (farm-yard manure), 3 (nil fertilizers), and 8 (mineral fertilizers)] within each of two sections under continuous winter wheat, grown with (section 1) and without (section 6) spring or summer fungicides, but including fungicide seed treatments. In addition, 30 strains were isolated from soils taken from the Park Grass Continuous Hay Experiment (permanent grass land, plot 3d - no liming and fertilizers) at Rothamsted (Macdonald et al., 2018). MIC testing using spiral plating showed for the wild-type (WT-NL), TR_{34}/L98H (TR34-NL), and TR_{46}/Y121F/T289A (TR46-NL) reference strains the following average values in μg/ml: 0.338, 0.180, and 0.286 for terbinafine, 1.056, >6.113, and >6.113 for itraconazole, 0.342, 1.505, and >19.120 for voriconazole, 0.978, 3.156, and >43.153 for imazalil, 0.829, 6.876, and >17.349 for tebuconazole, and 1.029, 1.048, and >11.464 for carbendazim, respectively. High levels of resistance to all four azoles and, unexpectedly, carbendazim were measured for the reference strain TR46-NL. Except for itraconazole, strain TR34-NL showed more moderate levels of resistance to azoles in comparison with strains WT-NL and TR46-NL, but similar levels of sensitivity to terbinafine were recorded in all reference strains. The Broadbalk and Park Grass isolates showed no significant differences in the sensitivity levels between the six different populations tested, with most isolates showing similar levels of control as the wild-type reference strain in typical dose-response curves (**Figure 1**). The dynamic range was 0.092 – 0.53, 0.059 – 4.757, 0.1 – 0.965, <0.249 – 1.622, 0.198 – 3.341, and 0.433 – 1.453 μg/ml for terbinafine, itraconazole, voriconazole, imazalil, tebuconazole and carbendazim, respectively. Only two strains, sampled from section 1 plot 3 (isolate BB1-3-B9) and section 6 plot 8 (isolate BB6-8-C7) showed resistance to itraconazole (MICs >6.113 μg/ml) and tebuconazole (MICs of 4.227 and 4.755 μg/ml) but not to voriconazole (MICs of 0.675 and 0.418 μg/ml) and imazalil (MICs of 1.015 and 0.714 μg/ml) in the first screen.

Isolation and Fungicide Sensitivity Testing of *A. fumigatus* Isolates From the Long-Term Amounts of Straw Experiments at Rothamsted and Woburn

In total 84 strains were isolated from the wheat straw incorporation experiment at Rothamsted, 35 came from three control plots (plots 1, 8, and 12) and 49 from three plots where straw was incorporated (plots 3, 5, and 9) (**Table 1**). The soils sampled at the Woburn Experimental Farm (Woburn, Bedfordshire) contained less strains and only 24 and 14 strains were isolated from untreated (plots 19, 21, and 28) and straw incorporated plots (20, 23, and 27), respectively (**Table 1**). Fungicide sensitivity was carried out as before except itraconazole, for which a higher spiral plate concentration range of 0.1–22.324 μg/ml was used in subsequent studies. The sensitivity profiles were similar for all populations tested showing no differences between untreated and straw incorporated plots (**Figure 2**). A significant number of isolates, 18 out of 122 tested, were highly resistant to itraconazole with MIC values >10 μg/ml. Only four isolates, three from untreated plots (two at Woburn and one from Rothamsted), and one from a straw incorporated plot at Rothamsted, showed moderate to high levels of resistance to voriconazole, imazalil, and tebuconazole using cut-off MIC values of 1.0, 2.5, and 3.0 μg/ml, respectively. Three of these isolates, RS3-3, WN19-3, and WN28-6, showing the highest MIC for all four azoles tested (all out of range), were also highly resistant to carbendazim with MIC values >11.464 μg/ml, which is similar to the profile of the TR_{46}/Y121F/T289A reference strain. A lower level of azole resistance was measured for the carbendazim sensitive isolate RN18-8 which has a similar sensitivity profile to the TR_{34}/L98H reference strain. All strains tested were sensitive to terbinafine, with MIC values between 0.041 and 0.322 μg/ml.

Isolation and Fungicide Sensitivity Testing of *A. fumigatus* Isolates From Soils of Commercial Wheat Fields in Germany, France, and the UK

In total 428 strains were isolated, of which 149, 139 and 140 came from Germany (locations Burscheid, Vechta, Göttingen, Dormagen, and Ergolding) France (Tierce, Obenheim, Grisolles, Lignon, and Reims) and the UK (Kent, Suffolk, Somerset, Norfolk, and Herefordshire), respectively. Thirty strains were isolated from all locations with exception of Ergolding (29), Grisolles (29), Reims (10 because subsamples were pooled), and Suffolk (20, only two subsamples available). The fungicide sensitivity profiles of the populations were similar for all locations tested (**Figure 3**). All strains were sensitive to terbinafine having MIC values between 0.082 and 0.669 μg/ml. A high number of isolates, 12 from Germany, 25 from France and 11 from the UK, showed MIC values >10 μg/ml for itraconazole. Only a few strains showed low levels of resistance to voriconazole, imazalil and tebuconazole using cut-off MIC values of 1.0, 2.5, and 3.0 μg/ml, respectively. Regarding voriconazole, only two

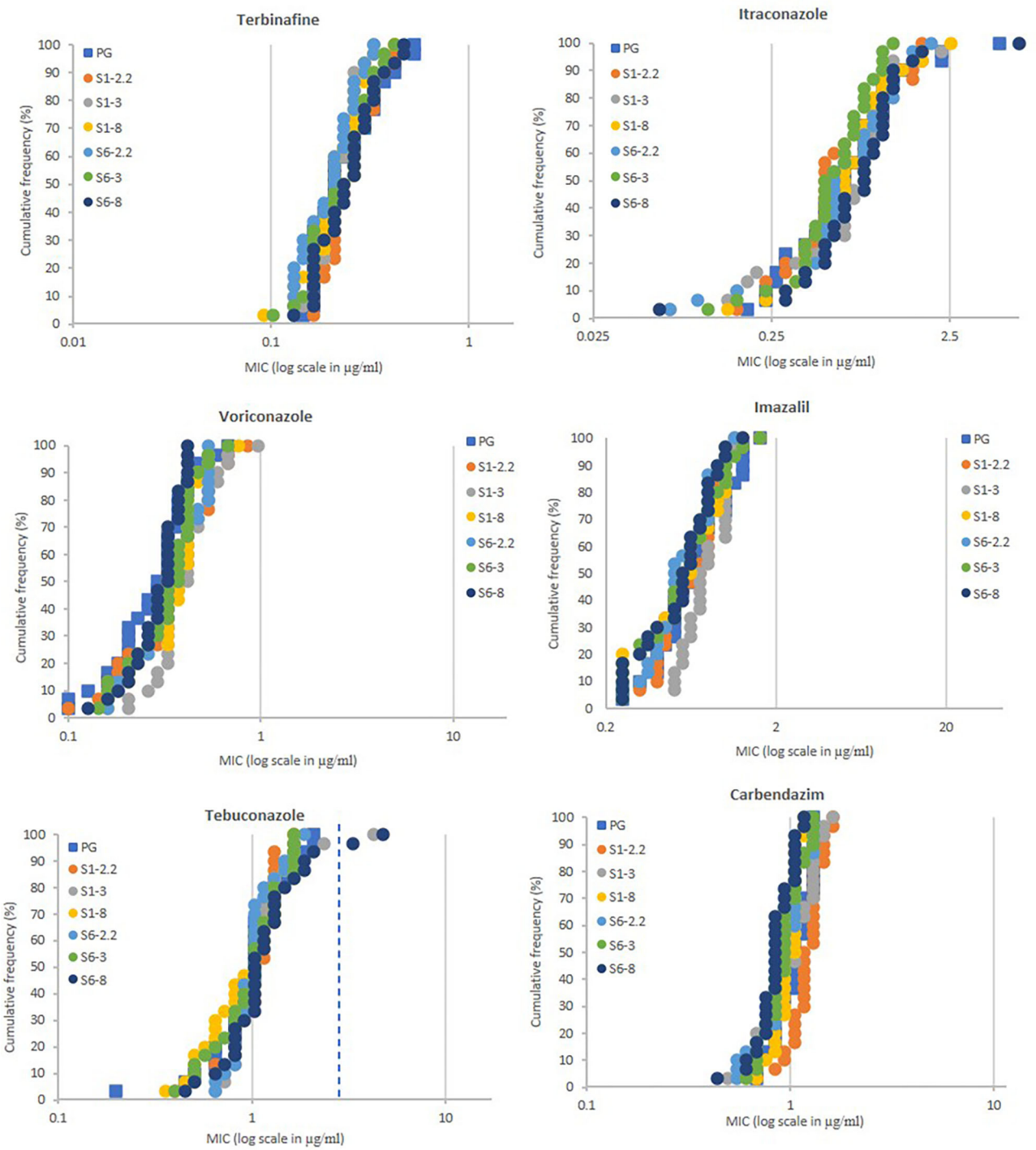

FIGURE 1 | Azole sensitivity profiling of *A. fumigatus* populations (each $n = 30$) sampled from soils of the Broadbalk (continuous wheat) and Park Grass (permanent grass land) long-term experiments at Rothamsted. MIC values of individual isolates (X-axis in µg/ml) are plotted against the proportion of the population (Y-axis in %). PG, Park Grass, S1 (section 1 with fungicides at Broadbalk), S6 (section 6 without fungicides at Broadbalk) with treatments 2.2 (farmyard manure), 3 (untreated) and 8 (standard fertilizers). MIC values (ppm) for highly resistant isolates to itraconazole (>6.113) and sensitive to voriconazole (<0.1) and imazalil (<0.25) are displayed as 6.113, 0.1, and 0.25, respectively. Extra dotted line for tebuconazole shows cut-off value of 3.0 ppm.

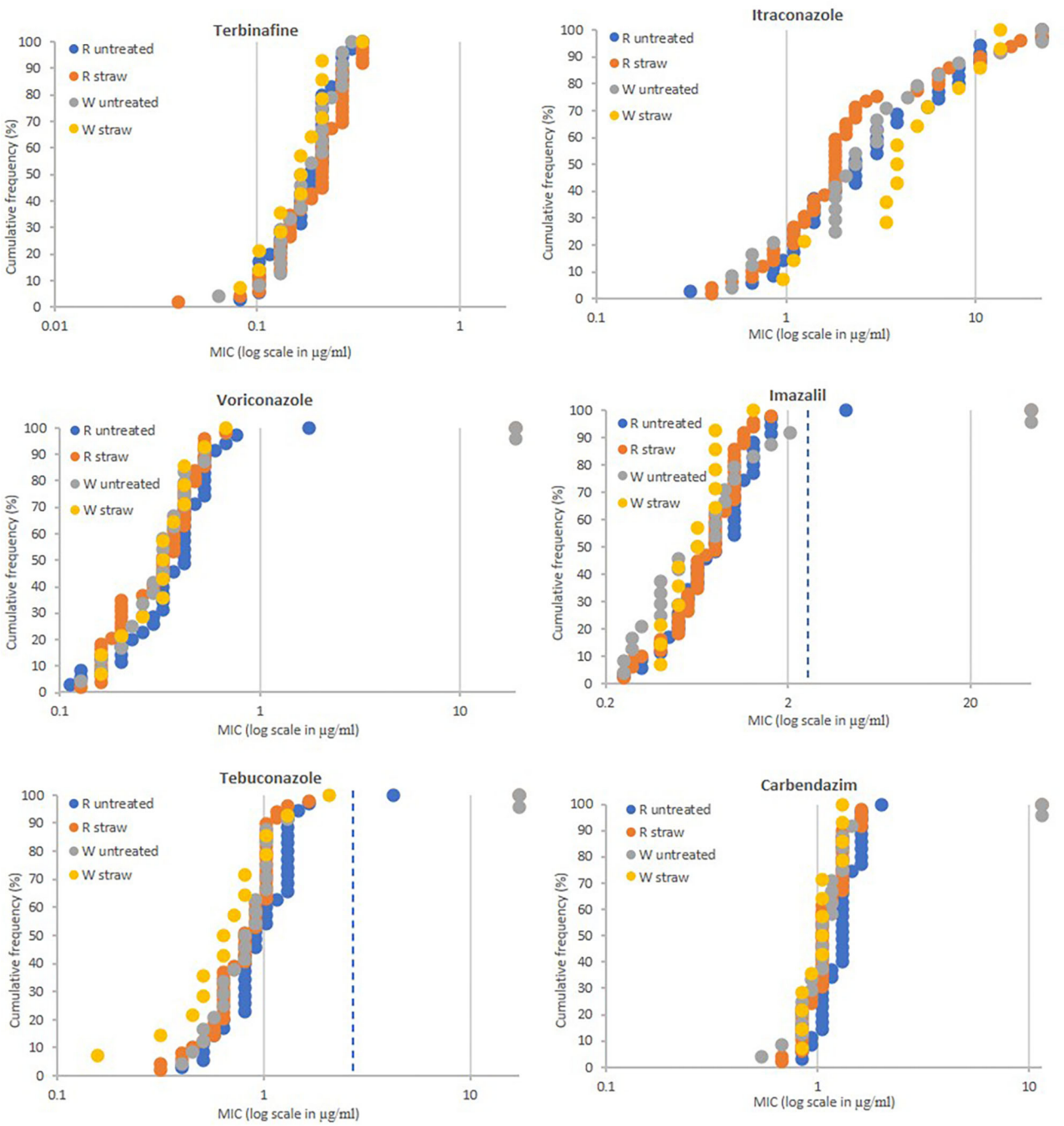

FIGURE 2 | Fungicide sensitivity profiling of *A. fumigatus* populations sampled from soils of the Long-term Amounts of Straw Experiments at the Rothamsted ($n = 84$) and Woburn farms ($n = 38$). MIC values of individual isolates (X-axis in ppm) are plotted against the proportion of the population (Y-axis in %). Populations from Rothamsted (R) with straw incorporation (straw) ($n = 49$) and without straw (untreated) ($n = 35$) and Woburn (W) with straw incorporation (straw) ($n = 14$) and without straw (untreated) ($n = 24$). MIC values (µg/ml) for highly resistant isolates to itraconazole (>22.324), voriconazole (>19.120), imazalil (>43.153), tebuconazole (>17.349), and carbendazim (>11.464), and sensitive to imazalil (<0.25) are displayed as 22.324, 19.120, 43.153, 17.349, 11.464, and 0.25, respectively. Extra dotted line for imazalil and tebuconazole show cut-off values of 2.5 and 3.0 ppm, respectively.

strains from Germany (G1-A1 and G1-A9 from Burscheid) and two from France (F1-C5 from Tierce and F5-B5 from Reims) showed low resistance levels with MICs between 1.0 and 2.0 µg/ml. Two, three and four strains from Germany, France and the UK, respectively, were moderately resistant to imazalil with MICs between 2.5 and 5.0 µg/ml. One, five and

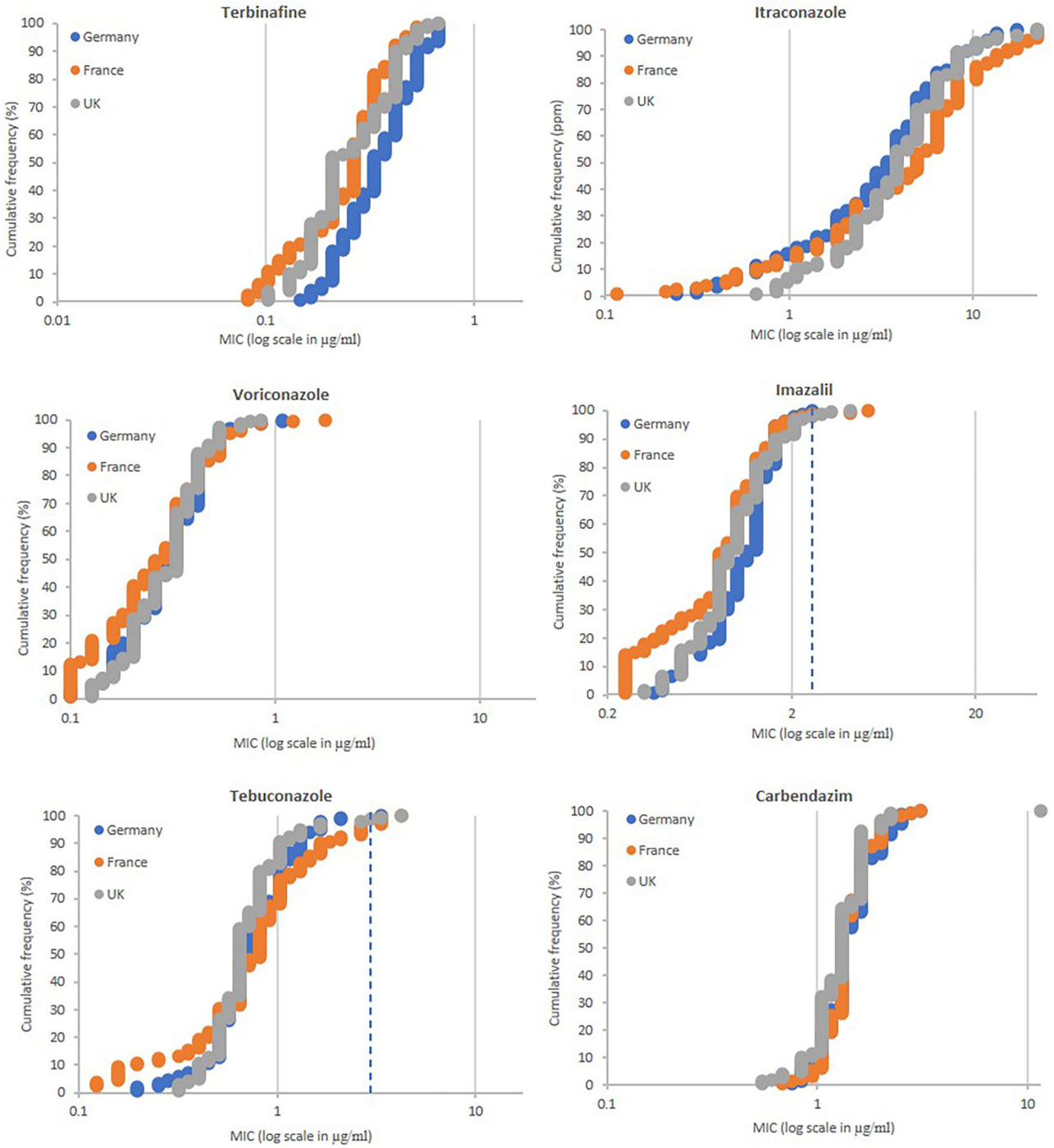

FIGURE 3 | Fungicide sensitivity profiling of *A. fumigatus* populations sampled from soils of commerial wheat fields in Germany ($n = 149$), France ($n = 129$), and the UK ($n = 140$). MIC values of individual isolates (X-axis in ppm) are plotted against the proportion of the population (Y-axis in %). MIC values (ppm) for highly resistant isolates to itraconazole (>22.324) and carbendazim (>11.464) are displayed as 22.324 and 11.464, respectively. MIC values (µg/ml) for highly resistant isolates to itraconazole (>22.324), voriconazole (>19.120), imazalil (>43.153), tebuconazole (>17.349), and carbendazim (>11.464), and sensitive to voriconazole (<0.1) and imazalil (<0.25) are displayed as 22.324, 19.120, 43.153, 17.349, 11.464, 0.1, and 0.25, respectively. Extra dotted line for imazalil and tebuconazole show cut-off values of 2.5 and 3.0 ppm, respectively.

two strains from Germany, France and the UK, respectively, were moderately resistant for tebuconazole with MICs between 3.0 and 6.0 µg/ml. None of the strains tested were resistant to all four azoles tested, but isolates UK5-B5 (Herefordshire, UK) and F1-C5 (Tierce, France), both highly resistant to itraconazole (MIC >22.324 µg/ml) were the only strains showing

resistance to two out of the three other azoles tested. UK5-B5 was the only strain with resistance to carbendazim (MIC >11.464 μg/ml).

Isolation and Fungicide Sensitivity Testing of *A. fumigatus* Isolates From Soils at Different Locations in Europe

Strains of *A. fumigatus* were isolated from soils sampled at 14 different locations in the Netherlands, Belgium, Germany, Austria and Hungary (**Table 2**). Ten or more strains per sample (154 strains in total) were further tested for sensitivity to terbinafine, itraconazole, voriconazole, imazalil, tebuconazole, and carbendazim (data not shown). All isolates were sensitive to terbinafine and carbendazim. Ten strains from locations in Hungary (Kenyeri), Austria (Kemmelbach), Germany (Hösbach), Belgium (Waremme), and the Netherlands (Afferden) showed itraconazole MICs >10.0 μg/ml, but only two of those strains, SS8-7 from a sugar beet field near Waremme in Belgium, and SS10-6 from a corn field near Afferden in the Netherlands, showed voriconazole MICs >1.0 μg/ml and were also less sensitive to imazalil and tebuconazole with MICs just above 2.5 and 3.0 μg/ml, respectively. Two strains from a sugar beet field near Adinkerke (Belgium) showed only a slightly raised MIC value of 3.341 μg/ml for tebuconazole. All other strains were sensitive to all azoles tested.

Isolation and Fungicide Sensitivity Testing of *A. fumigatus* Isolates From Aerosols

During 11–14 February 2018, 26–29 May 2018, and 17–20 May 2019, airborne spores were captured in Boskoop (the Netherlands), Boxtel (the Netherlands), or Harpenden (UK) on untreated and fungicide amended Sabouraud dextrose agar plates from air volumes of 5,000 L using mobile spin air samplers (IUL, Spain). Assuming an adult air intake of 14,000 L, the daily exposure to *A. fumigatus* varied between 14 and 193 conidia in Boskoop under cold and wet conditions in the afternoon on 11 February 2018 and in Boxtel during the evening on 20 February 2019, respectively. Only a few colonies were growing fast on tebuconazole amended plates on several occasions, which was compared to the recorded colony numbers on untreated plates equivalent to frequencies of up to 4%.

Five isolates, captured on carbendazim amended agar in Boxtel (BTCa-1) and Boskoop (BKCb-1), tebuconazole amended agar in Boxtel (BTTa-1) and pyraclostrobin amended agar in Harpenden (HPPb-1 and HPPb-2) in February 2018 were further tested for fungicide sensitivity. All five were highly resistant to both carbendazim and pyraclostrobin with MICs >11.464 and >20.120 μg/ml, respectively. BTTe-1 and BKCb1 were also highly resistant to imazalil (MIC >43.153 μg/ml), voriconazole (MIC >19.120 μg/ml), and tebuconazole (MIC >17.349 μg/ml), similar to the profile of the TR_{46}/Y121F/T289A reference strain. BTCa-1, HPPb-1, and HPPb-2 showed low to moderate levels of resistance to two or more of the azoles tested. All strains tested were sensitive to terbinafine with MICs between 0.116 and 0.595 μg/ml.

Cell Surface Protein Typing of *A. fumigatus* Strains Isolated From the Long-Term Broadbalk and Park Grass Experiments

A selection of isolates, 58 in total, was further characterized using cell surface protein (CSP) PCR amplicon sequencing (see primers in **Supplementary Table 1**). **Figure 4** shows the relatedness amongst the different CSP types identified in this study. Of the 57 strains tested, 14 belonged to CSP type t03, 11–t04A, 9–t18A, but they all came exclusively from a farm yard manure treated plot, 8–t02, 7–t01, 4–t05, 2–t06A, 2–t11, and one each to t08, t19 and a new CSP type. The new CSP type was named as t02* because the same tandem repeat succession as type t02 was found, but with changes in the flanking regions of the tandem repeat region at codon−14 (*C*TC instead of GTC), +1 (CC*G* instead of CCA), and +3 (CCT duplication) (Kidd et al., 2009). The itraconazole insensitive Broadbalk strains BB1-3-B9 and BB6-8-C7 belonged to CSP t02* and t19, respectively. When additional itraconazole insensitive isolates from commercial wheat fields in Germany, France and the UK were tested, a high proportion belonged to CSP t08, followed by t13, t15, t19, t02*, and t07 (data not shown). All these CSP types cluster together and have also a SNP at codon−55 of the flanking region (TG*T* instead of TGC) in common (**Figure 4**).

Azole Resistance Phenotype-to-Genotype Relationship of Isolates

A selection of 30 azole insensitive and sensitive isolates, including six older reference strains, were further characterized using an additional genotyping assays and phenotyping screens (**Tables 3**, **4**). Cross-resistance was observed for all four azoles tested, especially between voriconazole, tebuconazole and imazalil (**Table 4**). For itraconazole, two strains (BTTa-1 and BKCb-1) highly insensitive for voriconazole, tebuconazole and imazalil showed only moderate levels of insensitivity to itraconazole, whereas several strains sensitive or moderately insensitive to voriconazole, tebuconazole, and imazalil (e.g., UK2-B4 and G1-A9) were highly insensitive to itraconazole. CYP51A sequencing showed a clear pheno-to-genotype trend, with TR_{46}/Y121F/T289A, TR_{46}/Y121F/M172V/T289A/G448S, and TR_{46}/Y121F/T289A/S363P/I364V/G448S isolates showing high levels of insensitivity to imazalil, voriconazole and tebuconazole (**Table 4**). Mutations leading to S363P (serine (TCT) replaced by proline (*C*CT) at codon 363) and I364V (isoleucine (ATT) replaced by valine (*G*TT) at codon 364) have not been reported before (see GenBank MW119308). Lower levels of insensitivity were measured for TR_{34}/L98H strains, while some strains carrying F46Y/M172V/E427K showed insensitivity to tebuconazole and/or itraconazole with MIC values >3.0 and 10 μg/ml, respectively. D262Y was the only mutation found in sensitive strains. CYP51B sequencing of isolates BB1-3-B9, RN8-18, RS3-3, and WN19-9 revealed no mutations.

Resistance to MBC, QoI, and SDHI Fungicides

Insensitivity to carbendazim, pyraclostrobin and boscalid was also measured in a proportion of isolates (**Table 4**). All six

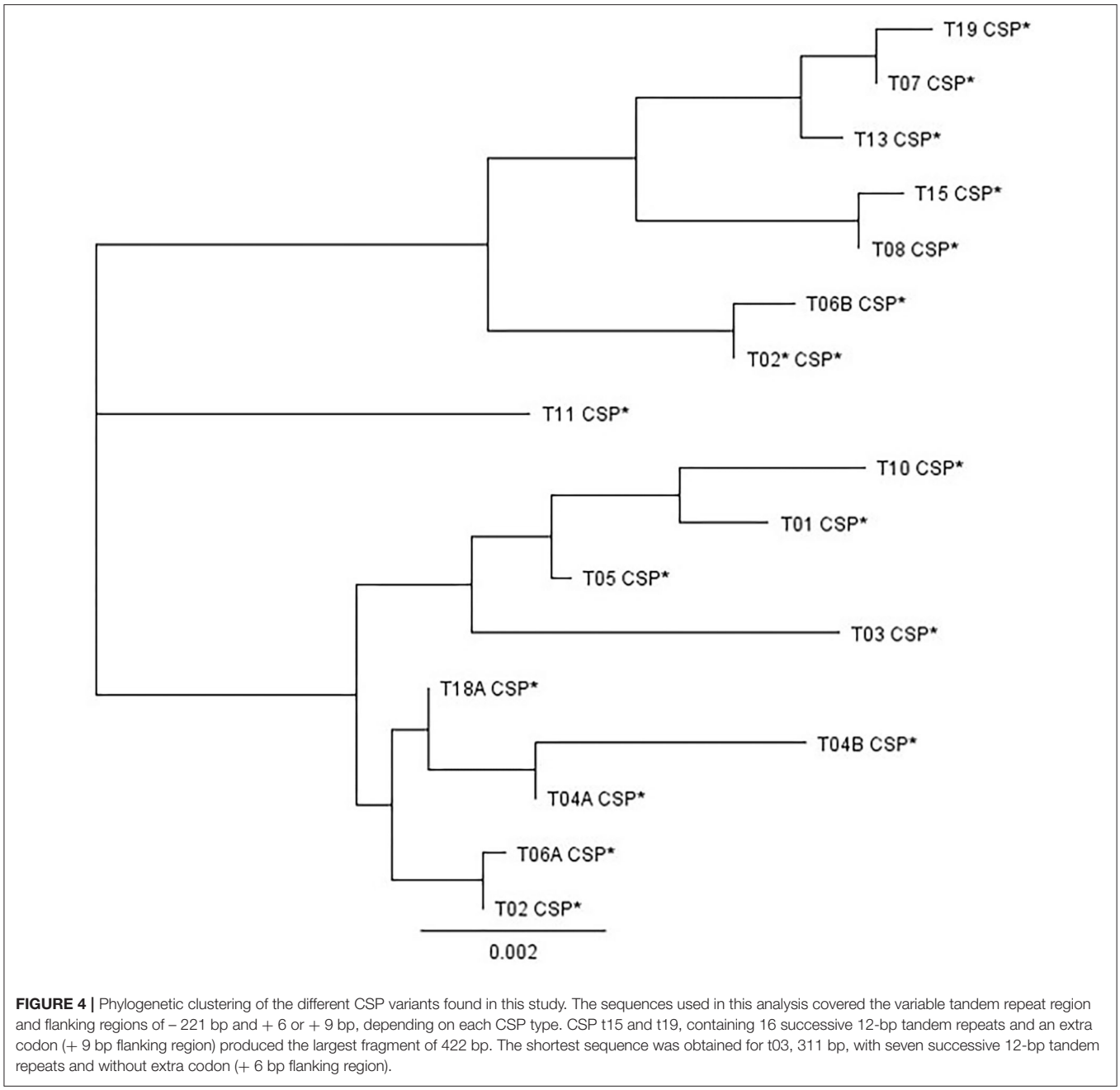

FIGURE 4 | Phylogenetic clustering of the different CSP variants found in this study. The sequences used in this analysis covered the variable tandem repeat region and flanking regions of – 221 bp and + 6 or + 9 bp, depending on each CSP type. CSP t15 and t19, containing 16 successive 12-bp tandem repeats and an extra codon (+ 9 bp flanking region) produced the largest fragment of 422 bp. The shortest sequence was obtained for t03, 311 bp, with seven successive 12-bp tandem repeats and without extra codon (+ 6 bp flanking region).

TR_{46} strains (TR46-NL included) were highly resistant to the MBC fungicide carbendazim (MIC > 11.464 μg/ml), with five of them also resistant to the QoI fungicide pyraclostrobin (MIC > 11.464 μg/ml). Two of these strains, BKCb-1 and WN19-3, were also moderately or highly resistant to the SDHI fungicide boscalid with MIC values of 5.606 and >18.469 μg/ml, respectively. Carbendazim, pyraclostrobin and boscalid resistance was also detected in several TR_{34} isolates but not in wild-type and F46Y/M172V/E427K isolates. Cytochrome *b* gene sequence analysis (MW119309 and MW119310) showed the presence of a mutation leading to the replacement of glycine (GGT) by alanine (GCT) at codon 143 (G143A) of the protein in five pyraclostrobin resistant strains tested (UK5-B5, HPPb-1, BTTa-1, RS3-3, and WN19-3), all showing MICs >20.120 μg/ml. G143A was not detected in two pyraclostrobin sensitive strains (RN8-18 and 08-19-02-10) with MICs of 0.423 and 1.110 μg/ml, respectively. Six carbendazim resistant isolates tested (HPPb-1, BTTa-1, BKCb-1, RS3-3, WN19-3, and WN28-6), all with MICs >11.464 μg/ml, carried a mutation that resulted in the replacement of phenylalanine (TTC) by tyrosine (TAC) at codon 200 (F200Y) of beta-tubulin (MW119311 and MW119312). No target site alterations were found in the sequence of the

TABLE 3 | Origin and characterization of *Aspergillus fumigatus* isolates using CYP51A sequencing, CSP typing, and STR*Af* profiling.

Isolate[a]	Origin/year	CYP51A	CSP	STR*Af* marker profile								
				2A	2B	2C	3A	3B	3C	4A	4B	4C
WT-NL	Netherlands, before 2014	Wt	t01	-	-	-	-	-	-	-	-	-
PG3-3	UK, 2015	Wt	t01	27	18	15	8	11	31	26	10	8
AF65	UK, 1997	Wt	t02	14	20	12	35	9	10	8	10	21
PG2-10	UK, 2015	Wt	t04B	18	12	8	27	10	18	9	9	5
BB1-2.2-B1	UK, 2015	Wt	t18A	13	21	11	31	27	8	10	9	8
BB6-8-B1	UK, 2015	D262Y	t03	20	19	8	36	14	22	9	9	5
SS5-2A	Austria, 2015	D262Y	t05	18	12	9	10	10	12	8	10	7
PG2-6	UK, 2015	D262Y	t05	15	20	9	10	10	6	8	10	10
BB1-3-B9	UK, 2015	F46Y/M172V/E427K	t02*	10	14	10	17	13	8	7	5	6
G1-A9	Germany, 2016	F46Y/M172V/E427K	t02*	10	14	10	17	13	8	7	5	6
SS5-7C	Austria, 2016	F46Y/M172V/E427K	t08	10	16	10	17	13	20	7	5	6
UK2-B4	UK, 2016	F46Y/M172V/E427K	t08	10	15	10	26	11	8	7	5	5
F5-C6	France, 2016	F46Y/M172V/E427K	t15	10	14	10	17	13	13.1	7	5	5
BB6-8-C7	UK, 2015	F46Y/M172V/E427K	t19	10	15	10	19	12	12	7	5	6
AF293	UK, 1993	F46Y/M172V/N284T/ D255E/E427K	t06A	26	18	18	46	21	23	11	10	8
TR34-NL	Netherlands, before 2014	TR_{34}/L98H	-	-	-	-	-	-	-	-	-	-
UK5-B5	UK, 2016	TR_{34}/L98H	t02	14	20	8	31	9	10	8	10	11
BTCa-1	Netherlands, 2018	TR_{34}/L98H	t02	-	-	-	-	-	-	-	-	-
HPPb-1	UK, 2018	TR_{34}/L98H	t02	25	20	18	31	9	10	10	14	5
08-19-02-10	Netherlands, 2008	TR_{34}/L98H	t04B	25	24	12	84	9	9	8	10	11
RN8-18	UK, 2016	TR_{34}/L98H	t04B	25	24	12	84	9	9	8	10	11
SS10-6A	Netherlands, 2016	TR_{34}/L98H	t11	20	21	16	16	12	7	16 3	24	33
SS8-7A	Belgium, 2016	TR_{34}/L98H	t11	20	21	16	77	12	11	16 3	11	21
F1-C5	France, 2016	TR_{34}/L98H	t11	-	-	-	-	-	-	-	-	-
BTTa-1	Netherlands, 2018	TR_{46}/Y121F/M172I/ T289A/G448S	t01	26	21	12	26	10	6	13	9	20
TR46-NL	Netherlands, before 2014	TR_{46}/Y121F/T289A	-	-	-	-	-	-	-	-	-	-
WN19-3	UK, 2016	TR_{46}/Y121F/T289A	t01	10	19	12	45	9	50	8	10	10
WN28-6	UK, 2016	TR_{46}/Y121F/T289A	t01	20	20	14	49	9	36	8	9	9
RS3-3	UK, 2016	TR_{46}/Y121F/T289A	t02	10	20	8	42	9	10	12	10	20
BKCb-1	Netherlands, 2018	TR_{46}/Y121F/T289A/ S363P/I364V/G448S	t01	26	20	12	43	11	11	12	9	9

Isolates grouped according to CYP51A sequence and CSP type.
[a]*AF65 and AF293 are clinical isolates; -, unknown or not determined.*

carbendazim sensitive strain RN8-18 with a MIC of 1.048 μg/ml. Only three out of 20 strains further characterized were insensitive to boscalid. Two strains, UK5-B5 and WN19-3, showed high levels of resistance with MICs >18.469 μg/ml, while strain BKCb-1 with a MIC of 5.606 μg/ml was moderately resistant. Sequencing the SdhB, C and D encoding genes from a boscalid sensitive (RN8-18), moderate resistant (BKCb-1) and highly resistant strain (WN19-3) revealed two different *SdhB* mutations causing alterations at codon 270 of the protein (MW119305, MW119306, and MW119307). SdhB alteration H270Y, histidine (CAC) replaced by tyrosine (*T*AC) was found in WN19-3, while H270R, histidine (CAC) replaced by arginine (C*G*C) was identified in BKCb-1.

Molecular Characterization of *A. fumigatus* Isolates Using CSP and STR*Af* Typing

CSP typing showed a high level of diversity among the selected isolates (**Table 3**). Four CSP types, t02*, t08, t15, and t19, were detected in F46Y/M172V/E427K strains. In addition to these, we also found additional F46Y/M172V/E427K strains with CSP t07 or t13 as part of this study (data not shown). All these six CSP types are closely related (**Figure 4**). STR*Af* profiling showed that several markers were conserved (2A, 2C, 4A, and 4B) in all six F46Y/M172V/E427K strains that were further characterized (**Table 3**). CSP types t02, t04B, and t11 were detected in TR_{34}/L98H strains and t01 and t02 in TR_{46}/Y121F/T289A strains. The CSP types detected in

TABLE 4 | CYP51A variants and sensitivity (MIC values in μg/ml) *of Aspergillus fumigatus* isolates to a panel of fungicides belonging to different modes of action.

Isolate	Origin	IMA	VRC	TEB	ITC	TRB	CAR	PYR	BOS
BB6-8-B1	D262Y	0.249	0.127	0.572	1.602	0.165	0.843	0.477	-
SS5-2A	D262Y	0.398	0.531	0.318	0.666	0.295	1.619	0.375	0.199
BB1-2.2-B1	Wt	0.398	0.181	0.814	0.301	0.185	1.048	1.110	0.407
PG2-6	D262Y	0.447	0.230	0.198	0.266	0.165	0.843	0.423	-
WT-NL	Wt	0.978	0.342	0.829	1.056	0.338	1.029	2.291	0.321
PG3-3	Wt	1.015	0.531	0.814	0.518	0.332	1.303	1.799	0.517
AF65	Wt	1.141	0.329	0.814	1.413	0.332	1.619	1.413	0.157
PG2-10	Wt	1.283	0.161	2.086	2.241	0.419	1.303	-	-
BB1-3-B9	F46Y/M172V/E427K	1.283	0.857	4.227	10.517	0.263	1.619	1.110	0.321
SS5-7C	F46Y/M172V/E427K	1.620	0.418	1.649	3.401	0.263	1.619	1.413	-
BB6-8-C7	F46Y/M172V/E427K	1.622	0.531	1.466	3.856	0.295	0.609	1.413	-
G1-A9	F46Y/M172V/E427K	1.622	1.088	3.341	17.371	0.332	1.303	1.799	-
UK2-B4	F46Y/M172V/E427K	1.824	0.329	2.970	>22.324	0.471	1.169	0.984	0.407
F5-C6	F46Y/M172V/E427K	2.306	0.531	2.086	8.184	0.419	1.619	1.799	-
AF293	F46Y/M172V/N284T/D255E/E427K	2.915	0.531	1.649	13.516	0.419	1.303	0.538	-
SS10-6A	TR_{34}/L98H	2.915	1.381	4.227	>22.324	0.208	1.303	0.231	0.321
SS8-7A	TR_{34}/L98H	2.915	2.227	5.348	>22.324	0.208	1.303	2.291	0.407
TR34-NL	TR_{34}/L98H	3.156	1.505	6.876	7.219	0.180	1.048	0.872	0.224
08-19-02-10	TR_{34}/L98H	3.277	1.754	5.348	>22.324	0.208	1.619	1.110	0.407
F1-C5	TR_{34}/L98H	4.142	1.754	2.640	>22.324	0.332	1.619	0.984	0.199
UK5-B5	TR_{34}/L98H	4.142	1.754	4.227	>22.324	0.295	>11.464	>20.120	>18.469
RN8-18	TR_{34}/L98H	4.142	1.754	4.227	>22.324	0.103	1.048	0.423	0.407
BTCa-1	TR_{34}/L98H	5.236	0.857	3.341	4.955	0.595	>11.464	>20.120	-
HPPb-1	TR_{34}/L98H	5.236	3.591	5.348	>22.324	0.165	>11.464	>20.120	-
BTTa-1	TR_{46}/Y121F/M172I/T289A/G448S	>43.153	>19.120	>17.349	3.000	0.263	>11.464	>20.120	0.199
BKCb-1	TR_{46}/Y121F/T289A/S363P/I364V/G448S	>43.153	>19.120	>17.349	1.100	0.116	>11.464	>20.120	5.606
TR46-NL	TR_{46}/Y121F/T289A	>43.153	>19.120	>17.349	>22.324	0.286	>11.464	>20.120	0.407
RS3-3	TR_{46}/Y121F/T289A	>43.153	>19.120	>17.349	>22.324	0.185	>11.464	>20.120	0.253
WN19-3	TR_{46}/Y121F/T289A	>43.153	>19.120	>17.349	>22.324	0.263	>11.464	>20.120	>18.469
WN28-6	TR_{46}/Y121F/T289A	>43.153	>19.120	>17.349	>22.324	0.208	>11.464	0.685	0.157

Isolates ranked according to imazalil sensitivity (low to high MIC values).

IMA (imazalil), VRC (voriconazole), TEB (tebuconazole) and ITC (itraconazole) are azoles, inhibiting 14α-demethylase (sterol biosynthesis); TRB (terbinafine) inhibits squalene-oxidase (sterol biosynthesis); CAR (carbendazim) is a MBC fungicide, inhibiting β-tubulin assembly (cytoskeleton); PYR (pyraclostrobin) is a QoI fungicide, inhibiting respiration (complex III); BOS (boscalid) is a SDHI fungicide, inhibiting respiration (complex II); -, not determined.

the TR_{34}/L98H and TR_{46}/Y121F/T289A strains are different from those detected in F46Y/M172V/E427K strains and cluster together in one or two different groups with t11 separated (**Figure 4**). Two pairs of strains with identical CYP51A, CSP type, and STR*Af* profile were detected. BB-1-3-B9 and G1-A9 having F46Y/M172V/E427K, CSP t02* and STR*Af* profile [10-14-10-17-13-8-7-5-6] in common, as well as mating type MAT1-1. TR_{34}/L98H strains 08-19-02-10 and RN8-18 have STR*Af* profile [25-24-12-84-9-9-8-10-11] and have also CSP t04B and mating type MAT1-2 in common. TR_{34}/L98H strains SS10-6 and SSB8-7 carry both CSP t11 and have five out of nine STR*Af* markers identical.

DISCUSSION

Flower bulb waste, green waste and wood chippings have recently been reported as "hotspots" for azole resistance selection in the Netherlands but more information on other hotspots will be needed to reduce the further selection and spread of fungicide resistant alleles. The aim of this study was to investigate if fungicide applications on cereals can be regarded as a hotspot for azole resistance selection.

None of the 180 strains isolated from soil samples at Broadbalk, taken from either untreated wheat crops ($n = 90$) or from plots sprayed with foliar fungicides ($n = 90$), tested positive for pan-azole resistant TR_{34}- or TR_{46}-based CYP51A variants. Pan-azole resistant strains were also not detected amongst the 30 strains isolated from Park Grass experiment (permanent grass land). Furthermore, only two out of 418 strains (0.5 %) isolated from soils sampled from commercial wheat fields in France, Germany and the UK were pan-azole resistant. Both strains, one from France (F1-C5) and one from the UK (UK5-B5), carried TR_{34}/L98H (**Table 3**). Straw incorporation did not increase the incidence of pan-azole resistant strains in soil samples taken

from winter wheat experiments carried out in Harpenden and Woburn (UK). Three strains [one TR_{34}/L98H (RN8-18) and two TR_{46}/Y121F/T289A (WN19-3 and WN28-6)] out of 59 isolates (5.1%) were detected in soils from fungicide treated plots without straw incorporation, while only one TR_{46}/Y121F/T289A strain (RS3-3) out of 63 isolates (1.6%) was found in soils of fungicide treated plots with straw incorporation. Only two out of 154 strains (1.3%) sampled from grassland, forest and other arable crop soils in different European countries were pan-azole resistant. Both isolates, one from a Dutch corn field (SS10-6A) and one from a sugar beet field in Belgium (SS8-7A), carried TR_{34}/L98H. Low frequencies of pan-azole resistant strains between 0 and 4.0% were found in air samples obtained at different urban locations in the Netherlands and the UK. This low background level of pan-azole resistant isolates in air samples is similar to the frequencies of resistant isolates found in soil samples of wheat crops but much lower than the frequencies reported for azole-containing flower bulb waste heaps (6.2–24.5%), where high numbers of spores are present and can be released into the air (Schoustra et al., 2019). We also did not detect an impact of long-term azole-based foliar fungicide applications on the selection of resistant strains in the Broadbalk experiment, comparing treated with untreated plots, and conclude that cereal production is not a hotspot for azole resistance development in *A. fumigatus* as predicted by Gisi (2014).

In addition to wild-type, five different CYP51A variants were found in this study. Regarding azole sensitivity, variant D262Y was equally or less sensitive to azoles in comparison with wild-type isolates. Except itraconazole, for which different resistance mechanisms have been reported, TR_{46}/Y121F/T289A isolates showed higher levels or resistance to the azoles voriconazole, imazalil, and tebuconazole than TR_{34}/L98H isolates (**Table 4**). Similar patterns of MIC distributions to itraconazole and voriconazole have also been reported for wildtype, TR_{34}/L98H and TR_{46}/Y121F/T289A strains using methods described by the European Committee on Antimicrobial Susceptibility Testing (EUCAST) (van Ingen et al., 2015) and the Clinical and Laboratory Standards Institute (CLSI) M38-A2 document (Buil et al., 2018). A TR_{46}/Y121F/M172I/T289A/G448S isolate (BTTa-1) and a TR_{46}/Y121F/T289A/S363P/I364V/G448S isolate (BKCb-1) were also found in this study. These more complex variants show similarities with the evolution of azole resistance in the plant pathogen *Zymoseptoria tritici*, where a stepwise accumulation of CYP51 mutations, determined by a negative trade-off between enzyme stability through reduced azole binding and enzyme functionality, has been reported to adapt to selection pressure exerted by different azoles entering and dominating the market (Cools and Fraaije, 2013). CYP51A amino acid substitutions Y121F, I364V, and G448S have homologous CYP51 position counterparts in other plant pathogens that have developed azole resistance (Mair et al., 2016). For example, G448S is equivalent to G460S in CYP51B of *Pyrenopeziza brassicae* conferring resistance to different azoles in this fungus (Carter et al., 2014). Mutations equivalent to Y121F and I364V have also evolved in *Z. tritici* (CYP51B Y137F and I381V), conferring resistance to triadimenol and tebuconazole, respectively (Mullins et al., 2011; Cools and Fraaije, 2013). Modeling of the *A. fumigatus* CYP51A protein showed that S363 is one of the key residues anchoring the heme and, therefore, likely to affect azole binding (Fraczek et al., 2011), while other studies showed that I364 forms part of the azole binding pocket (Liu et al., 2016). As CYP51s are less conserved than other fungicide target proteins such as beta-tubulin and cytochrome *b*, *in vitro* gene modification techniques can be undertaken to establish the precise impact of single and multiple target-site changes on inhibitor binding.

In addition to pan-azole resistant TR_{34} and TR_{46} strains, a proportion of strains isolated from the different soil samples showed high MIC values for itraconazole and, often, also elevated MICs for tebuconazole and, to a lesser extent, imazalil and voriconazole (**Table 4**). F46Y/M172V/E427K was identified in most of these strains and this variant has been reported for both clinical and environmental strains in Europe and Australia since 2001 (Garcia-Rubio et al., 2018). F46Y/M172V/E427K isolates are generally not considered resistant (Rodriguez-Tudela et al., 2008), but resistant isolates exceeding the EUCAST susceptibility break points for itraconazole (2.0 μg/ml), voriconazole (2.0 μg/ml), and/or posaconazole (0.25 μg/ml) have been reported in other studies (Howard et al., 2009; Garcia-Rubio et al., 2018). One new CSP variant t02* was found in this study. This new type, only found in F46Y/M172V/E427K isolates so far, can be distinguished from t02 by its flanking sequences (**Figure 4**). Based on the current nomenclature describing 29 different CSP types (Duarte-Escalante et al., 2020), t02 can be renamed as t02A and t02* as t02B. All F46Y/M172V/E427K strains carried closely related CSP types, t02*, t08, t13, t15, and t19 (**Figure 4**), and had identical or similar STR*Af* profiles (**Table 3**), indicating a separate lineage or cryptic sister species as suggested in other studies using whole genome sequencing (Garcia-Rubio et al., 2018). We recently established that strain IMI 16152 (NRRL 163), isolated in 1911 from chicken lung by C. Thom (Peterson, 1992), is also carrying CYP51A F46Y/M172V/E427K. Because of its presence long before the introduction of azole fungicides in both agricultural and clinical settings in the 1970's and early 1980's (Maertens, 2004; Russell, 2005), respectively, we consider F46Y/M172V/E427K as an example of standing variation rather than acquired resistance.

Acquired resistance against azoles can take place both in patient and in agricultural settings in response to exposure to azole compounds (Hagiwara et al., 2016). The genetic variation measured among TR_{34}/L98H and TR_{46}/Y121F/T289A isolates has been less in comparison with wild-type isolates indicating single recent origins of the resistant genotypes (Snelders et al., 2008; Chowdhary et al., 2013). Although *A. fumigatus* can undergo asexual, parasexual and sexual stages, some populations, including a lineage harboring TR_{34}/L98H isolates, seem to reproduce predominantly asexually (Klaassen et al., 2012). A close association with CSP types and isolates carrying CYP51A TR_{34}/L98H (CSP t02, t03, t04A, t04B, and t11) or TR_{46}/Y121F/T289A (CSP t01, t02, and t04A) was also observed in other studies (Camps et al., 2012b; Bader et al., 2015). The presence of identical clones in different countries supports clonal expansion of resistant genotypes over long distances by

airborne dispersal and/or transport of colonized agricultural produce (Chowdhary et al., 2012; Dunne et al., 2017; Sewell et al., 2019). Two identical clones were found in this study based on STR*Af* profiling (**Table 3**). One clone represented by isolates BB-1-3-B9 and G1-A9, originating from wheat fields in the UK and Germany, respectively, have also MAT1-1, CSP type t02*, and F46Y/M172V/E427K in common, and showed a close resemblance to Danish clinical F46Y/M172V/E427K and TR_{120}/F46Y/M172V/E427K strains with only one out of nine STR*Af* markers different (14 instead of 13 at 2B) (Hare et al., 2019). The other clone was formed by isolate RN8-18, isolated from a wheat field in the UK, and reference strain 08-19-02-10, a Dutch environmental isolate from 2008 (Abdolrasouli et al., 2015), with also TR_{34}/L98H, CSP t04B, and MAT1-2 in common. TR_{34}/L98H strain HPPB-1, isolated from an UK air sample, is very similar to an Australian clinical TR_{34}/L98H strain isolated in 2012 (Kidd et al., 2015) with only one STR*Af* marker different (19 for 18 at 2C). A clonal expansion based on an identical STR*Af* profile was also found for TR_{46}/Y121F/T289A strain RS3-3, sampled from an UK wheat field, matching with a German clinical TR_{46}/Y121F/T289A isolate dating back to 2012 (Steinmann et al., 2015) and several French clinical TR_{46}/Y121F/T289A strains in 2013 (Lavergne et al., 2015). With exception of STR*Af* marker 3C (21 instead of 22), one of the two markers for which low levels of instability have recently been reported (De Groot and Meis, 2019), soil isolates from India carrying TR_{46}/Y121F/T289A also showed the same profile as RS3-3 (Steinmann et al., 2015).

In addition to azoles, resistance to MBC, QoI, and SDHI fungicides, commonly used in agriculture and, with exception of SDHIs, also for material preservation but not in clinical settings, was also detected in several pan-azole resistant isolates (**Table 4**). This confirms that *A. fumigatus* as a non-target organism can evolve acquired resistance to agricultural fungicides in the environment. Selection for MBC resistance is currently expected to be minimal for cereal production because the use of this fungicide group as seed treatment or in foliar spray applications in the UK has been very low since 2006 due to resistance development in a range of target pathogens (Hawkins and Fraaije, 2018). All six TR_{46} and three out of nine TR_{34} strains tested (reference strains included) showed high levels of resistance to carbendazim associated with beta-tubulin F200Y, a mutation commonly found in other plant pathogens that have evolved resistance to MBC fungicides after exposure (Hawkins and Fraaije, 2016; Mair et al., 2016). In contrast to beta-tubulin E198A, which is associated with high levels of resistance to carbendazim but sensitivity to the N-phenyl carbamate diethofencarb in several plant pathogens, F200Y confers resistance to both carbendazim and diethofencarb (Koenraadt et al., 1992). While the use of carbendazim as a plant protection product is no longer authorized in the EU, selection for MBC resistance can further occur elsewhere and in areas of crop protection where thiabendazole and thiophanate-methyl, which is degraded to carbendazim, are used. Diethofencarb has been used for treatment of flower bulbs to control *Penicillium* sp. and is still being used in foliar sprays to control diseases like *Botrytis* sp. in fruit and vegetables. Most of MBC-resistant *A. fumigatus* strains were also resistant to pyraclostrobin and this was linked to the presence of cytochrome *b* G143A, a mutation associated with field resistance to QoI fungicides in a range of plant pathogens (Gisi et al., 2002). Only three strains showed insensitivity to boscalid. SdhB H270Y was detected in a strain highly resistant to boscalid (WN19-3; MIC $>18.469\,\mu g/ml$), whereas SdhB H270Y was detected in a strain with moderate levels of boscalid resistance (BKCb-1; MIC $= 5.606\,\mu g/ml$). Many different mutations can evolve after exposure to SDHI fungicides in experimental evolution experiments with fungi, including *Z. tritici* (Fraaije et al., 2012), and orthologous mutations to both SdhB H270Y and H270R have been reported in resistant field isolates of several plant pathogens, including *Botrytis* sp. on strawberries and tulips, *Alternaria alternata* on almonds and *Stemphylium botryosum* on asparagus (Sierotzki and Scalliet, 2013; Mair et al., 2016). Broad spectrum azole, MBC, QoI, and SDHI fungicides were introduced into the market in 1973, 1976, 1992, and 2003, respectively (Russell, 2005; Sierotzki and Scalliet, 2013). Isolates with resistance to multiple groups of fungicides have an advantage in habitats where there is abundant growth and sporulation in the presence of different fungicides such as compost and flower bulb waste heaps, and stockpiles of other fungicide-containing plant waste, the so called hotspots (Zhang et al., 2017; Schoustra et al., 2019). Favorable environmental conditions for the sexual stage can occur during composting and new azole resistant genotypes have been detected as well in this environment in the Netherlands. These included TR_{46}/Y121F/T289A/I364V, TR_{46}/Y121F/M172I/T289A/G448S, a variant reported in the Netherlands in 2010 (Zhang et al., 2017) and recently in Iran (Ahangarkani et al., 2020), and TR^2_{46}/Y121F/M172I/T289A/G448S and TR^3_{46}/Y121F/M172I/T289A/T289A/G448S, multiple 46-bp promoter repeat variants (Schoustra et al., 2019). The TR^3_{46} variant has also been found in Dutch clinical isolates since 2012 (Zhang et al., 2017). We found low numbers of pan-azole resistant isolates in soils from cereal fields and no new azole-resistant genotypes were identified. However, TR_{46}/Y121F/M172I/T289A/G448S and TR_{46}/Y121F/T289A/S363P/I364V/G448S, a novel CYP51A variant not reported before, were found in aerosols sampled at two urban locations in the Netherlands, indicating that new pan-azole resistant genotypes are evolving in habitats other than cereals, which can be regarded as a coldspot.

The latest report of a clinical case of infection with an azole resistant *A. fumigatus* strain carrying F46Y/M172V/E427K that acquired a 120-bp tandem repeat during long-term azole treatment, shows that the TR-mediated resistance mechanism is not restricted to environmental isolates only (Hare et al., 2019). In addition, the recent findings of airborne transmission of *A. fumigatus* by patients through coughs and sputum shows that not only spread of resistance mechanisms from environment-to-patient should be considered but also the spread from patient-to-environment and patient-to-patient (Lemaire et al., 2018; Engel et al., 2019). The origin of TR_{34} and TR_{46} based resistance mechanisms might be difficult to determine, however, the evolution of fungicide resistance is a continuous process in both clinical and environment settings where no borders exist for

A. fumigatus. Monitoring the presence and dynamics of alleles linked with resistance to azole, MBC, QoI, and SDHI in *A. fumigatus* populations will be useful to identify hotspots and coldspots for resistance development in the wider environment. Measures to reduce inoculum build-up, to prevent dispersal and minimize resistance development using tailored fungicide resistance management strategies can then be introduced and validated. A one-health approach, taking into account the relationship between health and disease at the human, animal and environment interfaces, will be needed to tackle the further spread of antifungal resistance and to safeguard the value of azoles for both human health and food security.

DATA AVAILABILITY STATEMENT

The original contributions presented in the study are included in the article/**Supplementary Material**, further inquiries can be directed to the corresponding author/s.

AUTHOR CONTRIBUTIONS

BF and AM designed the experiments. SA, BF, and SH performed the experiments. BF and SH analyzed the data. BF, AM, and JL participated in writing and/or editing the manuscript. All authors contributed to the article and approved the submitted version.

FUNDING

This work was supported by Crop Life International (grant 14209). BF received funding from the Newton Fund through grant BB/S018867/2 awarded by Biotechnology and Biological Sciences research Council (BBSRC) of the UK under the BBSRC-FAPESP AMR and Insecticide Pest Resistance in Livestock and Agriculture Programme. Rothamsted Research receives strategic funding from the BBSRC. The Rothamsted Long-term Experiments National Capability was supported by BBSRC Grant BBS/E/00005198. The funders played no role in the design of the study, the collection, analysis, or interpretation of data, or in writing the manuscript.

ACKNOWLEDGMENTS

We thank all members of Scientific Advisory Board (SAB) consisting of representatives of the Agrochemical Industry [Dr. Martin Semar (BASF), Dr. Klaus Stenzel and Dr. Andreas Goertz (Bayer CropScience), and Dr. Helge Sierotzki (Syngenta)] and experts from the *A. fumigatus* research community [Prof. Paul Verweij (Radboud University Medical Centre, The Netherlands), Prof. Paul Bowyer (University of Manchester), and Prof. Paul Dyer (University of Nottingham, UK)] for their valuable advice, support, and provision of samples. We also thank Dr. Jacques Meis (Canisius Wilhelmina Hospital, Nijmegen, The Netherlands) and Prof. Matt Fisher (Imperial College London, UK) for providing reference isolates and Ir. Peter Verkade for air sampling in Boskoop, The Netherlands.

SUPPLEMENTARY MATERIAL

The Supplementary Material for this article can be found online at: https://www.frontiersin.org/articles/10.3389/fmicb.2020.599233/full#supplementary-material

REFERENCES

Abdolrasouli, A., Rhodes, J., Beale, M. A., Hagen, F., Rogers, T. R., Chowdhary, A., et al. (2015). Genomic context of azole resistance mutations in *Aspergillus fumigatus* determined by using whole-genome sequencing. *MBio* 6:e00536. doi: 10.1128/mBio.00939-15

Ahangarkani, F., Puts, Y., Nabili, M., Khodavaisy, S., Moazeni, M., Salehi, Z., et al. (2020). First azole-resistant *Aspergillus fumigatus* with the environmental TR46/Y121F/T289A mutation in Iran. *Mycoses* 63, 430–436. doi: 10.1111/myc.13064

Bader, O., Tünnermann, J., Dudakova, A., Tangwattanachuleeporn, M., Weig, M., and Groß, U. (2015). Environmental isolates of azole-resistant *Aspergillus fumigatus* in Germany. *Antimicrob. Agents Chemother.* 59, 4356–4359. doi: 10.1128/AAC.00100-15

Balajee, S. A., Tay, S. T., Lasker, B. A., Hurst, S. F., and Rooney, A. P. (2007). Characterization of a novel gene for strain typing reveals substructuring of *Aspergillus fumigatus* across North America. *Eukaryot. Cell* 6, 1392–1399. doi: 10.1128/EC.00164-07

Berger, S., Chazli, Y. E., Babu, A. F., and Coste, A. T. (2017). Azole resistance in *Aspergillus fumigatus*: a consequence of antifungal use in agriculture? *Front. Microbiol.* 8:1024. doi: 10.3389/fmicb.2017.01024

Bromley, M. J., van Muijlwijk, G., Fraczek, M. G., Robson, G., Verweij, P. E., Denning, D. W., et al. (2014). Occurrence of azole-resistant species of *Aspergillus* in the UK environment. *J. Glob. Antimicrob. Resist.* 2, 276–279. doi: 10.1016/j.jgar.2014.05.004

Buied, A., Moore, C. B., Denning, D. W., and Bowyer, P. (2013). High-level expression of cyp51B in azole-resistant clinical *Aspergillus fumigatus* isolates. *J. Antimicrob. Chemother.* 68, 512–514. doi: 10.1093/jac/dks451

Buil, J. B., Hagen, F., Chowdhary, A., Verweij, P. E., and Meis, J. F. (2018). Itraconazole, voriconazole and posaconazole CLSI MIC distributions for wild-type and azole-resistant *Aspergillus fumigatus* isolates. *J. Fungi.* 4:103. doi: 10.3390/jof4030103

Camps, S. M. T., Dutilh, B. E., Arendrup, M. C., Rijs, A. J. M. M., Snelders, E., Huynen, M. A., et al. (2012a). Discovery of a hapE mutation that causes azole resistance in *Aspergillus fumigatus* through whole genome sequencing and sexual crossing. *PLoS ONE* 7:e50034. doi: 10.1371/journal.pone.0050034

Camps, S. M. T., Rijs, A. J. M. M., Klaassen, C. H. W., Meis, J. F., O'Gorman, C. M., Dyer, P. S., et al. (2012b). Molecular epidemiology of *Aspergillus fumigatus* isolates harboring the TR34/L98H azole resistance mechanism. *J. Clin. Microbiol.* 50, 2674–2680. doi: 10.1128/JCM.00335-12

Carter, H. E., Fraaije, B. A., West, J. S., Kelly, S., Mehl, A., Shaw, M. W., et al. (2014). Alterations in predicted regulatory and coding regions of the sterol. 14α-demethylase gene (CYP51) confer decreased azole sensitivity in the oilseed rape pathogen Pyrenopeziza brassicae. *Mol. Plant Pathol.* 15, 513–522. doi: 10.1111/mpp.12106

Chowdhary, A., Kathuria, S., Xu, J., and Meis, J. F. (2013). Emergence of azole-resistant *Aspergillus fumigatus* strains due to agricultural azole use creates an increasing threat to human health. *PLoS Pathog.* 9:e1003633. doi: 10.1371/annotation/4ffcf1da-b180-4149-834c-9c723c5dbf9b

Chowdhary, A., Kathuria, S., Xu, J., Sharma, C., Sundar, G., Singh, P. K., et al. (2012). Clonal expansion and emergence of environmental multiple-triazole-resistant *Aspergillus fumigatus* strains carrying the TR34/L98H mutations in the cyp51A gene in India. *PLoS ONE* 7:e52871. doi: 10.1371/journal.pone.0052871

Chowdhary, A., and Meis, J. F. (2018). Emergence of azole resistant *Aspergillus fumigatus* and one health: time to implement environmental stewardship. *Environ. Microbiol.* 20, 1299–1301. doi: 10.1111/1462-2920.14055

Cools, H. J., and Fraaije, B. A. (2013). Update on mechanisms of azole resistance in *Mycosphaerella graminicola* and implications for future control. *Pest Manage Sci.* 69, 150–155. doi: 10.1002/ps.3348

De Groot, T., and Meis, J. F. (2019). Microsatellite stability in STR analysis *Aspergillus fumigatus* depends on number of repeat units. *Front. Cell. Infect. Microbiol.* 9:82. doi: 10.3389/fcimb.2019.00082

De Valk, H. A., Meis, J. F. G. M., Curfs, I. M., Muehlethaler, K., Mouton, J. W., and Klaassen, C. H. W. (2005). Use of a novel panel of nine short tandem repeats for exact and high-resolution fingerprinting of *Aspergillus fumigatus* isolates. *J. Clin. Microbiol.* 43, 4112–4120. doi: 10.1128/JCM.43.8.4112-4120.2005

Denning, D. W., Venkateswarlu, K., Oakley, K. L., Anderson, M. J., Manning, N. J., Stevens, D. A., et al. (1997). Itraconazole resistance in *Aspergillus fumigatus*. *Antimicrob. Agents Chemother.* 41, 1364–1368. doi: 10.1128/AAC.41.6.1364

Duarte-Escalante, E., Frías-De-León, M. G., Martínez-Herrera, E., Acosta-Altamirano, G., Rosas de Paz, E., Reséndiz-Sánchez, J., et al. (2020). Identification of CSP types and genotypic variability of clinical and environmental isolates of *Aspergillus fumigatus* from different geographic origins. *Microorganisms* 8:688. doi: 10.3390/microorganisms8050688

Dunne, K., Hagen, F., Pomeroy, N., Meis, J. F., and Rogers, T. R. (2017). Intercountry transfer of triazole-resistant *Aspergillus fumigatus* on plant bulbs. *Clin. Infect. Dis.* 65, 147–149. doi: 10.1093/cid/cix257

Engel, T. G. P., Erren, E., Vanden Driessche, K. S. J., Melchers, W. J. G., Reijers, M. H., Merkus, P., et al. (2019). Aerosol transmission of *Aspergillus fumigatus* in cystic fibrosis patients in the Netherlands. *Emerg Inf. Dis.* 25, 797–799. doi: 10.3201/eid2504.181110

Förster, H., Kanetis, L., and Adaskaveg, J. E. (2004). Spiral gradient dilution, a rapid method for determining growth responses and 50% effective concentration values in fungus-fungicide interactions. *Phytopathology*. 94, 163–170. doi: 10.1094/PHYTO.2004.94.2.163

Fraaije, B. A., Bayon, C., Atkins, S., Cools, H. J., Lucas, J. A., and Fraaije, M. W. (2012). Risk assessment studies on succinate dehydrogenase inhibitors, the new weapons in the battle to control Septoria leaf blotch in wheat. *Mol. Plant Pathol.* 13, 263–275. doi: 10.1111/j.1364-3703.2011.00746.x

Fraczek, M. G., Bromley, M., and Bowyer, P. (2011). An improved model of the *Aspergillus fumigatus* CYP51A protein. *Antimicrob Agents and Chemother.* 55, 2483–2486. doi: 10.1128/AAC.01651-10

Fraczek, M. G., Bromley, M., Buied, A., Moore, C. B., Rajendran, R., Rautemaa, R., et al. (2013). The crd1B efflux transporter is associated with non-cyp51a-mediated itraconazole resistance in *Aspergillus fumigatus*. *J. Antimicrob. Chemother.* 68, 1486–1496. doi: 10.1093/jac/dkt075

Garcia-Rubio, R., Alcazar-Fuoli, L., Monteiro, M. C., Monzon, S., Cuesta, I., Peleaz, T., et al. (2018). Insight into the significance of *Aspergillus fumigatus* cyp51A polymorphisms. *Antimicrob. Agents Chemother.* 62:e00241. doi: 10.1128/AAC.00241-18

Gisi, U. (2014). Assessment of selection and resistance risk for demethylation inhibitor fungicides in *Aspergillus fumigatus* in agriculture and medicine: a critical review. *Pest Manage Sci.* 70, 352–364. doi: 10.1002/ps.3664

Gisi, U., Sierotzki, H., Cook, A., and McCaffery, A. (2002). Mechanisms influencing the evolution to Qo inhibitor fungicides. *Pest Manage Sci.* 58, 859–867. doi: 10.1002/ps.565

Hagiwara, D., Arai, T., Takahashi, H., Kusuya, Y., Watanabe, A., and Kamei, K. (2018). Non-cyp51A azole-resistant *Aspergillus fumigatus* isolates with mutation in HMG-CoA reductase. *Emerging Infect. Dis.* 24, 1889–1897. doi: 10.3201/eid2410.180730

Hagiwara, D., Watanabe, A., Kamei, K., and Goldman, G. H. (2016). Epidemiological and genomic landscape of azole resistance mechanisms in *Aspergillus fungi*. *Front. Microbiol.* 7:1382. doi: 10.3389/fmicb.2016.01382

Hare, R. K., Gertsen, J. B., Astvad, K. M. T., Degn, K. B., Løkke, A., Stegger, M., et al. (2019). In vivo selection of a unique tandem repeat mediated azole resistance mechanism (TR120) in *Aspergillus fumigatus* cyp51A, Denmark. *Emerg. Infect. Dis.* 25, 577–580. doi: 10.3201/eid2503.180297

Hawkins, N. J., and Fraaije, B. A. (2016). Predicting resistance by mutagenesis: lessons from. 45 years of MBC resistance. *Front. Microbiol.* 7:1814. doi: 10.3389/fmicb.2016.01814

Hawkins, N. J., and Fraaije, B. A. (2018). Fitness penalties in the evolution of fungicide resistance. *Annu. Rev. Phytopathol.* 56, 339–360. doi: 10.1146/annurev-phyto-080417-050012

Hollomon, D. (2017). Does agricultural use of azole fungicides contribute to resistance in the human pathogen *Aspergillus fumigatus*? *Pest Manage Sci.* 73, 1987–1993. doi: 10.1002/ps.4607

Howard, S. J., Cerar, D., Anderson, M. J., Albarrag, A., Fisher, M. C., Pasqualotto, A. C., et al. (2009). Frequency and evolution of azole resistance in *Aspergillus fumigatus* associated with treatment failure. *Emerging Infect. Dis.* 15, 1068–1076. doi: 10.3201/eid1507.090043

Kidd, S. E., Goeman, E., Meis, J. F., Slavin, M. A., and Verweij, P. (2015). Multi-triazole-resistant *Aspergillus fumigatus* infections in Australia. *Mycoses* 58, 350–355. doi: 10.1111/myc.12324

Kidd, S. E., Nik Zulkepeli, N. A. A., Slavin, M. A., and Morrissey, C. O. (2009). Utility of a proposed CSP typing nomenclature for Australian *Aspergillus fumigatus* isolates: Identification of additional CSP types and suggested modifications. *J. Microbiol. Methods* 78, 223–226. doi: 10.1016/j.mimet.2009.06.003

Klaassen, C. H. W., de Valk, H. A., Balajee, S. A., and Meis, J. F. G. M. (2009). Utility of CSP typing to sub-type clinical *Aspergillus fumigatus* isolates and proposal for a new CSP type nomenclature. *J. Microbiol. Methods* 77, 292–296. doi: 10.1016/j.mimet.2009.03.004

Klaassen, C. H. W., Gibbons, J. G., Fedorova, N. D., Meis, J. F., and Rokas, A. (2012). Evidence for genetic differentiation and variable recombination rates among Dutch populations of the opportunistic human pathogen *Aspergillus fumigatus*. *Mol. Ecol.* 21, 57–70. doi: 10.1111/j.1365-294X.2011.05364.x

Koenraadt, H., Somerville, S. C., and Jones, A. L. (1992). Characterisation of mutations in the β-tubulin gene of benomyl-resistant field strains of *Venturia inaequalis* and other plant pathogenic fungi. *Phytopathology* 82, 1348–1354. doi: 10.1094/Phyto-82-1348

Lavergne, R.-A., Morio, F., Favennec, L., Dominique, S., Meis, J. F., Gargala, G., et al. (2015). First description of azole-resistant *Aspergillus fumigatus* due to TR46/Y121F/T289A mutation in France. *Antimicrob. Agents Chemother.* 59, 4331–4335. doi: 10.1128/AAC.00127-15

Lazzarini, C., Esposto, M. C., Prigitano, A., Cogliati, M., De Lorenzis, G., and Tortorano, A. M. (2016). Azole resistance in *Aspergillus fumigatus* clinical isolates from an Italian culture collection. *Antimicrob. Agents Chemother.* 60, 682–685. doi: 10.1128/AAC.02234-15

Lemaire, B., Normand, A.-C., Forel, J.-M., Cassir, N., Piarroux, R., and Ranque, S. (2018). Hospitalized patient as source of *Aspergillus fumigatus*, 2015. *Emerging Infect. Dis.* 24, 1524–1527. doi: 10.3201/eid2408.171865

Liu, M., Zheng, N., Li, D., Zheng, H., Zhang, L., Ge, H., et al. (2016). Cyp51A-based mechanism of azole resistance in *Aspergillus fumigatus*: illustration by a new. 3D structural model of *Aspergillus fumigatus* CYP51A protein. *Med. Mycol.* 54, 400–408. doi: 10.1093/mmy/myv102

Macdonald, A., Poulton, P., Clark, I., Scott, T., Glendining, M., Perryman, S., et al. (2018). *Guide to the Classical and Other Long-term experiments, Datasets and Sample Archive*. (Harpenden, UK: Rothamsted Research).

Maertens, J. A. (2004). History of the development of azole derivatives. *Clin. Microbiol. Infect.* 10, 1–10. doi: 10.1111/j.1470-9465.2004.00841.x

Mair, W., Lopez-Ruiz, F., Stammler, G., Clark, W., Burnett, F., Hollomon, D., et al. (2016). Proposal for a unified nomenclature for target site mutations associated with resistance to fungicides. *Pest Manage Sci.* 8, 1449–1459. doi: 10.1002/ps.4301

Meneau, I., Coste, A. T., and Sanglard, D. (2016). Identification of *Aspergillus fumigatus* multidrug transporter genes and their potential involvement in antifungal resistance. *Med. Mycol.* 54, 616–627. doi: 10.1093/mmy/myw005

Mullins, J. G. L., Parker, J. E., Cools, H. J., Martel, C. M., Togawa, R. C., Lucas, J. A., et al. (2011). Molecular modelling of the emergence of azole resistance in *Mycosphaerella graminicola*. *PLoS ONE* 6:e20973. doi: 10.1371/journal.pone.0020973

Peterson, S. W. (1992). Neosartorya pseudofischeri sp. nov. and its relationship to other species in *Aspergilius* section Fumigati. *Mycol. Res.* 96, 547–554. doi: 10.1016/S0953-7562(09)80979-9

Pong, R., Boost, M. V., O'Donoghue, M. M., and Appelbaum, P. C. (2010). Spiral gradient endpoint susceptibility testing: a fresh look at a neglected technique. *J. Antimicrob. Chemother.* 65, 1959–1963. doi: 10.1093/jac/dkq239

Powlson, D. S., Glendining, M. J., Coleman, K., and Whitmore, A. P. (2011). Implications for soil properties of removing cereal straw: results from long-term studies. *J. Agron.* 103, 279–287. doi: 10.2134/agronj2010.0146s

Rocchi, S., Daguindau, E., Grenouillet, F., Deconinck, E., Bellanger, A.-P., Garcia-Hermoso, D., et al. (2014). Azole-resistant *Aspergillus fumigatus* isolate with the TR34/L98H mutation in both a fungicide-sprayed field and the lung of a hematopoietic stem cell transplant recipient with invasive Aspergillosis. *J. Clin. Microbiol.* 52, 1724–1726. doi: 10.1128/JCM.03182-13

Rodriguez-Tudela, J. L., Alcazar-Fuoli, L., Mellado, E., Alastruey-Izquierdo, A., Monzon, A., and Cuenca-Estrella, M. (2008). Epidemiological cutoffs and cross-resistance to azole drugs in *Aspergillus fumigatus*. *Antimicrob. Agents Chemother.* 52, 2468–2472. doi: 10.1128/AAC.00156-08

Russell, P. E. (2005). A century of fungicide evolution. *J. Agric. Sci.* 143, 11–25. doi: 10.1017/S0021859605004971

Rybak, J. M., Ge, W., Wiederhold, N. P., Parker, J. E., Kelly, S. L., Rogers, P. D., et al. (2019). Mutations in hmg1, (2019) Challenging the paradigm of clinical triazole resistance in *Aspergillus fumigatus*. *MBio* 10:e00437. doi: 10.1128/mBio.00437-19

Schoustra, S. E., Debets, A. J. M., Rijs, A. J. M. M., Zhang, J., Snelders, E., Leendertse, P. C., et al. (2019). Environmental hotspots for azole resistance selection of *Aspergillus fumigatus*, the Netherlands. *Emerging Infect. Dis.* 25, 1347–1353. doi: 10.3201/eid2507.181625

Sewell, T. R., Zhu, J., Rhodes, J., Hagen, F., Meis, J. F., Fisher, M. C., et al. (2019). Nonrandom distribution of azole resistance across the global population of *Aspergillus fumigatus*. *MBio* 10:e00392. doi: 10.1128/mBio.00392-19

Sierotzki, H., and Scalliet, G. (2013). A review of current knowledge of resistance aspects for the next-generation succinate dehydrogenase inhibitor fungicides. *Phytopathology* 103, 880-887. doi: 10.1094/PHYTO-01-13-0009-RVW

Snelders, E., Camps, S. M. T., Karawajczyk, A., Schaftenaar, G., Kema, G. H. J., van der Lee, H. A., et al. (2012). Triazole fungicides can induce cross-resistance to medical triazoles in *Aspergillus fumigatus*. *PLoS ONE* 7:e31801. doi: 10.1371/journal.pone.0031801

Snelders, E., van der Lee, H. A. L., Kuijpers, J., Rijs, A. J. M. M., Varga, J., Samson, R. A., et al. (2008). Emergence of azole resistance in *Aspergillus fumigatus* and spread of a single resistance mechanism. *PLoS Med.* 5:e219. doi: 10.1371/journal.pmed.0050219

Steinmann, J., Hamprecht, A., Vehreschild, M. J. G. T., Cornely, O. A., Buchheidt, D., Spiess, B., et al. (2015). Emergence of azole-resistant invasive aspergillosis in HSCT recipients in Germany. *J. Antimicrob. Chemother.* 70, 1522–1526. doi: 10.1093/jac/dku566

Tsitsopoulou, A., Posso, R., Vale, L., Bebb, S., Johnson, E., and White, P. L. (2018). Determination of the prevalence of triazole resistance in environmental *Aspergillus fumigatus* strains isolated in South Wales, UK. *Front. Microbiol.* 9:1395. doi: 10.3389/fmicb.2018.01395

Van der Linden, J. W. M., Snelders, E., Kampinga, G. A., Rijnders, B. J., Mattsson, E., Debets-Ossenkopp, Y. J., et al. (2011). Clinical implications of azole resistance in *Aspergillus fumigatus*, the Netherlands, 2007-2009. *Emerging Infect. Dis.* 10, 1846–1854. doi: 10.3201/eid1710.110226

van Ingen, J., van der Lee, H. A., Rijs, T. A., Zoll, J., Leenstra, T., Melchers, W. J. G., et al. (2015). Azole, polyene and echinocandin MIC distributions for wild-type, TR34/L98H and TR46/Y121F/T289A *Aspergillus fumigatus* isolates in the Netherlands. *J. Antimicrob. Chemother.* 70, 178–181. doi: 10.1093/jac/dku364

Verweij, P. E., Chowdhary, A., Melchers, W. J. G., and Meis, J. F. (2016). Azole resistance in *Aspergillus fumigatus*: can we retain the clinical use of mold-active antifungal azoles? *Clin. Infect. Dis.* 62, 362–368. doi: 10.1093/cid/civ885

Verweij, P. E., Snelders, E., Kema, G. H. J., Mellado, E., and Melchers, W. J. G. (2009). Azole resistance in *Aspergillus fumigatus*: a side-effect of environmental fungicide use? *Lancet Infect. Dis.* 9, 789–795. doi: 10.1016/S1473-3099(09)70265-8

Wei, X., Chen, P., Gao, R., Li, Y., Zhang, A., Liu, F., et al. (2017). Screening and characterization of a non-cyp51A mutation in an *Aspergillus fumigatus* cox10 strain conferring azole resistance. *Antimicrob. Agents Chemother.* 61:e02101-16. doi: 10.1128/AAC.02101-16

Wiederhold, N. P., Gil, V. G., Gutierrez, F., Lindner, J. R., Albataineh, M. T., McCarthy, D. I., et al. (2016). First detection of TR34 L98H and TR46 Y121F T289A cyp51 mutations in *Aspergillus fumigatus* isolates in the United States. *J. Clin. Microbiol.* 54, 168–171. doi: 10.1128/JCM.02478-15

Zhang, J., Snelders, E., Zwaan, B. J., Schoustra, S. E., Meis, J. F., van Dijk, K., et al. (2017). A novel environmental azole resistance mutation in *Aspergillus fumigatus* and a possible role of sexual reproduction in its emergence. *MBio* 8:e00791-17. doi: 10.1128/mBio.00791-17

Conflict of Interest: The authors declare that the research was conducted in the absence of any commercial or financial relationships that could be construed as a potential conflict of interest.

frontiers in Microbiology

ORIGINAL RESEARCH
published: 04 March 2021
doi: 10.3389/fmicb.2021.644000

Prevalence and Antifungal Susceptibility of *Candida parapsilosis* Species Complex in Eastern China: A 15-Year Retrospective Study by ECIFIG

Jian Guo[1†], Min Zhang[1†], Dan Qiao[2†], Hui Shen[1], Lili Wang[1], Dongjiang Wang[1], Li Li[2], Yun Liu[3], Huaiwei Lu[4], Chun Wang[5], Hui Ding[6], Shuping Zhou[7], Wanqing Zhou[8], Yingjue Wei[9], Haomin Zhang[9], Wei Xi[9], Yi Zheng[10], Yueling Wang[11], Rong Tang[12], Lingbing Zeng[13], Heping Xu[14]* and Wenjuan Wu[1]**

[1] Department of Laboratory Medicine, Shanghai East Hospital, Tongji University School of Medicine, Shanghai, China, [2] Department of Laboratory Medicine, Ruijin Hospital, Shanghai Jiao Tong University School of Medicine, Shanghai, China, [3] Department of Laboratory Medicine, Changhai Hospital, Naval Medical University (Second Military Medical University), Shanghai, China, [4] Department of Laboratory Medicine, The First Affiliated Hospital of USTC, Hefei, China, [5] Department of Laboratory Medicine, Children's Hospital, Shanghai Jiao Tong University School of Medicine, Shanghai, China, [6] Department of Laboratory Medicine, Lishui Municipal Central Hospital, Lishui, China, [7] Department of Laboratory Medicine, Jiangxi Provincial Children's Hospital, Nanchang, China, [8] Department of Laboratory Medicine, Nanjing Drum Tower Hospital, The Affiliated Hospital of Nanjing University Medical School, Nanjing University, Nanjing, China, [9] Department of Laboratory Medicine, Renji Hospital, Shanghai Jiao Tong University School of Medicine, Shanghai, China, [10] Department of Clinical Laboratory, The Second Affiliated Hospital of Soochow University, Suzhou, China, [11] Department of Clinical Laboratory, Shandong Provincial Hospital Affiliated to Shandong First Medical University, Jinan, China, [12] Department of Laboratory Medicine, Shanghai General Hospital, Shanghai Jiao Tong University School of Medicine, Shanghai, China, [13] Department of Laboratory Medicine, The First Affiliated Hospital of Nanchang University, Nanchang, China, [14] Department of Laboratory Medicine, The First Affiliated Hospital of Xiamen University, Xiamen, China*

OPEN ACCESS

Edited by:
Ying-Chun Xu, Peking Union Medical College Hospital (CAMS), China

Reviewed by:
Ping Zhan, Jiangxi Provincial People's Hospital, China
Changbin Chen, Institut Pasteur of Shanghai (CAS), China

***Correspondence:**
Wenjuan Wu
wwj1210@126.com
Heping Xu
xmsunxhp@163.com
Lingbing Zeng
lingbing_zeng@163.com

[†] These authors have contributed equally to this work

Specialty section:
This article was submitted to Antimicrobials, Resistance and Chemotherapy, a section of the journal Frontiers in Microbiology

Received: *19 December 2020*
Accepted: *26 January 2021*
Published: *04 March 2021*

Citation:
Guo J, Zhang M, Qiao D, Shen H, Wang L, Wang D, Li L, Liu Y, Lu H, Wang C, Ding H, Zhou S, Zhou W, Wei Y, Zhang H, Xi W, Zheng Y, Wang Y, Tang R, Zeng L, Xu H and Wu W (2021) Prevalence and Antifungal Susceptibility of Candida parapsilosis Species Complex in Eastern China: A 15-Year Retrospective Study by ECIFIG. Front. Microbiol. 12:644000. doi: 10.3389/fmicb.2021.644000

Candida parapsilosis complex is one of the most common non-*albicans Candida* species that cause candidemia, especially invasive candidiasis. The purpose of this study was to evaluate the antifungal susceptibilities of both colonized and invasive clinical *C. parapsilosis* complex isolates to 10 drugs: amphotericin (AMB), anidulafungin (AFG), caspofungin (CAS), micafungin (MFG), fluconazole (FLZ), voriconazole (VRZ), itraconazole (ITZ), posaconazole (POZ), 5-flucytosine (FCY), and isaconazole (ISA). In total, 884 *C. parapsilosis* species complex isolates were gathered between January 2005 and December 2020. *C. parapsilosis*, *Candida metapsilosis*, and *Candida orthopsilosis* accounted for 86.3, 8.1, and 5.5% of the cryptic species, respectively. The resistance/non-wild-type rate of bloodstream *C. parapsilosis* to the drugs was 3.5%, of *C. metapsilosis* to AFG and CAS was 7.7%, and of *C. orthopsilosis* to FLZ and VRZ was 15% and to CAS, MFG, and POZ was 5%. The geometric mean (GM) minimum inhibitory concentrations (MICs) of non-bloodstream *C. parapsilosis* for CAS (0.555 mg/L), MFG (0.853 mg/L), FLZ (0.816 mg/L), VRZ (0.017 mg/L), ITZ (0.076 mg/L), and POZ (0.042 mg/L) were significantly higher than those of bloodstream *C. parapsilosis*, for which the GM MICs were 0.464, 0.745, 0.704, 0.015, 0.061, and 0.033 mg/L, respectively ($P < 0.05$). The MIC distribution of the bloodstream *C. parapsilosis* strains collected from 2019 to 2020 for VRZ, POZ, and ITZ were

0.018, 0.040, and 0.073 mg/L, significantly higher than those from 2005 to 2018, which were 0.013, 0.028, and 0.052 mg/L ($P < 0.05$). Additionally, MIC distributions of *C. parapsilosis* with FLZ and the distributions of *C. orthopsilosis* with ITZ and POZ might be higher than those in Clinical and Laboratory Standards Institute studies. Furthermore, a total of 143 *C. parapsilosis* complex isolates showed great susceptibility to ISA. Overall, antifungal treatment of the non-bloodstream *C. parapsilosis* complex isolates should be managed and improved. The clinicians are suggested to pay more attention on azoles usage for the *C. parapsilosis* complex isolates. In addition, establishing the epidemiological cutoff values (ECVs) for azoles used in Eastern China may offer better guidance for clinical treatments. Although ISA acts on the same target as other azoles, it may be used as an alternative therapy for cases caused by FLZ- or VRZ-resistant *C. parapsilosis* complex strains.

Keywords: antifungal susceptibility, *Candida parapsilosis*, *Candida metapsilosis*, *Candida orthopsilosis*, China

INTRODUCTION

Candida albicans and emerging non-*albicans Candida* species can result in superficial infections of the oral and vaginal mucosa, as well as invasive candidiasis, such as bloodstream infections and deep-tissue infections. These invasive infections are associated with high mortality of about 70% (Pappas et al., 2018). *C. albicans* is the most common and aggressive species causing *Candida* infections around the world. However, over the past few decades, non-*albicans Candida* species such as *Candida glabrata*, *Candida parapsilosis*, and *Candida tropicalis* have also become health concern (Chow et al., 2008; Silva et al., 2012; Guinea, 2014; Guo et al., 2017). Among them, *C. parapsilosis* is well known for its threat to the patients undergoing invasive medical interventions, as it is considered to be one of the leading causes of catheter-related infections and can form enhanced biofilms on central venous catheters (CVCs) and other medical implants (Trofa et al., 2008; Pfaller et al., 2014; Strollo et al., 2016; Tóth et al., 2019). *C. parapsilosis* is also the second or third most commonly isolated *Candida* species in the intensive care units (ICUs) (Magobo et al., 2017; Asadzadeh et al., 2019). In contrast to *C. albicans*, horizontal transmission is another characteristic of *C. parapsilosis*, which allows the species to spread through contaminated medical equipment and medical staff in the clinic, leading to crossover infections between patients (García San Miguel et al., 2004; Kuhn et al., 2004; Vaz et al., 2011).

Candida parapsilosis, *C. metapsilosis*, and *C. orthopsilosis* are three species of the *C. parapsilosis* species complex (Tavanti et al., 2005). The prevalence of *C. parapsilosis* is the highest among the cryptic species. A 6-year multicenter study in Iran reported that the proportions of *C. orthopsilosis* and *C. metapsilosis* were quite small, comprising 5.3 and 0.17% of all *C. parapsilosis* species complex isolates (Arastehfar et al., 2019). While in Argentina and India, *C. orthopsilosis* may account for a higher proportion, reaching 40% of the cryptic species (Maria et al., 2018; Vigezzi et al., 2019). *C. parapsilosis* complex isolates were found susceptible to most of the antifungal agents (Modiri et al., 2019; Vigezzi et al., 2019). The multicenter studies in China by the China Hospital Invasive Fungal Surveillance Net (CHIF-NET) performed in 2015, 2018, and 2020 all reported low resistance/non-wild-type (NWT) rate of *C. parapsilosis* complex isolates to azoles (<6%) (Xiao et al., 2015, 2018, 2020). The multicenter study in Iran also reported four NWT *C. orthopsilosis* isolates for itraconazole (ITZ) (Arastehfar et al., 2019). Yet, the work in India reported high resistance to fluconazole (FLZ) of *C. parapsilosis* (Maria et al., 2018). However, all of the studies lasted only 2–6 years, lacking long-term studies.

Additionally, the difference in antifungal susceptibilities between the three cryptic species were described. Vigezzi et al. (2019) reported lower minimal inhibitory concentrations (MICs) with *C. parapsilosis* than *C. orthopsilosis* for ITZ and higher MIC values for echinocandins ($P < 0.01$). Similarly, Gil-Alonso et al. (2019) reported that *C. metapsilosis* was the most susceptible species to echinocandins, followed by *C. orthopsilosis* and *C. parapsilosis*. However, the number of strains used in these studies were quite limited so that these results may not able to uncover the difference clearly.

Furthermore, the Clinical and Laboratory Standards Institute (CLSI) updated its document M60-Ed2 in June 2020, illustrating that the clinical breakpoints can only be used for *C. parapsilosis*; otherwise, the epidemiological cutoff values (ECVs) recommended by M59-Ed3 should be applied for *C. metapsilosis* and *C. orthopsilosis*. No large-scale study, except the programs associated with CLSI, has been performed since then.

Notably, only the *C. parapsilosis* complex isolates from invasive candidiasis have been studied for their antifungal susceptibilities so far. *C. parapsilosis* complex are opportunistic pathogens that may transition from colonization to invasion; therefore, we believe that it is also worth studying colonized isolates. We launched the Eastern China Invasive Fungi Infection Group (ECIFIG), a multicenter institute, in 2019 in Shanghai to supervise the *Candida* strains isolated from both colonization and invasion sites and to improve rapid fungal diagnosis, therapeutic drug monitoring, and clinical intervention teams.

Therefore, this 15-year multicenter study collected a total of 884 colonized and invasive *C. parapsilosis* complex isolates in eastern China, with the aim of investigating their

epidemiological characteristics and antifungal susceptibility distributions systematically with nine common antifungal drugs as well as isavuconazole (ISA), a drug whose ECV was first reported in CLSI M59-Ed3 for *C. duobushaemulonii* only, applying the clinical breakpoints and ECVs updated in CLSI M60-Ed2 and M59-Ed3.

MATERIALS AND METHODS

Strains

For this retrospective study, a total of 884 *C. parapsilosis* complex clinical isolates (763 *C. parapsilosis*, 49 *C. orthopsilosis*, and 72 *C. metapsilosis*) were collected from 835 patients with more than one episode of candidiasis. The isolates were gathered from different tertiary hospitals of ECIFIG between 2005 and 2020. Among the seven provinces in Eastern China, the majority of the isolates were from Shanghai (n = 520), Jiangxi (n = 240), and Fujian (n = 64) (**Table 1**). For each isolate, the collected information included age and gender of the patient, date of sample collection, specimen type, body site of isolation, and the ward location of the patient at the time of sample collection. Strains were isolated from clinical samples of patients with bloodstream and non-bloodstream fungal infections.

Strains Identification

All isolates were first identified by biochemical methods and then confirmed by matrix-assisted laser desorption ionization–time of flight mass spectrometry (MALDI-TOF) (Autof ms1000, Autobio). Sequencing of the internal transcribed spacer (ITS) ribosomal DNA (rDNA) (ITS1/ITS4) region was performed for definitive species identification.

TABLE 1 | Number of *C. parapsilosis* complex isolates collected from different hospitals.

Hospitals		No. of isolates (%)		
		***C. parapsilosis* (*n* = 763)**	***C. metapsilosis* (*n* = 72)**	***C. orthopsilosis* (*n* = 49)**
Shanghai	East Hospital	185 (24.2)	2 (2.8)	4 (8.2)
	Ruijin Hospital	35 (4.6)		6 (12.2)
	Shanghai Children's Hospital	34 (4.5)	1 (1.4)	1 (2)
	Changhai Hospital	26 (3.4)	1 (1.4)	11 (22.4)
	Changzheng Hospital	26 (3.4)		
	Shanghai General Hospital	26 (3.4)	1 (1.4)	
	Shanghai Tenth People's Hospital	23 (3)	3 (4.2)	
	Eye and Ent Hospital of Fudan University	19 (2.5)	5 (6.9)	2 (4.1)
	East Brach of Renji Hospital	14 (1.8)	2 (2.8)	1 (2)
	Shanghai Public Health Clinical Center	13 (1.7)		
	West Brach of Renji Hospital	12 (1.6)	3 (4.2)	
	Zhongshan Hospital	11 (1.4)		
	Children's Hospital of Fudan University	9 (1.2)		1 (2)
	Huadong Hospital	9 (1.2)		
	Shanghai Children's Medical Center	8 (1)		
	South Brach of Renji Hospital	6 (0.8)		
	Huashan Hospital	5 (0.7)		
	Shanghai Eastern Hepatobiliary Surgery Hospital	4 (0.5)		
	Shanghai Chest Hospital	4 (0.5)		
	Shanghai Cancer Center	4 (0.5)		
	Shanghai Pudong New Area Gongli Hospital	3 (0.4)		
	Total	476 (62.4)	18 (25)	26 (53.1)
Jiangxi	The First Affiliated Hospital of Nanchang University	168 (22)	41 (56.9)	21 (42.9)
	Jiangxi Provincial People's Hospital	9 (1.2)		
	Jiangxi Provincial Children's Hospital	1 (0.1)		
	Total	178 (23.3)		
Fujian	The First Affiliated Hospital of Xiamen University	51 (6.7)	11 (15.3)	2 (4.1)
Zhejiang	Zhejiang Lishui Central Hospital	19 (2.5)		
Anhui	Anhui Provincial Hospital	18 (2.4)	2 (2.8)	
Jiangsu	The First Affiliated Hospital of Soochow University	9 (1.2)		
	Nanjing Drum Tower Hospital	8 (1)		
	Total	17 (2.2)		
Shandong	Shandong Provincial Hospital	4 (0.5)		

Criteria for Study Inclusion

We collected all *C. parapsilosis* complex isolates recovered from the blood and non-blood of patients and included them in this study. Isolates from bronchoalveolar lavage fluid (BALF), CVC tips, and the gastrointestinal tracts of patients with invasive infections were tested. Isolates from sputum, urine, genital tract, and other places considered to be colonizers were also collected as non-blood strains. Isolates of the same species with the same susceptibility or resistance biotype profile from the same site of the same patient at different times were considered duplicates and were excluded.

Criteria for Grouping

Since ECIFIG was launched in 2019 and started to collect all the strains isolated clinically, we divide the bloodstream *C. parapsilosis* isolates into two groups—2005–2018 and 2019–2020—to study the difference for MIC distributions between the two groups.

Antifungal Susceptibility Testing

The *in vitro* susceptibility of the 741 *C. parapsilosis* complex strains to nine antifungal drugs, amphotericin B (AMB, 0.12–8 mg/L), anidulafungin (AFG, 0.015–8 mg/L), caspofungin (CAS, 0.008–8 mg/L), micafungin (MFG, 0.008–8 mg/L), FLZ (0.12–256 mg/L), VRZ (0.008–8 mg/L), ITZ (0.015–16 mg/L), posaconazole (POZ, 0.008–8 mg/L), and 5-flucytosine (FCY, 0.06–64 mg/L) were determined by the Sensititre YeastOne™ YO10 methodology (Thermo Fisher Scientific, Waltham, MA, United States) following the manufacturer's instructions. The *in vitro* antifungal susceptibility tests of the other 143 *C. parapsilosis* complex strains collected in 2020 were conducted using the Sensititre YeastOne™ CMC1JHY methodology (Thermo Fisher Scientific), which is a new plate for research only, in which AMB is replaced with isavuconazole (ISA, 0.015–16 mg/L), and the concentration of CAS is changed from 0.008–8 mg/L to 0.06–4 mg/L. For these 143 strains, the *in vitro* susceptibilities to AMB were determined by the AMB microbroth dilution kit (BIO-KONT®, Wenzhou, China), which is also for scientific research only, with the drug concentrations ranging from 0.125 to 8 mg/L. *C. parapsilosis* (ATCC 22019) and *C. krusei* (ATCC 6258) standard strains were used as quality controls. After being incubated at 35°C for 24 h, the MIC endpoints were determined following the manufacturer's instructions. For Sensititre YeastOne™ YO10 and CMC1JHY (Thermo Fisher Scientific), MIC was defined as the lowest drug concentration at which the color in the well changed from red to blue. For the AMB microbroth dilution kit (BIO-KONT®), MIC was defined as the lowest concentration at which there was 100% growth inhibition. MIC_{50} and MIC_{90} were defined as the MICs required to inhibit the growth of 50 and 90% of the organisms, respectively. Data were interpreted based on the clinical breakpoints recommended by the CLSI M60-Ed2. Accordingly, the ECVs recommended by CLSI M59-Ed3 were applied if further species determination identified one of the cryptic species within the complex.

Ethical Approval

This retrospective study was approved by the ethics committee of Shanghai East Hospital, Tongji University School of Medicine. The need for informed consents was waived by the Clinical Research Ethics Committee [(2017) Pre-examination No. 026].

Statistical Analysis

The results were initially evaluated to assess if the data exhibited asymmetry and/or high variances using the Mann–Whitney test to compare the MIC distributions between non-bloodstream and bloodstream isolates as well as to compare the MIC distributions of bloodstream *C. parapsilosis* isolates between 2015–2018 and 2019–2020. The Kruskal–Wallis tests were used to compare the MIC distributions between the three cryptic species. $P < 0.05$ indicated statistical significance. Statistical analyses were performed using IBM SPSS for Windows v22.0 (IBM, Armonk, NY, United States). Antifungal susceptibility results that were "≤ the lowest concentration" were defaulted as "= the lowest concentration" for statistical analysis. Figures were made using GraphPad Prism v8.0 (GraphPad Software, Inc., San Diego, CA, United States).

RESULTS

Epidemiological Characteristics

The number of *C. parapsilosis* strains isolated were 334 (43.8%) from 2019 to 2020 and 429 (56.2%) from 2005 to 2018; *C. metapsilosis* 30 (41.7%) from 2019 to 2020 and 42 (58.3%) from 2005 to 2018; and *C. orthopsilosis* 15 (30.6%) from 2019 to 2020 and 34 (69.4%) from 2005 to 2018 (**Table 2**). Regarding patients with isolated strains, the age distributions among the three species were similar: 54.46 ± 23.29 years for *C. parapsilosis*, 52.38 ± 19 years for *C. metapsilosis*, and 51.21 ± 23.98 years for *C. orthopsilosis*. In addition, strains were nearly two times more frequently isolated from male than female patients. The variety of sample sources of *C. parapsilosis* was higher than that of *C. orthopsilosis* and *C. metapsilosis*. *C. parapsilosis* strains were mainly isolated from blood (37.1%), followed by sputum (11.5%), urine (10.4%), stool (7.2%), and CVC (6.6%). The proportion of *C. orthopsilosis* strains isolated from blood was highest (40.8%), followed by stool (14.3%), vagina (10.2%), sputum (8.2%), urine (8.2%), and CVC (4.1%). The percentage of strains isolated from blood was the lowest for *C. metapsilosis* among the three species (18.1%), followed by sputum (18.1%), stool (15.3%), and vagina (11.1%). The proportion of *C. metapsilosis* isolated from CVC was also the lowest among the three species (2.8%). The top 10 ward where *C. parapsilosis* complexes were isolated were ICU (12.4%), Oncology (11.5%), Emergency Medicine (8.9%), Gynecology (7.8%), Gastroenterology (7.0%), Respiratory Medicine (6.9%), Nephrology (5.9%), Hepatobiliary and Pancreatic Surgery (5.3%), Neonatology (4.0%), and Otorhinolaryngology (3.6%).

TABLE 2 | Epidemiological characteristics of the *C. parapsilosis* complex isolates.

Characteristics		No. of isolates (%)		
		***C. parapsilosis* (*n* = 763)**	***C. metapsilosis* (*n* = 72)**	***C. orthopsilosis* (*n* = 49)**
Year	2005–2018	429 (56.2)	42 (58.3)	34 (69.4)
	2019–2020	334 (43.8)	30 (41.7)	15 (30.6)
Gender	Male	491 (64.4)	49 (68.1)	31 (63.3)
	Female	272 (35.6)	23 (31.9)	18 (36.7)
Source	Blood	283 (37.1)	13 (18.1)	20 (40.8)
	Sputum	88 (11.5)	13 (18.1)	4 (8.2)
	Urine	79 (10.4)	6 (8.3)	4 (8.2)
	Stool	55 (7.2)	11 (15.3)	7 (14.3)
	Central venous catheter	50 (6.6)	2 (2.8)	2 (4.1)
	Secretions	33 (4.3)		2 (4.1)
	Ear	21 (2.8)	6 (8.3)	2 (4.1)
	Pus	20 (2.6)	2 (2.8)	
	Ascites	19 (2.5)	1 (1.4)	
	Bile	18 (2.4)		
	Vagina	15 (2)	8 (11.1)	5 (10.2)
	Drainage	15 (2)	3 (4.2)	
	Pleural fluid	11 (1.4)	1 (1.4)	
	Tissue	11 (1.4)	1 (1.4)	1 (2)
	Peritoneal dialysis fluid	8 (1)		1 (2)
	Cerebrospinal fluid	8 (1)		
	Wound	6 (0.8)		
	Bronchoalveolar lavage fluid	4 (0.5)		
	Puncture fluid	4 (0.5)		
	Synovial fluid	4 (0.5)	1 (1.4)	
	Puncture needle	3 (0.4)		
	Nail	3 (0.4)	3 (4.2)	1 (2)
	Dialyzate	2 (0.3)		
	Donor kidney lavage fluid	1 (0.1)	1 (1.4)	
	Gastric juice	1 (0.1)		
	Suction tube	1 (0.1)		

Antifungal Susceptibility Results

Resistance/NWT Rates of the *Candida parapsilosis* Complex Isolates

Among the 283 bloodstream *C. parapsilosis*, there were 3.2% SDD and 3.5% R to FLZ, 1.4% I and 2.5% R to VRZ, 0.4% I to MFG, 0.4% NWT to ITZ, 1.4% NWT to POZ, and 1.1% NWT to AMB (**Supplementary Table 2**). Among the 13 bloodstream *C. metapsilosis*, there were 7.7% NWT to AFG and 7.7% NWT to CAS. Among the 20 bloodstream *C. orthopsilosis*, there were 5% NWT to CAS, 5% NWT to MFG, 15% NWT to FLZ, 15% NWT to VRZ, and 5% NWT to POZ.

Among the 480 non-bloodstream *C. parapsilosis*, there were 4.4% SDD and 3.1% R to FLZ, 1.3% I and 1.5% R to VRZ, 0.4% I and 0.2% R to CAS, 1.5% I to AFG, 0.2% NWT to ITZ, 0.6% NWT to POZ, and 7.3% NWT to AMB. Among the 59 non-bloodstream *C. metapsilosis*, there were 10.2% NWT to AFG, 20.3% NWT to CAS, 3.4% NWT to VRZ, and 1.7% NWT to AMB. Among the 29 non-bloodstream *C. orthopsilosis*, there were 3.4% NWT to CAS, 3.4% NWT to MFG, 10.3% NWT to FLZ, 6.9% NWT to VRZ, and 3.4% NWT to POZ.

MIC Values of the Nine Drugs Compared by Source (Non-bloodstream vs. Bloodstream)

Although the general trend of the MIC ranges of the nine drugs for *C. parapsilosis*, *C. metapsilosis*, and *C. orthopsilosis* isolates were similar between bloodstream and non-bloodstream sources (**Figure 1** and **Supplementary Table 1**), for some drugs, their MIC values differed between the two sources. The GM MICs of non-bloodstream *C. parapsilosis* for CAS, MFG, FLZ, VRZ, ITZ, and POZ were 0.555, 0.853, 0.816, 0.017, 0.076, and 0.042 mg/L, respectively. These GM MICs were significantly higher than those of bloodstream *C. parapsilosis*, for which the GM MICs were 0.464, 0.745, 0.704, 0.015, 0.061, and 0.033 mg/L, respectively, for CAS, MFG, FLZ, VRZ, ITZ, and POZ ($P < 0.05$).

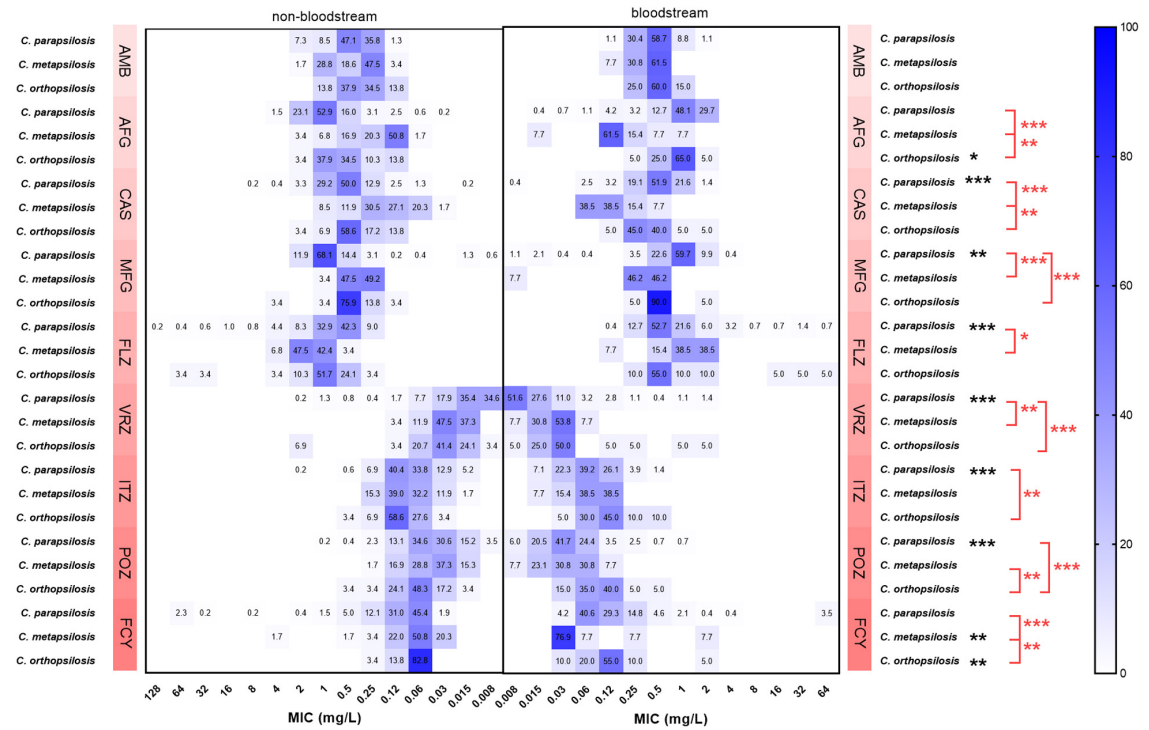

FIGURE 1 | Comparison of the proportions of minimum inhibitory concentration (MIC) distributions of *C. parapsilosis* complex isolates between bloodstream and non-bloodstream samples. Black *indicates $0.01 < P < 0.5$, statistically significant differences of MIC values between bloodstream and non-bloodstream isolates; black **indicates $0.001 < P < 0.01$, black ***indicates $P < 0.001$. Red *indicates $0.01 < P < 0.5$, statistically significant differences of MIC values between bloodstream *C. parapsilosis* complex species; red **indicates $0.001 < P < 0.01$, red ***indicates $P < 0.001$. FLZ, fluconazole; VRZ, voriconazole; ITZ, itraconazole; POZ, posaconazole; MFG, micafungin; AFG, anidulafungin; CAS, caspofungin; AMB, amphotericin B; FCY, 5-flucytosine.

The GM MIC of non-bloodstream *C. metapsilosis* for FCY (0.071 mg/L) was significantly higher than that of bloodstream isolates (0.051 mg/L) ($P < 0.05$). In contrast, the GM MICs of non-bloodstream *C. orthopsilosis* for AFG and FCY were 0.522 and 0.069 mg/L, respectively, which were significantly lower than those of bloodstream isolates, 0.812 and 0.113 mg/L, respectively ($P < 0.05$).

MIC Values of the Nine Drugs Compared Within *Candida parapsilosis* Complex Isolates

The GM MIC of bloodstream *C. parapsilosis* for FLZ (0.704 mg/L) was significantly lower than that of *C. metapsilosis* (0.997 mg/L) ($P < 0.05$, **Figure 1** and **Supplementary Table 1**). The GM MIC of bloodstream *C. parapsilosis* for MFG (0.745 mg/L) was significantly higher than those of *C. metapsilosis* (0.264 mg/L) and *C. orthopsilosis* (0.518 mg/L) ($P < 0.05$). The GM MIC of bloodstream *C. parapsilosis* for VRZ (0.015 mg/L) was significantly lower than those of *C. metapsilosis* (0.023 mg/L) and *C. orthopsilosis* (0.041 mg/L) ($P < 0.05$). The GM MIC of bloodstream *C. orthopsilosis* for ITZ (0.113 mg/L) was significantly higher than that of *C. parapsilosis* (0.061 mg/L) ($P < 0.05$). The GM MIC of bloodstream *C. orthopsilosis* for POZ (0.085 mg/L) was significantly higher than those of *C. parapsilosis* (0.033 mg/L) and *C. metapsilosis* (0.032 mg/L) ($P < 0.05$). The GM MICs of bloodstream *C. metapsilosis* for CAS (0.115 mg/L), AFG (0.150 mg/L), and FCY (0.051 mg/L) were significantly lower than those of *C. parapsilosis* (0.464, 0.918, and 0.136 mg/L, respectively) and *C. orthopsilosis* (0.378, 0.812, and 0.113 mg/L, respectively) ($P < 0.05$).

MIC Values of Bloodstream *Candida parapsilosis* Isolates With the Nine Drugs Compared Over Time

The MIC distributions of *C. parapsilosis* isolates with the nine drugs were different between 2005–2018 (152 strains) and 2019–2020 (131 strains) (**Figure 2**). The GM MICs of strains collected from 2019 to 2020 for VRZ, POZ, and ITZ were 0.018, 0.040, and 0.073 mg/L, respectively, which were significantly higher than those from 2005 to 2018 (0.013, 0.028, and 0.052 mg/L, respectively) ($P < 0.05$). In contrast, GM MICs of the strains collected from 2019 to 2020 for AMB, AFG, CAS, and FCY were 0.382, 0.801, 0.401, and 0.096 mg/L, respectively, which were significantly lower than those from 2005 to 2018 (0.430, 0.918, 0.464, and 0.136 mg/L, respectively) ($P < 0.05$).

MIC Results for ISA

A total of 143 *C. parapsilosis* complex isolates were tested for antifungal susceptibility to ISA (**Table 3**). The isolates all showed great susceptibility to the drug, with MIC ranges ≤ 0.008–1 mg/L.

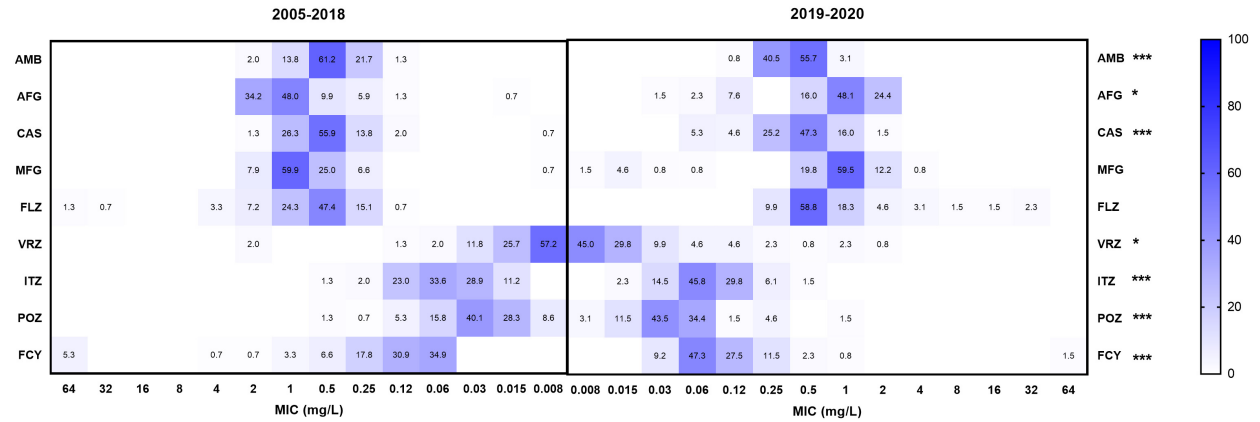

FIGURE 2 | Comparison of the proportions of minimum inhibitory concentration (MIC) distributions of bloodstream *C. parapsilosis* isolates between 2005–2018 and 2019–2020. *Indicates $0.01 < P < 0.5$, statistically significant differences of MIC values between 2005–2018 and 2019–2020; **indicates $0.001 < P < 0.01$, ***indicates $P < 0.001$. FLZ, fluconazole; VRZ, voriconazole; ITZ, itraconazole; POZ, posaconazole; MFG, micafungin; AFG, anidulafungin; CAS, caspofungin; AMB, amphotericin B; FCY, 5-flucytosine.

TABLE 3 | *In vitro* susceptibilities to isaconazole of the 143 *C. parapsilosis* complex isolates.

MIC terms (mg/L)	*C. parapsilosis*		*C. metapsilosis*		*C. orthopsilosis*	
	Blood (*n* = 61)	Non-blood (*n* = 56)	Blood (*n* = 10)	Non-blood (*n* = 12)	Blood (*n* = 2)	Non-blood (*n* = 2)
MIC range	≤0.008–1	≤0.008–0.12	≤0.008–0.03	≤0.008–0.03	≤0.008–0.06	0.015–0.12
MIC50	≤0.008	0.015	≤0.008	≤0.008		
MIC90	0.015	0.03	0.03	0.015		
Modal MIC	≤0.008	0.015	≤0.008	≤0.008	≤0.008, 0.06	0.015, 0.12
GM MIC	0.012	0.012	0.012	0.010	0.022	0.042

MIC, minimum inhibitory concentration; MIC50, the MICs required to inhibit the growth of 50% of the organisms; MIC90, the MICs required to inhibit the growth of 90% of the organisms; GM, geometric mean value.

DISCUSSION

Candida parapsilosis has become the second most prevalent non-*albicans Candida* species that causes invasive infections worldwide, ranging from 24.3% in Latin America to 12.9% in Asia-Pacific. From 2010 to 2019 in Beijing, the most frequently identified non-*albicans Candida* species were *C. parapsilosis*, *C. tropicalis*, and *C. glabrata* (Song et al., 2020). *C. orthopsilosis* and *C. metapsilosis* were reported to have much lower proportions (<1% of all *Candida* species) (Pfaller et al., 2019; Castanheira et al., 2020). Among the *C. parapsilosis* complexes that cause candidemia, *C. orthopsilosis* is responsible for approximately 40% in other countries, following *C. parapsilosis* with about 60%, both of which are much higher than the results in this study (Maria et al., 2018; Vigezzi et al., 2019). The distribution of *C. parapsilosis* (89.6%), *C. metapsilosis* (4.1%), and *C. orthopsilosis* (6.3%) from bloodstream (**Table 2**) is similar to what has been reported in Iran and Venezuela (Moreno et al., 2017; Arastehfar et al., 2019). Furthermore, this study also investigated the non-bloodstream *C. parapsilosis* complex, and there were nearly 1.8 times more of these isolates than bloodstream ones (**Supplementary Table 1**). The non-bloodstream sources included sputum, urine, stool, CVC, secretions, and the ear, by rank. Our data are consistent with the theory that *C. parapsilosis* complex species are a group of opportunistic invasive pathogenic fungi that often colonize the skin, mucous membranes, respiratory tract, intestinal tract, and reproductive tract, causing infections when the host's immunity is impaired. The species can also form biofilms on CVC and other medically implanted devices. The possibility of nosocomial cross-infections *via* the hands of the medical staff is alarming (Trofa et al., 2008; van Asbeck et al., 2009; Wang et al., 2016; Escribano et al., 2018; Tóth et al., 2019; Zhang et al., 2020).

The increasing number of nosocomial *C. parapsilosis* complex infections has raised concerns about conducting antifungal susceptibility tests to optimize clinical treatments (van Asbeck et al., 2008; Gonçalves et al., 2010; Cantón et al., 2011; Pemán et al., 2012; Ruiz et al., 2013; Gago et al., 2014). CLSI M60-Ed2 updated the application rules for clinical breakpoints of *C. parapsilosis* complex: if a cryptic species of the complex is identified, the ECVs should be used instead of the breakpoints (CLSI, 2020). Therefore, this study categorized *C. metapsilosis* and *C. orthopsilosis* as WT and NWT based on the ECVs. Overall, the susceptible rates of bloodstream *C. parapsilosis* to AFG, CAS, MFG, FLZ, and VRZ ranged between 93.3 and 100%, its WT rates to ITZ, POZ, and AMB were between 98.6 and 99.6%, similar to the findings of other studies (da Silva et al., 2015; Moreno et al., 2017; Pfaller et al., 2019). The WT rates for

bloodstream *C. metapsilosis* and *C. orthopsilosis* were between 92.3 and 100%, while there were 15% NWT for *C. orthopsilosis* for both FLZ and VRZ (**Supplementary Table 2**). Similarly, the data by the Shanghai Invasive Fungi Infection Group (IFIG) showed that the resistance rate of *C. parapsilosis* increased from 0 to approximately 5% between 2017 and 2019 (data not published).

In this study, we also investigated the antifungal susceptibilities of non-bloodstream isolates. Notably, the MICs of non-bloodstream *C. parapsilosis* to CAS, MFG, FLZ, VRZ, ITZ, and POZ were significantly higher than those of bloodstream isolates ($P < 0.05$). This was also true for the MICs of *C. metapsilosis* to FCY ($P < 0.05$). However, MICs of non-bloodstream *C. orthopsilosis* to AFG and FCY were significantly lower than those of bloodstream isolates ($P < 0.05$, **Figure 1**). Interestingly, the resistance rate of *Klebsiella pneumoniae* isolated from sputum also tends to be higher than those isolated from blood (Zhao-Yun et al., 2017; Feng et al., 2020). Because *C. parapsilosis* complex can transform from colonizing to invasive phenotypes (Escribano et al., 2018), the antifungal treatment and management of non-bloodstream species should be subject to strict supervision as for bloodstream species (Zhang et al., 2015; Pappas et al., 2018).

The supervision and management of antifungal treatments was performed by ECIFIG, which was launched in 2019 in Shanghai. Since launching, ECIFIG has been identifying organisms, testing their antifungal susceptibilities, and advocating the correct and rational use of antifungal drugs. It is believed that inappropriate drug exposure drives resistance. The mechanisms that cause drug resistance may naturally occur in less susceptible species and are then acquired in strains of susceptible organisms. Compared with MICs from 2005 to 2018, MIC values of bloodstream *C. parapsilosis* isolates collected from 2019 to 2020 decreased significantly for AMB, AFG, CAS, and FCY but increased significantly for VRZ, POZ, and ITZ ($P < 0.05$, **Figure 2**). This change indicated that attention should be paid to the clinical and agricultural use of azoles in Eastern China. It is also reflected in the opinion that an effective antifungal stewardship program is significant for controlling drug resistance.

The ECVs published in CLSI M59 are different among *C. parapsilosis* complex species for AMB, AFG, CAS, FLZ, ITZ, MFG, and VRZ. In this study, similar to the findings in CLSI M59, the MIC values of bloodstream *C. metapsilosis* were significantly lower than those of *C. parapsilosis* and *C. orthopsilosis* for AFG and CAS. MICs of *C. parapsilosis* were significantly higher than those of *C. metapsilosis* and *C. orthopsilosis* for MFG (**Figure 1**). However, MIC values of *C. parapsilosis* were significantly higher than those of *C. metapsilosis* for FLZ, while the ECV of *C. parapsilosis* for FLZ was lower than that of *C. metapsilosis*. Additionally, MICs of *C. orthopsilosis* were significantly higher than those of *C. parapsilosis* for ITZ and were also significantly higher than those of *C. parapsilosis* and *C. metapsilosis* for POZ. The ECVs for ITZ were equal for *C. parapsilosis* and *C. orthopsilosis*, and the ECVs for POZ were the same for all three species. This indicated that the MIC distributions of *C. parapsilosis* for FLZ and the distributions of *C. orthopsilosis* for ITZ and POZ might be higher than those in the CLSI SENTRY program (Pfaller et al., 2011a,b, 2012, 2019; Pfaller, 2012; Castanheira et al., 2016). FLZ is recommended as first-line therapy for candidemia (Pappas et al., 2016), and clonal transmission of FLZ-resistant strains has been reported in Brazil and India (Govender et al., 2016; Thomaz et al., 2018; Singh et al., 2019). Therefore, the higher MIC distributions for azoles in this study is concerning. Apart from that, the MIC values for ISA in this study seemed quite low for *C. parapsilosis* complex isolates. This drug has shown potential as an alternative for candidemia treatment.

CONCLUSION

In summary, the higher MIC values of non-bloodstream isolates compared with bloodstream isolates should arouse attention for antifungal treatment and management of non-bloodstream isolates. Additionally, the increased MIC values for azoles of bloodstream *C. parapsilosis* isolates over the years and the higher MIC distributions for azoles in this study than in CLSI M59 raise concerns about the proper use of azoles in the clinic and environment. It may be worth establishing Eastern China's own ECV for *C. parapsilosis* complex to incorporate better clinical treatment and therapeutic drug monitoring. Finally, ISA has the potential to be an alternative treatment for candidemia.

DATA AVAILABILITY STATEMENT

The original contributions presented in the study are included in the article/**Supplementary Material**, further inquiries can be directed to the corresponding author/s.

ETHICS STATEMENT

All strains isolated from patients were preserved in the ECIFIG at Shanghai East Hospital. We conducted a retrospective study on the isolates and patient data, including age and gender from electronic laboratory records. The need for informed consent was waived by the Clinical Research Ethics Committee.

AUTHOR CONTRIBUTIONS

WW, LZ, and HX designed the experiments and supervised data analysis. JG, HS, DQ, and LW performed the antifungal susceptibility testing. JG and MZ wrote the manuscript. HX, LL, YL, CW, HD, HL, WZ, YWe, HZ, WX, YZ, SZ, RT, DW, and YWa collected and analyzed the data. All authors discussed the results and commented on the manuscript.

FUNDING

This study was supported by the National Natural Science Foundation of China (grant number 81971990), National Science and Technology Major Project (grant number 2018ZX10305409-005-002), Shanghai Key Public Health Discipline (grant number

GWV-10.1-XK04), Shanghai Excellent Technology Leader (grant number 20XD1434500), Clinical Laboratory Diagnostics (grant number PWZxk2017-09-1), and the Top-Level Clinical Discipline Project of Shanghai Pudong (grant number PWYgf 2018-05).

SUPPLEMENTARY MATERIAL

The Supplementary Material for this article can be found online at: https://www.frontiersin.org/articles/10.3389/fmicb.2021.644000/full#supplementary-material

REFERENCES

Arastehfar, A., Khodavaisy, S., Daneshnia, F., Najafzadeh, M. J., Mahmoudi, S., Charsizadeh, A., et al. (2019). Molecular identification, genotypic diversity, antifungal susceptibility, and clinical outcomes of infections caused by clinically underrated yeasts, *Candida orthopsilosis*, and *Candida metapsilosis*: an iranian multicenter study (2014-2019). *Front. Cell Infect. Microbiol.* 9:264. doi: 10.3389/fcimb.2019.00264

Asadzadeh, M., Ahmad, S., Al-Sweih, N., Hagen, F., Meis, J. F., and Khan, Z. (2019). High-resolution fingerprinting of *Candida parapsilosis* isolates suggests persistence and transmission of infections among neonatal intensive care unit patients in Kuwait. *Sci. Rep.* 9:1340.

Cantón, E., Pemán, J., Quindós, G., Eraso, E., Miranda-Zapico, I., Álvarez, M., et al. (2011). Prospective multicenter study of the epidemiology, molecular identification, and antifungal susceptibility of *Candida parapsilosis*, *Candida orthopsilosis*, and *Candida metapsilosis* isolated from patients with candidemia. *Antimicrob. Agents Chemother.* 55, 5590–5596. doi: 10.1128/aac.00466-11

Castanheira, M., Deshpande, L. M., Messer, S. A., Rhomberg, P. R., and Pfaller, M. A. (2020). Analysis of global antifungal surveillance results reveals predominance of Erg11 Y132F alteration among azole-resistant *Candida parapsilosis* and *Candida tropicalis* and country-specific isolate dissemination. *Int. J. Antimicrob. Agents* 55:105799. doi: 10.1016/j.ijantimicag.2019.09.003

Castanheira, M., Messer, S. A., Rhomberg, P. R., and Pfaller, M. A. (2016). Antifungal susceptibility patterns of a global collection of fungal isolates: results of the SENTRY Antifungal Surveillance Program (2013). *Diagn. Microbiol. Infect Dis.* 85, 200–204. doi: 10.1016/j.diagmicrobio.2016.02.009

Chow, J. K., Golan, Y., Ruthazer, R., Karchmer, A. W., Carmeli, Y., Lichtenberg, D., et al. (2008). Factors associated with candidemia caused by non-*albicans Candida* species versus *Candida albicans* in the intensive care unit. *Clin. Infect. Dis.* 46, 1206–1213.

CLSI (2020). *Epidemiological Cutoff Values for Antifungal Susceptibility Testing*, 3rd Edn. Wayne, PA: Clinical and Laboratory Standards Institute.

da Silva, B. V., Silva, L. B., De Oliveira, D. B., Da Silva, P. R., Ferreira-Paim, K., Andrade-Silva, L. E., et al. (2015). Species distribution, virulence factors, and antifungal susceptibility among *Candida parapsilosis* complex isolates recovered from clinical specimens. *Mycopathologia* 180, 333–343. doi: 10.1007/s11046-015-9916-z

Escribano, P., Sánchez-Carrillo, C., Muñoz, P., Bouza, E., and Guinea, J. (2018). Reduction in percentage of Clusters of *Candida albicans* and *Candida parapsilosis* causing candidemia in a general hospital in Madrid, Spain. *J. Clin. Microbiol.* 56:e00574–18.

Feng, L., Su, B., Chang-Feng, Z., Shi-Jie, Z., and Xing-Xing, H. (2020). Clinical distribution characteristics and drug resistance analysis of *Klebsiella pneumoniae*. *Chin. J. Clin. Pulmonol.* 25, 1329–1332.

Gago, S., García-Rodas, R., Cuesta, I., Mellado, E., and Alastruey-Izquierdo, A. (2014). *Candida parapsilosis*, *Candida orthopsilosis*, and *Candida metapsilosis* virulence in the non-conventional host Galleria mellonella. *Virulence* 5, 278–285. doi: 10.4161/viru.26973

García San Miguel, L., Pla, J., Cobo, J., Navarro, F., Sánchez-Sousa, A., Alvarez, M. E., et al. (2004). Morphotypic and genotypic characterization of sequential *Candida parapsilosis* isolates from an outbreak in a pediatric intensive care unit. *Diagn. Microbiol. Infect. Dis.* 49, 189–196. doi: 10.1016/j.diagmicrobio.2004.03.017

Gil-Alonso, S., Quindós, G., Cantón, E., Eraso, E., and Jauregizar, N. (2019). Killing kinetics of anidulafungin, caspofungin and micafungin against *Candida parapsilosis* species complex: evaluation of the fungicidal activity. *Rev. Iberoam. Micol.* 36, 24–29. doi: 10.1016/j.riam.2018.12.001

Gonçalves, S. S., Amorim, C. S., Nucci, M., Padovan, A. C., Briones, M. R., Melo, A. S., et al. (2010). Prevalence rates and antifungal susceptibility profiles of the *Candida parapsilosis* species complex: results from a nationwide surveillance of candidaemia in Brazil. *Clin. Microbiol. Infect.* 16, 885–887. doi: 10.1111/j.1469-0691.2009.03020.x

Govender, N. P., Patel, J., Magobo, R. E., Naicker, S., Wadula, J., Whitelaw, A., et al. (2016). Emergence of azole-resistant *Candida parapsilosis* causing bloodstream infection: results from laboratory-based sentinel surveillance in South Africa. *J. Antimicrob. Chemother.* 71, 1994–2004. doi: 10.1093/jac/dkw091

Guinea, J. (2014). Global trends in the distribution of *Candida* species causing candidemia. *Clin. Microbiol. Infect.* 20(Suppl. 6), 5–10. doi: 10.1111/1469-0691.12539

Guo, L. N., Xiao, M., Cao, B., Qu, F., Zhan, Y. L., Hu, Y. J., et al. (2017). Epidemiology and antifungal susceptibilities of yeast isolates causing invasive infections across urban Beijing. *China. Future Microbiol.* 12, 1075–1086. doi: 10.2217/fmb-2017-0036

Kuhn, D. M., Mikherjee, P. K., Clark, T. A., Pujol, C., Chandra, J., Hajjeh, R. A., et al. (2004). *Candida parapsilosis* characterization in an outbreak setting. *Emerg. Infect. Dis.* 10, 1074–1081.

Magobo, R. E., Naicker, S. D., Wadula, J., Nchabeleng, M., Coovadia, Y., Hoosen, A., et al. (2017). Detection of neonatal unit clusters of *Candida parapsilosis* fungaemia by microsatellite genotyping: results from laboratory-based sentinel surveillance, South Africa, 2009-2010. *Mycoses* 60, 320–327. doi: 10.1111/myc.12596

Maria, S., Barnwal, G., Kumar, A., Mohan, K., Vinod, V., Varghese, A., et al. (2018). Species distribution and antifungal susceptibility among clinical isolates of *Candida parapsilosis* complex from India. *Rev. Iberoam. Micol.* 35, 147–150. doi: 10.1016/j.riam.2018.01.004

Modiri, M., Hashemi, S. J., Ghazvin, I. R., Khodavaisy, S., Ahmadi, A., Ghaffari, M., et al. (2019). Antifungal susceptibility pattern and biofilm-related genes expression in planktonic and biofilm cells of *Candida parapsilosis* species complex. *Curr. Med. Mycol.* 5, 35–42.

Moreno, X., Reviakina, V., Panizo, M. M., Ferrara, G., García, N., Alarcón, V., et al. (2017). Molecular identification and in vitro antifungal susceptibility of blood isolates of the *Candida parapsilosis* species complex in Venezuela. *Rev. Iberoam. Micol.* 34, 165–170.

Pappas, P. G., Kauffman, C. A., Andes, D. R., Clancy, C. J., Marr, K. A., Ostrosky-Zeichner, L., et al. (2016). Clinical practice guideline for the management of Candidiasis: 2016 update by the infectious diseases society of America. *Clin. Infect. Dis.* 62, e1–e50.

Pappas, P. G., Lionakis, M. S., Arendrup, M. C., Ostrosky-Zeichner, L., and Kullberg, B. J. (2018). Invasive candidiasis. *Nat. Rev. Dis. Primers* 4:18026.

Pemán, J., Cantón, E., Quindós, G., Eraso, E., Alcoba, J., Guinea, J., et al. (2012). Epidemiology, species distribution and in vitro antifungal susceptibility of fungaemia in a Spanish multicentre prospective survey. *J. Antimicrob. Chemother.* 67, 1181–1187. doi: 10.1093/jac/dks019

Pfaller, M. A. (2012). Antifungal drug resistance: mechanisms, epidemiology, and consequences for treatment. *Am. J. Med.* 125, S3–S13.

Pfaller, M. A., Andes, D. R., Diekema, D. J., Horn, D. L., Reboli, A. C., Rotstein, C., et al. (2014). Epidemiology and outcomes of invasive candidiasis due to non-*albicans* species of *Candida* in 2,496 patients: data from the Prospective Antifungal Therapy (PATH) registry 2004–2008. *PLoS One* 9:e101510. doi: 10.1371/journal.pone.0101510

Pfaller, M. A., Diekema, D. J., Turnidge, J. D., Castanheira, M., and Jones, R. N. (2019). Twenty years of the SENTRY antifungal surveillance program: results for *candida* species from 1997-2016. *Open Forum. Infect. Dis.* 6, S79–S94.

Pfaller, M. A., Espinel-Ingroff, A., Canton, E., Castanheira, M., Cuenca-Estrella, M., Diekema, D. J., et al. (2012). Wild-type MIC distributions and epidemiological cutoff values for amphotericin B, flucytosine, and itraconazole and *Candida* spp. as determined by CLSI broth microdilution. *J. Clin. Microbiol.* 50, 2040–2046. doi: 10.1128/jcm.00248-12

Pfaller, M. A., Messer, S. A., Moet, G. J., Jones, R. N., and Castanheira, M. (2011a). *Candida* bloodstream infections: comparison of species distribution

and resistance to echinocandin and azole antifungal agents in intensive care unit (ICU) and non-ICU settings in the SENTRY antimicrobial surveillance program (2008-2009). *Int. J. Antimicrob. Agents* 38, 65–69. doi: 10.1016/j.ijantimicag.2011.02.016

Pfaller, M. A., Moet, G. J., Messer, S. A., Jones, R. N., and Castanheira, M. (2011b). Geographic variations in species distribution and echinocandin and azole antifungal resistance rates among *Candida* bloodstream infection isolates: report from the SENTRY antimicrobial surveillance program (2008 to 2009). *J. Clin. Microbiol.* 49, 396–399. doi: 10.1128/jcm.01398-10

Ruiz, L. S., Khouri, S., Hahn, R. C., Da Silva, E. G., De Oliveira, V. K., Gandra, R. F., et al. (2013). Candidemia by species of the *Candida parapsilosis* complex in children's hospital: prevalence, biofilm production and antifungal susceptibility. *Mycopathologia* 175, 231–239. doi: 10.1007/s11046-013-9616-5

Silva, S., Negri, M., Henriques, M., Oliveira, R., Williams, D. W., and Azeredo, J. (2012). *Candida glabrata*, *Candida parapsilosis* and *Candida tropicalis*: biology, epidemiology, pathogenicity and antifungal resistance. *FEMS Microbiol. Rev.* 36, 288–305. doi: 10.1111/j.1574-6976.2011.00278.x

Singh, A., Singh, P. K., De Groot, T., Kumar, A., Mathur, P., Tarai, B., et al. (2019). Emergence of clonal fluconazole-resistant *Candida parapsilosis* clinical isolates in a multicentre laboratory-based surveillance study in India. *J. Antimicrob. Chemother.* 74, 1260–1268. doi: 10.1093/jac/dkz029

Song, Y., Chen, X., Yan, Y., Wan, Z., Liu, W., and Li, R. (2020). Prevalence and antifungal susceptibility of pathogenic yeasts in China: a 10-year retrospective study in a teaching hospital. *Front. Microbiol.* 11:1401. doi: 10.3389/fmicb.2020.01401

Strollo, S., Lionakis, M. S., Adjemian, J., Steiner, C. A., and Prevots, D. R. (2016). Epidemiology of hospitalizations associated with invasive Candidiasis, United States, 2002-2012(1). *Emerg. Infect. Dis.* 23, 7–13. doi: 10.3201/eid2301.161198

Tavanti, A., Davidson, A. D., Gow, N. A., Maiden, M. C., and Odds, F. C. (2005). *Candida orthopsilosis* and *Candida metapsilosis* spp. nov. to replace *Candida parapsilosis* groups II and III. *J. Clin. Microbiol.* 43, 284–292. doi: 10.1128/jcm.43.1.284-292.2005

Thomaz, D. Y., De Almeida, J. N. Jr., Lima, G. M. E., Nunes, M. O., Camargo, C. H., Grenfell, R. C., et al. (2018). An azole-resistant *Candida parapsilosis* outbreak: clonal persistence in the intensive care unit of a Brazilian teaching hospital. *Front. Microbiol.* 9:2997. doi: 10.3389/fmicb.2018.02997

Tóth, R., Nosek, J., Mora-Montes, H. M., Gabaldon, T., Bliss, J. M., Nosanchuk, J. D., et al. (2019). *Candida parapsilosis*: from genes to the bedside. *Clin. Microbiol. Rev.* 32:e00111–18.

Trofa, D., Gácser, A., and Nosanchuk, J. D. (2008). *Candida parapsilosis*, an emerging fungal pathogen. *Clin. Microbiol. Rev.* 21, 606–625. doi: 10.1128/cmr.00013-08

van Asbeck, E., Clemons, K. V., Martinez, M., Tong, A. J., and Stevens, D. A. (2008). Significant differences in drug susceptibility among species in the *Candida parapsilosis* group. *Diagn. Microbiol. Infect. Dis.* 62, 106–109. doi: 10.1016/j.diagmicrobio.2008.04.019

van Asbeck, E. C., Clemons, K. V., and Stevens, D. A. (2009). *Candida parapsilosis*: a review of its epidemiology, pathogenesis, clinical aspects, typing and antimicrobial susceptibility. *Crit. Rev. Microbiol.* 35, 283–309. doi: 10.3109/10408410903213393

Vaz, C., Sampaio, P., Clemons, K. V., Huang, Y. C., Stevens, D. A., and Pais, C. (2011). Microsatellite multilocus genotyping clarifies the relationship of *Candida parapsilosis* strains involved in a neonatal intensive care unit outbreak. *Diagn. Microbiol. Infect. Dis.* 71, 159–162. doi: 10.1016/j.diagmicrobio.2011.05.014

Vigezzi, C., Icely, P. A., Dudiuk, C., Rodríguez, E., Miró, M. S., Castillo, G. D. V., et al. (2019). Frequency, virulence factors and antifungal susceptibility of *Candida parapsilosis* species complex isolated from patients with candidemia in the central region of Argentina. *J. Mycol. Med.* 29, 285–291. doi: 10.1016/j.mycmed.2019.100907

Wang, H., Zhang, L., Kudinha, T., Kong, F., Ma, X. J., Chu, Y. Z., et al. (2016). Investigation of an unrecognized large-scale outbreak of *Candida parapsilosis sensu stricto* fungaemia in a tertiary-care hospital in China. *Sci. Rep.* 6:27099.

Xiao, M., Chen, S. C., Kong, F., Xu, X. L., Yan, L., Kong, H. S., et al. (2020). Distribution and antifungal susceptibility of *Candida* Species causing Candidemia in China: an update from the CHIF-NET study. *J. Infect. Dis.* 221, S139–S147.

Xiao, M., Fan, X., Chen, S. C., Wang, H., Sun, Z. Y., Liao, K., et al. (2015). Antifungal susceptibilities of *Candida glabrata* species complex, *Candida krusei*, *Candida parapsilosis* species complex and *Candida tropicalis* causing invasive candidiasis in China: 3 year national surveillance. *J. Antimicrob. Chemother.* 70, 802–810. doi: 10.1093/jac/dku460

Xiao, M., Sun, Z. Y., Kang, M., Guo, D. W., Liao, K., Chen, S. C., et al. (2018). Five-year national surveillance of invasive Candidiasis: species distribution and azole susceptibility from the China hospital invasive fungal surveillance net (CHIF-NET) study. *J. Clin. Microbiol.* 56:e00577–18.

Zhang, L., Xiao, M., Watts, M. R., Wang, H., Fan, X., Kong, F., et al. (2015). Development of fluconazole resistance in a series of *Candida parapsilosis* isolates from a persistent candidemia patient with prolonged antifungal therapy. *BMC Infect. Dis.* 15:340. doi: 10.1186/s12879-015-1086-6

Zhang, L., Yu, S.-Y., Chen, S. C.-A., Xiao, M., Kong, F., Wang, H., et al. (2020). Molecular characterization of *Candida parapsilosis* by microsatellite typing and emergence of clonal antifungal drug resistant strains in a multicenter surveillance in China. *Front. Microbiol.* 11:1320. doi: 10.3389/fmicb.2020.01320

Zhao-Yun, X., Huai, Y., Yun, X., Jing, S., Zhong-Ling, Y., and Yang, H. (2017). Clinical distribution and drug resistance of *Klebsiella pneumoniae* in non-sputum samples. *Chin. J. Hosp. Infect.* 27, 1689–1692.

Conflict of Interest: The authors declare that the research was conducted in the absence of any commercial or financial relationships that could be construed as a potential conflict of interest.

frontiers in Microbiology

ORIGINAL RESEARCH
published: 28 April 2021
doi: 10.3389/fmicb.2021.655069

A High Rate of Recurrent Vulvovaginal Candidiasis and Therapeutic Failure of Azole Derivatives Among Iranian Women

Amir Arastehfar[1†], Melika Laal Kargar[2†], Shahla Roudbar Mohammadi[2], Maryam Roudbary[3*], Nayereh Ghods[2], Ladan Haghighi[4], Farnaz Daneshnia[1], Mahin Tavakoli[2], Jalal Jafarzadeh[5], Mohammad Taghi Hedayati[6], Huiwei Wang[7,8], Wenjie Fang[7,8*], Agostinho Carvalho[9,10], Macit Ilkit[11], David S. Perlin[1] and Cornelia Lass-Flörl[12]*

[1] Center for Discovery and Innovation, Hackensack Meridian Health, Nutley, NJ, United States, [2] Department of Mycology, Faculty of Medical Science, Tarbiat Modares University, Tehran, Iran, [3] Department of Parasitology and Mycology, School of Medicine, Iran University of Medical Sciences, Tehran, Iran, [4] Department of Obstetrics and Gynecology, School of Medicine, Iran University of Medical Sciences, Tehran, Iran, [5] Department of Medical Mycology and Parasitology, School of Medicine, Babol University of Medical Sciences, Babol, Iran, [6] Invasive Fungi Research Center, Department of Medical Mycology, School of Medicine, Mazandaran University of Medical Sciences, Sari, Iran, [7] Shanghai Key Laboratory of Molecular Medical Mycology, Shanghai Institute of Mycology, Shanghai Changzheng Hospital, Second Military Medical University, Shanghai, China, [8] Department of Dermatology, Shanghai Changzheng Hospital, Second Military Medical University, Shanghai, China, [9] Life and Health Sciences Research Institute (ICVS), School of Medicine, University of Minho, Braga, Portugal, [10] ICVS/3B's – PT Government Associate Laboratory, Guimarães/Braga, Portugal, [11] Division of Mycology, University of Çukurova, Adana, Turkey, [12] Division of Hygiene and Medical Microbiology, Medical University of Innsbruck, Innsbruck, Austria

Recurrent vulvovaginal candidiasis (RVVC) is one of the most prevalent fungal infections in humans, especially in developing countries; however, it is underestimated and regarded as an easy-to-treat condition. RVVC may be caused by dysbiosis of the microbiome and other host-, pathogen-, and antifungal drug-related factors. Although multiple studies on host-related factors affecting the outcome have been conducted, such studies on *Candida*-derived factors and their association with RVVC are lacking. Thus, fluconazole-tolerant (FLZT) isolates may cause fluconazole therapeutic failure (FTF), but this concept has not been assessed in the context of *Candida*-associated vaginitis. Iran is among the countries with the highest burden of RVVC; however, comprehensive studies detailing the clinical and microbiological features of this complication are scarce. Therefore, we conducted a 1-year prospective study with the aim to determine the RVVC burden among women referred to a gynecology hospital in Tehran, the association of the previous exposure to clotrimazole and fluconazole with the emergence of FLZT and fluconazole-resistant (FLZR) *Candida* isolates, and the relevance of these phenotypes to FTF. The results indicated that about 53% of the patients (43/81) experienced RVVC. *Candida albicans* and *C. glabrata* constituted approximately 90% of the yeast isolates (72 patients). Except for one FLZT *C. tropicalis* isolate, FLZR and FLZT phenotypes were detected exclusively in patients with RVVC; among them, 27.9% (12/43) harbored FLZR strains. *C. albicans* constituted 81.2% of FLZR (13/16) and 100% of the FLZT (13/13) isolates, respectively, and both phenotypes were likely responsible for FTF, which was also observed among patients with RVVC infected with fluconazole-susceptible isolates. Thus, FTF could be due to host-, drug-,

OPEN ACCESS

Edited by:
Jack Wong,
Caritas Institute of Higher Education,
Hong Kong

Reviewed by:
Somanon Bhattacharya,
Stony Brook University, United States
Ashutosh Singh,
University of Lucknow, India

***Correspondence:**
Shahla Roubar Mohammadi
Sh.mohammadi@modares.ac.ir
Maryam Roudbary
m_roudbary@yahoo.com;
roudbari.mr@iums.ac.ir
Wenjie Fang
fangwenjie1990@126.com

[†] These authors have contributed equally to this work

Specialty section:
This article was submitted to Antimicrobials, Resistance and Chemotherapy, a section of the journal Frontiers in Microbiology

Received: 18 January 2021
Accepted: 22 March 2021
Published: 28 April 2021

Citation:
Arastehfar A, Kargar ML, Mohammadi SR, Roudbary M, Ghods N, Haghighi L, Daneshnia F, Tavakoli M, Jafarzadeh J, Hedayati MT, Wang H, Fang W, Carvalho A, Ilkit M, Perlin DS and Lass-Flörl C (2021) A High Rate of Recurrent Vulvovaginal Candidiasis and Therapeutic Failure of Azole Derivatives Among Iranian Women. Front. Microbiol. 12:655069. doi: 10.3389/fmicb.2021.655069

and pathogen-related characteristics. Our study indicates that FLZT and FLZR isolates may arise following the exposure to over-the-counter (OTC) topical azole (clotrimazole) and that both phenotypes can cause FTF. Therefore, the widespread use of OTC azoles can influence fluconazole therapeutic success, highlighting the necessity of controlling the use of weak topical antifungals among Iranian women.

Keywords: recurrent vulvovaginal candidiasis, *Candida albicans*, *Candida glabrata*, fluconazole therapeutic failure, fluconazole tolerance, fluconazole resistance

INTRODUCTION

Fungi are major components of the human microbiome (Rolling et al., 2020) and are associated with approximately 1.7 billion superficial fungal infections (SFIs) and 1.5 million deaths due to invasive fungal infections (IFIs) (Brown et al., 2012). While IFIs have received notable attention of medical mycologists (Brown et al., 2012), SFIs are somewhat neglected, being considered as mild and easily treatable conditions. Vulvovaginal candidiasis (VVC) is one of the most prevalent manifestations of SFIs, and it is estimated that 75% of women experience at least one VVC episode during their lifetime (Brown et al., 2012; Denning et al., 2018). Furthermore, approximately 138 million women suffer from recurrent vulvovaginal candidiasis (RVVC) annually, and this number is projected to reach 158 million by 2030 (Denning et al., 2018). RVVC can severely affect the quality of life for the afflicted patients and imposes a significant economic burden, which exceeds 14.39 billion USD in developed countries (Denning et al., 2018).

Antibiotic overuse, diabetes, pregnancy, and cystic fibrosis are among the risk factors for RVVC (Denning et al., 2018). In addition, immunodeficiency due to genetic aberrations (Jaeger et al., 2016; Tian et al., 2017), local immune overreaction (Rosati et al., 2020), the inefficiency of prescribed antifungal agents, and, to a lesser extent, the development of antifungal resistance contribute to RVVC. Numerous studies have evaluated the association between host-related factors and RVVC (Rosati et al., 2020); however, there is a lack of similar studies on *Candida*-related factors such as drug resistance and tolerance, which limits our understanding of their relevance to RVVC. Recently, it has been reported that tolerance to the principal antifungal agent fluconazole among a subpopulation of susceptible isolates may promote colonization, thus increasing therapeutic failure and mortality rates (Astvad et al., 2018; Rosenberg et al., 2018). Fluconazole resistance phenotype is due to stable genomic changes with visible growth of higher than minimum inhibitory concentration (MIC) at 24 h endpoint in the presence of drug. Fluconazole tolerance, on the other hand, is mainly due to physiologic changes allowing a subpopulation of cells, called tolerant cells, to grow slowly at concentrations above MIC for which the data MIC are recorded at 48 h (Rosenberg et al., 2018; Arastehfar et al., 2020c). Therefore, fluconazole tolerance may not be detected using standard broth microdilution assays in which the scoring endpoint is 24 h, indicating the necessity of alternative analytical methods (Rosenberg et al., 2018). Although drug tolerance has been studied in the context of candidemia, its role in VVC remains unclear.

Treatment of fungal infections depends on clinical manifestations, disease severity, and causative yeast/*Candida* species (Pappas et al., 2016). A single 150 mg dose of fluconazole is recommended for treating VVC, whereas 10–14-day induction with topical fluconazole or other agents, followed by 150 mg oral fluconazole weekly for a period of 6 months is recommended for RVVC (Pappas et al., 2016). Since some *Candida* species such as *Candida glabrata* can rapidly develop resistance to azoles (Arastehfar et al., 2020c), therefore the treatment of VVC consists of topical intravaginal nystatin or boric acid or 17% flucytosine cream alone or in combination with 3% amphotericin B cream for 14 days (Pappas et al., 2016). Although *Candida albicans* has been historically known as the most prevalent causative agent of fungal vulvovaginitis, new lines of evidence reveal an increasing incidence of non-*albicans Candida* (NAC) species, which generally respond to higher MICs of azoles (Makanjuola et al., 2018) and which may contribute to complications associated with RVVC. Since the vast majority of RVVC cases are recorded in developing countries (Denning et al., 2018), the shift toward NAC species could be problematic for their healthcare institutions, where the diagnosis and treatment of fungal infections are inadequate (Arastehfar et al., 2019a,b,c,d; Arastehfar et al., 2020d; Kord et al., 2020; Megri et al., 2020).

Iran, a developing country with a population of 85 million people, has been estimated to be among the countries with the highest RVVC prevalence (>4,300 cases per 100,000 women) (Denning et al., 2018); however, there is a lack of comprehensive epidemiological studies detailing the clinical and microbiological characteristics of VVC and RVVC. Therefore, the aim of the current prospective study conducted in Tehran was to determine the prevalence of VVC and RVVC and the rate of therapeutic failure for commonly used antifungals. We also assessed the proportion of fluconazole-resistant (FLZR) and fluconazole-tolerant (FLZT) isolates and examined their association with prior azole exposure and azole therapeutic failure. Thus, the novelty of our study was the focus on fungal factors affecting the efficacy of treatment.

MATERIALS AND METHODS

Patients, Definitions, and Treatment Strategies

Women referred to the Shahid Akbar-Abadi Obstetrics and Gynecology Hospital in Tehran, Iran, between January 30, 2018 and January 30, 2019 were included in the current prospective

study. Swab samples were obtained from patients with symptoms including but not limited to vulvar pruritus, burning vaginal soreness, dyspareunia and dysuria, edema, fissures, and vulvar and vaginal erythema. VVC was confirmed by microscopic detection of yeast structures and yeast/*Candida*-positive cultures (Gonçalves et al., 2016; Denning et al., 2018). Cases of bacterial vaginosis were excluded from this study.

Antifungal treatment did not depend on culture results and was empirically prescribed by the treating gynecologist based on gynecologic examination and microscopic observations. Patients were treated at the discretion of the treating gynecologists. Initial antifungal treatment included two 150-mg doses of oral fluconazole (the 1st and 4th days) or 1% topical clotrimazole (for 10–12 days). Patients showing remission after clotrimazole treatment were switched to two 150-mg doses of fluconazole, whereas those with remission after receiving oral fluconazole were switched to two doses of fluconazole + clotrimazole. If remission persisted after 3 months, patients were prescribed two 150-mg doses of fluconazole biweekly for 6 months.

Recurrent vulvovaginal candidiasis was diagnosed by treating physicians based on the following criteria: the patient developed ≥3 episodes per year (Rosati et al., 2020), the initial antifungal treatment did not result in improvement, and *Candida* species were detected by both microscopy and culture. Moreover, patients who used over-the-counter (OTC) clotrimazole for a long time (over 1 year) to treat recurrent complications prior to this study were considered as having RVVC. Short-term exposure was defined when patients (had) completed clotrimazole therapy (10–12 days). Follow-up was conducted by the phone every 2 weeks to evaluate the overall improvement and patients with complaints despite treatment were requested to come to the hospital for examination and swab test. Patients with remission who dropped out of the study after completion of the second course of antifungal treatment were monitored by phone calls.

This study was approved by the human subject hospital review board of Shahid Akbar-Abadi Obstetrics and Gynecology Hospital (IR.MODARES.REC.1397.225). Informed consents were obtained from all patients included in the current study, and researchers were blinded to patient identifiers.

Yeast Isolation and Identification

Vaginal samples were taken from symptomatic patients using sterile cotton swabs and transferred immediately to Falcon tubes containing PBS. Sampling was performed in accordance with institutional safety protocols. First, the specimens were observed directly under a microscope to reveal yeast structures and then cultured on Sabouraud dextrose agar and CHROMagar (Candiselect, Bio-Rad, Hercules, CA, United States) at 35°C for 48 h. DNA was extracted using a acetyl trimethylammonium bromide-based method described previously (Arastehfar et al., 2018). Isolates were primarily identified by a previously developed multiplex PCR, which can identify 21 yeast species associated with human infections (Arastehfar et al., 2019c). This assay includes three multiplex PCR reactions in which the first multiplex PCR identifies the main *Candida* species, the second one identifies the emerging *Candida* species, and the third multiplex PCR identifies basidiomycetous yeast species. Details regarding this assay were presented in details previously and primers used are listed in **Supplementary Tables 1–3**. Isolates were further identified by MALDI-TOF MS using a full-extraction method (Arastehfar et al., 2019b) to confirm the accuracy of the results obtained by PCR.

Antifungal Susceptibility Testing

Antifungal susceptibility testing (AFST) was conducted according to the Clinical Laboratory Standards Institute (CLSI-M27) protocol, fourth edition [Clinical and Laboratory Standards Institute (CLSI), 2017]. MIC values were interpreted based on CLSI-M60, second edition [Clinical and Laboratory Standards Institute (CLSI), 2020], previously reported clinical breakpoints (CBPs), and epidemiological cutoff values (ECVs) (Pfaller and Diekema, 2012). AFST included fluconazole and itraconazole (both from Sigma-Aldrich, St. Louis, MO, United States) but not echinocandins and amphotericin B, since patients did not receive these antifungals. Of note, clotrimazole was not included in our AFST scheme due to the lack of CBPs and ECVs to interpret MICs obtained for this antifungal. Antifungal drugs were dissolved in RPMI1640 (Sigma-Aldrich). Plates were incubated at 35°C and MICs were determined after 24 h. *Candida parapsilosis* (ATCC 22019) and *Candida krusei* (ATCC 6258) were used for quality control purposes. The MIC values for species lacking CBPs were interpreted based on ECVs, and isolates showing MICs > ECV or <ECV were considered as non-wild type (NWT) or wild-type (WT), respectively [Pfaller and Diekema, 2012; CLSI, 2nd ed. CLSI supplement M60 Clinical and Laboratory Standards Institute (CLSI), 2017]. Non-susceptible *C. albicans*, *C. parapsilosis*, and *C. tropicalis* isolates were denoted when the MICs were ≥4 μg/ml, while fluconazole-resistant *C. glabrata* isolates had MICs ≥ 64 μg/ml. *C. albicans* isolates with itraconazole MICs ≥ 1 μg/ml were considered as resistant and *C. glabrata* isolates showing MICs > 2 μg/ml and *C. parapsilosis* and *C. tropicalis* with MICs > 0.5 μg/ml were regarded as NWT to itraconazole. Since there is no CBPs for *C. krusei*, the MIC data were reported per ECVs, where *C. krusei* isolates with MICs > 64 μg/ml and >1 μg/ml were noted as NWT to fluconazole and itraconazole (Pfaller and Diekema, 2012).

Isolates growing at concentrations above the MIC after 48 h were considered as FLZT (Arastehfar et al., 2020b; Berman and Krysan, 2020). Fluconazole-tolerance for *C. albicans*, *C. parapsilosis*, and *C. tropicalis* was noted when the 48 h fluconazole MICs were ≥4 μg/ml, while fluconazole tolerance of *C. glabrata* was defined when the MICs of 48 h were ≥64 μg/ml (Rosenberg et al., 2018; Arastehfar et al., 2020b).

RESULTS

Patients' Characteristics

During the study period, 300 patients referred to the clinic were screened; 81 had confirmed VVC and over half of them

TABLE 1 | Isolate and patient numbers and *Candida* species distribution among patients with VVC and RVVC.

Species (number of isolates;%)	VVC number of cases (number of isolate)	RVVC number of cases (number of isolate)	Total number of patients (%)
Candida albicans (*n* = 114; 78.6%)	29 (*n* = 29)	35 (*n* = 85)	(64/81; 79%)
Candida glabrata (*n* = 17; 11.7%)	3 (*n* = 3)	5 (*n* = 14)	(8/81; 9.9%)
Candida krusei (*n* = 11; 7.5%)	3 (*n* = 3)	3 (*n* = 8)	(6/81; 7.4%)
Candida parapsilosis (*n* = 2; 1.3%)	2 (*n* = 2)	0	(2/81; 2.4%)
Candida tropicalis (*n* = 1; 0.68%)	1 (*n* = 1)	0	(1/81; 1.2%)
(*n* = 145; 100%)	38 (*n* = 38) (38/107; 35.5%)	43 (*n* = 107) (107/145; 73.7%)	(81; 100%)

VVC, vulvovaginal candidiasis; RVVC, recurrent vulvovaginal candidiasis.

were diagnosed with RVVC (43/81; 53%) (**Table 1**). The median age for RVVC patients was 35 years (20–68 years) and for patients with VVC only (38/81; 47%), the median age was 39 years (19–63 years). About 88% of patients with VVC and RVVC were healthy; the underlying conditions in the minority of patients included hypothyroidism (4/81, 4.8%; two in each group), diabetes (2/81, 2.4%; one in each group), anemia (2/81, 2.4%; one in each group), fatty liver (1/81, 1.2%; the VVC group), and hypertension (1/81, 1.2%; the VVC group). There was no significant difference in age and the underlying conditions between the VVC and RVVC groups. Among the 43 patients with RVVC, 12 had prior exposure to OTC topical clotrimazole for ≥1 year (**Table 2**). During the study period, nine and 15 patients with RVVC dropped out of the study after completing the second and third course of treatment, respectively. Approximately 62% of patients with RVVC had persistent vaginal candidiasis (28/43), whereas for all patients with VVC the infection was cleared after the first use of azoles and no signs of infection were recorded through the entire follow-up period.

Bacterial co-infection was observed in 15.8 and 30.2% of patients with VVC (6/38) and RVVC (13/43), respectively; it was completely resolved in the VVC group after antibiotic treatment but persisted in the RVVC group up to the second (7/13; 54%) and third (2/13; 15.4%) follow-up. Moreover, four new incidences of bacterial co-infection were detected at the second follow-up; these cases were successfully treated with antibiotics.

Candida Species Distribution

In total, 145 yeast isolates were recovered from 43 patients with RVVC (107/145; 73.7%) and 38 patients with VVC (38/145; 26.2%); among them, *C. albicans* was the most prevalent species (114/145; 78.6%), followed by *C. glabrata* (17/145; 11.7%), *C. krusei* (11/145; 7.6%), *C. parapsilosis* (2/145; 1.3%), and *C. tropicalis* (1/145; 0.7%) (**Tables 1**, **2** and **Figure 1**).

The same trend was observed among the 81 patients: *C. albicans* was the most prevalent species in both VVC (29/38; 76.3%) and RVVC (35/43; 81.3%) groups (**Table 1** and **Figure 1**). However, most of *C. glabrata* (14/17; 82.3%) and *C. krusei* (8/11; 72.2%) isolates were recovered from patients with RVVC (**Table 1**), whereas *C. parapsilosis* and *C. tropicalis* were only observed among those with VVC. All patients with RVVC carried the same species throughout the study period and mixed infections due to multiple yeast/*Candida* species were not observed.

Association of FLZR and FLZT Phenotypes With Azole Therapeutic Failure

Resistance was noted only to fluconazole and only among patients with RVVC, whereas all *Candida* isolates recovered from patients with VVC were fluconazole-susceptible (**Tables 2**, **3**). In total, 25.5% of RVVC cases (11/43) were due to fluconazole-non-susceptible (FNS) *C. albicans* (≥4 μg/ml) representing 15.3% of *C. albicans* isolates (13/85) recovered from the RVVC group (excluding cases due to mixed FLZR and FLZT isolates) (**Tables 2**, **3**). Moreover, only one RVVC case was due to FLZR *C. glabrata* (MIC ≥ 64 μg/ml); this patient had a prior exposure to clotrimazole. Some of the FLZR isolates were obtained from patients who were repeatedly exposed to topical clotrimazole for a period of ≥1 year, but all the infections were cleared after two doses of fluconazole (patients # 26, 60, 62, 63, 102, 118, and 125) (**Table 2**). The other FLZR isolates emerged during the course of treatment with clotrimazole and/or fluconazole and both azoles showed therapeutic failure in the infected patients. Approximately 42% of patients with RVVC were infected with fluconazole-sensitive (FLZS) isolates, which were not tolerant to fluconazole (**Table 2**). On the other hand, all patients with VVC were successfully treated with either topical clotrimazole or oral fluconazole (**Table 2**). Although categorized as WT, 100 and 66.6% of *C. krusei* isolates recovered from patients with RVVC and VVC, respectively, responded to fluconazole MIC of 64 μg/ml. None of the isolates showed itraconazole resistance and 2.6% of *C. albicans* isolates showed susceptible dose-dependent phenotype (MICs 0.25–0.5 μg/ml) (**Table 3**).

The FLZT phenotype was only observed for *C. albicans* (13/114; 11.4%) and *C. tropicalis* (1/1; 100%) and was not detected among *C. glabrata*, *C. krusei*, and *C. parapsilosis* isolates. Interestingly, except for one *C. tropicalis* isolate from a patient with VVC who was successfully treated with two 150-mg doses of fluconazole, all FLZT *C. albicans* isolates were recovered from patients with RVVC (**Table 2**). The FLZT phenotype, similar to the FLZR phenotype, emerged either in the course of treatment or prior to the study, when the infected patients had long-term exposure to clotrimazole and already carried FLZT isolates before the recruitment to this study. Although two of the patients with prior clotrimazole exposure (# 37 and 89) were successfully treated with two doses of fluconazole, FLZT isolates which emerged during the course of treatment caused therapeutic failure of both fluconazole and clotrimazole (**Table 2**). Finally, FLZS isolates initially carried

TABLE 2 | Clinical and microbiological characteristics of patients included in this study.

Patient #	Age (years)	Species (MIC, μ g/ml)/ (isolate number)	Treatment	Final outcome
Patients with RVVC harboring resistant or high fluconazole MIC-responding isolates with/without prior short-term exposure to 1% topical clotrimazole (*n* = 5).				
29	29	*C. glabrata* (64)[A]	CLT 1% (12 days)	Persistent
		C. glabrata (64)	FLC 150 mg (first and fourth days = 2 doses)	
		C. glabrata (64)	FLC 150 mg (1 dose per week for 6 months = 24 doses)	
31	25	*C. krusei* (64)[A]	FLC 150 mg (2 doses)	Persistent
		C. krusei (64)	FLC 150 mg (2 doses)	
		C. krusei (64)	FLC 150 mg (24 doses)	
32	31	*C. krusei* (64)[A]	FLC 150 mg (2 doses)	Cleared
		C. krusei (64)	FLC 150 mg (24 doses)[B]	
34	31	*C. krusei* (64)[A]	Oral fluconazole 150 mg (first and fourth days)	Persistent
		C. krusei (64)	FLC 150 mg (2 doses) + CLT1% (10 days)	
		C. krusei (64)	FLC 150 mg (24 doses)	
41	41	*C. albicans* (0.125)	CLT 1% (12 days)	Cleared
Patients with RVVC harboring fluconazole-non-susceptible isolates with prior long-term exposure to 1% topical clotrimazole (*n* = 7).				
26	40	*C. albicans* (64)	FLC 150 mg (2 doses)	Cleared
60	27	*C. albicans* (16)	FLC 150 mg (2 doses)	Cleared
62	52	*C. albicans* (64)	FLC 150 mg (2 doses)	Cleared
63	38	*C. albicans* (64)	FLC 150 mg (2 doses)	Cleared
102	31	*C. albicans* (64)	FLC 150 mg (2 doses)	Cleared
118	29	*C. albicans* (4)	FLC 150 mg (2 doses)	Cleared
125	29	*C. albicans* (4)	FLC 150 mg (2 doses)	Cleared
Patients with RVVC harboring fluconazole-tolerant isolates that became fluconazole-non-susceptible during the course of treatment (*n* = 3).				
3	46	*C. albicans* (0.25)	CLT1% (12 days)	Persistent
		C. albicans (0.5)	FLC 150 mg (2 doses) + CLT 1% (10 days)	
		C. albicans (2) (tolerant)	FLC 150 mg (2 doses)	
		C. albicans (16)	FLC 150 mg (24 doses)	
4	35	*C. albicans* (0.25)	CLT 1% (12 days)	Persistent
		C. albicans (2) (tolerant)	FLC 150 mg (2 doses)	
		C. albicans (4)	FLC 150 mg (24 doses)	
20	20	*C. albicans* (0.25) (tolerant)[A]	FLC 150 mg (2 doses)	Persistent
		C. albicans (64)	FLC 150 mg (2 doses) + CLT 1% (10 days)	
		C. albicans (64)	FLC 150 mg (24 doses)	
Patients with RVVC harboring tolerant isolates with/without prior short-term exposure to 1% topical clotrimazole (*n* = 8).				
19	34	*C. albicans* (0.25)	FLC 150 mg (2 doses)	Persistent
		C. albicans (0.5)	FLC 150 mg (2 doses) + CLT 1% (10 days)	
		C. albicans (2) (tolerant)	FLC 150 mg (24 doses)	
43	24	*C. albicans* (0.5)	FLC 150 mg (2 doses)	Persistent
		C. albicans (0.5)	FLC 150 mg (2 doses) + CLT 1% (10 days)	
		C. albicans (2)[A] (tolerant)	FLC 150 mg (24 doses)	
59	42	*C. albicans* (0.5)[A] (tolerant)	CLT 1% (12 days)	Persistent
		C. albicans (1)[A] (tolerant)	FLC 150 mg (2 doses)	
		C. albicans (0.125)[A] (tolerant)	FLC 150 mg (24 doses)	
73	30	*C. albicans* (0.125)	CLT 1% (12 days)	Persistent
		C. albicans (0.125)	FLC 150 mg (2 doses)	
		C. albicans (0.125) (tolerant)	FLC 150 mg (24 doses)	
101	35	*C. albicans* (0.125)	FLC 150 mg (2 doses)	Persistent
		C. albicans (0.125)	FLC 150 mg (2 doses) + CLT 1% (10 days)	
		C. albicans (0.25) (tolerant)	FLC 150 mg (24 doses)	

(Continued)

TABLE 2 | Continued

Patient #	Age (years)	Species (MIC, μ g/ml)/ (isolate number)	Treatment	Final outcome
110	40	*C. albicans* (0.25)	FLC 150 mg (2 doses) + CLT 1% (10 days)	Persistent
		C. albicans (0.25) (tolerant)	FLC 150 mg (2 doses) + CLT 1% (10 days)	
		C. albicans (0.5) (tolerant)	FLC 150 mg (24 doses)	
134	23	*C. albicans* (0.125)	FLC 150 mg (2 doses)	Persistent
		C. albicans (0.125)	FLC 150 mg (2 doses) + CLT 1% (10 days)	
		C. albicans (0.25) (tolerant)	FLC 150 mg (24 doses)	
138	68	*C. albicans* (0.25)	CLT 1% (12 days)	Persistent
		C. albicans (0.25)	FLC 150 mg (2 doses)	
		C. albicans (1) (tolerant)	FLC 150 mg (24 doses)	
Patients with RVVC harboring fluconazole-tolerant isolates with prior long-term exposure to 1% topical clotrimazole (*n* = 2).				
37	31	*C. albicans* (0.125)	FLC 150 mg (2 doses)	Cleared
89	44	*C. albicans* (2)	FLC 150 mg (2 doses)	Cleared
Patients with RVVC harboring fluconazole susceptible (fluconazole-non-tolerant) isolates (*n* = 18).				
NA	24–55	*C. albicans* (0.125–1) (*n* = 39)	FLC (2 doses)→ FLC (2 doses) + CLT 1% (10 days)→ FLC (24 doses) (*n* = 10) FLC (2 doses)→ FLC (2 doses) + CLT 1% (2 doses) (*n* = 1) CLT 1%(10 days)→ FLC (2 doses)→ FLC (24 doses) (*n* = 2) CLT 1% (10 days)→ FLC (2 doses) (*n* = 1)	Cleared (*n* = 4) Persistent (*n* = 10)
NA	29–35	*C. glabrata* (1–2) (*n* = 11)	CLT 1%(10 days)→ FLC (2 doses)→ FLC (24 doses) (*n* = 2) Oral fluconazole 150 mg (2 doses)→ Oral FLC (2 doses)→ FLC (2 doses) + CLT 1% (24 doses) (*n* = 1) CLT 1%(10 days)→ FLC (2 doses) (*n* = 1)	Persistent (*n* = 4)
Patients with VVC without prior exposure to 1% topical clotrimazole successfully treated during the first course (*n* = 38).				
29 patients	20–57	*C. albicans* (0.125–2) (*n* = 29)	FLC (2 doses) (*n* = 15) CLT 1% (12 days) (*n* = 14)	Cleared
3 patients	19–41	*C. glabrata* (1–16) (*n* = 3)	CLT 1% (12 days) (*n* = 2) FLC 150 mg (2 doses) (*n* = 1)	Cleared
2 patients	38, 63	*C. parapsilosis* (0.125) (*n* = 2)	CLT 1% (12 days) (*n* = 1) FLC 150 mg (2 doses) (*n* = 1)	Cleared
3 patients	29–52	*C. krusei* (4–64)[A] (*n* = 3)	FLC 150 mg (2 doses) (*n* = 2) CLT 1% (12 days) (*n* = 1)	Cleared
1 patient	42	*C. tropicalis* (1) (*n* = 1)	FLC 150 mg (2 doses) (*n* = 1)	Cleared

[A]*These isolates were recovered from a patient who had previous short-term exposure to intravaginal topical 1% clotrimazole.* [B]*These patients were only examined by a gynecologist and refused to provide swab samples during follow-up. FLZ: fluconazole; CLT: clotrimazole.*

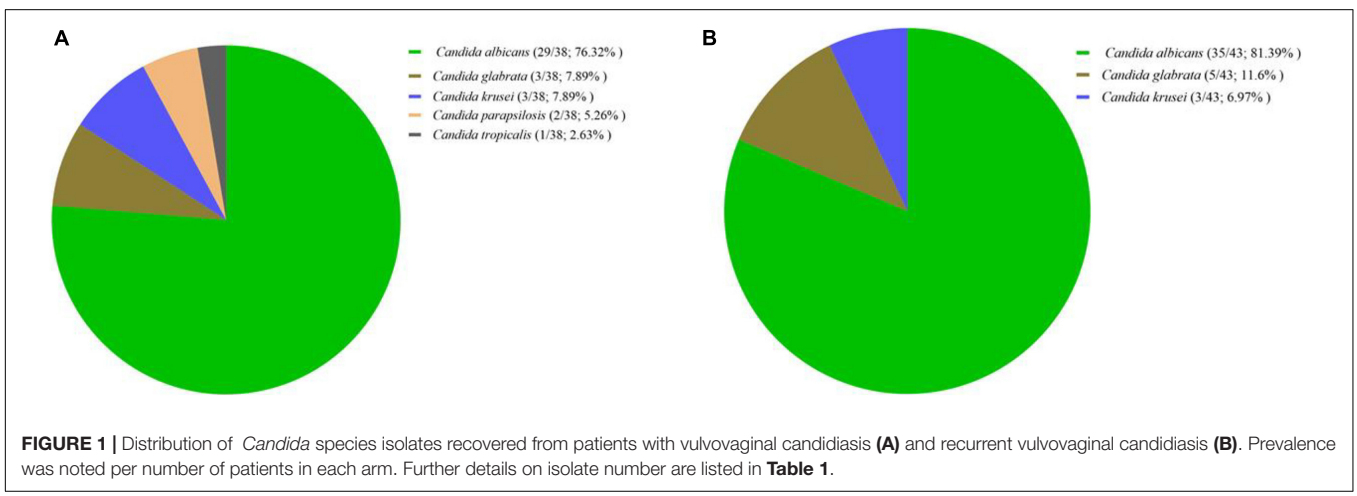

FIGURE 1 | Distribution of *Candida* species isolates recovered from patients with vulvovaginal candidiasis **(A)** and recurrent vulvovaginal candidiasis **(B)**. Prevalence was noted per number of patients in each arm. Further details on isolate number are listed in **Table 1**.

by some patients with RVVC acquired the FLZT and then the FLZR phenotype during the course of treatment, both of which were responsible for fluconazole and/or clotrimazole therapeutic failure.

DISCUSSION

Our study revealed that RVVC was dominant among the VVC cases, which, we believe, could be attributed to the

TABLE 3 | Species distribution and fluconazole and itraconazole susceptibility patterns of *Candida* isolates recovered from Iranian women suffering from VVC and RVVC.

Species	Susceptibility status	Fluconazole	Itraconazole
C. albicans (*n* = 114)	Susceptible	101	94
	Susceptible dose-dependent	3	20
	Resistant	10	0
	Range	0.125–64	0.032–0.25
C. glabrata (*n* = 17)	<ECV	14	17
	>ECV	3	0
	Susceptible dose-dependent	14	NA
	Resistant	3	NA
	Range	1–64	0.064–0.25
C. krusei (*n* = 11)	<ECV	11	11
	>ECV	0	0
	Range	4–64	0.032–0.25
C. parapsilosis (*n* = 2)	<ECV	2	2
	>ECV	0	0
	Susceptible	2	0
	Range	0.125	0.032
C. tropicalis (*n* = 1)	<ECV	1	1
	>ECV	0	0
	Susceptible	1	NA
	Range	NA	NA

ECV, epidemiological cutoff value.

disproportionate use of OTC topical clotrimazole, resulting in the emergence of FLZT and FLZR isolates. Moreover, we showed that, similar to the FLZR phenotype, the FLZT phenotype might predict azole therapeutic failure. Thus, our data confirm the multifactorial nature of RVVC, whose outcome can be influenced, along with host- and drug-related factors, by fungal characteristics such as FLZR and FLZT phenotypes.

Consistent with previous estimations (Denning et al., 2018), we showed that RVVC was a serious issue among Iranian women. Because VVC is considered a superficial and easy-to-treat fungal infection, most of the affected women refrain from visiting gynecologists and take OTC topical clotrimazole after consultation with pharmacists. Therefore, we assume that the prevalence of RVVC has been overestimated because of the low referral rate of patients with VVC, who have already been using topical clotrimazole. These findings highlight the importance of conducting nationwide observational prospective studies to define the actual prevalence of VVC and RVVC among Iranian women.

Our analysis of the yeast species causing vaginitis among Iranian patients revealed that *C. albicans* constituted 79% of the isolates and was the most abundant *Candida* species responsible for VVC and RVVC. This observation is consistent with previous studies on VVC (Sharifynia et al., 2017; Ghajari et al., 2018), oral candidiasis (Arastehfar et al., 2019a), and candidemia (Arastehfar et al., 2020d; Kord et al., 2020) in Iran, which documented the abundance of *C. albicans* among Iranian patients, whereas *C. glabrata* was reported the most prevalent *Candida* species among Indian patients (Mohanty et al., 2007). Of note, we observed that approximately 83% of *C. glabrata* and 73% of *C. krusei* isolates, which intrinsically respond to high MICs of azoles, were obtained from patients with RVVC. Altogether, this epidemiological profile indicates that *C. albicans* is the dominant yeast species in Iranian patients suffering from both VVC and RVVC; however, NAC species should also be a matter of concern.

Assessment of the azole susceptibility profiles of *Candida* isolates showed that *C. albicans* had the highest rate of the FLZR phenotype and was recovered only from patients with RVVC. This observation is in contrast with the typical situation in patients with candidemia, when *C. albicans* is rarely resistant to antifungal agents and fluconazole is the optimal treatment drug (Pfaller et al., 2019). Fluconazole resistance is most likely caused by repeated exposure to azoles, either fluconazole or OTC azoles. Similar to our findings, previous studies from Iran also reported a relatively high rate of fluconazole resistance among Iranian patients (Sharifynia et al., 2017). Since resistance to antifungal agents in general and to fluconazole in particular is associated with therapeutic failure, we assessed the clinical profiles of our patients, which showed that FLZR isolates mostly emerged after treatment with clotrimazole and some after that with fluconazole and were potentially associated with persistent RVVC. Bearing in mind that there is no ECV or CBP established for clotrimazole and that clotrimazole and fluconazole belong to various subset of azoles, imidazoles, and triazoles, respectively (Crowley and Gallagher, 2014), yet some clinical isolates with elevated MIC values against clotrimazole shown to be FLZR (Vazquez et al., 2001) and in some cases were cross-resistant to all azoles tested (Martel et al., 2010). Of note, none of our *Candida* isolates were itraconazole-resistant. Observing such heterogeneity in terms of resistance to a single or multiple azoles might be explained by underlying azole resistance mechanisms involved. For instance, some *Candida* isolates cross-resistant to multiple azoles harbor mutations in various *ERG* genes implicated in ergosterol biosynthetic pathway (Martel et al., 2010) in tandem with overexpression of efflux pumps, while some harboring a single mutation in *ERG11* may only confer resistance to fluconazole (Arastehfar et al., 2020a). Moreover, the structural differences noted among short-tailed, such as fluconazole, and long-tailed, such as itraconazole, may dictate the interaction with drug target followed by mutation type and hence the resistance to a single or multiple azoles, which may also vary depending on the species studied (Sagatova et al., 2015).

Along with drug resistance, drug tolerance has been revealed as an underestimated factor complicating patient treatment (Rosenberg et al., 2018; Arastehfar et al., 2020c; Berman and Krysan, 2020). Antifungal tolerance has not been evaluated in the context of VVC to clarify whether it is associated with azole exposure and can cause azole therapeutic failure. Our analysis of the antifungal tolerance rate and its correlation with the previous exposure to azoles and azole therapeutic failure showed that *C. albicans* was the only species developing tolerance

against fluconazole among RVVC and that both short- and long-term exposure to azoles was associated with the development of tolerance. More importantly, FLZT isolates were likely associated with both fluconazole and clotrimazole therapeutic failure. Furthermore, in some cases *C. albicans* FLZT isolates showed an intermediate phenotype between FLZS and FLZR, further supporting the notion that drug tolerance paves the way for the emergence of drug resistance (Levin-Reisman et al., 2017; Windels et al., 2019). Indeed, studies in bacteria have indicated the importance of antibiotic tolerance and its contribution to higher resistance and therapeutic failure rates, as well as longer hospital stay and increased healthcare-related expenses (Levin-Reisman et al., 2017; Windels et al., 2019). Thus, antifungal tolerance is an emerging issue of significant clinical relevance, which necessitates the development of fast and straightforward techniques for accurate and rapid measurement of drug tolerance with the ultimate goal of improving patients' outcomes.

Collectively, our and previous data indicate that FLZT and FLZR phenotypes may contribute to azole therapeutic failure in VVC treatment and that precautions, especially concerning the broad use of OTC topical azole preparations, should be taken. Moreover, *C. albicans* infections should not be regarded as easily treatable in the context of VVC, because the vast majority of persistent RVVC cases found in this study were caused by this species.

Another issue further complicating the management of VVC is the prescription of antifungal agents in the absence of species identification and AFST, which has also been revealed in a previous study of Iranian patients with candidemia (Arastehfar et al., 2020d), suggesting that VVC is an underestimated complication and a growing challenge for the healthcare in Iran.

Of note, approximately 42% of patients with RVVC recruited to this study were infected with azole susceptible non-tolerant isolates, but still showed persistent vaginitis despite treatment with fluconazole and/or clotrimazole, which is in line with the reports that host-related factors such as specific mutations causing immune deficiency and/or local immune overreaction may result in therapeutic failure (Jaeger et al., 2013; Costa-de-Oliveira and Rodrigues, 2020). This aspect will be the subject of our future studies, where we will try to categorize the most important mutations in the genes involved in host immunity. Furthermore, the fact that some patients with RVVC may not have adhered to the prescribed antifungal regimen could also explain a relatively high rate of therapeutic failure in the absence of fluconazole resistance or tolerance.

Since this was a single-center study, we admit that some VVC cases may have been missed, which is a limitation. We believe that a multicenter nationwide study would further the knowledge on the prevalence and severity of RVVC in Iran.

DATA AVAILABILITY STATEMENT

The original contributions presented in the study are included in the article/**Supplementary Material**, further inquiries can be directed to the corresponding author/s.

ETHICS STATEMENT

The studies involving human participants were reviewed and approved by the human subject hospital review board of Shahid Akbar-Abadi Obstetrics and Gynecology Hospital (IR.MODARES.REC.1397.225). The patients/participants provided their written informed consent to participate in this study.

AUTHOR CONTRIBUTIONS

AA, MR, SM, WF, DP, and CL-F designed and coordinated the study. MK, NG, MR, and SM collected the isolates and clinical data. AA, FD, CL-F, MI, MT, MH, JJ, LH, HW, WF, and AC performed the species identification and antifungal susceptibility testing. AA drafted the manuscript and all authors revised the draft. WF and SM funded the study. All authors contributed to the article and approved the submitted version.

FUNDING

This study received funding support from Tarbiat Modarres University (Grant#MED_76444).

SUPPLEMENTARY MATERIAL

The Supplementary Material for this article can be found online at: https://www.frontiersin.org/articles/10.3389/fmicb.2021.655069/full#supplementary-material

REFERENCES

Arastehfar, A., Daneshnia, F., Farahyar, S., Fang, W., Salimi, M., and Salehi, M. (2019a). Incidence and spectrum of yeast species isolated from the oral cavity of Iranian patients suffering from hematological malignancies. *J. Oral Microbiol.* 11:1601061. doi: 10.1080/20002297.2019.1601061

Arastehfar, A., Daneshnia, F., Hilmioğlu-Polat, S., Fang, W., Yaşar, M., Polat, F., et al. (2020a). First report of candidemia clonal outbreak caused by emerging fluconazole-resistant *Candida parapsilosis* isolates harboring Y132F and/or Y132F+K143R in Turkey. *Antimicrob. Agents Chemother.* 64, e01001–20. doi: 10.1128/AAC.01001-20

Arastehfar, A., Daneshnia, F., Kord, M., Roudbary, M., Zarrinfar, H., Fang, W., et al. (2019b). Comparison of 21-Plex PCR and API 20C AUX, MALDI-TOF MS, and rDNA sequencing for a wide range of clinically isolated yeast species: improved identification by combining 21-Plex PCR and API 20C AUX as an alternative strategy for developing countries. *Front. Cell. Infect. Microbiol.* 9:176. doi: 10.3389/fcimb.2019.00176

Arastehfar, A., Fang, W., Pan, W., Lackner, M., Liao, W., Badiee, P., et al. (2019c). YEAST PANEL multiplex PCR for identification of clinically important yeast species: stepwise diagnostic strategy, useful for developing countries. *Diagn. Microbiol. Infect. Dis.* 93, 112–119. doi: 10.1016/j.diagmicrobio.2018.09.007

Arastehfar, A., Fang, W., Pan, W., Liao, W., Yan, L., and Boekhout, T. (2018). Identification of nine cryptic species of *Candida albicans*, *C. glabrata*, and

C. parapsilosis complexes using one-step multiplex PCR. *BMC Infect. Dis.* 18:480. doi: 10.1186/s12879-018-3381-5

Arastehfar, A., Hilmioglu-Polat, S., Daneshnia, F., Salehi, M., Polat, F., Yasar, M., et al. (2020b). Recent increase in the prevalence of *Candida tropicalis* blood isolates in Turkey: clinical implication of azole-non-susceptible and fluconazole tolerant phenotypes and genotyping. *Front. Microbiol.* 11:587278. doi: 10.3389/fmicb.2020.587278

Arastehfar, A., Lass-Flörl, C., Garcia-Rubio, R., Daneshnia, F., Ilkit, M., and Boekhout, T. (2020c). The quiet and underappreciated rise of drug-resistant invasive fungal pathogens. *J. Fungi* 6:138. doi: 10.3390/jof6030138

Arastehfar, A., Wickes, B. L., Ilkit, M., Pincus, D. H., Daneshnia, F., Pan, W., et al. (2019d). Identification of mycoses in developing countries. *J. Fungi* 5:90. doi: 10.3390/jof5040090

Arastehfar, A., Yazdanpanah, S., Bakhtiari, M., Fang, W., Pan, W., and Mahmoudi, S. (2020d). Epidemiology of candidemia in Shiraz, southern Iran: a prospective multicenter study (2016–2018). *Med. Mycol.* Myaa059. doi: 10.1093/mmy/myaa059 [Epub ahead of print].

Astvad, K. M. T., Sanglard, D., Delarze, E., Hare, R. K., and Arendrup, M. C. (2018). Implications of the EUCAST trailing phenomenon in *Candida tropicalis* for the in vivo susceptibility in invertebrate and murine models. *Antimicrob. Agents Chemother.* 62, e01624–18. doi: 10.1128/AAC.01624-18

Berman, J., and Krysan, D. J. (2020). Drug resistance and tolerance in fungi. *Nat. Rev. Microbiol.* 18, 319–331. doi: 10.1038/s41579-019-0322-2

Brown, G. D., Denning, D. W., Gow, N. A. R., Levitz, S. M., Netea, M. G., and White, T. C. (2012). Hidden killers: human fungal infections. *Sci. Transl. Med.* 4:165rv13. doi: 10.1126/scitranslmed.3004404

Clinical and Laboratory Standards Institute (CLSI) (2017). *Reference Method for Broth Dilution Antifungal Susceptibility Testing of Yeasts*, 4th Edn. CLSI standard M27. Wayne, PA: Clinical and Laboratory Standards Institute.

Clinical and Laboratory Standards Institute (CLSI) (2020). *Performance Standards for Antifungal Susceptibility Testing of Yeasts*, 2nd Edn. CLSI supplement M60. Wayne, PA: Clinical and Laboratory Standards Institute.

Costa-de-Oliveira, S., and Rodrigues, A. G. (2020). *Candida albicans* antifungal resistance and tolerance in bloodstream infections: the triad yeast-host-antifungal. *Microorganisms* 8:154. doi: 10.3390/microorganisms8020154

Crowley, P. D., and Gallagher, H. C. (2014). Clotrimazole as a pharmaceutical: past, present and future. *J. Appl. Microbiol.* 117, 611–617. doi: 10.1111/jam.12554

Denning, D. W., Kneale, M., Sobel, J. D., and Rautemaa-Richardson, R. (2018). Global burden of recurrent vulvovaginal candidiasis: a systematic review. *Lancet Infect. Dis.* 18, e339–e347. doi: 10.1016/S1473-3099(18)30103-8

Ghajari, A., Lotfali, E., Ahmadi, N. A., Fassihi, P. N., Shahmohammadi, N., Ansari, S., et al. (2018). Isolation of different species of *Candida* in patients with vulvovaginal candidiasis from Damavand, Iran. *Arch. Clin. Infect. Dis.* 13:e59291. doi: 10.5812/archcid.59291

Gonçalves, B., Ferreira, C., Alves, C. T., Henriques, M., Azeredo, J., and Silva, S. (2016). Vulvovaginal candidiasis: epidemiology, microbiology and risk factors. *Crit. Rev. Microbiol.* 42, 905–927. doi: 10.3109/1040841X.2015.1091805

Jaeger, M., Carvalho, A., Cunha, C., Plantinga, T. S., Veerdonk, F., Puccetti, M., et al. (2016). Association of a variable number tandem repeat in the NLRP3 gene in women with susceptibility to RVVC. *Eur. J. Clin. Microbiol. Infect. Dis.* 35, 797–801. doi: 10.1007/s10096-016-2600-5

Jaeger, M., Plantinga, T. S., Joosten, L. A., Kullberg, B. J., and Netea, M. G. (2013). Genetic basis for recurrent vulvo-vaginal candidiasis. *Curr. Infect. Dis. Rep.* 15, 136–142. doi: 10.1007/s11908-013-0319-3

Kord, M., Salehi, M., Khodavaisy, S., Hashemi, S. J., Ghazvini, R. D., and Rezaei, S. (2020). Epidemiology of yeast species causing bloodstream infection in Tehran, Iran (2015– 2017); superiority of 21-plex PCR over the Vitek 2 system for yeast identification. *J. Med. Microbiol.* 69, 712–720. doi: 10.1099/jmm.0.001189

Levin-Reisman, I., Ronin, I., Gefen, O., Braniss, I., Shoresh, N., and Balaban, N. Q. (2017). Antibiotic tolerance facilitates the evolution of resistance. *Science* 355, 826–830. doi: 10.1126/science.aaj2191

Makanjuola, O., Bongomin, F., and Fayemiwo, S. A. (2018). An update on the roles of non-albicans Candida species in vulvovaginitis. *J. Fungi* 4:121. doi: 10.3390/jof4040121

Martel, C. M., Parker, J. E., Bader, O., Weig, M., Gross, U., Warrilow, A. G., et al. (2010). A clinical isolate of *Candida albicans* with mutations in ERG11 (encoding sterol 14α-demethylase) and ERG5 (encoding C22 desaturase) is cross resistant to azoles and amphotericin B. *Antimicrob. Agents Chemother.* 54, 3578–3583. doi: 10.1128/AAC.00303-10

Megri, Y., Arastehfar, A., Boekhout, T., Daneshnia, F., Hörtnagl, C., Sartori, B., et al. (2020). *Candida tropicalis* is the most prevalent yeast species causing candidemia in Algeria: the urgent need for antifungal stewardship and infection control measures. *Antimicrob. Resist. Infect. Control* 9:50. doi: 10.1186/s13756-020-00710-z

Mohanty, S., Xess, I., Hasan, F., Kapil, A., Mittal, S., and Tolosa, J. E. (2007). Prevalence and susceptibility to fluconazole of *Candida* species causing vulvovaginitis. *Indian J. Med. Res.* 126, 216–219.

Pappas, P. G., Kauffman, C. A., Andes, D. R., Clancy, C. J., Marr, K. A., Ostrosky-Zeichner, L., et al. (2016). Clinical practice guideline for the management of candidiasis: 2016 update by the infectious diseases society of America. *Clin. Infect. Dis.* 62, e1–50. doi: 10.1093/cid/civ933

Pfaller, M. A., and Diekema, D. J. (2012). Progress in antifungal susceptibility testing of *Candida spp*. by use of Clinical and Laboratory Standards Institute broth microdilution methods, 2010 to 2012. *J. Clin. Microbiol.* 50, 2846–2856. doi: 10.1128/JCM.00937-12

Pfaller, M. A., Diekema, D. J., Turnidge, J. D., Castanheira, M., and Jones, R. N. (2019). Twenty years of the SENTRY antifungal surveillance program: results for candida species from 1997–2016. *Open Forum Infect. Dis.* 6, S79–S94. doi: 10.1093/ofid/ofy358

Rolling, T., Hohl, T. M., and Zhai, B. (2020). Minority report: the intestinal mycobiota in systemic infections. *Curr. Opin. Microbiol.* 56, 1–6. doi: 10.1016/j.mib.2020.05.004

Rosati, D., Bruno, M., Jaeger, M., Ten Oever, J., and Netea, M. G. (2020). Recurrent vulvovaginal candidiasis: an immunological perspective. *Microorganisms* 8:144. doi: 10.3390/microorganisms8020144

Rosenberg, A., Ene, I. V., Bibi, M., Zakin, S., Segal, E. S., Ziv, N., et al. (2018). Antifungal tolerance is a subpopulation effect distinct from resistance and is associated with persistent candidemia. *Nat. Commun.* 9:2470. doi: 10.1038/s41467-018-04926-x

Sagatova, A. A., Keniya, M. V., Wilson, R. K., Monk, B. C., and Tyndall, J. D. (2015). Structural insights into binding of the antifungal drug fluconazole to *Saccharomyces cerevisiae* lanosterol 14α-demethylase. *Antimicrob. Agents Chemother.* 59, 4982–4989. doi: 10.1128/AAC.00925-15

Sharifynia, S., Falahati, M., Akhlaghi, L., Foroumadi, A., and Fateh, R. (2017). Molecular identification and antifungal susceptibility profile of *Candida* species isolated from patients with vulvovaginitis in Tehran, Iran. *J. Res. Med. Sci.* 22:132. doi: 10.4103/jrms.JRMS

Tian, C., Hromatka, B. S., Kiefer, A. K., Eriksson, N., Noble, S. M., Tung, J. Y., et al. (2017). Genome-wide association and HLA region finemapping studies identify susceptibility loci for multiple common infections. *Nat. Commun.* 8:599. doi: 10.1038/s41467-017-00257-5

Vazquez, J. A., Peng, G., Sobel, J. D., Steele-Moore, L., Schuman, P., Holloway, W., et al. (2001). Evolution of antifungal susceptibility among *Candida* species isolates recovered from human immunodeficiency virus-infected women receiving fluconazole prophylaxis. *Clin. Infect. Dis.* 33, 1069–1075. doi: 10.1086/322641

Windels, E. M., Michiels, J. E., Van den Bergh, B., Fauvart, M., and Michiels, J. (2019). Antibiotics: combatting tolerance to stop resistance. *mBio* 10:e02095–19. doi: 10.1128/mBio.02095-19

Conflict of Interest: DP receives research support and/or serves on advisory boards for Amplyx, Cidara, Scynexis, N8 Medical, Merck, Regeneron, and Pfizer.

The remaining authors declare that the research was conducted in the absence of any commercial or financial relationships that could be construed as a potential conflict of interest.

frontiers in Microbiology

ORIGINAL RESEARCH
published: 29 April 2021
doi: 10.3389/fmicb.2021.655242

ALS3 Expression as an Indicator for *Candida albicans* Biofilm Formation and Drug Resistance

Keke Deng[1], Wei Jiang[2], Yanyu Jiang[3], Qi Deng[3], Jinzhong Cao[1], Wenjie Yang[2]* and Xuequn Zhao[2]**

[1] Department of Respiratory, Tianjin Third Central Hospital Branch, Tianjin, China, [2] Department of Infectious Disease, Tianjin First Central Hospital, School of Medicine, Nankai University, Tianjin, China, [3] Department of Hematology, Tianjin First Central Hospital, School of Medicine, Nankai University, Tianjin, China

Resistance caused by the formation of the *Candida albicans* (*C. albicans*) biofilm is one of the main reasons for antifungal therapy failure. Thus, it is important to find indicators that predict *C. albicans* biofilm formation to provide evidence for the early prevention and treatment of the *C. albicans* biofilms. In this study, *C. albicans* samples were selected from *C. albicans* septicemia that were sensitive to common antifungal agents. It was found that the agglutinin-like sequence 3 (*ALS3)* gene was differentially expressed in free, antifungal, drug-sensitive *C. albicans*. The average *ALS3* gene expression was higher in the *C. albicans* strains with biofilm formation than that in the *C. albicans* strains without biofilm formation. Then, it was further confirmed that the rate of biofilm formation was higher in the high *ALS3* gene expression group than that in the low *ALS3* gene expression group. It was found that *C. albicans* with biofilm formation was more resistant to fluconazole, voriconazole, and itraconazole. However, it maintained its sensitivity to caspofungin and micafungin *in vitro* and in mice. Further experiments regarding the prevention of *C. albicans* biofilm formation were performed in mice, in which only caspofungin and micafungin prevented *C. albicans* biofilm formation. These results suggest that the expression level of *ALS3* in *C. albicans* may be used as an indicator to determine whether *C. albicans* will form biofilms. The results also show that the biofilm formation of *C. albicans* remained sensitive to caspofungin and micafungin, which may help to guide the selection of clinical antifungal agents for prevention and therapy.

Keywords: *Candida albicans*, biofilms, resistance, gene expression, *ALS3* gene

OPEN ACCESS

Edited by:
Keke Huo,
Fudan University, China

Reviewed by:
Laura Judith Marcos Zambrano,
IMDEA Food Institute, Spain
Ravikumar Bapurao Shinde,
Shri Pundlik Maharaj Mahavidyalaya, India

****Correspondence:***
Qi Deng
kachydeng@126.com
Wenjie Yang
yangm8006@sina.com
Xuequn Zhao
15522321896@163.com

Specialty section:
This article was submitted to Antimicrobials, Resistance and Chemotherapy, a section of the journal Frontiers in Microbiology

Received: *18 January 2021*
Accepted: *08 April 2021*
Published: *29 April 2021*

Citation:
Deng K, Jiang W, Jiang Y, Deng Q, Cao J, Yang W and Zhao X (2021) ALS3 Expression as an Indicator for Candida albicans Biofilm Formation and Drug Resistance. Front. Microbiol. 12:655242. doi: 10.3389/fmicb.2021.655242

INTRODUCTION

Infection is one of the most common serious complications associated with the use of medical devices retained in the body, particularly central venous catheters. As a major cause of catheter-related bloodstream infections, *Candida albicans* (*C. albicans*) has the propensity to form biofilms. Compared with its planktonic form, the biofilm formation of *C. albicans* is up to 1,000 times more resistant to azole antifungal agents (Lamfon, 2004) and up to 20 times more resistant to echinocandins (Nett et al., 2010; Tobudic et al., 2010; Taff et al., 2013). Because of its ability to form biofilms, the treatment of *C. albicans* catheter-related infections is challenging (Walraven and Lee, 2013). Recent evidence suggested that even when the minimal inhibitory concentration (MIC50)

increases, *C. albicans* biofilm formation remains sensitive to echinocandins (Ramage et al., 2005; Choi et al., 2007; Katragkou et al., 2008).

It is important to identify which *C. albicans* strains have the tendency to form biofilms. A goal of this study was to find some indicators that could predict the biofilm formation of *C. albicans*, which may provide a basis for the early prevention and treatment of *C. albicans* biofilm formation. In previous studies (Deng et al., 2016, 2017), *C. albicans* was resistant to fluconazole, voriconazole, and itraconazole after biofilm formation. The MIC50 of caspofungin and micafungin to 50% of the tested *C. albicans* biofilm increased to different degrees, but they did not reach drug resistance. Further studies found that there were differences in the expression levels of genes in the ALS gene family, particularly *ALS3*, between *C. albicans* strains before biofilm formation. *C. albicans* with higher *ALS3* expression levels tended to form biofilms.

This study selected sensitive *C. albicans* that were isolated from blood samples of *C. albicans* septicemia to investigate the correlation between *ALS3* expression and *C. albicans* biofilm formation and resistance. Then, an *in vivo* experiment to study the prevention of *C. albicans* biofilm formation in mice was performed.

MATERIALS AND METHODS

Source of *Candida albicans* Strains

A total of 55 strains of *C. albicans* isolated from the blood samples of 55 patients with *C. albicans* septicemia who were admitted to the hospital from January 2017 to December 2018 were collected. The patients had not received antifungal therapy before the diagnosis of *C. albicans* septicemia and had not received catheter therapy. All *C. albicans* strains were sensitive to common antifungal agents.

Strains and Purification

A small number of clinically isolated *C. albicans* was selected via inoculation ring. *C. albicans* were inoculated on Sabouraud dextrose agar (SDA) using a three-zone scribing method and placed into a temperature box at 37°C overnight. The following day, one of the growing strains was transplanted into 5 mL of yeast peptone glucose (YPG) medium and cultured overnight in a shaking table at a speed of 200 rpm at 35°C. On the third day, the medium was removed from the shaker and centrifuged for 5 min at 3,000 rpm to collect the thalli. The obtained thalli were rinsed with saline solution three times and diluted with RPMI-1640 medium. *C. albicans* were then subcultured in yeast peptone and glucose medium at 150 rpm and 35°C in a shaking table overnight (Deng et al., 2016, 2017). The concentration of *C. albicans* solution was adjusted to 1×10^7 cells/mL.

Drug Sensitivity Test *in vitro*

The susceptibilities of *C. albicans* strains to antifungal agents, including fluconazole (Diflucan, Pfizer Manufacturing Deut.), voriconazole (Vfend, Pfizer Manufacturing Deut.), itraconazole (Sporanox, Xian-Janssen Pharmaceutical Ltd.), caspofungin (Concidas, Merck & Co., Inc.), and micafungin (Mycamine, Astellas Pharma Tech Co., Ltd), were assayed *in vitro* using a microliquid-based dilution method M27-A3 [Clinical and Laboratory Standards Institute (CLSI), 2008]. The ATCC control used in this study was AT0CC10231.

Expression of *ALS3* in 55 Strains *C. albicans*

To detect *ALS3* expression levels, total RNA extracted from grinded fungi with TRIzol reagent (Invitrogen, Carlsbad, CA, United States) was used as the template for all reverse transcriptase reactions. The cDNA was synthesized with random priming using 10 μL of total RNA and RevertAid First Strand cDNA Synthesis Kit (Fermentas, CA, United States) following the manufacturer's protocol. The upstream primer of *ALS3* was 5′-CCGGTTTCATCTGAATCATTTAGTT-3′. The downstream primer of *ALS3* was 5′-ACGACAAGGTGTACGAATTAACATCT-3′. The upstream primer of the internal gene (*ACT1*) was 5′-TGGGCCAAAAGGATTCTTATG-3′. The downstream primer of the internal gene was 5′-AGATCTTTTCCATATCATCCCAG-3′. The housekeeping gene fragments of *C. albicans* consisted of *AAT1A, ACC1, ADP1, MPIB, SYA1, VPS13*, and *ZWF1B* (Bougnoux et al., 2003). Quantitative expression of *ALS3* levels was conducted by real-time RT-PCR with a LightCycler 96 system (Roche, Switzerland). The amplification consisted of denaturation at 95°C for 30 s (s), annealing at 95°C for 3 s, and extension at 60°C for 30 s (40 cycles). Each reaction was run in triplicate. *ALS3* expression was normalized to *ACT1*. Expression levels of the regulatory gene and *ALS3* were determined using the delta-delta Ct ($2^{-\Delta\Delta Ct}$) method. Ct indicates the average threshold period of the genes obtained in three independent experiments (Escribano et al., 2017). Data are presented as mRNA transcripts (arbitrary units) relative to *ACT1* (Hosseini et al., 2019).

Biofilm Formation Experiment *in vitro*

All 55 strains *C. albicans* were added to 12-well culture plates at 2 mL/well. A 10 mm sterile indwelling catheter was placed in each well. The culture plates were incubated in a 150 rpm shaking table at 35°C for 90 min (min). Then, culture plates and catheters were washed three times using aseptic saline and cultured in YPG medium for 72 h (h) at 37°C. Biofilm formation *in vitro* was completed in the 12-well culture plates (Deng et al., 2016, 2017).

Biofilm Formation Experiment *in vivo*

Six-week-old male C57 mice weighing 20.24 g ± 1.78 g (n = 50, Beijing Vitonlihua Experimental Animal Technology Co., Ltd., Beijing, China) were randomly divided into three groups. On the basis of *ALS3* expression in *C. albicans*, mice were grouped into either the high *ALS3* expression group (20 mice), low *ALS3* expression group (20 mice), or blank control group (10 mice). A 20 mm long sterile indwelling catheter was placed into the abdominal cavity of each mouse. Mice in the two experimental groups received 1×10^7 *C. albicans* with either high or low *ALS3* expression by intraperitoneal injection 48 h later. Mice in the

control group did not receive *C. albicans* injection. In all three groups, catheters were kept in the abdominal cavity.

After feeding under the same conditions for 2 weeks, all the three groups of mice were sacrificed by cervical dislocation. Catheters were taken out, washed three times using saline solution, then cultured in YPG medium for 48 h at 37°C. After catheters were cultured, the growing colonies of *C. albicans* were isolated. The randomly amplified polymorphic DNA (RAPD) method (Perrone et al., 2009) was used to determine whether *C. albicans* isolated *in vitro* were the same as those inoculated in abdominal cavities of the mice. Four arbitrary promoters (LEG2, CDL6s, Leptopatho, and CDL6as) were selected for the RAPD method (Vrioni and Matsiota-Bemard, 2001). Finally, *ALS3* expression in *C. albicans* strains was detected, also we performed a drug sensitivity test.

Prevention of Biofilm Formation in Mice

Six-week-old male C57 mice weighing 21.02 ± 1.12 g (n = 40, Beijing Vitonlihua Experimental Animal Technology Co., Ltd, Beijing, China) were divided into four groups in the prevention of biofilm formation experiment. The mice were divided into the voriconazole group, caspofungin group, micafungin group, and control group, with 10 mice in each group. Ten *C. albicans* strains with high *ALS3* expression were selected for the prevention experiment. A 20 mm long sterile indwelling catheter was placed into the abdominal cavity of each mouse. Ten mice in each group received a dose of 1×10^7 *C. albicans* by intraperitoneal injection 48 h later. All mice in the experiment groups received preventive therapy consisting of different antifungal agents, which included voriconazole (10 mg/kg per day), caspofungin (1.5 mg/kg per day), and micafungin (1.5 mg/kg per day) in each group. After feeding under the same conditions for 2 weeks, *C. albicans* were extracted from the *in vitro* cultures.

Statistics

SPSS 17.0 (SPSS, Inc., Chicago, IL, United States) statistical software was used for statistical analysis. Data were expressed as the mean ± standard error and analyzed by t-tests and F-tests. Susceptibility tests for antifungal agents were compared using non-parametric tests for independent samples. $P < 0.05$ was considered a statistically significant difference.

RESULTS

Biofilm Formation and Morphological Structure *in vitro*

In the biofilm formation experiment, 29 *C. albicans* strains out of the 55 total strains formed biofilms *in vitro*. The *C. albicans* budded and began to form mycelium after 6 h of cell culture *in vitro* under observation with an inverted microscope. *C. albicans* colonies fused with each other and arranged into a network after 12 h of culture. *C. albicans* then clumped along the mycelium formation after 24 h of culture. Finally, the mycelium of *C. albicans* interlaced and formed a membrane network structure inside the entire catheter after 48 h of culture *in vitro*.

Observation of Ultrastructure Under Transmission Electron Microscope

Cell walls of *C. albicans* were broken in the 26 strains that did not form biofilms. The thickness of most cell walls was about 110–220 nm. Electron density in the strains was higher in structures with spores that sprouted (**Figure 1A**). In the 29 strains that formed biofilms *in vitro*, cell walls were about 200–350 nm. Electron density in these strains and in structures with spores were the same as those that did not form

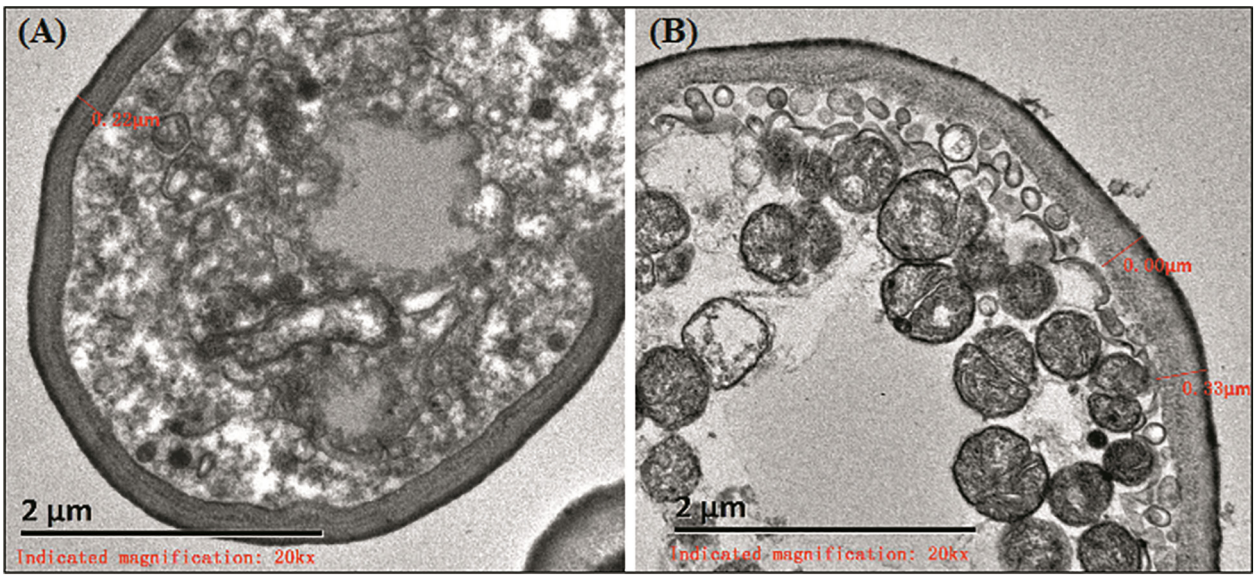

FIGURE 1 | Ultrastructure of biofilms. **(A)** The cell wall of strain that did not form biofilms was about 220 nm. **(B)** The biofilm formation strains were rich in mitochondria.

biofilms. However, the strains that formed biofilms were rich in mitochondria (**Figure 1B**).

ALS3 Expression in the 55 *C. albicans* Strains Prior to the Study

There were obvious differences among *ALS3* expression in the 55 *C. albicans* strains after they were collected from patients. The ratio of *ALS3* expression to the median of the 55 *C. albicans* strains is shown in **Figure 2**.

Changes in *ALS3* Expression Before and After Culture in all 55 *C. albicans* Strains

Objective stripes were presented at 100–200 bp after electrophoresis of gene amplification products with 2% sepharose gel. The average *ALS3* expression was higher in the 29 *C. albicans* with biofilm formation than that in the 26 *C. albicans* without biofilm formation (P = 0.000). The average *ALS3* expression declined after culture *in vitro* in the 29 strains with biofilm formation (P = 0.013). However, there were no differences in the 26 strains without biofilm formation before and after culturing (P = 0.167; **Figure 3**).

Biofilm Formation in Mice

During the biofilm formation experiment in mice, two mice in the high *ALS3* expression group died on the third and fourth days after the sterile indwelling catheter was placed into the abdominal cavity. No mice died in the low *ALS3* expression group or control group. After 2 weeks, the catheters were removed. A total of 14 *C. albicans* strains (14/18, 77.8%) in the high *ALS3* expression group formed biofilms with membrane structures attached to the catheters walls when observed under a microscope.

Three *C. albicans* strains (3/20, 15%) in the low *ALS3* expression group formed biofilms. The rate of biofilm formation

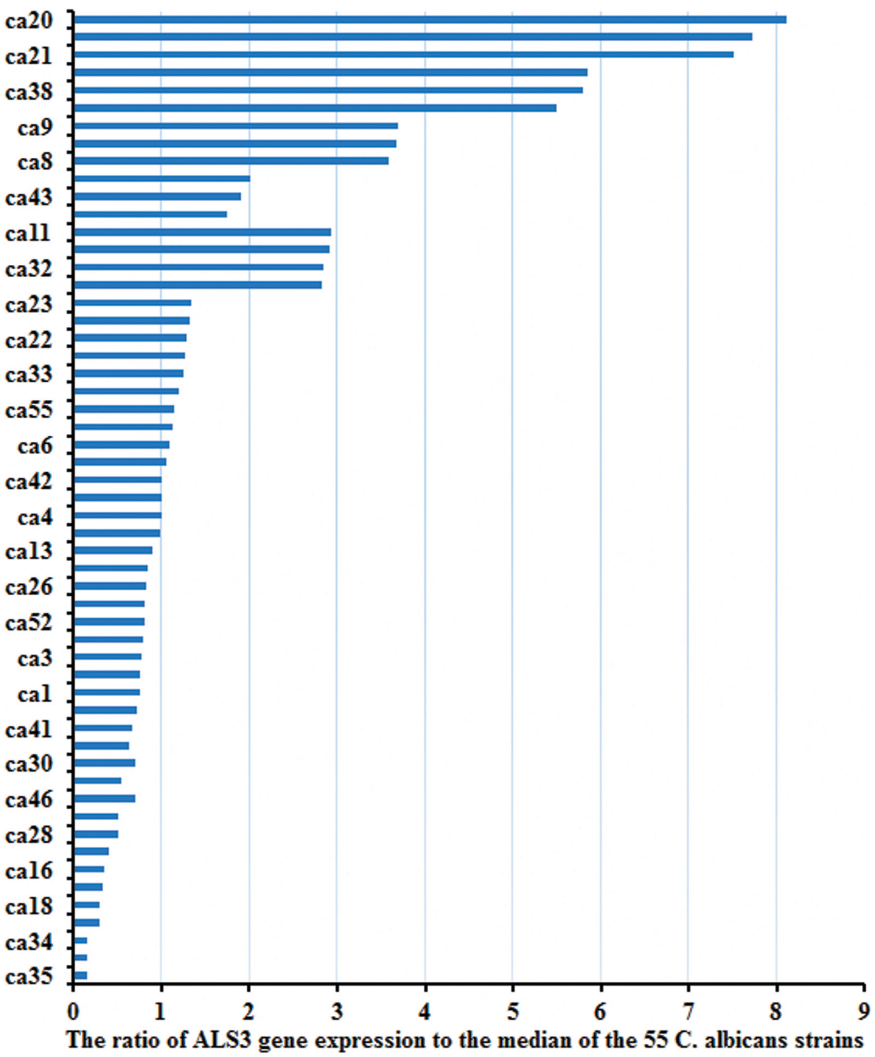

FIGURE 2 | The expression of *ALS3* gene was obvious differences in the 55 strains. There were obvious differences of the *ALS3* gene expression level in the 55 *C. albicans* when they were collected from patients.

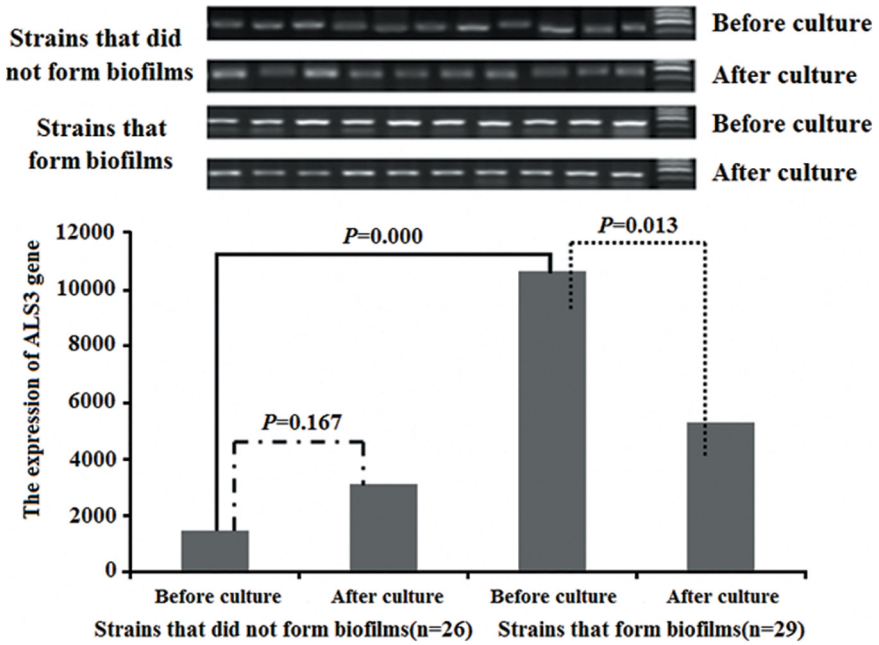

FIGURE 3 | The changes of the *ALS3* gene expression. The average of *ALS3* gene expression was higher in the 29 *C. albicans* with biofilm formation than that of in the 26 *C. albicans* without biofilm formation. The average of *ALS3* gene expression declined after culture in the 29 *C. albicans* with biofilm formation. But there was no different in the 26 *C. albicans* without biofilm formation before and after culture.

in the high *ALS3* expression group was higher than that in the low *ALS3* expression group (P = 0.000; **Figure 4A**). After the catheters were cultured, growing colonies of *C. albicans* were extracted. There were 12 *C. albicans* strains from catheters of the high *ALS3* expression group and eight *C. albicans* strains from catheters of the low *ALS3* expression group that were extracted from culture *in vitro* (**Figure 4B**). All *C. albicans* strains that were isolated from culture *in vitro* were identified by RAPD as having the same origins as *C. albicans* inoculated in the abdominal cavities of the mice.

Prevention of Biofilm Formation in Mice

In the prevention of biofilm formation experiment, eight *C. albicans* strains (8/10, 80%) in the voriconazole group, two *C. albicans* strains (2/10, 20%) in the caspofungin group, and three *C. albicans* strains (3/10, 30%) in the micafungin group formed biofilms with membrane structures attached to the catheter walls when observed under a microscope (**Figure 5**). The rates of biofilm formation in the caspofungin and micafungin groups were lower than that in voriconazole group ($P_{caspofungin}$ = 0.007 and $P_{micafungin}$ = 0.025). However, there were no differences in the biofilm formation rate between the caspofungin and micafungin groups (P = 0.606).

Changes in *ALS3* Expression in *C. albicans* Isolated From Catheters in Mice

After the catheters removed from the mice were cultured *in vitro*, growing colonies of *C. albicans* were isolated. A total of 12 *C. albicans* strains in the high *ALS3* expression group were isolated from the culture system, while eight *C. albicans* strains in the low *ALS3* expression group were isolated. All 12 *C. albicans* strains in the high *ALS3* expression group formed biofilms, while only one *C. albicans* strain formed biofilm in the low *ALS3* expression group. The average *ALS3* expression of 12 *C. albicans* strains in the high *ALS3* gene expression group declined from 13,710 ± 1,839 to 8,828 ± 1,680. The average *ALS3* expression of eight *C. albicans* in the low *ALS3* expression group was 1,860 ± 706, while it was 1,607 ± 324 in the same group before the biofilm formation experiment. There were no differences in average *ALS3* expression before and after the biofilm formation experiment in the low *ALS3* expression group (**Figures 4C,D**).

Drug Sensitivity Test *in vitro*

The susceptibility of *C. albicans* to antifungal agents (e.g., fluconazole, voriconazole, itraconazole, caspofungin, and micafungin) *in vitro* was assayed. The activities of antifungal agents against the planktonic form of 55 *C. albicans* strains isolated from blood samples of patients with candidaemia were examined. All antifungal agents showed high antifungal activity against the 55 *C. albicans* strains (**Table 1**). After the biofilm formation experiment *in vitro*, activities of antifungal agents against the 26 *C. albicans* strains without biofilm formation and 29 *C. albicans* strains with biofilm formation were compared. The *C. albicans* strains with biofilm formation were more resistant to fluconazole, voriconazole, and itraconazole. However, these strains remained sensitive to caspofungin and micafungin. The *C. albicans* strains without biofilm formation were sensitive to all antifungal agents (**Table 2**).

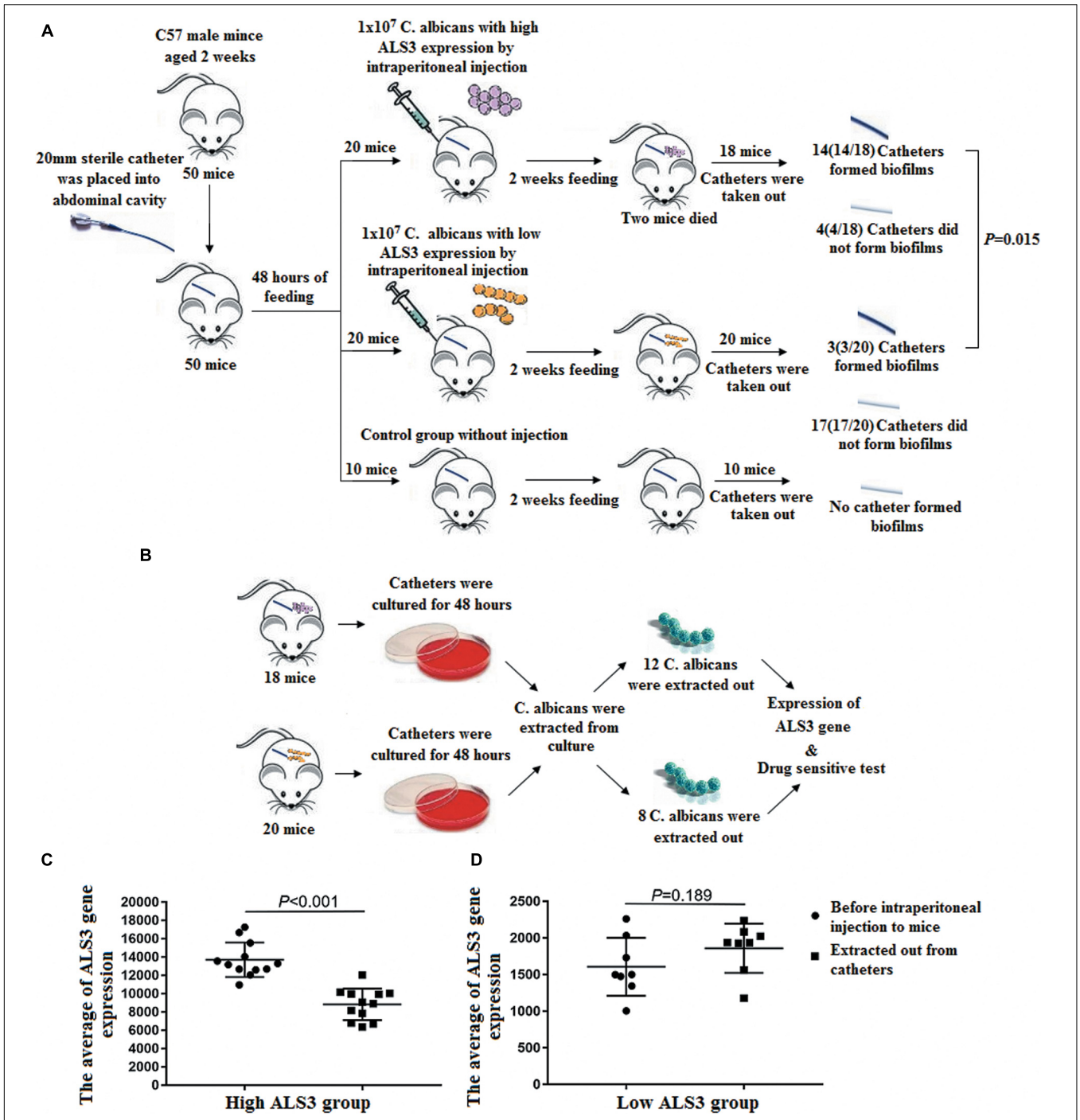

FIGURE 4 | Biofilm formation in mice. **(A)** A total of 14 *C. albicans* (14/18, 77.8%) in the high *ALS3* gene expression group formed biofilms. Three *C. albicans* strains (3/20, 15%) in the low *ALS3* gene expression group formed biofilms ($P = 0.000$). **(B)** After the catheters were cultured, there were 12 *C. albicans* strains from the catheters of the high *ALS3* expression group and the eight *C. albicans* strains from the catheters of the low *ALS3* expression group were isolated from culture *in vitro*. **(C)** The average of *ALS3* gene expression in 12 *C. albicans* from the catheters of the high *ALS3* expression group declined from 13710 ± 1839 to 8828 ± 1680 ($P < 0.001$). **(D)** The average of *ALS3* gene expression in eight *C. albicans* from the catheters of the low ALS3 expression group was 1860 ± 706. While before the biofilm formation experiment, it was 1607 ± 324 in this group ($P = 0.189$).

After the biofilm formation experiment in mice, activities of antifungal agents against the 12 *C. albicans* strains from the catheters in high *ALS3* expression group and the eight *C. albicans* strains from the catheters in low *ALS3* expression group were compared. The *C. albicans* from the catheters in the low *ALS3* expression group were sensitive to all antifungal agents. The

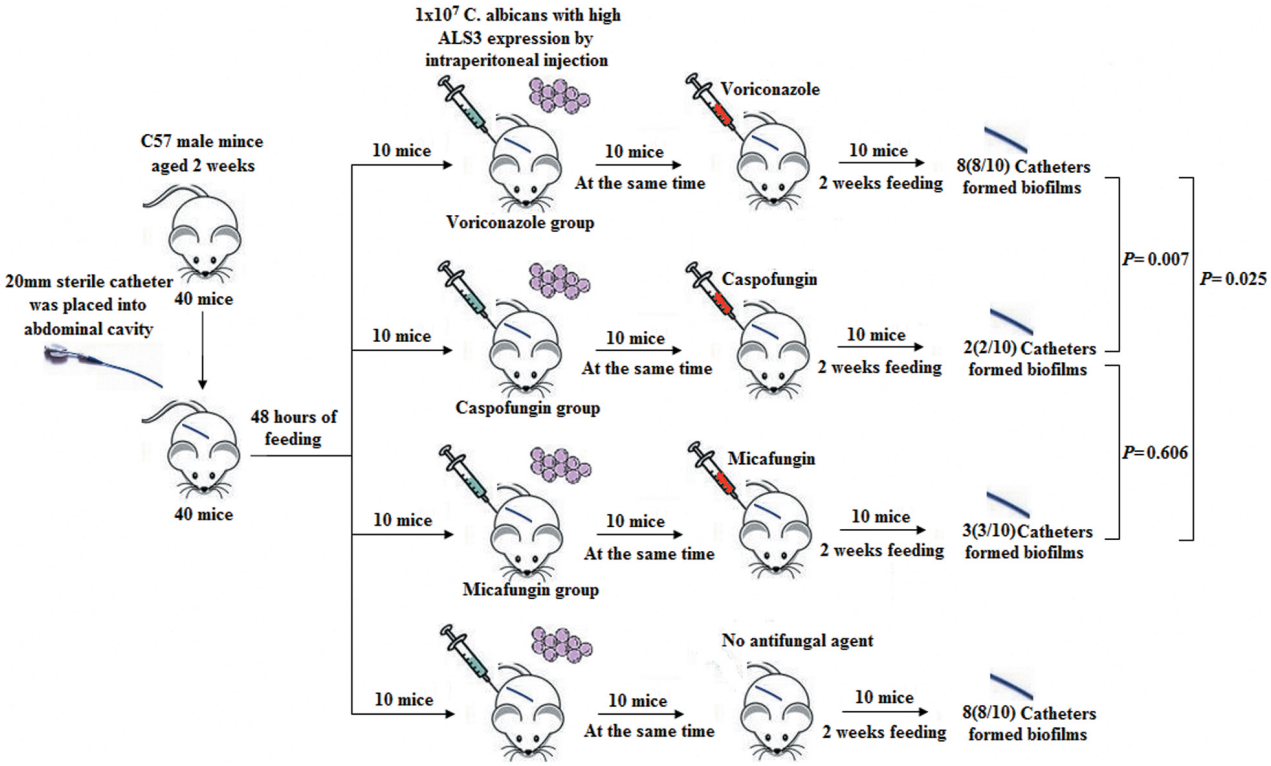

FIGURE 5 | Prevention of biofilm formation in mice. Eight *C. albicans* (8/10, 80%) in voriconazole group, two *C. albicans* (2/10, 20%) in caspofungin group and three *C. albicans* strains (3/10, 30%) in micafungin group formed biofilms with membrane structure attached in the wall of catheters under microscope. The rate of biofilm formation in the caspofungin group and in the micafungin group were lower than that of in the voriconazole group, respectively ($P_{caspofungin}$ = 0.007 and $P_{micafungin}$ = 0.025). But there was no different of the biofilm formation rate in the caspofungin and micafungin group (P = 0.606).

C. albicans strains from the catheters in high *ALS3* expression group were more resistant to fluconazole, voriconazole, and itraconazole. These strains remained sensitive to caspofungin and micafungin (**Table 3**).

DISCUSSION

Candida albicans biofilms are composed of a membranous multifungal complex adsorbed on the surface of biomaterials or a body cavity (Kojic and Darouiche, 2004; Gbelska et al., 2006; Uppuluri et al., 2010). *C. albicans* from biofilms are more invasive and resistant to azole antifungal agents than biofilms originating from planktonic *C. albicans* (Nett et al., 2010; Tobudic et al., 2010; Taff et al., 2013). Central venous catheter therapy is widely used in patients with malignant tumors. When *C. albicans* attaches to the surface of indwells *in vivo* (e.g., in catheters), it is easy to cause catheter-related candidiasis (Høiby et al., 2015). On this basis, *C. albicans* tends to form biofilms (Walraven and Lee, 2013). Biofilm-associated infections are difficult to eradicate because they are a self-perpetuating source of infection and are resistant to a variety of antifungal agents, particularly azole antifungal agents (Taff et al., 2013).

This study selected sensitive *C. albicans* isolated from blood samples from patients with candidiasis. The study intended to verify the results obtained from previous studies that *ALS3* is a predictor of *C. albicans* biofilm formation (Deng et al., 2016, 2017). Further studies plan to provide a theoretical basis for the prevention and treatment of *C. albicans* biofilm formation.

In this study, there was no significant thickening of *C. albicans* cell walls after biofilm formation. This result is different from previous reports (Hamza et al., 2006), in which cell walls after *C. albicans* biofilm formation are twice as thick as those before biofilm formation. However, it was found that after biofilm formation, the electron density and mitochondrial richness of *C. albicans* are high. Another study showed that the sensitivity of *C. albicans* during biofilm formation depends on the metabolic activity of *C. albicans* (Marcos-Zambrano et al., 2014). *C. albicans* biofilm with low metabolic activity was more sensitive to micafungin than that with high metabolic activity. In this study, the electron density and mitochondrial richness of *C. albicans* may have been related to the increased drug resistance after biofilm formation.

It has been reported (Tawara et al., 2000) that *C. albicans* is resistant to fluconazole, voriconazole, and itraconazole after biofilm formation. Although the MIC50 value of caspofungin and micafungin increased, *C. albicans* after biofilm formation remained sensitive to these two antifungal agents. Caspofungin and micafungin overcame the resistance of *C. albicans* after biofilm formation, which is consistent with prior results.

TABLE 1 | The number of strains with MIC50 value of different drugs in 55 planktonic *Candida albicans*.

	≤0.06	0.12	0.25	0.5	1	2	4	8	16	32	≥64
Micafungin	89	12	5	2	0	0	0	0	0	NT	NT
Caspofungin	42	51	9	5	1	0	0	0	0	NT	NT
Fluconazole	NT	2	12	21	67	6	0	0	0	0	NT
Itraconazole	NT	1	10	21	62	11	3	0	0	0	NT
Voriconazole	NT	NT	0	0	1	7	23	47	26	4	0

NT, not tested.

TABLE 2 | The number of strains with MIC50 value of different drugs in the 55 *Candida albicans* after biofilm formation experiment *in vitro*.

Concentration	No biofilm					Biofilm				
	Mica	CAS	VOR	ITC	FLU	Mica	CAS	VOR	ITC	FLU
0.06	11	12	NT	NT	NT	1	3	NT	NT	NT
0.12	8	9	0	0	NT	10	14	0	0	NT
0.25	5	4	4	2	0	11	8	0	0	0
0.5	2	1	6	6	0	6	3	2	1	0
1	0	0	11	10	0	1	1	4	5	0
2	0	0	4	6	2	0	0	5	3	0
4	0	0	1	2	6	0	0	11	7	2
8	0	0	0	0	9	0	0	6	10	3
16	0	0	0	0	5	0	0	1	3	4
32	NT	NT	0	0	3	NT	NT	0	1	8
64	NT	NT	NT	NT	1	NT	NT	NT	NT	12
Total	26	26	26	26	26	29	29	29	29	29

Independent predictors of biofilm formation candida bloodstream infections (CBSIs) were the presence of central venous catheters (CVCs) and urinary catheters (Tumbarello et al., 2012). However, not all *C. albicans* bloodstream infections form biofilms. This study showed that 29 *C. albicans* strains out of the 55 total strains (52.7%) formed biofilms *in vitro*. This result indicates that *C. albicans* had the heterogeneity of biofilm formation. A future goal is to find out the characteristics of *C. albicans* that can form biofilms easily.

The detection and analysis of gene expression is an important factor related to the study of biofilm formation (Sherry et al., 2014). ALS is the main gene family that controls the adhesion of biofilms (Klotz et al., 2007). It has been reported that the expression of *ALS3* is related to biofilm formation and that its expression gradually decreases after biofilm formation (Liu and Filler, 2011). In this experiment, the same results were obtained. This raised the issue of whether there is any difference in the *ALS3* expression before the biofilm formation of *C. albicans*, and whether this difference in *ALS3* expression can predict *C. albicans* biofilm formation? This study found a difference in the expression of *ALS3* in free, antifungal, drug-sensitive *C. albicans*. *In vitro* results showed that the average *ALS3* expression was higher in the 29 *C. albicans* strains with biofilm formation than that in the 26 *C. albicans* strains without biofilm formation. In the following experiments on biofilm formation in mice, similar results were obtained. The rate of biofilm formation was higher in the high *ALS3* expression group than that in the low *ALS3* expression group.

On the other hand, high expression of *ALS3* in *C. albicans* plays an important role not only in biofilm formation, but also in pathogenicity (Mukherjee et al., 2005). This study found that the *C. albicans* strains with biofilm formation were more resistant to fluconazole, voriconazole, and itraconazole. These strains remained sensitive to caspofungin and micafungin. *In vivo* tests in mice showed that the activities of antifungal agents against the 12 *C. albicans* strains from catheters in the high *ALS3* expression group were more resistant to fluconazole, voriconazole, and itraconazole than that in the eight strains from catheters in the low *ALS3* expression group. However, these strains remained sensitive to caspofungin and micafungin. This result regarding the activities of antifungal agents against *C. albicans* with biofilm formation is consistent with previous reports (Jacobson et al., 2009; Simitsopoulou et al., 2013).

It has been shown that the expression of *ALS3* is not significantly different among standard *C. albicans* strains, but

TABLE 3 | The number of strains with MIC50 value of different drugs in the *Candida albicans* after biofilm formation experiment in mice.

Concentration	Low *ALS3* expression group					High *ALS3* expression group				
	Mica	CAS	VOR	ITC	FLU	Mica	CAS	VOR	ITC	FLU
0.06	1	2	NT	NT	NT	1	2	NT	NT	NT
0.12	3	3	0	0	NT	3	5	0	0	NT
0.25	2	2	1	0	0	5	3	0	0	0
0.5	1	1	1	1	0	2	2	0	0	0
1	1	0	1	1	0	1	0	1	0	0
2	0	0	2	1	2	0	0	2	1	0
4	0	0	3	2	3	0	0	3	2	0
8	0	0	1	2	9	0	0	5	6	0
16	0	0	0	0	8	0	0	1	2	1
32	NT	NT	0	0	3	NT	NT	0	1	2
64	NT	NT	NT	NT	1	NT	NT	NT	NT	9
Total	8	8	8	8	8	12	12	12	12	12

there is a significant difference among clinical strains (Bruder-Nascimento et al., 2014), which was consistent with the results in this study. The *C. albicans* strains with high *ALS3* expression were more likely to form biofilms *in vitro* and in mice, leading to increased resistance to azole antifungal drugs but maintenance of sensitivity to caspofungin and micafungin. In the further prevention experiments on biofilm formation in mice, only caspofungin and micafungin prevented *C. albicans* biofilm formation.

Whether the differential expression of *ALS3* in *C. albicans* is a predictor of biofilm formation and whether its expression can further guide the selection of clinical antifungal agents remain to be further explored.

CONCLUSION

ALS3 is differentially expressed in *C. albicans* and *C. albicans* strains with high *ALS3* expression are associated with biofilm formation *in vitro* and in mice. *C. albicans* strains with biofilm formation remain sensitive to caspofungin and micafungin. In the prevention of the biofilm formation experiment, only caspofungin and micafungin prevented formation biofilm formation.

DATA AVAILABILITY STATEMENT

The datasets presented in this study can be found in online repositories. The names of the repository/repositories and accession number(s) can be found below: https://www.ncbi.nlm.nih.gov/genbank/, XM_705343.2.

ETHICS STATEMENT

The patient gave their written informed consent in accordance with the Declaration of Helsinki. The patient agreed to the use of his specimens and data for our study. The animal study was reviewed and approved by the Tianjin First Central Hospital Medical Ethics Committee.

AUTHOR CONTRIBUTIONS

QD: concept and design. KD and WJ: drafting or revising the manuscript. YJ and JC: acquisition of data. WY and XZ: analysis and interpretation of data. All authors contributed to writing, review, and/or revision of the manuscript. QD, WY, and XZ: study supervision. All the authors listed have made a substantial, direct and intellectual contribution to this work, and approved it for publication.

FUNDING

This study was supported by grants from the Tianjin Municipal Health Bureau of Science and Technology Fund 2015 Project (No. 15KG135). The project title is: The establishment of the individualized programs to prevent invasive fungal disease in acute leukemia. This study was supported by the Science and Technology Fund of Tianjin Health and Family Planning Commission (Grant 2012KZ022). The project title is: Study on fungal bilfilm and antifungal drug resistance. This study was also supported by the Science and Technology Foud of Tianjin Health and Family Planning Commission (Grant 2014KZ029). The project title is: Molecular biology research of carbapenemase producing Klebsiella pneumoniae.

ACKNOWLEDGMENTS

We thank the patients for the blood culture specimens and data provided in our experimental study. We also thank LetPub (www.letpub.com) for its linguistic assistance during the preparation of this manuscript.

REFERENCES

Bougnoux, M. E., Tavanti, A., Bouchier, C., Gow, N. A. R., Magnier, A., Davidson, A. D., et al. (2003). Collaborative consensus for optimized multilocus sequence typing of *Candida albicans*[J]. *J. Clin. Microbiol.* 41, 5265–5266. doi: 10.1128/JCM.41.11.5265-5266.2003

Bruder-Nascimento, A., Camargo, C. H., Mondelli, A. L., Sugizaki, M. F., Sadatsune, T., and Bagagli, E. (2014). Candida species biofilm and *Candida albicans* als3 polymorphisms in clinical isolates. *Braz. J. Microbiol.* 45, 1371–1377. doi: 10.1590/S1517-83822014000400030

Choi, H. W., Shin, J. H., Jung, S. I., Kee, C. S., Cho, D., Kee, S. J., et al. (2007). Species-specific differences in the susceptibilities of biofilms formed by *Candida* bloodstream isolates to echinocandin antifungals. *Antimicrob. Agents Chemother.* 51, 1520–1523. doi: 10.1128/AAC.01141-06

Clinical and Laboratory Standards Institute (CLSI) (2008). Reference Method for Broth Dilution Antifungal Susceptibility Testing of Yeasts; Approved Standard. CLSI Document M27-A3. Wayne, IL: Clinical and Laboratory Standards Institute.

Deng, K. K., Deng, Q., Zhang, J. L., Chen, J. Y., and Jiang, Y. Y. (2016). The drug resistance of *Candida albicans* biofilm and the correlation of ALS3 gene expression and film forming. *Chin. J. Infect. Dis.* 34, 603–608. doi: 10.3760/cma.j.issn.1000-6680.2016.10.007

Deng, K. K., Deng, Q., Zhang, J. L., Chen, J. Y., Jiang, Y. Y., and Xing, Y. (2017). The als3 gene expression and the *Candida albicans* biofilm film forming in mice vivo. *Chin. J. Infect. Dis.* 34, 603–608. doi: 10.3760/cma.j.issn.1000-6680.2017.05.009

Escribano, P., Marcos-Zambrano, L. J., Gómez, A., Sánchez, C., Martínez-Jiménez, M. C., Bouza, E., et al. (2017). The etest performed directly on blood culture bottles is a reliable tool for detection of fluconazole-resistant *Candida albicans* isolates. *Antimicrob. Agents Chemother.* 61:e00400-17. doi: 10.1128/AAC.00400-17

Gbelska, Y., Krijger, J. J., and Breunig, K. D. (2006). Evolution of gene families: the multidrug resistance transporter genes in five related yeast species. *FEMS Yeast Res.* 6, 345–355. doi: 10.1111/j.1567-1364.2006.00058.x

Hamza, O. J., Van den Bout-van, C. J., Matee, M. I., Moshi, M. J., Mikx, F. H., Selemani, H. O., et al. (2006). Antifungal activity of some Tanzanian plants used traditionally for the treatment of fungal infections. *J. Ethnopharmacol.* 108, 124–132. doi: 10.1016/j.jep.2006.04.026

Høiby, N., Bjarnsholt, T., Moser, C., Bassi, G. L., Coenye, T., Donelli, G., et al. (2015). ESCMID guideline for the diagnosis and treatment of biofilm

infections 2014. *Clin. Microbiol. Infect.* 21, S1–S25. doi: 10.1016/j.cmi.2014.10.024

Hosseini, S. S., Ghaemi, E., Noroozi, A., and Niknejad, F. (2019). Zinc oxide nanoparticles inhibition of initial adhesion and ALS1 and ALS3 gene expression in *Candida albicans* strains from urinary tract infections. *Mycopathologia* 184, 261–271. doi: 10.1007/s11046-019-00327-w

Jacobson, M. J., Steckelberg, K. E., Piper, K. E., Steckelberg, J. M., and Patel, R. (2009). In vitro activity of micafungin against planktonic and sessile *Candida albicans* isolates. *Antimicrob. Agents Chemother.* 53, 2638–2639. doi: 10.1128/AAC.01724-08

Katragkou, A., Chatzimoschou, A., Simitsopoulou, M., Dalakiouridou, M., Diza-Mataftsi, E., Tsantali, C., et al. (2008). Differential activities of newer antifungal agents against *Candida albicans* and *Candida parapsilosis* biofilms. *Antimicrob. Agents Chemother.* 52, 357–360. doi: 10.1128/AAC.00856-07

Klotz, S. A., Gaur, N. K., De Armond, R., Sheppard, D., Khardori, N., Edwards, J. E., et al. (2007). *Candida albicans* Als proteins mediate aggregation with bacteria and yeasts. *Med. Mycol.* 45, 363–370. doi: 10.1080/13693780701299333

Kojic, E. M., and Darouiche, R. O. (2004). *Candida* infections of medical devices. *Clin. Microbiol. Rev.* 17, 255–267. doi: 10.1128/CMR.17.2.255-267.2004

Lamfon, H. (2004). Susceptibility of *Candida albicans* biofilms grown in a constant depth film fermentor to chlorhexidine, fluconazole and miconazole: a longitudinal study. *J. Antimicrob. Chemother.* 53, 383–385. doi: 10.1093/jac/dkh071

Liu, Y., and Filler, S. G. (2011). *Candida albicans* Als3, a multifunctional adhesin and invasin. *Eukaryot. Cell* 10, 168–173. doi: 10.1128/EC.00279-10

Marcos-Zambrano, L. J., Escribano, P., González del Vecchio, M., and Guinea, J. (2014). Micafungin is more active against *Candida albicans* biofilms with high metabolic activity. *J. Antimicrob. Chemother.* 69, 2984–2987. doi: 10.1093/jac/dku222

Mukherjee, P. K., Zhou, G., Munyon, R., and Ghannoum, M. A. (2005). Candida biofilm: a well-designed protected environment. *Med Mycol.* 43, 191–208. doi: 10.1080/13693780500107554

Nett, J. E., Crawford, K., Marchillo, K., and Andes, D. R. (2010). Role of Fks1p and matrix glucan in *Candida albicans* biofilm resistance to an echinocandin, pyrimidine, and polyene. *Antimicrob. Agents Chemother.* 54, 3505–3508. doi: 10.1128/AAC.00227-10

Perrone, T. M., Gonzatti, M. I., Villamizar, G., Escalante, A., and Aso, P. M. (2009). Molecular profiles of Venezuelan isolates of *Trypanosoma* sp. by random amplified polymorphic DNA method. *Vet. Parasitol.* 161, 194–200. doi: 10.1016/j.vetpar.2009.01.034

Ramage, G., Saville, S. P., Thomas, D. P., and López-Ribot, J. L. (2005). *Candida* biofilms: an update. *Eukaryot. Cell* 4, 633–638. doi: 10.1128/EC.4.4.633-638.2005

Sherry, L., Rajendran, R., Lappin, D. F., Borghi, E., Perdoni, F., Falleni, M., et al. (2014). Biofilms formed by *Candida albicans* bloodstream isolates display phenotypic and transcriptional heterogeneity that are associated with resistance and pathogenicity. *BMC Microbiol.* 14:182. doi: 10.1186/1471-2180-14-182

Simitsopoulou, M., Peshkova, P., Tasina, E., Katragkou, A., Kyrpitzi, D., Velegraki, A., et al. (2013). Species-specific and drugspecific differences in susceptibility of *Candida* biofilms to echinocandins: characterization of less common bloodstream isolates. *Antimicrob. Agents Chemother.* 57, 2562–2570. doi: 10.1128/AAC.02541-12

Taff, H. T., Mitchell, K. F., Edward, J. A., and Andes, D. R. (2013). Mechanisms of *Candida* biofilm drug resistance. *Future Microbiol.* 8, 1325–1337. doi: 10.2217/fmb.13.101

Tawara, S., Ikeda, F., Maki, K., Morishita, Y., Otomo, K., Teratani, N., et al. (2000). In vitro activities of a new lipopeptide antifungal agent, FK463, against a variety of clinically important fungi. *Antimicrob. Agents Chemother.* 44, 57–62. doi: 10.1128/AAC.44.1.57-62.2000

Tobudic, S., Kratzer, C., Lassnigg, A., Graninger, W., and Presterl, E. (2010). In vitro activity of antifungal combinations against *Candida albicans* biofilms. *J. Antimicrob. Chemother.* 65, 271–274. doi: 10.1093/jac/dkp429

Tumbarello, M., Fiori, B., Trecarichi, E. M., Posteraro, P. P., Losito, A. R., Luca, A. D., et al. (2012). Risk factors and outcomes of candidemia caused by biofilm-forming isolates in a tertiary care hospital. *PLoS One.* 7:e33705. doi: 10.1371/journal.pone.0033705

Uppuluri, P., Chaturvedi, A. K., Srinivasan, A., Banerjee, M., Ramasubramaniam, A. K., Köhler, J. R., et al. (2010). Dispersion as an important step in the *Candida albicans* biofilm developmental cycle. *PLoS Pathog.* 6:e1000828. doi: 10.1371/journal.ppat.1000828

Vrioni, G., and Matsiota-Bemard, P. (2001). Molecular typing of *Candida* isolates from patients hospitalized in an intensive care unit. *J. Infect.* 42, 50–56. doi: 10.1053/jinf.2000.0778

Walraven, C. J., and Lee, S. A. (2013). Antifungal lock therapy. *Antimicrob. Agents Chemother.* 57, 1–8. doi: 10.1128/AAC.01351-12

Conflict of Interest: The authors declare that the research was conducted in the absence of any commercial or financial relationships that could be construed as a potential conflict of interest.

frontiers in Microbiology

ORIGINAL RESEARCH
published: 13 May 2021
doi: 10.3389/fmicb.2021.649026

Antifungal Activity of Minocycline and Azoles Against Fluconazole-Resistant *Candida* Species

Jingwen Tan[1], Shaojie Jiang[2], Lihua Tan[3], Haiyan Shi[3], Lianjuan Yang[1], Yi Sun[3] and Xiuli Wang[4]**

[1]Department of Medical Mycology, Shanghai Skin Disease Hospital, Tongji University School of Medicine, Shanghai, China, [2]Department of Gastroenterology, Jingzhou Central Hospital, The Second Clinical Medical College, Yangtze University, Jingzhou, China, [3]Department of Dermatology, Jingzhou Central Hospital, The Second Clinical Medical College, Yangtze University, Jingzhou, China, [4]Institute of Photomedicine, Shanghai Skin Disease Hospital, Tongji University School of Medicine, Shanghai, China

OPEN ACCESS

Edited by:
David Perlin,
Hackensack Meridian Health,
United States

Reviewed by:
Amir Arastehfar,
Westerdijk Fungal Biodiversity Institute, Netherlands
Cheshta Sharma,
The University of Texas Health Science Center at San Antonio,
United States

***Correspondence:**
Xiuli Wang
wangxiuli_1400023@tongji.edu.cn
Yi Sun
jzzxyysy@163.com

Specialty section:
This article was submitted to Antimicrobials, Resistance and Chemotherapy, a section of the journal Frontiers in Microbiology

Received: 03 January 2021
Accepted: 21 April 2021
Published: 13 May 2021

Citation:
Tan J, Jiang S, Tan L, Shi H, Yang L, Sun Y and Wang X (2021) Antifungal Activity of Minocycline and Azoles Against Fluconazole-Resistant Candida Species. Front. Microbiol. 12:649026. doi: 10.3389/fmicb.2021.649026

Candida species are the most common fungal pathogens to infect humans, and can cause life-threatening illnesses in individuals with compromised immune systems. Fluconazole (FLU) is the most frequently administered antifungal drug, but its therapeutic efficacy has been limited by the emergence of drug-resistant strains. When co-administered with minocycline (MIN), FLU can synergistically treat clinical *Candida albicans* isolates *in vitro* and *in vivo*. However, there have been few reports regarding the synergistic efficacy of MIN and azoles when used to treat FLU-resistant *Candida* species, including *Candida auris*. Herein, we conducted a microdilution assay wherein we found that MIN and posaconazole (POS) showed the best *in vitro* synergy effect, functioning against 94% (29/31) of tested strains, whereas combinations of MIN+itraconazole (ITC), MIN+voriconazole (VOR), and MIN+VOR exhibited synergistic activity against 84 (26/31), 65 (20/31), and 45% (14/31) of tested strains, respectively. No antagonistic activity was observed for any of these combinations. *In vivo* experiments were conducted in *Galleria mellonella*, revealing that combination treatment with MIN and azoles improved survival rates of larvae infected with FLU-resistant *Candida*. Together, these results highlight MIN as a promising synergistic compound that can be used to improve the efficacy of azoles in the treatment of FLU-resistant *Candida* infections.

Keywords: minocycline, fluconazole resistant *Candida* spp., *Candida auris*, antifungal, azole, synergy

INTRODUCTION

Invasive fungal infections represent an increasingly common threat to human health (Firacative, 2020), with *Candida* species serving as the leading cause of fungal infections and the fourth most prominent source of bloodstream infections globally, resulting in over 750,000 infections and a 40% mortality rate globally each year (McCarty and Pappas, 2016; Tsay et al., 2020). *Candida albicans* is the leading pathogenic member of this family, accounting for roughly half of these infections, followed by *Candida glabrata*, *Candida tropicalis*, *Candida parapsilosis*, and *Candida krusei*. In total, these five species cause 90% of candidaemia and other forms of invasive candidiasis (Goemaere et al., 2018).

Fluconazole (FLU) is the most commonly prescribed antifungal drug, but its utility is increasingly limited by the emergence of drug-resistant strains (Perfect and Ghannoum, 2020). Approximately 0.5–2% of *C. albicans* isolates are resistant to FLU, while these resistance frequencies, respectively, range from 4 to 9, 2 to 6, and 11 to 13% for *C. tropicalis*, *C. parapsilosis*, and *C. glabrata* (Berkow and Lockhart, 2017). *Candida auris* is an emerging pathogen, and 93% of these isolates are resistant to FLU with varying levels of resistance to other azoles, making it a particularly dangerous nosocomial pathogen with mortality rates of 30–60% (Berkow and Lockhart, 2017; Forsberg et al., 2019). As such, there is a clear need to identify reliable antifungal agents or compounds capable of enhancing the antifungal activity of extant compounds in order to improve patient outcomes.

Minocycline (MIN) is a second-generation semi-synthetic tetracycline analog that is widely used in clinical settings (Asadi et al., 2020). It exhibits a high degree of fat solubility, and can readily pass through the blood-brain barrier (Yong et al., 2004). MIN exhibits broad-spectrum antibacterial activity, and can be used to combat multidrug-resistant Gram-positive and Gram-negative bacteria (Sapadin and Fleischmajer, 2006). Importantly, MIN has also been shown to function synergistically with FLU when treating clinical *C. albicans* isolates *in vitro* and *in vivo* (Shi et al., 2010; Gu et al., 2018). As such, MIN may represent a promising drug that can be administered in combination with other azoles to treat infections caused by *C. auris* and other pathogenic *Candida* species.

In order to test this hypothesis, we explored the *in vitro* activity of MIN alone or in combination with FLU, itraconazole (ITC), voriconazole (VOR), or posaconazole (POS) against FLU-resistant *Candida* isolates. The *in vivo* effect of drug combination was evaluated using *Galleria mellonella*, as it is an ideal model system for studies of antifungal drug activity.

MATERIALS AND METHODS

Fungal Isolates

In total, 31 *Candida* isolates were utilized in the present analysis, including eight FLU resistant *C. albicans*, three FLU resistant *C. parapsilosis*, four FLU resistant *C. tropicalis*, six FLU susceptible dose-dependent *C. glabrata* strains, and 10 *C. auris* strains. All of these strains were clinical isolates, with the *C. auris* strains having been obtained from the CDC and FDA Antibiotic Resistance Isolate Bank. The identities of all strains were confirmed based on morphological evaluation and sequencing of the ITS and D1/D2 regions. *Candida parapsilosis* (ATCC22019) was included to ensure quality control.

Antifungal Agents

FLU (No. S1131), VOR (No. S1442), ITC (No. S2476), POS (No. S1257), and MIN (No. S4226) were obtained in a powdered form from Selleck Chemicals (TX, United States), and were prepared as detailed in M27-A4 (CLSI, 2017). Working concentration ranges were 0.03–16 μg/ml for ITC, VOR, and POS, and 0.25–64 μg/ml for FLU and MIN.

Inoculum Preparation

Yeast conidia were collected from isolates incubated for 24 h on potato dextrose agar (PDA) at 30°C. Yeast conidia were resuspended at 1–5 × 10^6 cfu/ml in sterile saline, and were then diluted 1,000-fold using RPMI-1640 to yield a suspension that was twice as concentrated as required (1–5 × 10^3 cfu/ml).

Testing the *in vitro* Synergy of MIN and Azoles

A broth microdilution checkerboard assay approach was used for the present study, having been adapted from the Clinical and Laboratory Standards Institute (CLSI) M27-A4 (CLSI, 2017). First, 50 μl volumes of MIN serial dilutions were applied horizontally to the wells of a 96-well plate containing 100 μl of prepared inoculum suspension, after which 50 μl volumes of azole serial dilutions were applied vertically to the wells of this same plate. Results were then analyzed after a 24 h incubation at 35°C.

Minimum inhibitory concentration (MIC) values were the lowest drug concentrations that suppressed fungal growth by 50% relative to control treatment at the end of the 24 h incubation. The fractional inhibitory concentration index (FICI) was used to assess MIN and azole interactions, and was calculated with the equation: FICI = (Ac/Aa) + (Bc/Ba), where Ac and Bc are the MIC values of tested agents in combination, while Aa and Ba correspond to these values for single-agent A and B treatments. A FICI of ≤0.5 is considered to indicate synergy, while a FICI of >0.5 to ≤4 is indicative of a lack of any interaction, and a FICI of >4 corresponds to an antagonistic interaction. Experiments were conducted in triplicate.

Assessment of the *in vivo* Activity of MIN Alone and in Combination With Azoles

As discussed previously (Jiang et al., 2020), survival tests were conducted with sixth instar larvae (300 mg; Sichuan, China) to evaluate the efficacy of MIN as a single-agent and in combination with azole drugs on *G. mellonella* infected with *C. albicans* R14, *C. parapsilosis* N101, *C. tropicalis* 00279, *C. glabrata* 05448, and *C. auris* AR385. Larvae were stored in the dark at room temperature with shavings prior to experimental use, while *Candida* strains had been grown for 2 days on PDA, after which the colony surface was scraped with a sterile plastic loop, washed two times, and adjusted to 1 × 10^8 cfu/ml using sterile saline. Control larval groups injected with saline, conidial suspensions, or nothing were established.

To explore the *in vivo* synergistic activity of MIN and azoles against pathogenic fungi, nine treatment groups were established: MIN, FLU, ITC, POS, VOR, MIN+FLU, MIN+ITC, MIN+POS, and MIN+VOR groups. Conidia suspensions were inoculated into larvae (10 μl per larvae) using a Hamilton syringe (25 gauge, 50 μl), and antifungal agents or a control solution (1 μg per larvae; drug concentration = 200 mg/L) was introduced into the larvae through the last left proleg after the area was cleaned with an alcohol swab. Within 120 h following infection, larval survival rates were recorded every 24 h. *Galleria mellonella* survival curves were assessed *via* the Kaplan-Meier method

TABLE 1 | Minimum inhibitory concentration (MIC) values pertaining to combinations of minocycline (MIN) and azoles when used to treat *Candida* spp.

No.	Species	MICs (μg/ml)[1]								
		Agent alone					Combination[2]			
		MIN	ITC	VOR	POS	FLU	MIN/ITC	MIN/VOR	MIN/POS	MIN/FLU
ATCC 64550	*C.albicans*	>64	1	0.5	0.5	8	16/0.5(I)	1/0.25(I)	16/0.125(S)	1/8(I)
R1		>64	8	2	2	16	4/1(S)	16/0.5(S)	4/0.5(S)	4/2(S)
R3		>64	2	1	2	32	4/1(I)	32/0.125(I)	4/0.25(S)	1/16(I)
R4		>64	4	1	2	16	8/0.5(S)	32/0.5(I)	4/0.25(S)	16/4(S)
R9		>64	>16	16	8	>64	8/0.5(S)	8/0.25(S)	4/0.125(S)	2/1(S)
R14		>64	4	8	2	16	2/0.5(S)	2/0.5(S)	2/0.25(S)	1/4(S)
R15		>64	2	2	1	32	4/0.5(S)	4/0.25(S)	4/0.125(S)	8/4(S)
N175		>64	4	1	1	8	4/0.5(S)	2/0.5(I)	4/0.25(S)	16/0.5(S)
N87	*C.parapsilosis*	>64	4	0.5	1	16	4/0.5(S)	32/0.5(I)	4/0.125(S)	16/4(S)
N101		>64	4	1	1	>32	8/1(S)	32/0.125(I)	4/0.125(S)	32/1(I)
N112		>64	4	1	0.5	16	8/0.5(S)	8/0.5(I)	4/0.125(S)	32/1(I)
00279	*C.tropicalis*	>64	1	0.5	0.5	64	16/0.5(S)	1/0.5(I)	8/0.125(S)	32/64(I)
N205		>64	4	0.5	1	32	32/1(I)	32/0.5(I)	8/0.25(S)	8/2(S)
N331		>64	2	0.5	1	32	4/0.5(S)	32/0.25(I)	8/0.25(S)	32/1(I)
N336		>64	4	1	1	32	8/0.5(S)	32/1(I)	4/0.25(S)	16/4(S)
05448	*C. glabrata*	64	4	0.5	2	8	8/0.5(S)	4/0.125(S)	8/0.125(S)	16/0.5(S)
C5		>64	1	0.5	1	8	2/0.5(I)	32/0.125(I)	8/0.125(S)	16/1(S)
C35		>64	2	0.5	1	8	8/0.5(S)	32/0.5(I)	4/0.25(S)	16/2(S)
C128		>64	1	2	1	8	8/0.25(S)	4/0.5(S)	8/0.25(S)	16/1(S)
N180		>64	2	1	1	8	2/0.5(S)	32/0.125(I)	4/0.125(S)	4/4(I)
N199		>64	4	1	1	>32	8/0.5(S)	32/0.5(I)	2/0.25(S)	16/16(I)
AR381	*C. auris*	>64	0.125	0.125	0.125	4	1/0.125(I)	1/0.125(I)	1/0.125(I)	16/2(I)
AR382		>64	0.5	1	0.5	16	8/0.125(S)	2/0.25(S)	1/0.125(S)	8/1(S)
AR383		>64	1	4	0.25	128	4/0.25(S)	4/1(S)	1/0.125(I)	8/8(S)
AR384		>64	2	0.5	0.5	128	8/0.125(S)	2/0.125(S)	8/0.125(S)	16/2(S)
AR385		>64	1	8	1	128	8/0.25(S)	1/1(S)	4/0.125(S)	16/4(S)
AR386		>64	1	16	0.5	128	4/0.125(S)	1/1(S)	4/0.125(S)	32/8(I)
AR387		>64	1	1	0.5	8	2/0.125(S)	2/0.125(S)	2/0.125(S)	4/1(S)
AR388		>64	2	4	0.5	128	8/0.5(S)	16/4(I)	8/0.125(S)	16/4(S)
AR389		>64	1	4	0.5	128	16/0.25(S)	16/1(S)	8/0.125(S)	8/2(S)
AR390		>64	0.5	4	0.5	128	8/0.125(S)	4/0.125(S)	8/0.125(S)	32/8(I)

[1]*The MIC is the concentration resulting in 50% growth inhibition.*

[2]*fractional inhibitory concentration index (FICI) results are shown in parentheses. S, synergy (FICI <0.5); I, no interaction (indifference, 0.5 < FICI < 4).*

and the log-rank (Mantel-Cox) test, with $p < 0.05$ as a significance threshold.

RESULTS

MIN and Azoles Interactions *in vitro*

A checkerboard microdilution assay was initially performed to explore the antifungal activity levels of different azoles alone and in combination with MIN when used to treat different *Candida* spp. *in vitro* (**Tables 1** and **2**). POS showed the best synergistic activity with MIN, achieving activity against 100% of tested *C. albicans*, *C. parapsilosis*, *C. tropicalis*, and *C. glabrata* strains and against 80% of tested *C. auris* strains. A combination of MIN and ITC exhibited synergistic activity against 100% of *C. parapsilosis* strains, 90% of *C. auris* strains, 83% of *C. glabrata* strains, and 75% of *C. albicans* and *C. tropicalis* strains. In combination with FLU, MIN exhibited synergistic efficacy against 75% of *C. albicans*, 70% of *C. auris*, 67% *C. glabrata*, 50% *C. tropicalis*, and 33% *C. parapsilosis* strains. Combination MIN and VOR treatment exhibited the poorest synergistic activity, affecting just 80% of *C. auris*, 50% of *C. albicans*, 33% of *C. glabrata*, and 0% of *C. parapsilosis* and *C. tropicalis* strains.

MIN and Azoles Interactions *in vivo*

Next, we performed *in vivo* antifungal activity assays using *G. mellonella* as a model system, with survival rates for the larvae in each group being shown in **Table 3** and **Figure 1**. Treatment with MIN alone had no effect on any of the five *Candida* spp. groups. When combined with FLU, however, this treatment significantly prolonged the survival of larvae infected with *C. albicans*, *C. glabrata*, and *C. auris* ($p < 0.05$), with a particularly noteworthy increase in the survival rate of larvae infected with *C. glabrata* from 5 to 25%. Combination treatment with ITC was associated with significantly prolonged larval survival rates in all groups ($p < 0.05$), with a particularly pronounced increase of 30% in the *C. glabrata* group. Combination MIN + VOR treatment significantly prolonged the survival ($p < 0.05$) of all larvae other than those infected with *C. parapsilosis*, with maximal synergy being observed for larvae infected with *C. tropicalis* for which the survival rate rose by 30%. Combination MIN + POS treatment also significantly ($p < 0.05$) increased survival in all groups, particularly in the *C. auris* group in which the survival rate reached 51.67%.

TABLE 2 | Summary of *in vitro* drug interactions.

Species(*n*)	*n* (%) of isolates showing synergism for the combination			
	MIN/ITC	MIN/VOR	MIN/POS	MIN/FLU
C.albicans (8)	6(75%)	4(50%)	8(100%)	6(75%)
C.parapsilosis (3)	3(100%)	0(0%)	3(100%)	1(33%)
C.tropicalis (4)	3(75%)	0(0%)	4(100%)	2(50%)
C.glabrata (6)	5(83%)	2(33%)	6(100%)	4(67%)
C.auris (10)	9(90%)	8(80%)	8(80%)	7(70%)
Total (31)	26(84%)	14(45%)	29(94%)	20(65%)

DISCUSSION

Minocycline was first identified as an inhibitor of *C. albicans* growth in 1974 (Waterworth, 1974), and several studies have further highlighted the antifungal activity of this compound. Shi et al. (2010) and Gu et al. (2018) demonstrated the ability of MIN to synergize with FLU against *C. albicans in vitro* and *in vivo* and Gao et al. (2013) observed synergy between tetracycline and FLU when treating *C. albicans* biofilms. MIN has also been shown to synergize with azoles in the treatment of other fungal species. Kong et al. (2020) determined that MIN was able to synergize with FLU *in vivo* and *in vitro* when treating *Cryptococcus neoformans*, while Gao et al. (2020) reported synergy between MIN and azoles when treating clinically important *Aspergillus*, *Fusarium*, and *Exophiala dermatitidis* isolates. Herein, we explored the synergistic activity of MIN in combination with azoles when treating FLU-resistant *C. albicans*, *C. parapsilosis*, *C. tropicalis*, *C. glabrata*, and *C. auris*.

Consistent with other studies, we found that MIN was able to enhance fungal sensitivity to azole treatment both *in vitro* and *in vivo*. In our *in vitro* analyses, MIN and POS showed 100% *in vitro* synergy effect in *C. albicans*, *C. parapsilosis*, *C. tropicalis*, *C. glabrata* group, functioning against 94% (29/31) of tested strains, whereas combinations of MIN+ITC, MIN+FLU, and MIN+VOR exhibited synergistic activity against 84 (26/31), 65 (20/31), and 45% (14/31) of tested strains, respectively. The *C. auris* strains used in this study belonged to four different clusters, with AR382, AR387, AR388, AR389, and AR390

TABLE 3 | Summary of *in vivo* drug interactions.

Drugs	Survival rate				
	C. abicans	*C. parapsilosis*	*C. tropicalis*	*C. glabrata*	*C. auris*
FLU	0.00%	10.00%	5.00%	5.00%	0.00%
FLU+MIN	20.00%	5.00%	5.00%	25.00%	5.00%
ITC	15.00%	5.00%	5.00%	10.00%	30.00%
ITC+MIN	30.00%	25.00%	30.00%	40.00%	48.33%
VOR	35.00%	10.00%	5.00%	10.00%	20.00%
VOR+MIN	50.00%	20.00%	35.00%	25.00%	41.67%
POS	10.00%	10.00%	10.00%	15.00%	26.67%
POS+MIN	25.00%	30.00%	30.00%	35.00%	51.67%

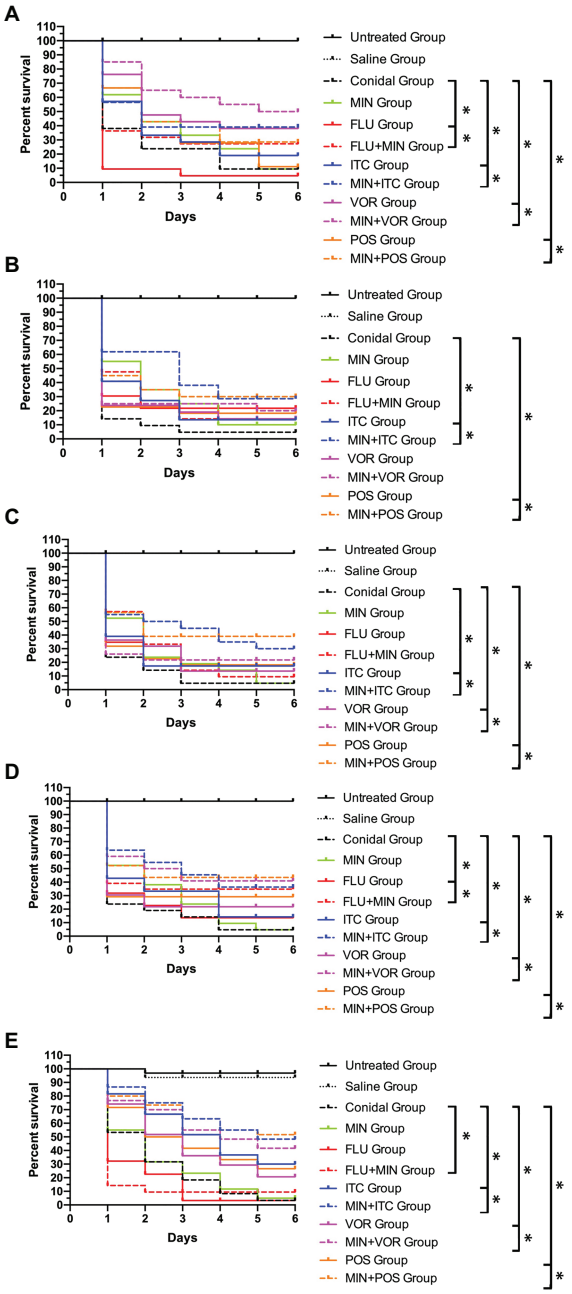

FIGURE 1 | *Galleria mellonella* survival curves following infection with *Candida* spp. **(A)** *Candida albicans* R14; **(B)** *Candida parapsilosis* N101; **(C)** *Candida tropicalis* 00279; **(D)** *Candida glabrata* 05448; **(E)** *Candida auris* AR385; Untreated Group, wild type uninfected larvae; Saline Group, wild type larvae injected with saline; Conidial Group, larvae infected with *Candida* without any treatment; MIN Group, *Candida*-infected larvae treated with MIN only; fluconazole (FLU) Group, *Candida*-infected larvae treated with FLU only; itraconazole (ITC) Group, *Candida*-infected larvae treated with ITC only; voriconazole (VOR) Group, *Candida*-infected larvae treated with VOR only; posaconazole (POS) Group, *Candida*-infected larvae treated with POS only; MIN+FLU Group, *Candida*-infected larvae treated with MIN combined with FLU; MIN+ITC Group, *Candida*-infected larvae treated with MIN combined with ITC; MIN+VOR Group, *Candida*-infected larvae treated with MIN combined with VOR; MIN+POS Group, *Candida*-infected larvae treated with MIN combined with POS. $^{*}p < 0.05$.

belonging in cluster I, AR381 belonging in cluster II, AR383 and AR384 belonging in cluster III, and AR385 and AR386 belonging in cluster IV (Vatanshenassan et al., 2020). No differences among these clusters were detected in our *in vitro* analyses.

Our *in vivo* experiment utilized *G. mellonella* as an animal model, given that these larvae exhibit similar responses to those of mammals and can be used as an ideal model system for studies of antifungal drug activity. Our data indicated that MIN and VOR combination treatment exhibited the best synergistic efficacy in the context of *C. albicans* and *C. tropicalis* infections, while MIN+POS was most effective against *C. parapsilosis* and *C. auris*. For *C. glabrata*, a combination of MIN+ITC was most effective. However, our *in vitro* data were not in full accordance with our *in vivo* data, potentially because too few strains were used when conducting our *in vivo* study. Additionally, further studies that using mice as infection models are required.

In our data, MIN can reduce the MIC of azoles in some tested strains, while there was no change for the others. That can observed in others study either, Shi et al. (2010) showed MIN can reduce MIC of FLU in 50% tested *C. albicans* strains. We speculate that might associate with the mechanism of synergistic action. Though remains incompletely understood, the ability of MIN to enhance FLU efficacy may be related to efflux pump blockade, the stimulation of high levels of intracellular calcium, iron chelation, or the inhibition of mitochondrial functionality (Oliver et al., 2008; Shi et al., 2010; Fiori and Van Dijck, 2012; Gao et al., 2013). Further research that can clarify the mechanisms might help to address this question.

In summary, we found that MIN can synergize with azoles to improve the antifungal activity of these agents against azole-resistant *Candida* species, with particular efficacy against *C. auris in vitro* and *in vivo*. Given that resistance to azoles is associated with significant increases in treatment failure and mortality rates, overcoming drug resistance is a critical public health issue. Our results highlight the potential of MIN as a tool that can overcome such azole resistance when used to treat *Candida* infections, although further work will be required to confirm these results and to elucidate the underlying mechanisms. Even so, our results hold great promise, suggesting that MIN can be used to reliably enhance efforts to cure invasive azole-resistant *Candida* infections in clinical settings.

DATA AVAILABILITY STATEMENT

The original contributions presented in the study are included in the article/supplementary material; further inquiries can be directed to the corresponding authors.

AUTHOR CONTRIBUTIONS

JT, SJ, and LT carried out the *in vitro* and *in vivo* antifungal experiment. JT and HS collected and analyzed the experiment

data. YS and XW designed and interpreted the experiment data and wrote the manuscript. LY and XW revised the manuscript critically for important content. All authors contributed to the article and approved the submitted version.

FUNDING

This work was supported by the Hubei Province Health and Family Planning Scientific Research Project (grant number WJ2018H178 to YS and WJ2019M082 to SJ); the Natural Science Foundation of Hubei Province (grant number 2019CFB567) to YS; and Shanghai Municipal Commission of Health and Family Planning (grant number 201940476) to LY.

ACKNOWLEDGMENTS

We gratefully acknowledge Professor Haoping Liu from University of California, Irvine, for kindly providing us with isolates studied.

REFERENCES

Asadi, A., Abdi, M., Kouhsari, E., Panahi, P., Sholeh, M., Sadeghifard, N., et al. (2020). Minocycline, focus on mechanisms of resistance, antibacterial activity, and clinical effectiveness: Back to the future. *J. Glob. Antimicrob. Resist.* 22, 161–174. doi: 10.1016/j.jgar.2020.01.022

Berkow, E. L., and Lockhart, S. R. (2017). Fluconazole resistance in *Candida* species: a current perspective. *Infect Drug Resist.* 10, 237–245. doi: 10.2147/IDR.S118892

CLSI (2017). *Reference Method for Broth Dilution Antifungal Susceptibility Testing of Yeasts. 4th Edn.* Wayne, PA: Clinical and Laboratory Standards Institute.

Fiori, A., and Van Dijck, P. (2012). Potent synergistic effect of doxycycline with fluconazole against *Candida albicans* is mediated by interference with iron homeostasis. *Antimicrob. Agents Chemother.* 56, 3785–3796. doi: 10.1128/AAC.06017-11

Firacative, C. (2020). Invasive fungal disease in humans: are we aware of the real impact? *Mem. Inst. Oswaldo Cruz* 115:e200430. doi: 10.1590/0074-02760200430

Forsberg, K., Woodworth, K., Walters, M., Berkow, E. L., Jackson, B., Chiller, T., et al. (2019). *Candida auris*: The recent emergence of a multidrug-resistant fungal pathogen. *Med. Mycol.* 57, 1–12. doi: 10.1093/mmy/myy054

Gao, L. j., Sun, Y., Yuan, M. Z., Li, M., and Zeng, T. X. (2020). *In Vitro* and *In Vivo* study on the synergistic effect of minocycline and azoles against pathogenic fungi. *Antimicrob. Agents Chemother.* 64:e00290-20. doi: 10.1128/AAC.00290-20

Gao, Y., Zhang, C. Q., Lu, C. Y., Liu, P., Li, Y., Li, H., et al. (2013). Synergistic effect of doxycycline and fluconazole against *Candida albicans* biofilms and the impact of calcium channel blockers. *FEMS Yeast Res.* 13, 453–462. doi: 10.1111/1567-1364.12048

Goemaere, B., Becker, P., Van, W. E., Maertens, J., Spriet, I., Hendrickx, M., et al. (2018). Increasing candidaemia incidence from 2004 to 2015 with a shift in epidemiology in patients preexposed to antifungals. *Mycoses* 61, 127–133. doi: 10.1111/myc.12714

Gu, W. R., Yu, Q., Yu, C. X., and Sun, S. J. (2018). *In vivo* activity of fluconazole/tetracycline combinations in *Galleria mellonella* with resistant *Candida albicans* infection. *J. Glob. Antimicrob. Resist.* 13, 74–80. doi: 10.1016/j.jgar.2017.11.011

Jiang, T., Tang, J., Wu, Z. Q., Sun, Y., Tan, J. W., and Yang, L. J. (2020). The combined utilization of Chlorhexidine and Voriconazole or Natamycin to combat *Fusarium* infections. *BMC Microbiol.* 20:275. doi: 10.1186/s12866-020-01960-y

Kong, Q. X., Cao, Z. B., Lv, N., Zhang, H., Liu, Y. Y., Hu, L. F., et al. (2020). Minocycline and fluconazole have a synergistic effect against *Cryptococcus neoformans* both *in vitro* and *in vivo*. *Front. Microbiol.* 11:836. doi: 10.3389/fmicb.2020.00836

McCarty, T. P., and Pappas, P. G. (2016). Invasive candidiasis. *Infect. Dis. Clin. N. Am.* 30, 103–124. doi: 10.1016/j.idc.2015.10.013

Oliver, B. G., Silver, P. M., Marie, C., Hoot, S. J., Leyde, S. E., and White, T. C. (2008). Tetracycline alters drug susceptibility in *Candida albicans* and other pathogenic fungi. *Microbiology* 154, 960–970. doi: 10.1099/mic.0.2007/013805-0

Perfect, J. R., and Ghannoum, M. (2020). Emerging issues in antifungal resistance. *Infect. Dis. Clin. N. Am.* 34, 921–943. doi: 10.1016/j.idc.2020.05.003

Sapadin, A. N., and Fleischmajer, R. (2006). Tetracyclines: nonantibiotic properties and their clinical implications. *J. Am. Acad. Dermatol.* 54, 258–265. doi: 10.1016/j.jaad.2005.10.004

Shi, W. N., Chen, Z. Z., Chen, X., Cao, L. L., Liu, P., and Sun, S. J. (2010). The combination of minocycline and fluconazole causes synergistic growth inhibition against *Candida albicans*: an *in vitro* interaction of antifungal and antibacterial agents. *FEMS Yeast Res.* 10, 885–893. doi: 10.1111/j.1567-1364.2010.00664.x

Tsay, S. V., Mu, Y., Williams, S., Epson, E., Nadle, J., Bamberg, W. M., et al. (2020). Burden of Candidemia in the United States, 2017. *Clin. Infect. Dis.* 71, e449–e453. doi: 10.1093/cid/ciaa193

Vatanshenassan, M., Boekhout, T., Mauder, N., Robert, V., Maier, T., Meis, J. F., et al. (2020). Evaluation of microsatellite typing, ITS sequencing, AFLP fingerprinting, MALDI-TOF MS, and Fourier-transform infrared spectroscopy analysis of *Candida auris*. *J. fungi* 6:146. doi: 10.3390/jof6030146

Waterworth, P. M. (1974). The effect of minocycline on *Candida albicans*. *J. Clin. Pathol.* 27, 269–272. doi: 10.1136/jcp.27.4.269

Yong, V. W., Wells, J., Giuliani, F., Casha, S., Power, C., and Metz, L. M. (2004). The promise of minocycline in neurology. *Lancet Neurol.* 3, 744–751. doi: 10.1016/S1474-4422(04)00937-8

Conflict of Interest: The authors declare that the research was conducted in the absence of any commercial or financial relationships that could be construed as a potential conflict of interest.

frontiers in Microbiology

ORIGINAL RESEARCH
published: 20 May 2021
doi: 10.3389/fmicb.2021.680382

Effects of Hsp90 Inhibitor Ganetespib on Inhibition of Azole-Resistant *Candida albicans*

Rui Yuan[1], *Jie Tu*[2], *Chunquan Sheng*[2], *Xi Chen*[1]* *and Na Liu*[2]*

[1] Key Laboratory of Synthetic and Natural Functional Molecule of the Ministry of Education, College of Chemistry and Materials Science, Northwest University, Xi'an, China, [2] School of Pharmacy, Second Military Medical University, Shanghai, China

Candida albicans is the most common fungal pathogen. Recently, drug resistance of *C. albicans* is increasingly severe. Hsp90 is a promising antifungal target to overcome this problem. To evaluate the effects of Hsp90 inhibitor ganetespib on the inhibition of azole-resistant *C. albicans*, the microdilution checkerboard method was used to measure the *in vitro* synergistic efficacy of ganetespib. The XTT/menadione reduction assay, microscopic observation, and Rh6G efflux assay were established to investigate the effects of ganetespib on azole-resistant *C. albicans* biofilm formation, filamentation, and efflux pump. Real-time RT-PCR analysis was employed to clarify the mechanism of antagonizing drug resistance. The *in vivo* antifungal efficacy of ganetespib was determined by the infectious model of azole-resistant *C. albicans*. Ganetespib showed an excellent synergistic antifungal activity *in vitro* and significantly inhibited the fungal biofilm formation, whereas it had no inhibitory effect on fungal hypha formation. Expression of azole-targeting enzyme gene *ERG11* and efflux pump genes *CDR1*, *CDR2*, and *MDR1* was significantly down-regulated when ganetespib was used in combination with FLC. In a mouse model infected with FLC-resistant *C. albicans*, the combination of ganetespib and FLC effectively reversed the FLC resistance and significantly decreased the kidney fungal load of mouse.

Keywords: Hsp90, *Candida albicans*, antifungal activity, ganetespib, drug resistance

OPEN ACCESS

Edited by:
Ying-Chun Xu,
Peking Union Medical College Hospital (CAMS), China

Reviewed by:
Hai-Bin Luo,
Sun Yat-Sen University, China
Jian Li,
East China University of Science and Technology, China

***Correspondence:**
Xi Chen
xchen@nwu.edu.cn
Na Liu
liuna@smmu.edu.cn

Specialty section:
This article was submitted to Antimicrobials, Resistance and Chemotherapy, a section of the journal Frontiers in Microbiology

Received: *14 March 2021*
Accepted: *28 April 2021*
Published: *20 May 2021*

Citation:
Yuan R, Tu J, Sheng C, Chen X and Liu N (2021) Effects of Hsp90 Inhibitor Ganetespib on Inhibition of Azole-Resistant Candida albicans. Front. Microbiol. 12:680382. doi: 10.3389/fmicb.2021.680382

INTRODUCTION

Invasive fungal infections (IFIs) are emerging as a severe threat in the clinic due to the increasing number of immune-impaired patients (Miceli et al., 2011; Brown et al., 2012). It is estimated that fungi killed 1.5 million individuals per year (Denning and Bromley, 2015; Enoch et al., 2017; Bassetti et al., 2018). *Candida albicans* (*C. albicans*) is the most common fungal pathogen in IFIs. Currently, only three classes of antifungal drugs are available for the treatment of infectious *C. albicans*: polyenes (e.g., amphotericin B), azoles (e.g., fluconazole), and echinocandins (e.g., caspofungin). Azoles are the first-line clinical drugs used to treat IFIs. Extensive and prophylactic use of antifungal agents, especially azoles, could easily lead to the emergence of fungal resistance, which has become a serious concern (Odds, 2005; Perfect, 2017). The resistance problem is particularly severe in *Candida* species (Revie et al., 2018). Thus, there is an urgent need to explore new treatments for resistant candidiasis.

Molecular mechanisms of drug resistance to azoles mainly include drug target (Erg11) alteration, Erg11overexpression, and efflux pump overexpression (Cuenca-Estrella, 2014; Wu et al., 2017; Lee et al., 2020). In addition, the modulation of stress responses is inextricably linked to fungal resistance. Heat shock protein 90 (Hsp90), an essential molecular chaperone in all eukaryotes, regulates the form and function of diversified client proteins (Li and Buchner, 2013; Taddei et al., 2014). Hsp90 in fungi controls stress response and enables drug resistance (Cowen, 2013; Tiwari et al., 2015). Hsp90 also acts as the enigmatic thermal sensor to govern morphological transformation in *C. albicans*, which in turn causes biofilm formation-related resistance (Cowen and Lindquist, 2005; Nett et al., 2011; Whitesell et al., 2019). The structure of nucleotide-binding domain (NBD) of *C. albicans* Hsp90 was reported, which is similar to the structure of human Hsp90 NBD (Huang et al., 2020). Targeting Hsp90 is a promising antifungal strategy to find new antiresistant agents. However, effective antifungal Hsp90 inhibitors, especially with *in vivo* antifungal activity, are still rather limited.

In this study, we evaluated the antifungal activities of four Hsp90 inhibitors. Among them, ganetespib showed the best synergistic antifungal activity both *in vitro* and *in vivo*, and its antiresistant mechanism was preliminarily clarified. The therapeutic potential of antifungal sensitizer targeting Hsp90 against azole-resistant fungi was confirmed as a promising strategy to develop novel antifungal agents.

MATERIALS AND METHODS

Strains, Culture, and Agents

Candida tropicalis (*C. tropicalis*) 5008, *C. albicans* (strain numbers: 0304103 and 7781), *Cryptococcus neoformans* (*Cry.neoformans*), and *Candida glabrata* (*C. glabrata*) 9703 were provided by Changzheng Hospital of Shanghai, China. *Candida auris* (*C. auris*) 0029 was provided by Fudan University of Shanghai, China. All the strains were cultivated in yeast extract–peptone–dextrose (YEPD) medium (1% yeast extract, 2% peptone, and 2% dextrose) at 30°C in a shaking incubator (200 rpm/min). All tested compounds were purchased commercially from Topscience (Shanghai) and dissolved in DMSO at 2 mg/mL as stock solutions.

In vitro Synergistic Antifungal Activity Test

The *in vitro* synergistic efficacy was measured by the microdilution checkerboard method according to the reported protocol (Huang et al., 2018). Exponentially growing fungal cells were harvested and resuspended to 1×10^3 CFU/mL with RPMI 1640 medium. The tested compounds were prepared in different concentrations and transferred to the 96-well plates along the abscissa. Then, FLC was serially double-diluted into the 96-well plates along the ordinate. The azole-resistant *C. albicans* suspension containing the drug combinations was incubated at 35°C for 48 h. Then, the OD_{630} was measured by a spectrophotometer, and the synergistic inhibition efficacy was calculated using the fractional inhibitory concentration index (FICI). Each compound was tested in triplicate. FICI < 0.5 indicates the synergistic effect, FICI > 4 indicates the antagonistic effect, and $0.5 \leq$ FICI ≤ 4 indicates irrelevant.

Cell Viability Assay

C. albicans cells during the exponential growth phase were harvested and resuspended in fresh YPD liquid medium to an OD_{600} of about 0.40; then, the cells were diluted five times to six different concentrations in 96-well plates. About 3 μL of *C. albicans* cell suspension at different concentrations was coated on the surface of the YPD solid medium plate containing different concentrations of compounds. Then, the YPD solid medium plate was incubated at 30°C for 24 h. The growth of *C. albicans* cell colony was photographed.

Biofilm Formation Assay

The assay was performed according to the reported protocol (Tu et al., 2019). Exponentially growing *C. albicans* 0304103 cells were harvested and diluted in RPMI 1640 medium to a concentration of 1×10^6 CFU/mL. The fungal cells were transferred to the 96-well culture plates and incubated at 37°C. After 1.5 h of adhesion, the RPMI 1640 medium was aspirated to remove the non-adherent cells. Different concentrations of FLC and ganetespib were added, and the cells were further incubated at 37°C for 24 h. Then, the XTT/menadione reduction assay was used to examine the formation of biofilms. The assay was performed in triplicate.

Filamentation Assay

The assay was performed according to the reported protocol (Ji et al., 2020). Exponentially growing *C. albicans* 0304103 were harvested and diluted in Spider medium to a concentration of 1×10^6 CFU/mL. Different concentrations of FLC and ganetespib were added to the 24-well culture plate, and the plates were incubated at 37°C for 3 h. The differences in microscopic observation studies between groups were recorded on the Axio Observer D1 inverted microscope (Carl Zeiss, Inc. Thornwood, NY).

Rh6G Efflux Assay

Exponentially growing *C. albicans* 0304103 cells were harvested and diluted in YEPD medium (8 mL). Different concentrations of FLC and ganetespib were added and incubated at 35°C for 16 h. Then, fungal cells were harvested, diluted with phosphate-buffered saline (PBS), and incubated at 35°C for 2 h, and 10 μM of Rh6G was added. After further incubation at 35°C for 30 min, 2 mM of D-glucose was added to each group. Then, the fluorescence intensity of each group was measured at 0, 20, 40, and 60 min to investigate the amount of Rh6G efflux. The assay was performed in triplicate.

In vivo Antifungal Potency

Female ICR mice (4–6 weeks old and weighing 18–22 g) from the Shanghai Experimental Animal Center were housed and fed. Cyclophosphamide [100 mg/kg, in normal saline (NS)] was intraperitoneally injected to destroy the immune system of mice. After 24 h, the mice were inoculated via the tail vein with 0.2 mL of yeast suspension of *C. albicans* 0304103 (1×10^6 CFU/mL). The infectious mice were divided into four groups and treated daily with saline, FLC (0.3 mg/kg, in NS), ganetespib group (25

mg/kg, suspended in NS with 1.5% glycerin and 0.5% Tween 80), and the coadministration of FLC and ganetespib until the 5th day. On day 6, all the mice were euthanized and dissected; then their left kidneys were homogenized in NS (1 mL) and diluted in different concentrations of normal saline (NS). The dilutions of kidney homogenates were inoculated on sabourauds agar (SDA) plates containing chloromycetin (100 μg/mL). The number of CFU/mL of the kidney tissue was counted to calculate the fungal burden. The differences between the groups were analyzed by analysis of variance (ANOVA).

Real-Time RT-PCR Analysis

The analysis was performed using the reported protocol with some modifications (Han et al., 2020). Exponentially growing *C. albicans* 0304103 cells were harvested and diluted in YEPD medium at a concentration of 1×10^6 CFU/mL. Different concentrations of FLC and ganetespib were added, and the blank group was made without any compound. After incubations at 30°C for 24 h, the total RNA of fungal cells were extracted according to the manufacturer's instructions (RNeasy Plant Mini kit, QIAGEN, Germany), and cDNA of cells were obtained according to the reverse transcription kit (TaKaRa, Biotechnology, China). Real-time RT-PCR was performed on LightCycler Real-time PCR system (Roche diagnostics, GmbH Mannheim, Germany) according to the protocol of the PCR amplification kit. The fluorescence change of SYBR Green I and the circulating threshold (CT) were measured (fluorescence indicator: SYBR Green I, internal control gene: ACT1). The formula $2(-\Delta\Delta CT)$ was used to calculate the changes in the gene expression level, compared with ACT1. The assay was performed in triplicate. The primers are shown in **Table 1**.

TABLE 1 | Primers for real-time RT-PCR (5′ to 3′).

Name	Sequence
ERG11-F	ACTCATGGGGTTGCCAATGT
ERG11-R	GAGCAGCATCACGTCTCCAA
CDR1-F	TCCACGGTCGTGAATTCCAATGTG
CDR1-R	GCCAGCAACAGGACCAGCTTC
CDR2-F	GCTACTGCCATGTCACTCTCCAC
CDR2-R	GGACAACTGTGCTTCCAGGAGTAG
MDR1-F	CCACTGGTGGTGCAAGTGTT
MDR1-R	TCGTTACCGGTGATGGCTCT
ALS1-F	GTGTCGGTTGTCAGAAGAGC
ALS1-R	TTGTTCACGTTGAGCCATGG
ALS3-F	ACTTTGTGGTCTACAACTTGGG
ALS3-R	CCAGATGGGGATTGTAAAGTGG
HWP1-F	CTGAACCTTCCCCAGTTGCT
HWP1-R	CGACAGCACTAGATTCCGGA
EAP1-F	TCCTACACGACTGACACTGC
EAP1-R	TGACACCCGTAGTTACTGCTG
BCR1-F	TCCTTTACGTGCACCACCTC
BCR1-R	ATGCCGACGATTCAGCTGAT
ACE2-F	ACTTTGTGGTCTACAACTTGGG
ACE2-R	CCAGATGGGGATTGTAAAGTGG
RLM1-F	GTGCCTGCGAATGTTCCAAA
RLM1-R	TGCATTGCTTCCTCCTGTCA
ZAP1-F	TACCGCGACTACAAACCACC
ZAP1-R	TGCCCCTGTTGCTCATGTTT
ACT1-F	GGTTTGGAAGCTGCTGGTAT
ACT1-R	ACCACCAATCCAGACAGAGT

RESULTS

In vitro Antifungal Activity of Hsp90 Inhibitor Ganetespib

Four commercial Hsp90 inhibitors AUY922, ganetespib, PU-H71, and CH5138303 were selected to test the antifungal activities. The antifungal activities of Hsp90 inhibitors used alone or in combination with FLC are listed in **Table 2**. When used alone, four Hsp90 inhibitors had no direct effect on the growth of azole-resistant *C. albicans* ($MIC_{80} > 64$ μg/mL). When used in combination with FLC, FICI of AUY922, ganetespib, PU-H71, and CH5138303 was 0.039, 0.023, 2.000, and 0.500, respectively. Among them, AUY922 and ganetespib showed excellent synergistic activities. Time–growth curve revealed that the growth of azole-resistant *C. albicans* was inhibited obviously using the combination of ganetespib and FLC (8+8 μg/mL, **Supplementary Figure 1**). Hence, we also tested their synergistic activities against the other four azole-resistant clinically isolated *C. tropicalis*, *C. albicans*, *C. auris*, and *C. glabrata* strains. The results showed that the FICI of ganetespib was 0.039 and 0.035 against *C. tropicalis* and *C. albicans*, respectively, and ganetespib has no synergistic effect with FLC against *C. auris* and *C. glabrata* (**Table 3**). Furthermore, ganetespib showed moderate antifungal activity against *C. neoformans in vitro* ($MIC_{50} = 8$ μg/mL, **Supplementary Table 1**).

TABLE 2 | *In vitro* antifungal activity of Hsp90 inhibitors used alone or in combination with FLC against azole-resistant *C. albicans* strain (0304103).

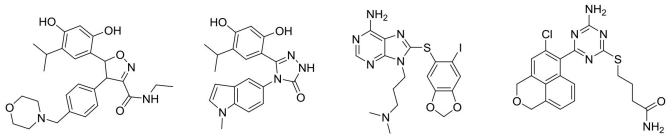

Compounds	Azole-resistant *C. albicans* 0304103			
	MIC_{80} (μg/mL)	FIC_{FLC} (μg/mL)	$FIC_{compd.}$ (μg/mL)	FICI[a]
AUY-922	>64	2	0.5	0.039
Ganetespib	>64	1	0.5	0.023
PU-H71	>64	>64	>64	2.000
CH5138303	>64	16	16	0.500

[a] *Synergism was defined by FICI of ≤ 0.5 and > 4, respectively. An FICI > 0.5 but < 4 is considered irrelevant.*

Ganetespib Affected Cell Viability

Since the ganetespib showed an excellent synergistic antifungal activity, the inhibitory effect of cell viability was then evaluated. Cell growth was monitored in the plate assay. As shown

in **Figure 1**, *C. albicans* cells were treated with ganetespib (32 μg/mL), FLC (32 μg/mL), as well as in combination of ganetespib and FLC (32+32 μg/mL). Compared with the blank control group, the ganetespib group (32 μg/mL) had little effect on the cell growth, and the FLC group (32 μg/mL) showed slightly reduced cell growth. In contrast, the simultaneous influence of ganetespib and FLC (32+32 μg/mL) resulted in an obvious decrease in the cell growth of *C. albicans*.

Comparison of the Binding Mode of Ganetespib With Human and *C. albicans* Hsp90

To probe the interactions of ganetespib with *C. albicans* Hsp90, computational glide docking studies were performed by the previous docking protocols (He et al., 2018). In the crystal structure of ganetespib/human Hsp90α complex (**Figure 2**), the *m*-diphenol and triazolone of ganetespib were compactly bound to Hsp90α. The *m*-diphenol group interacted with Asp93 through a hydrogen bond, and the triazolone group formed two hydrogen bonds with Thr184 and Lys58. The pyrrole ring was located in the solvent-exposed region. As depicted in **Figure 2**, ganetespib fit well within the NBD of *C. albicans* Hsp90. The phenolic hydroxyl group of *m*-diphenol, oxygen atom, and NH of triazolone formed hydrogen bonds with Lys47, Thr174, and Asp82, respectively.

TABLE 3 | *In vitro* antifungal activity of ganetespib used alone or in combination with FLC against azole-resistant clinically isolated strains.

Strains	MIC_{80} (μg/mL)	FIC_{FLC} (μg/mL)	FIC_{compd} (μg/mL)	FICI
C. tropicalis 5008	>64	0.5	2	0.039
C. albicans 7781	>64	0.25	2	0.035
C. auris 0029	>64	32	64	1.500
C. glabrata 9703	>64	16	8	1.125

Ganetespib Inhibited Fungal Biofilm Formation

Formation of fungal biofilms is a critical factor in the emergence of fungal drug resistance (Kelly et al., 2004; Nobile et al., 2006a,b; Nobile et al., 2009; Liu and Filler, 2011; Roudbarmohammadi et al., 2016; Araujo et al., 2017; Oliveira-Pacheco et al., 2018). Therefore, a biofilm formation assay was performed to clarify the mechanism of antagonizing drug resistance. The result showed that ganetespib significantly inhibited the biofilm formation at high concentration (32–64 μg/mL). Furthermore, the synergistic effect of the inhibition of biofilm formation was investigated using the treatment of ganetespib in combination with FLC. The result revealed that biofilm formation was effectively inhibited at 4 μg/mL of ganetespib and FLC, respectively ($P < 0.01$), and nearly 80% inhibition could be achieved at 64 μg/mL of ganetespib in combination with 4 μg/mL of FLC ($P < 0.001$, **Figure 3A**). However, the growth of fungal hypha was not inhibited by the ganetespib or FLC used alone or in combination at the concentration of 32 μg/mL (**Figure 3B**). To further investigate the mechanism of inhibition of biofilm formation, the expression of eight biofilm-related genes was evaluated by the real-time RT-PCR. As shown in **Figure 3C**, *ALS1*, *ALS3*, *HWP1*, *BCR1*, *ACE2*, and *RLM1* were down-regulated, while *EAP1* and *ZAP1* were up-regulated.

Ganetespib Obstructed Drug Resistance by Down-Regulating the Expression of Target Enzyme and Efflux Pump-Related Genes

The expression of FLC target gene *ERG11* was evaluated by the real-time RT-PCR. As shown in **Figure 4**, under the pressure of FLC, the expression of *ERG11* was obviously up-regulated.

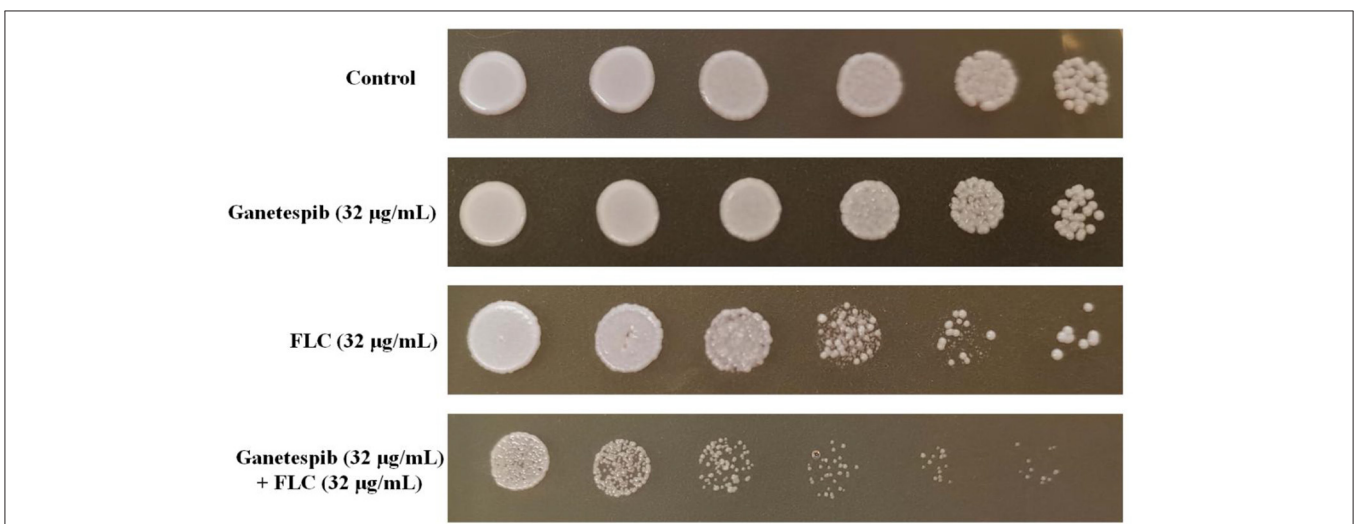

FIGURE 1 | Inhibitory effect of different compounds on the cell viability of *C. albicans* 0304103. Five-fold dilutions of cells (from 1×10^6/mL) were spotted on YPD.

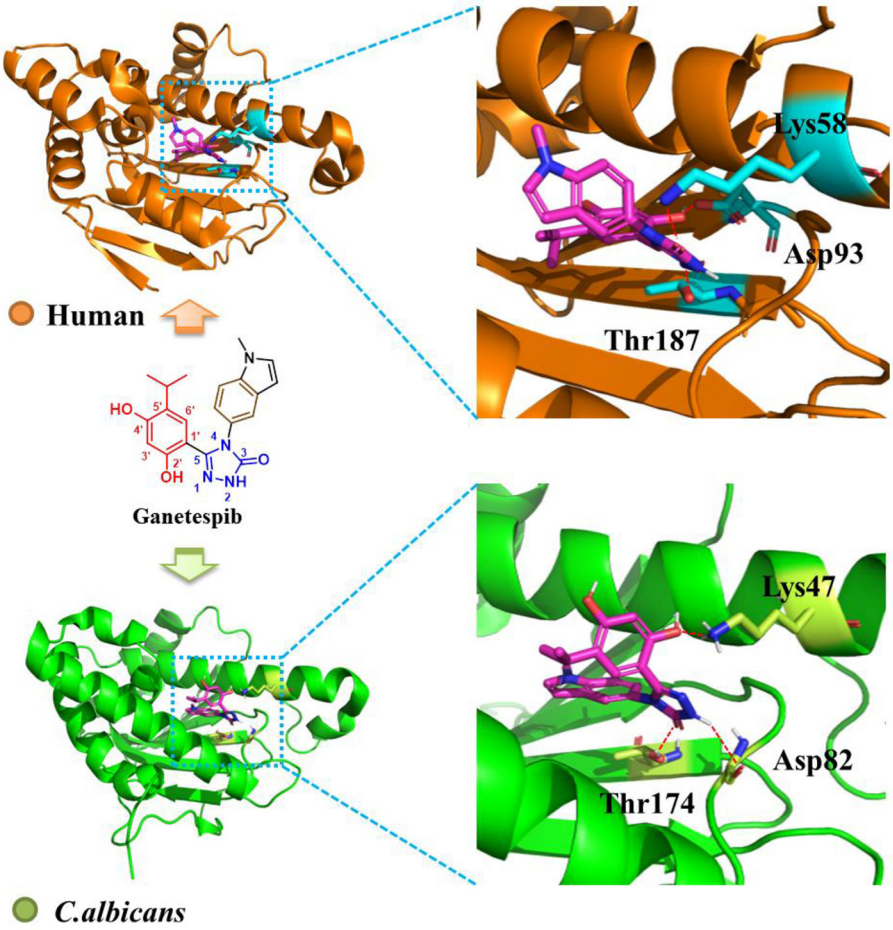

FIGURE 2 | Binding mode of ganetespib with human Hsp90 (orange, PDB code: 3UTH) and *C. albicans* Hsp90 (green, PDB code: 6CJS). The carbons of ganetespib are colored in magenta, nitrogen atoms in blue, and oxygen atoms in red. Red dashed lines represent the hydrogen bonding interactions. The figure was generated using PyMol (http://www.pymol.org/).

Interestingly, under the combinational action of FLC and ganetespib, the expression of *ERG11* was dramatically down-regulated. The overexpression of the efflux pump is a key factor of azole resistance in most fungal pathogens. ATP-binding cassette (ABC) superfamily and the major facilitator (MF) superfamily are the two main classes of efflux pumps contributing to azole resistance (Lee et al., 2020). In *C. albicans*, Cdr1 and Cdr2, two homologous ABC transporters, are closely associated with azole resistance. Besides, FLC resistance is also relevant to the MF transporter Mdr1 (multidrug resistance 1). Therefore, the expression of *CDR1*, *CDR2*, and *MDR1* was evaluated by the real-time RT-PCR. The results showed that the expression of *CDR1*, *CDR2*, and *MDR1* was significantly down-regulated when the FLC was used in combination with ganetespib.

Rhodamine 6G (Rh6G) Efflux Assay

By monitoring the fluorescence intensity, the extracellular Rh6G content was obtained. As shown in **Figure 5**, compared with FLC used alone, the fluorescence intensity was obviously lower when used in combination with ganetespib. The results indicated that the Rh6G excretion was decreased after the addition of ganetespib. As a result, the expression of efflux pumps was significantly declined under the action of ganetespib.

In vivo Antifungal Activity of Hsp90 Inhibitor Ganetespib

IFI mice model was constructed to investigate the *in vivo* antifungal activity of Hsp90 inhibitor ganetespib. Count of kidney fungal load was used as the evaluation index (**Figure 6**). The mice were divided into four groups: vehicle group, ganetespib group, FLC group, and the combination of ganetespib and FLC group. Compared with the blank group, ganetespib (25 mg/kg) used alone had no *in vivo* activity, however, treatment in combination with ganetespib (25 mg/kg) and FLC (0.3 mg/kg) could significantly decrease the kidney fungal load of mouse ($P < 0.001$), which was better than FLC used alone ($P < 0.05$).

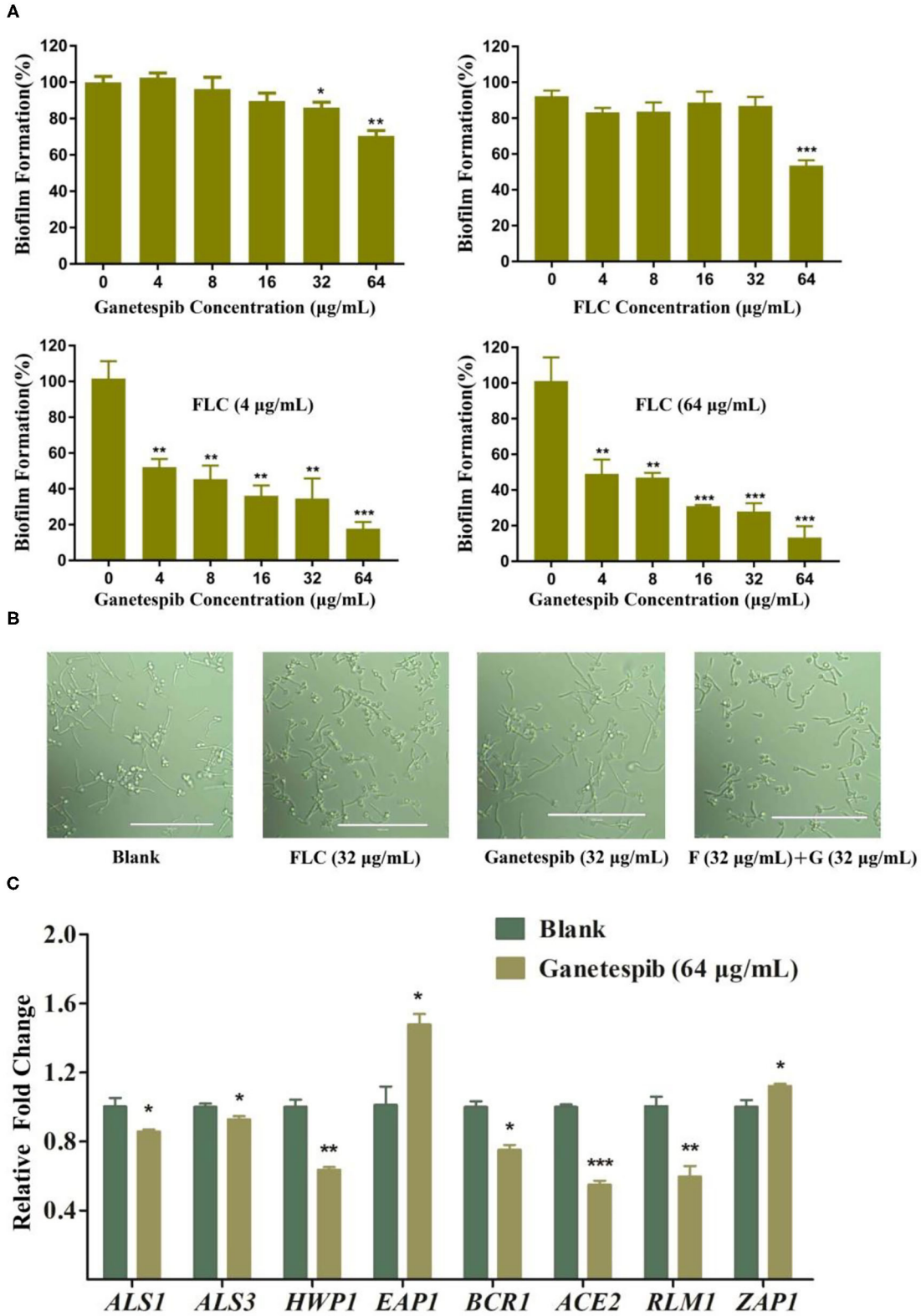

FIGURE 3 | (A) Effect of ganetespib, FLC, or both on the *C. albicans* 0304103 biofilm formation. **(B)** Filamentation microscopic observation of *C. albicans* 0304103 treated with FLC (F), ganetespib (G), or their combination. **(C)** Expression levels of biofilm formation-related and filamentation genes (*$P < 0.05$, **$P < 0.01$, ***$P < 0.001$, determined by Student's *t*-test).

DISCUSSION

Currently, the IFIs are a serious threat to public health in the clinic. *C. albicans* is the most common pathogenic fungi of IFIs. In recent years, drug resistance of abusive use of antifungal agents is becoming a serious problem. Thus, the antifungal efficacy of current drugs for the treatment of azole-resistant *C. albicans* in the clinic is limited (Arendrup and Patterson, 2017). Therefore, the discovery of new antifungal agents against resistant fungi is highly desirable.

Hsp90, a highly conserved molecular chaperone, plays an important role in antifungal drug tolerance and resistance in *Candida spp.*, and is regarded as a promising antifungal target. In this study, we assayed four Hsp90 inhibitors for the direct and synergistic antifungal activity. Ganetespib was validated to possess excellent synergistic activities when used in combination with FLC against azole-resistant *C. albicans* clinical isolates.

The crystal structures of human and *C. albicans* Hsp90 have been reported (Lee et al., 2015). We performed the docking study to compare the binding modes of ganetespib with human and *C. albicans* Hsp90. The result indicated that ganetespib fit well within the NBD of *C. albicans* Hsp90. Therefore, the cytotoxicity of ganetespib might hamper its potential application as an antifungal enhancer. Herein, *in vitro* antitumor activity and Hsp90α enzyme inhibition activity of ganetespib were also tested (**Supplementary Table 2** and **Supplementary Figure 2**). The results indicated that ganetespib had an excellent antitumor activity against HEL cells (IC_{50} = 0.021 μM), HL60 cells (IC_{50} = 0.023 μM), and A549 cells (IC_{50} = 0.11 μM), and an excellent Hsp90α enzyme inhibition activity (IC_{50} = 0.010 μM). Thus, further structural optimization of ganetespib is required to reduce the cytotoxicity. Recently, fungal-selective HSP90 inhibitors have been reported (Huang et al., 2020; Marcyk et al., 2021). However, the improvement of selectivity seems to have little influence on reducing cytotoxicity. Thus, extensive medicinal chemistry efforts are essential to developing HSP90 inhibitors as new antifungal agents.

The mechanism of ganetespib in antagonizing drug resistance was preliminarily investigated. Ganetespib significantly inhibited the biofilm formation used alone or in combination with FLC, but the growth of fungal hypha was not inhibited. It is inferred that ganetespib inhibited the biofilm formation not through acting on hypha formation. The effects of ganetespib on the expression of biofilm-related genes indicated that the ganetespib inhibited the biofilm formation relevant to cell adhesion.

Currently, molecular mechanisms of azole resistance included drug target alteration, drug target overexpression, and efflux pump overexpression (Vila et al., 2017). Overexpression of drug target (Erg11) of azoles is common in azole-resistant *C. albicans*

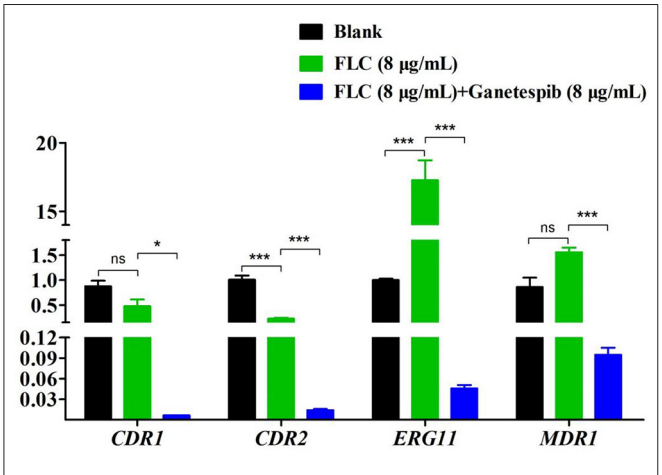

FIGURE 4 | Relative expression levels of azole resistance-related genes of *C. albicans* 0304103 after the treatment of ganetespib (*$P < 0.05$, ***$P < 0.001$, determined by Student's *t*-test).

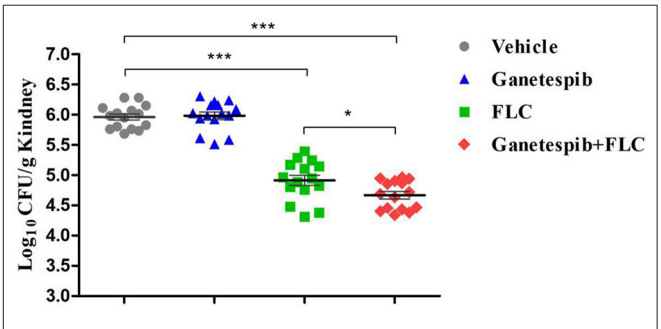

FIGURE 6 | *In vivo* therapeutic efficacy of ganetespib against IFI mice model infected with azole-resistant *C. albicans* 0304103 (*$P < 0.05$, ***$P < 0.001$, determined by ANOVA).

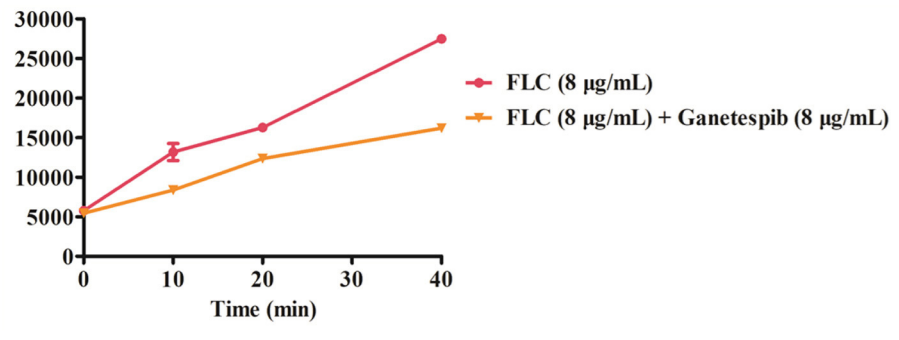

FIGURE 5 | Extracellular fluorescence intensity of Rh6G treated with ganetespib.

and leads to low drug sensitivity. Under the combinational treatment of FLC and ganetespib, the expression of *ERG11* and efflux pump genes *CDR1*, *CDR2,* and *MDR1* was significantly down-regulated. Though, the detailed mechanism of the drug combination in reversing *C. albicans* resistance remains to be clarified.

Taken together, this study investigated the *in vitro* and *in vivo* synergistic antifungal activities of ganetespib. Ganetespib could be used as a lead compound to develop a novel antifungal enhancer to treat resistant *Candida* infections.

DATA AVAILABILITY STATEMENT

The raw data supporting the conclusions of this article will be made available by the authors, without undue reservation, to any qualified researcher.

ETHICS STATEMENT

The animal study was reviewed and approved by Committee on Ethics of Medicine, Navy Medical University, PLA.

AUTHOR CONTRIBUTIONS

NL designed the experiments. RY and JT performed the experiments and interpreted the data. NL, XC, and CS wrote the manuscript. All authors contributed to the article and approved the submitted version.

FUNDING

This work was supported by the National Natural Science Foundation of China (Grants 81973175, 81725020, and 82003591), the Innovation Program of Shanghai Municipal Education Commission (Grant 2019-01-07-00-07-E00073), and the Science and Technology Commission of Shanghai Municipality (Grant 20S11900400).

SUPPLEMENTARY MATERIAL

The Supplementary Material for this article can be found online at: https://www.frontiersin.org/articles/10.3389/fmicb.2021.680382/full#supplementary-material

REFERENCES

Araujo, D., Henriques, M., and Silva, S. (2017). Portrait of *Candida* species biofilm regulatory network genes. *Trends Microbiol.* 25, 62–75. doi: 10.1016/j.tim.2016.09.004

Arendrup, M. C., and Patterson, T. F. (2017). Multidrug-resistant *Candida*: epidemiology, molecular mechanisms, and treatment. *J. Infect. Dis.* 216(Suppl. 3), S445–S451. doi: 10.1093/infdis/jix131

Bassetti, M., Righi, E., Montravers, P., and Cornely, O. A. (2018). What has changed in the treatment of invasive candidiasis? A look at the past 10 years and ahead. *J. Antimicrob. Chemother.* 73(Suppl. 1), i14–i25. doi: 10.1093/jac/dkx445

Brown, G. D., Denning, D. W., Gow, N. A., Levitz, S. M., Netea, M. G., and White, T. C. (2012). Hidden killers: human fungal infections. *Sci. Transl Med.* 4:165rv113. doi: 10.1126/scitranslmed.3004404

Cowen, L. E. (2013). The fungal Achilles' heel: targeting Hsp90 to cripple fungal pathogens. *Curr. Opin. Microbiol.* 16, 377–384. doi: 10.1016/j.mib.2013.03.005

Cowen, L. E., and Lindquist, S. (2005). Hsp90 potentiates the rapid evolution of new traits: drug resistance in diverse fungi. *Science* 309, 2185–2189. doi: 10.1126/science.1118370

Cuenca-Estrella, M. (2014). Antifungal drug resistance mechanisms in pathogenic fungi: from bench to bedside. *Clin. Microbiol. Infect.* 20(Suppl. 6), 54–59. doi: 10.1111/1469-0691.12495

Denning, D. W., and Bromley, M. J. (2015). Infectious disease. How to bolster the antifungal pipeline. *Science* 347, 1414–1416. doi: 10.1126/science.aaa6097

Enoch, D. A., Yang, H., Aliyu, S. H., and Micallef, C. (2017). The changing epidemiology of invasive fungal infections. *Methods Mol. Biol.* 1508, 17–65. doi: 10.1007/978-1-4939-6515-1_2

Han, G., Liu, N., Li, C., Tu, J., Li, Z., and Sheng, C. (2020). Discovery of novel fungal lanosterol 14alpha-demethylase (CYP51)/histone deacetylase dual inhibitors to treat azole-resistant candidiasis. *J. Med. Chem.* 63, 5341–5359. doi: 10.1021/acs.jmedchem.0c00102

He, S., Dong, G., Wu, S., Fang, K., Miao, Z., Wang, W., et al. (2018). Small molecules simultaneously inhibiting p53-murine double minute 2 (MDM2) interaction and Histone Deacetylases (HDACs): discovery of novel multitargeting antitumor agents. *J. Med. Chem.* 61, 7245–7260. doi: 10.1021/acs.jmedchem.8b00664

Huang, D. S., LeBlanc, E. V., Shekhar-Guturja, T., Robbins, N., Krysan, D. J., Pizarro, J., et al. (2020). Design and synthesis of fungal-selective resorcylate aminopyrazole Hsp90 inhibitors. *J. Med. Chem.* 63, 2139–2180. doi: 10.1021/acs.jmedchem.9b00826

Huang, Y., Dong, G., Li, H., Liu, N., Zhang, W., and Sheng, C. (2018). Discovery of Janus Kinase 2 (JAK2) and Histone Deacetylase (HDAC) dual inhibitors as a novel strategy for the combinational treatment of leukemia and invasive fungal infections. *J. Med. Chem.* 61, 6056–6074. doi: 10.1021/acs.jmedchem.8b00393

Ji, C., Liu, N., Tu, J., Li, Z., Han, G., Li, J., et al. (2020). Drug repurposing of haloperidol: discovery of new benzocyclane derivatives as potent antifungal agents against cryptococcosis and candidiasis. *ACS Infect. Dis.* 6, 768–786. doi: 10.1021/acsinfecdis.9b00197

Kelly, M. T., MacCallum, D. M., Clancy, S. D., Odds, F. C., Brown, A. J., and Butler, G. (2004). The *Candida albicans* CaACE2 gene affects morphogenesis, adherence and virulence. *Mol. Microbiol.* 53, 969–983. doi: 10.1111/j.1365-2958.2004.04185.x

Lee, C., Park, H. K., Jeong, H., Lim, J., Lee, A. J., Cheon, K. Y., et al. (2015). Development of a mitochondria-targeted Hsp90 inhibitor based on the crystal structures of human TRAP1. *J. Am. Chem. Soc.* 137, 4358–4367. doi: 10.1021/ja511893n

Lee, Y., Puumala, E., Robbins, N., and Cowen, L. E. (2020). Antifungal drug resistance: molecular mechanisms in *Candida albicans* and beyond. *Chem. Rev.* 121, 3390–3341. doi: 10.1021/acs.chemrev.0c00199

Li, J., and Buchner, J. (2013). Structure, function and regulation of the hsp90 machinery. *Biomed. J.* 36, 106–117. doi: 10.4103/2319-4170.113230

Liu, Y., and Filler, S. G. (2011). *Candida albicans* Als3, a multifunctional adhesin and invasin. *Eukaryot. Cell* 10, 168–173. doi: 10.1128/EC.00279-10

Marcyk, P. T., LeBlanc, E. V., Kuntz, D. A., Xue, A., Ortiz, F., Trilles, R., et al. (2021). Fungal-selective resorcylate aminopyrazole Hsp90 inhibitors: optimization of whole-cell anticryptococcal activity and insights into the structural origins of cryptococcal selectivity. *J. Med. Chem.* 64, 1139–1169. doi: 10.1021/acs.jmedchem.0c01777

Miceli, M. H., Díaz, J. A., and Lee, S. A. (2011). Emerging opportunistic yeast infections. *Lancet Infect. Dis.* 11, 142–151. doi: 10.1016/S1473-3099(10)70218-8

Nett, J. E., Sanchez, H., Cain, M. T., Ross, K. M., and Andes, D. R. (2011). Interface of *Candida albicans* biofilm matrix-associated drug resistance and cell wall integrity regulation. *Eukaryot. Cell* 10, 1660–1669. doi: 10.1128/EC.05126-11

Nobile, C. J., Andes, D. R., Nett, J. E., Smith, F. J., Yue, F., Phan, Q. T., et al. (2006a). Critical role of Bcr1-dependent adhesins in *C. albicans* biofilm formation in vitro and in vivo. *PLoS Pathog.* 2:e63. doi: 10.1371/journal.ppat.0020063

Nobile, C. J., Nett, J. E., Andes, D. R., and Mitchell, A. P. (2006b). Function of *Candida albicans* adhesin Hwp1 in biofilm formation. *Eukaryot. Cell* 5, 1604–1610. doi: 10.1128/EC.00194-06

Nobile, C. J., Nett, J. E., Herndday, A. D., Homann, O. R., Deneault, J. S., Nantel, A., et al. (2009). Biofilm matrix regulation by *Candida albicans* Zap1. *PLoS Biol.* 7:e1000133. doi: 10.1371/journal.pbio.1000133

Odds, F. C. (2005). Genomics, molecular targets and the discovery of antifungal drugs. *Rev. Iberoam. Micol.* 22, 229–237. doi: 10.1016/S1130-1406(05)70048-6

Oliveira-Pacheco, J., Alves, R., Costa-Barbosa, A., Cerqueira-Rodrigues, B., Pereira-Silva, P., Paiva, S., et al. (2018). The role of *Candida albicans* transcription factor RLM1 in response to carbon adaptation. *Front. Microbiol.* 9:1127. doi: 10.3389/fmicb.2018.01127

Perfect, J. R. (2017). The antifungal pipeline: a reality check. *Nat. Rev. Drug Discov.* 16, 603–616. doi: 10.1038/nrd.2017.46

Revie, N. M., Iyer, K. R., Robbins, N., and Cowen, L. E. (2018). Antifungal drug resistance: evolution, mechanisms and impact. *Curr. Opin. Microbiol.* 45, 70–76. doi: 10.1016/j.mib.2018.02.005

Roudbarmohammadi, S., Roudbary, M., Bakhshi, B., Katiraee, F., Mohammadi, R., and Falahati, M. (2016). ALS1 and ALS3 gene expression and biofilm formation in Candida albicans isolated from vulvovaginal candidiasis. *Adv. Biomed Res.* 5:105. doi: 10.4103/2277-9175.183666

Taddei, M., Ferrini, S., Giannotti, L., Corsi, M., Manetti, F., Giannini, G., et al. (2014). Synthesis and evaluation of new Hsp90 inhibitors based on a 1,4,5-trisubstituted 1,2,3-triazole scaffold. *J. Med. Chem.* 57, 2258–2274. doi: 10.1021/jm401536b

Tiwari, S., Thakur, R., and Shankar, J. (2015). Role of heat-shock proteins in cellular function and in the biology of fungi. *Biotechnol Res. Int.* 2015:132635. doi: 10.1155/2015/132635

Tu, J., Li, Z., Jiang, Y., Ji, C., Han, G., Wang, Y., et al. (2019). Discovery of carboline derivatives as potent antifungal agents for the treatment of cryptococcal meningitis. *J. Med. Chem.* 62, 2376–2389. doi: 10.1021/acs.jmedchem.8b01598

Vila, T., Romo, J. A., Pierce, C. G., McHardy, S. F., Saville, S. P., and Lopez-Ribot, J. L. (2017). Targeting *Candida albicans* filamentation for antifungal drug development. *Virulence* 8, 150–158. doi: 10.1080/21505594.2016.1197444

Whitesell, L., Robbins, N., Huang, D. S., McLellan, C. A., Shekhar-Guturja, T., LeBlanc, E. V., et al. (2019). Structural basis for species-selective targeting of Hsp90 in a pathogenic fungus. *Nat. Commun.* 10:402. doi: 10.1038/s41467-018-08248-w

Wu, S., Wang, Y., Liu, N., Dong, G., and Sheng, C. (2017). Tackling fungal resistance by biofilm inhibitors. *J. Med. Chem.* 60, 2193–2211. doi: 10.1021/acs.jmedchem.6b01203

Conflict of Interest: The authors declare that the research was conducted in the absence of any commercial or financial relationships that could be construed as a potential conflict of interest.

frontiers in Microbiology

ORIGINAL RESEARCH
published: 10 June 2021
doi: 10.3389/fmicb.2021.660645

Antifungal Combination of Ethyl Acetate Extract of *Poincianella pluviosa* (DC.) L. P. Queiros Stem Bark With Amphotericin B in *Cryptococcus neoformans*

*Gabriella Maria Andriani[1], Ana Elisa Belotto Morguette[1], Laís Fernanda Almeida Spoladori[1], Patrícia Morais Lopes Pereira[1], Weslei Roberto Correia Cabral[1], Bruna Terci Fernandes[1], Eliandro Reis Tavares[2,3], Ricardo Sérgio Almeida[1], Cesar Armando Contreras Lancheros[4], Celso Vataru Nakamura[1,4], João Carlos Palazzo Mello[5], Lucy Megumi Yamauchi[1,2] and Sueli Fumie Yamada-Ogatta[1,2]**

[1] Programa de Pós-graduação em Microbiologia, Departamento de Microbiologia, Centro de Ciências Biológicas, Universidade Estadual de Londrina, Londrina, Brazil, [2] Laboratório de Biologia Molecular de Microrganismos, Departamento de Microbiologia, Centro de Ciências Biológicas, Universidade Estadual de Londrina, Londrina, Brazil, [3] Programa Nacional de Pós-Doutorado, CAPES, Londrina, Brazil, [4] Laboratório de Inovação Tecnológica no Desenvolvimento de Fármacos e Cosméticos, Departamento de Ciências Básicas da Saúde, Centro de Ciências da Saúde, Universidade Estadual de Maringá, Maringá, Brazil, [5] Laboratório de Biologia Farmacêutica, Departamento de Farmácia, Universidade Estadual de Maringá, Maringá, Brazil

OPEN ACCESS

Edited by:
Ying-Chun Xu, Peking Union Medical College Hospital (CAMS), China

Reviewed by:
Fernanda Patrícia Gullo, UNESP – Universidade Estadual Paulista, Brazil
Liliana Scorzoni, São Paulo State University, Brazil

***Correspondence:**
Sueli Fumie Yamada-Ogatta
ogatta@uel.br

Specialty section:
This article was submitted to Antimicrobials, Resistance and Chemotherapy, a section of the journal Frontiers in Microbiology

Received: *29 January 2021*
Accepted: *06 May 2021*
Published: *10 June 2021*

Citation:
Andriani GM, Morguette AEB, Spoladori LFA, Pereira PML, Cabral WRC, Fernandes BT, Tavares ER, Almeida RS, Lancheros CAC, Nakamura CV, Mello JCP, Yamauchi LM and Yamada-Ogatta SF (2021) Antifungal Combination of Ethyl Acetate Extract of Poincianella pluviosa (DC.) L. P. Queiros Stem Bark With Amphotericin B in Cryptococcus neoformans. Front. Microbiol. 12:660645. doi: 10.3389/fmicb.2021.660645

Cryptococcus neoformans is the leading cause of cryptococcosis, an invasive and potentially fatal infectious disease. Therapeutic failures are due to the increase in antifungal resistance, the adverse effects of drugs, and the unavailability of therapeutic regimens in low-income countries, which limit the treatment of cryptococcosis, increasing the morbidity and mortality associated with these infections. Thus, new antifungal drugs and innovative strategies for the cryptococcosis treatment are urgently needed. The aim of the present study was to evaluate the effect of ethyl acetate fraction (EAF) of *Poincianella pluviosa* stem bark on planktonic and biofilm mode of growth of *C. neoformans*. Furthermore, the interaction between the EAF and amphotericin B (AmB) was evaluated *in vitro* and in *Galleria mellonella* infection model. Minimal inhibitory concentrations (MICs) of EAF ranged from 125.0 to >1,000.0 μg/ml and >1,000.0 μg/ml for planktonic and sessile cells, respectively. The combination between EAF and AmB exhibited a synergistic fungicidal activity toward *C. neoformans*, with a fractional inhibitory concentration index (FICI) ranging from 0.03 to 0.06 and 0.08 to 0.28 for planktonic and sessile cells, respectively. Microscopy analyses of planktonic *C. neoformans* cells treated with EAF, alone or combined with AmB, revealed morphological and ultrastructural alterations, including loss of integrity of the cell wall and cell membrane detachment, suggesting leakage of intracellular content, reduction

of capsule size, and presence of vacuoles. Moreover, EAF alone or combined with AmB prolonged the survival rate of *C. neoformans*-infected *G. mellonella* larvae. These findings indicate that *P. pluviosa* may be an important source of new compounds that can be used as a fungus-specific adjuvant for the treatment of cryptococcosis.

Keywords: antibiofilm, antivirulence, *Caesalpinia pluviosa*, cryptococcosis, *Galleria mellonella*, synergism

INTRODUCTION

Cryptococcosis is a potentially fatal fungal infection caused mainly by species of the *Cryptococcus gattii* and *Cryptococcus neoformans* complexes (Maziarz and Perfect, 2016). Currently, cryptococcosis ranks as the second most prevalent disease in human immunodeficiency virus (HIV)-infected individuals, with approximately 223,100 new cases and 181,000 deaths per year, particularly in low- and middle-income countries (WHO, 2018). The main contributors to the high mortality associated with cryptococcosis in these countries include delayed diagnosis, limited access and high cost of the drugs used in the induction phase and difficulty in monitoring drug toxicity (WHO, 2018). In fact, the etiological treatment of cryptococcosis is of paramount importance to reduce the mortality rate of this disease, and the use of a potent fungicidal agent during the induction (initial) phase is highly recommended (Maziarz and Perfect, 2016; Bermas and Geddes-McAlister, 2020). However, antifungals commonly used for induction and maintenance therapy schemes exhibit toxicity due to prolonged use, which is generally required (Bermas and Geddes-McAlister, 2020).

Clinically, cryptococcal meningitis is the most common presentation of cryptococcosis, followed by pulmonary cryptococcosis. Moreover, skin, lymph node, and bone involvement can also occur (Maziarz and Perfect, 2016). The etiological treatment of cryptococcosis is based on and limited to the use (alone or combined) of the polyene amphotericin B (AmB), azoles derivatives (mainly fluconazole), and the pyrimidine analog flucytosine, whose treatment regimens depend on the clinical presentation and the immune status of the patient (Perfect et al., 2010; Bermas and Geddes-McAlister, 2020).

Amphotericin B, a fungicidal agent, is considered the gold standard for the treatment of disseminated fungal infections (WHO, 2018). Although antifungal resistance to this drug is rare among cryptococcal isolates, cases of therapeutic failure have been documented (Singhal et al., 2016; Bandaranayake et al., 2018). Furthermore, prolonged treatment with AmB can lead to renal failure, hypokalemia, hypomagnesemia, and anemia (Bermas and Geddes-McAlister, 2020). Fluconazole, a fungistatic agent, is the second line for cryptococcosis treatment. Although it is a well-tolerated drug, gastrointestinal symptoms are frequently reported as adverse effects (Govindarajan et al., 2020). Unlike AmB, prophylactic or subinhibitory doses of fluconazole have led to the selection of resistant cryptococcal isolates, as well as being associated with the recurrence of infections (Perfect et al., 2010; Cheong and McCormack, 2013). Regarding flucytosine, the major drawback is related to the frequent development of resistance, so it is always used combined with another antifungal agent. Moreover, hematological and hepatic toxicities are adverse effects related to this drug (Padda and Parmar, 2020).

Due to this critical scenario and the fact that new classes of antifungals have not been made available by the pharmaceutical industry over the past two decades, there is an urgent need in researching and developing new drugs or strategies that are effective, safe, and affordable for the treatment of cryptococcosis. Thus, in recent decades, we have seen renewed interest in active compounds isolated from natural products, especially plants. In fact, plants are a source of different chemical classes of biologically active molecules, many of which have been proven to present antimicrobial activities against different microorganisms (Biasi-Garbin et al., 2016; Kokoska et al., 2018; Morguette et al., 2019).

Brazilian biomes exhibit a wide biodiversity of native or exotic flora and a high capacity for their sustainable exploitation, and many plants are used in folk medicine to treat different diseases (Savi et al., 2019; Ribeiro Neto et al., 2020). The *Caesalpinia* genus (Fabaceae family) consists of more than 500 species, of which only about 30 species have been studied. Various biological activities have been attributed to extracts or phytochemicals obtained from different species of *Caesalpinia*, such as antimicrobial, anti-inflammatory, antioxidant, anticancer, antidiabetic, antirheumatic, and analgesic activities (Zanin et al., 2012). *Poincianella pluviosa* (DC.) L. P. Queiros [also named *Caesalpinia pluviosa* DC. var. *peltophoroides* (Benth.) G. P. Lewis], popularly known as "sibipiruna" or "falso pau brasil," is a domesticated plant in Brazil found mainly in the Atlantic forest and Pantanal biomes; it is widely used in ornamentation and is known for its high wood potential (Carvalho, 2014). Few studies on the pharmacological activities of *P. pluviosa* are described in the literature, and the following activities have been specifically attributed to stem bark extract of *P. pluviosa*, including antimalarial (Deharo et al., 2001; Kayano et al., 2011), anti-staphylococcal (Guidi et al., 2020), wound healing *in vitro* and *in vivo* (Bueno et al., 2016; Guidi et al., 2020), and anti-inflammatory (Domingos et al., 2019).

The combination of two or more drugs that generate synergistic effects is another strategy that has been explored for the treatment of fungal infections (Longhi et al., 2016). This strategy may result in lower drug concentrations to produce an effect; reduction of the selection of resistant strains, thus increasing the efficacy of the treatment; and reduction of its toxicity by neutralizing or eliminating adverse effects (Mukherjee et al., 2005; Chen et al., 2014). Currently, studies on synergistic interactions of natural

products with clinically important antimicrobial agents have been carried out and are increasingly promising in the formulation of new therapeutic strategies (Chen et al., 2014; Longhi et al., 2016).

Therefore, the aim of the present study was to evaluate the antifungal potential of *P. pluviosa* stem bark extract and its combination with AmB on *C. neoformans*.

MATERIALS AND METHODS

Microorganisms and Culture Conditions

Cryptococcus neoformans serotype A ATCC 34872, *C. neoformans* serotype D ATCC 66031, and four isolates of *C. neoformans* (**Table 1**) recovered from human infections and belonging to the microbial collection of the Laboratory of Molecular Biology of the Microorganisms, Universidade Estadual de Londrina, Londrina, Brazil, were included in the present study. Yeasts were cultured in Sabouraud dextrose (SD) agar at 37°C and kept at 4°C. The clinical isolates were identified by PCR using specific primers complementary to intergenic spacer 1 (IGS1) of ribosomal DNA (Tavares et al., 2016). All fungal strains were also stored in SD broth containing 20% glycerol at −80°C. For the experiments, three to five colonies were transferred to SD broth and incubated at 37°C for 48 h. Cells were then centrifuged (10,000 × *g*, for 3 min) and resuspended in 0.85% NaCl solution (saline) to achieve a turbidity equivalent to 0.5 McFarland standard using the DensiCHEK^{TM} PLUS colorimeter (bioMérieux), which corresponded to approximately 1.0–2.0 × 10^6 colony-forming unit (CFU)/ml (standard fungal suspension). Each standard fungal suspension was then diluted in culture medium to achieve the cell density (inoculum) used in each assay, unless specified.

Poincianella pluviosa Extracts and Antifungals

Bark from *P. pluviosa* (DC.) L. P. Queiros was collected at the Universidade Estadual de Maringá (UEM), and a voucher species was deposited in the herbarium of UEM under the number 12492 HUEM. Access to the botanical material was registered in *Sistema Nacional de Gestão do Patrimônio Genético e do Conhecimento Tradicional Associado* (SISGEN, Brazil) under the number A6DD2D2. Moreover, field studies did not involve endangered or protected plant species. The extracts from stem bark of *P. pluviosa* were prepared according to Bueno et al. (2014). For all antifungal susceptibility assays, crude hydroalcoholic extract (CE) and ethyl acetate (EAF) fraction were dissolved in Roswell Park Memorial Institute 1640 (RPMI, Sigma-Aldrich, Brazil) buffered with 0.164 M 3-(*N*-morpholino) propanesulfonic acid, pH 7.2 (RPMI-MOPS) medium containing 10% dimethyl sulfoxide (DMSO) to obtain a stock solution of 4.0 mg/ml. Stock solution of AmB (1.6 mg/ml; Sigma, Brazil) was diluted in 10% DMSO solution in ultrapure water and maintained at −20°C. DMSO did not exceed 1% in all assays.

TABLE 1 | Minimal inhibitory concentration (MIC*) of *Poincianella pluviosa* stem bark extracts and amphotericin B against *Cryptococcus neoformans*.

Microorganism	Crude extract	Ethyl acetate fraction	Amphotericin B
C. neoformans ATCC 34872	>1,000.0	1,000.0	0.125
C. neoformans ATCC 66031	>1,000.0	1,000.0	0.125
C. neoformans 1172	>1,000.0	>1,000.0	0.250
C. neoformans 90889	>1,000.0	>1,000.0	0.250
C. neoformans CN01	>1,000.0	>1,000.0	0.125
C. neoformans CN12	1,000.0	125.0	0.125

**MIC was determined at the lowest concentration capable to inhibit the visual growth of fungal cells. The results were determined after 72 h of incubation and were expressed in μg/ml.*

Antifungal Susceptibility Testing on Planktonic Cells

Minimal inhibitory concentrations (MICs) of *P. pluviosa* extracts and AmB were determined by the broth microdilution method according to the Clinical and Laboratory Standards Institute [M27 document A3 (CLSI, 2008)] recommendations. An aliquot (100 μl) of fungal cells (0.5–2.5 × 10^3 CFU/ml) was added to the wells of 96-well U-bottom microtiter plates (Techno Plastic Products, Switzerland) containing two-fold serial dilutions of *P. pluviosa* extracts (1.95–1,000.0 μg/ml) and AmB (0.031–16.0 μg/ml) in RPMI-MOPS. Wells containing medium or medium plus DMSO 1% and wells without fungal cells were used as growth and sterility control, respectively. *Candida parapsilosis* ATCC 22019 was used as quality control. MIC was defined as the lowest concentration capable of inhibiting visual growth after 72 h of incubation at 37°C in comparison to untreated planktonic cells. Compounds with MIC values >1,000.0 μg/ml were considered inactive (Holetz et al., 2002). Here, 10-μl aliquots from the wells without visible growth were transferred onto SD agar to determine the minimal fungicidal concentration (MFC) (Miles et al., 1938). The plates were incubated at 37°C for 72 h, and MFC was determined as the concentration capable of reducing the CFU counts to zero.

Checkerboard Microdilution Assay

The antifungal effect of EAF combined with AmB was evaluated using the checkerboard broth microdilution assay in 96-well microtiter plates according to Scott et al. (1995). Two-fold serial dilutions of EAF (0.03–1,000.0 μg/ml) and AmB (0.000001–16.0 μg/ml) were, respectively, added across the plate rows and columns. Subsequently, the fungal inoculum (0.5–2.5 × 10^3 CFU/ml) was added, and the plates were incubated at 37°C for 72 h. The Fractional Inhibitory Concentration Index (FICI) was determined from the sum of FIC_{EAF} and FIC_{AmB}. The FIC of each compound is the concentration that presents the inhibitory effect when used combined with another compound divided by the concentration that has the same effect when used individually. The FICI values were interpreted as follows: synergism, FICI ≤ 0.5;

no interaction, 0.5 < FICI < 4.0; antagonism, FICI > 4.0 (Odds, 2003).

Characterization of the Synergistic Antifungal Interaction Between Ethyl Acetate Fraction and Amphotericin B

Time-Kill Kinetics

The rate of fungal killing in presence of EAF and AmB alone or combined at the MIC values was analyzed by the time-kill assay (CLSI, 2008). Planktonic cells (1.0×10^3 CFU/ml) were added in RPMI-MOPS containing the plant extract and/or the AmB and were incubated statically at 37°C. At specific time points (0, 24, and 48 h), 10 μl were removed from each well and serially diluted (1:10) in 0.15 M phosphate-buffered saline (PBS) pH 7.2. An aliquot of 10 μl of each dilution was inoculated onto SD agar, and the CFU counts were determined after incubation at 37°C for 48 h. Fungal cells incubated in the absence of the EAF and AmB were used as growth control. Data were averaged and plotted as $\log_{10}$ CFU/ml vs. time (h).

Fungal Cell Viability

Yeast viability was evaluated using the LIVE/DEAD® Yeast Viability Kit (Molecular Probes, Invitrogen) according to the manufacturer's recommendations. Fungal suspensions (1.0×10^7 CFU/ml) of *C. neoformans* ATCC 66031 and *C. neoformans* CN12 were treated with EAF (1,000.0 and 125.0 μg/ml, respectively), AmB (0.125 μg/ml for both strains), and the combination of EAF and AmB (3.9/0.003 μg/ml for both strains) for 12 h. Afterward, untreated and treated cells were incubated with FUN1® and Calcofluor White™ dyes and analyzed by fluorescence microscopy (LEICA DM2000) using fluorescein filters with excitation/emission of 480/530 nm.

Transmission Electron Microscopy (TEM) Analysis of Planktonic Cells

Morphological and ultrastructural changes induced by EAF (1,000.0 μg/ml), AmB (0.125 μg/ml), and the combination of EAF and AmB (3.9 μg/ml and 0.003 μg/ml, respectively) on planktonic cells after 48 h of treatment were analyzed by TEM. Yeast cells were fixed for 2 h at room temperature with 2.5% glutaraldehyde and 4% paraformaldehyde in 0.1 M sodium cacodylate buffer, pH 7.4. Postfixation in 1% OsO_4 in cacodylate buffer containing 0.8% potassium ferrocyanide and 5 mM $CaCl_2$ for 2 h. The cells were then dehydrated in a graded series of acetone and embedded in Epon resin for 72 h at 60°C. Ultrathin sections were obtained with a Leica ultramicrotome, and the sections were contrasted with 5% uranyl acetate and lead citrate for observation in a JEOL JEM-1400 Electron Microscope at 80 kV.

Effect of Ethyl Acetate Fraction and Amphotericin B on Capsule and Cell Size

Cryptococcus neoformans ATCC 66031 and *C. neoformans* CN12 were cultivated in minimal capsular induction medium (15 mM glucose, 10 mM $MgSO_4$, 29.4 mM KH_2PO_4, 13 mM glycine, and 3 μM thiamine-HCl, pH 5.5) for 7 days at 30°C (Frases et al., 2009). After incubation, a standard fungal suspension of each strain was prepared as described in section "Microorganisms and Culture Conditions," and yeast cells (1.0×10^7 CFU/ml) were treated with MIC values of EAF and AmB, alone or in combination at the MIC synergistic concentrations, in RPMI-MOPS for 48 h at 37°C. Untreated cells were used as control. Cells were centrifuged, suspended in Chinese ink, and observed in a Zeiss Axio Imager 2 microscope. Capsule size was measured in 100 cells using the ImageJ 1.49v software[1]. The capsule thickness was determined by the difference between the diameter of the cell, including the capsule, and the diameter of the body cell within the cell wall (Spadari et al., 2018).

Effect of Ethyl Acetate Fraction and Amphotericin B on Biofilms

The biofilms were formed on flat-bottomed 96-well polystyrene plates in SD broth according to Martinez and Casadevall (2006) at 37°C for 48 h statically, with an initial inoculum of 1.0×10^7 CFU/ml. After the incubation, non-adherent cells were removed by washing with sterile saline, and 200-μl aliquots of RPMI-MOPS containing different concentrations of EAF (31.25–1,000.0 μg/ml) or AmB (0.007–16.0 μg/ml) were added to the wells for determining the sessile minimal inhibitory concentration (SMIC). The checkerboard assays were used to evaluate the effect of EAF combined with AmB on 48-h biofilm, as described above. Untreated and treated biofilms were incubated at 37°C for 48 h and then washed with sterile saline. The viability of sessile cells was determined by using the dimethylthiazol diphenyltetrazolium bromide (MTT, Sigma) reduction assay according to the manufacturer's recommendations. The SMICs of EAF and AmB alone and combined were determined by the lowest concentration of the extract/antifungal capable of inhibiting 80% ($SCIM_{80}$) of the sessile cells when compared to the untreated control. The results of the combination were interpreted using the FICI as described above.

Scanning Electron Microscopy (SEM) Analysis of Biofilms

Morphological alterations induced by EAF alone and combined with AmB on *C. neoformans* ATCC 66031 biofilm were analyzed by SEM. The polystyrene strips (0.5 cm^2) and glass (round coverslip) were placed in wells of 24-well tissue culture plates containing 1.0 ml of SD broth, then the biofilm was formed as described above. The biofilms were fixed with 2.5% (v/v) glutaraldehyde in 0.1 M sodium cacodylate buffer pH 7.2 at room temperature and postfixed in 1% OsO_4, dehydrated with a series of ethanol washes (30, 50, 70, 90, and 100%), critical point dried in CO_2, coated with gold, and observed in a Shimadzu SS-550 scanning electron microscope.

Effect of Ethyl Acetate Fraction and Amphotericin B on Mammalian Cells

The cytotoxicity of EAF alone and combined with AmB was evaluated on human erythrocytes. Blood was collected from a healthy donor according to the Declaration of Helsinki principles, and 4% defibrinated blood was prepared in

[1]https://imagej.nih.gov/ij/

glycosylated saline (0.85% NaCl plus 5% glucose). Erythrocytes (100 μl) were inoculated in each well of 96-well microtiter plates containing different concentrations of EAF (1.95–1,000.0 μg/ml), AmB (0.015–16 μg/ml) alone or in combination. Wells without EAF and AmB and with 1% Triton X-100 were used as negative and positive hemolysis controls, respectively. After incubation for 3 h at 37°C, the optical density (OD) of the supernatant was determined at 550 nm with a microtiter plate reader (Synergy™ HT, BioTek). Thus, the plates were centrifuged at 1,000 × *g* for 10 min, and the supernatants were transferred to new microplates before spectrophotometric reading. The percentage of hemolysis was compared with the positive control wells using the equation: (OD_{550} of the treated supernatant – OD_{550} of the untreated control)/OD_{550} of the positive control – OD_{550} of the untreated control) × 100% (Izumi et al., 2012). The concentration of EAF capable of causing 90% hemolysis was used to calculate the selectivity index (IS) using the following equation: $IS = CC_{90}/MIC$.

Galleria mellonella Infection and Antifungal Treatment

The wax moth larvae killing assays were carried out as described previously with minor modifications (Fuchs et al., 2010). Groups of 10 larvae were used in all assays, and a volume of 5 μl containing the yeast inoculum or antifungals or PBS was inoculated with a Hamilton syringe (Hamilton, United States) into the hemocele. The larva abdomen was cleaned with 70% ethanol before the inoculation. First, the toxicity of EAF and AmB was evaluated by inoculating different concentrations of the compounds per kilogram of larvae as follows: a) 0.25 × MIC, 0.5 × MIC, and MIC values of EAF (*C. neoformans* ATCC 66031 250.0, 500.0, and 1,000.0 μg/ml, respectively; *C. neoformans* CN12 31.2, 62.5, and 125.0 μg/ml, respectively); b) MIC and 2 × MIC of AmB (0.125 and 0.25 μg/ml, respectively, for both strains); c) MIC values of EAF and AmB in the synergistic combination, 2 × MIC and 4 × MIC (3.9/0.003, 7.8/0.006, and 15.6/0.015 μg/ml, respectively, for both strains). All doses were inoculated in the last left proleg of larvae. A group of larvae inoculated with PBS was used as control. For larva infection and treatment, *C. neoformans* ATCC 66031 and *C. neoformans* CN12 were cultivated in minimal capsular induction medium as described in section "Effect of Ethyl Acetate Fraction and Amphotericin B on Capsule and Cell Size." Fungal cell suspension of each strain was prepared in PBS, and 5 × 10^8 cells were inoculated into the hemocele in the last left proleg. The treatment with EAF and AmB, alone and combined (as above), was carried out immediately post-infection by inoculating the compounds in the last right proleg. The larvae were incubated at 37°C, and survival was monitored every day up to 10 days. The larvae were considered dead when they did not respond to physical stimulation (slight pressure with forceps). A group of non-infected larvae and a group of infected larvae and treated with PBS were used as controls. Each experiment was carried out in triplicate, and the results presented are from a representative experiment.

Statistical Analysis

GraphPad Prism version 6.0 software (GraphPad Software, San Diego, CA, United States) was used for statistical analysis. Data of antifungal effect of EAF alone and combined with AmB on capsule and cell size and biofilm were analyzed by one-way ANOVA. The analysis of *G. mellonella* survival data was performed using the log-rank (Mantel–Cox). For all assays, a $p < 0.05$ was considered significant.

RESULTS

Crude Extract and Ethyl Acetate Fractions of *Poincianella pluviosa* Do Not Exhibit Antifungal Activity on Planktonic Cells of Most *Cryptococcus neoformans* Strains

To validate the MIC values obtained for EAF against *C. neoformans* strains, MIC values of fluconazole and AmB for the quality control *C. parapsilosis* ATCC 22019 were also determined. The MIC values of fluconazole (1.0 μg/ml) and AmB (0.25 μg/ml) identified for this fungal species were in accordance with CLSI guidelines (CLSI, 2008). The antimicrobial activity of CE and EAF of *P. pluviosa* stem bark was initially evaluated on planktonic cells of *C. neoformans*, and the MIC values are presented in **Table 1**. MICs ≥1,000.0 μg/ml for the plant compounds were detected for most cryptococcal strains, indicating that they were inactive against planktonic cells. *C. neoformans* CN12 strain was more sensitive to *P. pluviosa* extracts, judging by the MIC values equal to 1,000.0 and 125.0 μg/ml for CE and EAF, respectively. MFC values of EAF were ≥1,000.0 μg/ml for all strains tested, indicating a fungistatic effect.

Ethyl Acetate Fraction Combined With Amphotericin B Displays Synergistic Interaction Against Planktonic Cells of *Cryptococcus neoformans* Strains

Based on EAF MIC values, *C. neoformans* ATCC 66031 and *C. neoformans* CN12 were selected for analyzing the effect of simultaneous addition of plant extract and AmB during their planktonic growth by checkerboard assay. Thereafter, both strains were named ATCC 66031 and CN12, respectively. A remarkable reduction in MIC values of EAF and AmB combined was observed; a 32-fold reduction in MIC value of AmB was observed for both strains, whereas a 256-fold and 32-fold reduction in MIC values of EAF were detected for ATCC 66031 and CN12 strains, respectively. The calculated FICI of 0.03 (for ATCC 66031) and 0.06 (for CN12) indicated a synergistic antifungal interaction for the combination of 3.9 μg/ml EAF and 0.003 μg/ml AmB for both strains (**Table 2**). The results of time-kill studies confirmed this interaction and its fungicidal effect (**Figures 1A1,A2**). In the presence of MIC values of EAF, an inhibition of planktonic growth of both cryptococcal strains was observed over time compared to untreated control

TABLE 2 | Effect of ethyl acetate fraction (EAF) combined with amphotericin B (AmB) against planktonic cells and mature biofilm of *Cryptococcus neoformans*.

Microorganism	EAF (μg/ml)	AmB (μg/ml)	EAF/AmB (μg/ml)	FICI	Interaction
Planktonic cells*					
C. neoformans ATCC 66031	1,000.0	0.125	3.9/0.003	0.03	Synergism
C. neoformans CN12	125.0	0.125	3.9/0.003	0.05	Synergism
48-h biofilm**					
C. neoformans ATCC 66031	>1,000.0	2	31.25/0.5	0.28	Synergism
C. neoformans CN12	>1,000.0	4	15.6/0.25	0.07	Synergism

**Minimal inhibitory concentration. **Minimal inhibitory concentration capable to reduce the viability of 80% of sessile cells ($SMIC_{80}$). The results were determined after 72 h of incubation and were expressed in μg/ml. EAF, ethyl acetate fraction; AmB, amphotericin B; EAF/AmB, EAF combined with AmB; FICI, fractional inhibitory concentration index. Reference values: synergism, FICI ≤ 0.5; no interaction, 0.5 < FICI < 4.0; antagonism, FICI ≥ 4.0 (Odds, 2003).*

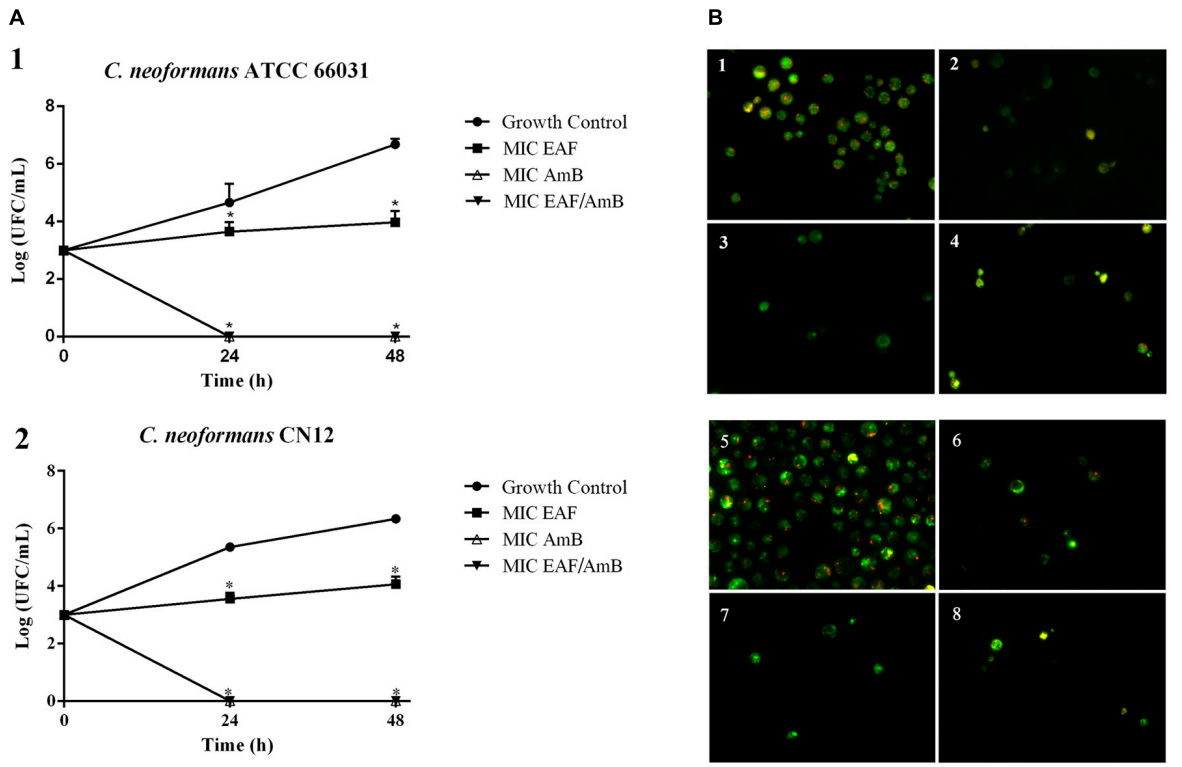

FIGURE 1 | Effect of ethyl acetate fraction (EAF) of *Poincianella pluviosa* bark and amphotericin B (AmB) alone or in combination against *Cryptococcus neoformans*. **(A)** Time-kill kinetics of EAF, AmB, and their combination at 0, 24, 48, and 72 h. **(1)** *C. neoformans* ATCC 66031; **(2)** *C. neoformans* CN12. The values are the mean ± standard deviation of two independent experiments in duplicate. Analysis of *C. neoformans* survival data was performed using two-way ANOVA, $^*p < 0.05$. **(B)** Cell viability analysis of *C. neoformans* ATCC 66031 **(1–4)** and *C. neoformans* CN12 **(5–8)** by fluorescence microscopy using FUN-1® dye. Yeasts were incubated with or without the minimal inhibitory concentrations (MICs) of the two compounds alone or combined for 12 h. Cells with diffuse greenish-yellow fluorescence characterize metabolically inactive cells, and cells containing red fluorescent structures in their vacuoles represent metabolically active yeast. **(1,5)** untreated viable cells; **(2)** 1,000.0 μg/ml EAF; **(3,7)** 0.125 μg/ml AmB; **(4,8)** 3.9/0.003 μg/ml EAF/AmB; **(6)** 125.0 μg/ml EAF.

cells. After 48-h incubation, there was a difference of 2 log in CFU counts in EAF-treated cells compared to the untreated ones ($p < 0.05$). At the synergistic combination, the CFU counts of both cryptococcal strains were zero after 24 h, indicating a fungicidal effect. Importantly, this fungicidal effect was similar to that obtained with AmB (MIC) but at lower concentrations of the drug.

The fungicidal effect of EAF combined with AmB was further supported by the analysis of cell viability of ATCC 66031 and CN12 using fluorescent dyes for differential labeling. The images show that untreated yeasts of both strains exhibited red fluorescent structures in their cytoplasm, indicating metabolically active cells with intact cytoplasmic membranes (**Figures 1B1,B5**). However, cells treated with EAF MIC exhibited bright, diffuse, green–yellow fluorescence staining, suggesting cells with poor metabolic activity (**Figures 1B2,B6**). AmB treatment (**Figures 1B3,B7**) and the combination of both (**Figures 1B4,B8**) showed diffuse green staining, indicating cell death.

To corroborate the time-kill and fungal viability analyses, thus, to elucidate the possible mechanism of action of EAF alone

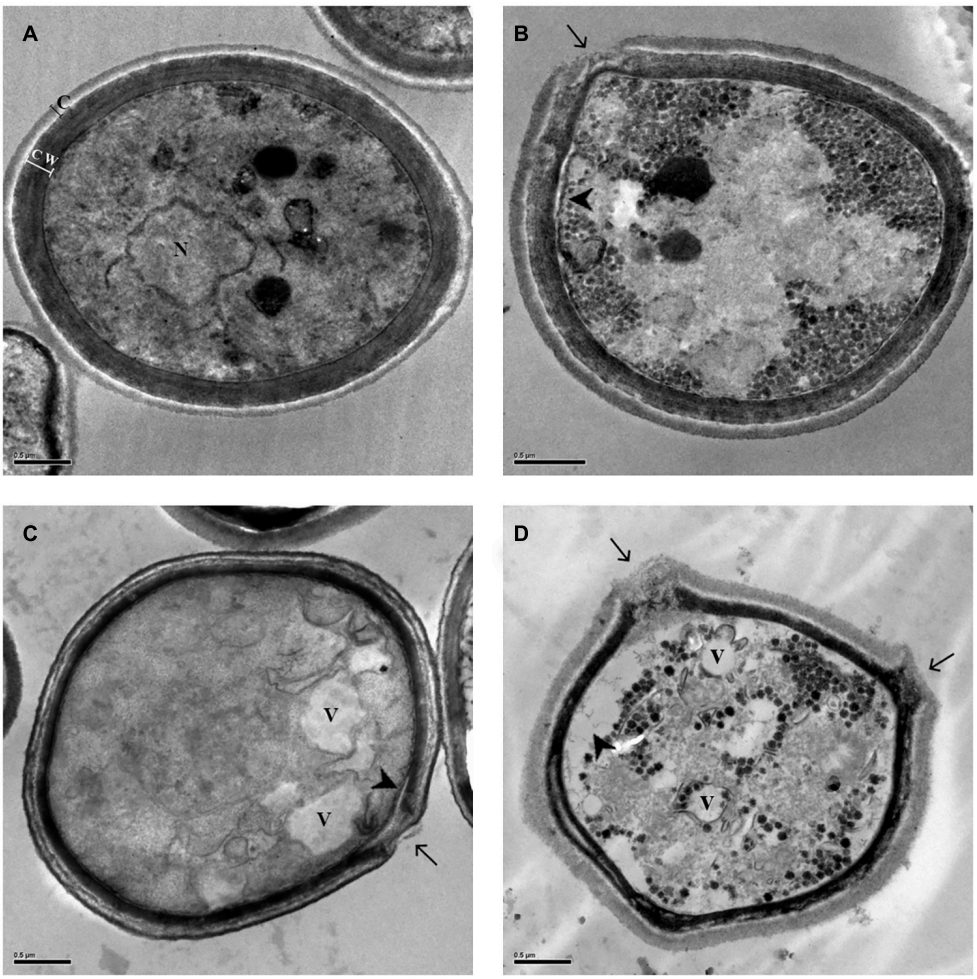

FIGURE 2 | Morphological and ultrastructural changes analyzed by transmission electron microscopy (TEM) in *Cryptococcus neoformans* ATCC 66031 after 48 h of treatment with ethyl acetate fraction (EAF) and amphotericin B (AmB) alone or combined. **(A)** Untreated control cells grown in RPMI-MOPS for 48 h at 37°C; **(B)** 1,000.0 μg/ml EAF; **(C)** 0.125 μg/ml AmB; **(D)** 3.9/0.003 μg/ml EAF/AmB. Capsule (c), cell wall (cw), nucleus (n), vacuole (v), loss of cell wall integrity (arrow), and cell membrane detachment (arrow head).

and combined with AmB, the ultrastructure of ATCC 66031 was examined by TEM. Untreated yeasts exhibited typical oval morphology with regular and compact cell wall (cw), surrounded by capsule (c), and normal electron density cytoplasm with evident nucleus (n) (**Figure 2A**). Treated cells showed significant morphological and ultrastructural alterations. The most observed changes in the treatment with EAF alone or combined with AmB were alterations in cryptococcal morphology, including irregularity of the cell wall with loss of integrity, suggesting leakage of intracellular content (arrow, **Figures 2B–D**) and cell membrane detachment (arrowhead, **Figures 2B–D**). Decreased electron density and presence of vacuoles were also observed in the treatment with the plant extract alone or combined with AmB (V, in **Figures 2C,D**).

To observe the effect of the EAF alone or combined with AmB on capsule, the thickness of this structure was measured using light microscopy in yeast cells negatively stained with Chinese ink. Untreated cells were typically round and were surrounded by a clear capsule (**Supplementary Figure 1**). Treatments with EAF and AmB, alone or in combination, lead to a significant ($p < 0.05$) reduction in capsule (**Figure 3A**) and cell size (**Figure 3B**) after 48 h of incubation when compared to the untreated control cells of both cryptococcal strains.

Ethyl Acetate Fraction Alone or Combined With Amphotericin B Exhibits Antibiofilm Activity in *Cryptococcus neoformans*

In addition to the antifungal effect on planktonic cells, EAF combined with AmB exhibited an inhibitory activity on 48-h biofilms of *C. neoformans*. The $SMIC_{80}$ of EAF alone was >1,000.0 μg/ml, as at this concentration, a percentage reduction of 69.8 and 9.1% in sessile cell viability was observed for ATCC 66031 and CN12 strains, respectively (**Figure 4** and **Supplementary Table 1**). Regarding AmB, the $SMIC_{80}$ values

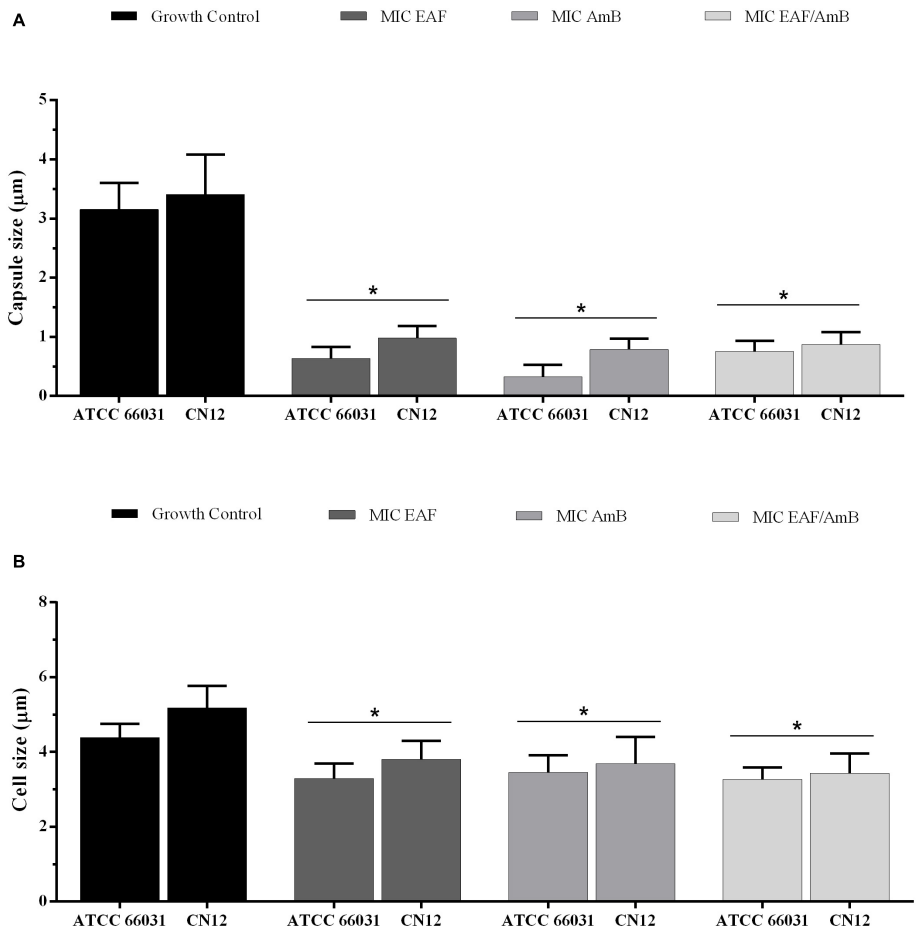

FIGURE 3 | Effect of ethyl acetate fraction (EAF) of *Poincianella pluviosa* bark and amphotericin B (AmB) alone or in combination on capsule **(A)** and cell **(B)** size. *Cryptococcus neoformans* ATCC 66031 and *C. neoformans* CN12 were treated with EAF minimal inhibitory concentration (MIC) (1,000.0 and 125 μg/ml, respectively), AmB MIC (0.125 μg/ml), and EAF combined with AmB (3.9/0.003 μg/ml), and the results were compared to untreated control. A total of 100 cells were measured, and the mean ± standard deviation was calculated and analyzed by one-way ANOVA. Asterisks indicate a significant reduction ($p < 0.05$) in the metabolic activity of treated sessile cells compared to untreated cells.

of 2.0 and 4.0 μg/ml were identified for ATCC 66031 and CN12 strains, respectively (**Table 2**). The simultaneous addition of EAF and AmB on 48-h biofilm provoked a significant reduction in MIC values of these compounds for both strains. For ATCC 66031, 32-fold and four-fold reductions in MIC values of EAF and AmB were, respectively, observed; for CN12, 64-fold and 16-fold reductions, respectively. Synergistic antifungal effect was observed on 48-h biofilm of *C. neoformans* strains, with calculated FICI values of 0.28 (ATCC 66031) and 0.08 (CN12) (**Table 2**).

Scanning electron microscopy (SEM) images showed the untreated and treated biofilms of ATCC 66031 formed on glass (**Figures 5A1–A4**) and polystyrene (**Figures 5B1–B4**) surfaces. On both surfaces, untreated biofilms (**Figures 5A1,B1**) consisted of cells firmly adhered to the surfaces, exhibiting typical spherical morphology after 48-h incubation. In contrast, a remarkable decrease in the number of cells within the biofilms treated with EAF (**Figures 5A2,B2**), AmB (**Figures 5A3,B3**), and their combination (**Figures 5A4,B4**) was visualized, which was consistent with the reduction of biofilm viability. Moreover, it was possible to observe severe damage with deformed cells and cell debris, indicating cell death (**Figures 5A2–A4,B2–B4**).

Ethyl Acetate Fraction Combined With Amphotericin B Does Not Induce Hemolysis on Human Erythrocytes

The effect of EAF alone and combined with AmB was evaluated in human erythrocytes. EAF in concentrations ranging from 1.95 to 500.0 μg/ml showed a percentage of hemolysis from 0.1 to 3% and were considered non-hemolytic (**Figure 6A**). However, at the highest concentration tested (1,000.0 μg/ml), a percentage of hemolysis of 21.2% was detected, indicating that the plant extract may induce erythrocyte lysis in higher concentrations. The combination of different concentrations of EAF and AmB caused around 3.0% hemolysis and were considered non-hemolytic. As it was not possible to calculate the CC_{90} of EAF on human erythrocytes, the highest concentration was used to calculate

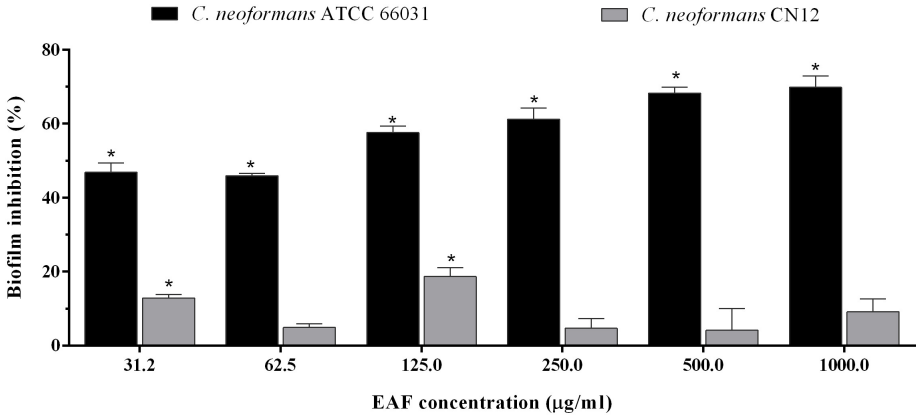

FIGURE 4 | Effect of ethyl acetate fraction (EAF) of *Poincianella pluviosa* on 48-h biofilm of *Cryptococcus neoformans*. Metabolic activity of sessile cells was assessed by the dimethylthiazol diphenyltetrazolium bromide (MTT) reduction method after 48-h incubation at 37°C with different concentrations of EAF. Values are mean ± standard deviation of two experiments in quintuplicate and were analyzed by one-way ANOVA. Asterisks indicate a significant reduction ($p < 0.05$) in the metabolic activity of treated sessile cells compared to untreated cells.

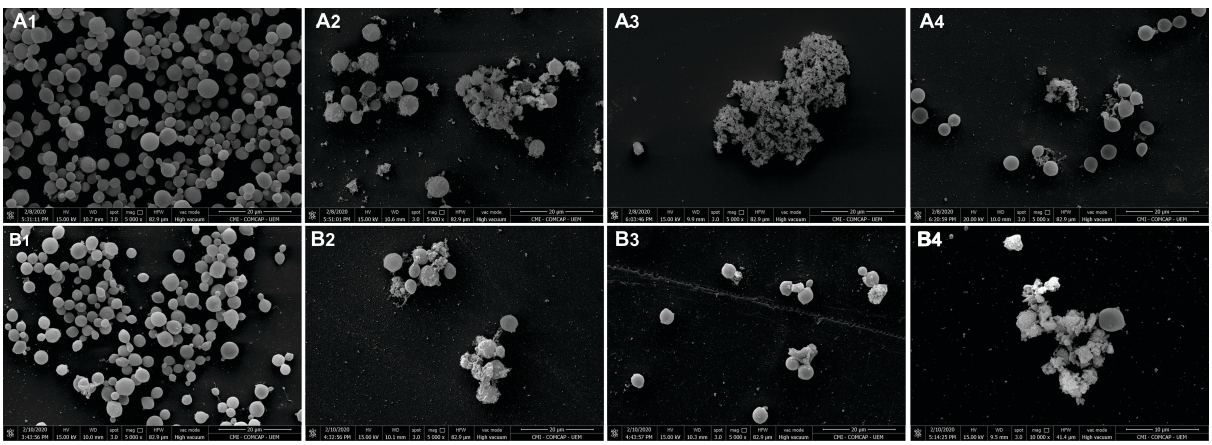

FIGURE 5 | Scanning electron microscopy (SEM) images of *Cryptococcus neoformans* ATCC 66031 biofilms on glass **(A1–A4)** and polystyrene **(B1–B4)** surfaces over 48 h of incubation at 37°C. **(1)** Untreated control; **(2)** 1,000.0 μg/ml ethyl acetate fraction (EAF); **(3)** 2.0 μg/ml amphotericin B (AmB); **(4)** 31.25/0.5 μg/ml EAF/AmB.

the IS. Thus, IS values greater than 8 were estimated for CN12 strain, while for ATCC 66031 and the other strains, the value was greater than 1, indicating that EAF may be more toxic toward the fungal species.

Ethyl Acetate Fraction Alone or Combined With Amphotericin B Does Not Exhibit Toxicity to *Galleria mellonella* Larvae and Reduces the Mortality of the Larvae Infected With *Cryptococcus neoformans*

Based on the MIC values and the results from mammalian cell tests, all treatments of the *G. mellonella* larvae were carried out using different concentrations of the compounds per kilogram of larvae, i.e., 0.25 × MIC, 0.5 × MIC, and MIC values of EAF; MIC and 2 × MIC of AmB; MIC values of EAF and AmB (at the synergistic combination), 2 × MIC and 4 × MIC.

First, the *G. mellonella* larvae were inoculated with EAF and AmB, alone and in combination, to determine the toxicity of the plant extract/antifungal for the larvae. Similar to the control group treated with PBS, a survival rate of 100% was observed with most EAF/AmB treatments after 10 days. Survival rates of 70, 80, and 90% were observed for 1,000.0 μg/ml/kg EAF, 125.0 μg/ml/kg EAF, and 250.0 μg/ml/kg EAF and 0.25 μg/ml/kg AmB, respectively (**Figure 6B**). Considering these results, the efficacy of these compounds was evaluated in *G. mellonella* infected with ATCC 66031 and CN12 strains.

After 168-h post-infection with ATCC 66031, the mortality rate of infected and untreated larvae was 40%, which progressively increased over 240 h, resulting in 90% of mortality (**Figure 7A**). Treatment with AmB resulted in 50% survival rate

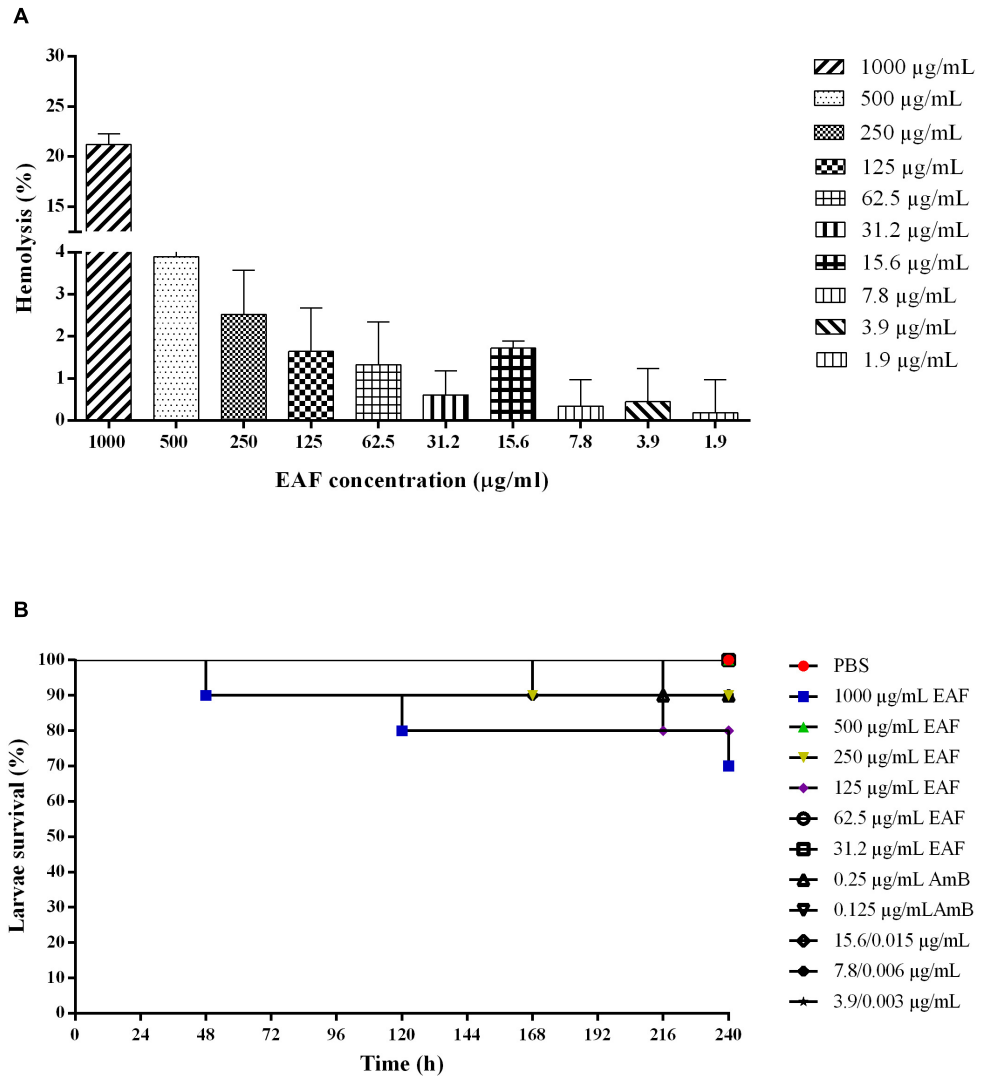

FIGURE 6 | Effect of ethyl acetate fraction (EAF) of *Poincianella pluviosa* bark and amphotericin B (AmB) alone or in combination against human erythrocytes **(A)** and *Galleria mellonella* larvae **(B)**. **(A)** Erythrocytes were treated with different concentrations (1,000.0–1.9 µg/ml) of EAF during 3 h at 37°C. The percentage hemolysis was calculated using untreated cells as control. Values are mean ± standard deviation of two experiments in duplicate. **(B)** Kaplan–Meier plots of survival curves of *G. mellonella* larvae treated with different concentrations of EAF (1,000.0–31.2 µg/kg of larvae), AmB (0.25 or 0.125 µg/kg of larvae), and EAF combined with AmB (15.6/0.015, 7.8/0.006, or 3.9/0.003 µg/kg of larvae) at the synergistic concentrations. Analysis of *G. mellonella* survival data was performed using the log-rank (Mantel–Cox) of representative experiment. PBS, phosphate-buffered saline.

of the larvae in both concentrations at the end of the experiment. Interestingly, the treatment of larvae with EAF significantly increased their survival rate in the three concentrations tested compared to the untreated group. After 240 h, 70% ($p < 0.01$), 80% ($p < 0.001$), and 70% ($p < 0.05$) of live larvae were observed for the treatment with MIC, 0.5 × MIC, and 0.25 × MIC of EAF, respectively. The EAF (15.6 µg/ml/kg) combined with AmB (0.015 µg/ml/kg) (4 × MIC) significantly ($p < 0.001$) prolonged larva survival compared to the untreated group (80%, EAF-treated vs. 10%, untreated). Furthermore, this survival rate was greater than those of the AmB (for both doses) and MIC EAF treatments. The combination 7.8 µg/ml/kg EAF with 0.006 µg/ml/kg AmB (2 × MIC) also significantly ($p < 0.05$) prolonged larva survival, with 60% of live larvae, being a better treatment than AmB as well. The other EAF/AmB combination (3.9/0.003 µg/ml) resulted in 40% survival rate (**Figure 7A**).

All larvae infected with CN12 and untreated died after 240 h of infection (100% mortality rate; **Figure 7B**). Treatment with AmB resulted in a survival rate of 50% ($p < 0.01$) for 2 × MIC and of 70% ($p < 0.001$) for MIC. EAF treatment was effective in all concentrations tested compared to the untreated group. At the end of the experiment, MIC, 0.5 × MIC, and 0.25 × MIC led to a survival rate of 50% ($p < 0.05$), 70% ($p < 0.001$), and 80% ($p < 0.0001$), respectively. Unlike the infection with ATCC 66031, treatment with all EAF and AmB combinations induced

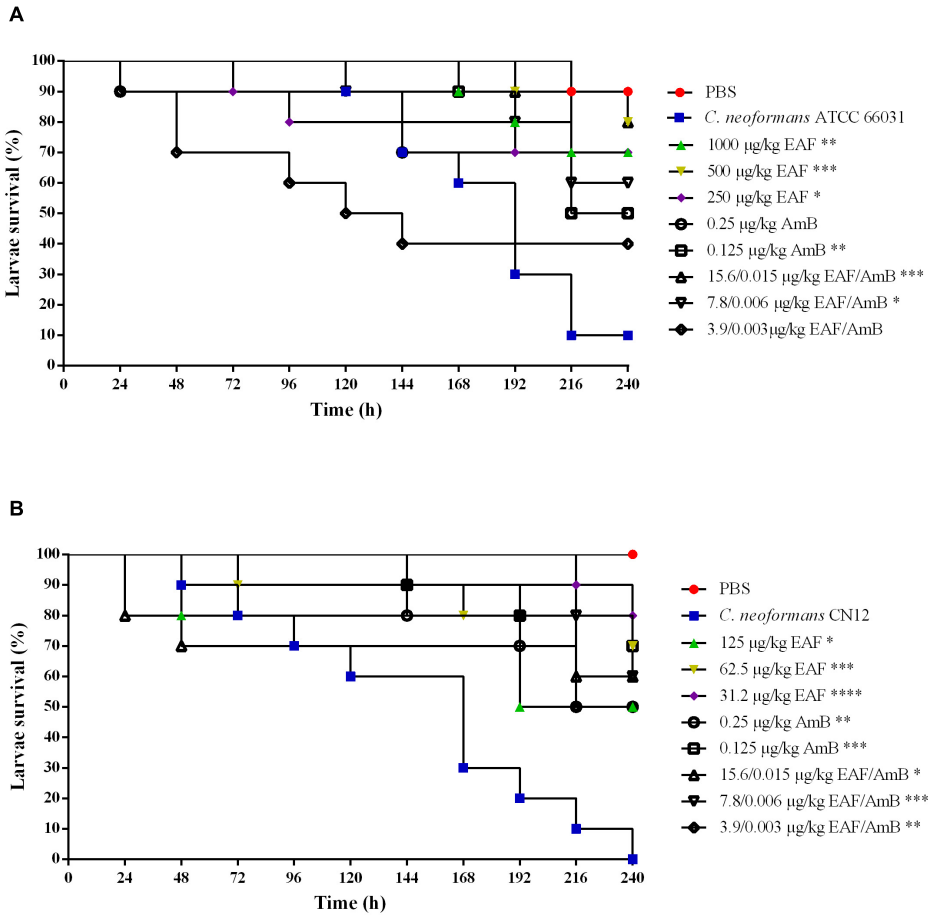

FIGURE 7 | Effect of ethyl acetate fraction (EAF) of *Poincianella pluviosa* bark and amphotericin B (AmB) alone or in combination against *Galleria mellonella* larvae infected with *Cryptococcus neoformans* ATCC 66031 **(A)** and *Cryptococcus neoformans* CN12 **(B)**. All groups were compared with infected and untreated larvae. Analysis of *G. mellonella* survival data was performed using the log-rank (Mantel–Cox) of representative experiment. The asterisks indicate a significant reduction in mortality rate of infected and treated group compared with the infected and untreated group (*$p < 0.05$; **$p < 0.01$; ***$p < 0.001$; ****$p < 0.0001$). **(A)** Kaplan–Meier plots of survival curves of *G. mellonella* larvae infected with *Cryptococcus neoformans* ATCC 66031. The larvae were infected with fungal cells and concomitantly treated with minimal inhibitory concentration (MIC), 0.5 × MIC, or 0.25 × MIC of EAF (1,000.0, 500.0, or 250.0 µg/ml/kg of larvae, respectively), 2 × MIC and MIC AmB (0.25 or 0.125 µg/ml/kg of larvae, respectively), and EAF combined with AmB (15.6/0.015, 7.8/0.006, or 3.9/0.003 µg/ml/kg of larvae) at the synergistic concentrations. **(B)** Kaplan–Meier plots of survival curves of *G. mellonella* larvae infected with *C. neoformans* CN12. The larvae were infected with fungal cells and concomitantly treated with MIC, 0.5 × MIC, or 0.25 × MIC of EAF (125.0, 62.5, or 31.2 µg/kg of larvae, respectively), AmB (0.25 or 0.125 µg/kg of larvae, respectively), and EAF combined with AmB (15.6/0.015, 7.8/0.006, or 3.9/0.003 µg/kg of larvae) at the synergistic concentrations.

an increase in CN12-infected larvae survival rates compared to untreated larvae. After the treatment with the combination of 4 × MIC ($p < 0.05$) and 2 × MIC ($p < 0.001$), 60% of live larvae were identified, which was a better treatment than 2 × MIC of AmB. At the MIC combination, 50% survival rate ($p < 0.01$) was observed.

DISCUSSION

The combination therapy has been used to improve the efficacy of drugs and to reduce their adverse effects (Chen et al., 2014), and this strategy has been widely applied for the treatment of different diseases, including those caused by microbial pathogens (Brennan-Krohn and Kirby, 2019). Indeed, the combination of AmB and 5-flucytosine is the recommended antifungal therapy for the treatment of cryptococcal meningitis (Perfect et al., 2010; Bermas and Geddes-McAlister, 2020).

The antifungal potential of *Poincianella* (*Caesalpinia*) species has been previously described. Different parts of *Caesalpinia sappan* (Niranjan Reddy et al., 2003), *Caesalpinia pyramidalis* (Cruz et al., 2007), *Caesalpinia bonducella* (Shukla et al., 2011), *Caesalpinia ferrea* Martius (Macêdo et al., 2020), and *Caesalpinia pulcherrima* (de Melo et al., 2020) showed antifungal effect *in vitro* against planktonic cells of several fungal species, which can cause infections in humans such as *Trichophyton rubrum*, *Candida guilliermondii*, *Candida albicans*, *Candida parapsilosis*, and *Fonsecaea pedrosoi*. Among these plant species, the inhibitory activity of only two species was evaluated on growth of planktonic cells of *C. neoformans*. The aqueous extract (water infusion) of

leaves from *C. pyramidalis* inhibited the growth of *C. neoformans* T_1-444, a clinical isolate, displaying a MIC of 12.5 μg/ml (Cruz et al., 2007). Lignin extracted from the leaves of *C. pulcherrima* inhibited the growth of three *C. neoformans* strains (HC43, HC44, and HC47) with MIC of 15.6 μg/ml (de Melo et al., 2020).

In the present study, the EAF obtained from *P. pluviosa* stem bark exhibited low intrinsic antifungal activity on planktonic cells of *C. neoformans*, presenting a fungistatic effect. However, EAF acted synergistically in combination with AmB, inhibiting the growth of planktonic and viability of sessile (biofilm) cells of this fungal species. Importantly, the fungicidal effect was maintained at lower concentrations of AmB (32-fold and at least four-fold lower for planktonic and sessile cells, respectively) and similar to those death kinetic produced by AmB alone. The combined antifungal effect on 48-h biofilm is an important finding of the present study, since the biofilm formation ability of *Cryptococcus* species is associated with both fungal virulence and reduced susceptibility to antifungals (Martinez and Casadevall, 2015; Benaducci et al., 2016; Tavares et al., 2019), as in other species of several genera of fungi including *Candida*, *Rhodotorula*, *Aspergillus*, *Fusarium*, *Trichosporon*, *Malassezia*, *Histoplasma*, *and Paracocidioides* (Bizerra et al., 2008; Sardi et al., 2014). In fact, the successful eradication of biofilms often requires concentrations of antimicrobial agents that are usually toxic to the host (Sardi et al., 2014; Martinez and Casadevall, 2015). Accordingly, biofilm-related human infections are difficult to treat and have been associated with high mortality rates (Tumbarello et al., 2012). Therefore, the combination of EAF and AmB may be useful for the treatment of biofilm-related cryptococcal infection.

Previous studies reported the antimalarial (Kayano et al., 2011) and anti-staphylococcal (Guidi et al., 2020) activities of the extracts from *P. pluviosa* stem bark. In addition, the combination of *P. pluviosa* extract with artesunate, an artemisinin derivative, reduced the parasitemia of *Plasmodium chabaudi*-infected mice (Kayano et al., 2011); however, there are no reports described for *C. neoformans*.

The mode of action of EAF combined with AmB is unclear. The polyphenol content of EAF from *P. pluviosa* was determined to be 27.98% ± 0.52% (w/w) (Bueno et al., 2012). Flavonoids such as quercetin (Kayano et al., 2011), caesalpinioflavone (Zanin et al., 2015), and hydrolyzable tannins (Bueno et al., 2014) such as pyrogallol, ellagic acid, and gallic acid (Sereia et al., 2019) were identified in the plant extracts, including CE and EAF. Polyphenols are widely distributed in plants, where they participate in various functions related to growth and protection against pathogens, predators, and UV radiation. Several studies indicate that the mechanism by which the plant polyphenols exert their biological activities are due to the ability to bind directly to target proteins, which can affect different processes related to cell function (Quideau et al., 2011). Although data in the literature indicate a possible mechanism of action for EAF, a limitation of our study is that we have not investigated which phytochemical is active against *C. neoformans*. Future studies will be necessary to unveil the active constituent of EAF and its mechanism of action against this fungal species. However, we cannot rule out that the antifungal activity observed in this study can be attributed to the various phytochemicals of *P. pluviosa* EAF acting synergistically with AmB.

Aside from the direct antimicrobial effect, different polyphenolic compounds have been studied for their potential as an adjuvant to clinically used drugs (Zacchino et al., 2017). For instance, epigallocatechin gallate with fluconazole/ketoconazole exhibited synergistic antifungal effect against planktonic and sessile cells of *Candida* spp. *in vitro* (Behbehani et al., 2019). The combination of this polyphenol with AmB significantly decreased the growth of *Candida albicans in vitro* (Hirasawa and Takada, 2004) and increased the survival of mice with disseminated candidiasis caused by this species (Han, 2007). The efficacy of combined therapy *in vivo* was also observed in mice infected with *C. gattii*; although the synergistic effect has not been observed *in vitro*, treatment of infected mice with curcumin and fluconazole reduced and eliminated the fungal burden in lung and brain tissues, respectively, increasing the animals survival (da Silva et al., 2016).

The analysis of the *C. neoformans* ultrastructure by transmission electron microscopy (TEM) revealed that EAF alone or combined with AmB induced important changes in yeast morphology, such as plasma membrane detachment, loss of cell wall integrity causing its rupture, and vacuole formation. Ishida et al. (2009) found similar changes through the exposure of *Cryptococcus* to tannins present in an extract of *Stryphnodendron adstringens*. Treatment with the allylamine terbinafine alone or in combination with fluconazole or AmB also generated similar alterations in the cellular ultrastructure. These changes may be related to altered ergosterols in the plasma membrane, impairing the integrity and function of the cell wall (Guerra et al., 2012).

In the present study, larvae of *G. mellonella* were used to evaluate the efficacy of combined therapy of EAF and AmB *in vivo* through the survival assay. This non-mammalian model can be maintained easily and inexpensively in laboratory conditions, at different temperatures, including the human temperature 37°C. Similarly to mammalian models, this insect develops a specific immune response against different microbial infections (Pereira et al., 2018). Therefore, this insect has been used to study the fungal virulence and pathogenesis (Benaducci et al., 2016; Firacative et al., 2020; Grizante Barião et al., 2020) and to evaluate the efficacy of the antifungal agents against different fungal species (Singulani et al., 2019; de Castro Spadari et al., 2020). The results reported in the present study showed that early treatment with EAF from *P. pluviosa* combined with AmB was effective in controlling *C. neoformans* infection with no toxicity to larvae, supporting the *in vitro* results. The combined therapy (2 × MIC and 4 × MIC) was slightly more effective than monotherapy with both AmB concentrations in larvae infected with ATCC 66031.

Interestingly, EAF monotherapy was the most effective treatment for larvae infected with both strains (survival rates of 80% and 70% with 0.5 × MIC, and 0.25 × MIC and MIC doses for ATCC 66031, respectively; survival rates of 70% and 80% with 0.5 × MIC and 0.25 × MIC doses for CN12, respectively), although a weak inhibitory activity was observed *in vitro*. A significant reduction in capsule size was also observed with the treatment of EAF alone or combined with AmB. Previous

studies have shown that AmB treatment reduced the capsule size of *C. neoformans in vitro* (Nosanchuk et al., 1999) and in murine infection (Zaragoza et al., 2005). The polysaccharide capsule is essential for the virulence of *C. neoformans*, contributing to the evasion of immune defenses and survival within the host (Zaragoza et al., 2009). Moreover, it has been shown that the capsule is important for the adhesion of the fungus on abiotic and biotic surfaces, triggering the formation of biofilm (Martinez and Casadevall, 2015; Camacho and Casadevall, 2018). Therefore, the reduction in the size of the *C. neoformans* capsule observed in the present study indicates that the treatment with EAF, alone or combined with AmB, may interfere with the virulence of both planktonic and biofilm cells. Moreover, as described above, hydrolyzable tannins (Bueno et al., 2014) such as pyrogallol, ellagic acid, and gallic acid (Sereia et al., 2019) were identified in the EAF from *P. pluviosa* stem bark. The antifungal activity of all these compounds has already been described for different species of fungi (de Paula E Silva et al., 2014; Yang et al., 2020); besides, the immunomodulatory activity of polyphenols was also well-known (Ding et al., 2018). Particularly, gallic acid inhibits the growth of *C. neoformans* (de Paula E Silva et al., 2014) and can modulate the host innate immune response, increasing defense against microbial infections (Yang et al., 2020). Therefore, the combined antivirulence and immunomodulatory activities of the polyphenols may be responsible for the therapeutic effect of EAF from *P. pluviosa* stem bark observed in *G. mellonella* infection in the present study. Further studies using mammalian models of *C. neoformans* infection should be carried out to support these findings.

In summary, the results of the present study report for the first time the antifungal activity of EAF of *P. pluviosa* stem bark against *C. neoformans*; its combination with AmB exhibited a potent and synergistic antifungal and antivirulence interaction toward *C. neoformans*, reducing significantly the inhibitory concentrations of both compounds for planktonic and sessile cells and preserving the fungicidal activity of AmB. Moreover, EAF alone or combined with AmB prolonged the survival rate of *C. neoformans*-infected *G. mellonella*. Despite the limitations of the present study, the results expand the knowledge about this legume bark's antimicrobial properties, highlighting the potential of this plant extract for the development of new strategies for the treatment of cryptococcosis.

DATA AVAILABILITY STATEMENT

The original contributions presented in the study are included in the article/**Supplementary Material**, further inquiries can be directed to the corresponding author.

AUTHOR CONTRIBUTIONS

GA and SY-O performed the conception, experimental design, analysis and interpretation of data, and writing of the manuscript. All authors have read and approved the final manuscript, and have made a substantial methodological and intellectual contribution to the study.

FUNDING

The present study was supported by grants from the Coordenação de Aperfeiçoamento de Pessoal de Nível Superior (CAPES, Financial Code 01). GA, LS, WC, and BF were funded by a graduate scholarship from CAPES. AM was funded by a graduate scholarship from Conselho Nacional de Desenvolvimento Científico e Tecnológico (CNPq). PP and ET were funded by a postgraduate scholarship from CAPES. CN, JM, LY, and SY-O were funded by a research fellowship from CNPq.

ACKNOWLEDGMENTS

We thank the Complexo de Centrais de Apoio à Pesquisa (COMCAP-UEM) for the support provided for the transmission and scanning electron microscopy techniques and the Instituto Nacional de Controle de Qualidade em Saúde (INCQS), Fundação Oswaldo Cruz-Rio de Janeiro, Brazil, for kindly donating the reference strains of *C. neoformans*. We also thank K. W. Hoepers for proofreading the manuscript.

SUPPLEMENTARY MATERIAL

The Supplementary Material for this article can be found online at: https://www.frontiersin.org/articles/10.3389/fmicb.2021.660645/full#supplementary-material

REFERENCES

Bandaranayake, T. D., Ogbuagu, O. E., Mahajan, A., Vortmeyer, A. O., and Villanueva, M. S. (2018). Fatal cryptococcal meningitis in an AIDS patient complicated with immune reconstitution syndrome refractory to prolonged amphotericin B treatment. *Int. J. STD AIDS* 29, 1250–1254. doi: 10.1177/0956462418773219

Behbehani, J. M., Irshad, M., Shreaz, S., and Karched, M. (2019). Synergistic effects of tea polyphenol epigallocatechin 3-O-gallate and azole drugs against oral *Candida* isolates. *J. Mycol. Med.* 29, 158–167. doi: 10.1016/j.mycmed.2019.01.011

Benaducci, T., Sardi, J. C., Lourencetti, N. M., Scorzoni, L., Gullo, F. P., et al. (2016). Virulence of *Cryptococcus* sp. biofilms *in vitro* and *in vivo* using *Galleria mellonella* as an alternative model. *Front. Microbiol.* 7:290. doi: 10.3389/fmicb.2016.00290

Bermas, A., and Geddes-McAlister, J. (2020). Combatting the evolution of antifungal resistance in *Cryptococcus neoformans*. *Mol. Microbiol.* 114, 721–734. doi: 10.1111/mmi.14565

Biasi-Garbin, R. P., Demitto F de, O., Amaral, R. C., Ferreira, M. R., Soares, L. A., Svidzinski, T. I., et al. (2016). Antifungal potential of plant species from brazilian caatinga against dermatophytes. *Rev. Inst. Med. Trop. Sao Paulo* 58:18. doi: 10.1590/S1678-9946201658018

Bizerra, F. C., Nakamura, C. V., de Poersch, C., Svidzinski, T. I. E., Borsato Quesada, R. M., Goldenberg, S., et al. (2008). Characteristics of biofilm formation by *Candida tropicalis* and antifungal resistance. *FEMS Yeast Res.* 8, 442–450. doi: 10.1111/j.1567-1364.2007.00347.x

Brennan-Krohn, T., and Kirby, J. E. (2019). Synergistic combinations and repurposed antibiotics active against the pandrug-resistant *Klebsiella pneumoniae* Nevada strain. *Antimicrob. Agents Chemother.* 63:e01374-19. doi: 10.1128/AAC.01374-19

Bueno, F. G., Machareth, M. A. D., Panizzon, G. P., Lopes, G. C., Mello, J. C. P., and Leite-Mello, E. V. S. (2012). Development of a UV/Vis spectrophotometric method for analysis of total polyphenols from *Caesalpinia peltophoroides* Benth. *Quim. Nova* 35, 822–826. doi: 10.1590/s0100-40422012000400031

Bueno, F. G., Moreira, E. A., De Morais, G. R., Pacheco, I. A., Baesso, M. L., De Souza Leite-Mello, E. V., et al. (2016). Enhanced cutaneous wound healing in vivo by standardized crude extract of *Poincianella pluviosa*. *PLoS One* 11:e0149223. doi: 10.1371/journal.pone.0149223

Bueno, F. G., Panizzon, G. P., Mello, E. V. S. D. L., Lechtenberg, M., Petereit, F., Mello, J. C. P., et al. (2014). Hydrolyzable tannins from hydroalcoholic extract from *Poincianella pluviosa* stem bark and its wound-healing properties: phytochemical investigations and influence on *in vitro* cell physiology of human keratinocytes and dermal fibroblasts. *Fitoterapia* 99, 252–260. doi: 10.1016/j.fitote.2014.10.007

Camacho, E., and Casadevall, A. (2018). Cryptococcal traits mediating adherence to biotic and abiotic surfaces. *J. Fungi (Basel)* 4:88. doi: 10.3390/jof4030088

Carvalho, P. E. R. (2014). *Espécies Arbóreas Brasileiras*. Colombo: EMBRAPA Florestas.

Chen, X., Ren, B., Chen, M., Liu, M. X., Ren, W., Wang, Q. X., et al. (2014). ASDCD: antifungal synergistic drug combination database. *PLoS One* 9:e86499. doi: 10.1371/journal.pone.0086499

Cheong, J. W., and McCormack, J. (2013). Fluconazole resistance in cryptococcal disease: emerging or intrinsic? *Med. Mycol.* 51, 261–269. doi: 10.3109/13693786.2012.715763

Clinical and Laboratory Standards Institute (CLSI) (2008). *Reference Method for Broth Dilution Antifungal Susceptibility Testing of Yeasts; Third Informational Supplement - M27-A3*. Wayne, PA: Clin. Lab. Standars Inst. - CLSI.

Cruz, M. C. S., Santos, P. O., Barbosa, A. M., de Mélo, D. L. F. M., Alviano, C. S., Antoniolli, A. R., et al. (2007). Antifungal activity of Brazilian medicinal plants involved in popular treatment of mycoses. *J. Ethnopharmacol.* 111, 409–412. doi: 10.1016/j.jep.2006.12.005

da Silva, D. L., Magalhães, T. F. F., dos Santos, J. R. A., de Paula, T. P., Modolo, L. V., de Fátima, A., et al. (2016). Curcumin enhances the activity of fluconazole against *Cryptococcus gattii*-induced cryptococcosis infection in mice. *J. Appl. Microbiol.* 120, 41–48. doi: 10.1111/jam.12966

de Castro Spadari, C., da Silva de Bastiani, F. W. M., Pisani, P. B. B., de Azevedo Melo, A. S., and Ishida, K. (2020). Efficacy of voriconazole in vitro and in invertebrate model of cryptococcosis. *Arch. Microbiol.* 202, 773–784. doi: 10.1007/s00203-019-01789-8

de Melo, C. M. L., da Cruz Filho, I. J., de Sousa, G. F., de Souza Silva, G. A., do Nascimento Santos, D. K. D., da Silva, R. S., et al. (2020). Lignin isolated from *Caesalpinia pulcherrima* leaves has antioxidant, antifungal and immunostimulatory activities. *Int. J. Biol. Macromol.* 1, 1725–1733. doi: 10.1016/j.ijbiomac.2020.08.003

de Paula E Silva, A. C., Costa-Orlandi, C. B., Gullo, F. P., Sangalli-Leite, F., de Oliveira, H. C., da Silva, J. F., et al. (2014). Antifungal activity of decyl gallate against several species of pathogenic fungi. *Evid. Based Complement. Altern. Med.* 2014:506273. doi: 10.1155/2014/506273

Deharo, E., Bourdy, G., Quenevo, C., Muñoz, V., Ruiz, G., and Sauvain, M. (2001). A search for natural bioactive compounds in Bolivia through a multidisciplinary approach. Part V. Evaluation of the antimalarial activity of plants used by the Tacana Indians. *J. Ethnopharmacol.* 77, 91–98. doi: 10.1016/S0378-8741(01)00270-7

Ding, S., Jiang, H., and Fang, J. (2018). Regulation of immune function by polyphenols. *J. Immunol. Res.* 2018:1264074. doi: 10.1155/2018/1264074

Domingos, O. D. S., Alcântara, B. G. V., Santos, M. F. C., Maiolini, T. C. S., Dias, D. F., Baldim, J. L., et al. (2019). Anti-inflammatory derivatives with dual mechanism of action from the metabolomic screening of *Poincianella pluviosa*. *Molecules* 24:4375. doi: 10.3390/molecules24234375

Firacative, C., Khan, A., Duan, S., Ferreira-Paim, K., Leemon, D., and Meyer, W. (2020). Rearing and maintenance of *Galleria mellonella* and its application to study fungal virulence. *J. Fungi* 6:130. doi: 10.3390/jof6030130

Frases, S., Pontes, B., Nimrichter, L., Viana, N. B., Rodrigues, M. L., and Casadevall, A. (2009). Capsule of *Cryptococcus neoformans* grows by enlargement of polysaccharide molecules. *Proc. Natl. Acad. Sci. U.S.A.* 106, 1228–1233. doi: 10.1073/pnas.0808995106

Fuchs, B. B., O'Brien, E., Khoury, J. B., and Mylonakis, E. (2010). Methods for using *Galleria mellonella* as a model host to study fungal pathogenesis. *Virulence* 1, 475–482. doi: 10.4161/viru.1.6.12985

Govindarajan, A., Bistas, K. G., and Aboeed, A. (2020). *Fluconazole*. StatPearls Publishing. Available online at: https://www.ncbi.nlm.nih.gov/books/NBK537158/ (accessed December 12, 2019).

Grizante Barião, P. H., Tonani, L., Cocio, T. A., Martinez, R., Nascimento, E., and von Zeska Kress, M. R. (2020). Molecular typing, in vitro susceptibility and virulence of *Cryptococcus neoformans/Cryptococcus gattii* species complex clinical isolates from south-eastern Brazil. *Mycoses* 63, 1341–1351. doi: 10.1111/myc.13174

Guerra, C. R., Ishida, K., Nucci, M., and Rozental, S. (2012). Terbinafine inhibits *Cryptococcus neoformans* growth and modulates fungal morphology. *Mem. Inst. Oswaldo Cruz* 107, 582–590. doi: 10.1590/S0074-02762012000500003

Guidi, A. C., de Paula, M. N., Mosela, M., Delanora, L. A., Soares, G. C. A., de Morais, G. R., et al. (2020). Stem bark extract of *Poincianella pluviosa* incorporated in polymer film: evaluation of wound healing and anti-staphylococcal activities. *Injury* 51, 840–849. doi: 10.1016/j.injury.2020.02.027

Han, Y. (2007). Synergic effect of grape seed extract with amphotericin B against disseminated candidiasis due to *Candida albicans*. *Phytomedicine* 14, 733–738. doi: 10.1016/j.phymed.2007.08.004

Hirasawa, M., and Takada, K. (2004). Multiple effects of green tea catechin on the antifungal activity of antimycotics against *Candida albicans*. *J. Antimicrob. Chemother.* 53, 225–229. doi: 10.1093/jac/dkh046

Holetz, F. B., Pessini, G. L., Sanches, N. R., Cortez, D. A. G., Nakamura, C. V., and Filho, B. P. (2002). Screening of some plants used in the Brazilian folk medicine for the treatment of infectious diseases. *Mem. Inst. Oswaldo Cruz* 97, 1027–1031. doi: 10.1590/s0074-02762002000700017

Ishida, K., Rozental, S., de Mello, J. C. P., and Nakamura, C. V. (2009). Activity of tannins from *Stryphnodendron adstringens* on *Cryptococcus neoformans*: effects on growth, capsule size and pigmentation. *Ann. Clin. Microbiol. Antimicrob.* 8:29. doi: 10.1186/1476-0711-8-29

Izumi, E., Ueda-Nakamura, T., Veiga, V. F., Pinto, A. C., and Nakamura, C. V. (2012). Terpenes from *Copaifera* demonstrated in vitro antiparasitic and synergic activity. *J. Med. Chem.* 55, 2994–3001. doi: 10.1021/jm201451h

Kayano, A. C. A. V., Lopes, S. C. P., Bueno, F. G., Cabral, E. C., Souza-Neiras, W. C., Yamauchi, L. M., et al. (2011). In vitro and in vivo assessment of the anti-malarial activity of *Caesalpinia pluviosa*. *Malar. J.* 10:112. doi: 10.1186/1475-2875-10-112

Kokoska, L., Kloucek, P., Leuner, O., and Novy, P. (2018). Plant-derived products as antibacterial and antifungal agents in human health care. *Curr. Med. Chem.* 26, 5501–5541. doi: 10.2174/0929867325666180831144344

Longhi, C., Santos, J. P., Morey, A. T., Marcato, P. D., Duran, N., Pinge-Filho, P., et al. (2016). Combination of fluconazole with silver nanoparticles produced by *Fusarium oxysporum* improves antifungal effect against planktonic cells and biofilm of drug-resistant *Candida albicans*. *Med. Mycol.* 54, 428–432. doi: 10.1093/mmy/myv036

Macêdo, N. S., de Sousa Silveira, Z., Bezerra, A. H., da Costa, J. G. M., Coutinho, H. D. M., Romano, B., et al. (2020). *Caesalpinia ferrea* C. Mart. (Fabaceae) phytochemistry, ethnobotany, and bioactivities: a review. *Molecules* 25:3831. doi: 10.3390/molecules25173831

Martinez, L. R., and Casadevall, A. (2006). Susceptibility of *Cryptococcus neoformans* biofilms to antifungal agents in vitro. *Antimicrob. Agents Chemother.* 50, 1021–1033. doi: 10.1128/AAC.50.3.1021-1033.2006

Martinez, L. R., and Casadevall, A. (2015). Biofilm formation by *Cryptococcus neoformans*. *Microbiol. Spectr.* 3, 1–11. doi: 10.1128/microbiolspec.mb-0006-2014

Maziarz, E. K., and Perfect, J. R. (2016). Cryptococcosis. *Infect. Dis. Clin. North Am.* 30, 179–206. doi: 10.1016/j.idc.2015.10.006

Miles, A. A., Misra, S. S., and Irwin, J. O. (1938). The estimation of the bactericidal power of the blood. *J. Hyg.* 38, 732–749. doi: 10.1017/s0022172400011158x

Morguette, A. E. B., Bigotto, B. G., Varella, R., de, L., Andriani, G. M., Spoladori, L. F., et al. (2019). Hydrogel containing oleoresin from *Copaifera officinalis* presents antibacterial activity against *Streptococcus agalactiae*. *Front. Microbiol.* 10:2806. doi: 10.3389/fmicb.2019.02806

Mukherjee, P. K., Sheehan, D. J., Hitchcock, C. A., and Ghannoum, M. A. (2005). Combination treatment of invasive fungal infections. *Clin. Microbiol. Rev.* 18, 163–194. doi: 10.1128/CMR.18.1.163-194.2005

Niranjan Reddy, V. L., Ravikanth, V., Jansi Lakshmi, V. V. N. S., Suryanarayan Murty, U., and Venkateswarlu, Y. (2003). Inhibitory activity of homoisoflavonoids from *Caesalpinia sappan* against *Beauveria bassiana*. *Fitoterapia* 74, 600–602. doi: 10.1016/S0367-326X(03)00153-9

Nosanchuk, J. D., Cleare, W., Franzot, S. P., and Casadevall, A. (1999). Amphotericin B and fluconazole affect cellular charge, macrophage phagocytosis, and cellular morphology of *Cryptococcus neoformans* at subinhibitory concentrations. *Antimicrob. Agents Chemother.* 43, 233–239. doi: 10.1128/AAC.43.2.233

Odds, F. C. (2003). Synergy, antagonism, and what the chequerboard puts between them. *J. Antimicrob. Chemother.* 52:1. doi: 10.1093/jac/dkg301

Padda, I. S., and Parmar, M. (2020). *Flucytosine*. StatPearls Publishing. Available online at: www.ncbi.nlm.nih.gov/books/NBK557607/ (accessed December 12, 2019).

Pereira, T. C., de Barros, P. P., Fugisaki, L. R. O., Rossoni, R. D., Ribeiro, F. C., de Menezes, R. T., et al. (2018). Recent advances in the use of *Galleria mellonella* model to study immune responses against human pathogens. *J. Fungi (Basel)* 4:128. doi: 10.3390/jof4040128

Perfect, J. R., Dismukes, W. E., Dromer, F., Goldman, D. L., Graybill, J. R., Hamill, R. J., et al. (2010). Clinical practice guidelines for the management of cryptococcal disease: 2010 update by the infectious diseases society of America. *Clin. Infect. Dis.* 50, 291–322. doi: 10.1086/649858

Quideau, S., Deffieux, D., Douat-Casassus, C., and Pouységu, L. (2011). Plant polyphenols: chemical properties, biological activities, and synthesis. *Angew. Chem. Int. Ed.* 50, 586–621. doi: 10.1002/anie.201000044

Ribeiro Neto, J. A., Pimenta Tarôco, B. R., Batista dos Santos, H., Thomé, R. G., Wolfram, E., and Ribeiro, R. I. M. A. (2020). Using the plants of Brazilian Cerrado for wound healing: from traditional use to scientific approach. *J. Ethnopharmacol.* 260:112547. doi: 10.1016/j.jep.2020.112547

Sardi, J. C., Pitangui, N. S., Rodríguez-Arellanes, G., Taylor, M. L., Fusco-Almeida, A. M., and Mendes-Giannini, M. J. (2014). Highlights in pathogenic fungal biofilms. *Rev. Iberoam. Micol.* 31, 22–29. doi: 10.1016/j.riam.2013.09.014

Savi, D. C., Aluizio, R., and Glienke, C. (2019). Brazilian plants: an unexplored source of endophytes as producers of active metabolites. *Planta Med.* 85, 619–636. doi: 10.1055/a-0847-1532

Scott, E. M., Tariq, V. N., and McCrory, R. M. (1995). Demonstration of synergy with fluconazole and either ibuprofen, sodium salicylate, or propylparaben against *Candida albicans in vitro*. *Antimicrob. Agents Chemother.* 39, 2610–2614. doi: 10.1128/AAC.39.12.2610

Sereia, A. L., de Oliveira, M. T., Baranoski, A., Medeiros Marques, L. L., Ribeiro, F. M., Isolani, R. G., et al. (2019). In vitro evaluation of the protective effects of plant extracts against amyloid-beta peptide-induced toxicity in human neuroblastoma SH-SY5Y cells. *PLoS One* 14:e0212089. doi: 10.1371/journal.pone.0212089

Shukla, S., Mehta, P., Mehta, A., Vyas, S. P., and Bajpai, V. K. (2011). Preliminary phytochemical and antifungal screening of various organic extracts of *Caesalpinia bonducella* seeds. *Rom. Biotechnol. Lett.* 16, 6384–6389.

Singhal, S., Gupta, P., Lamba, B. S., Singh, P., Chouhan, M. I., and Meher, D. (2016). Rare case of amphotericin-B resistant cryptococcal meningitis in HIV non reactive patient. *Int. J. Infect. Dis.* 45, 199–200. doi: 10.1016/j.ijid.2016.02.459

Singulani, J., de, L., Galeane, M. C., Ramos, M. D., Gomes, P. C., dos Santos, C. T., et al. (2019). Antifungal activity, toxicity, and membranolytic action of a mastoparan analog peptide. *Front. Cell. Infect. Microbiol.* 6:419. doi: 10.3389/fcimb.2019.00419

Spadari, C. C., Vila, T., Rozental, S., and Ishida, K. (2018). Miltefosine has a postantifungal effect and induces apoptosis in *Cryptococcus* yeasts. *Antimicrob. Agents Chemother.* 62:e00312-18. doi: 10.1128/AAC.00312-18

Tavares, E. R., Azevedo, C. S., Panagio, L. A., Pelisson, M., Pinge-Filho, P., Venancio, E. J., et al. (2016). Accurate and sensitive real-time PCR assays using intergenic spacer 1 region to differentiate *Cryptococcus gattii* sensu lato and *Cryptococcus neoformans* sensu lato. *Med. Mycol.* 54, 89–96. doi: 10.1093/mmy/myv078

Tavares, E. R., Gionco, B., Morguette, A. E. B., Andriani, G. M., Morey, A. T., do Carmo, A. O., et al. (2019). Phenotypic characteristics and transcriptome profile of *Cryptococcus gattii* biofilm. *Sci. Rep.* 9:6438. doi: 10.1038/s41598-019-42896-2

Tumbarello, M., Fiori, B., Trecarichi, E. M., Posteraro, P., Losito, A. R., De Luca, A., et al. (2012). Risk factors and outcomes of candidemia caused by biofilm-forming isolates in a tertiary care hospital. *PLoS One* 7:e33705. doi: 10.1371/journal.pone.0033705

World Health Organization (WHO) (2018). *Guidelines for the Diagnosis, Prevention and Management of Cryptococcal Disease in HIV-Infected Adults, Adolescents and Children: Supplement to the 2016 Consolidated Guidelines on the Use of Antiretroviral Drugs for Treating and Preventing HIV Infection*. Available online at: https://apps.who.int/iris/bitstream/handle/10665/260399/9789241550277-eng.pdf;jsessionid=1F42F942BA955CAF6B3CF1189E63713D?sequence=1 (accessed December 12, 2019).

Yang, Y., Wang, C., Gao, N., Lyu, Y., Zhang, L., Zhang, S., et al. (2020). A novel dual-targeted α-helical peptide with potent antifungal activity against fluconazole-resistant *Candida albicans* clinical isolates. *Front. Microbiol.* 11:548620. doi: 10.3389/fmicb.2020.548620

Zacchino, S. A., Butassi, E., Di Liberto, M., Raimondi, M., Postigo, A., and Sortino, M. (2017). Plant phenolics and terpenoids as adjuvants of antibacterial and antifungal drugs. *Phytomedicine* 15, 27–48. doi: 10.1016/j.phymed.2017.10.018

Zanin, J. L. B., De Carvalho, B. A., Salles Martineli, P., Dos Santos, M. H., Lago, J. H. G., Sartorelli, P., et al. (2012). The genus *Caesalpinia* L. (Caesalpiniaceae): phytochemical and pharmacological characteristics. *Molecules* 17, 7887–7902. doi: 10.3390/molecules17077887

Zanin, J. L. B., Massoni, M., dos Santos, M. H., de Freitas, G. C., Niero, E. L. O., Schefer, R. R., et al. (2015). Caesalpinioflavone, a new cytotoxic biflavonoid isolated from *Caesalpinia pluviosa* var. *peltophoroides*. *J. Braz. Chem. Soc.* 26, 804–809. doi: 10.5935/0103-5053.20150043

Zaragoza, O., Mihu, C., Casadevall, A., and Nosanchuk, J. D. (2005). Effect of amphotericin B on capsule and cell size in *Cryptococcus neoformans* during murine infection. *Antimicrob. Agents Chemother.* 49, 4358–4361. doi: 10.1128/AAC.49.10.4358-4361.2005

Zaragoza, O., Rodrigues, M. L., de Jesus, M., Frases, S., Dadachova, E., and Casadevall, A. (2009). The capsule of the fungal pathogen *Cryptococcus neoformans*. *Adv. Appl. Microbiol.* 68, 133–216. doi: 10.1016/S0065-2164(09)01204-0

Conflict of Interest: The authors declare that the research was conducted in the absence of any commercial or financial relationships that could be construed as a potential conflict of interest.

frontiers in Microbiology

METHODS
published: 28 June 2021
doi: 10.3389/fmicb.2021.658144

A Novel Diagnostic Method for Invasive Fungal Disease Using the Factor G Alpha Subunit From *Limulus polyphemus*

*Fang Cui[1], Peng Luo[1], Yao Bai[1] and Jiangping Meng[2]**

[1] Department of Laboratory Medicine, The First Affiliated Hospital of Chongqing Medical University, Chongqing, China, [2] Assisted Reproductive Center, Department of Obstetrics and Gynecology, The First Affiliated Hospital of Chongqing Medical University, Chongqing, China

Deaths due to invasive fungal disease (IFD) have been increasing every year. Early and rapid detection is important to reduce the mortality rate associated with IFD. In this study, we explored a novel diagnostic method for detecting IFD, which involves the G Factor α subunit (GFαSub) from *Limulus polyphemus*. The GFαSub double-sandwich method was developed to detect (1,3)-β-D-glucans in human serum using purified GFαSub and horseradish peroxidase-labeled GFαSub. The GFαSub double-sandwich method and the G test were performed and compared. Using GFαSub sequence analysis, the expression plasmid pET30a-GFαSub252-668 was synthesized, and GFαSub252-668 was expressed and purified *via* isopropyl-β-d-thiogalactoside induction and nickel-nitrilotriacetic acid affinity. The optimization method was established *via* the orthogonal method. Using this method, the sera of 36 patients with IFD and 92 volunteers without IFD underwent detection, and the receiver operating characteristic curve of the GFαSub252-668 double-sandwich method was described. The sensitivity and specificity of the GFαSub252-668 double-sandwich method were 91.67 and 82.61%, respectively, and there was good correlation with the G test for the serum specimens of 36 patients with pulmonary IFD (R^2 = 0.7592). In conclusion, our study suggests that the GFαSub252-668 double-sandwich method was satisfactory at detecting IFD cases. This method can be promoted and further developed as a novel method for diagnosing IFD.

Keywords: invasive fungal disease, G Factor α subunit, sandwich method, diagnosis, methodology

OPEN ACCESS

Edited by:
David Perlin, Hackensack Meridian Health, United States

Reviewed by:
Brunella Posteraro, Catholic University of the Sacred Heart, Italy
P. Lewis White, Public Health Wales NHS Trust, United Kingdom

***Correspondence:**
Jiangping Meng
278471655@qq.com;
txl831120@wnmc.edu.cn

Specialty section:
This article was submitted to Antimicrobials, Resistance and Chemotherapy, a section of the journal Frontiers in Microbiology

Received: *25 January 2021*
Accepted: *28 April 2021*
Published: *28 June 2021*

Citation:
Cui F, Luo P, Bai Y and Meng J (2021) A Novel Diagnostic Method for Invasive Fungal Disease Using the Factor G Alpha Subunit From Limulus polyphemus. Front. Microbiol. 12:658144. doi: 10.3389/fmicb.2021.658144

INTRODUCTION

The incidence rate of invasive fungal infections (IFD) in the general population has remained static year-on-year; however, with respect to at-risk individuals, the incidence rate has risen every year. Although most fungi do not cause infection in healthy individuals, IFD most commonly occurs in immunocompromised persons and those with autoimmune disorders (Enoch et al., 2017; Posch et al., 2017; Scriven et al., 2017). Lungs are the most common site of IFD, and it is difficult to differentiate pulmonary IFD from bacterial infections because of their similar clinical presentations (Schelenz et al., 2015; Acharige et al., 2018; Ajmal et al., 2018). The clinical consequences of IFD

are severe; therefore, the differential diagnosis of IFD is critical for guiding clinical treatment. To identify IFD, imaging and laboratory examinations are employed (Calitri et al., 2017; Calley and Warris, 2017; Katragkou et al., 2017). Other examinations include fungal smears, cultures, serological tests, and the G test. Despite the ability of these tests to accurately detect IFD, they have certain limitations. Fungal cultures generally require 2 days, whereas fungal smears only take few minutes but have high false-negative rates. Moreover, serological tests cannot distinguish current infections from past infections, particularly if only one test is utilized. The antifungal antibody or antigen also depends on a person's immunity level. Polymerase chain reaction (PCR) testing is sensitive but cannot identify the proliferation and survival of the fungus. In our clinic, the G test is used to detect and diagnose IFD. The principle behind this method is that (1,3)-β-D-glucan in the fungal cell wall can activate the G factor to catalyze the coagulation cascade in the *Limulus* plasma; the subsequent conversion of fibrinogen into fibrin is detected *via* a dynamic turbidimeter.

During IFD, phagocytes consume fungal spores and release (1,3)-β-D-glucan, a highly abundant fungal cell wall component, into the circulatory system. Measuring (1,3)-β-D-glucan levels, in combination with clinical signs and symptoms, might aid in diagnosing IFD (Shi et al., 2016; Verma et al., 2019). Hence, a method with high sensitivity that can accurately diagnose IFD should be developed. Because (1,3)-β-D-glucan is a sugar with varying degrees of polymerization, it may be difficult to obtain a specific antibody for this purpose. Glucan-binding proteins (GBPs) are natural proteins that are bound to glucan and are found in animals, plants, bacteria, and even in humans. In our previous study, we verified the binding forces of several GBPs for detecting (1,3)-β-D-glucan. The results showed that the clotting factor G alpha subunit (GFαSub) from *Limulus polyphemus* was better detected than other GBPs. In addition, based on the structural domains and functions of GfαSub, its truncated version can be an excellent ligand for research and clinical examination.

In the present study, we used the truncated GfαSub to quantify (1,3)-β-D-glucan in clinical samples (Ueda et al., 2009; Adachi et al., 2019). The study was designed to utilize the high specificity and sensitivity of the immunoassay to improve the clinical and laboratory diagnosis of IFD.

MATERIALS AND METHODS

Subjects

We selected 36 patients with deep respiratory tract fungal infections from January 2017 to December 2019 and classified them as the positive group. In total, 92 volunteers were assigned to the negative group: 52 had bacterial lung infection, which was confirmed by the clinical laboratory, and 40 were healthy volunteers without any infection.

Invasive fungal disease was diagnosed as per the guidelines of the European Organization for Research and Treatment of Cancer/Mycoses Study Group (EORTC/MSG) (Donnelly et al., 2020). The inclusion criteria for patients with IFD were as follows: (1) a recent history of IFD diagnosis, treatment, radiotherapy, chemotherapy, or hormone use accompanied by fever, cough, shortness of breath, and other respiratory symptoms; (2) positive sputum fungal culture and/or sputum fungal smear; (3) positive G test; and (4) detection of elevated levels of interleukin-6, procalcitonin, or both (Patterson et al., 2016). Patients with pulmonary bacterial infection were those who showed pathogenic gram-negative bacilli or gram-positive cocci on culture and had been treated effectively as per the information on drug sensitivity. However, patients with concurrent pulmonary bacterial and fungal infections were excluded. The clinical information of the 36 patients with IFD is listed in **Table 1**. A total of 128 subjects were included in this study, and their physiological information is shown in **Table 2**. In a fasting state, 4 mL whole blood was obtained in a procoagulant tube from each participant. Serum was separated and stored at −80°C until use. (1,3)-β-D-glucan levels were measured using the G test with commercial kits (Zhanjiang A&C Biological Co., Ltd) and the in-house developed GFαSub double-sandwich method.

Materials

The expression plasmid of pET30a-GFαSub252-668 was synthesized by Shanghai Biotechnology Company (China), and *Escherichia coli* BL21 (DE3) was maintained in our laboratory. (1,3)-β-D-glucan was purchased from Elicityl Co., Ltd., (France), and restriction endonucleases and digestion buffer were purchased from Fermentas Co., Ltd (Canada). The monoclonal antibody of anti-His tag was purchased from Beijing Zhongshan Jinqiao Biological Co., Ltd (China), whereas the horseradish peroxidase (HRP)-labeling kit, protein-free blocking solution, 3,3′,5,5′-tetramethylbenzidine chromogenic solution,

TABLE 1 | The basic information of 36 IFD patients.

Items		Total	Molds	Yeasts
		36	(*n* = 6)	(*n* = 30)
Sputum smear		Positive results (*n*)	3	26
Sputum culture			6	30
Blood culture			1	2
G-test			5	30
Imaging			6	30
Co-infection	G^-b		5	26
	G^+c		–	3

TABLE 2 | The comparison of the basic information of the 128 subjects.

	Pulmonary with IFD (*n* = 36)	Pulmonary with BI (*n* = 52)	Healthy donors (*n* = 40)	*F, t,* χ^2*/p*
Gender (M/F)	7/2	9/4	3/1	0.3348, 0.8459
Age (year)	46.9 ± 15.2	49.1 ± 20.8	48.3 ± 17.3	0.1543, 0.8572
BMI	23.2 ± 9.1	22.6 ± 7.2	28.3 ± 8.6	2.554, 0.2789
Yeast/Mould	5/1	–	–	–
G^-b/G^+c	31/3	21/5	–	–

M/F, male and female; BMI, Body Mass Index; G^-b/G^+c, gram-negative bacillus and gram-positive cocci; BI, bacterial infection.

and termination solution were purchased from Jinan Taitianhe Biological Co., Ltd (China). The nickel-nitrilotriacetic acid (Ni-NTA) purification column was purchased from Qiagen (Germany). The sodium dodecyl sulfate-polyacrylamide gel electrophoresis (SDS-PAGE) preparation kit and kanamycin were purchased from Solibao Biological Company (China). Protein and DNA ladder markers were purchased from ThermoFisher (United States). Phenylmethylsulfonyl fluoride (PMSF), protease inhibitor cocktail, and isopropyl-β-D-thiogalactoside (IPTG) were purchased from Aladdin (China). The remaining chemical reagents were purchased from Sinopharm Chemical Group Corporation (China).

Characterization of the GFαSub252-668 Expression Plasmid

Based on the clone site information about the constructed plasmid pET30a-GFαSub252-668, a double restriction enzyme digestion using NedI and *Hin*dIII was performed for characterization. The reaction system was as follows: 10 mL of plasmid, 1 mL each of NedI and *Hin*dIII, 2 mL of 10 × buffer, and 6 mL of deionized water. The system was placed in a water bath at 37°C for 30 min, and then heated at 95°C for 5 min to terminate the reaction. Products were identified by electrophoresis on 1% agarose gels.

Expression and Purification of GFαSub252-668

The plasmid pET30a-GFαSub252-668 was transfected into *E. coli* BL21 (DE3). Next, the strain underwent heat shock at 42°C for 90 s. Positive clones were screened on kanamycin-resistant Luria–Bertani (LB) solid medium and then inoculated into LB liquid medium. IPTG was added when the turbidity value of optical density $(OD)_{600\ nm}$ reached 0.8 with a final concentration of 0.8 mM. The strains were then induced overnight at room temperature (25°C). The strains were subsequently collected by centrifugation at 10,000 × *g* for 30 min and rinsed twice with sterile pre-cooled phosphate-buffered saline (PBS). Strains were then treated by repeated freezing (−80°C) and thawing followed by another ultrasonic fragmentation for 10 min. Finally, the supernatants and precipitates were collected separately by centrifugation at 10,000 × *g* for 30 min. SDS-PAGE was performed, and the target protein was identified using Coomassie brilliant blue staining. The lysed supernatants and Ni-NTA purification column were placed on a 4°C mixer and continuously mixed for 2 h at room temperature. PMSF and protease inhibitor cocktail were added during the mixing. Then, the column was subjected to washing and eluting with various concentrations of imidazole buffer. The eluent was identified again by SDS-PAGE and stained using Coomassie brilliant blue staining.

Establishing the Double-Sandwich Testing System

The purified protein of GFαSub was quantified and then labeled using an HRP-labeling kit as per its molar concentration. Next, a double-sandwich testing method for GFαSub252-668 was established *via* the chessboard method: the measurement was performed by coating with various concentrations of GFαSub252-668, and GFαSub252-668 was then labeled with HRP. PBS containing 10% dimethyl sulfoxide (DMSO) served as the negative control, while (1,3)-β-D-glucan diluted in 200 pg/mL of PBS containing 10% DMSO served as the positive control. After determining the optimal coating and detection concentrations, the sera of healthy controls and the final concentration of 200 pg/mL (1,3)-β-D-glucan were used as negative and positive samples, respectively, and six multiple wells were set for each group to verify testing efficiency.

Comparison of Testing Efficiency Between the Double-Sandwich and G Test Methods

We performed a double-sandwich assay of GFαSub252-668 in 128 human serum samples. Meanwhile, 0, 50, 100, 200, and 400 pg/mL of (1,3)-β-D-glucan were used for quantitative standard curves. We calculated correlations between the levels of measured (1,3)-β-D-glucan using the double-sandwich and G test methods.

Statistical Analysis

Statistical analyses were performed using SPSS 15.0. The comparison of quantitative data between the two groups was determined using a *t*-test, while differences in the constituent ratio among various groups were compared *via* the chi-square test. Correlation analysis between the two groups of quantitative data was performed using Spearman's method. All *p*-values were considered statistically significant if $p < 0.05$.

RESULTS

Establishing the GFαSub252-668 Double-Sandwich Method

GFαSub252-668 was inserted into pET30a, and the presence of the inserted gene was confirmed by restriction digestion (**Supplementary Figure 1**). The identity of the inserted gene was verified by sequencing. The expression of recombinant GFαSub252-668 was induced by IPTG (**Supplementary Figure 2**), purified using the Ni-NTA column (**Supplementary Figure 3**), and detected with the anti-His tag monoclonal antibody (**Supplementary Figure 4**).

The coating concentration of GFαSub252-668 and the testing concentration of GFαSub252-668-HRP were optimized using the orthogonal method with the uniform conditions of incubation, blocking, rinsing, and coloration. Based on the value of absorbance in the 450 nm wavelength and the ratio of absorbance positive/absorbance negative, the maximum value of the ratio of absorbance positive/absorbance negative was 5.064 when the coating concentration of GFαSub252-668 and working concentration of GFαSub252-668-HRP were 0.8 and 1.6 ng/mL, respectively (**Table 3**). To verify the influence of the matrix effect on the method, healthy human serum containing 200 pg/mL of (1,3)-β-D-glucan was considered as a positive sample and healthy

TABLE 3 | Determination of the working concentrations of the reagent for coating and testing in the GFαSub252-668 double sandwich method using the orthogonal method.

Coating (ng/mL)	Testing (ng/mL) (Absorbance of Positive team)					Testing (ng/mL) (Absorbance of Negative team)				
	0.1	0.2	0.4	0.8	1.6	0.1	0.2	0.4	0.8	1.6
0.1	0.289	0.391	0.466	0.583	0.636	0.087	0.102	0.116	0.122	0.146
0.2	0.339	0.447	0.529	0.613	0.738	0.107	0.125	0.131	0.148	0.182
0.4	0.395	0.501	0.627	0.706	0.892	0.133	0.154	0.161	0.189	0.205
0.8	0.413	0.613	0.736	0.866	**1.094**	0.169	0.181	0.196	0.209	**0.216**
1.6	0.484	0.705	0.843	1.003	1.246	0.205	0.213	0.227	0.235	0.285

Underlined number stands for optimum concentration of coating and testing, MAX = Abs_P/Abs_N.

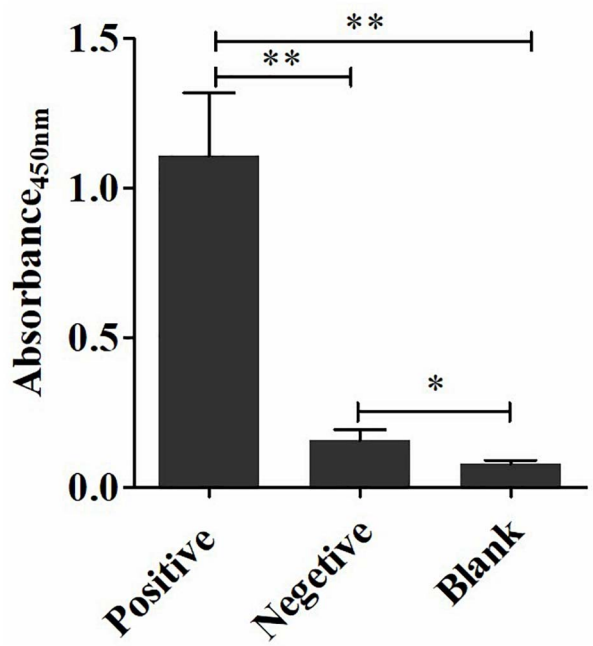

FIGURE 1 | Determination of (1,3)-β-D-glucan serum levels using the GFαSub252-668 double-sandwich method. * $P < 0.05$, ** $P < 0.01$.

human serum was taken as a negative sample. The GFαSub252-668 double-sandwich method was used for testing, and the OD ratio for positive to negative samples was approximately 6, which clearly distinguished the negative and positive samples (**Figure 1**).

Comparison of the Clinical Testing Efficiency Between the GFαSub252-668 Double-Sandwich and G Test Methods

The quantitative analysis of (1,3)-β-D-glucan in the samples was performed by establishing a standard fitting curve. The value of R^2 was 0.9672, and the equation was $y = 1/239.8 \times x + 0.2586$ (**Figure 2**). Serum samples from 36 patients with pulmonary IFD and 92 patients without IFD were included, and the basic

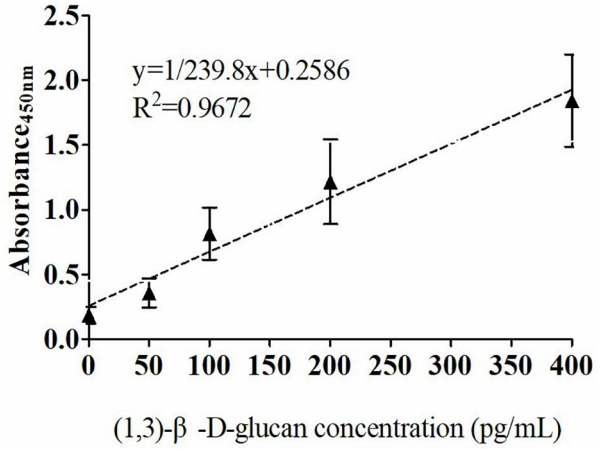

FIGURE 2 | Standard curve of the GFαSub252-668 double-sandwich method for determining the level of (1,3)-β-D-glucan in serum.

information of the subjects is shown in **Tables 1**, **2**. Of the 128 serum samples tested using the double-sandwich method, the levels of (1,3)-β-D-glucan in patients with IFD were significantly higher than those in patients with bacterial infections and healthy subjects (**Figure 3**). The measured results were fit using a receiver operating characteristic curve, and the sensitivity and specificity of the GFαSub252-668 double-sandwich method were 91.67% [95% confidence interval (CI): 77.53–98.25%] and 82.61% (95% CI: 73.3–89.72%), respectively. The area under the curve was 0.9423 (95% CI: 0.8999–0.9848) (**Figure 4**). The levels of serum (1,3)-β-D-glucan were determined in the 36 patients with pulmonary IFD using the two methods, and correlation analysis of the results showed that the value of R^2 was 0.7592 ($p < 0.001$) (**Figure 5**).

DISCUSSION

The clinical course of IFD of the respiratory tract may be severe with poor outcomes. Making a timely diagnosis and initiating appropriate treatment greatly improves survival (Ueda et al., 2009; Shi et al., 2016; Calley and Warris, 2017; Acharige et al., 2018; Ajmal et al., 2018). Clinically, histological analysis is the gold standard, and the G test is more widely used presently (Ueda et al., 2009; Shi et al., 2016). Nevertheless, there are some limitations to these laboratory testing methods, including the low detection rate of fungal culture and smear and the long culture periods. In addition, fungus-specific antibodies in serological examinations cannot fully reflect the infection status. Until recently, the detection of fungus-specific antigens was based on the G test (Ueda et al., 2009; Calley and Warris, 2017; Katragkou et al., 2017; Adachi et al., 2019). In this process, factor G from the serum of *L. polyphemus* is activated by (1,3)-β-D-glucan, which in turn catalyzes the conversion of fibrinogen to fibrin. The assay is highly sensitive for quantifying glucan using dynamic turbidimetric. Nevertheless, the assay principle suggests that it cannot avoid the interference of testing environment,

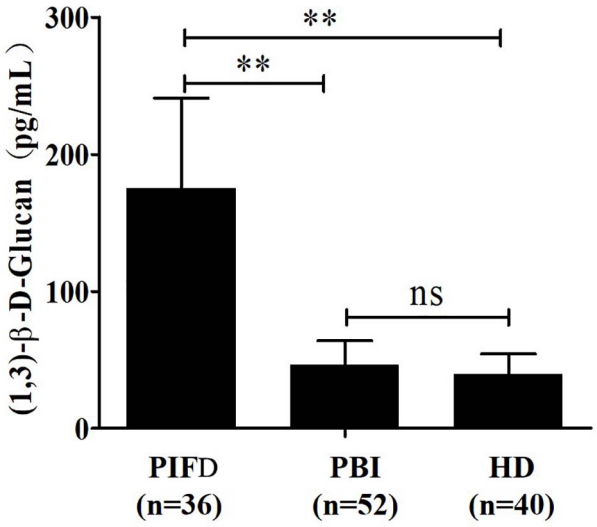

FIGURE 3 | Determination of serum (1,3)-β-D-glucan levels in 128 subjects using the GFαSub252-668 double-sandwich method. PIFD, pulmonary invasive fungal disease; PBI, pulmonary bacterial infection; HD, healthy donors; ns, not significant; $^{**}p < 0.001$. IFD group vs. bacterial infection group: $t = 13.47$, $p < 0.001$; IFD group vs. healthy group: $t = 12.7$, $p < 0.001$; bacterial infection group vs. healthy group: $t = 1.983$, $p = 0.0504$.

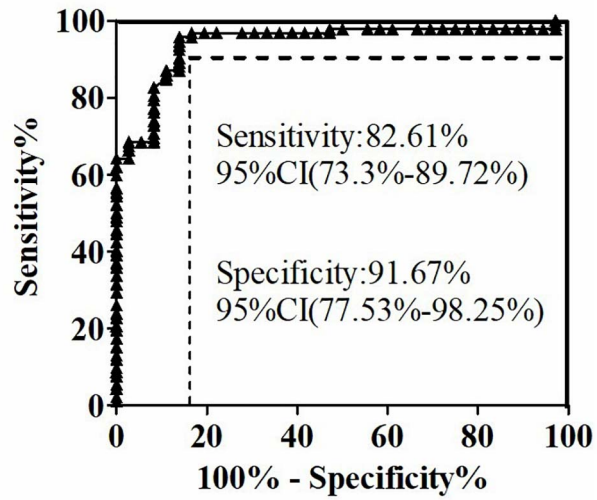

FIGURE 4 | Receiver operating characteristic curve of serum (1,3)-β-D-glucan levels in 128 subjects using the GFαSub252-668 double-sandwich method.

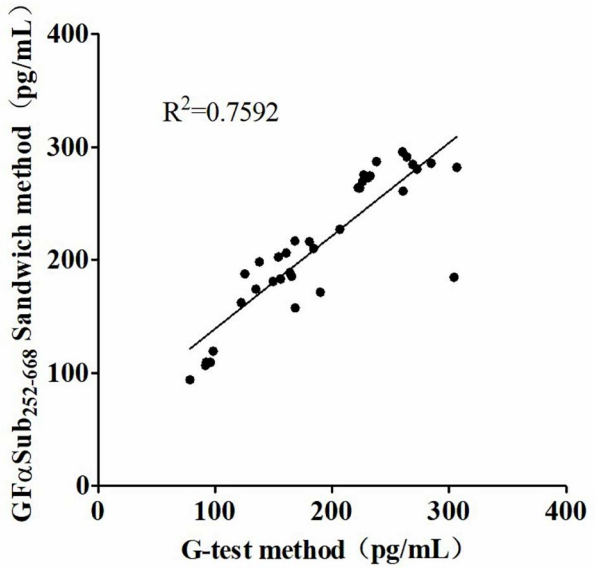

FIGURE 5 | Correlation analysis of serum (1,3)-β-D-glucan levels in 36 patients with invasive fungal disease using the two methods.

fungal food, drugs, and even some medical equipment. The serum physical properties of patients with abnormalities, such as severe lipidemia, hemolysis, or jaundice, have a substantial impact on the results (Lo Cascio et al., 2015), The present study was designed to immunologically determine the abundance of (1,3)-β-D-glucan in fungal cell walls and to evaluate the status of IFD. Immunoassay can complement the methods described above with its relatively high sensitivity and specificity and can eliminate some interference from other substances in the testing process (Mattos-Graner et al., 2001; Lo Cascio et al., 2015; Anjugam et al., 2018).

Studies have shown that GFαSub derived from marine organisms is efficiently recognizable and binds to glucan with various structures (Ueda et al., 2009; Adachi et al., 2019). In our previous studies, GFαSub from *L. polyphemus*, nematodes, plants, and other species was cloned and expressed, and the results showed that these GFαSub proteins could recognize and bind to (1,3)-β-D-glucan. However, their recognition and binding abilities differed. Subsequently, GFαSub from *L. polyphemus* was selected as the ligand of (1,3)-β-D-glucan based on a comprehensive evaluation of the specificity of recognition and binding capacity. Thus, GFαSub from *L. polyphemus* with these characteristics could be industrialized *via* genetic engineering.

The ID number of the GFαSub provided by the National Center for Biotechnology Information is NM_001314167.1. The full length of the mRNA sequence is 2,007 bp, and it encodes a peptide chain of 668 amino acids. Amino acids 1–20 are signal peptides, 27–253 have glycohydrolase activity, and the rest comprise three glucan-binding domains. Based on this, amino acids 252–668 of the active binding domain of GFαSub252-668 were synthesized and cloned into a prokaryotic expression plasmid and their expression was then induced. After purifying the product, GFαSub252-668 protein was obtained. By constructing a GFαSub double-sandwich system, standard samples and clinical serum samples were tested, and the results showed both high sensitivity and a wide linear range. In the present study, 128 clinical serum samples were tested using this method, and its sensitivity and specificity were 91.67 and 82.61%, respectively, both of which were higher than those of the G test reported in previous studies (Martín-Mazuelos et al., 2015;

Lahmer et al., 2016; Shabaan et al., 2018; Ge et al., 2019). The possible reasons for the discrepancy are as follows: (1) the principle of the method: a specific spatial conformation between a ligand and a target is recognized in the GFαSub double-sandwich method, whereas in the G test, the cascade catalytic reaction is activated and initiated by factor G; (2) the quality of the samples: some unknown factors may influence the process of clinical sample collection and delivery that may lead to changes in its characteristics, including severe hemolysis, jaundice, and severe lipidemia; (3) the source of target materials: GFαSub can only bind to glucan with a specific structure; however, the activation of factor G in the G test has no such characteristics, and glucan contained in diets, the environment, drugs, and others may thus interfere with the detection; (4) the protocol of the double-sandwich method in this study is simple, and the entire process is facilitated using an automated enzyme-linked immunoassay instrument that greatly reduces the error. By contrast, all steps of the G test are performed manually, except for the testing step, and the time difference to process samples is likely to cause errors in the final result.

The two methods were subsequently used to determine the amount of (1,3)-β-D-glucan from the serum of 36 patients with IFD, and the correlation analysis of their values showed a good correlation (R^2 = 0.7592). During the analysis, an interesting phenomenon was found in that the levels of serum (1,3)-β-D-glucan in patients with pulmonary Mucor infections (n = 6) were slightly lower than in those with yeast-type fungal infections (n = 30), which may be because of the difference of (1,3)-β-D-glucan abundance in the cell walls of different species of fungi (Free, 2013). Nevertheless, the method could still be used as an effective means to distinguish IFD.

The findings of the present study showed that our method has a good correlation with the G test. However, because of funding limitations, the G test was performed only in the 36 samples of patients with IFD but not in all the 92 control samples. We will measure the performance of our method in the next stage. Furthermore, HRP was used for signal detection, which limits the sensitivity of our method. In the future, we plan to use luminescent groups for labeling to improve the sensitivity of the detection system.

In summary, we preliminarily tested the application of a specific target *in vivo* to recognize a ligand in clinical testing. This concept provides a solution to the problem of target antibody preparation for small molecular polysaccharides or oligosaccharides, such as (1,3)-β-D-glucan. We hope to develop a new kit for IFD detection that may provide data support for the differential diagnosis of clinical IFD.

DATA AVAILABILITY STATEMENT

The original contributions presented in the study are included in the article/**Supplementary Material**, further inquiries can be directed to the corresponding author/s.

ETHICS STATEMENT

The studies involving human participants were reviewed and approved by The First Affiliated Hospital of Chongqing Medical University. The patients/participants provided their written informed consent to participate in this study.

AUTHOR CONTRIBUTIONS

JM designed the experiments. FC, PL, and YB performed the experiments and the statistical analysis. FC wrote and edited the manuscript. JM supervised the study. All authors have read and approved the final version of the manuscript.

ACKNOWLEDGMENTS

We would like to thank all patients and medical staff who volunteered to provides specimens for this study. We would also like to thank the scientific research center of our hospital for its support.

SUPPLEMENTARY MATERIAL

The Supplementary Material for this article can be found online at: https://www.frontiersin.org/articles/10.3389/fmicb.2021.658144/full#supplementary-material

REFERENCES

Acharige, M. J. T., Koshy, S., Ismail, N., Aloum, O., Jazaerly, M., Astudillo, C. L., et al. (2018). Breath-based diagnosis of fungal infections. *J. Breath Res.* 12:027108. doi: 10.1088/1752-7163/aa98a1

Adachi, Y., Ishii, M., Kanno, T., Tetsui, J., Ishibashi, K.-I., Yamanaka, D., et al. (2019). N-terminal (1→3)-β-d-glucan recognition proteins from insects recognize the difference in ultra-structures of (1→3)-β-d-glucan. *Int. J. Mol. Sci.* 20:3498. doi: 10.3390/ijms20143498

Ajmal, S., Mahmood, M., Saleh, O. A., Larson, J., and Sohail, M. R. (2018). Invasive fungal infections associated with prior respiratory viral infections in immunocompromised hosts. *Infection* 46, 555–558. doi: 10.1007/s15010-018-1138-0

Anjugam, M., Vaseeharan, B., Iswarya, A., Divya, M., Prabhu, N. M., and Sankaranarayanan, K. (2018). Biological synthesis of silver nanoparticles using β-1, 3 glucan binding protein and their antibacterial, antibiofilm and cytotoxic potential. *Microb. Pathog.* 115, 31–40. doi: 10.1016/j.micpath.2017.12.003

Calitri, C., Caviglia, I., Cangemi, G., Furfaro, E., Bandettini, R., Fioredda, F., et al. (2017). Performance of 1, 3-β-D-glucan for diagnosing invasive fungal diseases in children. *Mycoses* 60, 789–795. doi: 10.1111/myc.12664

Calley, J. L., and Warris, A. (2017). Recognition and diagnosis of invasive fungal infections in neonates. *J. Infect.* 74, S108–S113.

Donnelly, J. P., Chen, S. C., Kauffman, C. A., Steinbach, W. J., Baddley, J. W., Verweij, P. E., et al. (2020). Revision and update of the consensus definitions of invasive fungal disease from the European Organization for Research and Treatment of Cancer and the Mycoses Study Group Education and Research Consortium. *Clin. Infect. Dis.* 71, 1367–1376.

Enoch, D. A., Yang, H., Aliyu, S. H., and Micallef, C. (2017). "The changing epidemiology of invasive fungal infections," in *Human Fungal Pathogen*

Identification. Methods in Molecular Biology, ed. T. Lion (New York, NY: Humana Press).

Free, S. J. (2013). Fungal cell wall organization and biosynthesis. *Adv. Genet.* 81, 33–82. doi: 10.1016/b978-0-12-407677-8.00002-6

Ge, Y. L., Zhu, X. Y., Hu, K., Zhang, Q., Li, W. Q., Zhang, C., et al. (2019). Positive serum beta-d-glucan by G test and Aspergillus fumigatus sputum culture mimic invasive pulmonary aspergillosis in a pulmonary nocardia patient: a case report and literature review. *Clin. Lab.* 65:31232022.

Katragkou, A., Fisher, B. T., Groll, A. H., Roilides, E., and Walsh, T. J. (2017). Diagnostic imaging and invasive fungal diseases in children. *J. Pediatric Infect. Dis. Soc.* 6, S22–S31.

Lahmer, T., Neuenhahn, M., Held, J., Rasch, S., Schmid, R. M., and Huber, W. (2016). Comparison of 1, 3-β-d-glucan with galactomannan in serum and bronchoalveolar fluid for the detection of Aspergillus species in immunosuppressed mechanical ventilated critically ill patients. *J. Crit. Care* 36, 259–264. doi: 10.1016/j.jcrc.2016.06.026

Lo Cascio, G., Koncan, R., Stringari, G., Russo, A., Azzini, A., Ugolini, A., et al. (2015). Interference of confounding factors on the use of (1,3)-beta-D-glucan in the diagnosis of invasive candidiasis in the intensive care unit. *Eur. J. Clin. Microbiol. Infect. Dis.* 34, 357–365. doi: 10.1007/s10096-014-2239-z

Martín-Mazuelos, E., Loza, A., Castro, C., Macías, D., Zakariya, I., Saavedra, P., et al. (2015). β-D-glucan and Candida albicans germ tube antibody in ICU patients with invasive candidiasis. *Intensive Care Med.* 41, 1424–1432. doi: 10.1007/s00134-015-3922-y

Mattos-Graner, R. O., Jin, S., King, W. F., Chen, T., Smith, D. J., and Duncan, M. J. (2001). Cloning of the Streptococcus mutans gene encoding glucan binding protein B and analysis of genetic diversity and protein production in clinical isolates. *Infect. Immun.* 69, 6931–6941. doi: 10.1128/iai.69.11.6931-6941.2001

Patterson, T. F., Thompson, G. R., Denning, D. W., Fishman, J. A., Hadley, S., Herbrecht, R., et al. (2016). Practice guidelines for the diagnosis and management of aspergillosis: 2016 update by the Infectious Diseases Society of America. *Clin. Infect. Dis.* 63, e1–e60.

Posch, W., Steger, M., Wilflingseder, D., and Lass-Flörl, C. (2017). Promising immunotherapy against fungal diseases. *Expert Opin. Biol. Ther.* 17, 861–870. doi: 10.1080/14712598.2017.1322576

Schelenz, S., Barnes, R. A., Barton, R. C., Cleverley, J. R., Lucas, S. B., Kibbler, C. C., et al. (2015). British Society for Medical Mycology best practice recommendations for the diagnosis of serious fungal diseases. *Lancet Infect. Dis.* 15, 461–474. doi: 10.1016/s1473-3099(15)70006-x

Scriven, J. E., Tenforde, M. W., Levitz, S. M., and Jarvis, J. N. (2017). Modulating host immune responses to fight invasive fungal infections. *Curr. Opin. Microbiol.* 40, 95–103. doi: 10.1016/j.mib.2017.10.018

Shabaan, A. E., Elbaz, L. M., El-Emshaty, W. M., and Shouman, B. (2018). Role of serum (1, 3)-β-d-glucan assay in early diagnosis of invasive fungal infections in a neonatal intensive care unit. *J. Pediatr.* 94, 559–565. doi: 10.1016/j.jpedp.2017.07.007

Shi, X. Y., Liu, Y., Gu, X. M., Hao, S. Y., Wang, Y. H., Yan, D., et al. (2016). Diagnostic value of (1→3)-β-D-glucan in bronchoalveolar lavage fluid for invasive fungal disease: a meta-analysis. *Respir. Med.* 117, 48–53. doi: 10.1016/j.rmed.2016.05.017

Ueda, Y., Ohwada, S., Abe, Y., Shibata, T., Iijima, M., Yoshimitsu, Y., et al. (2009). Factor G utilizes a carbohydrate-binding cleft that is conserved between horseshoe crab and bacteria for the recognition of β-1, 3-d-glucans. *J. Immunol.* 183, 3810–3818. doi: 10.4049/jimmunol.0900430

Verma, N., Singh, S., Taneja, S., Duseja, A., Singh, V., Dhiman, R. K., et al. (2019). Invasive fungal infections amongst patients with acute-on-chronic liver failure at high risk for fungal infections. *Liver Int.* 39, 503–513. doi: 10.1111/liv.13981

Conflict of Interest: The authors declare that the research was conducted in the absence of any commercial or financial relationships that could be construed as a potential conflict of interest.

frontiers in Microbiology

ORIGINAL RESEARCH
published: 02 July 2021
doi: 10.3389/fmicb.2021.679563

Mechanism of Growth Regulation of Yeast Involving Hydrogen Sulfide From *S*-Propargyl-Cysteine Catalyzed by Cystathionine-γ-Lyase

Zhongkai Gu[1], Yufan Sun[2†], Feizhen Wu[1†] and Xiaomo Wu[3]**

[1] The Institute of Biomedical Sciences, Fudan University, Shanghai, China, [2] Key Laboratory of Medical Molecular Virology of Ministries of Education and Health, Department of Medical Microbiology, School of Basic Medical Sciences, Fudan University, Shanghai, China, [3] Dermatology Institute of Fuzhou, Dermatology Hospital of Fuzhou, Fuzhou, China

OPEN ACCESS

Edited by:
David Perlin,
Hackensack Meridian Health Center for Discovery and Innovation, United States

Reviewed by:
Weimin Shi,
Shanghai General Hospital, China
Yongbing Cao,
Shanghai University of Traditional Chinese Medicine, China
Bing Du,
South China Agricultural University, China

***Correspondence:**
Zhongkai Gu
zhongkaigu@fudan.edu.cn
Xiaomo Wu
xiaomo.wu@gmail.com

† These authors have contributed equally to this work

Specialty section:
This article was submitted to Antimicrobials, Resistance and Chemotherapy, a section of the journal Frontiers in Microbiology

Received: 12 March 2021
Accepted: 11 June 2021
Published: 02 July 2021

Citation:
Gu Z, Sun Y, Wu F and Wu X (2021) Mechanism of Growth Regulation of Yeast Involving Hydrogen Sulfide From S-Propargyl-Cysteine Catalyzed by Cystathionine-γ-Lyase. Front. Microbiol. 12:679563. doi: 10.3389/fmicb.2021.679563

Pathogenic fungi are recognized as a progressive threat to humans, particularly those with the immunocompromised condition. The growth of fungi is controlled by several factors, one of which is signaling molecules, such as hydrogen sulfide (H_2S), which was traditionally regarded as a toxic gas without physiological function. However, recent studies have revealed that H_2S is produced enzymatically and endogenously in several species, where it serves as a gaseous signaling molecule performing a variety of critical biological functions. However, the influence of this endogenous H_2S on the biological activities occurring within the pathogenic fungi, such as transcriptomic and phenotypic alternations, has not been elucidated so far. Therefore, the present study was aimed to decipher this concern by utilizing *S*-propargyl-cysteine (SPRC) as a novel and stable donor of H_2S and *Saccharomyces cerevisiae* as a fungal model. The results revealed that the yeast could produce H_2S by catabolizing SPRC, which facilitated the growth of the yeast cells. This implies that the additional intracellularly generated H_2S is generated primarily from the enhanced sulfur-amino-acid-biosynthesis pathways and serves to increase the growth rate of the yeast, and presumably the growth of the other fungi as well. In addition, by deciphering the implicated pathways and analyzing the *in vitro* enzymatic activities, cystathionine-γ-lyase (*CYS3*) was identified as the enzyme responsible for catabolizing SPRC into H_2S in the yeast, which suggested that cystathionine-γ-lyase might play a significant role in the regulation of H_2S-related transcriptomic and phenotypic alterations occurring in yeast. These findings provide important information regarding the mechanism underlying the influence of the gaseous signaling molecules such as H_2S on fungal growth. In addition, the findings provide a better insight to the *in vivo* metabolism of H_2S-related drugs, which would be useful for the future development of anti-fungal drugs.

Keywords: hydrogen sulfide, H_2S metabolism, fungal growth rate, SPRC, cystathionine-γ-lyase, fungal growth

INTRODUCTION

Many fungi are recognized as opportunistic pathogens, causing invasive infections and critical illness in humans (Romani, 2011; Köhler et al., 2017). The growth of fungi is subject to several factors, one of which is signaling molecules, including hydrogen sulfide (H_2S), which plays a central role in intercellular communication and intracellular redox balancing in yeast, a member of kingdom fungi (Lloyd, 2006). H_2S ranks the third as a gaseous signal molecule after nitric oxide (NO) and carbon monoxide (CO). H_2S is reported to be canonically involved in regulating a variety of physiological functions in mammals (Abe and Kimura, 1996; Hosoki et al., 1997; Kimura and Kimura, 2004; Li et al., 2005; Luan et al., 2012; Olas, 2015; Yu et al., 2014). However, despite the promising results observed with the use of H_2S in animal models, the influence of endogenously-generated H_2S on the transcriptomic and phenotypic alternations in fungi has been largely overlooked. Moreover, the canonical donors of exogenous H_2S, such as sulfide salts, are reported to cause a spike in the generation of H_2S, resulting in an unstable level of H_2S concentration (Li et al., 2009; Zhao et al., 2013). *S*-propargyl-cysteine (SPRC) was developed to replace sulfide salts for a gentle and stable generation of H_2S (Wang et al., 2009). In this context, the present study employed SPRC as the donor of H_2S and budding yeast *Saccharomyces cerevisiae* as the model organism to investigate the influence of H_2S on the transcriptome and phenotype alterations in the yeast to identify any potential H_2S-related factor for inhibition by drugs (Denoth Lippuner et al., 2014; Mulla et al., 2014; Voisset and Blondel, 2014).

The existing literature on endogenous H_2S in yeast mainly concerns the mechanism principally regarding the enhanced generation of H_2S during yeast fermentation and the strategies and approaches for reducing the H_2S production in the wine industry (Huang et al., 2017; Huo et al., 2018). The phenotypical alterations occurring in yeast due to the generation of H_2S have not been thoroughly studied so far. In addition, the transcriptomic variations in yeast upon H_2S production from an H_2S donor also require further exploration and investigation.

Interestingly, the results of the present study revealed that H_2S is intracellularly generated during the metabolism of SPRC and it can significantly enhance the growth of the yeast cells compared to NaHS. This phenomenon was initially inferred as a possibility that the growth of yeast and even that of other fungi could be inhibited by suppressing the generation of H_2S. Moreover, the transcriptome analysis and the functional assays elucidated the molecular mechanism underlying the H_2S-mediated growth enhancement, which further revealed that H_2S-mediated upregulation of certain genes resulted in the enrichment of the sulfur-amino-acid biosynthesis pathways. Consequently, a pathway analysis was conducted, which identified cystathionine-γ-lyase (*CYS3*) as the catabolic enzyme candidate that could utilize SPRC as a substrate for the production of H_2S with the enhancement the growth rate of yeast, and a further confirmation of this was provided by *in vitro* catalysis assay. Furthermore, the evolutionary analysis revealed that cystathionine-γ-lyase is highly conserved among various species of fungi (Krück et al., 2009), suggesting that Cys3p could be worth of consideration for anti-fungal drug development to inhibit fungal growth in the future.

MATERIALS AND METHODS

Yeast Culture Conditions

The budding yeast *S. cerevisiae* strain S288C was cultured in the SD medium (Yeast Protocols Handbook, Clontech, Protocol No.: PT3024–1, Version No.: PR973283). SPRC was provided by Prof. Yizhun Zhu. Sodium hydrosulfide (NaHS) was a domestic product of Sinopharm (Shanghai, China). The S288C strain was inoculated in each well of a 96-well plate at the starting concentration of 1.7×10^5 cells/mL in 150 μL medium, and the plate was subsequently incubated at 30°C in a Higro 220V incubator (DigiLab, Marlborough, MA, United States) at 600 rpm. The medium in each well contained SPRC (0.1–10 mM) or NaHS (1–8 μM) or no drug, and each well had a triplication. Every 2 h, $OD_{595\ nm}$ measurements were performed by placing the plate in a DTX880 plate reader (Beckman Coulter, Brea, CA, United States) after being subjected to shaking at 950 rpm for 1 min in the shaking module of an automation workstation (Beckman Coulter, Brea, CA, United States) (**Supplementary Tables 1, 2**). The experiment was performed for a minimum of 24 h. Besides, another set of yeast cells was simultaneously growing in SD medium without any drug for 30 h for the consequent standard curve measurement. A hemocytometer was applied to the measurement, and the cell density in the 1× medium suspension was known as 2.75×10^8. Subsequently, a series dilution was performed by accurate pipetting from 0.8 to 0.2× and the theoretical cell densities of the diluted suspensions were known by calculation. Following, all the suspension samples, including a blank SD medium sample, were injected to 3 wells of a 96-well plate for a triplication, and each well contained a volume of 150 μL, which was followed by the $OD_{595\ nm}$ measurement (**Supplementary Table 3**). All the OD values together with the calculated densities were carried out for a linear regression calculation to obtain the standard curve (**Supplementary Figure 1**), which converted each OD value above to a corresponding cell density number.

Transcriptome Analysis

The budding yeast cells were cultured for 16 h in a medium containing 2 mM SPRC, after which the cells were collected through centrifugation, fixed in 75% ethanol, and finally maintained at 4°C until the subsequent RNA extraction procedure. The total-RNA samples were extracted using the Biomiga Yeast RNA kit (Cat. No.: R6617, San Diego, CA, United States). The RNA-Seq library constructions were performed on the RNA samples by an RNA library prep kit (Illumina, San Diego, CA, United States Cat. No.: RS-122-2001). The library samples were sequenced by an Illumina HiSeq 2500 sequencer (San Diego, CA, United States). The raw data were

consequently examined for the sequencing quality by the FastQC v0.11.9[1], and all the reads were trimmed by the Trim_galore v0.6.6[2] with the default setting for a better quality. The trimmed data was aligned against the *S. cerevisiae* reference genome and annotation (R64-1-1[3]) by the software Tophat v2.1.1 (Trapnell et al., 2012), and the generated FPKM data was transferred into the TPM format by TPMCalculator (Vera Alvarez et al., 2018), which was used for the generation of the enrichment heatmap by Clustvis (Metsalu and Vilo, 2015). Meanwhile, the Tophat-generated data was processed using Cuffdiff (Trapnell et al., 2012) to generate the data of gene expression differences, which was utilized to generate the volcano plot using the Origin 2018 software (OriginLab Co., Northampton, MA, United States). Subsequently, certain genes with *p*-values below 0.05 and the values of $\log_2$(fold change) ≥ 0.585 or ≤ -0.585 were selected from the matrix for the following analyses (**Supplementary Table 5**). The gene ontology (GO) and KEGG analyses were performed using DAVID (Huang da et al., 2009a,b). The GSEA analysis was performed using the GSEA software (Mootha et al., 2003; Subramanian et al., 2005). The enrichment gene ontology (GO) network was deciphered using Metascape.org (Tripathi et al., 2015), and the network file was processed and visualized in Cytoscape (Shannon et al., 2003).

Cystathionine-γ-Lyase Cloning, Expression and Purification

The gDNA of the S288C strain was extracted from the yeast cells and purified using a gDNA kit (Biomiga, San Diego, CA, United States). Subsequently, the open reading frame of the yeast cystathionine-γ-lyase *CYS3* gene was amplified by performing a primary PCR reaction with the gDNA of the S288C strain using the Q5 HF DNA polymerase (New England BioLabs, Cat. No.: M0491, Ipswich, MA, United States), the forward primer 5′-ATGACTCTACAAGAATCTGA-3′, and the reverse primer 5′-TTAGTTGGTGGCTTGTTTCA-3′. The primary PCR reaction conditions were: initial denaturation at 98°C for 30 s, followed by 35 cycles of 98°C for 10 s, 55°C for 30 s, and 72°C for 75 s, and then a final extension at 72°C for 10 min followed by reservation 4°C. The resultant PCR product was analyzed using agarose gel electrophoresis. Next, the restriction enzyme sites for *Bam*HI and *Xho*I were introduced to the ends of these amplified fragments in a secondary PCR reaction conducted using KOD Plus polymerase (TOYOBO, Japan), the forward primer 5′-CGGGATCCATGACTC TACAAGAATCTGATAAATTTG-3′, and the reverse primer 5′-CCGCTCGAGTTAGTTGGTGGCTTGTTTCAAG-3′. The secondary PCR reaction conditions were as follows: initial denaturation at 94°C for 5 min, followed by 30 cycles of 94°C for 30 s, 57°C for 30 s, and 68°C for 90 s, and then a final extension at 68°C for 10 min and reservation at 4°C. The amplified fragments from the secondary PCR reaction and an *Escherichia coli* expression vector, which was a modified pET-28a plasmid vector with a His_6-tag and a SUMO-tag (Cheng et al., 2015), were individually digested by *Bam*HI and *Xho*I restriction enzymes (New England Biolabs, Ipswich, MA, United States), and all the digested products were examined together on agarose gel. Next, the digested fragments and the vector plasmid were ligated by overnight incubation with T4 DNA ligase (Ipswich, MA, United States) at 16°C. The constructs were transformed into Top10 competent *E. coli* and then placed onto LB agar plates containing kanamycin. A single colony was transferred to the liquid LB medium containing kanamycin for plasmid amplification and then purified using a plasmid kit (Qiagen, Hilden, Germany). After confirmation of the plasmid in the sequencing test conducted with T7 primers, the plasmid was transformed into another competent *E. coli* strain, BL21 (DE3), and then placed onto LB agarose plates containing kanamycin. On the next day, a single colony was selected for inoculation in the liquid LB medium containing kanamycin. Massive cell culture was subsequently prepared in Erlenmeyer flasks of 1 L capacity. After 18 h of culturing, when the medium OD_{600} was over 0.4, protein expression was induced by adding 0.1 mM IPTG to the culture (Isopropyl β-D-1-thiogalactopyranoside), followed by incubation at 37°C for 3 h.

The cells were harvested through centrifugation, resuspended in lysis buffer [40 mM Tris-HCl pH = 8.0, 300 mM NaCl, 6 mM $MgCl_2$, 1 mM β-mercaptoethanol, 10 μM pyridoxal-phosphate, and 10 mg/mL DNase], and disrupted using a high atmospheric compressor (AH-100B, ATS Engineering Ltd., Suzhou, China) at 1,500 bar. The cell debris was removed through centrifugation at 15,000 rpm for 35 min. The proteins suspended in the supernatant were examined by SDS-PAGE, and the lysate was subsequently loaded onto a nickel column (Thermo Fisher, Waltham, MA, United States). Next, the SUMO-tag was digested by overnight incubation with SUMO proteinase (or ULP1, Thermo Fisher, Waltham, MA, United States) at 4°C, and then the elution buffer [20 mM Tris-HCl pH = 8.0, 150 mM NaCl, 6 mM $MgCl_2$, and 1 mM β-mercaptoethanol] was loaded onto the column for elution. The eluted protein was diluted to 12.8% (v/v) using the dilution buffer [40 mM Tris-HCl pH = 8.0, 6 mM $MgCl_2$, and 1 mM β-mercaptoethanol] and then applied to an ÄKTApurifier UPC-100 purification system (GE Healthcare, Chicago, IL, United States) equipped with a Source Q column (GE Healthcare, Chicago, IL, United States) at 4°C, using Washing Buffer A [20 mM Tris-HCl pH = 8.0, 6 mM $MgCl_2$, and 1 mM β-mercaptoethanol], Washing Buffer B [20 mM Tris-HCl pH = 8.0, 1 M NaCl, 6 mM $MgCl_2$, and 1 mM β-mercaptoethanol], and an interception tube (Merck-Millipore, Burlington, MA, United States). Next, the concentrated solution was centrifuged at 13,000 rpm and 4°C for 10 min, and the resultant supernatant was loaded onto a SuperdexTM 200 column (GE Healthcare, Chicago, IL, United States) that had been previously installed onto the ÄKTApurifier UPC-100 purification system, followed by washing with the washing buffer [40 mM HEPES pH = 7.5, 100 mM NaCl, 2 mM $MgCl_2$, and 1 mM β-mercaptoethanol] at the rate of 0.5 mL/min. The samples were examined using SDS-PAGE and then stored at −80°C. The identity of the protein sample was confirmed using a mass spectrometer (LTQ Orbitrap XL, Thermo Fisher, Waltham, MA, United States).

[1]https://www.bioinformatics.babraham.ac.uk/projects/fastqc/

[2]https://www.bioinformatics.babraham.ac.uk/projects/trim_galore/

[3]https://support.illumina.com/sequencing/sequencing_software/igenome.html

In vitro Catalytic Functional Assay

The purified cystathionine-γ-lyase protein (Cys3p) solution was measured for A_{280} by an Eppendorf BioSpectrometer® (Eppendorf, Hamburg, Germany Cat.: 6135000009) and the value was 2.3. Meanwhile, the Abs 0.1% of Cys3p was known of 0.611 on ExPaSy (Artimo et al., 2012). By these values, the concentration of the purified protein was identified as 89 μM. Consequently, for the catalysis assay, the purified Cys3p solution was diluted to 5 μM and incubated with 500 μM of SPRC or cystathionine at 37°C on a shaking incubator (ThermoMixer® C, Eppendorf, Hamburg, Germany Cat.: 5382000023) for the duration from 0 to 24 h. On the contrary, for the control assay of the inhibition of Cys3p, 500 μM of PAG (propargylglycine) was added into the mixture of 5 μM Cys3p and 500 μM SPRC, which served as the specific inhibitor to Cys3p. At each time point, a small volume was aliquoted from each sample and stored immediately at −20°C. The LC-MS/MS analysis methods for detecting SPRC, H_2S, and cystathionine described in a previous report were used (Tan et al., 2017).

Evolutionary Analysis of the Cystathionine-γ-Lyase of Multiple Species

The protein sequences of the cystathionine-γ-lyase of 12 species were retrieved from the protein database of NCBI (National Center of Biotechnology Information). The multiple alignment analysis was performed using COBALT (Constraint-based Multiple Alignment Tool) (Papadopoulos and Agarwala, 2007) on NCBI with default parameter settings. The consensus motifs were analyzed using ClustalΩ (Sievers et al., 2011) on EMBL (Li et al., 2015) with default parameter settings, and the generated result file from EMBL-ClustalΩ was opened and visualized in Jalview (Waterhouse et al., 2009). A phylogenetic tree in rooted format was also generated simultaneously from the EMBL-ClustalΩ using default parameter settings and subsequently visualized in Dendroscope (Huson et al., 2007; Huson and Scornavacca, 2012; Huson and Linz, 2018).

RESULTS

Emission of Intracellular H_2S Generated From Catabolized SPRC in Yeast

In order to elucidate the influence of H_2S on fungi, the S288C strain of budding yeast *S. cerevisiae* was employed as the model organism first to examine if H_2S could be generated during the catabolization of SPRC by the yeast and then to explore if any transcriptomic and phenotypic alterations occurred in the yeast when H_2S was served. After inoculation, the yeast cells were cultivated in the presence or absence of 2 mM SPRC for 16–48 h before harvest. After centrifugation of the harvested culture, the supernatant samples were collected and subjected to the mass-spectrometry measurement to detect SPRC and H_2S. As depicted in **Figure 1A**, the SPRC signal did not change in the yeast culture for 16 h after the inoculation, following which a substantial decrease was observed in the next 32 h with an 80% decline in the signal. The control group showed no such decrease, suggesting that SPRC was catabolized by the yeast cells, presumably during the exponential growth phase. Meanwhile, the signal of H_2S increased significantly during the same period (**Figure 1B**) in the SPRC-serving yeast cells, suggesting that the additionally elevated H_2S concentrations were linked with SPRC, which was the only extracellular source of sulfur, thereby confirming that the extra H_2S was derived intracellularly from the catabolism of SPRC within the yeast cells.

Yeast Growth Enhancement With SPRC-Generated H_2S

Although the results above have confirmed that H_2S is generated via SPRC catabolism, no previous studies have reported any potential phenotype alteration in the yeast upon the generation of H_2S. Therefore, in the present study, the growth curves of the yeast cells were measured in the presence or absence of SPRC. As depicted in **Figure 1C**, comparing to the control condition, the presence of SPRC enhanced the growth rate of yeast with the generation of H_2S, particularly at the working concentrations above 0.5 mM. This growth-enhancing effect was largely dose-dependent, with 2 mM of SPRC being the most effective concentration presenting the highest growth. Interestingly, when the concentration of SPRC was above 2 mM, the enhancement of growth was undermined. The growth enhancement began to appear at the time point of around 10 h, with the highest effect observed at 16 h, which lasted for approximately 10 h. In comparison, supplementation with NaHS, a sulfide salt with rapid and uncontrolled reactivity, exhibited only a minor growth-stimulation effect on the yeast cells (**Figure 1D**). Therefore, it was inferred that, as a catabolic product of SPRC, the generated H_2S was found accompanying the enhancement of the growth rate of yeast as a phenotypic alternation, while the exogenously-supplied H_2S could not achieve this effect.

SPRC-Generated H_2S Led to Elevated Expression of Genes Involved in Sulfur–Amino Acid Biosynthesis

After the confirmation of the phenotypic alteration in the yeast upon the generation of H_2S from SPRC, the transcriptomic analysis was performed to delineate the molecular mechanism underlying the yeast growth rate enhancement with the intracellular generation of H_2S. The cell culture of the S288C strain supplemented with or without 2 mM SPRC for 16 h before the transcriptome assay was used. As depicted in **Figure 2A**, a total of 270 genes with significant differences in the expression levels with $\log_2$(fold change) values larger than 0.585 and less than −0.585 ($p < 0.05$) were obtained, among which 162 genes were upregulated, while the remaining 108 genes were downregulated, implying that the generated H_2S from SPRC exerted the yeast growth enhancement effect mainly through the upregulated genes. This finding was further confirmed by the heatmap analysis (**Figure 2B**) and by the well-clustered triplicate samples of each group, in which the number of upregulated genes was larger than that of the downregulated genes upon the generation of H_2S.

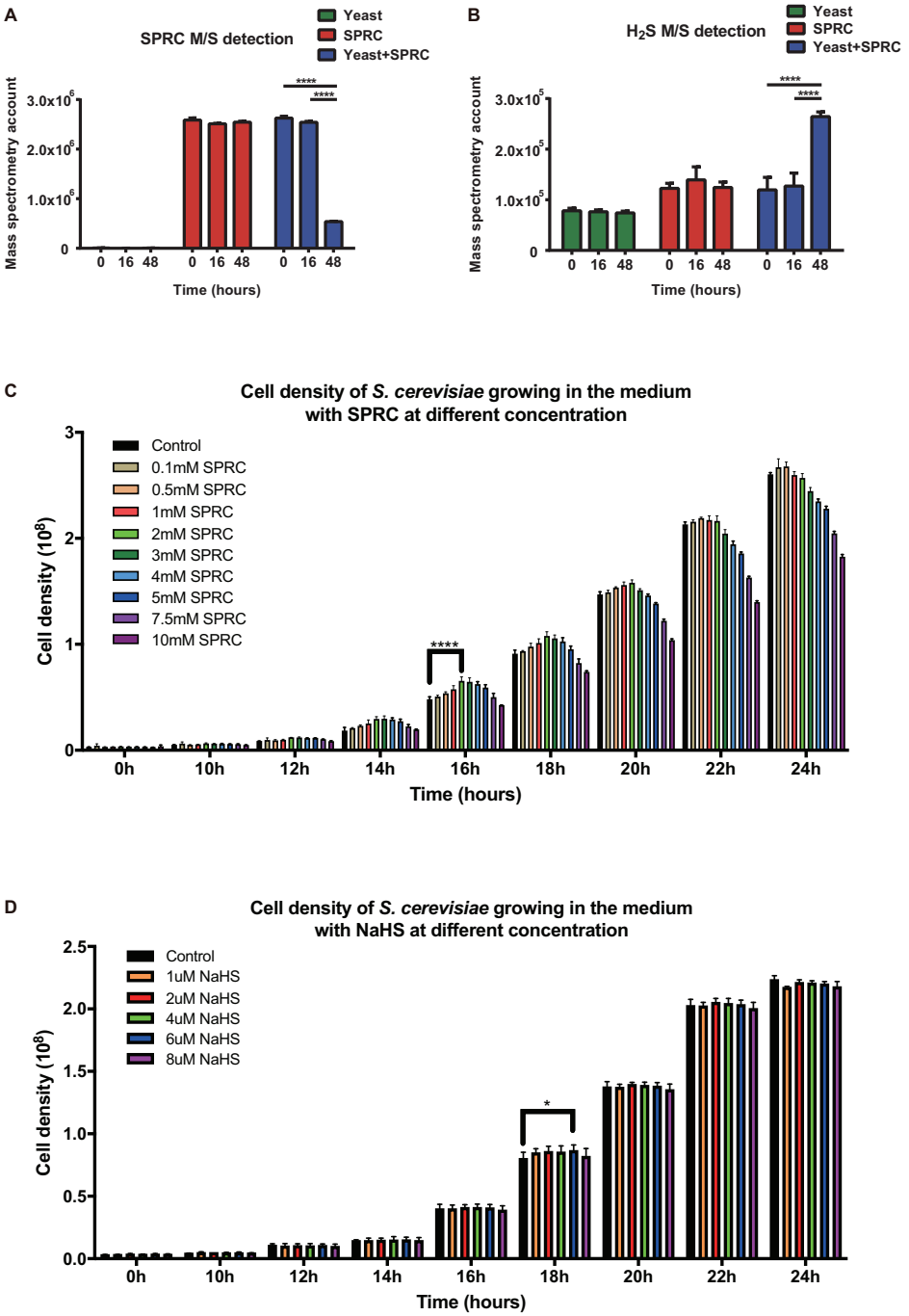

FIGURE 1 | Yeast capable of catalyzing SPRC (*S*-propargyl-cysteine) and emitting H_2S. **(A)** The mass spectrometry detection of SPRC shows the decreasing SPRC M/S signals when metabolized by the yeast cells. The horizontal axis shows the time group. The vertical axis shows the M/S signal counts. The data of triplicates was represented as the mean ± SD (Two-way ANOVA, *p*-values are of the 0 h group and 18 h in comparison to the 48 h group individually, $^{****}p \leq 0.0001$). The green bars show the SPRC signals in the supernatant SD medium when yeast cells were cultivated. The red bars show the SPRC signals in the supernatant SD medium without any yeast cells. The blue bars show the SPRC signals in the supernatant SD medium containing SPRC when yeast cells were cultivated. **(B)** The mass spectrometry detection of H_2S showed the increasing H_2S M/S signals when SPRC is metabolized by the yeast cells. The horizontal axis shows the time group. The vertical axis shows the M/S signal counts. The data of triplicates was represented as the mean ± SD (Two-way ANOVA, *p*-values are of the 0 h group and 18 h in comparison to the 48 h group individually, $^{****}p \leq 0.0001$). The green bars show the H_2S signals in the supernatant SD medium when yeast cells were cultivated. The red bars show the H_2S signals in the supernatant SD medium without any yeast cells. The blue bars show the H_2S signals in the supernatant SD medium containing SPRC when yeast cells were cultivated. **(C)** The growth rate of the yeast cells at 0–24 h with the 0.1–3 mM SPRC (Two-way ANOVA, *p*-values are of the 0.5–3.0 mM SPRC group in comparison to the 0.1 mM SPRC group individually, $^{****}p \leq 0.0001$). **(D)** The growth rate of the yeast cells at 0–24 h with the 1–8 μM NaHS (Two-way ANOVA, *p*-values are of the 2–8 μM NaHS group in comparison to the 1 μM NaHS group individually, $^{*}p \leq 0.1$).

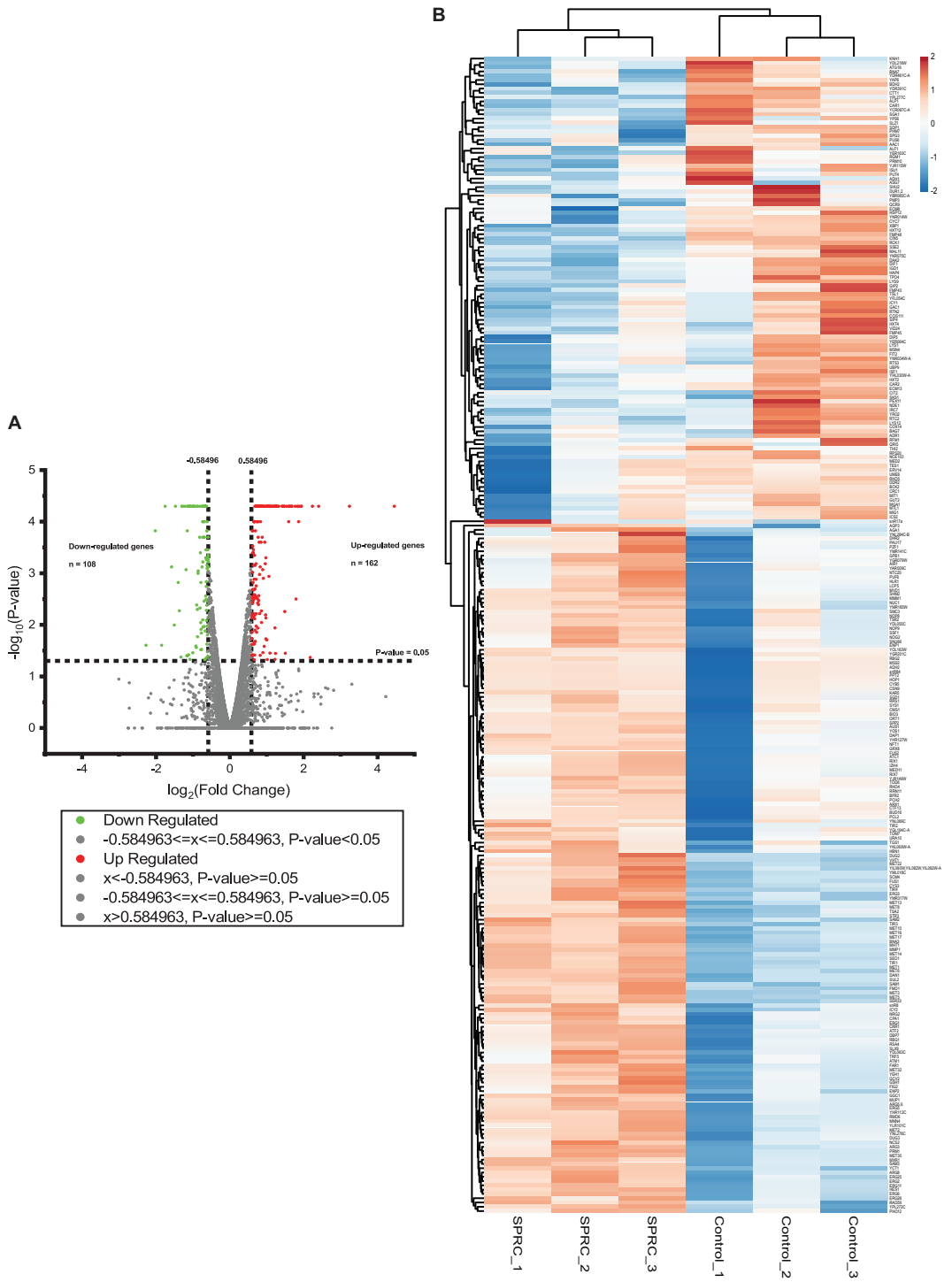

FIGURE 2 | The volcano plot and the heatmap of differentially expressed genes in response to SPRC display that SPRC-upregulated genes are more than SPRC-downregulated genes. **(A)** The volcano plot represents the differentially expressed genes under the SPRC treatment comparing with the control condition. The horizontal axis shows the value of $\log_2$(fold change) of each gene which is represented by a spot, and the cut-off values are set to ±0.584963. The vertical axis shows the $-\log_{10}$(*p*-value) of each gene calculated by the Cuffdiff program, and the cut-off value is set to *p*-value = 0.05. The number of SPRC-upregulated genes colored in red is 162, whose *p*-values are smaller than 0.05. The number of SPRC-downregulated genes colored in green is 108, whose *p*-values are smaller than 0.05. **(B)** The heatmap of the enrichment of the differentially expressed genes under the SPRC treatment comparing with the control condition whose $\log_2$(fold changes) are larger than +0.585 or smaller than –0.585. The enrichment illustrates a good triplicates situation and more SPRC-upregulated genes than SPRC-downregulated genes. The legend of the color bar displays the $\log_2$ values of the fold change of each replicate of each gene, from –2 to 2.

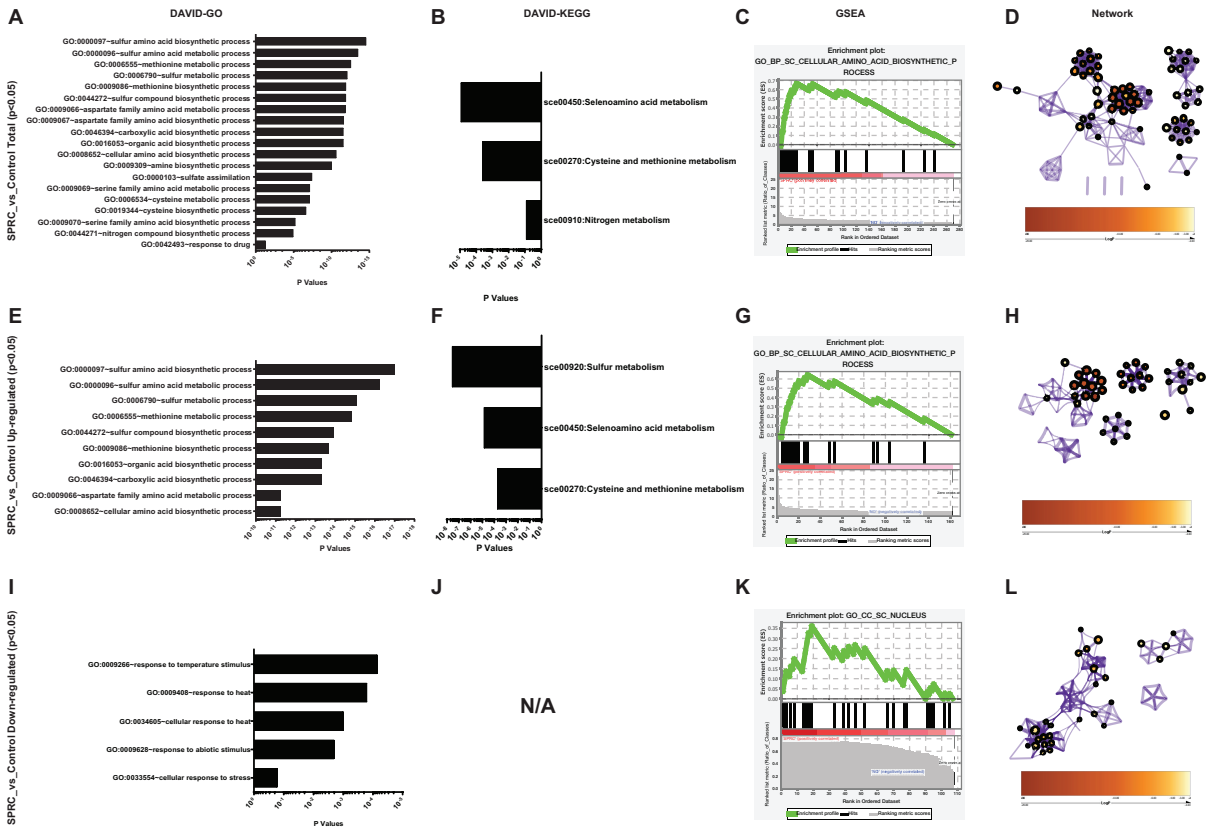

FIGURE 3 | *S*-propargyl-cysteine (SPRC) elevating the expression of the genes involved in sulfur-amino-acid biosynthesis. **(A)** DAVID-GO analysis result of the total SPRC-significantly-influenced genes highlights the "GO:0000097" term of "sulfur amino acid biosynthetic process." The horizontal axis shows the *p*-values of each enriched GO terms. **(B)** DAVID-KEGG analysis result of the total SPRC-significantly-influenced genes highlights the "sce00450" pathway of "Selenoamino acid metabolism." The horizontal axis shows the *p*-values of each KEGG pathway. **(C)** The GSEA result showed the total SPRC-significantly-influenced genes are enriched into the Top-1-ranked GO term of "cellular amino acid biosynthetic process" with the enrichment score of 0.669408 and the nominal *p*-value of 0.00101833. **(D)** In Metascape-generated GO network, the total SPRC-significantly-influenced genes are mainly enriched in the GO terms related to sulfur-amino-acid biosynthetic process with a relatively small logP-value (**Table 1**). **(E)** DAVID-GO analysis result of the SPRC-upregulated genes. **(F)** DAVID-KEGG analysis result of the SPRC-upregulated genes. **(G)** The GSEA result showed the SPRC-upregulated genes. **(H)** In Metascape-generated GO network, the SPRC-upregulated are mainly enriched in the GO terms related to sulfur-amino-acid biosynthetic process with a small logP-value (**Table 2**). **(I)** DAVID-GO analysis result of the SPRC-downregulated genes. **(J)** DAVID-KEGG analysis result of the SPRC-downregulated genes fail to be enriched in any KEGG pathway even when the "classification stringency" is set to "lowest," which implies that the SPRC-downregulated genes are not pathway-directed. **(K)** The GSEA result showed the SPRC-downregulated genes. **(L)** In Metascape-generated GO network, the SPRC-downregulated are mainly enriched in the GO terms related to energy and oxidation processes with a relatively large logP-values (**Table 3**).

Using these 270 genes with significant differences in their expression levels, including both the upregulated and downregulated genes (**Supplementary Table 5**), the functional information analysis was performed using DAVID-Gene Ontology. As illustrated in **Figure 3A**, these genes were significantly enriched into the sulfur-amino-acid-related GO terms, including the "sulfur amino acid biosynthetic process" and the "sulfur amino acid metabolic process." A similar conclusion was reached in the DAVID-KEGG pathway analysis, in which the "seleno-amino acid metabolism" and the "cysteine and methionine metabolism" were significantly enriched (**Figure 3B**). Besides, these 270 genes together with their expression values were processed using GSEA, which revealed "cellular amino acid biosynthetic process" as the top-enriched GO term with a high enrichment score of over 0.6, thereby corroborating the results of the DAVID analysis (**Figure 3C**). The above results were supported by an additional analysis conducted using Metascape, in which the top 10 nodes in the darkest red with the highest *p*-values, including the node number 1–9 and node 97, were clustered within the networks, including the leading GO terms of "sulfur-amino-acids metabolic process" and "sulfur-compound biosynthetic process" with low *p*-values (**Figure 3D** and **Table 1**). Furthermore, all 10 enriched terms were related to the amino acid biological process (**Figure 3D** and **Table 1**).

In particular, the 162 upregulated genes among the total 270 genes were analyzed to specifically reveal the properties of the transcriptomic upregulation of these genes. The "sulfur amino acid biosynthetic process" remained the top-enriched GO term in this analysis as well (**Figure 3E**), similar to the one in the analysis of the total number of genes (**Figure 3A**).

TABLE 1 | The information of the nudes clustered in **Figure 3D**.

Nude ID	#Gene hit list	Description	GO term	Group ID	LogP	STDV	*Z* score
97	21	Sulfur amino acid metabolic process	GO:0000096	1	−15.4057	1.774673	12.98227
1	31	Sulfur compound metabolic process	GO:0006790	1	−13.9626	2.10796	10.57599
2	35	Alpha-amino acid metabolic process	GO:1901605	1	−13.8483	2.218996	10.18649
3	18	Methionine metabolic process	GO:0006555	1	−13.8105	1.653897	12.45484
4	17	Sulfur amino acid biosynthetic process	GO:0000097	1	−12.7771	1.610805	11.86046
5	19	Aspartate family amino acid biosynthetic process	GO:0009067	1	−12.5129	1.695504	11.19716
6	21	Aspartate family amino acid metabolic process	GO:0009066	1	−12.4005	1.774673	10.7511
7	16	Methionine biosynthetic process	GO:0009086	1	−12.1777	1.566104	11.6122
8	27	Alpha-amino acid biosynthetic process	GO:1901607	1	−12.1738	1.985399	9.84303
9	22	Sulfur compound biosynthetic process	GO:0044272	1	−12.1097	1.812413	10.38678

TABLE 2 | The information of the nudes clustered in **Figure 3H**.

Nude ID	#Gene hit list	Description	GO term	Group ID	LogP	STDV	*Z* score
2	20	Sulfur amino acid metabolic process	GO:0000096	1	−18.4759	2.758578	16.33831
63	17	Methionine metabolic process	GO:0006555	1	−16.1884	2.57224	15.49488
62	26	Sulfur compound metabolic process	GO:0006790	1	−15.0493	3.072389	11.97794
61	16	Sulfur amino acid biosynthetic process	GO:0000097	1	−14.9489	2.504733	14.7213
60	20	Sulfur compound biosynthetic process	GO:0044272	1	−14.2937	2.758578	12.68996
59	15	Methionine biosynthetic process	GO:0009086	1	−14.1238	2.434163	14.34356
58	28	Alpha-amino acid metabolic process	GO:1901605	1	−14.0886	3.162759	11.02434
57	22	Alpha-amino acid biosynthetic process	GO:1901607	1	−12.459	2.87105	10.77938
56	30	Cellular amino acid metabolic process	GO:0006520	1	−12.1864	3.247042	9.588036
55	17	Aspartate family amino acid metabolic process	GO:0009066	1	−11.9671	2.57224	11.48193

TABLE 3 | The information of the nudes clustered in **Figure 3L**.

Nude ID	#Gene hit list	Description	GO term	Group ID	LogP	STDV	*Z* score
5	13	Energy derivation by oxidation of organic compounds	GO:0015980	1	−5.63141	3.492238	6.400214
69	21	Oxidation-reduction process	GO:0055114	1	−4.81791	4.219232	5.068667
68	13	Generation of precursor metabolites and energy	GO:0006091	1	−4.30953	3.492238	5.115331
67	6	Cellular respiration	GO:0045333	1	−2.01229	2.470529	3.135611

However, the *p*-values of the enriched GO terms of the upregulated genes were much smaller than the ones of the total 270 genes, which implied higher credibility of the result for the GO terms of the 162 upregulated genes. A similar phenomenon was demonstrated in the KEGG analysis of the enriched pathways of upregulated genes (**Figure 3F**), with the obtained smaller *p*-values being more convincing than the larger ones obtained in the analysis of total genes (**Figure 3B**). The subsequent GSEA analysis of the upregulated genes (**Figure 3G**) also highlighted the "cellular amino acid biosynthetic process" as the top-enriched GO term, thereby corroborating the GSEA result obtained in the analysis of the total 270 genes (**Figure 3C**). These 162 genes were then processed in the Metascape network analysis, in which they were enriched to the "sulfur amino acid metabolic process" pathway (**Figure 3H** and **Table 2**) with a much smaller *p*-value compared to the one generated from the analysis of total genes (**Figure 3D** and **Table 1**), implying higher credibility of the enrichment result for the SPRC-upregulated genes compared to that for the total genes.

In contrast to the above results, the analyzed 108 downregulated genes presented opposite ones. These genes were enriched into certain GO terms such as "response to temperature stimulus" (**Figure 3I**) with considerably high *p*-values compared to those obtained from the total genes, particularly those obtained from upregulated genes. Furthermore, the KEGG terms of the downregulated genes simply failed to be enriched onto any pathway even when the "classification stringency" settings in the DAVID system were set to "lowest," which implied that the downregulated genes had less significant biological importance compared to the upregulated ones upon the generation of H_2S (**Figure 3J**). This finding was supported by the GSEA analysis with "CC_SC_nucleus" as the top-enriched GO term with a low enrichment score and a low ranked list metric (**Figure 3K**). The network analysis also illustrated the enriched nodes of temperature-stimulus-related in the light color region of higher *p*-values (**Figure 3L**). In general, the H_2S generation from SPRC catabolism in yeast occurred with the upregulation of the expressions of genes in sulfur amino acid-related pathways,

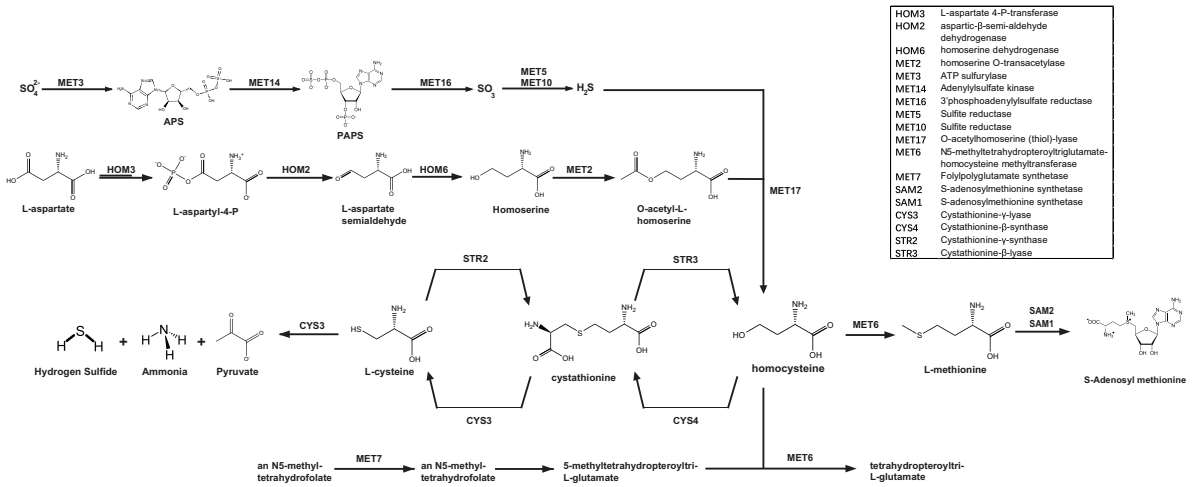

FIGURE 4 | "Sulfur amino acid biosynthesis superpathway" of *S. cerevisiae*. The re-organized sulfur amino acid biosynthesis superpathway of *S. cerevisiae* illustrates the sulfur metabolism in the yeast cells. The inorganic sulfur is initially metabolized in the sub-branch pathway by *MET3* and the subsequent enzyme genes (*MET14*, *MET16*, *MET5*, and *MET10*) and then generate H_2S, which will be synthesized to be homocysteine synthesized from the non-sulfur L-aspartate in the sub-branch pathway by *HOM3* and the downstream enzyme genes (*HOM2*, *HOM6*, *MET2*, and *MET17*). For the sub-branch pathway begun with *MET7*, the structure of the initial substrate, an N^5-methyl-tetrahydrofolate, is far from the one of SPRC, and this sub-branch generate no H_2S. Whereas the substrates in the sub-branch pathway (*CYS3*, *CYS4*, *STR2*, and *STR3*) are all sulfur-amino-acids and are structurally similar to SPRC, and also whereas *CYS3* is capable to catalyze L-cysteine to generate H_2S, this sub-branch is expected to be the metabolism pathway to SPRC and CYS3 is selected to be the catabolic enzyme candidate to SPRC for the consequent assays.

which was accompanied by the phenotype of enhanced growth rate in the yeast.

H_2S Presumed to Be Generated Because of the Catabolic Action of Cystathionine-γ-Lyase, a Potential Enzyme for SPRC Metabolism

Although the analyses conducted in the present study revealed that the sulfur amino acid-related pathways were upregulated upon H_2S generation from SPRC catabolism, a metabolic map based on the *Saccharomyces* Genome Database (SGD) is summarized in **Figure 4** for comprehension, as the sulfur amino acid biosynthesis in *S. cerevisiae* involves numerous enzymes required for *de novo* biosynthesis of sulfur amino acids as well as for transferring the organic sulfur among the metabolites. As illustrated in the upper portion of **Figure 4**, only a reduced sulfur atom can be incorporated into carbon chains via sulfate adenylation to lower the electron potential and a further reduction by the oxidation of NADPH. Since this process of assimilation aimed at reducing the electro-redox state of the inorganic sulfate, the enzymes involved in the activation of this process were excluded from being the SPRC-consuming protein candidates. Subsequently, S^{2-} could be incorporated into four-carbon chain homocysteine, which is interconverted by the *trans*-sulfuration pathway into L-cysteine via the intermediary formation of cystathionine. As depicted in **Figure 4**, SPRC is an analog of L-cysteine, suggesting that cystathionine-γ-lyase could be responsible for catabolizing SPRC and generating the H_2S detected in the yeast. Cystathionine-γ-lyase is one of the three enzymes (cystathionine β-synthase and 3-MST being the other two enzymes) involved in producing H_2S (Yu et al., 2014). In addition to catalyzing L-cystathionine into L-cysteine (EC 4.4.1.1, ID: RXN-15130), cystathionine-γ-lyase causes the further breakdown of L-cysteine into pyruvate, NH_3, and H_2S (EC 4.4.1.1/4.4.1.28 ID: LCYSDESULF-RXN). Therefore, cystathionine-γ-lyase was preliminarily considered for application as the catabolic enzyme, as it was presumed to be involved in the generation of H_2S by catabolizing SPRC and thereby enhancing the yeast growth rate.

H_2S Confirmed to Be Generated Through the Catabolic Action of Yeast Cystathionine-γ-Lyase

The cystathionine-γ-lyase of *S. cerevisiae* (abbreviated as *CYS3*) was expressed in *E. coli* (**Supplementary Figures 2–5**), purified, and then subjected to mass spectrometry identification (depicted in **Figure 5A** and **Supplementary Table 4**). Although Cys3p catalyzed both cystathionine and L-cysteine as substrates, the canonical one, i.e., cystathionine, was selected to be used as the control molecule for evaluating the enzymatic activity (Yamagata et al., 1993). In order to determine whether the purified Cys3p retained its enzymatic function, the catabolism of cystathionine was monitored in the presence or absence of Cys3p. As illustrated in **Figures 5B,C**, in the absence of Cys3p, cystathionine was chemically-stable, while α-ketobutyric acid, a well-recognized product of Cys3p catalysis on cystathionine (Yamagata et al., 1993), was undetectable. However, when Cys3p was added, the M/S signals of cystathionine decreased rapidly, while the concentration of α-ketobutyric acid increased, demonstrating the functional catalytic enzyme activity of purified Cys3p. Subsequently, SPRC degradation and H_2S generation could be

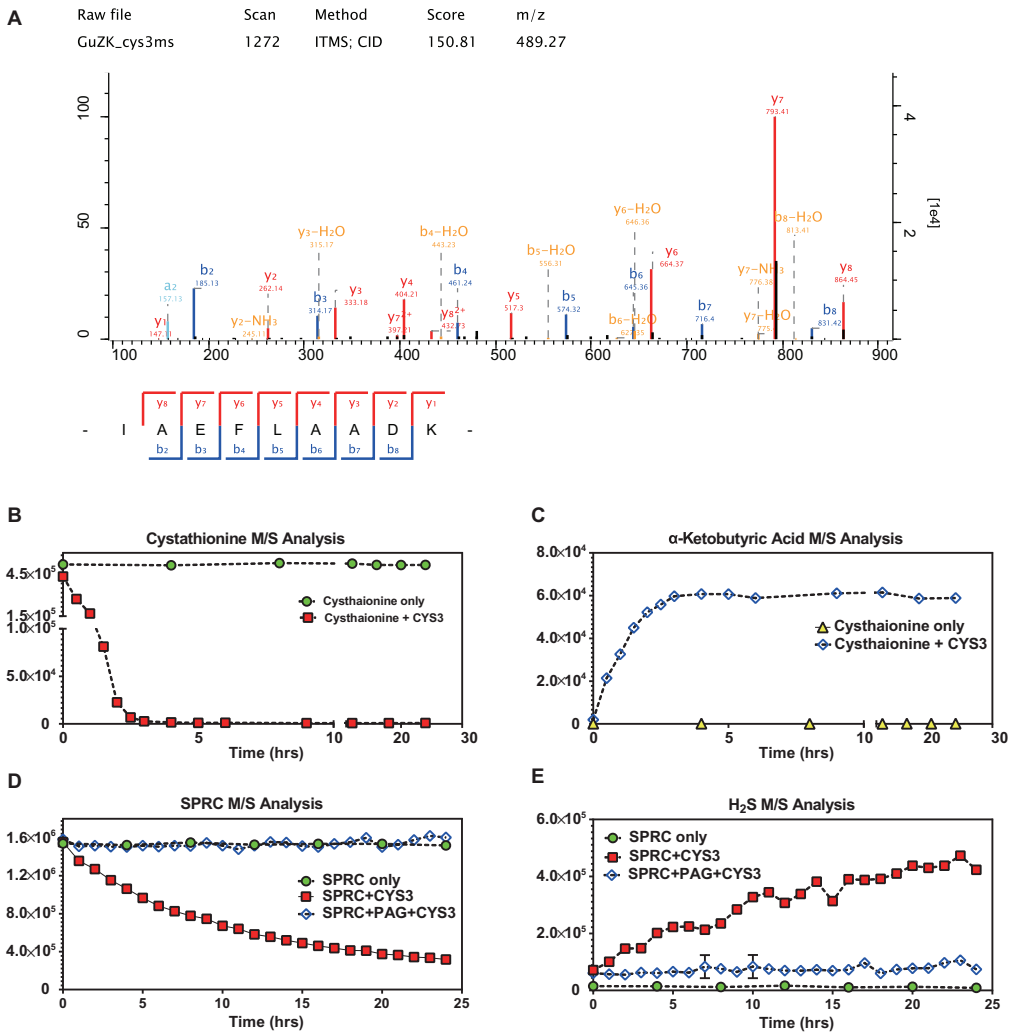

FIGURE 5 | *S*-propargyl-cysteine catalyzed by yeast cystathionine-γ-lyase. **(A)** The mass spectrometry analysis confirmed the identity of Cys3p (cystathionine-γ-lyase in S288C) purified from *E. coli* lysis. The sequence of the peptide of Cys3p has been identified as "IAEFLAADK," which matched to the sequence of Cys3p by NCBI-BLASTp. The horizontal axis shows the molecular weight, and the vertical axis shows the signal intensity. **(B)** The mass spectrometry analysis showed relatively rapid decreasing signals of cystathionine when cystathionine was being catalyzed by purified Cys3p from 0 to 24 h, and non-decreasing signals of cystathionine without the Cys3p incubation. **(C)** The mass spectrometry analysis showed relatively rapid increasing signals of α-ketobutyric acid when cystathionine was being catalyzed by purified Cys3p from 0 to 24 h, and non-increasing signals of α-ketobutyric acid without the Cys3p incubation. **(D)** The mass spectrometry analysis showed relatively stable decreasing signals of SPRC when SPRC was being catalyzed by purified Cys3p from 0 to 24 h, and non-decreasing signals of SPRC when the catalysis inhibited by PAG. **(E)** The mass spectrometry analysis showed relatively stable increasing signals of H_2S when SPRC was being catalyzed by purified Cys3p from 0 to 24 h, and non-increasing signals of H_2S when the catalysis inhibited by PAG. **(B–E)** The horizontal axes indicate the incubation time (0–24 h). The vertical axes indicate the M/S signals of the detected molecules, including cystathionine, α-ketobutyric acid, SPRC and H_2S. The data of triplicates was represented as mean ± SD.

observed upon Cys3p serving (**Figures 5D,E**), in contrast to the absence of it. Moreover, the Cys3p inhibitor PAG could specifically inhibit such enzymatic activity (Wang et al., 2009), which again confirmed the enzymatic activity of purified Cys3p. Taken together, these results confirmed the additional generation of H_2S upon the service of Cys3p *in vitro*, suggesting that Cys3p was an H_2S-generating enzyme in yeast, which acted by catalyzing the substrate SPRC, and implying that the growth rate of yeast could be reduced by inhibiting the activity of this enzyme.

Cystathionine-γ-Lyase Identified as a Potential Enzyme for Inhibition Owing to Its High Conservation Throughout Evolution

In order to obtain further insight into the possibility of using cystathionine-γ-lyase as a metabolic enzyme candidate for suppressing the generation of H_2S and inhibiting fungal growth rate, the NCBI-COBALT (Constraint-based Multiple Alignment Tool) analysis was performed to examine the conservation of

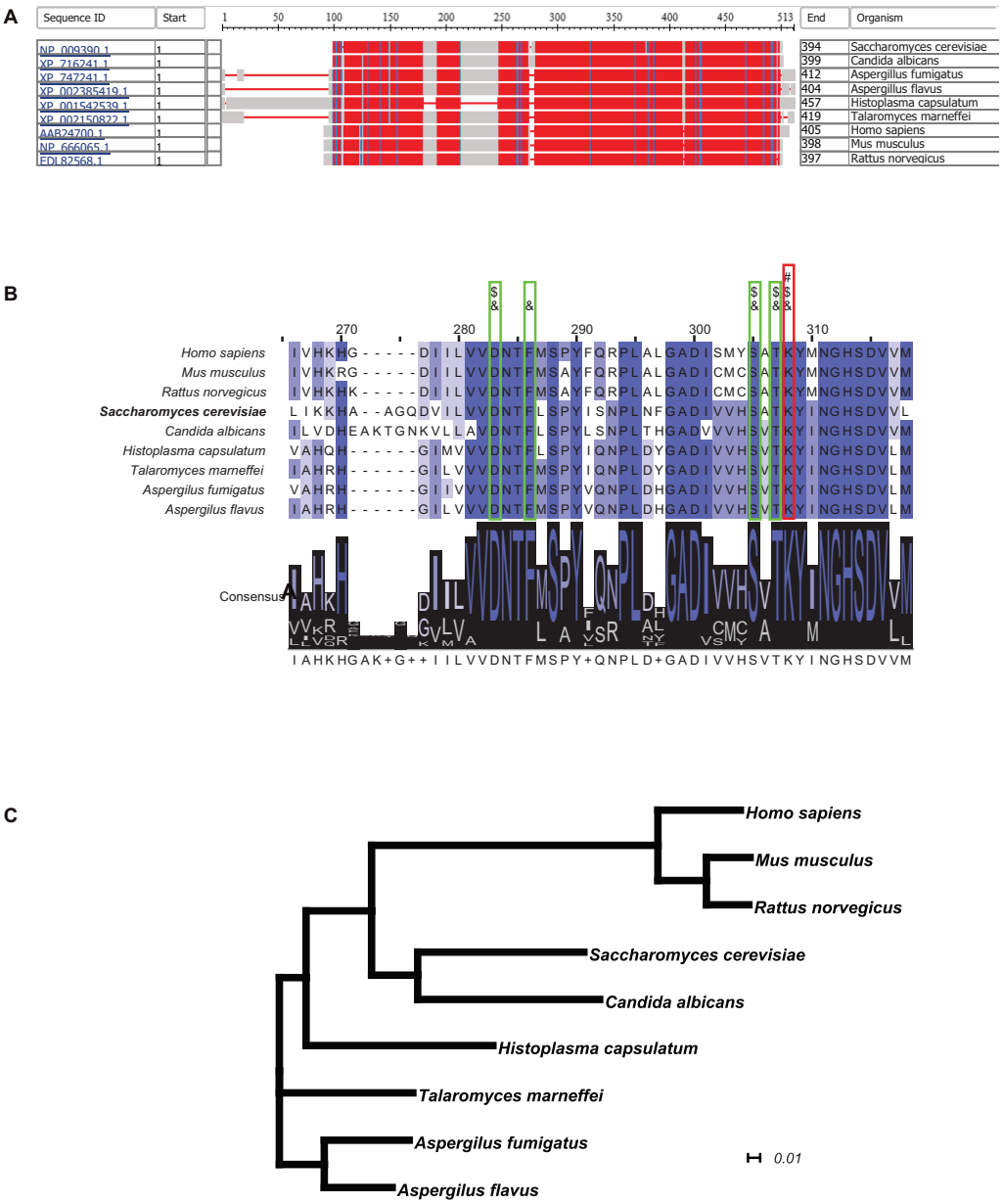

FIGURE 6 | Cystathionine-γ-lyase is a highly conserved enzyme throughout evolution. **(A)** The NCBI-COBALT (Constraint-based Multiple Alignment Tool) alignment display cystathionine-γ-lyase homologs from multiple species. The red parts show the highly conserved domains and the blue parts for less conserved domains, gray parts for no consensus of conservation. **(B)** The Conserved Protein Domain Family alignment revealed the key catalytic residues. The PID (Percentage Identity Color) codes for amino acid residue are as following: darkest cyan: the residues according to the percentage of the residues in each column that agree with the consensus sequence of a level of 80% or more; middle cyan between 60 and 80%; lightest cyan between 40 and 60%; no color when the consensus level below 40%. A "#" symbol represents a Schiff-base forming lysine residue at which PLP forms an internal aldimine bond. An "&" symbol represents an adjacent residue forming a hydrogen bond with the phosphate group of PLP for anchoring. A "$" symbol represents an adjacent residue involved in substrate-cofactor accommodation. **(C)** The phylogenetic analysis showed the evolutionary conservatism of the cystathionine-γ-lyase among the 12 species. The plotting scale shows the evolutionary distance of 0.1 K_{nuc}.

cystathionine-γ-lyase across different species. The full-length protein sequences of cystathionine-γ-lyase from 9 species, including 6 of pathogenic fungi and 3 of mammals, were retrieved and displayed in a bird's-eye scope. In **Figure 6A**, the parts with high degrees of sequence homology are depicted in red, while the parts with a relatively low level of homology are depicted in blue or gray. As hypothesized, cystathionine-γ-lyase was a highly conserved metabolic protein, as evidenced by all species sharing large parts of the protein sequence of this enzyme as the conserved domains. The sequences of the enzyme in the nine species were further clustered using the ClustalΩ algorithm, generating the consensus across the species, which are depicted in **Figure 6B**. The Schiff-base-forming lysine residue of *S. cerevisiae* labeled "#" (Messerschmidt et al., 2003) is the site at which PLP formed an internal aldimine bond that was invariably conserved across all nine species.

In addition, the adjacent residues forming hydrogen bonds with the phosphate group of PLP for anchoring were labeled "&" (Messerschmidt et al., 2003), and the ones involved in the substrate–cofactor accommodation were labeled "$" (Clausen et al., 1996). These residues were also completely identical among all nine species, demonstrating the motifs conserved through evolution. Moreover, for visualizing the evolutionary association among the selected species, a phylogenetic tree was generated using CLUSTALW (**Figure 6C**), which illustrated a narrow range of evolutionary distances of cystathionine-γ-lyase, particularly among the fungal species. In summary, cystathionine-γ-lyase was observed to be highly conserved across species, which suggested the importance of this enzyme in biological activities, particularly in those involved in the regulation of the growth of pathogenic fungi via influencing the sulfur metabolism for the intracellular generation of H_2S. In addition to producing the phenotype of yeast growth enhancement, the conservation of cystathionine-γ-lyase is expected to be useful for developing anti-fungal drugs in the future by serving as an enzyme candidate for inhibition.

DISCUSSION

Fungal infections lead to millions of cases of infection and deaths every year. The growth of fungi is subject to several factors, one of which is gaseous signaling molecules. H_2S is a well-recognized and extensively studied gaseous signaling molecule that ranks third after the signaling molecules NO and CO. H_2S is reported to be involved in physiological functions related to cardiovascular protection, such as homeostasis and smooth muscle relaxation. Moreover, since H_2S generation is a common phenomenon during the fermentation of yeast, it was reasonable to hypothesize that H_2S possibly regulates the growth of yeast and/or the other species of fungi. However, studies on the potential effect of H_2S on fungi encounters two limitations. One is that the H_2S generated from sulfide salts, such as NaHS, is gaseous and unstable for using dosage control, and owing to the exogenous generation, this H_2S exhibits properties different from the ones described for the endogenously-generated H_2S during yeast fermentation. The other limitation is that little is known regarding the effect of the phenotypic or transcriptomic alternations on the fungal growth enhancement by H_2S. Therefore, in the present study, SPRC, which is a stable donor that gently produces H_2S intracellularly under catalytic action *in vivo*, was employed to unravel the mechanism operating in the budding yeast *S. cerevisiae* S288C that was used as a fungal model.

The results demonstrated that the growth rate of yeast was enhanced upon the intracellular generation of H_2S, while the exogenously served H_2S offered little contribution. In addition, the transcriptomic study preliminarily revealed that the intracellularly-generated H_2S was produced with the elevation of the expression levels of the genes associated with the metabolism of cysteine-like substrates in the sulfur-amino-biosynthesis metabolism pathway. Finally, Cys3p was revealed and confirmed to be capable of catalyzing SPRC for H_2S production *in vitro*, which led to the inference that *CYS3* could serve to influences the growth rate of yeast and even that of the other fungi by regulating the sulfur metabolism in these fungi. These findings contribute a possibility to the pharmacological industry that *CYS3* has become worth of the development of anti-fungal drugs against fungal infections and providing relief to patients with fungal infections and diseases.

DATA AVAILABILITY STATEMENT

The datasets generated for this study can be found in online repositories. The names of the repository/repositories and accession number(s) can be found below: https://www.ncbi.nlm.nih.gov/, PRJNA714796.

AUTHOR CONTRIBUTIONS

ZG designed the total topic and all the experiments and took in charge of almost all the experiments and the data analyses. YS took in charge of the purification of Cys3p of budding yeast. FW took in charge of the direction on the data analyses. XW took in charge of the manuscript preparation. All the authors contributed to the article and approved the submitted version.

FUNDING

The study was funded in part by a grant from the National Key Basic Research Project of China [grant number: 2013CB531603]. This work was supported by Key Clinical Specialty Discipline Construction Program of Fuzhou (201807111) and Clinical Medicine Center Construction Program of Fuzhou (2018080309) to XW.

ACKNOWLEDGMENTS

We are greatly indebted to Yizhun Zhu in the School of Pharmacy of Macau University of Science and Technology for kindly offering SPRC as a H_2S donor.

SUPPLEMENTARY MATERIAL

The Supplementary Material for this article can be found online at: https://www.frontiersin.org/articles/10.3389/fmicb.2021.679563/full#supplementary-material

REFERENCES

Abe, K., and Kimura, H. (1996). The possible role of hydrogen sulfide as an endogenous neuromodulator. *J. Neurosci.* 16, 1066–1071. doi: 10.1523/jneurosci.16-03-01066.1996

Artimo, P., Jonnalagedda, M., Arnold, K., Baratin, D., Csardi, G., de Castro, E., et al. (2012). ExPASy: SIB bioinformatics resource portal. *Nucleic Acids Res.* 40, W597–W603.

Cheng, J., Yang, H., Fang, J., Ma, L., Gong, R., Wang, P., et al. (2015). Molecular mechanism for USP7-mediated

DNMT1 stabilization by acetylation. *Nat. Commun.* 6:7023.

Clausen, T., Huber, R., Laber, B., Pohlenz, H. D., and Messerschmidt, A. (1996). Crystal structure of the pyridoxal-5'-phosphate dependent cystathionine beta-lyase from *Escherichia coli* at 1.83 A. *J. Mol. Biol.* 262, 202–224.

Denoth Lippuner, A., Julou, T., and Barral, Y. (2014). Budding yeast as a model organism to study the effects of age. *FEMS Microbiol. Rev.* 38, 300–325. doi: 10.1111/1574-6976.12060

Hosoki, R., Matsuki, N., and Kimura., H. (1997). The possible role of hydrogen sulfide as an endogenous smooth muscle relaxant in synergy with nitric oxide. *Biochem. Biophys. Res. Commun.* 237, 527–531. doi: 10.1006/bbrc.1997.6878

Huang, C. W., Walker, M. E., Fedrizzi, B., Gardner, R. C., and Jiranek, V. (2017). Hydrogen sulfide and its roles in Saccharomyces cerevisiae in a winemaking context. *FEMS Yeast Res.* 17:fox058.

Huang da, W., Sherman, B. T., and Lempicki, R. A. (2009a). Bioinformatics enrichment tools: paths toward the comprehensive functional analysis of large gene lists. *Nucleic Acids Res.* 37, 1–13. doi: 10.1093/nar/gkn923

Huang da, W., Sherman, B. T., and Lempicki, R. A. (2009b). Systematic and integrative analysis of large gene lists using DAVID bioinformatics resources. *Nat. Protoc.* 4, 44–57. doi: 10.1038/nprot.2008.211

Huo, J., Huang, D., Zhang, J., Fang, H., Wang, B., Wang, C., et al. (2018). Hydrogen Sulfide: a Gaseous Molecule in Postharvest Freshness. *Front. Plant Sci.* 9:1172. doi: 10.3389/fpls.2018.01172

Huson, D. H., and Linz, S. (2018). Autumn Algorithm-Computation of Hybridization Networks for Realistic Phylogenetic Trees. *IEEE/ACM Trans. Comput. Biol. Bioinform.* 15, 398–410. doi: 10.1109/tcbb.2016.2537326

Huson, D. H., Richter, D. C., Rausch, C., Dezulian, T., Franz, M., and Rupp, R. (2007). Dendroscope: an interactive viewer for large phylogenetic trees. *BMC Bioinformatics* 8:460. doi: 10.1186/1471-2105-8-460

Huson, D. H., and Scornavacca, C. (2012). Dendroscope 3: an interactive tool for rooted phylogenetic trees and networks. *Syst. Biol.* 61, 1061–1067. doi: 10.1093/sysbio/sys062

Kimura, Y., and Kimura, H. (2004). Hydrogen sulfide protects neurons from oxidative stress. *FASEB J.* 18, 1165–1167. doi: 10.1096/fj.04-1815fje

Köhler, J. R., Hube, B., Puccia, R., Casadevall, A., and Perfect, J. R. (2017).Fungi that infect humans. *Microbiol. Spectr.* 5, 5.3.08. doi: 10.1128/microbiolspec.FUNK-0014-2016

Krück, S., Mittapalli, V. R., Pröls, F., and Scaal, M. (2009). Cystathionine gamma-lyase expression during avian embryogenesis. *J. Anat.* 215, 170–175. doi: 10.1111/j.1469-7580.2009.01092.x

Li, L., Bhatia, M., Zhu, Y. Z., Zhu, Y. C., Ramnath, R. D., Wang, Z. J., et al. (2005). Hydrogen sulfide is a novel mediator of lipopolysaccharide-induced inflammation in the mouse. *FASEB J.* 19, 1196–1198. doi: 10.1096/fj.04-3583fje

Li, L., Salto-Tellez, M., Tan, C.-H., Whiteman, M., and Moore, P. K. (2009). GYY4137, a novel hydrogen sulfide-releasing molecule, protects against endotoxic shock in the rat. *Free Radic. Biol. Med.* 47, 103–113. doi: 10.1016/j.freeradbiomed.2009.04.014

Li, W., Cowley, A., Uludag, M., Gur, T., McWilliam, H., Squizzato, S., et al. (2015). The EMBL-EBI bioinformatics web and programmatic tools framework. *Nucleic Acids Res.* 43, W580–W584.

Lloyd, D. (2006). Hydrogen sulfide: clandestine microbial messenger?. *Trends Microbiol.* 14, 456–462. doi: 10.1016/j.tim.2006.08.003

Luan, H. F., Zhao, Z. B., Zhao, Q. H., Zhu, P., Xiu, M. Y., and Ji, Y. (2012). Hydrogen sulfide postconditioning protects isolated rat hearts against ischemia and reperfusion injury mediated by the JAK2/STAT3 survival pathway. *Braz. J. Med. Biol. Res.* 45, 898–905. doi: 10.1590/s0100-879x2012001000003

Messerschmidt, A., Worbs, M., Steegborn, C., Wahl, M. C., Huber, R., Laber, B., et al. (2003). Determinants of enzymatic specificity in the Cys-Met-metabolism PLP-dependent enzymes family: crystal structure of cystathionine gamma-lyase from yeast and intrafamiliar structure comparison. *Biol. Chem.* 384, 373–386.

Metsalu, T., and Vilo, J. (2015). ClustVis: a web tool for visualizing clustering of multivariate data using Principal Component Analysis and heatmap. *Nucleic Acids Res.* 43, W566–W570.

Mootha, V. K., Lindgren, C. M., Eriksson, K. F., Subramanian, A., Sihag, S., Lehar, J., et al. (2003). PGC-1alpha-responsive genes involved in oxidative phosphorylation are coordinately downregulated in human diabetes. *Nat. Genet.* 34, 267–273. doi: 10.1038/ng1180

Mulla, W., Zhu, J., and Li, R. (2014). Yeast: a simple model system to study complex phenomena of aneuploidy. *FEMS Microbiol. Rev.* 38, 201–212. doi: 10.1111/1574-6976.12048

Olas, B. (2015). Hydrogen sulfide in signaling pathways. *Clin. Chim. Acta* 439, 212–218. doi: 10.1016/j.cca.2014.10.037

Papadopoulos, J. S., and Agarwala, R. (2007). COBALT: constraint-based alignment tool for multiple protein sequences. *Bioinformatics* 23, 1073–1079. doi: 10.1093/bioinformatics/btm076

Romani, L. (2011). Immunity to fungal infections. *Nat. Rev. Immunol.* 11, 275–288.

Shannon, P., Markiel, A., Ozier, O., Baliga, N. S., Wang, J. T., Ramage, D., et al. (2003). Cytoscape: a software environment for integrated models of biomolecular interaction networks. *Genome Res.* 13, 2498–2504. doi: 10.1101/gr.1239303

Sievers, F., Wilm, A., Dineen, D., Gibson, T. J., Karplus, K., Li, W., et al. (2011). Fast, scalable generation of high-quality protein multiple sequence alignments using Clustal Omega. *Mol. Syst. Biol.* 7:539. doi: 10.1038/msb.2011.75

Subramanian, A., Tamayo, P., Mootha, V. K., Mukherjee, S., Ebert, B. L., Gillette, M. A., et al. (2005). Gene set enrichment analysis: a knowledge-based approach for interpreting genome-wide expression profiles. *Proc. Natl. Acad. Sci. U. S. A.* 102, 15545–15550. doi: 10.1073/pnas.0506580102

Tan, B., Jin, S., Sun, J., Gu, Z., Sun, X., Zhu, Y., et al. (2017). New method for quantification of gasotransmitter hydrogen sulfide in biological matrices by LC-MS/MS. *Sci. Rep.* 7:46278.

Trapnell, C., Roberts, A., Goff, L., Pertea, G., Kim, D., Kelley, D. R., et al. (2012). Differential gene and transcript expression analysis of RNA-seq experiments with TopHat and Cufflinks. *Nat. Protoc.* 7, 562–578. doi: 10.1038/nprot.2012.016

Tripathi, S., Pohl, M. O., Zhou, Y., Rodriguez-Frandsen, A., Wang, G., Stein, D. A., et al. (2015). Meta- and Orthogonal Integration of Influenza "OMICs" Data Defines a Role for UBR4 in Virus Budding. *Cell Host Microbe* 18, 723–735. doi: 10.1016/j.chom.2015.11.002

Vera Alvarez, R., Pongor, L. S., Mariño-Ramírez, L., and Landsman, D. (2018). TPMCalculator: one-step software to quantify mRNA abundance of genomic features. *Bioinformatics* 35, 1960–1962. doi: 10.1093/bioinformatics/bty896

Voisset, C., and Blondel, M. (2014). [Chemobiology at happy hour: yeast as a model for pharmacological screening]. *Med. Sci.* 30, 1161–1168.

Wang, Q., Liu, H. R., Mu, Q., Rose, P., and Zhu, Y. Z. (2009). S-propargyl-cysteine protects both adult rat hearts and neonatal cardiomyocytes from ischemia/hypoxia injury: the contribution of the hydrogen sulfide-mediated pathway. *J. Cardiovasc. Pharmacol.* 54, 139–146. doi: 10.1097/fjc.0b013e3181ac8e12

Waterhouse, A. M., Procter, J. B., Martin, D. M., Clamp, M., and Barton, G. J. (2009). Jalview Version 2–a multiple sequence alignment editor and analysis workbench. *Bioinformatics* 25, 1189–1191. doi: 10.1093/bioinformatics/btp033

Yamagata, S., D'Andrea, R. J., Fujisaki, S., Isaji, M., and Nakamura, K. (1993). Cloning and bacterial expression of the CYS3 gene encoding cystathionine gamma-lyase of Saccharomyces cerevisiae and the physicochemical and enzymatic properties of the protein. *J. Bacteriol.* 175, 4800–4808. doi: 10.1128/jb.175.15.4800-4808.1993

Yu, X. H., Cui, L. B., Wu, K., Zheng, X. L., Cayabyab, F. S., Chen, Z. W., et al. (2014). Hydrogen sulfide as a potent cardiovascular protective agent. *Clin. Chim. Acta* 437, 78–87. doi: 10.1016/j.cca.2014.07.012

Zhao, Y., Bhushan, S., Yang, C., Otsuka, H., Stein, J. D., Pacheco, A., et al. (2013). Controllable hydrogen sulfide donors and their activity against myocardial ischemia-reperfusion injury. *ACS Chem. Biol.* 8, 1283–1290. doi: 10.1021/cb400090d

Conflict of Interest: The authors declare that the research was conducted in the absence of any commercial or financial relationships that could be construed as a potential conflict of interest.

frontiers in Microbiology

ORIGINAL RESEARCH
published: 09 July 2021
doi: 10.3389/fmicb.2021.702839

Continual Decline in Azole Susceptibility Rates in *Candida tropicalis* Over a 9-Year Period in China

Yao Wang[1,2,3†], Xin Fan[4†], He Wang[3], Timothy Kudinha[5,6], Ya-Ning Mei[7], Fang Ni[7], Yu-Hong Pan[8], Lan-Mei Gao[8], Hui Xu[9], Hai-Shen Kong[10], Qing Yang[10], Wei-Ping Wang[11], Hai-Yan Xi[11], Yan-Ping Luo[12], Li-Yan Ye[12], Meng Xiao[1,2,3] and China Hospital Invasive Fungal Surveillance Net (CHIF-NET) Study Group*

[1] Department of Laboratory Medicine, Peking Union Medical College Hospital, Chinese Academy of Medical Sciences, Beijing, China, [2] Beijing Key Laboratory for Mechanisms Research and Precision Diagnosis of Invasive Fungal Diseases, Peking Union Medical College Hospital, Chinese Academy of Medical Sciences, Beijing, China, [3] State Key Laboratory of Complex Severe and Rare Diseases, Peking Union Medical College Hospital, Chinese Academy of Medical Sciences, Beijing, China, [4] Department of Infectious Diseases and Clinical Microbiology, Beijing Chaoyang Hospital, Capital Medical University, Beijing, China, [5] School of Biomedical Sciences, Charles Sturt University, Orange, NSW, Australia, [6] New South Wales Health Pathology, Regional and Rural, Orange Hospital, Orange, NSW, Australia, [7] Department of Clinical Laboratory, Jiangsu Province Hospital, Nanjing, Jiangsu, China, [8] Department of Clinical Laboratory, Fujian Medical University Union Hospital, Fuzhou, China, [9] Department of Clinical Laboratory, First Affiliated Hospital of Zhengzhou University, Zhengzhou, China, [10] Department of Laboratory Medicine, First Affiliated Hospital of Zhejiang University School of Medicine, Hangzhou, China, [11] Institute of Laboratory Medicine, Jinling Hospital, Nanjing University School of Medicine, Nanjing, China, [12] Medical Laboratory Center, Chinese PLA General Hospital, Medical School of Chinese PLA, Beijing, China

OPEN ACCESS

Edited by:
Keke Huo,
Fudan University, China

Reviewed by:
Peiying Feng,
Sun Yat-sen University, China
Somanon Bhattacharya,
Stony Brook University, United States
Paul Rhomberg,
JMI Laboratories, United States

***Correspondence:**
Meng Xiao
cjtcxiaomeng@aliyun.com

[†] These authors have contributed equally to this work

Specialty section:
This article was submitted to Antimicrobials, Resistance and Chemotherapy, a section of the journal Frontiers in Microbiology

Received: 30 April 2021
Accepted: 09 June 2021
Published: 09 July 2021

Citation:
Wang Y, Fan X, Wang H, Kudinha T, Mei Y-N, Ni F, Pan Y-H, Gao L-M, Xu H, Kong H-S, Yang Q, Wang W-P, Xi H-Y, Luo Y-P, Ye L-Y, Xiao M and China Hospital Invasive Fungal Surveillance Net (CHIF-NET) Study Group (2021) Continual Decline in Azole Susceptibility Rates in Candida tropicalis Over a 9-Year Period in China. Front. Microbiol. 12:702839. doi: 10.3389/fmicb.2021.702839

Background: There have been reports of increasing azole resistance in *Candida tropicalis*, especially in the Asia-Pacific region. Here we report on the epidemiology and antifungal susceptibility of *C. tropicalis* causing invasive candidiasis in China, from a 9-year surveillance study.

Methods: From August 2009 to July 2018, *C. tropicalis* isolates (n = 3702) were collected from 87 hospitals across China. Species identification was carried out by mass spectrometry or rDNA sequencing. Antifungal susceptibility was determined by Clinical and Laboratory Standards Institute disk diffusion (CHIF-NET10–14, n = 1510) or Sensititre YeastOne (CHIF-NET15–18, n = 2192) methods.

Results: Overall, 22.2% (823/3702) of the isolates were resistant to fluconazole, with 90.4% (744/823) being cross-resistant to voriconazole. In addition, 16.9 (370/2192) and 71.7% (1572/2192) of the isolates were of non-wild-type phenotype to itraconazole and posaconazole, respectively. Over the 9 years of surveillance, the fluconazole resistance rate continued to increase, rising from 5.7 (7/122) to 31.8% (236/741), while that for voriconazole was almost the same, rising from 5.7 (7/122) to 29.1% (216/741), with no significant statistical differences across the geographic regions. However, significant difference in fluconazole resistance rate was noted between isolates cultured from blood (27.2%, 489/1799) and those from non-blood (17.6%, 334/1903) specimens (P-value < 0.05), and amongst isolates collected from medical wards (28.1%, 312/1110) versus intensive care units (19.6%, 214/1092) and surgical

wards (17.9%, 194/1086) (Bonferroni adjusted P-value < 0.05). Although echinocandin resistance remained low (0.8%, 18/2192) during the surveillance period, it was observed in most administrative regions, and one-third (6/18) of these isolates were simultaneously resistant to fluconazole.

Conclusion: The continual decrease in the rate of azole susceptibility among *C. tropicalis* strains has become a nationwide challenge in China, and the emergence of multi-drug resistance could pose further threats. These phenomena call for effective efforts in future interventions.

Keywords: *Candida tropicalis*, antifungal susceptibility, azole, echinocandin, antifungal resistance

INTRODUCTION

Candida species are leading fungal pathogens causing invasive fungal diseases worldwide, and can be life-threatening with notable mortality (Kullberg and Arendrup, 2015; Pappas et al., 2018). *Candida albicans* remains the predominant species implicated in invasive candidiasis (IC), and is generally susceptible to all antifungal agents, including azoles and echinocandins (Kullberg and Arendrup, 2015; Pappas et al., 2016, 2018; Perlin et al., 2017). However, a rising trend in the detection rates of non-*albicans Candida* species has been observed, mostly due to the wide use of antifungals, as many of these species are less susceptible (Perlin et al., 2017). The top three non-*albicans Candida* species most described worldwide are *Candida glabrata sensu stricto*, *Candida tropicalis*, and *Candida parapsilosis sensu stricto*, but with significant geographic variations (Kullberg and Arendrup, 2015; Perlin et al., 2017; Pappas et al., 2018). Amongst these species, *C. tropicalis* has been detected at significantly higher prevalence rates in Asia and Latin-America regions (Tan et al., 2016; Pfaller et al., 2019; Xiao et al., 2020).

To date, there are only four classes of antifungals used for IC, namely azoles, echinocandins, polyenes, and nucleoside analogs (Pappas et al., 2016). Without any other antifungal therapy alternatives, resistance to any of these antifungal classes could pose a great threat to patients (Pappas et al., 2016; Perlin et al., 2017). Previous studies have shown that antifungal resistance in *Candida* species varies across geographic regions worldwide. For *C. tropicalis*, low resistance rates to azoles have been reported in North America, Latin-America, and most European Countries (fluconazole resistant rate <5%) as per the SENTRY global surveillance program (Pfaller et al., 2019), but high rates (23.2% to fluconazole) were reported by Fernandez-Ruiz et al. (2015) in Spain. In contrast, a high azole resistance rate for *C. tropicalis* has been observed in the Asia-Pacific region, especially in mainland China and Taiwan (Fan et al., 2017; Chen et al., 2019; Pfaller et al., 2019; Xiao et al., 2020). In a recent report by Chen et al. (2019), 16.9% of *C. tropicalis* isolates collected in Taiwan were non-susceptible to fluconazole. Meanwhile, the fluconazole resistance rate of *C. tropicalis* in China mainland have exceeded 25%, with over 90% of these isolates cross-resistant to voriconazole (Wang et al., 2020; Xiao et al., 2020). In addition, echinocandin drugs including caspofungin, micafungin, and anidulafungin, have been commercially used for treatment of IC worldwide. Thus emergence of echinocandin- and multidrug-resistance in *C. tropicalis* raises further concerns for clinical management of patients (Jensen et al., 2013; Khan et al., 2018; Xiao et al., 2018; Pfaller et al., 2019; Arastehfar et al., 2020).

As growing challenges of antifungal resistance in *C. tropicalis* have been noted, it is important that continual surveillance targeting this species be implemented in all regions of China and elsewhere. The CHIF-NET study is a laboratory-based, nationwide multicenter study of invasive yeast infections, including IC in China, which was initiated in August 2009. As of July 2018, a total of 87 hospitals had participated in this program for a period of nine surveillance years (CHIF-NET10 to CHIF-NET18). Here we report essential findings on the epidemiology and antifungal susceptibility patterns of *C. tropicalis* causing IC from the CHIF-NET program. Of note and worrying, is the continual decreasing trend of azole susceptibility rate, and fluconazole non-susceptible rates, among *C. tropicalis* strains, which has risen to around 45% nationwide.

MATERIALS AND METHODS

Study Design

During August 2009 to July 2018, a total of 87 hospitals participated in CHIF-NET program, with 79.3% (69/87) of these sites having participated for at least 3 years or longer (median duration of participation, 5 years). Inclusion and exclusion criteria for the isolates were the same as previously described (Xiao et al., 2020). Of note, in the case of multiple *C. tropicalis* isolates from one patient, only one isolate was included in the analysis. In each surveillance year, all isolates from the participating hospitals were sent to a central laboratory (Department of Laboratory Medicine, Peking Union Medical College Hospital) for confirmative identification and antifungal susceptibility testing.

Species Identification

Isolates collected from CHIF-NET10 and CHIF-NET11 were identified by DNA sequencing of the fungal rDNA internal transcribed spacer region supplemented with D1/D2 domain of the 28S rRNA gene, as previously described (Wang et al., 2012). From CHIF-NET12 to CHIF-NET18, species identification was

carried out by matrix-assisted laser desorption ionization-time of flight mass spectrometry (MALDI-TOF MS) (Vitek MS, IVD database V2.0/2.1/3.0, bioMérieux, France, CHIF-NET12 to CHIF-NET16; and Autof MS 1000, Autof Acquirer Version V2.0.18, Autobio Diagnostics, China, CHIF-NET17 to CHIF-NET18). For any isolates that could not be identified or with uncertain identification results to species level by MALDI-TOF MS, rDNA sequencing was performed as "gold standard" (Xiao et al., 2020).

Antifungal Susceptibility Testing

Susceptibility to fluconazole and voriconazole was determined using the Clinical and Laboratory Standards Institute (CLSI) disk diffusion method (disks purchased from Oxoid, Thermo Fisher Scientific, Hampshire, United Kingdom) for isolates collected from CHIF-NET10 to CHIF-NET14 (CLSI, 2020b). From CHIF-NET15 to CHIF-NET18, the *in vitro* susceptibility to nine antifungal agents, including fluconazole, voriconazole, itraconazole, posaconazole, caspofungin, micafungin, anidulafungin, amphotericin B, and 5-flucytosine, was determined using Sensititre YeastOne^{TM} YO10 methodology (Thermo Scientific, Cleveland, OH, United States) following manufacturer's instructions. Current available clinical breakpoints (CBPs) or epidemiological cut-off values (ECVs) were used for interpretation of susceptibility results (Fan et al., 2017; CLSI, 2020a,b). *Candida parapsilosis* ATCC 22019 and *Candida krusei* ATCC 6258 were used for quality control for each run of susceptibility testing, and all quality control results were within published ranges.

Susceptibility Interpretation and Statistical Analysis

Disk diffusion diameter and minimum inhibitory concentration (MIC) results of fluconazole and voriconazole, and MICs of three echinocandin agents were interpreted as per the latest CLSI CBPs (CLSI, 2020b). In addition, ECVs were used for interpretation of itraconazole, posaconazole, amphotericin B (CLSI, 2020a), and 5-flucytocine (Xiao et al., 2020).

For statistical analyses, Chi-square test was performed using IBM SPSS software (version 22.0; IBM SPSS Inc., Armonk, NY, United States), and Bonferroni *post hoc* test was carried out for multiple comparisons when necessary. A *P*-value (or Bonferroni adjusted *P*-value) of <0.05 was considered significant.

RESULTS

Demography Characters

A total of 3702 *C. tropicalis* isolates were collected over a period of 9 years from 87 different hospitals in China. In each surveillance year, 122–741 *C. tropicalis* isolates were identified. The number of participating hospitals and isolates collected in each year are shown in **Supplementary Figure 1**. For patients with IC due to *C. tropicalis*, the majority (64.9%; 2404/3702) were male. Patient ages ranged from 0 to 103 years (median, 56; interquartile, 41–68).

Antifungal Susceptibilities in General

During the first five surveillance years of the CHIF-NET program (CHIF-NET10–14), only susceptibility to fluconazole and voriconazole was performed. However, from CHIF-NET15–18, susceptibilities to nine antifungal drugs were performed (**Table 1**).

Amongst the 3702 *C. tropicalis* isolates collected over 9 years, 22.2% (n = 823) were resistant to fluconazole, and 20.3% (n = 753) were resistant to voriconazole (**Table 1**). Moreover, 20.1% (744/3702) isolates were cross-resistant to both fluconazole and voriconazole. For 2192 isolates collected during CHIF-NET15–18, 16.9% (n = 370) of the isolates were of non-wild-type (NWT) phenotype to itraconazole, whilst a significantly larger proportion (n = 1572, 71.7%) of the isolates were of NWT phenotype to posaconazole, as per the latest CLSI ECVs (**Table 1**). About 16% (342/2192; 15.6%) of the isolates were resistant or of NWT phenotype to all four azoles tested.

Emerging resistance to echinocandins was observed in *C. tropicalis*, although the prevalence remained low, with 0.8% (18/2192) isolates identified in CHIF-NET15–18 being resistant to one or more echinocandin drugs, and 10 of 2192 (0.45%) isolates being resistant to all the 3 echinocandins (**Table 1**). In addition, 6 of 18 echinocandin resistant isolates (33.3%) were simultaneously resistant to fluconazole. Isolates of NWT phenotype to 5-flucytosine and amphotericin B were rare, with prevalence rates of 1.0% (22/2192) and 0.2% (5/2192), respectively (**Table 1**).

Trend of Decreasing Azole Susceptibility Rate

From CHIF-NET10–18 (9 years), we have observed a tremendous decreasing trend of azole susceptibility rate for *C. tropicalis* isolates collected in China. For fluconazole, the resistance rate was only 5.7% (7/122) in the first year (CHIF-NET 10), but this rose sharply (about six times) to 31.8% (236/741) by the ninth surveillance year ($P < 0.001$) (**Figure 1** and **Supplementary Table 1**), and the fluconazole non-susceptible rate had risen to 44.7% (331/741) (**Supplementary Table 1**). A similar picture was observed for voriconazole, with the resistance rate increasing from 5.7 (7/122) to 29.1% (216/741) over 9 years ($P < 0.001$) (**Figure 1** and **Supplementary Table 1**), and furthermore, the voriconazole non-susceptible rate was even higher than that of fluconazole (444/741, 59.9%) (**Supplementary Table 1**). During CHIF-NET15–18, we also observed a continual increase in the proportion of NWT phenotype strains to itraconazole [from 10.7 (62/577) to 20.4% (151/741)] and posaconazole [from 58.9% (340/577) to 76.8% (569/741)] (both $P < 0.001$) (**Figure 1** and **Supplementary Table 1**).

Antifungal Susceptibility Across Geographic Regions

As China is a vast country, we further analyzed the antifungal susceptibility data to assess whether trends of declining azole susceptibility rate among *C. tropicalis* isolates was associated with geographic origins. Among seven administrative regions in China, there were 152–1393 isolates collected

TABLE 1 | Distribution and antifungal susceptibility of *C. tropicalis* by clinical services and specimen types.

Characters	No. of isolates (%)		Antifungal susceptibility (%)																	
	CHIF-NET 10–18	CHIF-NET 15–18	Fluconazole[a]		Voriconazole[a]		Itraconazole[b]		Posaconazole[b]		Caspofungin[b]		Micafungin[b]		Anidulafungin[b]		5-Flucytosine[b]		Amphotericin B[b]	
			S	R	S	R	WT	NWT	WT	NWT	S	R	S	R	S	R	WT	NWT	WT	NWT
Overall	3702 (100.0)	2192 (100.0)	71.2	22.2	63.8	20.3	83.1	16.9	28.3	71.7	99.0	0.7	99.0	0.8	97.6	0.6	99.0	1.0	99.8	0.2
Clinical service																				
Inpatient	3491 (94.3)	2070 (94.4)	71.4	22.1	63.8	20.1	83.1	16.9	28.5	71.5	98.9	0.7	99.0	0.8	97.5	0.6	99.0	1.0	99.8	0.2
Medical	1110 (30.0)	703 (32.1)	65.7	28.1	58.5	26.5	76.4	23.6	26.9	73.1	98.9	0.9	98.9	0.9	97.6	1.0	99.4	0.6	99.4	0.6
ICU	1092 (29.5)	618 (28.2)	74.3	19.6	67.9	17.9	87.2	12.8	31.4	68.6	98.9	0.6	99.0	0.8	96.8	0.5	99.5	0.5	99.8	0.2
Surgical	1086 (29.3)	649 (29.6)	74.2	17.9	65.4	15.4	86.7	13.3	28.4	71.6	99.2	0.3	99.4	0.5	98.3	0.3	98.2	1.8	100.0	0.0
Other	203 (5.5)	100 (4.6)	71.4	24.6	63.1	22.7	82.0	18.0	22.0	78.0	98.0	2.0	98.0	2.0	97.0	1.0	98.0	2.0	100.0	0.0
Emergency department	162 (4.4)	100 (4.6)	65.4	26.5	58.0	26.5	84.0	16.0	24.0	76.0	99.0	1.0	99.0	1.0	99.0	1.0	99.0	1.0	100.0	0.0
Outpatient	49 (1.3)	22 (1.0)	79.6	20.4	77.6	16.3	77.3	22.7	31.8	68.2	100.0	0.0	100.0	0.0	100.0	0.0	100.0	0.0	100.0	0.0
Specimen type																				
Blood	1799 (48.6)	1122 (51.2)	66.7	27.2	58.6	25.6	79.4	20.6	27.1	72.9	98.8	0.9	98.8	0.9	97.2	1.0	99.2	0.8	99.7	0.3
Non-blood samples	1903 (51.4)	1070 (48.8)	75.5	17.6	68.7	15.4	87.0	13.0	29.5	70.5	99.2	0.5	99.3	0.7	98.0	0.3	98.8	1.2	99.8	0.2
Ascitic fluid	708 (19.1)	373 (17.0)	77.5	15.8	71.6	13.8	87.7	12.3	28.7	71.3	98.9	0.5	99.2	0.8	98.1	0.3	98.7	1.3	99.7	0.3
Pus	344 (9.3)	205 (9.4)	74.4	17.7	67.4	16.0	83.4	16.6	32.7	67.3	100.0	0.0	100.0	0.0	99.0	0.0	99.5	0.5	99.5	0.5
Bile	216 (5.8)	143 (6.5)	72.7	21.3	62.5	18.1	86.7	13.3	29.4	70.6	98.6	1.4	98.6	1.4	98.6	0.7	100.0	0.0	100.0	0.0
Pleural fluid	142 (3.8)	80 (3.6)	77.5	15.5	72.5	12.7	92.5	7.5	41.3	58.8	98.8	0.0	100.0	0.0	98.8	0.0	97.5	2.5	100.0	0.0
CVC	205 (5.5)	108 (4.9)	71.2	19.5	65.9	17.6	86.1	13.9	23.1	76.9	98.1	0.9	98.1	1.9	95.4	0.9	98.1	1.9	100.0	0.0
BALF	126 (3.4)	79 (3.6)	70.6	20.6	62.7	17.5	88.6	11.4	27.8	72.2	100.0	0.0	100.0	0.0	96.2	0.0	98.7	1.3	100.0	0.0
Tissue	70 (1.9)	38 (1.7)	80.0	17.1	72.9	14.3	89.5	10.5	23.7	76.3	100.0	0.0	100.0	0.0	100.0	0.0	100.0	0.0	100.0	0.0
CSF	65 (1.8)	31 (1.4)	76.9	18.5	70.8	18.5	83.9	16.1	29.0	71.0	100.0	0.0	100.0	0.0	100.0	0.0	96.8	3.2	100.0	0.0
Other	27 (0.7)	13 (0.6)	85.2	11.1	70.4	11.1	92.3	7.7	15.4	84.6	100.0	0.0	100.0	0.0	92.3	0.0	92.3	7.7	100.0	0.0

S, susceptible; R, resistant; WT, wild-type; NWT, non-wild-type; ICU, intensive care unit.

[a]*For isolates from CHIF-NET10–18.*

[b]*For isolates from CHIF-NET15–18.*

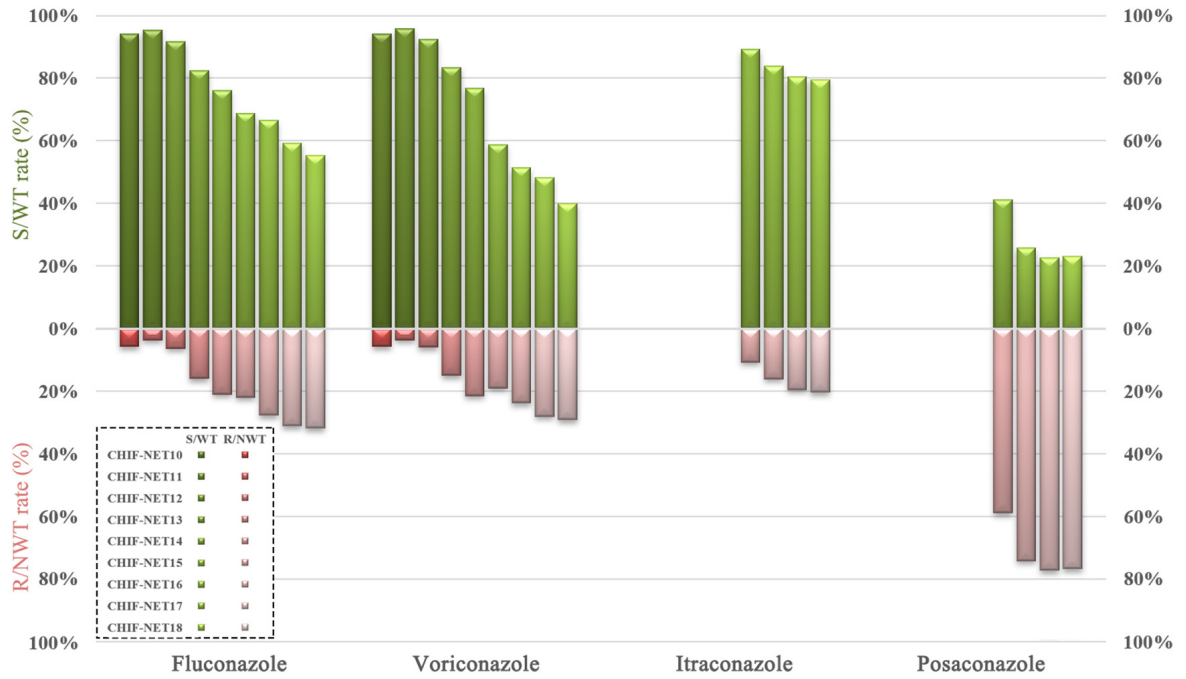

FIGURE 1 | Trends of azole susceptibility in *C. tropicalis* over a 9-year surveillance. S, susceptible; R, resistant; WT, wild-type; NWT, non-wild-type.

over nine surveillance years (**Figure 2** and **Supplementary Table 1**). Fluconazole resistance and non-susceptible rates ranged from 18.4 to 25.0%, and from 24.3 to 32.4%, respectively (**Figure 2** and **Supplementary Table 1**), although the differences were statistically insignificant (Chi-square test, $P > 0.05$). Voriconazole resistance rates, which ranged from 17.1 to 23.9% across different administrative regions, were also not significantly different (**Figure 2** and **Supplementary Table 1**). However, it was observed that voriconazole non-susceptible rate in South China region (41.9%) was significantly higher than in other regions (ranged from 30.8 to 37.7%) (Bonferroni adjusted P-value < 0.05).

For echinocandins, it was observed that resistance to this class had emerged in six of seven administrative regions except for Northwest China, and in all regions the resistance rates were below 3% (**Supplementary Table 1**).

Azole Susceptibility by Specimen Types and Clinical Services

Of 3702 *C. tropicalis* isolates collected, around half (1799/3702, 48.6%) was from blood cultures, and common non-blood specimen types included ascitic fluid (n = 708, 19.1%), pus (n = 344, 9.3%) and bile (n = 216, 5.8%) (**Table 1**). Of note, compared to isolates cultured from non-blood samples, isolates from blood cultures exhibited significantly higher azole resistance rate, which was 27.2% (489/1799) versus 17.6% (334/1903) for fluconazole ($P < 0.001$), and 25.6% (460/1799) versus 15.4% (293/1903) for voriconazole ($P < 0.001$) (**Table 1**). However, amongst different non-blood specimen types, there was no significant difference in azole resistance rate ($P > 0.05$). Moreover, both blood culture and non-blood culture isolates exhibited increasing resistance trends for fluconazole and voriconazole over 9 years (**Supplementary Figure 2**).

Overall, 94.3% of isolates collected over 9 years were from inpatient wards (3491/3702), and isolates from emergency department (4.4%, 162/3702) and outpatients (1.3%, 49/3702) were rare. Amongst strains collected in inpatient services, the proportion of isolates from medical wards, surgical wards and intensive care units (ICUs) was generally the same, ranging from 31.5 (1100/3491) to 31.1% (1086/3491) (**Table 1**). Statistical analysis revealed significant difference in azole resistance rates amongst medical, surgical wards, and ICUs ($P < 0.001$). *Post hoc* test indicated that the rate of azole resistance was higher in isolates from medical wards compared to those from surgical wards and ICUs. For instance, fluconazole resistance rate was 28.1% (312/1110) for isolates from medical wards, which was notably higher versus 19.6 (214/1092) and 17.9% (194/1086) for strains from ICUs and surgical wards, respectively (Bonferroni adjust P-value < 0.05) (**Table 1**).

DISCUSSION

Antifungal resistance has posed great challenges to clinical management of fungal infections including IC. Of note, there are significant geographic variations in the epidemiology and antifungal susceptibilities of fungal pathogens worldwide (Kullberg and Arendrup, 2015; Pappas et al., 2018). From the global SENTRY surveillance study, it was observed that *C. albicans* remained the predominant *Candida* species worldwide (overall prevalence 46.9%), and in comparison,

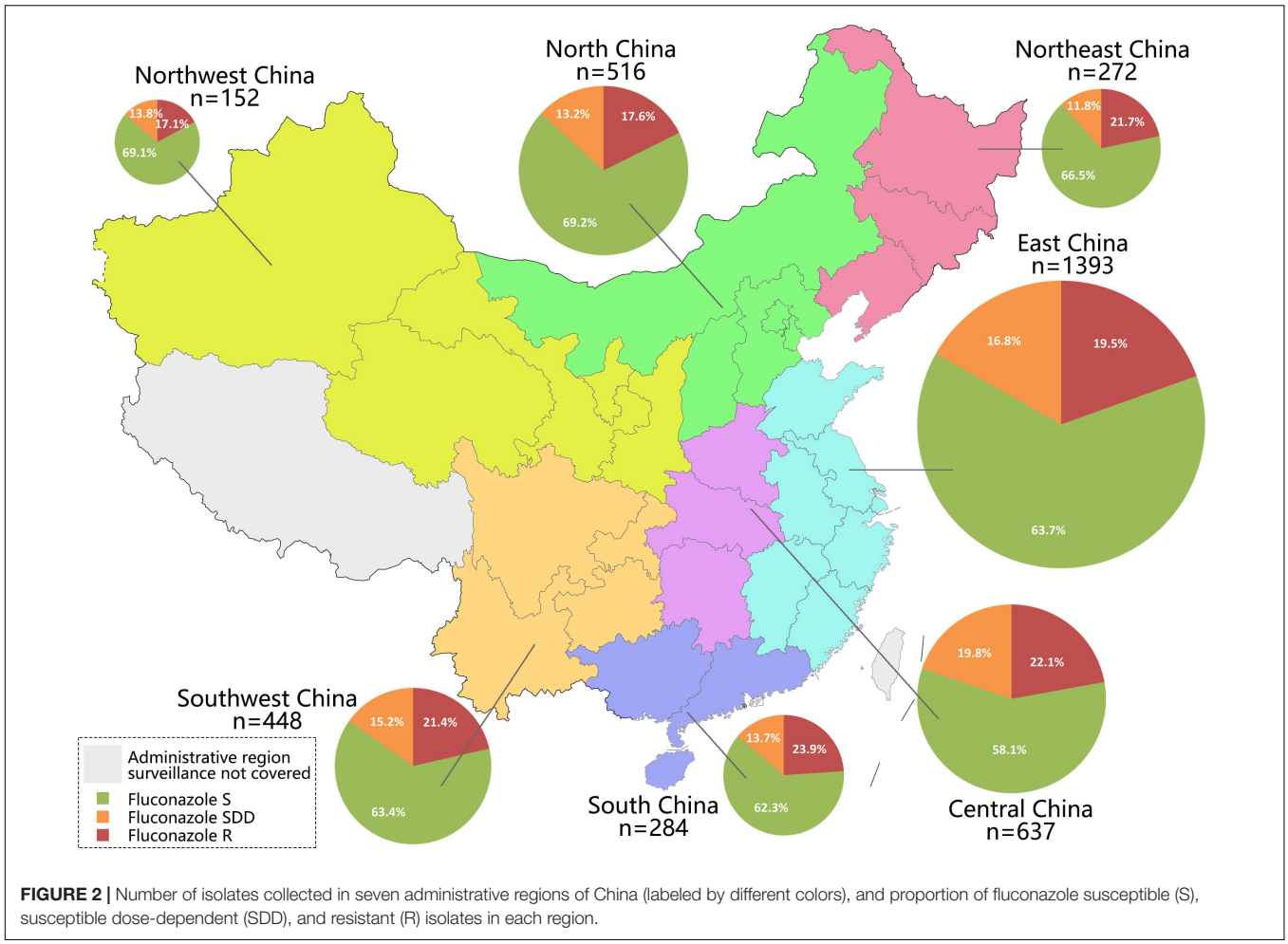

FIGURE 2 | Number of isolates collected in seven administrative regions of China (labeled by different colors), and proportion of fluconazole susceptible (S), susceptible dose-dependent (SDD), and resistant (R) isolates in each region.

C. tropicalis is the second to fourth most predominant species in different geographic regions, and is more commonly seen in Asia and Latin-America regions (14.1–17.0%) than in North America and Europe (7.5–8.0%) (Pfaller et al., 2019). However, in Asian countries like Pakistan and India, *C. tropicalis* has become the most frequently encountered *Candida* species causing candidemia (>30%) with even higher prevalence rates than *C. albicans*, while azole resistance in *C. tropicalis* remains low (<8%) in these regions (Farooqi et al., 2013; Wang et al., 2016a; Sridharan et al., 2021). Furthermore, an African country has also reported predominance of *C. tropicalis* (28.8%) in candidemia cases, but with notably high fluconazole resistance rate (31.6%) (Megri et al., 2020).

In China, *C. tropicalis* is the second to third commonest *Candida* pathogen causing IC nationwide (Liu et al., 2014; Xiao et al., 2020). But the continual rise in azole resistance rate in this species has become quite worrisome. CHIF-NET surveillance program, and a China-SCAN study (a multicenter study monitoring candidemia in ICUs in China), revealed that fluconazole resistance rate among *C. tropicalis* strains in China was steadily low (3–6%) around 2009–2012 (Wang et al., 2012; Liu et al., 2014), which was comparable to global azole resistance levels within this species (2–5% in general) (Pfaller et al., 2019). However, since then, the proportion of azole resistant *C. tropicalis* isolates in China has continued to rise. It has been reported that in 10 hospitals that consecutively participated in the first 5 years of the CHIF-NET program, fluconazole resistance rate had exceeded 20% by the fifth year (Fan et al., 2017). Further surveillance of *C. tropicalis* isolates causing candidemia revealed that >30% of strains were fluconazole-resistant by the eighth surveillance year (Xiao et al., 2020). During the same time period, there were no obvious changing trends found in fluconazole susceptibility amongst other commonly seen *Candida* species like *C. albicans*, *C. parapsilosis sensu stricto*, and *C. glabrata sensu stricto* (Song et al., 2020; Xiao et al., 2020).

In the present study, we expanded our analysis to include all IC cases. Although it was notable to find that a greater proportion of isolates from blood cultures were resistant to azoles than those from other clinical specimens (27.2 versus 17.6% for fluconazole and 25.6 versus 15.4% for voriconazole, respectively), there was also an increasing trend in the rate of resistance during the 9-year period. Furthermore, the fluconazole non-susceptible rate currently stands at over 44%, and nearly 60% of the strains were voriconazole non-susceptible nationwide in the last year. High azole resistance rates have also been reported in other recent studies in China (Song et al., 2020; Wang et al., 2020), with no

obvious geographic variations in azole resistance rate amongst *C. tropicalis* strains across the country.

Molecular methods, including multilocus sequence typing (MLST), microsatellite analysis and whole genome sequencing, have been applied to investigate the phylogenetic structure of fungal pathogens. It was demonstrated that *C. tropicalis* has an extensive genetic diversity using these molecular methods, but no evidence of association between clonal population structure and geographic origins was found (Fan et al., 2017; Wu et al., 2019; O'Brien et al., 2021). However, an association between certain *C. tropicalis* phylogenetic clades, and reduced azole susceptibility, has been reported. MLST studies carried out in Thailand, Singapore, China mainland, and Taiwan, have illustrated a distinct phylogenetic clade of diploid sequence types (DSTs), including DST225, DST 376, DST 505, DST 506, DST506, DST525, DST546, etc., that are associated with azole non-susceptibility (Wang et al., 2016b, 2020; Chew et al., 2017; Tulyaprawat et al., 2020). Microsatellite analysis also revealed an association between certain genetic clusters and decreasing azole susceptibility in China (Fan et al., 2017). It is worth noting that most of the related reports on *C. tropicalis* azole resistance are from Asian countries, suggesting that Asia is probably the geographic origin of these azole non-susceptible clones. Expansion of these clones is speculated to be responsible for the fall in azole susceptibility rate in China (Fan et al., 2017), while the described diversity in DST or microsatellite molecular types, suggests continual microevolution within these clones.

Several mechanisms for azole resistance in *Candida* species have been described. *ERG11* gene mutation remains one of the most common and well-understood azole resistance mechanisms in *C. tropicalis*. Azole non-susceptible *C. tropicalis* isolates carrying substitution Y132F in Erg11p have been reported in Turkey and Asian countries (Chew et al., 2017; Fan et al., 2019; Arastehfar et al., 2020; Castanheira et al., 2020), and this key amino acid change is also responsible for reduced azole susceptibility in many other *Candida* species, including the recently discovered "superbug" *Candida auris* (Castanheira et al., 2020; Chow et al., 2020). Of note, S154F substitution in Erg11p has consistently appeared together with Y132F in *C. tropicalis* isolates from China (Jiang et al., 2013; Fan et al., 2019), but presence of S154F alone did not change azole MICs (Chen et al., 2019). There have been other Erg11p amino acid substitutions reported, such as P56S and K143R, predominantly found in fluconazole resistant *C. tropicalis* isolates in Algeria and Brazil (Xisto et al., 2017; Megri et al., 2020). Other mechanisms, including modulation of *ERG* genes and up-regulation of drug efflux pumps, also influence azole susceptibility of *C. tropicalis* (Fan et al., 2019; Arastehfar et al., 2020; Silva et al., 2020).

The emergence of echinocandin resistance among the *C. tropicalis* isolates in this study, albeit small proportion of about 0.8%, is a cause for concern as this class of antifungal drugs is highly active against most *Candida* species with minimal adverse effects, and has been recommended as first-line therapy for candidemia by Infectious Diseases Society of America since 2016 (Pappas et al., 2016). However, an increase in echinocandin resistance rate has been observed in *C. glabrata* and *C. tropicalis* in North America (Pfaller et al., 2019). Moreover, apart from the fact that echinocandin resistance has emerged in six of seven administrative regions in China, we also observed that over 30% of echinocandin resistant isolates were also resistant to azoles, which has rarely been reported from other countries.

There are several limitations in this study. Firstly, there were disparities between numbers of participating hospitals and isolates collected from different geographic regions, which may affect the accuracy of the data used for analysis. Secondly, antifungal susceptibility testing was carried out using different methods in CHIF-NET10–14 and CHIF-NET15–18, although previous studies have shown good correlation between disk diffusion and commercial Sensititre YeastOne methods to CLSI standard broth microdilution method (Pfaller et al., 2003; Espinel-Ingroff et al., 2004; Xiao et al., 2015). Moreover, CHIF-NET study remains a laboratory-based surveillance to date, primarily focused on yeasts strains causing invasive infections, and detailed clinical data, including patient management and antifungal consumption, is not systematically collected. Therefore, we are unable to determine the exact reason for the sharp decline in azole susceptibility in China, but highly speculate that it is due to azole overuse resulting in accelerated development of resistance.

In conclusion, the continual decreasing trend in the rate of azole susceptibility amongst *C. tropicalis* isolates was observed over 9 years in China. The rate of resistance to azoles was higher in isolates from blood cultures and medical wards, whilst resistance rates were statistically insignificant across geographic regions. Emergence of echinocandin- and multidrug-resistant isolates was also noted and is a worrying trend needing further scrutiny so that urgent efforts can be directed at arresting the trend.

MEMBERS OF THE CHINA HOSPITAL INVASIVE FUNGAL SURVEILLANCE NET (CHIF-NET) STUDY GROUP

List of principal investigators in the participating hospitals from CHIF-NET study group (ranked by number of *C. tropicalis* isolates contributed): Zi-Yong Sun, Zhong-Jv Chen, Tongji Hospital, Tongji Medical College of Huazhong University of Science and Technology; Ying-Chun Xu, Meng Xiao, Peking Union Medical College Hospital, Chinese Academy of Medical Sciences; Mei Kang, Yu-Ling Xiao, West China Hospital, Sichuan University; Ya-Ning Mei, Fang Ni, Jiangsu Province Hospital; Yu-Hong Pan, Lan-Mei Gao, Fujian Medical University Union Hospital; Hui Xu, Hui Xu, First Affiliated Hospital of Zhengzhou University; Kang Liao, Peng-Hao Guo, First Affiliated Hospital, Sun Yat-sen University; Hai-Shen Kong, Qing Yang, First Affiliated Hospital, Zhejiang University School of Medicine; Wei-Ping Wang, Jinling Hospital, Nanjing University School of Medicine; Yan-Ping Luo, Li-Yan Ye, Chinese PLA General Hospital, Medical School of Chinese PLA; Hua Yu, Lin Yin, Sichuan Provincial People's Hospital, Sichuan Academy of Medical Sciences; Da-Wen Guo, Lan-Ying Cui, First Affiliated Hospital of Harbin Medical University; Peng-Peng Liu, Hong

He, Affiliated Hospital of Qingdao University; Yan Jin, Hui Fan, Shandong Provincial Hospital; Yun-Song Yu, Jie Lin, Sir Run Run Shaw Hospital; Ruo-Yu Li, Zhe Wan, Peking University First Hospital; Ling Ma, Shuai-Xian Du, Union Hospital, Tongji Medical College, Huazhong University of Science and Technology; Wen-En Liu, Yan-Ming Li, Xiangya Hospital, Central South University; Tie-Li Zhou, Qing Wu, First Affiliated Hospital of Wenzhou Medical University; Xin-Lan Hu, Ning Li, Fujian Provincial Hospital; Rong Zhang, Hong-Wei Zhou, Second Affiliated Hospital Zhejiang University School of Medicine; Yi-Min Li, Dan-Hong Su, First Affiliate Hospital of Guangzhou Medical University; Qiang-Qiang Zhang, Li Li, Huashan Hospital, Fudan University; Yun Xia, Li Yan, First Affiliated Hospital of Chongqing Medical University; Zhi-Dong Hu, Na Yue, Tianjin Medical University General Hospital; Yan Jiang, Tianjin First Central Hospital; Zhi-Yong Liu, Yu-Ting Zheng, Southwest Hospital of Army Medical University; Wei Cao, Second Xiangya Hospital of Central South University; Yun-Zhuo Chu, Fu-Shun Li, First Hospital of China Medical University; Yun Liu, Changhai Hospital; Yuan-Hong Xu, Ying Huang, First Affiliated Hospital of University of Science and Technology of China; Wei Jia, Gang Li, General Hospital of Ningxia Medical University; Huo-Xiang Lv, Qing-Feng Hu, Zhejiang Provincial People's Hospital; Xiu-Li Xu, Xiao-Yan Chen, Air Force Medical University; Xiao-Ling Ma, Huai-Wei Lu, First Affiliated Hospital of University of Science and Technology of China; Yin-Mei Yang, Hui-Ling Chen, Guangzhou First People's Hospital; Jian-Sheng Huang, Hui Jing, Lisui Municipal Central Hospital; Bin San, Yan Du, First Affiliated Hospital, Kunming Medical University; Hong-Jie Liang, First Affiliated Hospital of Guangxi Medical University; Bin Yang, Yu-Lan Lin, First Affiliated Hospital of Fujian Medical University; Shan-Mei Wang, Qiong Ma, Henan Provincial People's Hospital; Hong-Mei Zhao, Li-Wen Liu, People's Hospital of Liaoning Province; Qing Zhang, Fei Xia, Ruian People's Hospital; Jin-Ying Wu, Mao-Li Yi, Yantai Yuhuangding Hospital; Xiang-Yang Chen, People's Hospital of Zhengzhou; Wei-Ping Lu, Dao-Hong Zhou, Daping Hospital, Third Military Medical University; Xiao-Yan Zeng, Jing Zhang, First Affiliated Hospital of Xi'an Jiaotong University; Jing Wang, Xiao-Guang Xiao, First Affiliated Hospital of Dalian Medical University; Jia-Yin Liang, Fan-Hua Huang, Third Attached Hospital, Sun Yat-sen University; Gui-Ling Zou, Xue-Fei Du, Fourth Hospital of Harbin Medical University; Xiao-Ming Wang, Xu-Feng Ji, First Bethune Hospital of Jilin University; Yong Liu, Zhi-Jie Zhang, Shengjing Hospital of China Medical University; Yu-Xing Ni, Sheng-Yuan Zhao, Ruijin Hospital, Shanghai Jiao Tong University of Medicine; Xiu-Lan Song, First Hospital of Jiaxing; Chun-Yan Xu, Chun-Yan Xu, Taizhou Hospital of Zhejiang Province; Lin Meng, Lanzhou University Second Hospital; Xian-Feng Zhang, Ya-Lu Ren, First Affiliated Hospital of Soochow University; Jian-Hong Zhao, Hong-Lian Wei, Second Hospital of Hebei Medical University; Xue-Song Xu, Weil Li, China-Japan Union Hospital of Jilin University; Yu-Ping Wang, Mei Xu, Affiliated Hospital of Guizhou Medical University; Yun-Duo Wang, Jing Song, Dalian Municipal Central Hospital; Tian-Pen Cui, Zhi-Min Hu, WuHan No.1 Hospital; Ting-Yin Zhou, Hai-Qing Hu, Shanghai Changzheng Hospital; Xiao-Min Xu, Shan-Yan Liang, Hwa Mei Hospital, University of Chinese Academy of Sciences; Lin-Qiang Deng, Hui Chen, Jiangxi Province People's Hospital; Xiao-Jun Sun, First Affiliated Hospital of Shandong First Medical University; Hai-Bin Wang, Jing Zhu, Fouth Medical Center of PLA General Hospital; Jian-Bang Kang, Second Hospital of Shanxi Medical University; Tie-Ying Hou, Guangdong Provincial People's Hospital, Guangdong Academy of Medical Sciences; Ping Ji, Na Chen, First Affiliated Hospital of Xinjiang Medical University; Wen-Jun Sui, Hai-Tong Gu, Beijing Tongren Hospital, Capital Medical University; Xiao-Qin Ha, Yuan-Yuan Zhang, General Hospital of Lanzhou Military Region; Shu-Feng Wang, Hong Lu, First Hospital of Shanxi Medical University; Yi-Hai Gu, Xuan Hou, 3201 Hospital; Rong Tang, Shanghai General Hospital; Yan-Yan Guo, Fei Huang, Tangshan Gongren Hospital; Long-Hua Hu, Xiao-Yan Hu, Second Affiliated Hospital of Nanchang University; Juan Li, People's Hospital of Xinjiang; Lian-Hua Wei, Xin Wang, Gansu Provincial Hospital; Dan Liu, Jiujiang No.1 People's Hospital; Yan-Qiu Han, Jun-Rui Wang, Affiliated Hospital of Inner Mongolia Medical University; Yi-Hui Yao, Zhongshan Hospital, Xiamen University; Jian-Sheng Wang, Jie Wang, Hebei General Hospital; Wei Li, Qilu Hospital of Shandong University; Li-Ping Ning, 94th Hospital of Chinese PLA; Wei-Qing Song, Yu-Jie Wang, Qingdao Municipal Hospital; Liang Luan, General Hospital of Northern Theater Command.

DATA AVAILABILITY STATEMENT

The original contributions presented in the study are included in the article/**Supplementary Material**, further inquiries can be directed to the corresponding author/s.

ETHICS STATEMENT

The studies involving human participants were reviewed and approved by Ethics Committee of Peking Union Medical College Hospital. Written informed consent for participation was not required for this study in accordance with the national legislation and the institutional requirements.

AUTHOR CONTRIBUTIONS

YW, XF, HW, and MX conceived and designed the experiments. XF, Y-NM, FN, Y-HP, L-MG, HX, H-SK, QY, W-PW, H-YX, Y-PL, L-YY, and MX performed the experiments. YW, XF, TK, and MX performed the data analysis and wrote the manuscript. All authors participated in the critical review of this manuscript.

FUNDING

This work was supported by a Beijing Hospitals Authority Youth Programme (Grant No. QML20190301), Natural Science

Foundation of China (81802042), Special Foundation for National Science and Technology Basic Research Program of China (Grant No. 2019FY101200), Beijing Nova Program (Z201100006820127), and Beijing Key Clinical Specialty for Laboratory Medicine – Excellent Project (Grant No. ZK201000).

SUPPLEMENTARY MATERIAL

The Supplementary Material for this article can be found online at: https://www.frontiersin.org/articles/10.3389/fmicb.2021.702839/full#supplementary-material

REFERENCES

Arastehfar, A., Hilmioglu-Polat, S., Daneshnia, F., Hafez, A., Salehi, M., Polat, F., et al. (2020). Recent increase in the prevalence of Fluconazole-Non-susceptible candida tropicalis blood isolates in Turkey: clinical implication of azole-Non-susceptible and Fluconazole tolerant phenotypes and genotyping. *Front. Microbiol.* 11:587278. doi: 10.3389/fmicb.2020.587278

Castanheira, M., Deshpande, L. M., Messer, S. A., Rhomberg, P. R., and Pfaller, M. A. (2020). Analysis of global antifungal surveillance results reveals predominance of Erg11 Y132F alteration among azole-resistant Candida parapsilosis and Candida tropicalis and country-specific isolate dissemination. *Int. J. Antimicrob. Agents* 55:105799. doi: 10.1016/j.ijantimicag.2019.09.003

Chen, P. Y., Chuang, Y. C., Wu, U. I., Sun, H. Y., Wang, J. T., Sheng, W. H., et al. (2019). Clonality of Fluconazole-Non susceptible candida tropicalis in bloodstream infections, Taiwan, 2011–2017. *Emerg. Infect. Dis.* 25, 1660–1667. doi: 10.3201/eid2509.190520

Chew, K. L., Cheng, J. W. S., Jureen, R., Lin, R. T. P., and Teo, J. W. P. (2017). ERG11 mutations are associated with high- level azole resistance in clinical candida tropicalis isolates, a Singapore study. *Mycoscience* 58, 111–115. doi: 10.1016/j.myc.2016.11.001

Chow, N. A., Munoz, J. F., Gade, L., Berkow, E. L., Li, X., Welsh, R. M., et al. (2020). Tracing the evolutionary history and global expansion of candida auris using population genomic analyses. *Mbio* 11, 3364–3319. doi: 10.1128/mBio.03364-19

CLSI. (2020a). *M59. Epidemiological cutoff values for antifungal susceptibility testing*, 3rd Edn. Wayne, PA: CLSI.

CLSI. (2020b). *M60. Performance standards for antifungal susceptibility testing of yeasts*, 2nd Edn. Wayne, PA: CLSI.

Espinel-Ingroff, A., Pfaller, M., Messer, S. A., Knapp, C. C., Holliday, N., and Killian, S. B. (2004). Multicenter comparison of the sensititre yeastone colorimetric antifungal panel with the NCCLS M27-A2 reference method for testing new antifungal agents against clinical isolates of Candida spp. *J. Clin. Microbiol.* 42, 718–721. doi: 10.1128/jcm.42.2.718-721.2004

Fan, X., Xiao, M., Liao, K., Kudinha, T., Wang, H., Zhang, L., et al. (2017). Notable increasing trend in azole Non-susceptible candida tropicalis causing invasive candidiasis in China (August 2009 to July 2014): molecular epidemiology and clinical Azole consumption. *Front. Microbiol.* 8:464. doi: 10.3389/fmicb.2017.00464

Fan, X., Xiao, M., Zhang, D., Huang, J. J., Wang, H., Hou, X., et al. (2019). Molecular mechanisms of azole resistance in Candida tropicalis isolates causing invasive candidiasis in China. *Clin. Microbiol. Infect.* 25, 885–891. doi: 10.1016/j.cmi.2018.11.007

Farooqi, J. Q., Jabeen, K., Saeed, N., Iqbal, N., Malik, B., Lockhart, S. R., et al. (2013). Invasive candidiasis in Pakistan: clinical characteristics, species distribution and antifungal susceptibility. *J. Med. Microbiol.* 62, 259–268. doi: 10.1099/jmm.0.048785-0

Fernandez-Ruiz, M., Puig-Asensio, M., Guinea, J., Almirante, B., Padilla, B., Almela, M., et al. (2015). Candida tropicalis bloodstream infection: Incidence, risk factors and outcome in a population-based surveillance. *J. Infect.* 71, 385–394. doi: 10.1016/j.jinf.2015.05.009

Jensen, R. H., Johansen, H. K., and Arendrup, M. C. (2013). Stepwise development of a homozygous S80P substitution in Fks1p, conferring echinocandin resistance in Candida tropicalis. *Antimicrob. Agents Chemother.* 57, 614–617. doi: 10.1128/aac.01193-12

Jiang, C., Dong, D. F., Yu, B. Q., Cai, G., Wang, X. F., Ji, Y. H., et al. (2013). Mechanisms of azole resistance in 52 clinical isolates of Candida tropicalis in China. *J. Antimicrob. Chemother.* 68, 778–785. doi: 10.1093/jac/dks481

Khan, Z., Ahmad, S., Mokaddas, E., Meis, J. F., Joseph, L., Abdullah, A., et al. (2018). Development of echinocandin resistance in candida tropicalis following short-term exposure to caspofungin for empiric therapy. *Antimicrob. Agents Chemother.* 62:e1926–17. doi: 10.1128/AAC.01926-17

Kullberg, B. J., and Arendrup, M. C. (2015). Invasive candidiasis. *N. Engl. J. Med.* 373, 1445–1456.

Liu, W., Tan, J., Sun, J., Xu, Z., Li, M., Yang, Q., et al. (2014). Invasive candidiasis in intensive care units in China: in vitro antifungal susceptibility in the China-SCAN study. *J. Antimicrob. Chemother.* 69, 162–167.

Megri, Y., Arastehfar, A., Boekhout, T., Daneshnia, F., Hortnagl, C., Sartori, B., et al. (2020). Candida tropicalis is the most prevalent yeast species causing candidemia in Algeria: the urgent need for antifungal stewardship and infection control measures. *Antimicrob. Resist. Infect. Control* 9:50.

O'Brien, C. E., Oliveira-Pacheco, J., Ó Cinnéide, E., Haase, M. A. B., Hittinger, C. T., Rogers, T. R., et al. (2021). Population genomics of the pathogenic yeast Candida tropicalis identifies hybrid isolates in environmental samples. *PLoS Pathog.* 17:e1009138. doi: 10.1371/journal.ppat.1009138

Pappas, P. G., Kauffman, C. A., Andes, D. R., Clancy, C. J., Marr, K. A., Ostrosky-Zeichner, L., et al. (2016). Clinical practice guideline for the management of candidiasis: 2016 update by the Infectious Diseases Society of America. *Clin. Infect. Dis.* 62, e1–e50.

Pappas, P. G., Lionakis, M. S., Arendrup, M. C., Ostrosky-Zeichner, L., and Kullberg, B. J. (2018). Invasive candidiasis. *Nat. Rev. Dis. Primers* 4:18026.

Perlin, D. S., Rautemaa-Richardson, R., and Alastruey-Izquierdo, A. (2017). The global problem of antifungal resistance: prevalence, mechanisms, and management. *Lancet Infect. Dis.* 17, e383–e392.

Pfaller, M. A., Diekema, D. J., Messer, S. A., Boyken, L., and Hollis, R. J. (2003). Activities of fluconazole and voriconazole against 1,586 recent clinical isolates of Candida species determined by Broth microdilution, disk diffusion, and Etest methods: report from the ARTEMIS global antifungal susceptibility program, 2001. *J. Clin. Microbiol.* 41, 1440–1446. doi: 10.1128/jcm.41.4.1440-1446.2003

Pfaller, M. A., Diekema, D. J., Turnidge, J. D., Castanheira, M., and Jones, R. N. (2019). Twenty years of the SENTRY antifungal surveillance program: results for candida species from 1997-2016. *Open Forum. Infect. Dis.* 6, S79–S94.

Silva, M. C., Cardozo Bonfim Carbone, D., Diniz, P. F., Freitas Fernandes, F., Fuzo, C. A., Santos Pereira Cardoso Trindade, C., et al. (2020). Modulation of ERG genes expression in clinical isolates of candida tropicalis susceptible and resistant to fluconazole and itraconazole. *Mycopathologia* 185, 675–684.

Song, Y., Chen, X., Yan, Y., Wan, Z., Liu, W., and Li, R. (2020). Prevalence and antifungal susceptibility of pathogenic yeasts in china: A 10-year retrospective study in a teaching hospital. *Front. Microbiol.* 11:1401. doi: 10.3389/fmicb.2020.01401

Sridharan, S., Gopalakrishnan, R., Nambi, P. S., Kumar, S., Sethuraman, N., and Ramasubramanian, V. (2021). Clinical profile of Non-neutropenic patients with invasive Candidiasis: A retrospective study in a tertiary care center. *Indian J. Crit. Care Med.* 25, 267–272. doi: 10.5005/jp-journals-10071-23748

Tan, T. Y., Hsu, L. Y., Alejandria, M. M., Chaiwarith, R., Chinniah, T., Chayakulkeeree, M., et al. (2016). Antifungal susceptibility of invasive Candida bloodstream isolates from the Asia-Pacific region. *Med. Mycol.* 54, 471–477.

Tulyaprawat, O., Pharkjaksu, S., Chongtrakool, P., and Ngamskulrungroj, P. (2020). An Association of an eBURST group with Triazole resistance of candida tropicalis blood isolates. *Front. Microbiol.* 11:934. doi: 10.3389/fmicb.2020.00934

Wang, H., Xiao, M., Chen, S. C., Kong, F., Sun, Z. Y., Liao, K., et al. (2012). In vitro susceptibilities of yeast species to fluconazole and voriconazole as determined by the 2010 National China Hospital Invasive Fungal Surveillance Net (CHIF-NET) study. *J. Clin. Microbiol.* 50, 3952–3959. doi: 10.1128/jcm.01130-12

Wang, H., Xu, Y. C., and Hsueh, P. R. (2016a). Epidemiology of candidemia and antifungal susceptibility in invasive candida species in the Asia-Pacific region. *Future Microbiol.* 11, 1461–1477. doi: 10.2217/fmb-2016-0099

Wang, Y., Shi, C., Liu, J. Y., Li, W. J., Zhao, Y., and Xiang, M. J. (2016b). Multilocus sequence typing of Candida tropicalis shows clonal cluster enrichment in azole-resistant isolates from patients in Shanghai, China. *Infect. Genet. Evol.* 44, 418–424. doi: 10.1016/j.meegid.2016.07.026

Wang, Q., Tang, D., Tang, K., Guo, J., Huang, Y., and Li, C. (2020). Multilocus sequence typing reveals clonality of Fluconazole-Nonsusceptible Candida tropicalis: A study from wuhan to the global. *Front. Microbiol.* 11:554249. doi: 10.3389/fmicb.2020.554249

Wu, J. Y., Zhou, D. Y., Zhang, Y., Mi, F., and Xu, J. (2019). Analyses of the global multilocus genotypes of the human pathogenic yeast candida tropicalis. *Front. Microbiol.* 10:900. doi: 10.3389/fmicb.2019.00900

Xiao, M., Chen, S. C., Kong, F., Xu, X. L., Yan, L., Kong, H. S., et al. (2020). Distribution and antifungal susceptibility of candida species causing candidemia in China: An update from the CHIF-NET Study. *J. Infect. Dis.* 221, S139–S147.

Xiao, M., Fan, X., Chen, S. C., Wang, H., Sun, Z. Y., Liao, K., et al. (2015). Antifungal susceptibilities of Candida *Glabrata species* complex, Candida krusei, Candida *Parapsilosis species* complex and Candida tropicalis causing invasive candidiasis in China: 3 year national surveillance. *J. Antimicrob. Chemother.* 70, 802–810. doi: 10.1093/jac/dku460

Xiao, M., Fan, X., Hou, X., Chen, S. C., Wang, H., Kong, F., et al. (2018). Clinical characteristics of the first cases of invasive candidiasis in China due to pan-echinocandin-resistant Candida tropicalis and Candida glabrata isolates with delineation of their resistance mechanisms. *Infect. Drug Resist.* 11, 155–161. doi: 10.2147/idr.s152785

Xisto, M. I., Caramalho, R. D., Rocha, D. A., Ferreira-Pereira, A., Sartori, B., Barreto-Bergter, E., et al. (2017). Pan-azole-resistant Candida tropicalis carrying homozygous erg11 mutations at position K143R: a new emerging superbug? *J. Antimicrob. Chemother.* 72, 988–992.

Conflict of Interest: The authors declare that the research was conducted in the absence of any commercial or financial relationships that could be construed as a potential conflict of interest.

frontiers in Microbiology

ORIGINAL RESEARCH
published: 16 July 2021
doi: 10.3389/fmicb.2021.708009

A Comparative Transcriptome Between Anti-drug Sensitive and Resistant *Candida auris* in China

Wenkai Zhou[1†], Xiuzhen Li[2†], Yiqing Lin[1], Wei Yan[1], Shuling Jiang[1], Xiaotian Huang[2], Xinglong Yang[1], Dan Qiao[3]* and Na Li[1]**

[1] The First Affiliated Hospital of Nanchang University, Nanchang, China, [2] Department of Medical Microbiology, School of Medicine, Nanchang University, Nanchang, China, [3] Department of Laboratory Medicine, Ruijin Hospital, Shanghai Jiao Tong University School of Medicine, Shanghai, China

Candida auris emerged as a pathogenic species of fungus that causes severe and invasive outbreaks worldwide. The fungus exhibits high intrinsic resistance rates to various first-line antifungals, and the underlying molecular mechanism responsible for its multidrug resistance is still unclear. In this study, a transcriptomic analysis was performed between two *C. auris* isolates that exhibited different anti-drug patterns by RNA-sequencing, namely, CX1 (anti-drug sensitive) and CX2 (resistant). Transcriptomic analysis results revealed 541 upregulated and 453 downregulated genes in the resistant *C. auris* strain compared with the susceptible strain. In addition, our findings highlight the presence of potential differentially expressed genes (DEGs), which may play a role in drug resistance, including genes involved in ergosterol and efflux pump biosynthesis such as *SNQ2*, *CDR4*, *ARB1*, *MDR1*, *MRR1*, and *ERG* genes. We also found that Hsp related genes were upregulated for expression in the anti-drug-resistant strain. Biofilm formation and growth conditions were also compared between the two isolates. Our study provides novel clues for future studies in terms of understanding multidrug resistance mechanisms of *C. auris* strains.

Keywords: *Candida auris*, RNA-seq, drug resistance, transcriptome, virulence

OPEN ACCESS

Edited by:
Keke Huo,
Fudan University, China

Reviewed by:
Min Chen,
Shanghai Changzheng Hospital, China
Boyu Liu,
Anhui Medical University, China

****Correspondence:***
Xinglong Yang
xinglongyang0510@163.com
Dan Qiao
qiaodan840924@163.com
Na Li
pingguonana1999@163.com

[†] These authors have contributed equally to this work

Specialty section:
This article was submitted to Antimicrobials, Resistance and Chemotherapy, a section of the journal Frontiers in Microbiology

Received: *11 May 2021*
Accepted: *16 June 2021*
Published: *16 July 2021*

Citation:
Zhou W, Li X, Lin Y, Yan W, Jiang S, Huang X, Yang X, Qiao D and Li N (2021) A Comparative Transcriptome Between Anti-drug Sensitive and Resistant Candida auris in China. Front. Microbiol. 12:708009. doi: 10.3389/fmicb.2021.708009

INTRODUCTION

Candida auris is a species of fungus that was firstly isolated from a patient's external ear canal in Tokyo, Japan and represented a novel species within this genus in 2009 (Satoh et al., 2009). However, a study performed in 2011 revealed that *C. auris* already existed as a nosocomial infective agent in South Korea since 1996, in a case that the infection was treated as unidentified yeasts and which eventually caused nosocomial fungemia in a 1-year-old girl (Lee et al., 2011). Since its first description in 2009, the presence of *C. auris* was soon reported in all continents, except Antarctica, and which caused infections in more than 40 countries (Chow et al., 2018; Rhodes and Fisher, 2019; Vila et al., 2020). Genomic epidemiology revealed that *C. auris* exhibits five genetically diverse clades by genome sequencing. Consequently, this species was divided according to the following geographical clusters: Clade I (South Asian), Clade II (East Asian), Clade III (African), Clade IV (South American), and Clade V (Iran). Clade V was isolated from a patient in Iran and is the most recently identified clade (Lockhart et al., 2017; Chow et al., 2019). Genetic sequences of isolates from patients or environments are very important to trace the transmission of *C. auris* among different

countries, hospitals, and perhaps different patients' parts. What makes this species so important is its ability to spread and cause nosocomial outbreaks in hospitals and healthcare facilities in a similar manner to bacteria (Schelenz et al., 2016; Adams et al., 2018; Eyre et al., 2018; Ruiz-Gaitan et al., 2018, 2019; Armstrong et al., 2019; O'Connor et al., 2019). In fact, a recent review showed that the majority of the recovery sites in *C. auris* outbreaks involved candidemia (blood) and skin, which in turn underlines the ability of *C. auris* to induce invasive infections and colonization (Vila et al., 2020). Misidentification of *C. auris*, which unavoidably induces inappropriate and delayed treatment, is another important reason for these outbreaks. Unlike other yeasts, *C. auris* has often been confused with other pathogens such as *C. parapsilosis*, *C. haemulonii*, and *C. sake* by commercial systems (Lee et al., 2011; Kathuria et al., 2015; Mizusawa et al., 2017; Adams et al., 2018; Snayd et al., 2018; ElBaradei, 2020). Reliable identification methods involve systems with updated databases and molecular methods, which target the specific sequences of *C. auris* (Kathuria et al., 2015; Kordalewska et al., 2017; Sexton et al., 2018; Forsberg et al., 2019; Lima et al., 2019; Lone and Ahmad, 2019). However, the most worrying characteristic of *C. auris* pertains to its intrinsic or required resistance to a variety of first-line antifungals commonly used in clinical settings, including the three main categories of antifungals, i.e., azoles, echinocandins, and polyenes, thus limiting the underlying treatment options (Adams et al., 2018; Chaabane et al., 2019; Wickes, 2020). As a result, the misidentification and multidrug resistance of *C. auris* have both been prominent factors that enhance the ability of this fungus to cause infections with significant patient mortality, especially in patients that already suffer from concurrent diseases or receive invasive treatments (Lockhart et al., 2017; Armstrong et al., 2019; de Jong and Hagen, 2019; Taori et al., 2019).

Despite the fact that the multidrug resistance of *C. auris* has been a prevalent concern, there have only been a limited number of research studies performed to expound its mechanisms of antifungal resistance, and thus, these molecular mechanisms remain unknown (Chaabane et al., 2019; Kean and Ramage, 2019). For instance, several studies have focused on its phenotype. However, the majority of studies on antifungal resistance mechanisms are based on drug resistance-related genes in non-auris *Candida* species that have been previously reported (Arastehfar et al., 2020; Lee et al., 2020). Pertaining to azoles resistance, mutations in *ERG11* and *ERG11* overexpression play a distinct role in *C. auris* that facilitate drug target alteration and overexpression, respectively (Pristov and Ghannoum, 2019). Another common mechanism for azole resistance in *C. auris* involves efflux pumps enhanced overexpression including Major Facilitator Superfamily (MFS) and ATP Binding Cassette (ABC) that accelerate drug efflux (Kean et al., 2018; Lee et al., 2020). Echinocandin resistance in *C. auris* is the result of mutations in *FKS1* due to drug target alterations (Pristov and Ghannoum, 2019). However, the resistance mechanism to amphotericin B is still not confirmed, and it cannot be explained by any of the proposed mechanisms thus far. Apart from the pathways that the above genes participate in, certain genes play a role in triggering stress responses such as *HSP90*, which also confer resistance (Lee et al., 2020).

In this study, we performed transcriptome analysis on two *C. auris* strains using RNA-sequencing (RNA-seq). One strain showed elevated minimum inhibitory concentration (MIC) in fluconazole and micafungin, whereas the other strain was a susceptible strain. Until now, a limited number of research studies have been performed with RNA-seq between susceptible and resistant *C. auris* strains without imposing any conditions in China. Consequently, through the analysis of gene expression differences, we aimed to explore the resistance mechanism and identify genes that may play an important part of this process.

MATERIALS AND METHODS

Bacterial Strains and Identification

The first *C. auris* strain used in this study was isolated from the environment in China and was named CX1. The other *C. auris* strain was acquired from the NCCLs (National Center for Clinical Laboratories), was isolated from a patient's ascitic fluid, and was named CX2. Two isolates were identified as *C. auris* by sequencing ribosomal DNA internal transcribed spacer (ITS) combined with using matrix-assisted laser desorption/ionization time of flight mass spectrometry (Bruker Daltonics, Germany) (Schoch et al., 2012; Fraser et al., 2016). The Ethics Committee of The First Affiliated Hospital of Nanchang University (approval no. 2016026) approved the present study. All participants provided a written informed consent to participate in this study.

Antifungal Susceptibility Testing

In vitro antifungal susceptibility testing was performed with YeastOne plate (Thermo Fisher, United States) on three replicates of two strains according to the Clinical and Laboratory Standards Institute (CLSI) broth microdilution method M27-A3 (Clinical and Laboratory Standards Institute [CLSI], 2008). Several fully isolated strains were also selected from a yeast isolate of 24 h pure yeast culture species, emulsified in sterile water, and mixed with vortex. Then, we adjusted yeast suspension to 0.5 McFarland and Pipetted 20 μl to 11 ml fungus inoculation broth. Broth suspension (100 μl) was pipetted onto the drug sensitive plate and incubated in 35°C for 24 h. Finally, SensititreVizion system (Thermo Fisher, United States) was used to read the test results of the drug sensitive plate. The activities of nine antifungals against two *C. auris* isolates were tested, including fluconazole, itraconazole, voriconazole, posaconazole, micafungin, anidulafungin, caspofungin, amphotericin B, and 5-flucytosine. The MIC endpoints were interpreted in tentative breakpoints proposed by CDC[1], as follows: ≥32 for fluconazole, ≥2 for amphotericin B, ≥4 for anidulafungin and micafungin, and ≥2 for caspofungin.

RNA Extraction

Candida auris cells were inoculated in yeast–peptone–dextrose (YPD) broth medium with constant shaking at 220 rpm at

[1]https://www.cdc.gov/fungal/candida-auris/c-auris-antifungal.html

30S°C for 18 h. The fungus was collected at an approximate OD 600 = 0.7, transferred to the EP tube, and resuspended in 50 μl of sterile water preheated at 30°C. Cells were cooled quickly in the liquid nitrogen and grinded to powder in the pre-cooled grinding tool. Then, we added 1 ml of Trizol solution (Invitrogen, United Kingdom), grinded, sealed the mortar with tin foil, and let it stand. When the Trizol–bacteria mixture became liquid, we gently grinded this mixture again. Ribozyme-free pipette tips were used to suck the Trizo-bacterial mixture into new ribozyme-free 1.5 ml EP tubes, which were subsequently centrifuged at 12,000 rpm for 10 min at 4°C. We pipetted the water phase to new 1.5 ml EP tubes and added an equal volume of 25:24:1 phenol/chloroform/isoamyl alcohol, which was vigorously shook for 10 s and centrifuged at 4°C, 12,000 rpm for 5 min. Water phase was transferred to new 1.5 ml EP tubes, and an equal volume of isopropanol was added into an ice-bath for 10 min. We then centrifuged the tubes at 12,000 rpm at 4°C for 5 min, and we discarded the supernatant. The total RNA was then washed with 75% ethanol and centrifuged at 12,000 rpm for 5 min, and the supernatant was discarded. Total RNA was dried for 5–10 min, resuspended in 25 μl DEPC water, and temporarily stored at −20°C. Following this protocol for obtaining the total RNA, we used electrophoresis to observe the integrity of the RNA using 1.0% agarose gel. Quality and concentration of the isolated RNA were assessed by NanoDrop 2000c (Thermo Scientific, United Kingdom). CX1 and CX2 isolates were cultured in triplicates named CX1-1, CX1-2, CX1-3 and CX2-1, CX2-2, CX2-3, respectively.

Transcriptome Analysis

In total, six samples and three biological replicates for two strains were sent for cDNA library construction, transcriptome sequencing, and analysis conducted by OE biotech Co., Ltd. (Shanghai, China). Furthermore, TruSeq Stranded mRNA LT Sample Prep Kit (Illumina, San Diego, CA, United States) was used to construct cDNA library in accordance with the manufacturer's instructions. After the constructed library was qualified with Agilent 2100 Bioanalyzer, it was sequenced using Illumina HiSeq X Tento to generate 150 bp paired-end reads. Raw reads of fast format were preprocessed using Trimmomatic (Bolger et al., 2014), and the number of reads in the whole quality control was statistically summarized. Each sample's clean reads remained after quality pretreatment steps, including the removal of reads containing adaptor, low quality reads, and bases arranged in different ways from the 3′ end and 5′ end. HISAT2 (Kim et al., 2015) was used to compare the clean reads with the specific reference genome[2] to obtain the position information on the reference genome and the unique sequence feature information of the sequenced samples. The STRING (Search Tool for the Retrieval of Interacting Genes) database (Szklarczyk et al., 2019) was used to construct a protein–protein association network and to visualize the interactome network.

[2]http://www.candidagenome.org/download/chromosomal_feature_files/C_auris_B11221/

DEG Analysis

Each gene's FPKM (Roberts et al., 2011) value was calculated using Cufflinks (Trapnell et al., 2010), and its read counts were obtained by HTSeq-count (Anders et al., 2015). Cluster analysis was performed with the "pheatmap" package to explore gene expression pattern. Correlation test between samples was carried out using R language to calculate the Pearson correlation coefficient. DEseq (2012) R package was used to perform differential expression analysis. The threshold of significantly differential expression between samples was a false discovery rate (FDR) < 0.05 and fold change > 1.5.

Functional Annotation

Gene Ontology (GO) enrichment and Kyoto Encyclopedia of Gene and Genomes (KEGG) (Kanehisa et al., 2008) pathway enrichment analysis of differentially expressed genes (DEGs) were performed using R based on the hypergeometric distribution. Biological process, cellular component, and molecular function enrichment analysis in GO level 2 were performed on DEGs using the fisher algorithm.

Virulence Factor Prediction

We initially searched for genes associated with phospholipase, proteinase, hemolysin, adhesin, and biofilm formation in our transcriptome results. Subsequently, we searched for phospholipase, proteinase, hemolysin, and adhesin in Candida genome database (CGD). After retrieving related genes in other *Candida* species, we then searched for orthologous genes or best hits in *Candida auris*, shown in **Supplementary Table 2**. For biofilm formation, we downloaded the biofilm formation phenotype from CGD and performed a blastp with DEGs in the transcriptome. The criteria for filtering the blastp results were over 50% coverage and identity.

Biofilm Formation Experiment and Growth Experiment

Prior to developing the biofilm, we treated the 96-well plate (Corning, United Kingdom) with fetal bovine serum, blocked at 4°C for 72 h, and then washed with sterile phosphate buffer saline. Candida was inoculated in YPD medium broth, incubated with shaking at 220 rpm at 30°C overnight, and then resuspended with Spider medium to make OD_{600} = 0.5. We added 200 μl bacterial solutions to each well in the experimental group and 200 μl Spider medium in the control group. The plate was incubated at 37°C under shaking at 200 rpm for 90 min and then washed with PBS. Each hole was added with 200 μl Spider medium and sealed with sealing film. After being incubated at 37°C under shaking at 200 rpm for 48 h, the culture medium was discarded, and each hole was washed with PBS. We fixed each well with 200 μl methanol for 30 min and then used 200 μl 11% crystal violet to stain after discarding fixative. Then, we absorbed the crystal violet and washed each well with PBS after washing with slow water flow and then decolorized each well with glacial acetic acid for 30 min. Finally, biofilm formation was measured according to spectrophotometric methods using microplate reader (Biotek, United States).

TABLE 1 | Antifungal susceptibility.

Strain	MIC, μ g/ml								
	FLZ	ITZ	VRZ	PSZ	MCF	ANF	CSF	AMB	FC
CX1	2	0.03	0.015	0.015	0.06	0.12	0.06	0.25	≤0.06
CX2	64	≤0.015	0.06	≤0.008	8	2	1	1	≤0.06

FLZ, fluconazole; ITZ, itraconazole; VRZ, voriconazole; PSZ, posaconazole; MCF, micafungin; ANF, anidulafungin; CSF, caspofungin; AMB, amphotericin B; FC, 5-flucytosine.

A spot dilution assay was performed to compare the growth status of the two *C. auris* isolates and *C. albicans*. Candida was incubated in YPD liquid medium with constant shaking at 220 rpm at 30°C overnight. Then, we collected the bacteria by centrifugation at 3,000 rpm, washed with sterile PBS, and resuspended with PBS. The yeast suspension was adjusted to an optical density (OD_{600}) of 0.1 and was diluted by 10-fold serial in sterile PBS to a final OD_{600} of 10^{-2}, 10^{-3}, 10^{-4}, 10^{-5}, 10^{-6}, and 10^{-7}. A total of 1 μl suspension of each dilution was spotted on the YPD agar plate, and the plate was cultured at 30°C for 4 days before observing the growth differences of the two strains' colonies.

RESULTS

Antifungal Susceptibility

As demonstrated in **Table 1**, CX2 exhibits a higher MIC toward antifungals than CX1, except 5-flucytosine, itraconazole, and posaconazole, thus indicating that CX2 was a resistant strain as opposed to CX1. Apart from fluconazole (MIC = 2 μg/ml), CX1 exhibited high susceptibility to all three main categories of antifungals and 5-flucytosine. With respect to the antifungal susceptibility testing of azoles, fluconazole was the least active azole (MIC = 16 μg/ml) against CX2. Interestingly, CX2 exhibited higher susceptibility to itraconazole (MIC≤0.015 μg/ml) and posaconazole (≤0.008 μg/ml) compared to CX1. MICs of echinocandins were greater for CX2 compared to CX1: caspofungin (MIC = 1 μg/ml), anidulafungin (MIC = 2 μg/ml), and micafungin (MIC = 8 μg/ml). Furthermore, CX2 displayed significant resistance to micafungin, which may represent the underlying drug resistance mechanism. The MIC of amphotericin B was 1 μg/ml in CX2, whereas the MIC of 5-flucytosine was ≤0.06 μg/ml, both in CX1 and CX2 (**Table 1**).

Biofilm Formation and Growth Condition

As opposed to the two *C. auris* isolates that did not form any biofilm and were thus the same as the blank control, *C. albicans* (SC5314) formed biofilm in the 96-well plate (**Supplementary Figure 1A**). The spot assay was used to assess the growth status of the two *C. auris* isolates and *C. albicans* (SC5314) (**Supplementary Figure 1B**). No growth differences were found between the two *C. auris* strains and between *C. auris* and *C. albicans* strains.

Transcriptome Analysis

In this study, we performed a comparative RNA-seq analysis on two clinical types (CX1 and CX2) including six samples (CX1-1, CX1-2, CX1-3, CX2-1, CX2-2, and CX2-3) to identify DEGs that may potentially facilitate drug-related resistance. The Illumina sequencing of the transcriptome of these six samples produced raw RNA-seq reads. To minimize the effect of data error in our results, we used the Trimmomatic software to pre-process the original data, and the number of reads in the whole quality control process was statistically summarized (**Supplementary Table 1**).

Hisat2 was used to sequence the aligned Clean Reads with the specified reference genome to obtain the location information on the reference genome or gene, as well as the sequence characteristic information that was unique to the sequencing sample (**Supplementary Table 2**). The percentage of raw reads of samples mapped to the *C. auris* genome was high (over 98% in total mapped reads), thus indicating that these samples were consistent with *C. auris*.

Principal-component analysis and cluster analysis were used to demonstrate a visual representation of the correlation in transcriptome between the different replicates (**Figures 1A,B**). Samples from different isolates were clustered separately, whereas samples from the same isolates were clustered together. Furthermore, the protein coding gene expression level was used to generate a heatmap of correlation coefficient between samples (**Figure 1C**). The results obtained reflected a high-level of relevance among samples from the same strain and slight differences between CX1 and CX2.

RNA-seq data analysis clearly displayed a wide range of differences between CX1 and CX2 gene expression in the transcriptome. More specifically, genes with a 1.5-fold change (up or down) in the level of expression were considered to reflect differences in gene expression, and they were thus regarded as significantly regulated genes. A negative binomial distribution test revealed a P-value < 0.05. Nine hundred ninety-four statistically significant variation genes were found in expression between our samples, of which 541 were upregulated and 453 were downregulated (**Supplementary Table 3**). The volcano plot was used to demonstrate the number of significantly DEGs between CX1

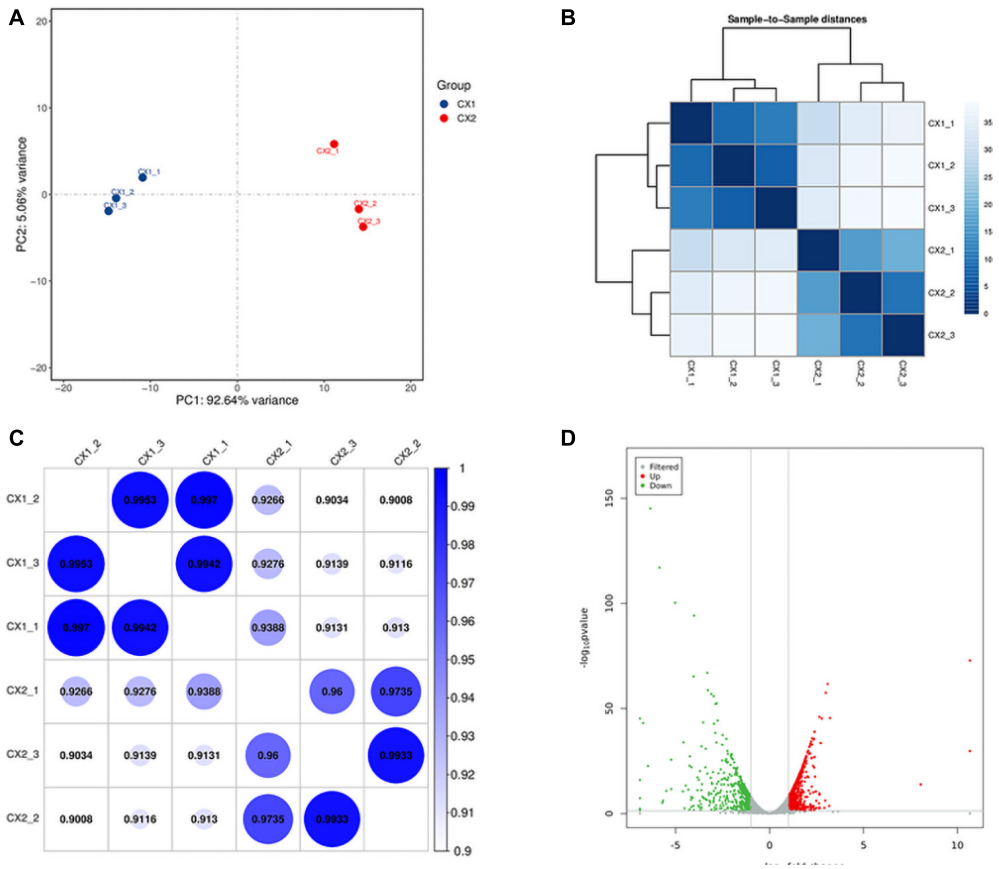

FIGURE 1 | Validation of *C. auris* transcriptome. **(A)** Principal component analysis (PCA) plot showing the level of correlation among CX1 (blue) and CX2 (red). The closer the PCA plot distance is, the more similar the samples are. **(B)** Cluster analysis of gene expression data. The chromaticity of the color represents the size of the correlation coefficient. **(C)** Heat map of correlation coefficient between samples. The color represents the size of the correlation coefficient. **(D)** Volcano plot. Every dot represents a differentially expressed gene. Gray dots were non-significantly different genes, and the green and red dots were significantly upregulated different genes in CX1 and CX2, respectively.

and CX2 (**Figure 1D**). Clustering analysis of the differential expression patterns showed that the DEGs were consistent across replicates, with a significant variation between CX1 and CX2 (**Figure 2**).

Enrichment Analysis of DEGs

After obtaining the statistically DEGs, the GO enrichment analysis was carried out on the DEGs to describe their respective functions (combined with the GO annotation results). The DEGs could be divided into three main GO categories, i.e., biological process, cellular component, and molecular function (**Figure 3**). The 669 downregulated differential expression genes were assigned to 43 GO terms, including 21 biological processes, 11 cellular components, and 11 molecular functions. More specifically, these genes were distributed as follows: biological processes included cellular processes (70.3%), single-organism processes (62.9%), and metabolic processes (53.7%); cellular components associated with cells (85.2%), cell parts (84.6%), and organelles (60.5%); and molecular functions containing catalytic activity (49.3%) and binding (49.0%). In contrast, the 885 upregulated differential expression genes were assigned to 41 GO terms, including 20 biological processes, 10 cellular components, and 11 molecular functions. More specifically, these genes were distributed as follows: biological processes, including cellular processes (84.0%) and metabolic processes (74.4%); cellular components associated with cells (93.6%), cell parts (93.6%), and organelles (76.0%); molecular functions contributing to binding (58.8%) and catalytic activity (42.7%).

Moreover, the pathway-analysis of differentially expressed protein coding genes using the KEGG database (combined with KEGG annotation results) could reveal the relationship between drug resistance and cellular pathway changes. A total of 427 downregulated genes and 558 upregulated genes were categorized into known KEGG pathways. Among the 427 downregulated genes, 82 DEGs were distributed in cellular processes that were mainly sub-categorized under transport and catabolism (17.1%), and cell growth and death (10.2%). In addition, 44 DEGs were distributed in environmental information processing that were mainly sub-categorized under signal transduction (17.1%), whereas 41 DEGs were distributed in genetic information processing that were mainly sub-categorized under folding, sorting, and degradation (9.8%). Finally, 260 DEGs were

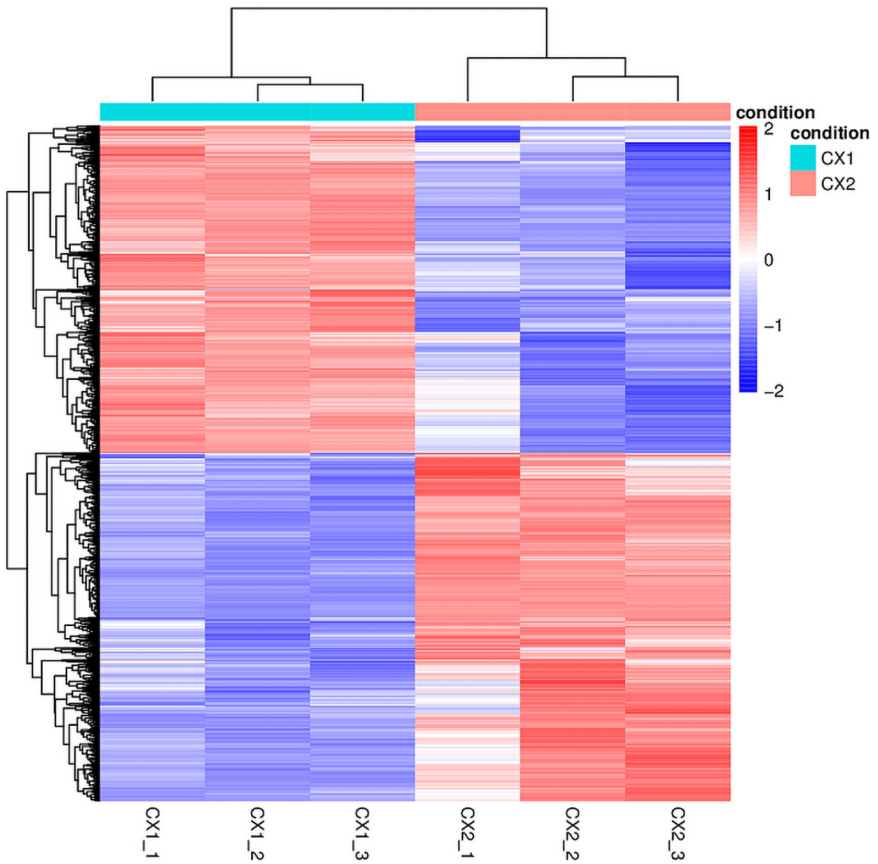

FIGURE 2 | The heatmap of DEGs identified in this study. In the heatmap, rows in red and blue represent upregulated and downregulated genes, respectively. The different depth of colors represents different level of DEG expression.

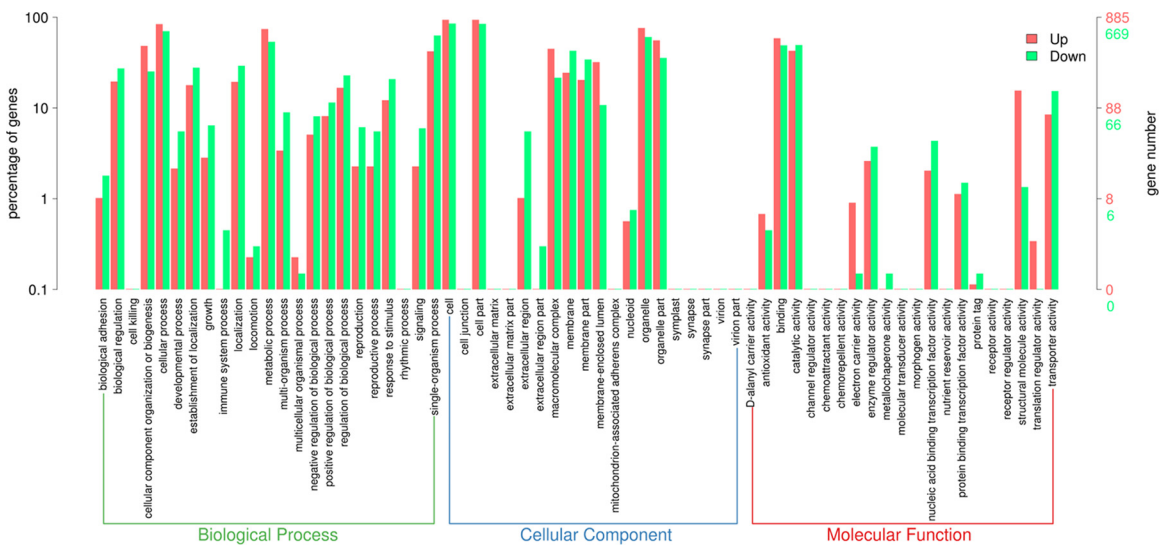

FIGURE 3 | Gene Ontology (GO) term enrichment of differentially expressed genes between sensitive and resistant strains. Three GO categories including molecular function, cellular component, and biological process were used to classify the DEGs. Red represented upregulated genes, and green represented downregulated genes.

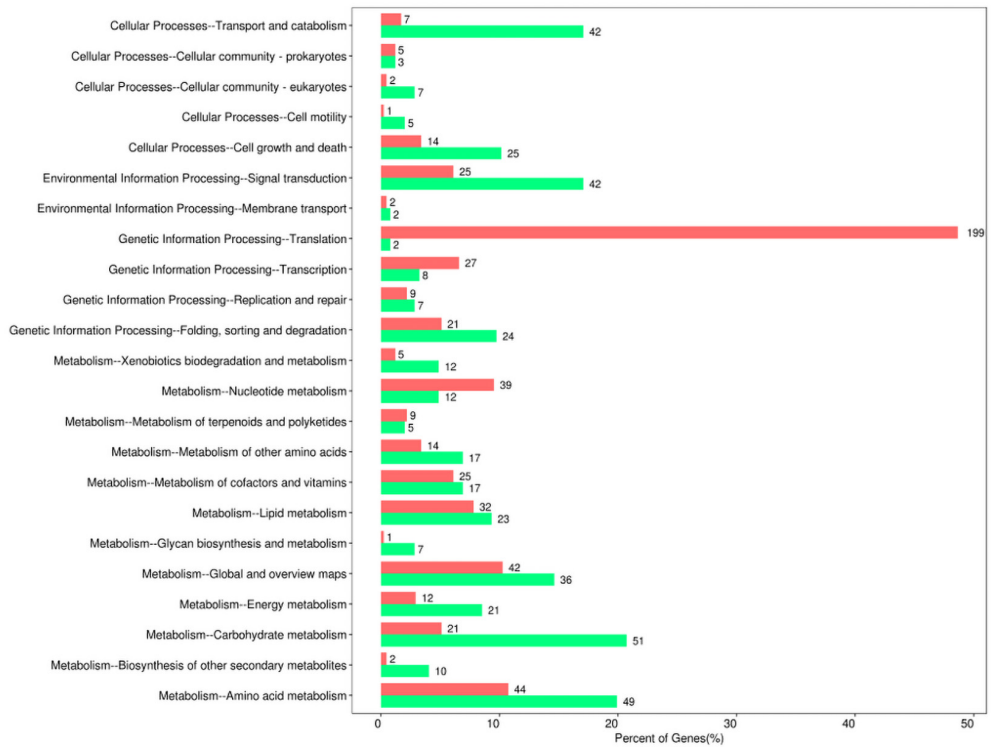

FIGURE 4 | Kyoto Encyclopedia of Gene and Genomes (KEGG) pathway enrichment of differentially expressed genes between sensitive and resistant strains. Red represented upregulated genes, and green represented downregulated genes.

distributed in metabolism, and they were mainly sub-categorized under carbohydrate metabolism (20.7%), amino acid metabolism (19.9%), and global and overview maps (14.6%). In contrast, among the 558 upregulated genes, 29 DEGs were distributed in cellular processes that were mainly sub-categorized under cell growth and death (3.4%), and 27 DEGs were distributed in environmental information processing that were mainly sub-categorized under signal transduction (6.1%). Furthermore, 256 DEGs were distributed in genetic information processing that were especially sub-categorized under translation (48.7%), and 246 DEGs were distributed in metabolism that were mainly sub-categorized under nucleotide metabolism (9.5%), amino acid metabolism (10.8%), and global and overview maps (10.3%) (**Figure 4**).

Virulence Factors

A previous study performed showed that *C. auris* exhibit phospholipase, proteinase, and hemolysin activity *in vitro* (Kumar et al., 2015). In another study, *C. auris* were found to produce phospholipase and proteinase that varied by strain (Larkin et al., 2017). The draft genome of *C. auris* revealed that virulence may be caused as a result of its diverse transporters, secreted aspartyl proteinases, secreted lipases, phosphatases, phospholipase, mannosyl transferases, integrins, adhesins, and transcription factors (Chatterjee et al., 2015). In this study, we investigated phospholipase, proteinase, hemolysin, adhesin, and biofilm formation-related genes in CGD. Initially, we did not identify hemolysin-related genes in DEGs between sensitive and resistant strains. However, a certain number of DEGs exist, which were related with phospholipase, proteinase, adhesion, and biofilm formation (**Table 2**). In fact, **Table 2** shows that a greater number of downregulated than upregulated genes were related with phospholipase, proteinase, and adhesin. These findings are consistent with the common knowledge that drug resistance strains possess fewer virulence factors and thus demonstrate wear virulence. Meanwhile, our findings regarding DEGs related with biofilm formation were inconsistent with previous results that suggested a slightly greater number of upregulated genes compared to downregulated genes.

Protein Interaction Network

In order to acquire a more accurate visualization of the molecular mechanism of multidrug resistance involved in *C. auris*, we used the STRING (Search Tool for the Retrieval of interacting Genes) database to generate a predicted protein interaction network that contained the top 20 downregulated DEGs and top 20 upregulated DEGs (**Figure 5**). The red and green nodes with gene names represented the upregulated and downregulated DEGs, respectively. The obtained picture shows that the proteins were divided into two clusters. Consequently, the core genes that more predicted associations with other genes and other remaining genes within the network were then investigated.

TABLE 2 | Upregulated and downregulated phospholipase-, proteinase-, adhesin-, and biofilm-associated genes (CX2 vs. CX1).

Gene-identifier	Gene symbol	Description	Function	Fold change (log_2)
B9J08_004010	PLB1	Lysophospholipase 1	Phospholipase	−2.88
B9J08_003621	PLB3	Lysophospholipase 3	Phospholipase	−0.86
B9J08_003289	SPAC6G10.03c	Probable cardiolipin-specific deacylase, mitochondrial	Phospholipase	−0.59
B9J08_003446	RAS1	Ras-like protein 1	Phospholipase	−0.69
B9J08_005379	ATG15	Putative lipase ATG15	Phospholipase	−0.92
B9J08_003305	CDC25	Cell division control protein 25	Phospholipase	−0.98
B9J08_000458	CEK1	Extracellular signal-regulated kinase 1	Phospholipase	−0.86
B9J08_005379	ATG15	Putative lipase ATG15	Phospholipase	−0.92
B9J08_003361	RHO1	GTP-binding protein RHO1	Phospholipase	0.60
B9J08_003959	SLC1	Probable 1-acyl-sn-glycerol-3-phosphate acyltransferase	Phospholipase	0.69
B9J08_004606	YOR059C	Putative lipase YOR059C	Phospholipase	0.69
B9J08_001064	PGC1	Phosphatidylglycerol phospholipase C	Phospholipase	0.63
B9J08_003873	PLC1	1-Phosphatidylinositol 4,5-bisphosphate phosphodiesterase 1	Phospholipase	0.85
B9J08_000871	LAP3	Cysteine proteinase 1, mitochondrial	Proteinase	−1.25
B9J08_005051	YIL108W	Putative zinc metalloproteinase YIL108W	Proteinase	−0.73
B9J08_002962	LAP3	Cysteine proteinase 1, mitochondrial	Proteinase	−1.11
B9J08_003912	YPS1	Aspartic proteinase 3	Proteinase	−0.75
B9J08_001019	RRT12	Subtilase-type proteinase RRT12	Proteinase	1.27
B9J08_002266	TRY4	Transcriptional regulator of yeast form adherence 4	Adhesin	−1.17
B9J08_000829	TRY5	Transcriptional regulator of yeast form adherence 5	Adhesin	−2.76
B9J08_002582	ALS4	Agglutinin-like protein 4 (fragments)	Adhesin	8.05
B9J08_001242	PGA1	Predicted GPI-anchored protein 1	Adhesin	−0.61
B9J08_001958	SAP9	Candidapepsin-9	Adhesin	−1.08
B9J08_002075	SDS3	Transcriptional regulatory protein SDS3	Adhesin	−0.98
B9J08_002266	TRY4	Transcriptional regulator of yeast form adherence 4	Adhesin	−1.17
B9J08_000829	TRY5	Transcriptional regulator of yeast form adherence 5	Adhesin	−2.76
B9J08_001192	SNF2	Transcription regulatory protein SNF2	Adhesin	−0.86
B9J08_002529	BRG1	Biofilm regulator 1	Adhesin	−1.73
B9J08_002596	MP65	Cell surface mannoprotein MP65	Adhesin	−2.63
B9J08_003278	MCM1	Transcription factor of morphogenesis MCM1	Adhesin	−0.77
B9J08_003305	CDC25	Cell division control protein 25	Adhesin	−0.98
B9J08_003836	HXK1	*N*-Acetylglucosamine kinase 1	Adhesin	−0.73
B9J08_003920	PKH2	Serine/threonine-protein kinase PKH2	Adhesin	−0.76
B9J08_004027	WOR1	White-opaque regulator 1	Adhesin	−2.03
B9J08_000458	CEK1	Extracellular signal-regulated kinase 1	Adhesin	−0.86
B9J08_000675	FLO9	Flocculation protein FLO9	Adhesin	−3.28
B9J08_000447	CRZ2	Transcriptional regulator CRZ2	Adhesin	1.48
B9J08_000592	UME6	Transcriptional regulatory protein UME6	Adhesin	2.49
B9J08_001918	AHR1	Adhesion and hyphal regulator 1	Adhesin	2.38
B9J08_001940	HSP12	12 kDa heat shock protein	Adhesin	1.56
B9J08_002582	ALS4	Agglutinin-like protein 4 (fragments)	Adhesin	8.05
B9J08_003361	RHO1	GTP-binding protein RHO1	Adhesin	0.60
B9J08_003550	YWP1	Yeast-form wall protein 1	Adhesin	2.96
B9J08_003772	CZF1	Zinc cluster transcription factor CZF1	Adhesin	1.42
B9J08_005078	AAH1	Adenine deaminase	Adhesin	0.79
B9J08_005458	ASC1	Guanine nucleotide-binding protein subunit beta-like protein	Adhesin	1.58
B9J08_001196	CSA1	Cell wall protein 1	Biofilm formation	−1.00
B9J08_000458	CEK1	Extracellular signal-regulated kinase 1	Biofilm formation	−0.86
B9J08_002788	TPK2	cAMP-dependent protein kinase type 2	Biofilm formation	−1.29
B9J08_004015	GAM1	Glucoamylase 1	Biofilm formation	−0.73

(continued)

TABLE 2 | continued

Gene-identifier	Gene symbol	Description	Function	Fold change (log_2)
B9J08_000003	zrt1	Zinc-regulated transporter 1	Biofilm formation	−1.41
B9J08_002763	FAA1	Long-chain-fatty-acid–CoA ligase 1	Biofilm formation	−0.70
B9J08_000860	TAF14	Transcription initiation factor TFIID subunit 14	Biofilm formation	−0.74
B9J08_000928	AQY1	Aquaporin-1	Biofilm formation	−1.90
B9J08_001383	ams1	Alpha-mannosidase	Biofilm formation	−1.86
B9J08_003563	ADH2	Alcohol dehydrogenase 2	Biofilm formation	−3.10
B9J08_001633	YMR315W	Uncharacterized protein YMR315W	Biofilm formation	−0.59
B9J08_004068	VPS4	Vacuolar protein sorting-associated protein 4	Biofilm formation	−1.06
B9J08_004334	PHO2	Regulatory protein PHO2	Biofilm formation	−1.09
B9J08_004477		Glucan 1,3-beta-glucosidase	Biofilm formation	−3.62
B9J08_005380	SUR7	Protein SUR7	Biofilm formation	−0.60
B9J08_003614	ADH2	Alcohol dehydrogenase 2	Biofilm formation	−3.61
B9J08_000384	EPD1	Protein EPD1	Biofilm formation	1.40
B9J08_000822	CBK1	Serine/threonine-protein kinase CBK1	Biofilm formation	0.60
B9J08_001624	ILS1	Isoleucine–tRNA ligase, cytoplasmic	Biofilm formation	1.28
B9J08_001686	RPS4A	40S ribosomal protein S4-A	Biofilm formation	1.39
B9J08_001939	RIX7	Ribosome biogenesis ATPase RIX7	Biofilm formation	1.18
B9J08_002042	At2g30170	Probable protein phosphatase 2C 26	Biofilm formation	1.44
B9J08_002043	ARO1	Pentafunctional AROM polypeptide	Biofilm formation	0.78
B9J08_002365	STH1	Nuclear protein STH1/NPS1	Biofilm formation	0.61
B9J08_002420	FAS2	Fatty acid synthase subunit alpha	Biofilm formation	0.90
B9J08_002855	PMA1	Plasma membrane ATPase 1	Biofilm formation	0.98
B9J08_003041	PDX1	Pyruvate dehydrogenase complex protein X component, mitochondrial	Biofilm formation	1.33
B9J08_003159	CPH1	Transcription factor CPH1	Biofilm formation	1.17
B9J08_003402	ZPR1	Zinc finger protein ZPR1	Biofilm formation	1.73
B9J08_003582	RPS4A	40S ribosomal protein S4-A	Biofilm formation	1.81
B9J08_003641	DUS3	tRNA-dihydrouridine(47) synthase [NAD(P)(+)]	Biofilm formation	1.12
B9J08_003772	CZF1	Zinc cluster transcription factor CZF1	Biofilm formation	1.42
B9J08_004640	SIM1	Secreted beta-glucosidase SIM1	Biofilm formation	0.79
B9J08_004918	HSP90	Heat shock protein 90 homolog	Biofilm formation	0.80
B9J08_005403	QDR3	MFS antiporter QDR3	Biofilm formation	0.84

DISCUSSION

Candida auris is a pathogen that has been known for more than 10 years, yet it continuously causes outbreaks and exhibits alarmingly high drug resistance rates and even pan-drug resistance, which has not been efficiently studied (Wickes, 2020). Despite the high mortality rates caused by *Candida auris* infections, due to the rapid spread and frequent worldwide outbreaks caused by this fungus, only a small number of drugs can appropriately treat fungal infections. To understand the mechanism that facilitates drug resistance, we performed transcriptome of two *Candida auris* isolates, one of which was found to be resistant to fluconazole (MIC = 64) and micafungin (MIC = 8), and the other was found to be susceptible to antifungal drugs based on CDC reports (see text footnote 1). Therefore, we focused on the underlying mechanism of resistance to azoles and echinocandins in *Candida auris*. Due to the fact that the two *Candida auris* strains were unable to form biofilms, we searched the agglutinin-like sequence (*ALS*) genes in DEGs that play an important role in biofilm formation after attachment to abiotic surfaces (Hoyer and Cota, 2016). As expected, we only found *ALS4*, which is the most frequently expressed gene in the *ALS* gene family and which is differentially expressed between these two strains (but with low expression levels) (Monroy-Perez et al., 2012). The average value of *ALS4* gene expression in three biological replicates of CX1 was 0.012, whereas the average value of *ALS4* gene expression in three biological replicates of CX2 was 4.069. The significantly low expression level of *ALS* genes may be the reason for their inability to form biofilms. Enrichment analysis of DEGs revealed abundant differential pathways and gene functions between strains. The comparison of the GO classification enriched by upregulated and downregulated genes revealed that more upregulated genes were found than downregulated genes involved in electron carrier activity, structure molecule activity, and translation regulator activity, which may be related with transmembrane transporters such as efflux pumps. In addition, more downregulated genes were involved in immune system processes, extra cellular regions, extracellular region parts, and metallochaperone activity; however, further research is required to validate these findings. Nonetheless, pertaining to the KEGG pathway classification, more upregulated genes were found in

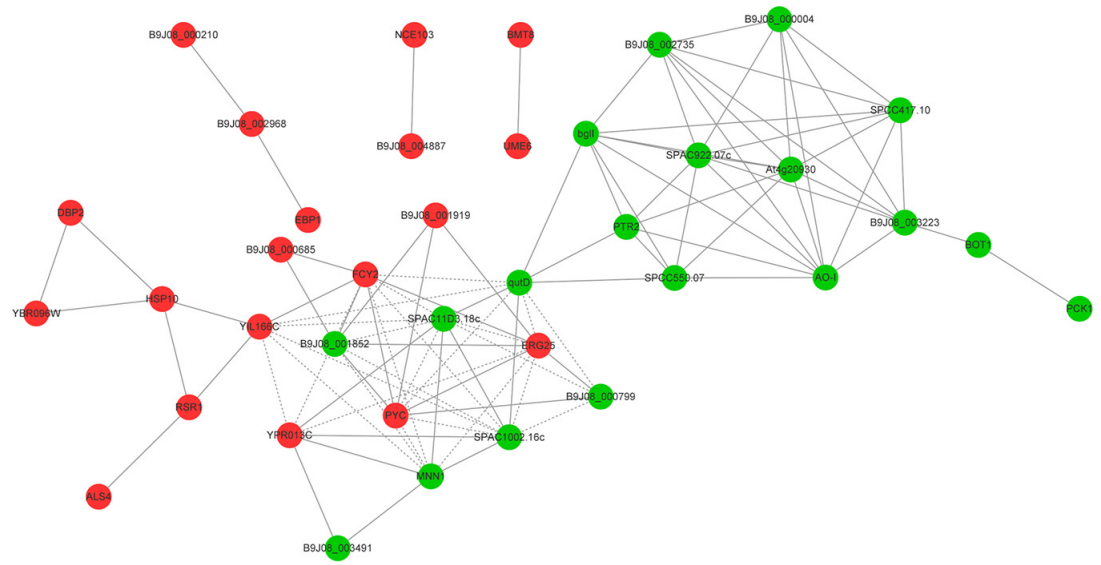

FIGURE 5 | A predicted protein–protein interaction network. The top 20 upregulated DEGs and top 20 downregulated DEGs constitute the predicted protein interaction network using the STRING (Search Tool for the Retrieval of interacting Genes) database. The red and green nodes with gene names represented upregulated and downregulated differentially expressed genes, respectively.

resistant *Candida auris* with respect to translation, transduction, and nucleotide metabolism. However, more downregulated genes were involved in transport and catabolism, signal transduction, folding, sorting and degradation, and most metabolism pathways, a finding indicating that the metabolism of resistant strain is less active compared to susceptible strains or that a lower number of genes can in fact play a more significant role.

The azoles inhibit the activity of the lanosterol 14-α-demethylase encoded by *ERG11*, thus blocking ergosterol synthesis. Known mechanisms of resistance to azole include point mutations in *ERG11* that lead to a decrease in the affinity of drugs and enzymes. Furthermore, overexpression of *ERG11* and efflux pump genes can also cause a decrease in azole susceptibility (Lee et al., 2020). In our results, we investigated genes that are involved in steroid biosynthesis and efflux pumps pathways, which may in turn facilitate resistance to fluconazole. We identified genes that are involved in ergosterol and efflux pump biosynthesis that were upregulated expressed in resistant *Candida auris* strains including *SNQ2*, *CDR4*, *ARB1*, *MDR1*, *MRR1*, and 9 (*ERG1*, *ERG7*, *ERG11*, *ERG24*, *ERG25*, *ERG6*, *ERG2*, *ERG3*, and *ERG5*) of 13 of the ergosterol synthesis genes, which were consistent with previous studies performed (Chowdhary et al., 2018; Kean et al., 2018; Rybak et al., 2019). SNQ2, CDR4, MDR1, and ARB1 were found to be present and upregulated in drug-resistant isolates of *C. auris* (Munoz et al., 2018; Wasi et al., 2019). The ATP binding cassette (ABC) superfamily and major facilitator (MF) superfamily are the two main classes of efflux pumps. RNA-seq analysis indicated that the downregulated efflux pump genes such as an ABC transporter gene (*ABCF3*) and two MFS transporter genes (*hxnP* and *ecdD*) may play an atypical role. However, these genes have not been previously reported, and thus, further investigating their properties is imperative. In addition to *ERG11* and efflux pump overexpression, we also identified point mutations in ERG11. The amino acid substitutions at Y132F, K143R, and F126L were considered the cause of the azole resistance in *C. auris*, with Y132F being the most widespread mutation associated with azole resistance (Lee et al., 2021). We found point mutations at T395A which led to the amino acid substitution at Y132F in all three biological replicates of drug-resistant strains; this was surprisingly consistent with previous studies. However, we did not identify any point mutations in ERG11 in the susceptible strains.

Echinocandins exert their antifungal effect by inhibiting beta (1,3) D-glucan synthase encoded by *FKS*, thus causing a defective cell wall. Unlike azole resistance, several studies exist, which demonstrate that amino acid substitutions at S639F, S639P, and S639Y in *FKS1* simply lead to elevated MIC levels of echinocandins, as opposed to the role played by efflux pumps (Berkow and Lockhart, 2018; Chowdhary et al., 2018; Kordalewska et al., 2018; Lee et al., 2021). However, our study detected one amino acid substitution at R464P in the sensitive strain, in addition to three point mutations, T588C, A897G, and G2458T (same-sense mutations), in the resistant strain. We tried to explain the high MIC of micafungin (MIC = 8 μg/ml) in CX2 with HSP-associated genes. Heat shock proteins (HSPs) contain a large number of proteins that are distributed widely and are involved in many cellular pathways to modulate stress responses (Gong et al., 2017; Lee et al., 2020). In transcriptome analysis, we found that all HSP related genes were upregulated in resistant *Candida auris* strains such as *HSP90*, a strain that has been studied before. However, the exact role of HSPs in the resistance mechanism needs to be further studied.

In addition, this study assessed the potential role of protein modification genes in the underlying resistance mechanism.

Epigenetics has been continuously studied in mammals; however, few studies have been performed that focus on fungal resistance mechanisms and epigenetics (Madhani, 2021). Therefore, we searched for genes that are involved in methylation, SUMOylation, ubiquitination, acetylation, glycosylation, and phosphorylation processes. Our results indicate that the number of DEGs related with methylation was the largest among the protein modification genes, whereas SUMOylation and ubiquitination did not reveal any significant differences. Although multi-omics studies of fungi can quickly obtain a lot of information, more experimental studies are still needed to evaluate the biological effects of these genes.

After searching for genes with relatively large differential expression in the network, we identified that the functions of most genes have not been individually studied in *C. auris* before. Consequently, we searched their orthologous genes in other *Candida* species and yeasts in Pubmed, CGD (Candida Genome Database), and SGD (Saccharomyces Genome Database). *FCY2* participated in the process of transmembrane transporting and converting 5-fluorocytosine (5FC) into toxic 5-fluorouracil (5FU). Furthermore, FCY2 mutations can mediate resistance to 5FC in both *Candida* species and Cryptococcus (Billmyre et al., 2020). In this study, although we did not know whether genetic mutations are present, we found that FCY2 (B9J08_002435) was upregulated in the resistant *C. auris* strain, a finding that is consistent with the drug sensitivity results obtained for 5FC (MIC$\leq$0.06 μg/ml). *EBP1* was also upregulated in the resistant *C. auris* strain, and previous studies identified that it plays an essential role in the yeast-to-hypha transition (Kurakado et al., 2017). Furthermore, pertaining to genes involved in CO_2 signaling in fungi, *NCE103* and *UME6* were upregulated in the resistant *C. auris* strain. *NCE103* and *UME6* not only are essential for ensuring the carbon supply required for cell metabolism but also play an important role in signal transduction process such as fungi's morphology and communication (Martin et al., 2017; Lu et al., 2019). Therefore, we believe that these two genes are perhaps involved in the drug resistance mechanism, yet their specific roles need to be further determined. Among the downregulated genes, we found certain genes or orthologous genes with transmembrane transporter activity, including B9J08_005345, B9J08_004188, B9J08_005571, B9J08_00002660, and B9J08_004099. These transmembrane transporter genes may reduce drug uptake and lead to drug resistance through a different approach than drug efflux. In addition, *ADY2*, which is assigned to the acetate uptake transporter family, was found to be downregulated in the resistant *C. auris* strain. So far, no pleiotropic drug resistance (PDR) transporters belonging to the ABC superfamily exist, which are found to be related with the export of carboxylates under acid stress conditions (Alves et al., 2020). Our research was also in line with a previous study that verified that PKC1 downregulation leads to defects in the formation of biofilms (Heinisch and Rodicio, 2018). Moreover, B9J08_004787 (orthologous gene: YPR013C) and B9J08_004804 (orthologous gene: At4g20930) downregulation may lead to reduced virulence, which is consistent with the weakened virulence of the resistant strain (Mao et al., 2008; Otzen et al., 2014).

Through transcriptome analysis between resistant and susceptible *Candida auris* strains, our study may provide some novel ideas for future studies with respect to understanding the mechanisms of drug resistance in *Candida auris*. The limitation of this study is that only one drug-resistant *C. auris* strain was compared with one susceptible *C. auris* strain. Future research should be performed to confirm the exact function of a certain DEG involved in molecular mechanism of multidrug resistance.

DATA AVAILABILITY STATEMENT

The datasets presented in this study can be found in online repositories. The names of the repository/repositories and accession number(s) can be found below: https://www.ncbi.nlm.nih.gov/, PRJNA735406.

ETHICS STATEMENT

The Ethics Committee of The First Affiliated Hospital of Nanchang University (approval no. 2016026) approved of the present study. The participants provided written informed consent to participate in this study.

AUTHOR CONTRIBUTIONS

XY, DQ, and NL designed the study. WZ, XL, and YL wrote the manuscript. NL reviewed the manuscript. WY, XH, and SJ were responsible for managing the strains and the subsequent data collection. WZ, YL, and WY prepared the figures and tables. All authors contributed to the article and approved the submitted version.

FUNDING

This work was supported by the Natural Science Foundation of Jiangxi Province (20171BBG70107), the Science and Technology Research Project of Education Department of Jiangxi Province (GJJ180130), and the Major Science and Technology Project of Jiangxi Province (20181BBG70030).

ACKNOWLEDGMENTS

We thank Ou Yi corporation for providing additional bioinformatics analysis for this study.

SUPPLEMENTARY MATERIAL

The Supplementary Material for this article can be found online at: https://www.frontiersin.org/articles/10.3389/fmicb.2021.708009/full#supplementary-material

REFERENCES

Adams, E., Quinn, M., Tsay, S., Poirot, E., Chaturvedi, S., Southwick, K., et al. (2018). *Candida auris* in healthcare facilities, New York, USA, 2013-2017. *Emerg. Infect. Dis.* 24, 1816–1824. doi: 10.3201/eid2410.180649

Alves, R., Sousa-Silva, M., Vieira, D., Soares, P., Chebaro, Y., Lorenz, M. C., et al. (2020). Carboxylic acid transporters in candida pathogenesis. *mBio* 11:e00156–20. doi: 10.1128/mBio.00156-20

Anders, S., Pyl, P. T., and Huber, W. (2015). HTSeq–a Python framework to work with high-throughput sequencing data. *Bioinformatics* 31, 166–169. doi: 10.1093/bioinformatics/btu638

Arastehfar, A., Lass-Florl, C., Garcia-Rubio, R., Daneshnia, F., Ilkit, M., Boekhout, T., et al. (2020). The quiet and underappreciated rise of drug-resistant invasive fungal pathogens. *J. Fungi (Basel)* 6:138. doi: 10.3390/jof6030138

Armstrong, P. A., Rivera, S. M., Escandon, P., Caceres, D. H., Chow, N., Stuckey, M. J., et al. (2019). Hospital-associated multicenter outbreak of emerging fungus *Candida auris*, Colombia, 2016. *Emerg. Infect. Dis.* 25, 1339–1346. doi: 10.3201/eid2507.180491

Berkow, E. L., and Lockhart, S. R. (2018). Activity of CD101, a long-acting echinocandin, against clinical isolates of *Candida auris*. *Diagn. Microbiol. Infect. Dis.* 90, 196–197. doi: 10.1016/j.diagmicrobio.2017.10.021

Billmyre, R. B., Applen Clancey, S., Li, L. X., Doering, T. L., and Heitman, J. (2020). 5-fluorocytosine resistance is associated with hypermutation and alterations in capsule biosynthesis in Cryptococcus. *Nat. Commun.* 11:127. doi: 10.1038/s41467-019-13890-z

Bolger, A. M., Lohse, M., and Usadel, B. (2014). Trimmomatic: a flexible trimmer for Illumina sequence data. *Bioinformatics* 30, 2114–2120. doi: 10.1093/bioinformatics/btu170

Chaabane, F., Graf, A., Jequier, L., and Coste, A. T. (2019). Review on antifungal resistance mechanisms in the emerging pathogen *Candida auris*. *Front. Microbiol.* 10:2788. doi: 10.3389/fmicb.2019.02788

Chatterjee, S., Alampalli, S. V., Nageshan, R. K., Chettiar, S. T., Joshi, S., and Tatu, U. S. (2015). Draft genome of a commonly misdiagnosed multidrug resistant pathogen *Candida auris*. *BMC Genomics* 16:686. doi: 10.1186/s12864-015-1863-z

Chow, N. A., de Groot, T., Badali, H., Abastabar, M., Chiller, T. M., and Meis, J. F. (2019). Potential fifth clade of *Candida auris*, Iran, 2018. *Emerg. Infect. Dis.* 25, 1780–1781. doi: 10.3201/eid2509.190686

Chow, N. A., Gade, L., Tsay, S. V., Forsberg, K., Greenko, J. A., Southwick, K. L., et al. (2018). Multiple introductions and subsequent transmission of multidrug-resistant *Candida auris* in the USA: a molecular epidemiological survey. *Lancet Infect. Dis.* 18, 1377–1384. doi: 10.1016/S1473-3099(18)30597-8

Chowdhary, A., Prakash, A., Sharma, C., Kordalewska, M., Kumar, A., Sarma, S., et al. (2018). A multicentre study of antifungal susceptibility patterns among 350 *Candida auris* isolates (2009-17) in India: role of the ERG11 and FKS1 genes in azole and echinocandin resistance. *J. Antimicrob. Chemother.* 73, 891–899. doi: 10.1093/jac/dkx480

Clinical and Laboratory Standards Institute [CLSI] (2008). *Reference Method for Broth Dilution Antifungal Susceptibility Testing of Yeasts. Approved Standard 3rd ed. CLSI Document M27-A3*. Wayne, PA: Humana Press.

de Jong, A. W., and Hagen, F. (2019). Attack, defend and persist: how the fungal pathogen *Candida auris* was able to emerge globally in healthcare environments. *Mycopathologia* 184, 353–365. doi: 10.1007/s11046-019-00351-w

ElBaradei, A. (2020). A decade after the emergence of *Candida auris*: what do we know? *Eur. J. Clin. Microbiol. Infect. Dis.* 39, 1617–1627. doi: 10.1007/s10096-020-03886-9

Eyre, D. W., Sheppard, A. E., Madder, H., Moir, I., Moroney, R., Quan, T. P., et al. (2018). A *Candida auris* outbreak and its control in an intensive care setting. *N. Engl. J. Med.* 379, 1322–1331. doi: 10.1056/NEJMoa1714373

Forsberg, K., Woodworth, K., Walters, M., Berkow, E. L., Jackson, B., Chiller, T., et al. (2019). *Candida auris*: the recent emergence of a multidrug-resistant fungal pathogen. *Med. Mycol.* 57, 1–12. doi: 10.1093/mmy/myy054

Fraser, M., Brown, Z., Houldsworth, M., Borman, A. M., and Johnson, E. M. (2016). Rapid identification of 6328 isolates of pathogenic yeasts using MALDI-ToF MS and a simplified, rapid extraction procedure that is compatible with the Bruker Biotyper platform and database. *Med. Mycol.* 54, 80–88. doi: 10.1093/mmy/myv085

Gong, Y., Li, T., Yu, C., and Sun, S. (2017). Candida albicans heat shock proteins and hsps-associated signaling pathways as potential antifungal targets. *Front. Cell Infect. Microbiol.* 7:520. doi: 10.3389/fcimb.2017.00520

Heinisch, J. J., and Rodicio, R. (2018). Protein kinase C in fungi-more than just cell wall integrity. *FEMS Microbiol. Rev.* 42:fux051. doi: 10.1093/femsre/fux051

Hoyer, L. L., and Cota, E. (2016). Candida albicans Agglutinin-Like Sequence (Als) family vignettes: a review of Als protein structure and function. *Front. Microbiol.* 7:280. doi: 10.3389/fmicb.2016.00280

Kanehisa, M., Araki, M., Goto, S., Hattori, M., Hirakawa, M., Itoh, M., et al. (2008). KEGG for linking genomes to life and the environment. *Nucleic Acids Res.* 36, D480–D484. doi: 10.1093/nar/gkm882

Kathuria, S., Singh, P. K., Sharma, C., Prakash, A., Masih, A., Kumar, A., et al. (2015). Multidrug-resistant *Candida auris* misidentified as *Candida haemulonii*: characterization by matrix-assisted laser desorption ionization-time of flight mass spectrometry and DNA sequencing and its antifungal susceptibility profile variability by Vitek 2, CLSI broth microdilution, and etest method. *J. Clin. Microbiol.* 53, 1823–1830. doi: 10.1128/JCM.00367-15

Kean, R., Delaney, C., Sherry, L., Borman, A., Johnson, E. M., Richardson, M. D., et al. (2018). Transcriptome assembly and profiling of *Candida auris* reveals novel insights into biofilm-mediated resistance. *mSphere* 3:e00334–18. doi: 10.1128/mSphere.00334-18

Kean, R., and Ramage, G. (2019). Combined antifungal resistance and biofilm tolerance: the global threat of *Candida auris*. *mSphere* 4:e00458–19. doi: 10.1128/mSphere.00458-19

Kim, D., Langmead, B., and Salzberg, S. L. (2015). HISAT: a fast spliced aligner with low memory requirements. *Nat. Methods* 12, 357–360. doi: 10.1038/nmeth.3317

Kordalewska, M., Lee, A., Park, S., Berrio, I., Chowdhary, A., Zhao, Y., et al. (2018). Understanding echinocandin resistance in the emerging pathogen *Candida auris*. *Antimicrob. Agents Chemother.* 62:e00238–18. doi: 10.1128/AAC.00238-18

Kordalewska, M., Zhao, Y., Lockhart, S. R., Chowdhary, A., Berrio, I., and Perlin, D. S. (2017). Rapid and accurate molecular identification of the emerging multidrug-resistant pathogen *Candida auris*. *J. Clin. Microbiol.* 55, 2445–2452. doi: 10.1128/JCM.00630-17

Kumar, D., Banerjee, T., Pratap, C. B., and Tilak, R. (2015). Itraconazole-resistant *Candida auris* with phospholipase, proteinase and hemolysin activity from a case of vulvovaginitis. *J. Infect. Dev. Ctries.* 9, 435–437. doi: 10.3855/jidc.4582

Kurakado, S., Kurogane, R., and Sugita, T. (2017). 17beta-Estradiol inhibits estrogen binding protein-mediated hypha formation in Candida albicans. *Microb. Pathog.* 109, 151–155. doi: 10.1016/j.micpath.2017.05.038

Larkin, E., Hager, C., Chandra, J., Mukherjee, P. K., Retuerto, M., Salem, I., et al. (2017). the emerging pathogen *Candida auris*: growth phenotype, virulence factors, activity of antifungals, and effect of SCY-078, a novel glucan synthesis inhibitor, on growth morphology and biofilm formation. *Antimicrob. Agents Chemother.* 61:e02396–16. doi: 10.1128/AAC.02396-16

Lee, W. G., Shin, J. H., Uh, Y., Kang, M. G., Kim, S. H., Park, K. H., et al. (2011). First three reported cases of nosocomial fungemia caused by *Candida auris*. *J. Clin. Microbiol.* 49, 3139–3142. doi: 10.1128/JCM.00319-11

Lee, Y., Puumala, E., Robbins, N., and Cowen, L. E. (2020). Antifungal drug resistance: molecular mechanisms in Candida albicans and beyond. *Chem. Rev.* 121, 3390–3411. doi: 10.1021/acs.chemrev.0c00199

Lee, Y., Puumala, E., Robbins, N., and Cowen, L. E. (2021). Antifungal drug resistance: molecular mechanisms in Candida albicans and beyond. *Chem. Rev.* 121, 3390–3411.

Lima, A., Widen, R., Vestal, G., Uy, D., and Silbert, S. (2019). A TaqMan probe-based real-time PCR assay for the rapid identification of the emerging multidrug-resistant pathogen *Candida auris* on the BD max system. *J. Clin. Microbiol.* 57:e01604–18. doi: 10.1128/JCM.01604-18

Lockhart, S. R., Etienne, K. A., Vallabhaneni, S., Farooqi, J., Chowdhary, A., Govender, N. P., et al. (2017). Simultaneous emergence of multidrug-resistant *Candida auris* on 3 continents confirmed by whole-genome sequencing and epidemiological analyses. *Clin. Infect. Dis.* 64, 134–140. doi: 10.1093/cid/ciw691

Lone, S. A., and Ahmad, A. (2019). *Candida auris*-the growing menace to global health. *Mycoses* 62, 620–637. doi: 10.1111/myc.12904

Lu, Y., Su, C., Ray, S., Yuan, Y., and Liu, H. (2019). CO2 signaling through the Ptc2-Ssn3 axis governs sustained hyphal development of candida albicans by

reducing Ume6 phosphorylation and degradation. *mBio* 10:e02320–18. doi: 10.1128/mBio.02320-18

Madhani, H. D. (2021). Unbelievable but true: epigenetics and chromatin in fungi. *Trends Genet.* 37, 12–20. doi: 10.1016/j.tig.2020.09.016

Mao, J., Habib, T., Shenwu, M., Kang, B., Allen, W., Robertson, L., et al. (2008). Transcriptome profiling of Saccharomyces cerevisiae mutants lacking C2H2 zinc finger proteins. *BMC Genomics* 9 Suppl 1:S14. doi: 10.1186/1471-2164-9-S1-S14

Martin, R., Pohlers, S., Muhlschlegel, F. A., and Kurzai, O. (2017). CO2 sensing in fungi: at the heart of metabolic signaling. *Curr. Genet.* 63, 965–972. doi: 10.1007/s00294-017-0700-0

Mizusawa, M., Miller, H., Green, R., Lee, R., Durante, M., Perkins, R., et al. (2017). Can multidrug-resistant *Candida auris* be reliably identified in clinical microbiology laboratories? *J. Clin. Microbiol.* 55, 638–640. doi: 10.1128/JCM.02202-16

Monroy-Perez, E., Sainz-Espunes, T., Paniagua-Contreras, G., Negrete-Abascal, E., Rodriguez-Moctezuma, J. R., and Vaca, S. (2012). Frequency and expression of ALS and HWP1 genotypes in Candida albicans strains isolated from Mexican patients suffering from vaginal candidosis. *Mycoses* 55, e151–e157. doi: 10.1111/j.1439-0507.2012.02188.x

Munoz, J. F., Gade, L., Chow, N. A., Loparev, V. N., Juieng, P., Berkow, E. L., et al. (2018). Genomic insights into multidrug-resistance, mating and virulence in *Candida auris* and related emerging species. *Nat. Commun.* 9:5346. doi: 10.1038/s41467-018-07779-6

O'Connor, C., Bicanic, T., Dave, J., Evans, T. J., Moxey, P., Adamu, U., et al. (2019). *Candida auris* outbreak on a vascular ward – the unexpected arrival of an anticipated pathogen. *J. Hosp. Infect.* 103, 106–108. doi: 10.1016/j.jhin.2019.06.002

Otzen, C., Bardl, B., Jacobsen, I. D., Nett, M., and Brock, M. (2014). Candida albicans utilizes a modified beta-oxidation pathway for the degradation of toxic propionyl-CoA. *J. Biol. Chem.* 289, 8151–8169. doi: 10.1074/jbc.M113.517672

Pristov, K. E., and Ghannoum, M. A. (2019). Resistance of Candida to azoles and echinocandins worldwide. *Clin. Microbiol. Infect.* 25, 792–798. doi: 10.1016/j.cmi.2019.03.028

Rhodes, J., and Fisher, M. C. (2019). Global epidemiology of emerging *Candida auris*. *Curr. Opin. Microbiol.* 52, 84–89. doi: 10.1016/j.mib.2019.05.008

Roberts, A., Trapnell, C., Donaghey, J., Rinn, J. L., and Pachter, L. (2011). Improving RNA-Seq expression estimates by correcting for fragment bias. *Genome Biol.* 12:R22. doi: 10.1186/gb-2011-12-3-r22

Ruiz-Gaitan, A., Moret, A. M., Tasias-Pitarch, M., Aleixandre-Lopez, A. I., Martinez-Morel, H., Calabuig, E., et al. (2018). An outbreak due to *Candida auris* with prolonged colonisation and candidaemia in a tertiary care European hospital. *Mycoses* 61, 498–505. doi: 10.1111/myc.12781

Ruiz-Gaitan, A. C., Canton, E., Fernandez-Rivero, M. E., Ramirez, P., and Peman, J. (2019). Outbreak of *Candida auris* in Spain: a comparison of antifungal activity by three methods with published data. *Int. J. Antimicrob. Agents* 53, 541–546. doi: 10.1016/j.ijantimicag.2019.02.005

Rybak, J. M., Doorley, L. A., Nishimoto, A. T., Barker, K. S., Palmer, G. E., and Rogers, P. D. (2019). Abrogation of triazole resistance upon deletion of CDR1 in a clinical isolate of *Candida auris*. *Antimicrob. Agents Chemother.* 63:e00057–19. doi: 10.1128/AAC.00057-19

Satoh, K., Makimura, K., Hasumi, Y., Nishiyama, Y., Uchida, K., and Yamaguchi, H. (2009). *Candida auris* sp. nov., a novel ascomycetous yeast isolated from the external ear canal of an inpatient in a Japanese hospital. *Microbiol. Immunol.* 53, 41–44. doi: 10.1111/j.1348-0421.2008.00083.x

Schelenz, S., Hagen, F., Rhodes, J. L., Abdolrasouli, A., Chowdhary, A., Hall, A., et al. (2016). First hospital outbreak of the globally emerging *Candida auris* in a European hospital. *Antimicrob. Resist. Infect. Control* 5:35. doi: 10.1186/s13756-016-0132-5

Schoch, C. L., Seifert, K. A., Huhndorf, S., Robert, V., Spouge, J. L., Levesque, C. A., et al. (2012). Nuclear ribosomal internal transcribed spacer (ITS) region as a universal DNA barcode marker for fungi. *Proc. Natl. Acad. Sci. U. S. A.* 109, 6241–6246. doi: 10.1073/pnas.1117018109

Sexton, D. J., Kordalewska, M., Bentz, M. L., Welsh, R. M., Perlin, D. S., and Litvintseva, A. P. (2018). Direct detection of emergent fungal pathogen *Candida auris* in clinical skin swabs by SYBR green-based quantitative PCR assay. *J. Clin. Microbiol.* 56:e01337–18. doi: 10.1128/JCM.01337-18

Snayd, M., Dias, F., Ryan, R. W., Clout, D., and Banach, D. B. (2018). Misidentification of *Candida auris* by RapID yeast plus, a commercial, biochemical enzyme-based manual rapid identification system. *J. Clin. Microbiol.* 56:e00080–18. doi: 10.1128/JCM.00080-18

Szklarczyk, D., Gable, A. L., Lyon, D., Junge, A., Wyder, S., Huerta-Cepas, J., et al. (2019). STRING v11: protein-protein association networks with increased coverage, supporting functional discovery in genome-wide experimental datasets. *Nucleic Acids Res.* 47, D607–D613. doi: 10.1093/nar/gky1131

Taori, S. K., Khonyongwa, K., Hayden, I., Athukorala, G. D. A., Letters, A., Fife, A., et al. (2019). *Candida auris* outbreak: mortality, interventions and cost of sustaining control. *J. Infect.* 79, 601–611. doi: 10.1016/j.jinf.2019.09.007

Trapnell, C., Williams, B. A., Pertea, G., Mortazavi, A., Kwan, G., van Baren, M. J., et al. (2010). Transcript assembly and quantification by RNA-Seq reveals unannotated transcripts and isoform switching during cell differentiation. *Nat. Biotechnol.* 28, 511–515. doi: 10.1038/nbt.1621

Vila, T., Sultan, A. S., Montelongo-Jauregui, D., and Jabra-Rizk, M. A. (2020). *Candida auris*: a fungus with identity crisis. *Pathog. Dis.* 78:ftaa034. doi: 10.1093/femspd/ftaa034

Wasi, M., Khandelwal, N. K., Moorhouse, A. J., Nair, R., Vishwakarma, P., Bravo Ruiz, G., et al. (2019). ABC transporter genes show upregulated expression in drug-resistant clinical isolates of *Candida auris*: a genome-wide characterization of ATP-Binding Cassette (ABC) transporter genes. *Front. Microbiol.* 10:1445. doi: 10.3389/fmicb.2019.01445

Wickes, B. L. (2020). Analysis of a *Candida auris* outbreak provides new insights into an emerging pathogen. *J. Clin. Microbiol.* 58:e02083–19. doi: 10.1128/JCM.02083-19

Conflict of Interest: The authors declare that the research was conducted in the absence of any commercial or financial relationships that could be construed as a potential conflict of interest.

frontiers in Microbiology

ORIGINAL RESEARCH
published: 22 July 2021
doi: 10.3389/fmicb.2021.680884

A 20-Year Antifungal Susceptibility Surveillance (From 1999 to 2019) for *Aspergillus* spp. and Proposed Epidemiological Cutoff Values for *Aspergillus fumigatus* and *Aspergillus flavus*: A Study in a Tertiary Hospital in China

*Xinyu Yang[1,2,3,4], Wei Chen[1,2,3,4], Tianyu Liang[1,2,3,4], JingWen Tan[1,2,3,4], Weixia Liu[1,2,3,4], Yi Sun[1,2,3,4], Qian Wang[1,2,3,4], Hui Xu[1,2,3,4], Lijuan Li[1,2,3,4], Yabin Zhou[1,2,3,4], Qiqi Wang[1,2,3,4], Zhe Wan[1,2,3,4], Yinggai Song[1,2,3,4], Ruoyu Li[1,2,3,4] and Wei Liu[1,2,3,4]**

[1] Department of Dermatology and Venereology, Peking University First Hospital, Beijing, China, [2] National Clinical Research Center for Skin and Immune Diseases, Beijing, China, [3] Research Center for Medical Mycology, Peking University, Beijing, China, [4] Beijing Key Laboratory of Molecular Diagnosis on Dermatoses, Beijing, China

OPEN ACCESS

Edited by:
Ying-Chun Xu,
Peking Union Medical College Hospital (CAMS), China

Reviewed by:
Iman Haghani,
Mazandaran University of Medical Sciences, Iran
Shahram Mahmoudi,
Iran University of Medical Sciences, Iran

***Correspondence:**
Wei Liu
liuwei@bjmu.edu.cn

Specialty section:
This article was submitted to Antimicrobials, Resistance and Chemotherapy, a section of the journal Frontiers in Microbiology

Received: 15 March 2021
Accepted: 23 June 2021
Published: 22 July 2021

Citation:
Yang X, Chen W, Liang T, Tan J, Liu W, Sun Y, Wang Q, Xu H, Li L, Zhou Y, Wang Q, Wan Z, Song Y, Li R and Liu W (2021) A 20-Year Antifungal Susceptibility Surveillance (From 1999 to 2019) for Aspergillus spp. and Proposed Epidemiological Cutoff Values for Aspergillus fumigatus and Aspergillus flavus: A Study in a Tertiary Hospital in China. Front. Microbiol. 12:680884. doi: 10.3389/fmicb.2021.680884

The emergence of resistant *Aspergillus* spp. is increasing worldwide. Long-term susceptibility surveillance for clinically isolated *Aspergillus* spp. strains is warranted for understanding the dynamic change in susceptibility and monitoring the emergence of resistance. Additionally, neither clinical breakpoints (CBPs) nor epidemiological cutoff values (ECVs) for *Aspergillus* spp. in China have been established. In this study, we performed a 20-year antifungal susceptibility surveillance for 706 isolates of *Aspergillus* spp. in a clinical laboratory at Peking University First Hospital from 1999 to 2019; and *in vitro* antifungal susceptibility to triazoles, caspofungin, and amphotericin B was determined by the Clinical and Laboratory Standards Institute (CLSI) broth microdilution method. It was observed that *Aspergillus fumigatus* was the most common species, followed by *Aspergillus flavus* and *Aspergillus terreus*. Forty isolates (5.7%), including *A. fumigatus*, *A. flavus*, *A. terreus*, *Aspergillus niger*, and *Aspergillus nidulans*, were classified as non-wild type (non-WT). Importantly, multidrug resistance was observed among *A. flavus*, *A. terreus*, and *A. niger* isolates. *Cyp51A* mutations were characterized for 19 non-WT *A. fumigatus* isolates, and TR_{34}/L98H/S297T/F495I was the most prevalent mutation during the 20-year surveillance period. The overall resistance trend of *A. fumigatus* increased over 20 years in China. Furthermore, based on ECV establishment principles, proposed ECVs for *A. fumigatus* and *A. flavus* were established using gathered minimum inhibitory concentration (MIC)/minimum effective concentration (MEC) data. Consequently, all the proposed ECVs were identical to the CLSI ECVs, with the exception of itraconazole against *A. flavus*, resulting in a decrease in the non-WT rate from 6.0 to 0.6%.

Keywords: *Aspergillus* spp., susceptibility surveillance, epidemiological cutoff values, non-wild-type, a single-center study

INTRODUCTION

Aspergillus species are saprophytic molds widely distributed throughout the environment and are easily transported in the air and inhaled into the airway due to the small size of spores (Chabi et al., 2015). *Aspergillus* spp. can cause many human diseases, ranging from non-invasive allergic bronchopulmonary aspergillosis (ABPA) and chronic pulmonary aspergillosis to invasive aspergillosis (IA), and their clinical manifestations and prognosis vary widely (Cadena et al., 2016). IA is a life-threatening opportunistic infection associated with high morbidity and mortality rates, occurring mainly in immunocompromised patients, such as those with organ transplants or hematological malignancy and those receiving certain types of chemotherapy or immunosuppression therapy (Verweij et al., 2016). *Aspergillus fumigatus* is the most common *Aspergillus* spp. causing infection in humans, accounting for 70–80% of cases. The incidences of infections with other species, such as *Aspergillus flavus*, *Aspergillus niger*, and *Aspergillus terreus*, have been increasing, especially in immunocompromised hosts (Richardson and Lass-Flörl, 2008).

Triazoles have a broad spectrum of *in vitro* antifungal activity against molds and are currently the first-line antifungals for the treatment of IA, including itraconazole (ITC), voriconazole (VRC), and posaconazole (POS). Caspofungin (CAS) and amphotericin B (AMB) are important therapeutic agents for the systemic treatment of refractory IA as well as empirical or prophylactic therapy (Walsh et al., 2008). Despite advances in IA treatment, the mortality rates remain high, especially in immunosuppressed hosts. Antifungal resistance development is one of the major threats (Verweij et al., 2016). Resistance has emerged during the past decade, and the prevalence is increasing in some areas of the world. Therefore, identifying strains of *Aspergillus* spp. with different susceptibilities has important implications for understanding the susceptibility trend and selecting the correct antifungal agents.

Antifungal susceptibility testing of *Aspergillus* spp. has been standardized by both the Clinical and Laboratory Standards Institute (CLSI) and European Committee on Antimicrobial Susceptibility Testing (EUCAST) (CLSI, 2017). Breakpoints are used to determine whether the microorganisms are susceptible or resistant to the tested antifungals, which is an important basis for clinicians to select antifungal agents for the treatment of pathogenic infections. Breakpoints include clinical breakpoints (CBPs) and epidemiological cutoff values (ECVs). Currently, CBPs based on the minimum inhibitory concentration (MIC) distributions, pharmacokinetic and pharmacodynamics (PK/PD) parameters, animal data, and clinical outcomes for molds have not been established by the CLSI except for the CBP of VRC for *A. fumigatus* (CLSI, 2020). In the absence of sufficient data such as (PK/PD) parameters and clinical outcomes, CBPs are unable to be established. ECVs are used to evaluate the susceptibility of strains, to distinguish wild-type (WT) strains from strains with decreased susceptibility or acquired resistance mechanisms, and to monitor resistance development. ECVs for AMB, ITC, VRC, POS, CAS, and *Aspergillus* spp. have been defined by the CLSI and EUCAST using the broth microdilution (BMD) method (Espinel-Ingroff et al., 2010, 2011a,b; CLSI, 2018).

In the present study, we analyzed the antifungal activities of AMB, triazoles, and CAS against an extensive, geographically diverse collection of 706 *Aspergillus* spp. isolates from a clinical laboratory in China collected from 1999 to 2019. Furthermore, we applied CLSI ECVs to detect the emergence of resistant isolates. More importantly, WT distributions and tentative ECVs for AMB, ITC, VRC, POS, and CAS against *A. fumigatus* and *A. flavus* were proposed for the first time based on the gathered MIC/minimum effective concentration (MEC) data obtained from 20 years of antifungal susceptibility surveillance in China.

MATERIALS AND METHODS

Isolation and Identification of *Aspergillus* Species

This study was a retrospective laboratory-based study of *Aspergillus* spp. infections from April 1999 to December 2019. All clinical isolates of *Aspergillus* spp. collected consecutively from unique patients in various Chinese hospitals were preserved at the Research Center for Medical Mycology at Peking University First Hospital, Beijing, China. The date of specimen collection, the type, and isolation site of the specimen were also recorded. This research was a surveillance study and did not involve human subjects.

To ensure the accuracy of species identification, all clinical isolates of *Aspergillus* spp. were identified to the species level in the central laboratory by a combination of morphological characteristics, matrix-assisted laser desorption/ionization–time of flight mass spectrometry (MALDI-TOF MS), and sequence analysis of the internal transcribed spacer (ITS), β-tubulin, and calmodulin genes (Sugui et al., 2014).

Antifungal Susceptibility Testing

In vitro antifungal susceptibility testing of AMB, ITC, VRC, POS, and CAS against *Aspergillus* spp. isolates was performed using the CLSI M38-A3 method for filamentous fungi (CLSI, 2017). The antifungals used were AMB, ITC, VRC, POS, and CAS (all from Harveybio Gene Technology Co. Ltd., Beijing, China). The MIC was read at 48 h as the lowest concentration inhibiting visible growth for AMB, ITC, VRC, and POS. The MEC for CAS was defined at 24 h as the lowest concentration causing the growth of small, rounded, compact hyphal forms as compared with the hyphal growth seen in the growth control well. According to the recommendations in CLSI document M38-A3, the *Candida parapsilosis* ATCC 22019 and *Candida krusei* ATCC 6258 strains were used as quality control strains. The susceptibilities to AMB, ITC, VRC, POS, and CAS of *Aspergillus* spp. were evaluated, and the MICs/MECs were determined in this study. MIC/MEC ranges, MIC_{50}/MEC_{50} (MIC causing inhibition of 50% of the isolates), and MIC_{90}/MEC_{90} (MIC causing inhibition of 90%

of the isolates) were also calculated. Because the CLSI has not established CBPs for *Aspergillus* species except the CBP of VRC for *A. fumigatus* (CLSI, 2020), CLSI ECVs were applied to classify the isolates as WT or non-wild type (non-WT) in terms of their antifungal susceptibilities (CLSI, 2018).

Cyp51A Gene Sequencing of Triazole-Resistant *Aspergillus fumigatus* Isolates

Genomic DNA of non-WT *A. fumigatus* strains was extracted using a Biospin Fungus Genomic DNA Extraction Kit (BioFlux, Beijing, China) following the manufacturer's instructions. The full sequences of the *cyp51A* gene with its promoter regions of non-WT *A. fumigatus* isolates were amplified using previously described PCR primers (**Supplementary Table 1**). The amplified products were sent to the BGI Company (Beijing, China) for sequencing. The DNA sequences of non-WT *A. fumigatus* isolates were aligned with those of the *A. fumigatus* reference strain (GenBank accession AF338659) using Clustal Omega.[1]

Definition of Proposed Epidemiological Cutoff Values

The highest WT MIC/MEC is defined as ECV, which should be established by statistical techniques (Turnidge et al., 2006) or conventional methods (Espinel-Ingroff et al., 2010, 2011a,b). Briefly, the modeled WT population established by the statistical method is based on fitting a normal distribution starting at the lower end of the MIC range and calculating the mean and standard deviation (SD) of the cumulative normal distribution. These values are used to estimate the ECVs that capture at least 95% of the modeled WT population (Espinel-Ingroff et al., 2010, 2011a,b). The conventional method, also known as the "eyeball" method, visually inspects the histograms of the MIC distribution for a single species. The "eyeball" method has been used widely to define the ECVs for triazoles and echinocandins (Espinel-Ingroff et al., 2010, 2011a,b). Importantly, ECVs defined by the CLSI must include MIC distributions (≥100 MIC results per species and antifungal agent) from multiple (≥3) independent laboratories. In this study, since the number of *A. fumigatus* and *A. flavus* isolates exceeded 100, the proposed ECVs for *A. fumigatus* and *A. flavus* were established by combining the statistical calculation and "eyeball" method in our single-center laboratory.

Statistical Analysis

All comparisons were performed using SPSS software version 18.0 (SPSS Inc., Chicago, IL, United States). Comparisons of continuous variables were performed using the Mann–Whitney test, and categorical variables were analyzed using the χ^2 test or Fisher's exact test. A p-value ≤ 0.05 was considered statistically significant.

[1]https://www.ebi.ac.uk/Tools/msa/clustalo/

RESULTS

Specimen Origin and Species Distribution of *Aspergillus* Isolates

A total of 706 non-duplicate *Aspergillus* spp. isolates from individual patients were preserved at the Research Center for Medical Mycology in Peking University First Hospital from April 1999 to December 2019. Of these, 688 *Aspergillus* strains were isolated from various clinical sources, while the sources of the remaining 18 isolates were unknown. Regarding specimen types, over 50% of the *Aspergillus* spp. isolates (416/706, 58.9%) were recovered from sputum, 13.6% (96/706 isolates) were from bronchoalveolar lavage fluid (BALF), 9.2% (65/706 isolates) were from ear canal secretions, 5.1% (36/706 isolates) were from sinus secretions, 4.2% (30/706 isolates) were from biopsy tissues, 2.7% (19/706 isolates) were from body fluids (pleural fluid, ascetic fluid, and pericardial effusion), and 2.4% (17/706 isolates) were from the skin. Nine isolates were obtained from other body sites, including blood, urine, maxillary sinuses, and stool, accounting for no more than 5% (**Table 1**).

Among 706 *Aspergillus* spp. isolates, the proportion of *A. fumigatus* (385/548 isolates, 70.3%) isolated from respiratory tract samples (sputum, BALF, and sinus secretions) was significantly higher than that of isolates recovered from other specimen types ($\chi^2 = 54.8$, $p < 0.05$). *A. terreus* (27/65 isolates, 41.5%) and *A. niger* (23/65 isolates, 35.4%) isolated from ear canal secretions accounted for a higher proportion than isolates recovered from other specimen types ($p < 0.05$). More specifically, *A. fumigatus* accounted for the majority of strains (18/19 isolates, 94.8%) isolated from body fluids (ascetic fluid, pleural fluid, and pericardial effusion) and was the only species isolated from urine, maxillary sinus secretions, blood, and stool (**Table 1**).

A. fumigatus was the most predominant species (445/706 isolates, 63.0%), and *A. flavus* (166/706 isolates, 23.5%) was the second most common species, followed by *A. terreus* (48/706 isolates, 6.7%), *A. niger* (35/706 isolates, 5.0%), and *Aspergillus nidulans* (8/706 isolates, 1.1%). The remaining four species were cryptic species, including each isolate of *Aspergillus sydowii*, *Aspergillus penicillioides*, *Aspergillus tamarii*, and *Aspergillus undagawae*; and the prevalence rates were collectively <1%. Additionally, cryptic species were isolated in the past 5 years.

Susceptibility to Triazoles, Amphotericin B, and Caspofungin

The antifungal activities of ITC, VRC, POS, AMB, and CAS against the 706 *Aspergillus* spp. isolates; and MIC/MEC_{50}, MIC/MEC_{90}, MIC/MEC ranges, and CLSI ECVs for the five agents tested against *Aspergillus* spp. isolates are presented in **Table 2**. A total of 666 isolates (94.3%) were susceptible to all tested antifungals. Since the CLSI M38-A3 method has not established ECVs for cryptic species, WT or non-WT strains were classified using CLSI ECVs at the *Aspergillus* species complex

TABLE 1 | *Aspergillus* spp. isolates recovered from clinical samples.

N (%)	Sputum	BALF	Ear canal	Sinus secretions	Tissues	Fluid	Skin (scales, pus)	Urine	Maxillary sinuses secretion	Blood	Stool	Unknown source	Total
Aspergillus fumigatus	300 (72.1)	62 (64.6)	0	23 (63.9)	20 (66.7)	18 (94.8)	6 (35.3)	3 (100)	3 (100)	2 (100)	1 (100)	7 (38.8)	445
Aspergillus flavus	91 (21.9)	26 (27.1)	14 (21.5)	13 (36.1)	7 (23.3)	0	7 (41.2)	0	0	0	0	8 (44.4)	166
Aspergillus terreus	15 (3.6)	3 (3.1)	27 (41.5)	0	1 (3.3)	0	1 (5.9)	0	0	0	0	1 (5.5)	48
Aspergillus niger	5 (1.2)	2 (2.1)	23 (35.4)	0	2 (6.6)	0	1 (5.9)	0	0	0	0	2 (11.1)	35
Aspergillus nidulans	4 (0.9)	2 (2.1)	0	0	0	1 (5.2)	1 (5.9)	0	0	0	0	0	8
Other rare species[a]	1 (0.2)	1 (1.0)	1 (1.5)	0	0	0	1 (5.9)	0	0	0	0	0	4
Total	416 (58.9)	96 (13.6)	65 (9.2)	36 (5.1)	30 (4.2)	19 (2.7)	17 (2.4)	3 (0.4)	3 (0.4)	2 (0.3)	1 (0.1)	18 (2.5)	706

BALF, bronchoalveolar lavage fluid.

[a]*Other rare species included each isolate of Aspergillus sydowii (from ear canal), Aspergillus penicillioides (from cutaneous pus), Aspergillus tamarii (from sputum), and Aspergillus undagawae (from BALF).*

level (Won et al., 2018), and four cryptic isolates were susceptible to all antifungals tested.

As shown in **Table 2**, for *A. fumigatus*, AMB was active against all isolates, and VRC exhibited more efficacy than ITC and POS. For *A. flavus*, VRC was more effective than ITC and AMB. For *A. terreus* and *A. niger*, triazoles were effective against 97.9 and 100% of strains, while AMB was active against 93.7 and 91.4% of strains, respectively.

Resistance to Triazoles, Amphotericin B, and Caspofungin

A total of 40 isolates (5.7%) displayed a non-WT phenotype for at least one antifungal tested (**Table 3**). Of these, 16 isolates (40.0%) showed multidrug resistance to antifungals, and 75% (12/16) were *A. fumigatus* (**Figure 1**).

The prevalence of triazole resistance was 4.3% (19/445 isolates) in *A. fumigatus*, 6.0% (10/166 isolates) in *A. flavus*, and 2.1% (1/48 isolates) in *A. terreus* (**Table 3**). Additionally, four *A. flavus*, three *A. niger*, and three *A. terreus* exhibited non-WT phenotypes to AMB (**Table 2**). All *Aspergillus* spp. isolates were susceptible to CAS except three isolates: one *A. flavus* (MEC of 4 μg/ml) isolated in 2014, one AMB co-resistant *A. niger* (MEC of 1 μg/ml) isolated in 2013, and one *A. nidulans* (MEC of 2 μg/ml) isolated in 2019 (**Table 2**), suggesting that CAS resistance in clinical *Aspergillus* spp. isolates has emerged in recent years.

As shown in **Figure 2**, the total isolates of *A. fumigatus* and *A. flavus* increased annually before 2012 but remained stable after 2012. Resistant strains of *A. fumigatus* and *A. flavus* were not isolated every year (**Figure 2**). Additionally, the 5-year proportion of resistant *A. fumigatus* isolates increased slightly from 5.06% (4/79 isolates) for 1999–2004 to 6.25% (7/112 isolates) for 2005–2009 and 8.43% (7/83 isolates) for 2015–2019 ($p > 0.05$). There was no statistically significant difference, while the increase in resistance for 2015–2019 compared with 2010–2014 (0.58%, 1/171 isolates) was statistically significant ($\chi^2 = 8.859$, $p < 0.05$). Although the triazole resistance rate of *A. fumigatus* decreased significantly from 6.25% for 2005–2009 to 0.58% for 2010–2014, the overall resistance trend increased slightly in the past 20 years. For *A. flavus*, the 5-year proportion of resistant *A. flavus* isolates decreased from 10.9% (10/92 isolates) for 2008–2013 to 5.4% (4/74 isolates) for 2014–2019 (**Figure 2**).

Cyp51A Mutations in Non-wild Type *Aspergillus fumigatus* Isolates

Of the 19 non-WT *A. fumigatus* isolates, six harbored the G54W mutation, three harbored the G54R mutation, four exhibited the TR_{34}/L98H/S297T/F495I mutation, three had the TR_{46}/Y121F/T289A mutation, one carried the TR_{34}/L98H mutation, and one carried the M220I mutation in the *cyp51A* gene. TR_{34}/L98H/S297T/F495I was the most prevalent mutation. Surprisingly, there were no mutations in the *cyp51A* gene of one strain isolated in 2019 (**Table 4**).

The Establishment of Epidemiological Cutoff Values for *Aspergillus fumigatus* and *Aspergillus flavus*

Based on the statistical approach and ≥95% inclusion eyeball method used in our study, as shown in **Table 2**, the proposed ECVs for *A. fumigatus* and *A. flavus* isolates were calculated. Since only 59 isolates of *A. flavus* were examined for POS susceptibilities, the ECV of POS was not evaluated for *A. flavus*. Of note, the calculated ECVs were in agreement with the ECVs established by the CLSI in prior studies (CLSI, 2018), except the proposed ECV of *A. flavus* for ITC. Therefore, the susceptibility of *A. flavus* isolates to ITC was re-evaluated using the proposed ITC ECV listed in **Table 2**. Since the calculated ECV was 2 μg/ml, which was higher than the ECV recommended by the CLSI, the non-WT rate of *A. flavus* for ITC decreased from 6.0 to 0.6%.

DISCUSSION

In the present study, *A. fumigatus* was the most frequently isolated species among 706 *Aspergillus* strains, accounting for 63% of the isolates collected in this study, similar to the rates observed in several epidemiological studies in other

TABLE 2 | *In vitro* susceptibilities of the 706 *Aspergillus* spp. isolates against five antifungal agents and proposed ECVs for *Aspergillus fumigatus* and *Aspergillus flavus* obtained using CLSI M38-A3 broth microdilution method.

Species (*N*)	Antifungal agents	No. of isolates													MIC/MEC (μg/ml)[d]			CLSI ECV[e] (μg/ml)	WT (%)	Non-WT	Calculated ECV[f] (μg/ml)	WT[g]
		MIC/MEC (μg/ml)																				
		0.008	0.015	0.03	0.06	0.125	0.25	0.5	1	2	4	8	16	32	50	90	Range					
Aspergillus fumigatus (445)	ITC			2	3	10	61	119	234				16		1	1	0.03–16	1	96.4	16 (3.6%)	1	96.4%
	VRC					15	101	232	88	4		2	3		0.5	1	0.125–16	1	98.0	9 (2.0%)	1	98.0%
	POS		1	27	69	220	77	39	5	1			6		0.125	0.5	0.015–16	0.5	97.3	12 (2.7%)	0.5	97.3%
	CAS	13	28	89	126	76	71	42							0.06	0.25	0.008–0.5	0.5	100	0	0.5	100%
	AMB					4	5	18	180	238					2	2	0.125–2	2	100	0	2	100%
Aspergillus flavus (166)	ITC		1	2	3	6	45	40	59	9	1				0.5	1	0.015–4	1	94.0	10 (6.0%)	2	99.4%
	VRC			1		7	39	75	39	3	1		1		0.5	1	0.03–16	2	98.8	2 (1.2%)	2	98.8%
	POS[a]		1	2	2	8	38	8							0.25	0.5	0.015–0.5	0.5	100	0	ND	ND
	CAS	36	20	17	31	32	22	7			1				0.06	0.25	0.008–4	0.5	99.4	1 (0.6%)	0.5	99.4%
	AMB					1	2	7	51	76	23		3	1	2	4	0.125–32	4	97.6	4 (2.4%)	4	97.6%
Aspergillus terreus (48)	ITC	2		3	7	5	6	1	19	4		1			0.5	2	0.008–8	2	97.9	1 (2.1%)	ND	ND
	VRC				1	10	24	8	4	1					0.25	1	0.06–2	2	100	0	ND	ND
	POS[b]		5	3	6	3	3								0.06	0.25	0.015–0.25	1	100	0	ND	ND
	CAS	12	3	8	11	11	3								0.06	0.125	0.008–0.25	0.25	100	0	ND	ND
	AMB						1	1	4	24	15	3			2	8	0.25–8	4	93.7	3 (6.3%)	ND	ND
Aspergillus niger (35)	ITC					1	1	13	13	3	4				1	4	0.125–4	4	100	0	ND	ND
	VRC					2	7	16	10						0.5	1	0.125–1	2	100	0	ND	ND
	POS[c]			1		4	6	7							0.25	0.25	0.03–0.5	2	100	0	ND	ND
	CAS	11	5	4	3	6	5		1						0.03	0.25	0.008–1	0.25	97.1	1 (2.9%)	ND	ND
	AMB						1	2	11	17		3			2	2	0.25–8	2	91.4	3 (8.6%)	ND	ND
Aspergillus nidulans (8)	ITC				1	2	5								ND	ND	0.06–0.25	1	100	0	ND	ND
	VRC				2	4	1	1							ND	ND	0.06–0.5	2	100	0	ND	ND
	POS			1	1	5	1								ND	ND	0.03–0.25	1	100	0	ND	ND
	CAS	2		5						1					ND	ND	0.008–2	0.5	87.5	1 (12.5%)	ND	ND
	AMB								4	3	2				ND	ND	1–4	4	100	0	ND	ND
Aspergillus sydowii (1)	ITC						1								ND	ND	ND	2	100	0	ND	ND
	VRC								1						ND	ND	ND	2	100	0	ND	ND
	POS					1									ND	ND	ND	1	100	0	ND	ND
	CAS		1												ND	ND	ND	0.25	100	0	ND	ND
	AMB									1					ND	ND	ND	2	100	0	ND	ND
Aspergillus penicillioides (1)	ITC						1								ND	ND	ND	ND	100	0	ND	ND
	VRC								1						ND	ND	ND	ND	100	0	ND	ND
	POS					1									ND	ND	ND	ND	100	0	ND	ND
	CAS	1													ND	ND	ND	ND	100	0	ND	ND
	AMB									1					ND	ND	ND	ND	100	0	ND	ND
Aspergillus tamarii (1)	ITC								1						ND	ND	ND	1	100	0	ND	ND
	VRC							1							ND	ND	ND	2	100	0	ND	ND

(Continued)

TABLE 2 | Continued

Species (*N*)	Antifungal agents	No. of isolates											MIC/MEC (μg/ml)[d]			CLSI ECV[e] (μg/ml)	WT (%)	Non-WT	Calculated ECV[f] (μg/ml)	WT[g]
		MIC/MEC (μg/ml)																		
		0.008	0.015	0.03	0.06	0.125	0.25	0.5	1	2	4	8	16	32	50	90	Range					
	POS							1							ND	ND	ND	0.5	100	0	ND	ND
	CAS	1													ND	ND	ND	0.5	100	0	ND	ND
	AMB								1						ND	ND	ND	4	100	0	ND	ND
Aspergillus undagawae (1)	ITC							1							ND	ND	ND	1	100	0	ND	ND
	VRC								1						ND	ND	ND	1	100	0	ND	ND
	POS							1							ND	ND	ND	0.5	100	0	ND	ND
	CAS				1										ND	ND	ND	0.5	100	0	ND	ND
	AMB									1					ND	ND	ND	2	100	0	ND	ND

$MIC_{50/90}$ was the MIC inhibiting the growth of 50 and 90% of the isolates, respectively.
ITC, itraconazole; VRC, voriconazole; POS, posaconazole; AMB, amphotericin B; CAS, caspofungin; MIC, minimum inhibitory concentration; MEC, minimum effective concentration; ECVs, epidemiological cutoff values; non-WT, non-wild type; ND, not determined.
[a]*The susceptibilities of 59 A. flavus isolates were tested using the CLSI broth microdilution method.*
[b]*The susceptibilities of 20 A. terreus isolates were tested using the CLSI broth microdilution method.*
[c]*The susceptibilities of 18 A. niger isolates were tested using the CLSI broth microdilution method.*
[d]*$MIC_{50/90}$ values were calculated for species with ≥10 isolates.*
[e]*The CLSI ECVs were recommended by CLSI M59 document.*
[f]*The calculated ECVs captured ≥97.5% of the statistically modeled population.*
[g]*The percentage of MICs less than the calculated ECVs.*

TABLE 3 | The single and multidrug resistance of 706 *Aspergillus* spp. isolates to antifungals.

***Aspergillus* species (number of isolates tested)**	**Number (%) of isolates with resistance to antifungals**
Aspergillus fumigatus (445)	19 (4.3%)
ITC	4 (0.9%)
VRC	3 (0.7%)
ITC + POS	6 (1.3%)
ITC + VRC + POS	6 (1.3%)
Aspergillus flavus (166)	14 (8.4%)
ITC	7 (4.2%)
VRC	1 (0.6%)
CAS	1 (0.6%)
AMB	3 (1.8%)
ITC + VRC	1 (0.6%)
ITC + AMB	1 (0.6%)
Aspergillus niger (35)	3 (8.6%)
AMB	2 (5.7%)
AMB + CAS	1 (2.9%)
Aspergillus terreus (48)	3 (6.3%)
AMB	2 (4.2%)
ITC + AMB	1 (2.1%)
Aspergillus nidulans (8)	1 (12.5%)
CAS	1 (12.5%)

countries (Krishnan et al., 2009; Alastruey-Izquierdo et al., 2013a). *A. flavus* was the second most commonly isolated species, which was in accordance with previous studies in the United States (Balajee et al., 2009), Europe (Alastruey-Izquierdo et al., 2013b), and Brazil (Negri et al., 2014). *A. terreus* and *A. niger* were the third and fourth most common isolates, respectively. However, *A. terreus* and *A. niger* were reported as the second most common species in Austria (Lackner et al., 2016) and Korea (Heo et al., 2015), respectively, indicating that there are geographical variations in the prevalence of different species. Additionally, sputum was the most common source of the clinically isolated *Aspergillus* spp. over the 20 years. *A. fumigatus* and *A. flavus* were mainly isolated from respiratory tract specimens. However, *A. terreus* and *A. niger* were mainly isolated from ear specimens.

The results of *in vitro* susceptibility testing listed in **Table 2** showed that AMB was the most active against 100% of *A. fumigatus* isolates and that triazoles were effective against 95.7% of *A. fumigatus* isolates. In agreement with our finding, the susceptibility profiles of 159 clinical *A. fumigatus* isolates collected from different areas in China also showed that all isolates were susceptible to AMB and that 95.6% were susceptible to triazoles (Deng et al., 2017). A retrospective surveillance study in Portugal also indicated that AMB MICs of all *A. fumigatus* isolates were ≤2 μg/ml, while ITC, VRC, and POS were effective against 95.8, 97.4, and 84.7% of *A. fumigatus* isolates, respectively (Pinto et al., 2018). Gomez-Lopez et al. (2003) also demonstrated that AMB inhibited all *A. fumigatus* isolates at a concentration of 2 μg/ml. Likewise, the susceptibility result of a study from multiple hospitals in Shanghai, China, also showed that AMB

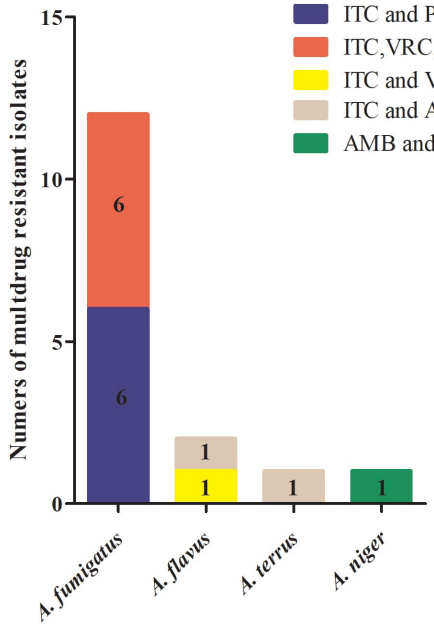

FIGURE 1 | Multidrug-resistant *Aspergillus* spp. isolates collected in China from 1999 to 2019. Among 16 multidrug-resistant isolates of *Aspergillus* spp., six *Aspergillus fumigatus* isolates were cross-resistant to itraconazole (ITC) and posaconazole (POS); six *A. fumigatus* isolates were cross-resistant to ITC, voriconazole (VRC), and POS; one *Aspergillus flavus* isolate was cross-resistant to ITC and VRC; one *A. flavus* and one *Aspergillus terreus* isolate were co-resistant to ITC and amphotericin B (AMB); and one *Aspergillus niger* isolate was co-resistant to AMB and caspofungin (CAS).

was more effective than triazoles against *A. fumigatus* (Xu et al., 2020). Therefore, AMB appears to be the most active antifungal agent against *A. fumigatus*. This may be due to the fact that AMB is a polyene fungicidal agent with excellent property of high activity, while azole compounds inhibit fungal growth (Wiederhold, 2017). The fungicidal ability of AMB is higher than that of triazoles (Perlin et al., 2017). On the other hand, since the clinical use of AMB is limited due to nephrotoxicity, triazoles are recommended as the first-line therapy for IA, leading to the emergence of triazole resistance (Perlin et al., 2017; Wiederhold, 2017).

As shown in **Table 4**, the mutations in the *cyp51A* gene are the most common reasons conferring resistance to triazoles in *A. fumigatus*. Among 19 non-WT *A. fumigatus* strains, six types of the *cyp51A* mutations (M220I, G54W, G54R, TR_{34}/L98H, TR_{34}/L98H/S297T/F495I, and TR_{46}/Y121F/T289A) were observed. The emergence of *A. fumigatus* harboring TR_{34}/L98H/S297T/F495I mutation in China was first reported from a global surveillance study conducted in 2008 and 2009 (Lockhart et al., 2011). Chen et al. (2015) reported the first isolation of TR_{46}/Y121F/T289A *A. fumigatus* strain from a Chinese patient without triazole exposure in 2015, which was related to two strains from clinical and environmental samples obtained in the Netherlands by genetic analysis based on microsatellite genotyping. Clinical and environmental *A. fumigatus* strains harboring TR_{34}/L98H and TR_{34}/L98H/S297T/F495I mutations were isolated in China; genetic typing and phylogenetic analysis showed that TR_{34}/L98H isolates had a clonal expansion worldwide, while the TR_{34}/L98H/S297T/F495I isolates harbored a distinct genetic background with resistant isolates from other countries (Chen et al., 2016). These mutations were also reported in many countries (Sharma et al., 2015; Chowdhary et al., 2017; Leonardelli et al., 2017). Additionally, one strain without mutations in the *cyp51A* gene was isolated in 2019 in this study. Recent studies have demonstrated the occurrence of triazole-resistant *A. fumigatus* without *cyp51A* gene mutations (Hagiwara et al., 2018; Sharma et al., 2019). Therefore, the strain may have non-*cyp51A*-mediated resistance mechanisms, and further research is worth conducting.

As shown in **Table 2**, triazoles were likely to be more effective than AMB against *A. flavus*, *A. terreus*, and *A. niger*. Since the total number of non-*fumigatus* strains isolated was low during the 10-year period and the susceptibility result of a single-center study was insufficient, it is difficult to consider triazoles as the potent agents against non-*fumigatus* strains, although the susceptibility result was in accordance with the previous study showing triazoles were the most active compounds against non-*fumigatus* species (Gomez-Lopez et al., 2003). However, the emergence of AMB resistance in *A. flavus* and *A. niger* strains should raise concerns. *A. terreus* is considered intrinsically resistant to AMB (Lass-Flörl et al., 2005; Blatzer et al., 2015).

As shown in **Figure 2**, the 5-year proportion of resistant *A. fumigatus* isolates was 5.06% for 1999–2004, 6.25% for 2005–2009, 0.58% for 2010–2014, and 8.43% for 2015–2019. The increase in resistance for 2015–2019 compared with 2010–2014 was statistically significant ($\chi^2 = 8.859$, $p < 0.05$). In various time periods, the prevalence of resistance was inconsistent and dynamic. Among 19 non-WT *A. fumigatus*, nine strains of BMU02731, BMU02810, BMU02816, BMU02998, BMU03908, BMU03941, BMU03942, BMU04053, and BMU04758, harboring the single point mutations in the *cyp51A* gene, were isolated from one patient with pulmonary aspergilloma and chronic cavitary tuberculosis before 2009 (Chen et al., 2005). The patient had a history of long-term ITC therapy (Chen et al., 2005). The presence of a cavity allows for asexual sporulation to occur; and with chronic azole exposure, numerous spontaneous mutations may occur in the conidia (Rivero-Menendez et al., 2016; Buil et al., 2019). Hence, due to ITC exposure, nine triazole-resistant strains were continuously isolated from the patient, resulting in high resistance rates in 1999–2004 (5.06%) and 2005–2009 (6.25%). Additionally, strains harboring TR_{34}/L98H and TR_{46}/Y121F/T289A were gradually isolated after 2009. Since TR_{34} or TR_{46} mutations are believed to be primarily driven by the use of azole fungicides in the environment (Chen et al., 2016; Rivero-Menendez et al., 2016), patients are infected by inhaling resistant conidia that already harbor azole resistance mechanisms under environmental exposure, presumably the consequence of exposure to azole fungicides used in agriculture (Chen et al., 2016; Rivero-Menendez et al., 2016).

Although the prevalence of resistance showed fluctuations, the overall trends toward decreasing susceptibility to triazoles were observed in *A. fumigatus* over the past 20 years. Previous studies

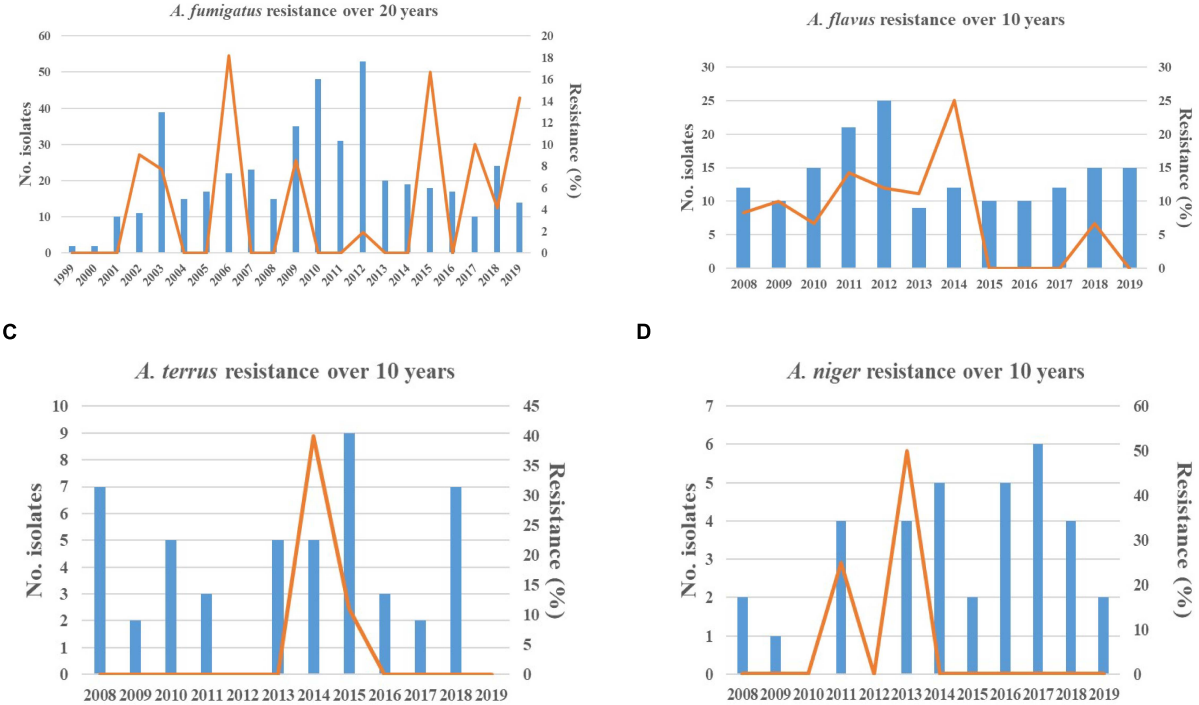

FIGURE 2 | Resistance trends of *Aspergillus* spp. isolates collected over 20 years. Blue histograms: the total number of *Aspergillus* isolates collected each year. Yellow solid line: the frequency of resistant *Aspergillus* isolates each year. **(A)** The increasing trend in resistance of *Aspergillus fumigatus* was observed. **(B)** The decreasing trend in resistance of *Aspergillus flavus* was observed. **(C,D)** The trends in susceptibility of *Aspergillus terreus* and *Aspergillus niger* were stable.

were consistent with our finding. Nine-year susceptibility trends of 1,789 clinical *Aspergillus* spp. isolates obtained from more than 60 medical centers worldwide showed that the proportion of non-WT *A. fumigatus* isolates ranged from 0.7 to 4.0% for ITC, from 1.1 to 5.7% for POS, and from 0.0 to 1.6% for VRC (Pfaller et al., 2011). A 23-year continuous surveillance study for *A. fumigatus* in the Netherlands also observed an increasing trend of triazole resistance in clinical *A. fumigatus* isolates (Buil et al., 2019). Hence, the increasing prevalence of triazole resistance is a worldwide concern (Choukri et al., 2015; Chowdhary et al., 2017; Buil et al., 2019). In 2018, Chen et al. (2020) reported that 10.2% of *A. fumigatus* isolates collected from 63 soil samples from agricultural farms or greenhouses were azole resistant, and 18 resistant strains were cultured from soil samples acquired from strawberry fields. In a study in the United Kingdom, azole-resistant *A. fumigatus* isolates were identified in several products that originated from China, including tea and pepper (Chen et al., 2020). The total amount of azole fungicides used in agriculture accounted for more than one-third of fungicides used in China during 2013–2016 (Zhang et al., 2011). All these findings suggested that more resistant *A. fumigatus*, harboring the TR_{34} or TR_{46} mutations, were isolated from the environment in China. Similarly, azole-resistant *A. fumigatus* isolates have been recovered from the environment in an increasing number of countries (Choukri et al., 2015; Rivero-Menendez et al., 2016; Verweij et al., 2016; Perlin et al., 2017), with the frequency of azole resistance varying widely. Additionally, it has been reported that more resistant strains from China harbored the identical genetic background with resistant isolates from other countries by genetic analysis based on microsatellite genotyping (Chen et al., 2016; Deng et al., 2017), suggesting that the spread of resistant strains in the environment is increasing worldwide. Considering that the TR_{34}/L98H was the most common type of mutation in this study, we speculated that the decreasing trend in susceptibility of *A. fumigatus* to triazoles shown in **Figure 2** may be correlated with the increased exposure and transmission of resistant strains in the environment.

The possible reasons for the fluctuations in the prevalence of resistance in this study are as follows. Firstly, the number of resistant strains in the environment is increasing. Secondly, the triazole exposure in patients is increasing. Thirdly, the number of isolates collected was low, and the susceptibility result of a single-center study was limited. Finally, all isolates of *Aspergillus* spp. were recovered from clinical samples only.

Additionally, since only four isolates of *A. flavus* were non-WT to AMB, the trend in susceptibility of *A. flavus* to AMB seemed to be stable over the 10-year period, which was inconsistent with other studies showing that more *A. flavus* isolates were resistant to AMB (Gonçalves et al., 2013; Reichert-Lima et al., 2018; Rudramurthy et al., 2019). Given that *A. flavus* was the second leading species in our collection, continuous susceptibility surveillance will be still needed.

TABLE 4 | *Cyp51A* mutations of non-WT *A. fumigatus* isolates.

Strains	GenBank accession numbers	*cyp51A* mutation	MIC (μg/ml)		
			ITC	VRC	POS
BMU02731	MW811158	M220I	16	1	0.25
BMU02810	MW811159	G54R	16	0.5	0.5
BMU02816	MW811160	G54R	16	0.5	0.5
BMU02998	MW814729	G54R	16	0.5	0.5
BMU03908	MW811161	G54W	16	0.5	16
BMU03941	MW811162	G54W	16	1	16
BMU03942	MW811163	G54W	16	1	16
BMU04053	MW814730	G54W	16	0.5	16
BMU04758	MW814731	G54W	16	1	16
BMU04835	MW811165	TR_{34}/L98H	16	8	1
BMU04836	MW811166	TR_{34}/L98H/S297T/F495I	16	2	1
BMU07160	MW814724	TR_{34}/L98H/S297T/F495I	16	2	1
BMU07945	MW814725	TR_{46}/Y121F/T289A	0.5	16	0.5
BMU07946	MW814726	TR_{46}/Y121F/T289A	0.5	16	0.5
BMU08181	MW814727	TR_{34}/L98H/S297T/F495I	16	2	1
BMU09386	MW811164	G54W	16	0.5	16
BMU09453	MW970052	TR_{46}/Y121F/T289A	0.5	16	0.5
BMU09691	MW814728	TR_{34}/L98H/S297T/F495I	16	2	1
BMU09765	MW788327	non-*cyp51A*	16	8	2

BMU02731, BMU02810, BMU02816, BMU02998, BMU03908, BMU03941, BMU03942, BMU04053, and BMU04758 were isolated from one patient with pulmonary aspergilloma and chronic cavitary tuberculosis; BMU07945 and BMU07946 were isolated from one patient with ANCA-associated vasculitis; BMU04835 and BMU04836 were isolated from one patient with acute lymphoblastic leukemia. WT, wild type; MIC, minimum inhibitory concentration; ITC, itraconazole; VRC, voriconazole; POS, posaconazole; ANCA, anti-neutrophil cytoplasmic antibody.

Cryptic species were found to account for over 10% of *Aspergillus* spp. clinical isolates and to be resistant to at least one of the antifungals available in Brazil, Spain, and Korea (Alastruey-Izquierdo et al., 2013a; Negri et al., 2014; Won et al., 2018). While only four isolates of cryptic species were identified, including *A. sydowii*, *A. penicillioides*, *A. tamarii*, and *A. undagawae*, and all were susceptible to the antifungals tested. Albeit the number of cryptic species was low in this study, attention should be paid to the emergence of resistant cryptic species.

Considering that the CBPs of *Aspergillus* spp. for common antifungals have not been determined except for the CBP of VRC for *A. fumigatus* (CLSI, 2020), the ECVs proposed for *A. fumigatus* and *A. flavus* were calculated. The proposed ECVs were in agreement with those defined by the CLSI except the ECV of ITC for *A. flavus* (Espinel-Ingroff et al., 2010, 2011a,b; CLSI, 2018). The susceptibility of *A. flavus* isolates to ITC was re-evaluated using the proposed ECV, showing that the prevalence of non-WT *A. flavus* isolates reduced significantly from 6 to 0.6%. The ECVs, established by CLSI using statistical methods combined with the "eyeball" method, must include MIC distributions (≥100 MIC results per species and antifungal agent) from multiple (≥3) independent laboratories (Espinel-Ingroff et al., 2010, 2011a,b), while the ECVs defined in this study were based on the gathered MIC data of strains collected from multiple geographic locations and preserved in a single center in China over 20 years. The proposed ITC ECV of *A. flavus* was higher than that defined by the CLSI, probably because the susceptibility of *A. flavus* isolates to ITC in China may be lower than that of other countries. On the other hand, the susceptibility result of a single-center study could not fully represent the susceptibility of *A. flavus* strains nationwide. Therefore, multicenter surveillance data in China need to be collected to establish accurate ECVs in the future.

In conclusion, this is the first 20-year retrospective surveillance study for clinically isolated *Aspergillus* spp. in China. Several species of *Aspergillus* spp. have developed drug resistance and even multidrug resistance, and the resistance mechanisms of non-WT *A. fumigatus* strains have been also described. Moreover, the proposed ECVs were established for *A. fumigatus* and *A. flavus*, which will be an essential step in developing CBPs and be useful for resistance surveillance in China. Hence, the significance of this study is to establish continuous susceptibility surveillance and determine antifungal susceptibility trends, providing a basis for clinical medication.

DATA AVAILABILITY STATEMENT

The datasets presented in this study can be found in online repositories. The names of the repository/repositories and accession number(s) can be found in the article/**Supplementary Material**.

AUTHOR CONTRIBUTIONS

XY, WC, TL, JT, WxL, YS, QW, HX, LL, YZ, QqW, and YgS contributed to the species identification and antifungal susceptibility testing. WL designed all the experiments of the study. XY, QW, and YZ contributed to molecular biology experiments. XY and WL contributed to writing and reviewing the manuscript. All authors read and approved the final manuscript.

FUNDING

This work was supported by the National Natural Science Foundation of China (grants 81861148028, 81671990, and 81971912) and Natural Science Foundation of Guangxi Province of China project Guangxi Innovation Research Team for Fungal Infectious Diseases Prevention and Treatment (grant 2020GXNSFGA238001).

SUPPLEMENTARY MATERIAL

The Supplementary Material for this article can be found online at: https://www.frontiersin.org/articles/10.3389/fmicb.2021.680884/full#supplementary-material

REFERENCES

Alastruey-Izquierdo, A., Mellado, E., Peláez, T., Pemán, J., Zapico, S., Alvarez, M., et al. (2013a). Population-based survey of filamentous fungi and antifungal resistance in Spain (FILPOP Study). *Antimicrob. Agents Chemother.* 57:4604. doi: 10.1128/aac.01287-13

Alastruey-Izquierdo, A., Mellado, E., Peláez, T., Pemán, J., Zapico, S., Alvarez, M., et al. (2013b). Population-based survey of filamentous fungi and antifungal resistance in Spain (FILPOP Study). *Antimicrob. Agents Chemother.* 57, 3380–3387. doi: 10.1128/aac.00383-13

Balajee, S. A., Kano, R., Baddley, J. W., Moser, S. A., Marr, K. A., Alexander, B. D., et al. (2009). Molecular identification of *Aspergillus* species collected for the transplant-associated infection surveillance network. *J. Clin. Microbiol.* 47, 3138–3141. doi: 10.1128/jcm.01070-09

Blatzer, M., Jukic, E., Posch, W., Schöpf, B., Binder, U., Steger, M., et al. (2015). Amphotericin B resistance in *Aspergillus terreus* is overpowered by coapplication of pro-oxidants. *Antioxid. Redox. Signal.* 23, 1424–1438. doi: 10.1089/ars.2014.6220

Buil, J. B., Snelders, E., Denardi, L. B., Melchers, W. J. G., and Verweij, P. E. (2019). Trends in azole resistance in *Aspergillus fumigatus*, the Netherlands, 1994-2016. *Emerg. Infect. Dis.* 25, 176–178. doi: 10.3201/eid2501.171925

Cadena, J., Thompson, G. R. III, and Patterson, T. F. (2016). Invasive aspergillosis: current strategies for diagnosis and management. *Infect. Dis. Clin. North Am.* 30, 125–142. doi: 10.1016/j.idc.2015.10.015

Chabi, M. L., Goracci, A., Roche, N., Paugam, A., Lupo, A., and Revel, M. P. (2015). Pulmonary aspergillosis. *Diagn. Intervent. Imaging* 96, 435–442. doi: 10.1016/j.diii.2015.01.005

Chen, J., Li, H., Li, R., Bu, D., and Wan, Z. (2005). Mutations in the cyp51A gene and susceptibility to itraconazole in *Aspergillus fumigatus* serially isolated from a patient with lung aspergilloma. *J. Antimicrob. Chemother.* 55, 31–37. doi: 10.1093/jac/dkh507

Chen, Y., Dong, F., Zhao, J., Fan, H., Qin, C., Li, R., et al. (2020). High azole resistance in *Aspergillus fumigatus* isolates from strawberry fields, China, 2018. *Emerg. Infect. Dis.* 26, 81–89. doi: 10.3201/eid2601.190885

Chen, Y., Lu, Z., Zhao, J., Zou, Z., Gong, Y., Qu, F., et al. (2016). Epidemiology and molecular characterizations of azole resistance in clinical and environmental *Aspergillus fumigatus* isolates from China. *Antimicrob. Agents Chemother.* 60, 5878–5884. doi: 10.1128/AAC.01005-16

Chen, Y., Wang, H., Lu, Z., Li, P., Zhang, Q., Jia, T., et al. (2015). Emergence of TR_{46}/Y121F/T289A in an *Aspergillus fumigatus* isolate from a Chinese patient. *Antimicrob. Agents Chemother.* 59, 7148–7150. doi: 10.1128/AAC.00887-15

Choukri, F., Botterel, F., Sitterlé, E., Bassinet, L., Foulet, F., Guillot, J., et al. (2015). Prospective evaluation of azole resistance in *Aspergillus fumigatus* clinical isolates in France. *Med. Mycol.* 53, 593–596. doi: 10.1093/mmy/myv029

Chowdhary, A., Sharma, C., and Meis, J. F. (2017). Azole-resistant aspergillosis: epidemiology, molecular mechanisms, and treatment. *J. Infect. Dis.* 216, S436–S444. doi: 10.1093/infdis/jix210

CLSI (2017). *M38: Reference Method for Broth Dilution Antifungal Susceptibility Testing of Filamentous Fungi*, 3rd Edn. Wayne, PA: Clinical and Laboratory Standards Institute.

CLSI (2018). *M59: Epidemiological Cutoff Values for Antifungal Susceptibility Testing*, 2nd Edn. Wayne, PA: Clinical and Laboratory Standards Institute.

CLSI (2020). *M61: Performance Standards for Antifungal Susceptibility Testing of Filamentous Fungi*, 2nd Edn. Wayne, PA: Clinical and Laboratory Standards Institute.

Deng, S., Zhang, L., Ji, Y., Verweij, P. E., Tsui, K. M., Hagen, F., et al. (2017). Triazole phenotypes and genotypic characterization of clinical *Aspergillus fumigatus* isolates in China. *Emerg. Microbes Infect.* 6:e109. doi: 10.1038/emi.2017.97

Espinel-Ingroff, A., Cuenca-Estrella, M., Fothergill, A., Fuller, J., Ghannoum, M., Johnson, E., et al. (2011a). Wild-type MIC distributions and epidemiological cutoff values for amphotericin B and *Aspergillus* spp. for the CLSI broth microdilution method (M38-A2 document). *Antimicrob. Agents Chemother.* 55, 5150–5154. doi: 10.1128/aac.00686-11

Espinel-Ingroff, A., Diekema, D. J., Fothergill, A., Johnson, E., Pelaez, T., Pfaller, M. A., et al. (2010). Wild-type MIC distributions and epidemiological cutoff values for the triazoles and six *Aspergillus* spp. for the CLSI broth microdilution method (M38-A2 document). *J. Clin. Microbiol.* 48, 3251–3257. doi: 10.1128/jcm.00536-10

Espinel-Ingroff, A., Fothergill, A., Fuller, J., Johnson, E., Pelaez, T., and Turnidge, J. (2011b). Wild-type MIC distributions and epidemiological cutoff values for caspofungin and *Aspergillus* spp. for the CLSI broth microdilution method (M38-A2 document). *Antimicrob. Agents Chemother.* 55, 2855–2859. doi: 10.1128/aac.01730-10

Gomez-Lopez, A., Garcia-Effron, G., Mellado, E., Monzon, A., Rodriguez-Tudela, J. L., and Cuenca-Estrella, M. (2003). In vitro activities of three licensed antifungal agents against Spanish clinical isolates of *Aspergillus* spp. *Antimicrob. Agents Chemother.* 47, 3085–3088. doi: 10.1128/aac.47.10.3085-3088.2003

Gonçalves, S. S., Stchigel, A. M., Cano, J., Guarro, J., and Colombo, A. L. (2013). In vitro antifungal susceptibility of clinically relevant species belonging to *Aspergillus* section Flavi. *Antimicrob. Agents Chemother.* 57, 1944–1947. doi: 10.1128/aac.01902-12

Hagiwara, D., Arai, T., Takahashi, H., Kusuya, Y., Watanabe, A., and Kamei, K. (2018). Non-cyp51A azole-resistant *Aspergillus fumigatus* isolates with mutation in HMG-CoA reductase. *Emerg. Infect. Dis.* 24, 1889–1897. doi: 10.3201/eid2410.180730

Heo, M. S., Shin, J. H., Choi, M. J., Park, Y. J., Lee, H. S., Koo, S. H., et al. (2015). Molecular identification and amphotericin B susceptibility testing of clinical isolates of *Aspergillus* from 11 hospitals in Korea. *Ann. Lab. Med.* 35, 602–610. doi: 10.3343/alm.2015.35.6.602

Krishnan, S., Manavathu, E. K., and Chandrasekar, P. H. (2009). *Aspergillus flavus*: an emerging non-fumigatus *Aspergillus* species of significance. *Mycoses* 52, 206–222. doi: 10.1111/j.1439-0507.2008.01642.x

Lackner, M., Coassin, S., Haun, M., Binder, U., Kronenberg, F., Haas, H., et al. (2016). Geographically predominant genotypes of *Aspergillus terreus* species complex in Austria: microsatellite typing study. *Clin. Microbiol. Infect.* 22, 270–276. doi: 10.1016/j.cmi.2015.10.021

Lass-Flörl, C., Griff, K., Mayr, A., Petzer, A., Gastl, G., Bonatti, H., et al. (2005). Epidemiology and outcome of infections due to *Aspergillus terreus*: 10-year single centre experience. *Br. J. Haematol.* 131, 201–207. doi: 10.1111/j.1365-2141.2005.05763.x

Leonardelli, F., Theill, L., Nardin, M. E., Macedo, D., Dudiuk, C., Mendez, E., et al. (2017). First itraconazole resistant *Aspergillus fumigatus* clinical isolate harbouring a G54E substitution in Cyp51Ap in South America. *Rev. Iberoam. Micol.* 34, 46–48. doi: 10.1016/j.riam.2016.05.005

Lockhart, S. R., Frade, J. P., Etienne, K. A., Pfaller, M. A., Diekema, D. J., and Balajee, S. A. (2011). Azole resistance in *Aspergillus fumigatus* isolates from the ARTEMIS global surveillance study is primarily due to the TR/L98H mutation in the cyp51A gene. *Antimicrob. Agents Chemother.* 55, 4465–4468. doi: 10.1128/AAC.00185-11

Negri, C. E., Gonçalves, S. S., Xafranski, H., Bergamasco, M. D., Aquino, V. R., Castro, P. T., et al. (2014). Cryptic and rare *Aspergillus* species in Brazil: prevalence in clinical samples and in vitro susceptibility to triazoles. *J. Clin. Microbiol.* 52, 3633–3640. doi: 10.1128/jcm.01582-14

Perlin, D. S., Rautemaa-Richardson, R., and Alastruey-Izquierdo, A. (2017). The global problem of antifungal resistance: prevalence, mechanisms, and management. *Lancet Infect. Dis.* 17, e383–e392. doi: 10.1016/S1473-3099(17)30316-X

Pfaller, M., Boyken, L., Hollis, R., Kroeger, J., Messer, S., Tendolkar, S., et al. (2011). Use of epidemiological cutoff values to examine 9-year trends in susceptibility of *Aspergillus* species to the triazoles. *J. Clin. Microbiol.* 49, 586–590. doi: 10.1128/jcm.02136-10

Pinto, E., Monteiro, C., Maia, M., Faria, M. A., Lopes, V., Lameiras, C., et al. (2018). *Aspergillus* species and antifungals susceptibility in clinical setting in the North of Portugal: cryptic species and emerging azoles resistance in *A. fumigatus*. *Front. Microbiol.* 9:1656. doi: 10.3389/fmicb.2018.01656

Reichert-Lima, F., Lyra, L., Pontes, L., Moretti, M. L., Pham, C. D., and Lockhart, S. R. (2018). Surveillance for azoles resistance in *Aspergillus* spp. highlights a high number of amphotericin B-resistant isolates. *Mycoses* 61, 360–365. doi: 10.1111/myc.12759

Richardson, M., and Lass-Flörl, C. (2008). Changing epidemiology of systemic fungal infections. *Clin. Microbiol. Infect.* 14(Suppl. 4), 5–24. doi: 10.1111/j.1469-0691.2008.01978.x

Rivero-Menendez, O., Alastruey-Izquierdo, A., Mellado, E., and Cuenca-Estrella, M. (2016). Triazole resistance in *Aspergillus* spp.: a worldwide problem? *J. Fungi* 2:21. doi: 10.3390/jof2030021

Rudramurthy, S. M., Paul, R. A., Chakrabarti, A., Mouton, J. W., and Meis, J. F. (2019). Invasive aspergillosis by *Aspergillus flavus*: epidemiology, diagnosis, antifungal resistance, and management. *J. Fungi* 5:55. doi: 10.3390/jof5030055

Sharma, C., Hagen, F., Moroti, R., Meis, J. F., and Chowdhary, A. (2015). Triazole-resistant *Aspergillus fumigatus* harbouring G54 mutation: is it de novo or environmentally acquired? *J. Glob. Antimicrob. Resist.* 3, 69–74. doi: 10.1016/j.jgar.2015.01.005

Sharma, C., Nelson-Sathi, S., Singh, A., Radhakrishna Pillai, M., and Chowdhary, A. (2019). Genomic perspective of triazole resistance in clinical and environmental *Aspergillus fumigatus* isolates without cyp51A mutations. *Fungal Genet. Biol.* 132:103265. doi: 10.1016/j.fgb.2019.103265

Sugui, J. A., Kwon-Chung, K. J., Juvvadi, P. R., Latgé, J. P., and Steinbach, W. J. (2014). *Aspergillus fumigatus* and related species. *Cold Spring Harb. Perspect. Med.* 5:a019786. doi: 10.1101/cshperspect.a019786

Turnidge, J., Kahlmeter, G., and Kronvall, G. (2006). Statistical characterisation of bacterial wild-type MIC value distributions and the determination of epidemiological cut-off values. *Clin. Microbiol. Infect.* 12, 418–425. doi: 10.1111/j.1469-0691.2006.01377.x

Verweij, P. E., Chowdhary, A., Melchers, W. J., and Meis, J. F. (2016). Azole resistance in *Aspergillus fumigatus*: can we retain the clinical use of mold-active antifungal azoles? *Clin. Infect. Dis.* 62, 362–368. doi: 10.1093/cid/civ885

Walsh, T. J., Anaissie, E. J., Denning, D. W., Herbrecht, R., Kontoyiannis, D. P., Marr, K. A., et al. (2008). Treatment of aspergillosis: clinical practice guidelines of the infectious diseases society of America. *Clin. Infect. Dis.* 46, 327–360. doi: 10.1086/525258

Wiederhold, N. P. (2017). The antifungal arsenal: alternative drugs and future targets. *Int. J. Antimicrob. Agents* 51, 333–339. doi: 10.1016/j.ijantimicag.2017.09.002

Won, E. J., Shin, J. H., Kim, S. H., Choi, M. J., Byun, S. A., Kim, M. N., et al. (2018). Antifungal susceptibilities to amphotericin B, triazoles and echinocandins of 77 clinical isolates of cryptic *Aspergillus* species in multicenter surveillance in Korea. *Med. Mycol.* 56, 501–505. doi: 10.1093/mmy/myx067

Xu, Y., Chen, M., Zhu, J., Gerrits van den Ende, B., Chen, A. J., Al-Hatmi, A. M. S., et al. (2020). *Aspergillus* species in lower respiratory tract of hospitalized patients from Shanghai, China: species diversity and emerging azole resistance. *Infect. Drug Resist.* 13, 4663–4672. doi: 10.2147/IDR.S281288

Zhang, W. J., Jiang, F. B., and Ou, J. F. (2011). Global pesticide consumption and pollution: with China as a focus. *Proc. Int. Acad. Ecol. Environ. Sci.* 1, 125–144. doi: 10.1016/j.scitotenv.2020.136856

Conflict of Interest: The authors declare that the research was conducted in the absence of any commercial or financial relationships that could be construed as a potential conflict of interest.

frontiers in Microbiology

ORIGINAL RESEARCH
published: 03 August 2021
doi: 10.3389/fmicb.2021.680749

The Elevated Endogenous Reactive Oxygen Species Contribute to the Sensitivity of the Amphotericin B-Resistant Isolate of *Aspergillus flavus* to Triazoles and Echinocandins

*Tianyu Liang, Wei Chen, Xinyu Yang, Qiqi Wang, Zhe Wan, Ruoyu Li and Wei Liu**

Department of Dermatology and Venerology, Peking University First Hospital, National Clinical Research Center for Skin and Immune Diseases, Research Center for Medical Mycology, Peking University, Beijing Key Laboratory of Molecular Diagnosis on Dermatoses, Beijing, China

OPEN ACCESS

Edited by:
Ying-Chun Xu,
Peking Union Medical College Hospital (CAMS), China

Reviewed by:
Jata Shankar,
Jaypee University of Information Technology, India
Stéphane Ranque,
Aix-Marseille Université, France

***Correspondence:**
Wei Liu
liuwei@bjmu.edu.cn

Specialty section:
This article was submitted to Antimicrobials, Resistance and Chemotherapy, a section of the journal Frontiers in Microbiology

Received: *15 March 2021*
Accepted: *13 July 2021*
Published: *03 August 2021*

Citation:
Liang T, Chen W, Yang X, Wang Q, Wan Z, Li R and Liu W (2021) The Elevated Endogenous Reactive Oxygen Species Contribute to the Sensitivity of the Amphotericin B-Resistant Isolate of Aspergillus flavus to Triazoles and Echinocandins. Front. Microbiol. 12:680749. doi: 10.3389/fmicb.2021.680749

Aspergillus flavus has been frequently reported as the second cause of invasive aspergillosis (IA), as well as the leading cause in certain tropical countries. Amphotericin B (AMB) is a clinically important therapy option for a range of invasive fungal infections including invasive aspergillosis, and *in vitro* resistance to AMB was associated with poor outcomes in IA patients treated with AMB. Compared with the AMB-susceptible isolates of *A. terreus*, the AMB-resistant isolates of *A. terreus* showed a lower level of AMB-induced endogenous reactive oxygen species (ROS), which was an important cause of AMB resistance. In this study, we obtained one AMB-resistant isolate of *A. flavus,* with an AMB MIC of 32 μg/mL, which was sensitive to triazoles and echinocandins. This isolate presented elevated endogenous ROS levels, which strongly suggested that no contribution of decreased AMB-induced endogenous ROS for AMB-resistance, opposite to those observed in *A. terreus*. Further, we confirmed that the elevated endogenous ROS contributed to the sensitivity of the AMB-resistant *A. flavus* isolate to triazoles and echinocandins. Further investigation is needed to elucidate the causes of elevated endogenous ROS and the resistance mechanism to AMB in *A. flavus*.

Keywords: *Aspergillus flavus*, amphotericin B, reactive oxygen species, triazoles, echinocandins

INTRODUCTION

Invasive aspergillosis (IA) is an important opportunistic fungal infection caused by *Aspergillus* with high mortality rates. Over the past few decades, the incidence of IA has been rising with the increasing number of immunosuppressed patients (Brown et al., 2012). *Aspergillus flavus* has been frequently reported as the second leading cause of IA, as well as the leading cause in certain tropical countries (Rudramurthy et al., 2019).

At present, there are three main classes of antifungal drugs used for the treatment of IA (Perlin et al., 2017): (i) polyenes, such as amphotericin B (AMB); (ii) triazoles, such as itraconazole (ITC), voriconazole (VRC) and posaconazole (POS); and (iii) echinocandins, such as caspofungin (CAS) and micafungin (MFG). Among them, AMB stood out due to its broad activity spectrum and less likely developed drug resistance. AMB has been a clinically important therapy option for a range of

invasive fungal diseases, including IA, since it was first approved in the 1950s (Perlin et al., 2017). Although dose-dependent toxic side effects, such as nephrotoxicity, limit the use of AMB, the lipid formulations of AMB with equal antifungal activity were therefore developed to reduce these toxicity issues (Stone et al., 2016; Grazziotin et al., 2018). Although AMB resistance is rare, the pathogenic *A. terreus* is intrinsically resistant to AMB (Vaezi et al., 2018) and the reports of the AMB-resistant *A. fumigatus* and *A. flavus* were also notable (Ashu et al., 2018; Rudramurthy et al., 2019). Moreover, *in vitro* resistance to AMB was associated with poor outcomes in IA patients treated with AMB (Hadrich et al., 2012). Therefore, it is important to elucidate the mechanisms of AMB resistance.

Until now, the mode of antifungal action of AMB has not been well understood, and the mechanisms of AMB resistance also need to be elucidated. In addition to binding to ergosterol directly (Gray et al., 2012) and forming ion channels (Kristanc et al., 2019) thereby disrupting the structural integrity of cell membranes, several studies have highlighted that AMB exert antifungal activity by inducing endogenous reactive oxygen species (ROS) production, therefore resulting in oxidative damage and fungal cell death (Belenky et al., 2013; Mesa-Arango et al., 2014; Shekhova et al., 2017). Studies on *A. terreus*, intrinsic resistance to AMB, revealed that the AMB-resistant clinical isolates of *A. terreus* could handle better with AMB-induced oxidative stress and thus showed a lower level of AMB-induced endogenous ROS, compared with AMB-susceptible clinical isolates of *A. terreus* (Blatzer et al., 2015; Jukic et al., 2017). These studies are important for understanding the mechanisms of resistance to AMB in pathogenic fungi, including *A. flavus*.

In this study, we screened the susceptibility of clinical isolates of *A. flavus* to AMB by using the broth microdilution method according to the Clinical and Laboratory Standards Institute (CLSI) M38-A3 guideline. From 117 clinical isolates of *A. flavus*, we obtained an AMB-resistant *A. flavus* isolate. To investigate the role of ROS in AMB resistance in this isolate, the sensitivity to oxidative stress and endogenous ROS levels with or without exposure to AMB were determined. Meanwhile, the expression level and activities of enzymes involved in ROS detoxification were also investigated. In addition, the endogenous ROS levels induced by triazoles and echinocandins were also measured, and the ROS scavenger N-acetylcysteine (NAC) was used to investigate the effect of ROS levels on *in vitro* antifungal susceptibility in AMB-resistant *A. flavus* isolate.

MATERIALS AND METHODS

Antifungal Susceptibility Testing

Antifungal susceptibility testing by the broth microdilution method was performed according to the recommendations of the CLSI M38-A3 document (Clinical and Laboratory Standards Institute (CLSI)., 2017), and the tested drugs included were ITC, VRC, POS, CAS, MFG (all from Harveybio Gene Technology Co., Ltd., Beijing, China) and AMB (North China Pharmaceutical Co., Ltd., Shijiazhuang, China). Briefly, antifungal drugs were dispensed into 96-well plates at final concentration ranges of 0.0625–32 μg/mL for AMB, 0.0313–16 μg/mL for ITC, VRC, and POS, and 0.008–4 μg/mL for CAS and MFG. All isolates of *A. flavus* were subcultured on potato dextrose agar (PDA) at 35°C for 3 to 7 days to yield good conidiation. Conidia were harvested by slightly scraping the surface of the *A. flavus* colonies with a sterile cotton swab and suspending the colonies in sterile saline solution with 0.05% Tween-20. Heavy particles were allowed to settle for 5 min, after which the upper homogenous suspensions were used as inoculum suspensions. Inoculum suspensions were diluted in RPMI 1640 medium at a final concentration of 1×10^4 CFU/mL, as determined by a hemocytometer, and transferred into 96-well plates containing drug dilutions. The 96-well plates were incubated at 35°C and examined visually for MIC (after 48 h) and MEC (after 24 h) determinations. The MIC endpoints for AMB and triazoles were determined as the lowest drug concentration that resulted in a 100% reduction in growth compared with that of the drug-free controls. The MEC endpoints for echinocandins were determined as the lowest drug concentration that led to the growth of small, rounded, compact hyphal forms compared with the hyphal growth seen in the growth control well.

Antifungal susceptibility testing by E-test was performed according to the manufacturer's instructions. Briefly, inoculum suspensions at a final concentration of 1×10^6 CFU/mL were inoculated on the entire surface of each 90-mm plate containing 25 mL of RPMI 1640 medium (in the presence or absence of 15 mM NAC) with a sterile cotton swab. The E-test strips (Autobio, Zhengzhou, China) were placed on the center of the plate and incubated at 35°C. The MIC or MEC (for CAS only) was determined from the inhibition ellipse that intersected the scale on the strip after 48 h.

Antifungal susceptibility testing by disk diffusion was performed on non-supplemented Muller-Hinton (NMH) agar refer to the method described previously (Qiao et al., 2007). When necessary, a 15 mM concentration of the antioxidant NAC was dissolved in NMH medium. Disks prepared in-house of AMB (50 μg), ITC (10 μg), VRC (5 μg), POS (5 μg), CAS (5 μg), and MFG (5 μg) were placed onto the surface of the inoculated (the same method as described in the E-test) NMH plate. The plates were incubated at 35°C, and the inhibition zone diameter was determined after 48 h.

Testing of Sensitivity to Oxidative Stress

Based on the reported studies that AMB-resistant *A. terreus* can handle oxidative stress better, two *A. terreus* clinical isolates with different susceptibilities to AMB, the AMB-susceptible *A. terreus* isolate BMU09523 (MIC = 2 μg/ml) and the AMB-resistant *A. terreus* isolate BMU05143 (MIC = 8 μg/mL) were included for comparison. We tested the sensitivity of *A. flavus* isolates and *A. terreus* isolates to H_2O_2 by spot assay. H_2O_2 at a final concentration of 1 mM was supplemented in PDA medium with or without antifungal drugs. Serially diluted inoculum suspensions (2 μl) were spotted onto PDA plates and incubated at 35°C for 48 h.

TABLE 1 | Primers used in this study.

Locus tag	Gene ID	Sequence (5′–3′)
AFLA_056170	*catA*	TGTGAAGGTCGCTACGTCTG
		ACGCTTGTAGTTCCGATGCT
AFLA_100250	*cat*	CGAGACACTGGCTCATTTCA
		ACCGGTGGTACTGATTCTGC
AFLA_090690	*cat1*	CTCCAAGCTCGTCAAGTTCC
		GATCGAAGCCAAACTTCAGC
AFLA_122110	*cat2*	TCAATCAGATGGAGCCTGTG
		GCCGGGTAGTAAACACTCCA
AFLA_096210	*cat3*	ATAATGTCGGTCGCAAGTCC
		CTTCGCATACTCTGGTGCAA
AFLA_034380	*cat4*	TGAGACTCTCGCCCATTTCT
		CCCAGTCCAAGTTACCCTCA
AFLA_044930	*sod1*	ATTGAAGGCTACGGTGTTGG
		CCCTCTTTGCTCTTCGACAC
AFLA_068080	*sod2*	GCGACATAAGCGGAAAACAT
		GTCTTCCTTCGCCTCTTCCT
AFLA_033420	*sod3*	ATGGAAATCCACCACCAAAA
		AGAGGGAGTGGTTGATGTGG
AFLA_027580	*sod4*	ACTCTGCCTGACCTGGCTTA
		AGTGGTGATGTCCTCCTTGG
AFLA_088150	*sod5*	GAGATGGCCTCCGTATTCAA
		CATCAATCCTTCCCTCTCCA
AFLA_099000	*sod6*	CACCAGTTCGGTGACAACAC
		GTACGGCCAAGTACGCTCTC

Measurement of Endogenous ROS Level

The endogenous ROS level of the AMB-resistant *A. flavus* isolate was determined by 2′,7′-dichlorofluorescin diacetate (DCF-DA) as previously described (Shekhova et al., 2017). In brief, 100 μL conidial suspensions at a concentration of 1×10^4 CFU/mL were dispensed into flat-bottom 96-well plates, followed by incubation at 37°C for 18 h. After a washing step with phosphate buffered saline (PBS), the cells were stained with 10 μM DCF-DA for 30 min at 37°C in the dark. After washing with PBS, different antifungal drugs prepared in PBS were added to the cells. PBS was used as a negative control and 2 mM H_2O_2 was used as a positive control. The fluorescence intensity (excitation filter at 485 nm and emission filter at 530 nm) was measured by a microtiter plate reader (Infinite 200 Pro, Tecan, Switzerland) and observed under fluorescence microscope simultaneously at 37°C. The maximum fluorescence intensity observed after 2 h of incubation with drugs was recorded as a reference to the endogenous ROS level.

Assessment of Genes Encoding Enzymes Involved in ROS Detoxification by RT-qPCR

To identify homologs of enzymes involved in ROS detoxification in *A. flavus*, the amino acid sequences of catalases (CATs) and superoxide dismutases (SODs) in *A. fumigatus* and *A. terreus* (Jukic et al., 2017) were used as queries to perform BLASTP analysis[1] in the genome database of *A. flavus*. The primers used in Reverse transcription-quantitative PCR (RT-qPCR) were designed on the Primer3Plus[2]. The identified putative genes encoding enzymes involved in ROS detoxification in *A. flavus* and the primers are listed in **Table 1**.

For assessment of expression of genes encoding enzymes involved in ROS detoxification, a total of 1×10^6 CFU conidia were dispensed into *Aspergillus* minimal medium followed by incubation at 37°C for 18 h on an orbital shaker at 200 rpm. Different antifungal drugs prepared in PBS or PBS were added at 37°C for an additional 2 h on an orbital shaker at 200 rpm. Then the hyphae were harvested and total RNA was extracted following liquid nitrogen crush using TRIzol reagent (Invitrogen). cDNA was synthesized using an Advantage RT-for-PCR kit (Clontech) according to the manufacturer's instructions. RT-qPCR was performed on an Applied Biosystems ViiA7 Real-Time PCR system using SYBR green reagent (Applied Biosystems). The cycling conditions were as follows: a 10-min initial denaturation at 95°C, followed by 40 cycles of denaturation at 95°C for 15 s, and annealing/extension at 60°C for 10 s. Changes in gene expression were calculated using the $2^{-\Delta\Delta Ct}$ method (Schmittgen and Livak, 2008). All experiments were performed in triplicate from biological triplicates.

Determination of CAT, SOD and GSH-Px Activity

To determine CAT, SOD and glutathione peroxidase (GSH-Px) activity of the *A. flavus* isolate, the hyphae were harvested as conditions described in the RT-qPCR assay. The enzyme activity was determined using the CAT activity assay kit (Abcam), the SOD activity assay kit (Abcam), and GSH-Px activity assay kit (Abcam) separately according to the manufacturer's instructions. The relative enzyme activities (%) were calculated relative to those of *A. flavus* NRRL3357 under basal conditions.

Statistical Analysis

Experiments were performed at least three independent biological replicates. A Welch two-sample *t* test was used for significance testing of two groups. *P*-values < 0.05 were considered statistically significant.

RESULTS

The AMB-Resistant Isolate of *A. flavus* Showed Sensitivity to Triazoles and Echinocandins

From 117 clinical isolates of *A. flavus*, we obtained one AMB-resistant isolate of *A. flavus*, named BMU09525, with an AMB MIC of 32 μg/mL. The MICs of ITC, VRC, and POS against *A. flavus* BMU09525 were 0.06, 0.25, and 0.03 μg/mL, respectively. The MECs of CAS and MFG for *A. flavus* BMU09525 were both 0.008 μg/mL (**Table 2**). The results showed that the AMB-resistant isolate of *A. flavus* BMU09525 was sensitive to triazoles (ITC, VRC, POS) and echinocandins

[1]https://blast.ncbi.nlm.nih.gov/Blast.cgi

[2]https://primer3plus.com/cgi-bin/dev/primer3plus.cgi

TABLE 2 | Antifungal susceptibility testing by the broth microdilution method (μg/mL), E-test (μg/mL), and disk diffusion (mm).

	Methods	NAC	NRRL3357	BMU09525
AMB	**BMM**	–	2	32
	E-test	–	2	>32
		+	2	>32
	DD	–	15	0
		+	12	0
ITC	**BMM**	–	0.25	0.06
	E-test	–	2	0.25
		+	4	0.75
	DD	–	33	47
		+	29	34
VRC	**BMM**	–	0.5	0.25
	E-test	–	0.032	0.024
		+	0.064	0.064
	DD	–	40	51
		+	34	44
POS	**BMM**	–	0.125	0.03
	E-test	–	NA	NA
		+	NA	NA
	DD	–	32	46
		+	33	30
CAS	**BMM**	–	0.03	0.008
	E-test	–	0.25	0.064
		+	0.5	0.25
	DD	–	27	25
		+	23	22
MFG	**BMM**	–	0.03	0.008
	E-test	–	NA	NA
		+	NA	NA
	DD	–	40	36
		+	40	28

BMM, broth microdilution method; DD, disk diffusion; NA, E-test strips were not available.

(CAS, MFG). Similar results were obtained by the disk diffusion method and E-test (**Figure 1** and **Table 2**). Interestingly, when testing echinocandins against the *A. flavus* strain NRRL3357, microcolonies within a well-defined zone of inhibition could be seen, while testing echinocandins against AMB-resistant isolate of *A. flavus*, the inhibition ellipse of E-test strip (CAS) or the inhibition zone of the disk (CAS and MFG) was as clean as that seen in triazoles against the AMB-resistant *A. flavus* isolate, suggesting that echinocandins may exert a fungicidal effect, instead of a fungistatic effect, against the AMB-resistant isolate of *A. flavus*.

The AMB-Resistant Isolate of *A. flavus* Showed Hypersensitivity to Oxidative Stress, Opposite to That Observed in the AMB-Resistant *A. terreus*

The AMB-resistant *A. terreus* isolate showed better tolerance to H_2O_2 than the AMB-susceptible *A. terreus* isolates (**Figure 2A**), consistent with previous studies on *A. terreus*. Surprisingly, when exposed to H_2O_2, the AMB-resistant *A. flavus* isolate showed more obvious growth inhibition than the *A. flavus* strain NRRL3357 (**Figure 2B**). When H_2O_2 was combined with antifungals, the *A. flavus* strain NRRL3357 showed merely slight growth inhibition compared to that using antifungals alone. However, H_2O_2 could significantly enhance the activity of antifungals against the AMB-resistant *A. flavus* isolate (**Figure 2B**). The above results indicated that the AMB-resistant *A. flavus* isolate was hypersensitive to oxidative stress, in contrast to the case reported for *A. terreus*. In addition, a decreased growth rate of the AMB-resistant *A. flavus* isolate could be observed compared to the *A. flavus* strain NRRL3357 (**Figure 2B**).

The AMB-Resistant Isolate of *A. flavus* Showed Elevated Basal Endogenous ROS

The basal endogenous ROS level of the AMB-resistant *A. terreus* isolate was comparable to that of the AMB-susceptible *A. terreus* isolate, while the basal endogenous ROS level of the AMB-resistant *A. flavus* isolate was significantly higher than that of both the *A. flavus* NRRL3357 and *A. terreus* (**Figures 3**, **4**). The elevated basal endogenous ROS in AMB-resistant *A. flavus* isolate suggested that the mechanisms of AMB resistance in AMB-resistant *A. flavus* isolate may differ from those mediating AMB resistance in *A. terreus*.

The AMB-Resistant Isolate of *A. flavus* Showed Comparable ROS Detoxification Enzyme Activities

Because the AMB-resistant *A. flavus* isolate showed elevated basal endogenous ROS level and was sensitive to oxidative stress, we further tested the expression level of *sod* and *cat* genes in *A. flavus*. A total of 6 *sod* and 6 *cat* genes were investigated in *A. flavus* (**Figure 5** and **Table 1**). And the ROS detoxification enzyme activities, including CAT, SOD, and GSH-Px (**Figure 6**), were also measured.

Except for *cat* gene, the basal level of *catA*, *cat1*, *cat2*, *cat3*, and *cat4* in the AMB-resistant *A. flavus* isolate were mildly higher than that of the *A. flavus* NRRL3357. Upon H_2O_2 exposure, *catA*, *cat2* and *cat3* expression level increased in both the AMB-resistant *A. flavus* isolate and the *A. flavus* NRRL3357, while no significant changes of *cat*, *cat1*, and *cat4* in both two strains. However, a different picture was observed in *sod* genes expression level. In the AMB-resistant *A. flavus* isolate, only *sod2* showed a higher basal level than that of the *A. flavus* NRRL3357, while the basal expression level of *sod1*, *sod5* and *sod6* were less than that of the *A. flavus* NRRL3357. The basal expression levels of both *sod3* and *sod4* did not differ between these two *A. flavus* strains. After exposure to H_2O_2, *sod1*, *sod2*, *sod5*, and *sod6* showed a significant increase in the AMB-resistant *A. flavus* isolate, while only *sod2* showed elevated transcript level in the *A. flavus* NRRL3357.

Next, we tested the enzyme activities of CAT, SOD, and GSH-Px using the commercially available kits (**Figure 5**). The basal enzyme activities of CAT, SOD or GSH-Px in the AMB-resistant *A. flavus* isolate were not significantly different from those in the *A. flavus* NRRL3357. After exposure to H_2O_2,

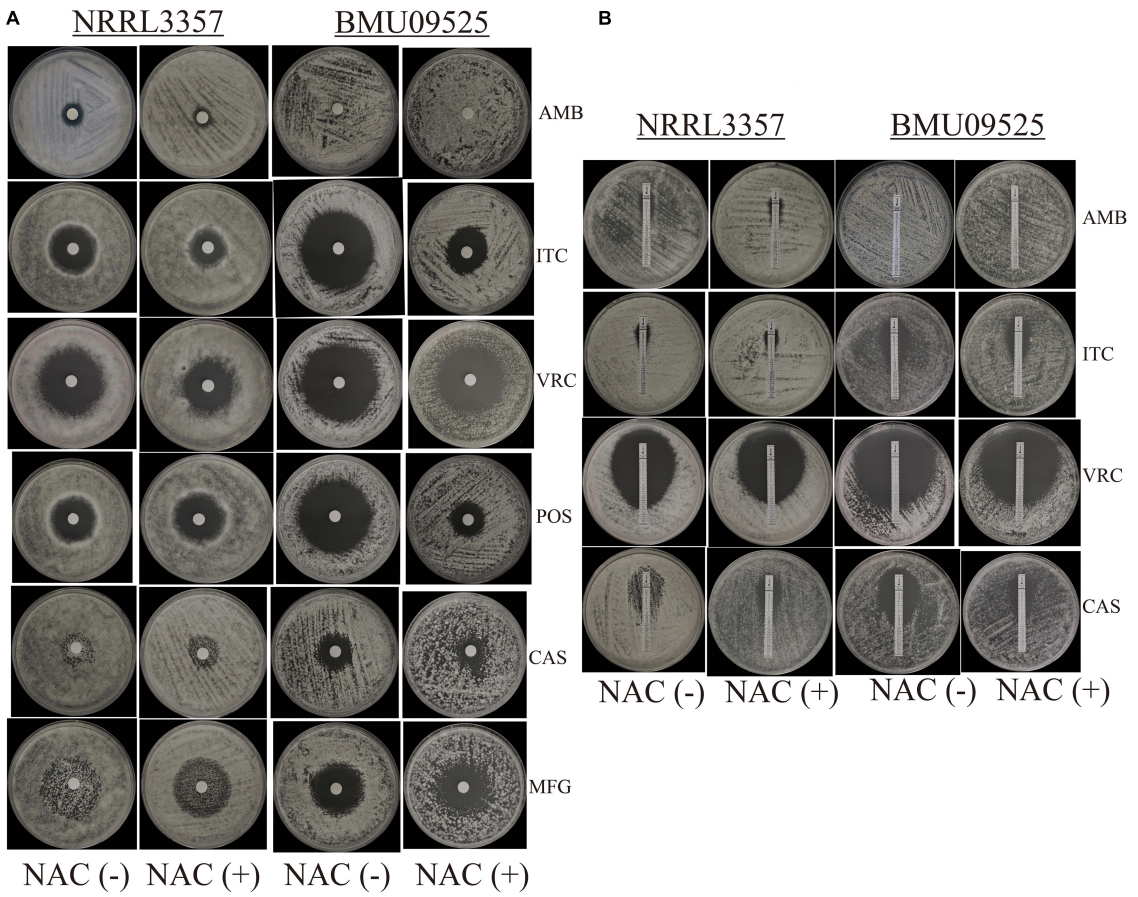

FIGURE 1 | *In vitro* antifungal susceptibility testing. **(A)** *In vitro* antifungal susceptibility testing determined by disk diffusion. The antioxidant N-Acetylcysteine (NAC) was added at a concentration of 15 mM. Disks of AMB (50 μg), ITC (10 μg), VRC (5 μg), POS (5 μg), CAS (5 μg), and MFG (5 μg) were placed onto the NMH medium. Plates were incubated at 35°C for 48 h. **(B)** *In vitro* antifungal susceptibility testing determined by E-test. Plates were incubated at 35°C for 48 h.

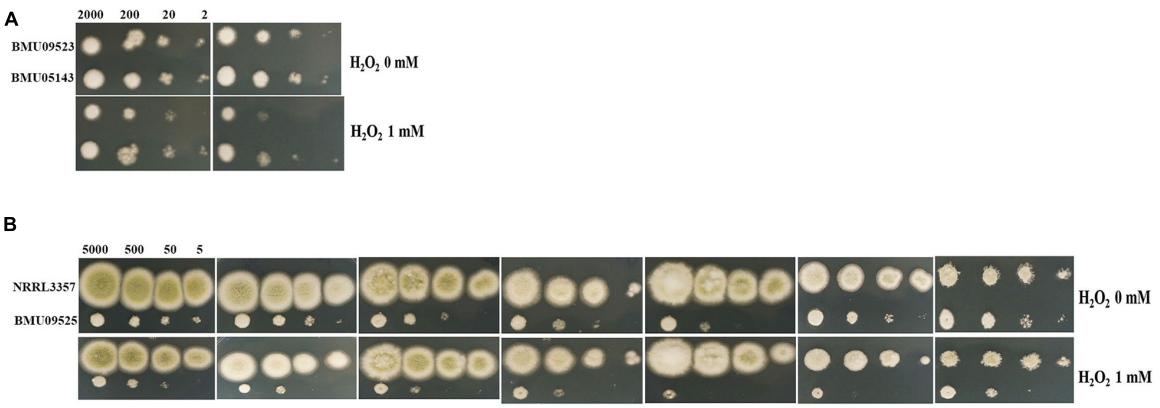

FIGURE 2 | The sensitivity to H_2O_2 determined by spot assay. Hydrogen peroxide (H_2O_2) at a concentration of 1 mM was supplemented in PDA medium with or without antifungal drugs. **(A)** A total of 2, 20, 200, and 2×10^3 conidia of *A. terreus* were spotted onto PDA medium, respectively. **(B)** A total of 5, 50, 500, and 5×10^3 conidia of *A. flavus* were spotted onto PDA medium, respectively. Plates were incubated at 35°C and documented after 48 h.

the activities of all these enzymes showed an increase but remained comparable between the two strains. Nevertheless, the increase of enzyme activities of CAT and GSH-Px in the *A. flavus* NRRL3357 was more significant than that in the AMB-resistant *A. flavus* isolate, which showed only a mild increase.

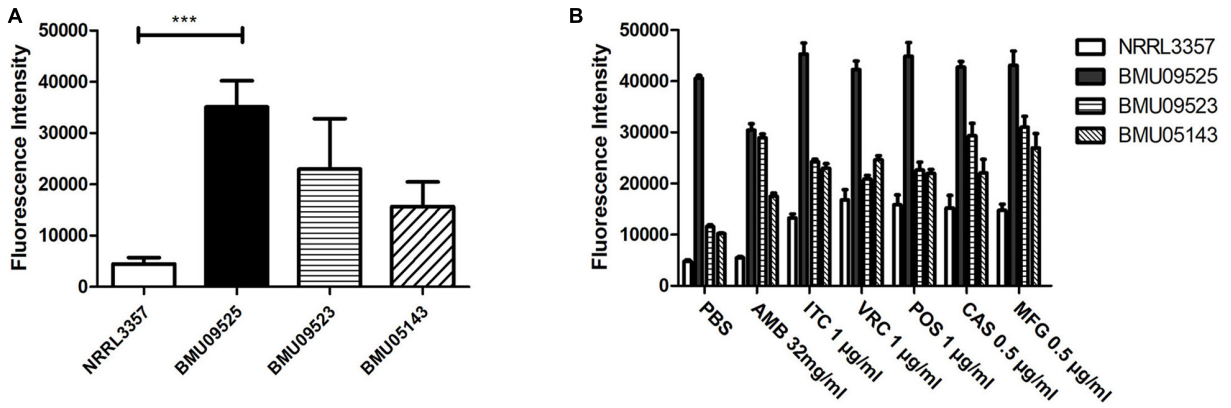

FIGURE 3 | Level of endogenous ROS determined by DCF-DA assay. **(A)** The level of basal endogenous ROS. **(B)** The level of endogenous ROS induced by antifungals. Conidial were incubated at 37°C for 18 h before stained with 10 μM DCF-DA for 30 min at 37°C in the dark. After a wash step, different antifungal drugs prepared in PBS were added to the cells. The fluorescence intensity peak was observed after 2 h of incubation with drugs.

Overall, these results indicate that the basal activities of the enzyme involved in ROS detoxification in the AMB-resistant *A. flavus* isolate were comparable to those in the *A. flavus* NRRL3357, despite the different expression levels were observed. And the elevated basal endogenous ROS level in the AMB-resistant *A. flavus* isolate may not be related to abnormal ROS detoxification enzyme activities. When exposure to H_2O_2, however, the less remarkable increase in enzyme activities of CAT and GSH-Px in the AMB-resistant *A. flavus* isolate may result in hypersensitivity to oxidative stress.

Triazoles and Echinocandins, Instead of AMB, Could Induce the Production of Endogenous ROS in the AMB-Resistant Isolate of *A. flavus*

To further investigate the relationships between ROS levels and antifungal susceptibilities in the AMB-resistant *A. flavus* isolate, the endogenous ROS levels induced by antifungals were determined (**Figures 3**, **4**). With exposure to AMB, the endogenous ROS level of the AMB-susceptible *A. terreus* isolate was significantly increased, while that in the AMB-resistant *A. terreus* isolate increased slightly, consistent with the literature reports on *A. terreus*. Surprisingly, the endogenous ROS level of the *A. flavus* strain NRRL3357 increased slightly, while the endogenous ROS level of the AMB-resistant *A. flavus* isolate even showed a minor decrease despite the ROS level in the AMB-resistant *A. flavus* isolate being significantly higher than that of the *A. flavus* strain NRRL3357. With exposure to triazoles and echinocandins, the endogenous ROS levels of both *A. terreus* and *A. flavus* isolates increased to different degrees. These results strongly suggested no contribution of AMB-induced endogenous ROS to AMB resistance in the AMB-resistant *A. flavus* isolate, in contrast to the situation observed in *A. terreus*. In addition, the elevated basal endogenous ROS in the AMB-resistant *A. flavus* isolate might result in its sensitivity to triazoles and echinocandins.

ROS Elimination by the Antioxidant NAC Decreased the Sensitivity of the AMB-Resistant *A. flavus* Isolate to Triazoles and Echinocandins

The antioxidant NAC can act as a non-specific sulfhydryl donor to scavenge intracellular ROS. Adding NAC to the medium did not show any impact on the susceptibility to AMB, corresponding to the result that no AMB-induced ROS production in the AMB-resistant *A. flavus* isolate (**Figure 1A** and **Table 2**). However, adding NAC to the medium reduced the inhibition zone of triazoles and echinocandins, indicating the decreased susceptibility of AMB-resistant *A. flavus* isolate to triazoles and echinocandins (**Figure 1A** and **Table 2**). Consistent results were obtained by E-test (**Figure 1B** and **Table 2**), which showed that NAC increased the MICs of triazoles and the MECs of echinocandins obtained from E-test strips. The above results confirmed our assumption that the increased level of endogenous ROS contributes to the sensitivity of the AMB-resistant *A. flavus* isolate to triazoles and echinocandins. Interestingly, the addition of NAC decreased the susceptibility of the *A. flavus* strain NRRL3357 to ITC, VRC, and CAS, similar to the AMB-resistant *A. flavus* isolate. Although adding NAC decreased the susceptibility of the *A. flavus* strain NRRL3357 to AMB, the addition of NAC did not change its susceptibility to POS or MFG, as no alteration in the inhibition zone diameter was observed by disk diffusion.

DISCUSSION

Several studies have reported that AMB can induce endogenous ROS production as its mode of action (Belenky et al., 2013; Mesa-Arango et al., 2014; Shekhova et al., 2017). Due to the intrinsic resistance of *A. terreus* to AMB, the impact of endogenous ROS production on the susceptibility of this species to AMB has been closely studied (Posch et al., 2018). Compared with AMB-susceptible *A. terreus* isolates, AMB-resistant *A. terreus*

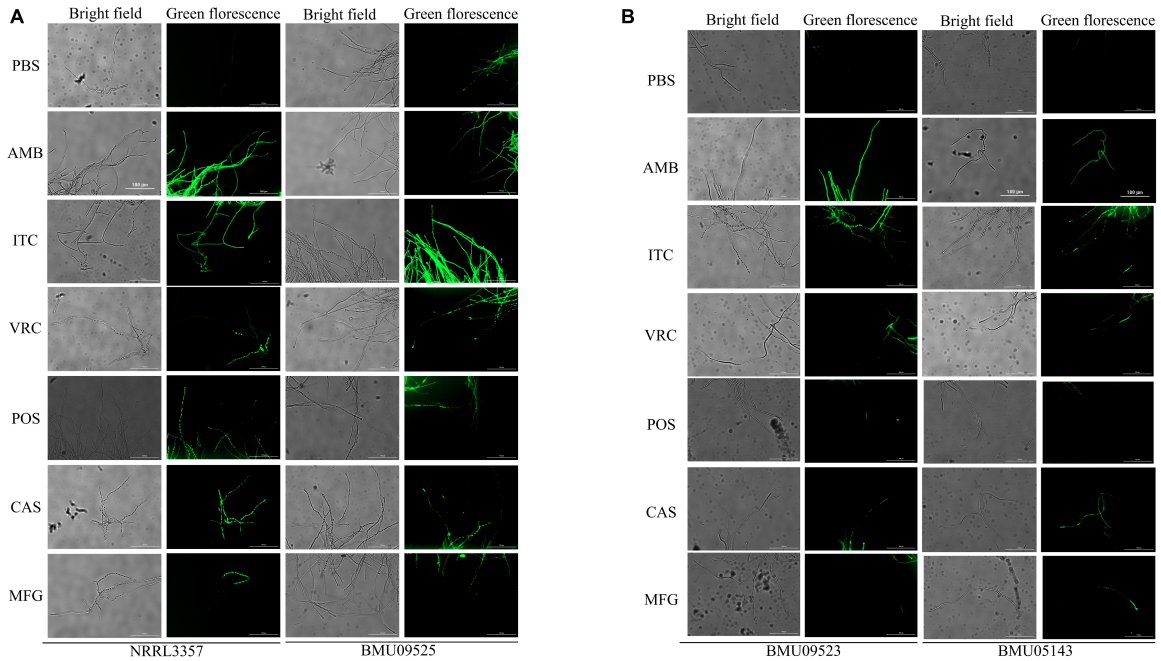

FIGURE 4 | Fluorescence microscope images showing endogenous ROS in **(A)** *A. flavus*. **(B)** *A. terreus*. Conidial were incubated at 37°C for 18 h before stained with 10 μM DCF-DA for 30 min at 37°C in the dark. After a wash step, Fluorescence images were recorded after 2 h of incubation with drugs. AMB (32 μg/ml), ITC (1 μg/ml), VRC (1 μg/ml), POS (1 μg/ml), CAS (0.5 μg/ml), MFG (0.5 μg/ml).

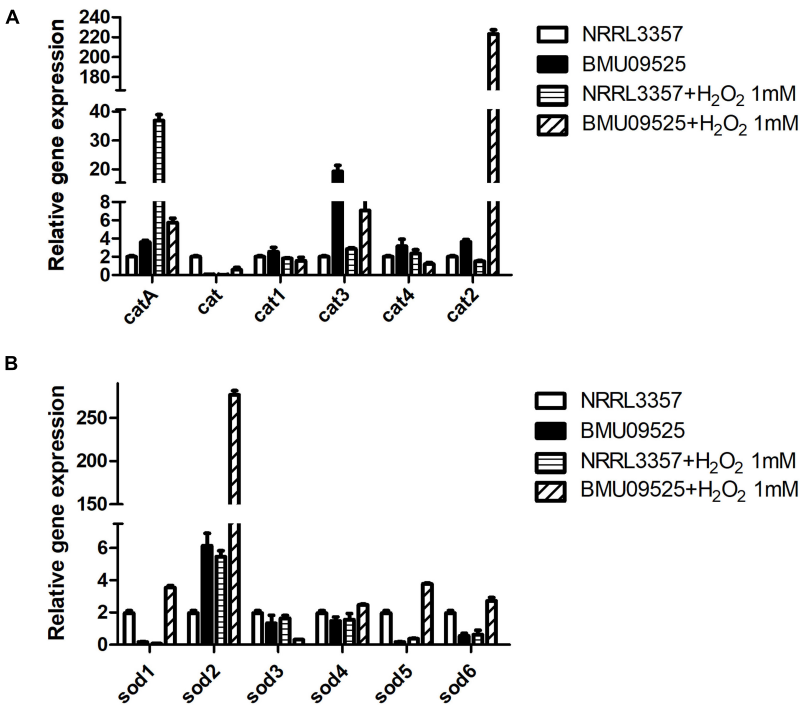

FIGURE 5 | The expression level of **(A)** *cat* genes and **(B)** *sod* genes in *A. flavus*. A total of 1 × 10^6 CFU *A. flavus* conidia were preincubated in *Aspergillus* minimal medium for 18 h at 37°C and 200 rpm before H_2O_2 (1 mM) was added for 2 h. Then the hyphae were harvested and total RNA was extracted following liquid nitrogen crush. Gene expression was normalized to that of beta-tubulin according to the $2^{-\Delta\Delta Ct}$ method. Data are presented as means ± standard deviations for three independent experiments with technical duplicates.

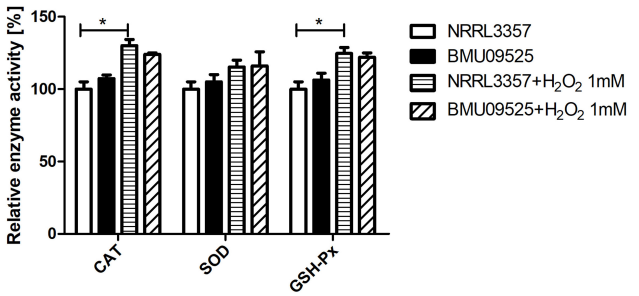

FIGURE 6 | Determination of the enzyme activities of SOD, CAT and GSH-Px. A total of 1×10^6 CFU *A. flavus* conidia were preincubated in *Aspergillus* minimal medium for 18 h at 37°C and 200 rpm before H_2O_2 (1 mM) was added for 2 h. Then the hyphae were harvested and enzyme activities were determined according to the manufacturer's instructions. The relative enzyme activities (%) were calculated relative to those of *A. flavus* NRRL3357 under basal conditions. CAT, catalase; SOD, superoxide dismutase; GHS-Px, glutathione peroxidase.

isolates presented decreased AMB-induced ROS production in mitochondria (Blatzer et al., 2015) and higher ROS-detoxifying enzyme activity (Jukic et al., 2017). However, the AMB-resistant isolate of *A. flavus* presented an elevated level of endogenous ROS regardless of exposure to AMB and was hypersensitive to oxidative stress. Further studies revealed that the less remarkable increase in enzyme activities of CAT and GSH-Px may result in its hypersensitivity to oxidative stress, compared to the observations in *A. terreus* (Blatzer et al., 2015; Jukic et al., 2017). These results suggested that the higher activity of ROS-detoxifying enzyme did not contribute to resistance to AMB in the AMB-resistant isolate of *A. flavus*. The above results indicate that the mechanisms underlying AMB resistance in AMB-resistant *A. flavus* isolate differ from those mediating AMB resistance in *A. terreus*. Although AMB resistance has not been reported to be associated with the missing ergosterol in *Aspergillus* spp. (Blum et al., 2008, 2013), the absence of ergosterol in *Candida* spp., caused by mutations in genes of the ergosterol biosynthesis (Geber et al., 1995; Sanglard et al., 2003; Martel et al., 2010a; Vincent et al., 2013; Silva et al., 2020), leading to AMB resistance and abnormal membrane structure and function, which also drastically diminished tolerance to oxidative stress (Vincent et al., 2013). These studies are consistent with the phenotypes observed in the AMB-resistant isolate of *A. flavus*. Further membrane sterol profile analysis is needed to elucidate its mechanisms of AMB resistance.

Triazoles exert antifungal effects by inhibiting sterol 14α-demethylase (CYP51A/ERG11), which prevents ergosterol biosynthesis and causes the accumulation of toxic sterols (Martel et al., 2010b; Warrilow et al., 2010, 2019). Echinocandins target the β-1,3-glucan synthase of the fungal cell wall and inhibit the synthesis of β-1,3-D glucan on the cell wall (Perlin, 2015). In addition to the above targets, several studies have reported that triazoles (Shirazi et al., 2013; Shekhova et al., 2017; Lee and Lee, 2018) and echinocandins (Belenky et al., 2013; Hao et al., 2013; Delattin et al., 2014) are capable of inducing endogenous ROS production. The AMB-resistant *A. flavus* isolate was sensitive to triazoles and echinocandins, while having elevated basal endogenous ROS. Further, H_2O_2 significantly enhanced the antifungal effects of triazoles and echinocandins *in vitro*, showing a synergistic effect against the AMB-resistant *A. flavus* isolate. Thus, we hypothesized that sensitivity of AMB-resistant *A. flavus* isolate to triazoles and echinocandins may be caused by elevated endogenous ROS levels. The antioxidant NAC can act as a non-specific sulfhydryl donor and is widely used to scavenge intracellular ROS (Dringen and Hamprecht, 1999; Dekhuijzen, 2004). Scavenging ROS by NAC decreased the sensitivity of AMB-resistant *A. flavus* isolate to triazoles and echinocandins confirmed our hypothesis. Interestingly, NAC did not affect the susceptibility of *A. flavus* strain NRRL3357 to POS and MFG, suggesting that ROS, albeit can be induced by POS and MFG, may not be necessary in antifungal mode of action.

Reactive oxygen species are derived from oxygen and known to be of biological importance in eukaryotic cells (Sena and Chandel, 2012). Mitochondria possess the oxidative phosphorylation system, which is the major origin of ROS generation (Zorov et al., 2014). Inappropriate electron transfer reactions in mitochondrial electron transport chain can produce excessive ROS. These highly reactive and toxic ROS can cause cellular damage, ultimately resulting in cell death (Zorov et al., 2014). Correspondingly, ROS can be eliminated by multiple antioxidant enzymes in eukaryotic cells, including SOD (Lambou et al., 2010), CAT (Shibuya et al., 2006), and GSH-Px (Margis et al., 2008). Studies in *A. terreus* (Blatzer et al., 2015; Jukic et al., 2017), the AMB-resistant *A. terreus* isolates exhibited distinct basal expression levels of *sod* and *cat* genes compared to the AMB-susceptible *A. terreus* isolates. However, the basal enzyme activities of CAT and SOD of the AMB-resistant *A. terreus* isolates were already higher than that of the AMB-susceptible *A. terreus* isolate. In this study, the two *A. flavus* strains also exhibited distinct basal expression levels of *sod* and *cat* genes. The basal expression level of *catA*, *cat3*, *cat4*, and *sod2* in the AMB-resistant *A. flavus* isolate were higher than that of the *A. flavus* NRRL3357, while the basal expression level of *cat*, *sod1*, *sod5*, and *sod6* were less than that of the *A. flavus* NRRL3357. However, the basal enzyme activities of CAT and SOD in the AMB-resistant *A. flavus* isolate were comparable to those in the *A. flavus* NRRL3357. Taken together, although no elevated enzyme activity was observed in the AMB-resistant *A. flavus* isolate in the basal condition as reported in the AMB-resistant *A. terreus,* the basal enzyme activity in the AMB-resistant *A. flavus* isolate was still comparable to the AMB-susceptible *A. terreus* isolates. Therefore, it is reasonable to speculate that the elevated basal endogenous ROS level is due to increased production rather than impaired clearance in the AMB-resistant *A. flavus* isolate. Since mitochondria are the main site of ROS production, it is likely that the elevated endogenous ROS level in the AMB-resistant *A. flavus* isolate may be caused by the dysfunction mitochondrial which may lead to overproduction of ROS. Also, the slowed growth observed in the AMB-resistant *A. flavus* isolate may be also due to mitochondrial abnormalities. However, additional studies are needed.

In conclusion, our results showed that the AMB-resistant *A. flavus* isolate presented elevated endogenous ROS levels, an opposite observation to that mediating AMB-resistance in *A. terreus*. The elevated endogenous ROS contributed to the sensitivity of the AMB-resistant *A. flavus* isolate to triazoles and echinocandins. However, further investigation is needed to elucidate the causes of elevated endogenous ROS and the resistance mechanism to AMB in *A. flavus*.

DATA AVAILABILITY STATEMENT

The original contributions presented in the study are included in the article/supplementary material, further inquiries can be directed to the corresponding author.

AUTHOR CONTRIBUTIONS

TL, WC, and ZW completed the experiments. TL wrote the manuscript. XY, QW, RL, and WL revised the manuscript. WL conducted the experiments and data analysis. All authors read and approved the manuscript.

FUNDING

This work was supported by the National Natural Science Foundation of China (grant 81861148028, 81671990, and 81971912) and Natural Science Foundation of Guangxi Province of China project Guangxi Innovation Research Team for Fungal Infectious Diseases Prevention and Treatment (grant 2020GXNSFGA238001).

REFERENCES

Ashu, E. E., Korfanty, G. A., Samarasinghe, H., Pum, N., You, M., Yamamura, D., et al. (2018). Widespread amphotericin B-resistant strains of *Aspergillus fumigatus* in Hamilton. *Canada. Infect. Drug Resist.* 11, 1549–1555. doi: 10.2147/IDR.S170952

Belenky, P., Camacho, D., and Collins, J. J. (2013). Fungicidal drugs induce a common oxidative-damage cellular death pathway. *Cell. Rep.* 3, 350–358. doi: 10.1016/j.celrep.2012.12.021

Blatzer, M., Jukic, E., Posch, W., Schopf, B., Binder, U., Steger, M., et al. (2015). Amphotericin B Resistance in *Aspergillus terreus* Is Overpowered by Coapplication of Pro-oxidants. *Antioxid. Redox. Signal.* 23, 1424–1438. doi: 10.1089/ars.2014.6220

Blum, G., Hortnagl, C., Jukic, E., Erbeznik, T., Pumpel, T., Dietrich, H., et al. (2013). New insight into amphotericin B resistance in *Aspergillus terreus*. *Antimicrob. Agents Chemother.* 57, 1583–1588. doi: 10.1128/AAC.01283-12

Blum, G., Perkhofer, S., Haas, H., Schrettl, M., Wurzner, R., Dierich, M. P., et al. (2008). Potential basis for amphotericin B resistance in *Aspergillus terreus*. *Antimicrob. Agents Chemother.* 52, 1553–1555. doi: 10.1128/AAC.01280-07

Brown, G. D., Denning, D. W., Gow, N. A., Levitz, S. M., Netea, M. G., and White, T. C. (2012). Hidden killers: human fungal infections. *Sci. Transl. Med.* 4:165rv113. doi: 10.1126/scitranslmed.3004404

Clinical and Laboratory Standards Institute (CLSI). (2017). *Reference Method for Broth Dilution Antifungal Susceptibility Testing of Filamentous Fungi. CLSI Standard M38*, 3rd Edn. Wayne: Clinical and Laboratory Standards Institute.

Dekhuijzen, P. N. (2004). Antioxidant properties of N-acetylcysteine: their relevance in relation to chronic obstructive pulmonary disease. *Eur. Respir. J.* 23, 629–636. doi: 10.1183/09031936.04.00016804

Delattin, N., Cammue, B. P., and Thevissen, K. (2014). Reactive oxygen species-inducing antifungal agents and their activity against fungal biofilms. *Future Med. Chem.* 6, 77–90. doi: 10.4155/fmc.13.189

Dringen, R., and Hamprecht, B. (1999). N-acetylcysteine, but not methionine or 2-oxothiazolidine-4-carboxylate, serves as cysteine donor for the synthesis of glutathione in cultured neurons derived from embryonal rat brain. *Neurosci. Lett.* 259, 79–82. doi: 10.1016/s0304-3940(98)00894-5

Geber, A., Hitchcock, C. A., Swartz, J. E., Pullen, F. S., Marsden, K. E., Kwon-Chung, K. J., et al. (1995). Deletion of the *Candida glabrata ERG3* and *ERG11* genes: effect on cell viability, cell growth, sterol composition, and antifungal susceptibility. *Antimicrob. Agents Chemother.* 39, 2708–2717. doi: 10.1128/aac.39.12.2708

Gray, K. C., Palacios, D. S., Dailey, I., Endo, M. M., Uno, B. E., Wilcock, B. C., et al. (2012). Amphotericin primarily kills yeast by simply binding ergosterol. *Proc. Natl. Acad. Sci. U. S. A.* 109, 2234–2239. doi: 10.1073/pnas.1117280109

Grazziotin, L. R., Moreira, L. B., and Ferreira, M. A. P. (2018). Comparative Effectiveness and Safety between Amphotericin B Lipid-Formulations: a Systematic Review. *Int. J. Technol. Assess. Health Care* 34, 343–351. doi: 10.1017/S026646231800034X

Hadrich, I., Makni, F., Neji, S., Cheikhrouhou, F., Bellaaj, H., Elloumi, M., et al. (2012). Amphotericin B *in vitro* resistance is associated with fatal *Aspergillus flavus* infection. *Med. Mycol.* 50, 829–834. doi: 10.3109/13693786.2012.684154

Hao, B., Cheng, S., Clancy, C. J., and Nguyen, M. H. (2013). Caspofungin kills *Candida albicans* by causing both cellular apoptosis and necrosis. *Antimicrob. Agents Chemother.* 57, 326–332. doi: 10.1128/AAC.01366-12

Jukic, E., Blatzer, M., Posch, W., Steger, M., Binder, U., Lass-Florl, C., et al. (2017). Oxidative Stress Response Tips the Balance in *Aspergillus terreus* Amphotericin B Resistance. *Antimicrob. Agents Chemother.* 61:e00670–17. doi: 10.1128/AAC.00670-17

Kristanc, L., Bozic, B., Jokhadar, S. Z., Dolenc, M. S., and Gomiscek, G. (2019). The pore-forming action of polyenes: from model membranes to living organisms. *Biochim. Biophys. Acta Biomembr.* 1861, 418–430. doi: 10.1016/j.bbamem.2018.11.006

Lambou, K., Lamarre, C., Beau, R., Dufour, N., and Latge, J. P. (2010). Functional analysis of the superoxide dismutase family in *Aspergillus fumigatus*. *Mol. Microbiol.* 75, 910–923. doi: 10.1111/j.1365-2958.2009.07024.x

Lee, W., and Lee, D. G. (2018). Reactive oxygen species modulate itraconazole-induced apoptosis via mitochondrial disruption in *Candida albicans*. *Free Radic. Res.* 52, 39–50. doi: 10.1080/10715762.2017.1407412

Margis, R., Dunand, C., Teixeira, F. K., and Margis-Pinheiro, M. (2008). Glutathione peroxidase family - an evolutionary overview. *FEBS J.* 275, 3959–3970. doi: 10.1111/j.1742-4658.2008.06542.x

Martel, C. M., Parker, J. E., Bader, O., Weig, M., Gross, U., Warrilow, A. G., et al. (2010a). A clinical isolate of *Candida albicans* with mutations in ERG11 (encoding sterol 14alpha-demethylase) and ERG5 (encoding C22 desaturase) is cross resistant to azoles and amphotericin B. *Antimicrob. Agents Chemother.* 54, 3578–3583. doi: 10.1128/AAC.00303-10

Martel, C. M., Parker, J. E., Warrilow, A. G., Rolley, N. J., Kelly, S. L., and Kelly, D. E. (2010b). Complementation of a *Saccharomyces cerevisiae* ERG11/CYP51 (sterol 14alpha-demethylase) doxycycline-regulated mutant and screening of the azole sensitivity of *Aspergillus fumigatus* isoenzymes CYP51A and CYP51B. *Antimicrob. Agents Chemother.* 54, 4920–4923. doi: 10.1128/AAC.00349-10

Mesa-Arango, A. C., Trevijano-Contador, N., Roman, E., Sanchez-Fresneda, R., Casas, C., Herrero, E., et al. (2014). The production of reactive oxygen species is a universal action mechanism of Amphotericin B against pathogenic yeasts and contributes to the fungicidal effect of this drug. *Antimicrob. Agents Chemother.* 58, 6627–6638. doi: 10.1128/AAC.03570-14

Perlin, D. S. (2015). Mechanisms of echinocandin antifungal drug resistance. *Ann. N. Y. Acad. Sci.* 1354, 1–11. doi: 10.1111/nyas.12831

Perlin, D. S., Rautemaa-Richardson, R., and Alastruey-Izquierdo, A. (2017). The global problem of antifungal resistance: prevalence, mechanisms, and management. *Lancet Infect. Dis.* 17, e383–e392. doi: 10.1016/S1473-3099(17)30316-X

Posch, W., Blatzer, M., Wilflingseder, D., and Lass-Florl, C. (2018). *Aspergillus terreus*: novel lessons learned on amphotericin B resistance. *Med. Mycol.* 56, 73–82. doi: 10.1093/mmy/myx119

Qiao, J., Kontoyiannis, D. P., Wan, Z., Li, R., and Liu, W. (2007). Antifungal activity of statins against *Aspergillus* species. *Med. Mycol.* 45, 589–593. doi: 10.1080/13693780701397673

Rudramurthy, S. M., Paul, R. A., Chakrabarti, A., Mouton, J. W., and Meis, J. F. (2019). Invasive Aspergillosis by *Aspergillus flavus*: epidemiology, Diagnosis, Antifungal Resistance, and Management. *J. Fungi.* 5:55. doi: 10.3390/jof5030055

Sanglard, D., Ischer, F., Parkinson, T., Falconer, D., and Bille, J. (2003). *Candida albicans* mutations in the ergosterol biosynthetic pathway and resistance to several antifungal agents. *Antimicrob. Agents Chemother.* 47, 2404–2412. doi: 10.1128/aac.47.8.2404-2412.2003

Schmittgen, T. D., and Livak, K. J. (2008). Analyzing real-time PCR data by the comparative C(T) method. *Nat. Protoc.* 3, 1101–1108. doi: 10.1038/nprot.2008.73

Sena, L. A., and Chandel, N. S. (2012). Physiological roles of mitochondrial reactive oxygen species. *Mol. Cell.* 48, 158–167. doi: 10.1016/j.molcel.2012.09.025

Shekhova, E., Kniemeyer, O., and Brakhage, A. A. (2017). Induction of Mitochondrial Reactive Oxygen Species Production by Itraconazole, Terbinafine, and Amphotericin B as a Mode of Action against *Aspergillus fumigatus*. *Antimicrob. Agents Chemother.* 61:e00978–17. doi: 10.1128/AAC.00978-17

Shibuya, K., Paris, S., Ando, T., Nakayama, H., Hatori, T., and Latge, J. P. (2006). Catalases of *Aspergillus fumigatus* and inflammation in aspergillosis. *Nihon. Ishinkin. Gakkai. Zasshi.* 47, 249–255. doi: 10.3314/jjmm.47.249

Shirazi, F., Pontikos, M. A., Walsh, T. J., Albert, N., Lewis, R. E., and Kontoyiannis, D. P. (2013). Hyperthermia sensitizes *Rhizopus oryzae* to posaconazole and itraconazole action through apoptosis. *Antimicrob. Agents Chemother.* 57, 4360–4368. doi: 10.1128/AAC.00571-13

Silva, L. N., Oliveira, S. S. C., Magalhaes, L. B., Andrade Neto, V. V., Torres-Santos, E. C., Carvalho, M. D. C., et al. (2020). Unmasking the Amphotericin B Resistance Mechanisms in *Candida haemulonii* Species Complex. *ACS Infect. Dis.* 6, 1273–1282. doi: 10.1021/acsinfecdis.0c00117

Stone, N. R., Bicanic, T., Salim, R., and Hope, W. (2016). Liposomal Amphotericin B (AmBisome(®)): a Review of the Pharmacokinetics, Pharmacodynamics, Clinical Experience and Future Directions. *Drugs* 76, 485–500. doi: 10.1007/s40265-016-0538-7

Vaezi, A., Fakhim, H., Arastehfar, A., Shokohi, T., Hedayati, M. T., Khodavaisy, S., et al. (2018). *In vitro* antifungal activity of amphotericin B and 11 comparators against *Aspergillus terreus* species complex. *Mycoses* 61, 134–142. doi: 10.1111/myc.12716

Vincent, B. M., Lancaster, A. K., Scherz-Shouval, R., Whitesell, L., and Lindquist, S. (2013). Fitness trade-offs restrict the evolution of resistance to amphotericin B. *PLoS Biol.* 11:e1001692. doi: 10.1371/journal.pbio.1001692

Warrilow, A. G., Melo, N., Martel, C. M., Parker, J. E., Nes, W. D., Kelly, S. L., et al. (2010). Expression, purification, and characterization of *Aspergillus fumigatus* sterol 14-alpha demethylase (CYP51) isoenzymes A and B. *Antimicrob. Agents Chemother.* 54, 4225–4234. doi: 10.1128/AAC.00316-10

Warrilow, A. G. S., Parker, J. E., Price, C. L., Rolley, N. J., Nes, W. D., Kelly, D. E., et al. (2019). Isavuconazole and voriconazole inhibition of sterol 14alpha-demethylases (CYP51) from *Aspergillus fumigatus* and *Homo sapiens*. *Int. J. Antimicrob. Agents* 54, 449–455. doi: 10.1016/j.ijantimicag.2019.07.011

Zorov, D. B., Juhaszova, M., and Sollott, S. J. (2014). Mitochondrial reactive oxygen species (ROS) and ROS-induced ROS release. *Physiol. Rev.* 94, 909–950. doi: 10.1152/physrev.00026.2013

Conflict of Interest: The authors declare that the research was conducted in the absence of any commercial or financial relationships that could be construed as a potential conflict of interest.

Publisher's Note: All claims expressed in this article are solely those of the authors and do not necessarily represent those of their affiliated organizations, or those of the publisher, the editors and the reviewers. Any product that may be evaluated in this article, or claim that may be made by its manufacturer, is not guaranteed or endorsed by the publisher.

frontiers in Microbiology

ORIGINAL RESEARCH
published: 10 August 2021
doi: 10.3389/fmicb.2021.708280

In vitro Antifungal Susceptibility Profiles of *Cryptococcus neoformans* var. *grubii* and *Cryptococcus gattii* Clinical Isolates in Guangxi, Southern China

Najwa Al-Odaini[1,2†], Xiu-ying Li[1,2†], Bing-kun Li[1,2], Xing-chun Chen[3], Chun-yang Huang[1,2], Chun-ying Lv[1,2], Kai-su Pan[1,2], Dong-yan Zheng[1,2], Yan-qing Zheng[2,4], Wan-qing Liao[5] and Cun-wei Cao[1,2]**

[1] Department of Dermatology and Venerology, First Affiliated Hospital, Guangxi Medical University, Nanning, China, [2] Guangxi Health Commission Key Lab of Fungi and Mycosis Research and Prevention, Nanning, China, [3] The People's Hospital of Guangxi Zhuang Autonomous Region, Nanning, China, [4] Fourth People's Hospital of Nanning, Nanning, China, [5] Shanghai Key Laboratory of Medical Fungal Molecular Biology, Second Military Medical University, Shanghai, China

OPEN ACCESS

Edited by:
Keke Huo,
Fudan University, China

Reviewed by:
Piriyaporn Chongtrakool,
Mahidol University, Thailand
Lujuan Gao,
Fudan University, China

***Correspondence:**
Wan-qing Liao
liaowanqing@sohu.com
Cun-wei Cao
caocunwei@yeah.net

† These authors have contributed equally to this work and share first authorship

Specialty section:
This article was submitted to Antimicrobials, Resistance and Chemotherapy, a section of the journal Frontiers in Microbiology

Received: 11 May 2021
Accepted: 05 July 2021
Published: 10 August 2021

Citation:
Al-Odaini N, Li X-y, Li B-k, Chen X-c, Huang C-y, Lv C-y, Pan K-s, Zheng D-y, Zheng Y-q, Liao W-q and Cao C-w (2021) In vitro Antifungal Susceptibility Profiles of Cryptococcus neoformans var. grubii and Cryptococcus gattii Clinical Isolates in Guangxi, Southern China. Front. Microbiol. 12:708280. doi: 10.3389/fmicb.2021.708280

This study analyzed the *in vitro* drug sensitivity of *Cryptococcus* spp. from Guangxi, Southern China. One hundred three strains of *Cryptococcus* were recovered from 86 patients; 14 were HIV positive and 72 were HIV negative. Ninety-two strains were identified as *Cryptococcus neoformans* var. *grubii*, while 11 strains were identified as *Cryptococcus gattii* (5 *C. gattii sensu stricto* and 6 *Cryptococcus deuterogattii*). The recovered strains were tested against commonly used antifungal drugs (fluconazole, amphotericin B, 5-fluorocytosine, itraconazole, and voriconazole) and to novel antifungal drugs (posaconazole and isavuconazole) using CLSI M27-A4 method. The results showed that all isolates were susceptible to most antifungal drugs, of which the minimum inhibitory concentration (MIC) ranges were as follows: 0.05–4 μg/ml for fluconazole, 0.25–1 μg/ml for amphotericin B; 0.0625–2 μg/ml for 5-fluorocytosine, 0.0625–0.25 μg/ml for itraconazole, 0.0078–0.25 μg/ml for voriconazole, 0.0313–0.5 μg/ml for posaconazole, 0.0020–0.125 μg/ml for isavuconazole for *C. neoformans* var. *grubii* isolates, and 1–16 μg/ml for fluconazole, 0.125–1 μg/ml for 5-fluorocytosine, 0.25–1 μg/ml for amphotericin B, 0.0625–0.25 μg/ml for itraconazole, 0.0156–0.125 μg/ml for voriconazole, 0.0156–0.25 μg/ml for posaconazole, and 0.0078–0.125 μg/ml for isavuconazole for *C. gattii* isolates. Furthermore, some *C. neoformans* var. *grubii* isolates were found to be susceptible-dose dependent to 5-fluorocytosine and itraconazole. In addition, a reduction in the potency of fluconazole against *C. gattii* is possible. We observed no statistical differences in susceptibility of *C. neoformans*

var. *grubii* and *C. gattii* in the tested strains. Continuous observation of antifungal susceptibility of *Cryptococcus* isolates is recommended to monitor the emergence of resistant strains.

Keywords: *Cryptococcus gattii*, variant identification, *in vitro* drug sensitivity, *C. neoformans* var. *grubii*, Guangxi

INTRODUCTION

Cryptococcosis is a common opportunistic invasive fungal infection caused mainly by *Cryptococcus neoformans* (*C. neoformans*, serotypes A, AD, and D) and *Cryptococcus gattii* (*C. gattii* serotypes B and C) (Guinea et al., 2010). The latter mainly affects otherwise healthy individuals, whereas *C. neoformans* is more common in immunocompromised patients (Park et al., 2009; Guinea et al., 2010; Maziarz and Perfect, 2016). Although the incidence of cryptococcosis has declined with the introduction of highly active antiretroviral therapy (HAART), immunocompromised individuals remain at risk, and mortality rate remain unacceptably high despite the continued research on cryptococcosis (Park et al., 2009; Selb et al., 2019). *C. neoformans* and *C. gattii* are genetically related to each other; however, they vary in the ecological niche geographic distribution, natural habitat, host infectivity, and pathogenicity (Gutch et al., 2015). For instance, *C. neoformans* has a global distribution, while *C. gattii* strains are more common in North America and Australia (Ellis and Pfeiffer, 1990). Moreover, *C. gattii* seems to be less sensitive to therapy and requires more aggressive management than *C. neoformans* (Speed and Dunt, 1995). China has the worlds' largest population with large humid tropical and subtropic regions rich with vegetation, a climate favorable for the growth and spread of fungi. In addition, the number of immunocompromised (HIV and non-HIV) populations in China has been increasing in the past several decades, leading to an increase in the incidence and prevalence of aggressive fungal infections such as cryptococcosis, which is a heavy burden to public health (Fang et al., 2015). Furthermore, cryptococcosis can be easily misdiagnosed due to the vague and diversity of the clinical manifestations, leading to the delay of proper treatment. Therefore, early diagnosis and timely treatment play an important role in the prognosis of the disease. Several studies have been performed to investigate the microbiological, epidemiological, and clinical characteristics of *C. neoformans* and *C. gattii* strains in China (Chen et al., 2008, 2018; Feng et al., 2008; Wu et al., 2015, 2021; Fang et al., 2020; Jin et al., 2020; Xu et al., 2021). Unfortunately, relatively little is known about the pathogenic *Cryptococcus* species and their sensitivity to antifungal chemotherapy in Guangxi, Southern China. Guangxi province is located in the subtropical zone with a warm, humid climate where cryptococcosis is significantly common but might be severely underreported. Recently, new antifungal agents have been introduced, suggesting that the antifungal susceptibility profiles need to be researched and updated. Therefore, the current study aims to analyze the clinical characteristics of *Cryptococcus* infection and *in vitro* drug susceptibility of *Cryptococcus* spp. in Guangxi, Southern China.

Abbreviations: FLC, fluconazole; AmB, amphotericin B; ITC, itraconazole; 5-FC, 5-flucytosine; VOC, voriconazole; POS, posaconazole; ISA, isavuconazole; SDA, Sabouraud dextrose agar medium; CGB, L-canavanine-glycine-bromothymol blue; MALDI-TOF MS, matrix-assisted laser desorption ionization-time of flight mass spectrometry; ECVs, epidemiological cutoff values.

MATERIALS AND METHODS

Ethics Statement

This study was approved by the Medical Ethics Committee of the First Affiliated Hospital of Guangxi Medical University. The clinical data in this study were obtained with written consent from the patients or their families, and data collected concerning them was anonymized.

Isolates and Clinical Data

Between May 2014 and May 2018, clinical isolates of *Cryptococcus* spp. from patients admitted to the First Affiliated Hospital of Guangxi Medical University, Nanning, Guangxi, the Fourth People's Hospital of Nanning, and People's Hospital of Guangxi Zhuang Autonomous Region were collected and recovered for this study. We assessed the patients' medical records to collect clinical information. Strains with insufficient clinical data of patients were excluded.

Strains Identification

Activation and Identification

A total of 120 *Cryptococcus* strains were taken out of the refrigerator at −80°C, resuscitated at 20°C for 24 h, transferred to Sabouraud dextrose agar (SDA) medium, and incubated at 27°C for 48–72 h, then transferred onto L-canavanine-glycine-bromothymol blue (CGB) medium for 3–7 days to differentiate *C. neoformans* from *C. gattii* species as previously mentioned (Klein et al., 2009). Three consecutive purifications were made using the streak plate technique to ensure the growth and purity of the strains. Multiple colonies were transferred to SDA medium for cultivation at 27°C and enrichment for later use.

Extraction of *Cryptococcus* Neoformans Protein

A sterile loop full of the purified isolated strains (about 5 mg) was added to an Eppendorf tube containing 300 μl of distilled H_2O and was mixed thoroughly. Nine hundred microliters of absolute ethanol was added to the tube, mixed, and centrifuged at 12,000 r/min for 2 min. After discarding the supernatant, the tube was centrifuged again at 12,000 r/min for 2 min and later placed at room temperature to dry. Following the addition of 50 μl of 70% formic acid and 50 μl of acetonitrile, the tube was centrifuged for 2 min at 12,000 r/min. The supernatant was then transferred to a new tube for use.

Matrix-Assisted Laser Desorption Ionization-Time of Flight Mass Spectrometry Identification

The samples were overlaid with 1 μl of matrix solution consisting of a saturated solution of α-cyano-4-hydroxycinnamic acid in 50% acetonitrile–2.5% trifluoroacetic acid and again allowed to air dry prior to analysis. For each isolate, a spectrum with a mass-to-charge range of 2,200–22,000 Da was generated as an average of 240 laser shots in an automatic acquisition mode. When poor spectra (fewer than 10 well-defined peaks above 1,000 arbitrary units) were obtained, analysis was repeated with an extra wash step during the protein extraction procedure, which improved the quality of the spectra. The MALDI Biotyper 3.0 database was used to compare the data and record the mass spectrometry identification results. According to the instruction manual, a log score ≥1.70 indicates correct identification; a log score <1.70 indicates that the identification is incorrect or unable to be identified (McTaggart et al., 2011).

DNA Extraction and ITS Sequencing

As a reference "gold standard," 20 strains of *Cryptococcus* were randomly selected to extract DNA for ITS sequencing. Strains were cultured on SDA medium at 27°C for 72 h for DNA extraction according to the operation steps of the fungal genomic DNA extraction kit produced by Jiangsu Kangwei Century Biotechnology Co., Ltd (Changping, Beijing, China). According to the operating manual, the concentration of genomic DNA is determined using a nucleic acid protein analyzer and then placed in a refrigerator at −20°C for later use. Ribosomal RNA (rRNA) internal transcribed spacer Region (rITS) sequencing is performed on the extracted DNA using primer sets (upstream primer sequence ITS1: 5′-TCCGTAGGTGAACCTGCGG-3′) and (downstream primer sequence ITS4: 5′-TCCTCCGCTTATTGATATGC-3′). A total volume of 50 μl (Taq-Mix, 25 μl; upper material, 2 μl; downstream primer, 2 μl; at least 100 ng of DNA extract and sterile deionized water) was used to perform polymerase chain reaction (PCR) for 35 cycles at 95°C with 3 min initial denaturation, 30 s denaturation at 95°C, 30 s annealing at 55°C, 2 min extension at 72°C, and final extension cycle for 10 min at 72°C, and then stored at 4°C. A total of 6 μl of PCR products was separated slowly into 1% agar gel spotting hole electrophoresis at 120 V for 30 min. The agar gel was placed under the UV gel imager to observe whether the PCR product and marker are clear and record the band length. PCR products are then sent with clear bands under electrophoresis to Guangzhou Kinco Biotechnology Co., Ltd. for two-way sequencing. Results were uploaded to the National Center for Biotechnology Information (NCBI) Genebank database[1] for comparison and identification.

Antifungal Susceptibility Test

Antifungal and Suspensions Preparation

The antifungal susceptibility testing was assessed by the checkerboard broth microdilution method performed according to the Clinical and Laboratory Standards Institute (CLSI) protocol M27-A4 (Clinical and Laboratory Standards Institute (CLSI), 2017). The minimum inhibitory concentration (MIC) value was determined for fluconazole (FLC), amphotericin B (AmB), 5-fluorocytosine (5-FC), itraconazole (ITC), voriconazole (VOC), posaconazole (POS), and isavuconazole (ISA). Antifungal drugs were provided as powders with known potency from Sigma Chemical Co. (St. Louis, MO, United States). Stock solutions were prepared as follows: FLC and 5-FC were dissolved in sterile distilled water to a drug storage solution of 1,280 μg/ml, while AmB, ITC, VOC, POS, and ISA were dissolved in dimethyl sulfoxide (DMSO) (Sigma Chemical Co., United States) into a stock solution of 1,600 μg/ml and stored at −20°C until needed. The final concentration ranges were 0.125–64 μg/ml for FLC, 0.00156–8 μg/ml for AmB and 5-FC, 0.0020–1 g/ml for ITC, VOC, POS, and ISA, respectively. The yeast inocula were adjusted to a concentration of 1×10^3–5×10^3 cfu/ml in Roswell Park Memorial Institute (RPMI) 1640 medium as measured by a hemocytometer, and an aliquot of 0.1 ml was added to each well containing various concentrations of antifungal drugs. The 96-well plates were incubated at 37°C. The assays were read 72 h after inoculation. *Candida parapsilosis* ATCC 22019 was used as a quality control strain for susceptibility tests.

MIC and MIC Interpretations

According to the CLSI M27-A4 protocol, the MIC of AmB was defined as the lowest concentration that produced complete growth inhibition, while the MIC for other antifungal agents were defined as the lowest concentrations at which there was 50% inhibition of growth (≥50%) compared with that of drug-free control (optical clear). The MIC_{50} and MIC_{90}, on the other hand, are the concentrations capable of inhibiting the growth of isolates by 50 and 90%, respectively (Favalessa et al., 2014). The interpretive MIC criteria for FLC were as follows: susceptible (S), ≤8 μg/ml; susceptible-dose dependent (SDD), 16–32 μg/ml; and resistance (R), ≥64 μg/ml; for 5-FC, ≤4 μg/ml (S), 8–16 μg/ml (SDD), and ≥32 μg/ml; for ITC, ≤0.125 μg/ml (S), 0.25–0.5 μg/ml (SDD), and ≥1 μg/ml; for VOR, ≤1 μg/ml (S) based on previous studies (Pfaller et al., 2005; Dias et al., 2006; Bertout et al., 2013; Gutch et al., 2015). For *Cryptococcus*, interpretative criteria have not been defined for POS, ISA, and AmB; hence, data available for *Candida* spp. were used, as previously reported (Revankar et al., 1988; Rodríguez-Tudela et al., 1995; Pfaller et al., 1999). Based on the recommendation of previous studies, the ECVs for *C. neoformans* var. *grubii* were 8.0 μg/ml for FLC, 1.0 μg/ml for AmB, 4 μg/ml for 5FC, 0.125 μg/ml for ITC, 1.0 μg/ml for VOR, 0.5 μg/ml for POS, and 0.25 μg/ml for ISA; and that for *C. gattii* were 8 μg/ml for FLC, 4 μg/ml for 5FC, 0.5 μg/ml for AmB, ITC, VOR, and POS, and 0.25 μg/ml for ISA (Espinel-Ingroff, 2012; Espinel-Ingroff et al., 2012, 2015; Lockhart et al., 2012). The susceptibility of each *Cryptococcus* spp. isolate was determined in triplicate at different times for optimal results.

Statistical Analysis

Statistical analysis was performed using SPSS 17.0 (SPSS Inc., Chicago, IL, United States) where $p < 0.05$ was considered statistically significant.

[1] http://www.ncbi.nlm.nih.gov/

RESULTS

Isolates and Clinical Data

A total of 103 strains from 86 patients were included in this study (**Table 1**). Fifty-nine of them were male, and twenty-seven were female. The age distribution ranged from 21 to 84 years. Of the 86 patients, 14 were HIV positive and 72 were HIV negative. A total of 55 had no underlying diseases, 21 had liver diseases, 7 were diabetic, 4 had systemic lupus erythematosus (SLE), 1 had a history of immunosuppressing therapy, 3 had liver cancer, and 1 had rheumatoid arthritis. All 86 patients came from 13 different cities in Guangxi province, Southern China (**Figure 1**). Of the 103 strains, 17 were episode strains (i.e., strains recovered from different parts of the same patient simultaneously or from the same part at different times). In total, 91 were isolated from cerebrospinal fluid, 7 were from lung tissue, 3 were from alveolar lavage, and 2 from the skin.

Strain Identification

Eleven strains successfully turned canavanine-glycine-bromothymol blue (CGB) medium to blue and were consequently identified as *C. gattii*. The remaining 92 strains were identified as *C. neoformans* var. *grubii* according to the MALDI-TOF MS technique, with mass spectrum scores $\geq$1.7. The DNA results on the database comparison result were 100% consistent with the MALDI-TOF MS identification result, making the results of MALDI-TOF MS in our study credible. The identification of *C. gattii* strains and their genotypes were analyzed in detail in our previous study using multilocus sequence typing (MLST) technique, where five isolates were identified as *C. gattii sensu stricto* (*C. gattii s.s.*), and six were identified as *C. deuterogattii* serotype (Huang et al., 2020).

Drug Susceptibility Results

The seven antifungal agents tested retained activity against all isolates. The MIC, MIC_{50}, and MIC_{90} values are presented in **Table 2**.

C. neoformans var. *grubii*

The MIC ranges of the 92 *C. neoformans* var. *grubii* strains for the 7 drugs were as follows: FLC, 0.05–4 μg/ml; AmB, 0.25–1 μg/ml; 5-FC, 0.0625–2 μg/ml; ITC, 0.0625–0.25 μg/ml; VOC, 0.0078–0.25 μg/ml; POS, 0.0313–0.5 μg/ml; and ISA, 0.0020–0.125 μg/ml. All 92 clinical strains of *C. neoformans* var. *grubii* were susceptible to FLC, AmB, VOC, POS, and ISA; 91 strains (98.91%) were susceptible to 5-FC, while 1 strain (1.09%) was susceptible-dose dependent; 85.87% (79/92) of the strains were susceptible to ITC; and the remaining 14.13% (13/92) strains were susceptible-dose dependent to ITC.

C. gattii

Similar to *C. neoformans* var. *grubii,* none of the strains demonstrated resistance to the antifungal drugs (**Table 2**). However, we observed an MIC value above the ECVs to FLC against a single *C. deuterogattii* isolate.

TABLE 1 | Demographic and clinical characteristics of the 86 patients with cryptococcosis.

Variables	*C. neoformans* var. *grubii* (*n* = 75)	*Cryptococcus gattii* (*n* = 11)
Age, year, average	46.58	38.09
Gender, male	51	8
HIV (+), *n*	14	–
Underlying diseases		
None, *n*	51	4
Diabetes mellitus, *n*	7	–
HBV, *n*	13	5
HCV, *n*	1	2
Liver diseases[a], *n*	4	1
Liver cancer, *n*	3	–
Corticosteroids administration, *n*	1	–
Autoimmune diseases[b], *n*	4	1
Clinical diagnosis		
Cryptococcal meningitis	47	10
Pulmonary cryptococcosis	8	1
Disseminated cryptococcosis	20	–
Clinical symptoms		
Neurological abnormalities[c], *n*	31	1
Headache, *n*	61	9
Fever, *n*	51	9
Cough, *n*	13	2
Vomiting, *n*	39	6
Abnormal vision, *n*	2	2
Skin lesions, *n*	1	–
Treatment outcome		
Survived, *n*	47	10
Died, *n*	27	1
Unknown, *n*	1	–
Specimen source	**(*n* = 92)**	**(*n* = 11)**
CSF, *n*	81	10
Lung tissue, *n*	6	1
BALF, *n*	3	–
Skin tissue, *n*	2	–

n, number; HBV, hepatitis B virus; HCV, hepatitis C virus; CSF, cerebrospinal fluid; BALF, bronchoalveolar lavage fluid.
[a]Liver cirrhosis, fatty liver.
[b]Systemic lupus erythematous, rheumatoid arthritis.
[c]Convulsion, altered consciousness, epilepsy.

DISCUSSION

This study analyzed the epidemiology and *in vitro* antifungal susceptibility profiles of *Cryptococcus* spp. in a large-scale population from Guangxi, Southern China. Consistent with previous reports from China, our study showed that the prevalence of cryptococcosis caused by *C. neoformans* is higher than those caused by *C. gattii* (Chen et al., 2008; Fang et al., 2015; Wu et al., 2015). In addition, the disease was more observed among otherwise healthy individuals.

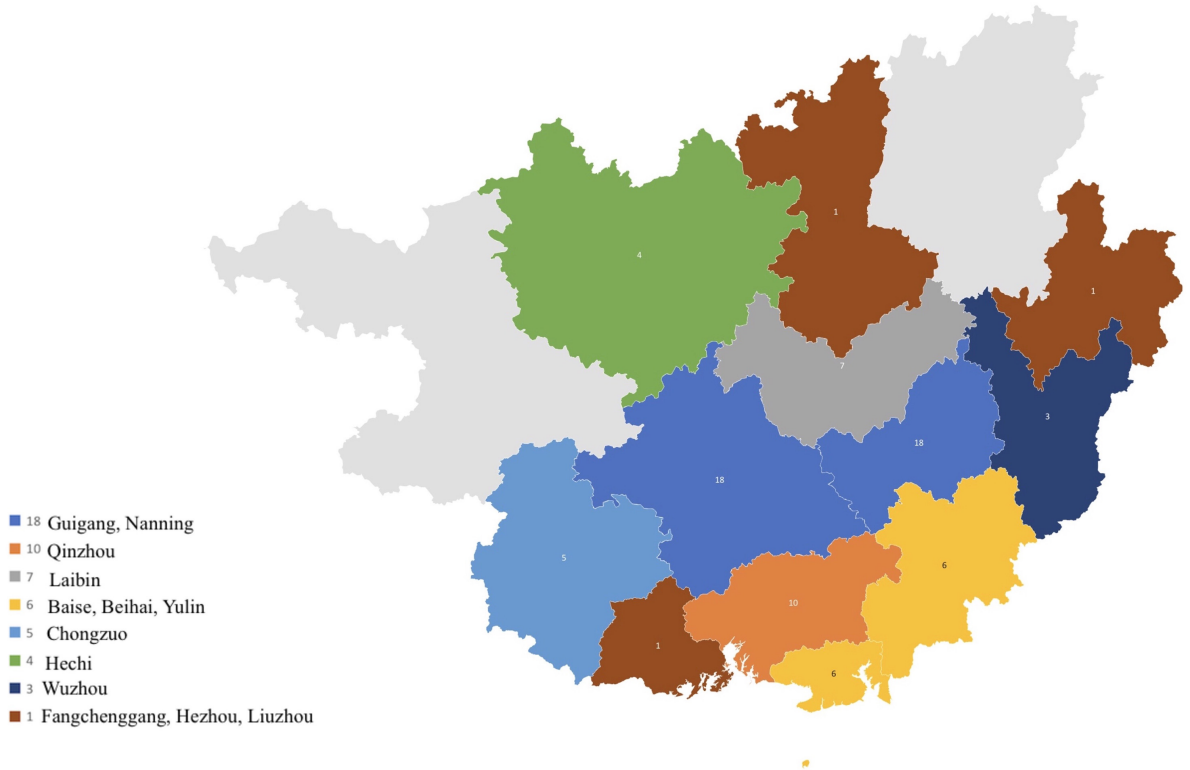

FIGURE 1 | Geographic distribution of cryptococcosis patients from Guangxi province, Southern China.

TABLE 2 | Antifungal susceptibilities for 130 *Cryptococcus* isolates.

Isolates and antifungal	MIC range	GM	MIC_{50}	MIC_{90}
	(μg/ml)	(μg/ml)	(μg/ml)	(μg/ml)
***C. neoformans* var. *grubii* (*n* = 92)**				
FLC	0.05–4	1.57	2	4
AmB	0.25–1	0.75	1	1
5-FC	0.0625–2	0.57	0.5	1
ITC	0.0625–0.25	0.08	0.0625	0.125
VOC	0.0078–0.25	0.03	0.0313	0.0625
POS	0.0313–0.5	0.13	0.125	0.25
ISA	0.0020–0.125	0.02	0.0156	0.0625
***Cryptococcus gattii* (*n* = 11)**				
FLC	1–16	2.57	2	4
AmB	0.25–1	0.47	0.5	0.5
5-FC	0.125–1	0.28	0.25	0.5
ITC	0.0625–0.25	0.18	0.25	0.25
VOC	0.0156–0.125	0.05	0.0625	0.125
POS	0.0156–0.25	0.07	0.0625	0.25
ISA	0.0078–0.125	0.04	0.0625	0.125

MIC_{50} and MIC_{90}, the concentration capable of inhibiting the growth of isolates by 50 and 90%, respectively. GM, geometric means.

Furthermore, our study demonstrated that *C. neoformans* was responsible for the infection in immunocompetent, which is contrary to the HIV-associated cryptococcosis cases reported in the United States, Africa, and Europe (Dromer et al., 1996; Moosa and Coovadia, 1997; Hajjeh et al., 1999). Similar to reports from other parts of China, *C. neoformans* var. *grubii* was the dominant pathogenic strain in Guangxi (Chen et al., 2008).

In recent years, MALDI-TOF MS has emerged as a rapid, accurate, and cost-effective method for microbial identification and diagnosis (Singhal et al., 2015). Additionally, MALDI-TOF MS can replace some traditional identification methods, which improves clinical diagnosis and treatment. Furthermore, MALDI-TOF MS can help predict drug-resistant fungal isolates by identifying inflicting fungal species (McTaggart et al., 2011). Moreover, MALDI-TOF MS correctly identified 100% of *Cryptococcus* spp. in previous studies (Firacative et al., 2012; van Belkum et al., 2015; Cheng et al., 2016). Similarly, our study demonstrated that MALDI-TOF MS method is reliable, as we obtained a 100% consistency with results obtained using DNA sequencing.

The antifungal agents tested retained activity against all *Cryptococcus* isolates. Both *C. neoformans* var. *grubii* and *C. gattii* showed susceptibility to amphotericin B (MIC, 0.25–1 μg/ml). These results are consistent with previous reports (Thompson et al., 2009; Favalessa et al., 2014; Nascimento et al., 2017); however, greater MIC values are reported in the literature and were associated with treatment failure (Lozano-Chiu et al., 1998; Perkins et al., 2005).

Studies conducted previously have shown low MIC_{50} and MIC_{90} values for fluconazole against *C. neoformans* (Datta et al., 2003; Tay et al., 2006; Lia et al., 2012). In this study, the MIC_{50} and MIC_{90} values for fluconazole were 2–4 μg/ml; however, higher MIC_{50} and MIC_{90} values (4–8 and 2–128 μg/ml) have been reported for *C. neoformans* isolates (Sar et al., 2004; Favalessa et al., 2014).

High MIC values (≥64 μg/ml) have been reported for fluconazole against *C. gattii* (Sar et al., 2004; Tay et al., 2006; Soares et al., 2008; Lia et al., 2012), in contrast to this study, where we determined MIC values of ≤ 16 μg/ml. It is worth mentioning that MIC ≥16 μg/ml is believed to be the resistance cutoff for fluconazole; this value was observed from a single *C. gattii* (*C. deuterogattii*) isolate in this study. This observation brings the resistance concerns to attention and suggests that FLC might lose its potency, especially if used as a single treatment.

The new azoles (voriconazole, posaconazole, and isavuconazole) showed high antifungal activity against all *C. neoformans* and *C. gattii* strains, with low MIC values of ≤0.5 μg/ml, which is consistent with previous reports (Pfaller et al., 2003, 2009; Sabatelli et al., 2006; Illnait-Zaragozi et al., 2008; Torres-Rodríguez et al., 2008). Itraconazole, on the other hand, showed high activity against all isolates with low MIC values of ≤0.25, which is similar or lower than those of previous reports (Alves et al., 2001; Souza et al., 2010; Chowdhary et al., 2011; Herkert et al., 2018); however, 13 *C. neoformans* strains (14.13%) showed to be susceptible-dose dependent to itraconazole. Similarly, *C. neoformans* strains from Serbia showed to be susceptible-dose dependent to itraconazole (Arsic Arsenijevic et al., 2014). Nevertheless, itraconazole is rarely used as a single drug, especially in the treatment of cryptococcal meningitis, due to low concentration in the cerebrospinal fluid.

Studies conducted in several parts of the world have shown MIC values of ≤64 μg/ml for 5-FC against *C. neoformans* and *C. gattii* (Thompson et al., 2009; Chowdhary et al., 2011; Arsic Arsenijevic et al., 2014). In this study, all isolates were susceptible to 5-FC with MIC values ≤2 μg/ml; however, one *C. neoformans* strain (1.09%) was susceptible-dose dependent to 5-FC.

We observed no statistically significant difference between *C. neoformans* var. *grubii* and *C. gattii*, nor between *C. gattii s.s.* and *C. deuterogattii* isolates against all seven antifungal drugs ($p > 0.05$). Overall, according to CLSI M27-A4, most strains in this study were of wild type, except for one that might acquire resistance to FLC. A follow-up study is required to confirm if it was of non-wild type.

In summary, cryptococcosis is a complicated disease that can be easily misdiagnosed due to the lack of specificity of the clinical manifestations. In China, healthy individuals are more prone to the infection. *C. neoformans* var. *grubii* is the most predominant strain in Guangxi. MALDI-TOF MS is a rapid and reliable method to identify *Cryptococcus* spp. All isolates showed no resistance to commonly used antifungal drugs and were highly susceptible to the new triazoles. Antifungal susceptibility tests are desirable to early detect any resistant strains in order to ensure proper and successful therapy of cryptococcosis.

DATA AVAILABILITY STATEMENT

The raw data supporting the conclusions of this article will be made available by the authors, without undue reservation.

ETHICS STATEMENT

Written informed consent was obtained from the individual(s) for the publication of any potentially identifiable images or data included in this article.

AUTHOR CONTRIBUTIONS

X-YL, NA-O, C-YL, and C-YH contributed to the data collection. X-YL, X-CC, B-KL, K-SP, Y-QZ, and D-YZ contributed to the laboratory work. NA-O and X-YL wrote the manuscript. W-QL and C-WC supervised and evaluated the process of the study. All authors contributed to manuscript revision and read and approved the submitted version.

ACKNOWLEDGMENTS

This study was supported by the National Natural Science Foundation of China (81960567), grants from the Natural Science Foundation of Guangxi Province of China (2020GXNSFGA238001), and The First Affiliated Hospital of Guangxi Medical University Provincial and Ministerial Key Laboratory Cultivation Project: Guangxi Key Laboratory of Tropical Fungi and Mycosis Research (No. YYZS2020006). The funders had no role in study design, data, collection and analysis, decision to publish, or preparation of the manuscript.

REFERENCES

Alves, S. H., Oliveir, L., Costa, J. M., Lubeck, I., Casali, A. K., and Vainstein, M. H. (2001). In vitro susceptibility to antifungal agents of clinical and environmental *Cryptococcus neoformans* isolated in Southern of Brazil. *Rev. Inst. Med. Trop. Sao Paulo* 43, 267–270. doi: 10.1590/s0036-46652001000500006

Arsic Arsenijevic, V., Pekmezovic, M. G., Meis, J. F., and Hagen, F. (2014). Molecular epidemiology and antifungal susceptibility of Serbian *Cryptococcus neoformans* isolates. *Mycoses* 57, 380–387.

Bertout, S., Drakulvoski, P., Kouanfack, C., Krasteva, D., Ngouana, T., and Dunyach-Rémy, C. (2013). Genotyping and antifungal susceptibility testing of *Cryptococcus neoformans* isolates from Cameroonian HIV-positive adult patients. *Clin. Microbiol. Infect.* 19, 763–769. doi: 10.1111/1469-0691.12019

Chen, J., Varma, A., Diaz, M. R., Litvintseva, A. P., Wollenberg, K. K., and Kwon-Chung, K. J. (2008). *Cryptococcus neoformans* strains and infection in apparently immunocompetent patients, China. *Emerg. Infect. Dis.* 14, 755–762. doi: 10.3201/eid1405.071312

Chen, Y., Yu, F., Bian, Z. Y., Hong, J. M., Zhang, N., Zhong, Q. S., et al. (2018). Multilocus sequence typing reveals both shared and unique genotypes of *Cryptococcus neoformans* in Jiangxi Province, China. *Sci. Rep.* 24:1495.

Cheng, K., Chui, H., Domish, L., Hernandez, D., and Wang, G. (2016). Recent development of mass spectrometry and proteomics applications in identification and typing of bacteria. *Proteomics Clin. Appl.* 10, 346–357. doi: 10.1002/prca.201500086

Chowdhary, A., Singh Randhawa, H., Sundar, G., Kathuria, S., Prakash, A., Khan, Z., et al. (2011). In vitro antifungal susceptibility profiles and genotypes of 308 clinical and environmental isolates of *Cryptococcus neoformans* var. grubii and *Cryptococcus gattii* serotype B from north-western India. *J. Med. Microbiol.* 60(Pt 7), 961–967. doi: 10.1099/jmm.0.029025-0

Clinical and Laboratory Standards Institute (CLSI) (2017). *Reference Method for Broth. (Dilution)Antifungal Susceptibility Testing of Yeasts. Approved Standard*, 4th Edn. Wayne, PA: CLSI.

Datta, K., Jain, N., Sethi, S., Rattan, A., Casadevall, A., and Banerjee, U. (2003). Fluconazole and itraconazole susceptibility of clinical isolates of *Cryptococcus neoformans* at a tertiary care centre in India: a need for care. *J. Antimicrob. Chemother.* 52, 683–686. doi: 10.1093/jac/dkg399

Dias, A. L. T., Mastumoto, F., Melhem, M. S. C., da Silva, E. G., Auler, M. E., de Siqueira, A. M., et al. (2006). Comparative analysis of Etest and broth microdilution method (AFST-EUCAST) for trends in antifungal drug susceptibility testing of Brazilian *Cryptococcus neoformans* isolates. *J. Med. Microbiol.* 55, 1693–1699. doi: 10.1099/jmm.0.46789-0

Dromer, F., Mathoulin, S., Dupont, B., and Laporte, A. (1996). Epidemiology of cryptococcosis in France: a 9-year survey (1985-1993). French Cryptococcosis study group. *Clin. Infect. Dis.* 23, 82–90. doi: 10.1093/clinids/23.1.82

Ellis, D. H., and Pfeiffer, T. (1990). Natural habitat of *Cryptococcus neoformans* var. gattii. *J. Clin. Microbiol.* 28, 1642–1644. doi: 10.1128/jcm.28.7.1642-1644.1990

Espinel-Ingroff, A. E. A. (2012). *Cryptococcus neoformans-Cryptococcus gattii* species complex: an international study of wild-type susceptibility endpoint distributions and epidemiological cutoff values for amphotericin B and flucytosine. *Antimicrob. Agents Chemother.* 56, 3107–3113. doi: 10.1128/aac.06252-11

Espinel-Ingroff, A., Aller, A. I., Canton, E., Castañón-Olivares, L. R., Chowdhary, A., and Cordoba, S. (2012). *Cryptococcus neoformans-Cryptococcus gattii* species complex: an international study of wild-type susceptibility endpoint distributions and epidemiological cutoff values for fluconazole, itraconazole, posaconazole, and voriconazole. *Antimicrob. Agents Chemother.* 56, 5898–5906. doi: 10.1128/aac.01115-12

Espinel-Ingroff, A., Chowdhary, A., Gonzalez, G. M., Guinea, J., Hagen, F., Meis, J. F., et al. (2015). Multicenter study of isavuconazole MIC distributions and epidemiological cutoff values for the *Cryptococcus neoformans-Cryptococcus gattii* species complex using the CLSI M27-A3 broth microdilution method. *Antimicrob. Agents Chemother.* 59, 666–668. doi: 10.1128/aac.04055-14

Fang, L. F., Zhang, P., Wang, J., Yang, Q., and Qu, T. T. (2020). Clinical and microbiological characteristics of cryptococcosis at an university hospital in China from 2013 to 2017. *Braz. J. Infect. Dis.* 24, 7–12. doi: 10.1016/j.bjid.2019.11.004

Fang, W., Fa, Z., and Liao, W. (2015). Epidemiology of Cryptococcus and cryptococcosis in China. *Fungal Genet. Biol.* 78, 7–15. doi: 10.1016/j.fgb.2014.10.017

Favalessa, O. C., de Paula, D. A., Dutra, V., Nakazato, L., Tadano, T., and Lazera Mdos, S. (2014). Molecular typing and in vitro antifungal susceptibility of Cryptococcus spp from patients in Midwest Brazi. *J. Infect. Dev. Ctries* 8, 1037–1043. doi: 10.3855/jidc.4446

Feng, X., Bo, L., and Daming, R. (2008). Analysis of variants, genotypes and mating types of 110 clinical strains of *Cryptococcus neoformans* in China. *Chin. J. Microbiol. Immunol.* 12, 193–197.

Firacative, C., Trilles, L., and Meyer, W. (2012). MALDI-TOF MS enables the rapid identification of the major molecular types within the *Cryptococcus neoformans*/C. gattii species complex. *PLoS One* 7:e37566. doi: 10.1371/journal.pone.0037566

Guinea, J., Hagen, F., Peláez, T., Boekhout, T., Tahoune, H., Torres-Narbona, M., et al. (2010). Antifungal susceptibility, serotyping, and genotyping of clinical *Cryptococcus neoformans* isolates collected during 18 years in a single institution in Madrid. Spain. *Med. Mycol.* 48, 942–948. doi: 10.3109/13693781003690067

Gutch, R. S., Nawange, S. R., Singh, S. M., Yadu, R., Tiwari, A., Gumasta, R., et al. (2015). Antifungal susceptibility of clinical and environmental *Cryptococcus neoformans* and *Cryptococcus gattii* isolates in Jabalpur, a city of Madhya Pradesh in Central India. *Braz. J. Microbiol.* 46, 1125–1133. doi: 10.1590/s1517-838246420140564

Hajjeh, R. A., Conn, L., Stephens, D. S., Baughman, W., Hamill, R., and Graviss, E. (1999). Cryptococcosis: population-based multistate active surveillance and risk factors in human immunodeficiency virus-infected persons. cryptococcal active surveillance group. *J. Infect Dis.* 179, 449–454. doi: 10.1086/314606

Herkert, P. F., Meis, J., Lucca, de Oliveira Salvador, G., Rodrigues Gomes, R., Aparecida Vicente, V., et al. (2018). Molecular characterization and antifungal susceptibility testing of *Cryptococcus neoformans* sensu stricto from southern Brazil. *J. Med. Microbiol.* 67, 560–569. doi: 10.1099/jmm.0.000698

Huang, C., Tusi, C., Chen, M., Pan, K., Li, X., and Wang, L. (2020). Emerging Cryptococcus gattii species complex infections in Guangxi, southern China. *PLoS Negl. Trop. Dis.* 14:e0008493. doi: 10.1371/journal.pntd.0008493

Illnait-Zaragozi, M. T., Martínez, G. F., Curfs-Breuker, I., Fernández, C. M., Boekhout, T., and Meis, J. F. (2008). In vitro activity of the new azole isavuconazole (BAL4815) compared with six other antifungal agents against 162 *Cryptococcus neoformans* isolates from Cuba. *Antimicrob. Agents Chemother.* 52, 1580–1582. doi: 10.1128/aac.01384-07

Jin, L., Cao, J. R., Xue, X. Y., Wu, H., Wang, L. F., and Guo, L. (2020). Clinical and microbiological characteristics of *Cryptococcus gattii* isolated from 7 hospitals in China. *BMC Microbiol.* 20:73.

Klein, K. R., Hall, L., Deml, S. M., Rysavy, J. M., Wohlfiel, S. L., and Wengenack, N. L. (2009). Identification of Cryptococcus gattii by use of L-canavanine glycine bromothymol blue medium and DNA sequencing. *J. Clin. Microbiol.* 47, 3669–3672. doi: 10.1128/jcm.01072-09

Lia, M., Liao, Y., Chena, M., Pana, W., and Weng, L. (2012). Antifungal susceptibilities of Cryptococcus species complex isolates from AIDS and non-AIDS patients in Southeast China. *Braz. J. Infect. Dis.* 16, 175–179. doi: 10.1590/s1413-86702012000200012

Lockhart, S. R., Bolden, C. B., DeBess, E. E., Marsden-Haug, N., Worhle, R., Thakur, R., et al. (2012). Cryptococcus gattii PNW Public health working group. epidemiologic cutoff values for triazole drugs in *Cryptococcus gattii*: correlation of molecular type and in vitro susceptibility. *Diagn Microbiol. Infect Dis.* 73, 144–148. doi: 10.1016/j.diagmicrobio.2012.02.018

Lozano-Chiu, M., Paetznick, V., Ghannoum, M. A., and Rex, J. H. (1998). Detection of resistance to amphotericin B among *Cryptococcus neoformans* clinical isolates: performances of three different media assessed by using E-test and national committee for clinical laboratory standards M27-A methodologies. *J. Clin. Microbiol.* 36, 2817–2822. doi: 10.1128/jcm.36.10.2817-2822.1998

Maziarz, E. K., and Perfect, J. (2016). Cryptococcosis. *Infect. Dis. Clin. North Am.* 30, 179–206.

McTaggart, L. R., Lei, E., Richardson, S. E., Hoang, L., Fothergill, A., and Zhang, S. X. (2011). Rapid identification of *Cryptococcus neoformans* and *Cryptococcus gattii* by matrix-assisted laser desorption ionization-time of flight mass spectrometry. *J. Clin. Microbiol.* 49, 3050–3053. doi: 10.1128/jcm.00651-11

Moosa, M. Y. S., and Coovadia, Y. (1997). Cryptococcal meningitis in Durban, South Africa: a comparison of clinical features, laboratory fi ndings, and outcome for human immunodefi ciency virus (HIV)-positive and HIV-negative patients. *Clin. Infect. Dis.* 24, 131–134. doi: 10.1093/clinids/24.2.131

Nascimento, E., Vitali, L., Kress, M. R. V. Z., and Martinez, R. (2017). *Cryptococcus neoformans* and C. gattii isolates from both HIV-infected and uninfected patients: antifungal susceptibility and outcome of cryptococcal disease. *Rev. Inst. Med. Trop. Sao Paulo* 59:e49.

Park, B. J., Wannemuehler, K., Marston, B. J., Govender, N., Pappas, P. G., and Chiller, T. M. (2009). Estimation of the current global burden of cryptococcal meningitis among persons living with HIV/AIDS. *AIDS* 23, 525–530. doi: 10.1097/qad.0b013e328322ffac

Perkins, A., Gomez-Lopez, A., Mellado, E., Rodriguez-Tudela, J. L., and Cuenca-Estrella, M. J. (2005). Rates of antifungal resistance among Spanish clinical isolates of *Cryptococcus neoformans* var. neoformans. *J. Antimicrob. Chemother.* 56, 1144–1147. doi: 10.1093/jac/dki393

Pfaller, M. A., Diekema, D., Gibbs, D. L., Newell, V. A., Bijie, H., and Dzierzanowska, D. (2009). Results from the ARTEMIS DISK Global antifungal

surveillance study, 1997 to 2007: 10.5-year analysis of susceptibilities of noncandidal yeast species to fluconazole and voriconazole determined by CLSI standardized disk diffusion testing. *J. Clin. Microbiol.* 47, 117–123. doi: 10.1128/jcm.01747-08

Pfaller, M. A., Messer, S., Boyken, L., Hollis, R. J., Rice, C., Tendolkar, S., et al. (2003). In vitro activities of voriconazole, posaconazole, and fluconazole against 4,169 clinical isolates of Candida spp. and *Cryptococcus neoformans* collected during 2001 and 2002 in the ARTEMIS global antifungal surveillance program. *Diagn. Microbiol. Infect. Dis.* 48, 201–205. doi: 10.1016/j.diagmicrobio.2003.09.008

Pfaller, M. A., Messer, S., Boyken, L., Rice, C., Tendolkar, S., Hollis, R. J., et al. (2005). Global trends in the antifungal susceptibility of *Cryptococcus neoformans* (1990 to 2004). *J. Clin. Microbiol.* 43, 2163–2167. doi: 10.1128/jcm.43.5.2163-2167.2005

Pfaller, M. A., Zhang, J., Messer, S. A., Brandt, M. E., Hajjeh, R. A., Jessup, C. J., et al. (1999). In vitro activities of voriconazole, fluconazole, and itraconazole against 566 clinical isolates of *Cryptococcus neoformans* from the United States and Africa. *Antimicrob. Agents Chemother.* 43, 169–171. doi: 10.1128/aac.43.1.169

Revankar, S. G., Kirkpatrick, W. R., McAtee, R. K., Fothergill, A. W., Redding, S. W., and Rinaldi, M. G. (1988). Interpretation of trailing endpoints in antifungal susceptibility testing by the national committee for clinical laboratory standards method. *J. Clin. Microbiol.* 36, 153–156. doi: 10.1128/jcm.36.1.153-156.1998

Rodríguez-Tudela, J. L., Martínez-Suárez, J. V., Dronda, F., Laguna, F., Chaves, F., and Valencia, E. (1995). Correlation of in-vitro susceptibility test results with clinical response: a study of azole therapy in AIDS patients. *J. Antimicrob. Chemother.* 35, 793–804. doi: 10.1093/jac/35.6.793

Sabatelli, F., Patel, R., Mann, P. A., Mendrick, C. A., Norris, C. C., Hare, R., et al. (2006). In vitro activities of posaconazole, fluconazole, itraconazole, voriconazole, and amphotericin B against a large collection of clinically important molds and yeasts. *Antimicrob. Agents Chemother.* 50, 2009–2015. doi: 10.1128/aac.00163-06

Sar, B., Monchy, D., Vann, M., Keo, C., Sarthou, J. L., and Buisson, Y. (2004). Increasing in vitro resistance to fluconazole in *Cryptococcus neoformans* Cambodian isolates: April 2000 to March 2002. *J. Antimicrob. Chemother.* 54, 563–565. doi: 10.1093/jac/dkh361

Selb, R., Fuchs, V., Graf, B., Hamprecht, A., Hogardt, M., Sedlacek, L., et al. (2019). Molecular typing and in vitro resistance of *Cryptococcus neoformans* clinical isolates obtained in Germany between 2011 and 2017. *Int. J. Med. Microbiol.* 309:151336. doi: 10.1016/j.ijmm.2019.151336

Singhal, N., Kumar, M., Kanaujia, P. K., and Virdi, J. S. (2015). MALDI-TOF mass spectrometry: an emerging technology for microbial identification and diagnosis. *Front. Microbiol.* 6:791.

Soares, B. M., Santos, D. A., Kohler, L. M., da Costa César, G., de Carvalho, I. R., dos Anjos Martins, M., et al. (2008). Cerebral infection caused by Cryptococcus gattii: a case report and antifungal susceptibility testing. *Rev. Iberoam. Micol* 25, 242–245.

Souza, L. K., Santos, J. A., Costa, C. R., Faganello, J., Vainstein, M. H., Chagas, A. L., et al. (2010). Molecular typing and antifungal susceptibility of clinical and environmental *Cryptococcus neoformans* species complex isolates in Goiania. Brazil. *Mycoses* 53, 62–67. doi: 10.1111/j.1439-0507.2008.01662.x

Speed, B., and Dunt, D. (1995). Clinical and host differences between infections with the two varieties of *Cryptococcus neoformans*. *Clin. Infect. Dis.* 21, 28–34. doi: 10.1093/clinids/21.1.28

Tay, S. T., Tanty Haryanty, T., Ng, K. P., Rohani, M. Y., and Hamimah, H. (2006). In vitro susceptibilities of Malaysian clinical isolates of *Cryptococcus neoformans* var. grubii and *Cryptococcus gattii* to five antifungal drugs. *Mycoses* 49, 324–330. doi: 10.1111/j.1439-0507.2006.01242.x

Thompson, G. R., Wiederhold, N. P., Fothergill, A. W., Vallor, A. C., Wickes, B. L., and Patterson, T. F. (2009). Antifungal susceptibilities among different serotypes of *Cryptococcus gattii* and *Cryptococcus neoformans*. *Antimicrob. Agents Chemother.* 53, 309–311. doi: 10.1128/aac.01216-08

Torres-Rodríguez, J. M., Alvarado-Ramírez, E., Murciano, F., and Sellart, M. (2008). MICs and minimum fungicidal concentrations of posaconazole, voriconazole and fluconazole for *Cryptococcus neoformans* and *Cryptococcus gattii*. *J. Antimicrob. Chemother.* 62, 205–206. doi: 10.1093/jac/dkn132

van Belkum, A., Chatellier, S., Girard, V., Pincus, D., Deol, P., and Dunne, W. M. (2015). Progress in proteomics for clinical microbiology: MALDI-TOF MS for microbial species identification and more. *Expert Rev. Proteomics* 12, 595–605. doi: 10.1586/14789450.2015.1091731

Wu, S. Y., Lei, Y., Kang, M., Xiao, Y. L., and Chen, Z. X. (2015). Molecular characterisation of clinical *Cryptococcus neoformans* and *Cryptococcus gattii* isolates from Sichuan province. China. *Mycoses* 58, 280–287.

Wu, S., Kang, M., Liu, Y., Chen, Z. X., Xiao, Y. L., and He, C. (2021). Molecular epidemiology and antifungal susceptibilities of Cryptococcus species isolates from HIV and non-HIV patients in Southwest China. *Eur. J. Clin. Microbiol. Infect. Dis.* 40, 287–295. doi: 10.1007/s10096-020-04013-4

Xu, X., Du, P., Wang, H., Yang, X., Liu, T., and Zhang, Y. (2021). Clinical characteristics, *Cryptococcus neoformans* genotypes, antifungal susceptibility, and outcomes in human immunodeficiency virus-positive patients in Beijing, China. *J. Int. Med. Res.* 49:3000605211016197.

Conflict of Interest: The authors declare that the research was conducted in the absence of any commercial or financial relationships that could be construed as a potential conflict of interest.

Publisher's Note: All claims expressed in this article are solely those of the authors and do not necessarily represent those of their affiliated organizations, or those of the publisher, the editors and the reviewers. Any product that may be evaluated in this article, or claim that may be made by its manufacturer, is not guaranteed or endorsed by the publisher.

frontiers in Microbiology

ORIGINAL RESEARCH
published: 17 August 2021
doi: 10.3389/fmicb.2021.692693

Antifungal Activity and Potential Mechanism of 6,7, 4′-O-Triacetylscutellarein Combined With Fluconazole Against Drug-Resistant *C. albicans*

Liu-Yan Su[1†], Guang-Hui Ni[1,2†], Yi-Chuan Liao[1], Liu-Qing Su[1], Jun Li[1], Jia-Sheng Li[1], Gao-Xiong Rao[1,2] and Rui-Rui Wang[1,2*]*

[1] School of Chinese Materia Medica, Yunnan University of Traditional Chinese Medicine, Kunming, China, [2] Engineering Laboratory for National Health Theory and Product of Yunnan Province, Yunnan University of Traditional Chinese Medicine, Kunming, China

OPEN ACCESS

Edited by:
Mohmmad Younus Wani, Jeddah University, Saudi Arabia

Reviewed by:
Somanon Bhattacharya, Stony Brook University, United States
Fahimeh Alizadeh, Islamic Azad University, Iran
Arif Mohammed, Jeddah University, Saudi Arabia

***Correspondence:**
Rui-Rui Wang
wangrryucm@126.com
Gao-Xiong Rao
Rao_gx@163.com

[†] These authors have contributed equally to this work

Specialty section:
This article was submitted to Antimicrobials, Resistance and Chemotherapy, a section of the journal Frontiers in Microbiology

Received: *09 April 2021*
Accepted: *12 July 2021*
Published: *17 August 2021*

Citation:
Su L-Y, Ni G-H, Liao Y-C, Su L-Q, Li J, Li J-S, Rao G-X and Wang R-R (2021) Antifungal Activity and Potential Mechanism of 6,7, 4′-O-Triacetylscutellarein Combined With Fluconazole Against Drug-Resistant C. albicans. Front. Microbiol. 12:692693. doi: 10.3389/fmicb.2021.692693

The increased resistance of *Candida albicans* to conventional antifungal drugs poses a huge challenge to the clinical treatment of this infection. In recent years, combination therapy, a potential treatment method to overcome *C. albicans* resistance, has gained traction. This study assessed the effect of 6,7,4′-O-triacetylscutellarein (TA) combined with fluconazole (FLC) on *C. albicans in vitro* and *in vivo*. TA combined with FLC showed good synergistic antifungal activity against drug-resistant *C. albicans in vitro*, with a partial inhibitory concentration index (FICI) of 0.0188–0.1800. In addition, the time-kill curve confirmed the synergistic effect of TA and FLC. TA combined with FLC showed a strong synergistic inhibitory effect on the biofilm formation of resistant *C. albicans*. The combined antifungal efficacy of TA and FLC was evaluated *in vivo* in a mouse systemic fungal infection model. TA combined with FLC prolonged the survival rate of mice infected with drug-resistant *C. albicans* and reduced tissue invasion. TA combined with FLC also significantly inhibited the yeast-hypha conversion of *C. albicans* and significantly reduced the expression of RAS-cAMP-PKA signaling pathway-related genes (RAS1 and EFG1) and hyphal-related genes (HWP1 and ECE1). Furthermore, the mycelium growth on TA combined with the FLC group recovered after adding exogenous db-cAMP. Collectively, these results show that TA combined with FLC inhibits the formation of hyphae and biofilms through the RAS-cAMP-PKA signaling pathway, resulting in reduced infectivity and resistance of *C. albicans*. Therefore, this study provides a basis for the treatment of drug-resistant *C. albicans* infections.

Keywords: *Candida albicans*, drug resistance, 6,7,4′-O-triacetylscutellarein, fluconazole, synergistic effect

INTRODUCTION

In recent years, the morbidity and mortality of invasive fungal infections have remained high, especially in patients with weakened immunity and hospitalized patients with severe illness (Noble et al., 2016). *Candida albicans* is the most common opportunistic fungal pathogen, which can cause superficial infections of the skin, oral cavity, and mucous membranes and potentially

life-threatening invasive infections (Rajasekharan et al., 2018). Fluconazole has become the first choice for treating *C. albicans* infection due to its good effects, few side effects, and broad antibacterial spectrum. However, long-term, high-dose use of fluconazole can lead to the emergence of drug-resistant strains, which poses a major challenge to the clinical prevention and treatment of *C. albicans* infection (Zhang et al., 2020). Therefore, it is necessary to find new antifungal drugs or effective treatment strategies for inhibiting fungal resistance.

Due to the limited therapeutic effects of existing antifungal drugs, more attempts have been made to identify effective antifungal drugs. Combination therapy has been widely studied and used to combat fungal resistance. Studies have shown that using natural compounds derived from traditional Chinese medicine and their derivatives combined with fluconazole has an excellent synergistic effect against drug-resistant *C. albicans* (Gong et al., 2019). As illustrated in **Figure 1**, the 6,7,4′-O-triacetylscutellarein (TA) is the structural modification of scutellarin (SL) (Ni et al., 2018). We studied the antifungal activity of TA and SL and unexpectedly found that TA combined with FLC has good antifungal activity against *C. albicans,* especially the resistant strains.

TA is a flavonoid. Previous reports have shown that flavonoids combined with FLC have significant antifungal effects against *C. albicans*, quercetin, baicalein, chalcone, etc. Besides, TA combined with FLC has a good synergistic inhibitory effect on drug-resistant *C. albicans* (Huang et al., 2008; Gao et al., 2016; Wang et al., 2016). Several reports have shown that the antifungal effects of flavonoids and their derivatives are related to the inhibition of biofilm formation, yeast-hyphae transition, and efflux pump activity. However, the anti-*C. albicans* activity of TA has not been explored. Therefore, this study investigated whether TA combined with FLC has antifungal activity against *C. albicans* and whether they can treat drug resistance *C. albicans* infection.

Herein, the antifungal activity of TA combined with FLC was determined both *in vitro* and *in vivo*. In addition, this study also investigated whether TA combined with FLC can inhibit yeast-hyphae transformation through the RAS-cAMP-PKA signaling pathway to combat drug-resistant *C. albicans*.

MATERIALS AND METHODS

Compounds, Strains, and Culture Conditions

We prepared a TA and SL solution (25 mg/mL) in DMSO (dimethyl sulfoxide). Fluconazole (FLC) was obtained from Helioeast company (Nanchang, China) and dissolved in DMSO (10 mg/mL). All drug solutions were stored at 4°C.

Professor Li Yu-ye of the First Affiliated Hospital of Kunming Medical University of China donated clinically resistant *C. albicans* strains including CA3511, CA602, A550, CA4508, CA381, CA187, CA800, CA799, CA3816, CA808, and CA23. In addition, the standard *C. albicans* strain SC5314 was sourced from Yunnan Denglou Technology Co., Ltd. All the strains were frozen with 30% glycerol in a refrigerator at −80°C.

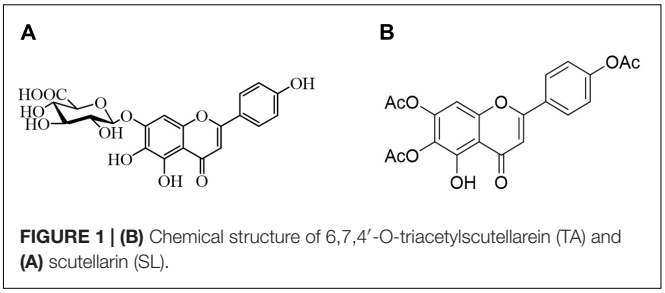

FIGURE 1 | (B) Chemical structure of 6,7,4′-O-triacetylscutellarein (TA) and **(A)** scutellarin (SL).

Before the experiment, the strains were incubated in an incubator at 37°C on Sabouraud-dextrose-agar (SDA) for at least 24 h.

Antifungal Susceptibility Testing

According to the Clinical and Laboratory Standards Institute (CLSI) M27-A3 method (Reyes and Ghannoum, 2000), a broth microdilution method was used to determine the minimum inhibitory concentration (MIC) of samples used alone and in combination with FLC against *C. albicans* strains. Here MIC is defined as the drug concentration that reduces growth by 80% compared to the control group. Serial five-fold dilutions of the samples were prepared using Sabouraud-dextrose-broth (SDB) medium (Weerasekera et al., 2016), with a final concentration of 0.32–1000 μg/mL. These were used in a preliminary study on the antifungal activity of TA and SL. Serial two-fold dilutions of the samples were then prepared using SDB to further analyze the antifungal activity of TA combined with FLC. The final concentration of the samples was 32–1000 μg/mL when used alone and 0.064–200 μg/mL and 0.0128–40 μg/mL when used in combination (TA and FLC, respectively). Each well contained 100 μL of 1×10^5 colony-forming units (CFU)/mL of yeast cell suspension. Then, we added 50 μL of TA and FLC to each well (200 μL). Subsequently, we incubated the flat bottom 96-well plate (701001, NEST, China) at 37°C for 24 h. The wells with only fungi (no drugs) were defined as the control and wells with only SDB as the blank. Further, we determined the growth rate in each well via visual observation and measuring the optical density at a wavelength of 625 nm using a multifunctional microplate reader (SpectraMax 340PC384, Molecular Devices Corporation, United States). We analyzed the antifungal effects using fractional inhibitory concentration index (FICI) to assess the *in vitro* interactions between TA and FLC. The FICI was calculated for each combination using the following formula: FICI = FICI TA + FICI FLC = (MIC of TA in combination/MIC of TA alone) + (MIC of FLC in combination/MIC of FLC alone). Here, synergy was defined as FICI $\leq$ 0.5. 0.5 < FICI < 1 indicated partial synergy, FICI = 1 indicated additive effect, 1 < FICI $\leq$ 4 indicated indifference, and antagonism was defined as FICI > 4 (Khodavandi et al., 2010).

Antifungal Kinetics Assay

The optical density (OD) of different drug treatment groups was measured at different time points. The time-course curve of fungal killing was plotted to study the dynamic inhibitory effect of TA on drug-resistant *C. albicans* CA23. Next, we diluted the overnight cultures of *C. albicans* strains with SDB medium to

1×10^5 CFU/mL and exposed them to TA (128 μg/mL), FLC (16 μg/mL), and a combination of TA (128 μg/mL) with FLC (16 μg/mL). It is worth noting that in the control group, only fungi were not added with drugs. Subsequently, we incubated the cells at 37°C with constant shaking (150 rpm), and 200 μL samples collected from each well after 0, 4, 8, 12, 24, 48, and 72 h to measure the OD at 625 nm (Li X. et al., 2020; Li et al., 2021). The experiment was performed thrice (independently), and each sample was assessed in three replicates.

The Effect of FLC Combined With TA on the Pre-formation and Formation of *C. albicans* Biofilm

We evaluated the effect of TA on the formation and pre-formation of the biofilm of drug-resistant *C. albicans* CA23 through microscopic observation and cell staining (Soll and Daniels, 2016; Wu et al., 2020). First, we cultured *C. albicans* CA23 in SDB medium overnight, then washed the fungal cells three times with PBS, resuspended them in RPMI-1640 (+10% FBS) medium, and adjusted it to 1×10^5 CFU/mL (final concentration). Next, we added 1 mL of the fungal cell suspension of different groups to the 24-well plate; statically incubated for 90 min at 37°C for adhesion; aspirated to remove non-adherent cells; then added the same volume of Fresh RPMI 1640 (+10% FBS) medium. The plate was incubated in a 37°C incubator for 24 h until a mature biofilm was formed. After 90 min of adhesion, we added fresh RPMI 1640 (+10% FBS) containing the drug to the 24-well plate, and the plate was incubated at 37°C for 24 h to detect the formation of biofilm by TA impact. In addition, after 90 min of adhesion, we added fresh RPMI 1640 (+10% FBS) to the 24-well plate, incubated the plate at 37°C for 24 h to form a mature biofilm then discarded the biofilm supernatant. Fresh RPMI 1640 medium (+10% FBS) containing the drug was then added. The incubation continued for 24 h to detect the effect of TA on pre-formation biofilm. Lastly, the plates were incubated at 37°C for 24 h to observe the antibiofilm effect of TA. We divided them into four groups: control, FLC, TA, and TA + FLC. Each experiment had three multiple holes per group.

Evaluation of Antifungal Activity *in vivo* Using Mouse Systemic Fungal Infection Model

Experimental Design and Mouse Model

We evaluated the antifungal activity of TA in a murine model of systemic infection *in vivo* (Kong et al., 2018; Khan et al., 2020). We raised and treated all mice following the guidelines approved by the China Animal Protection and Use Committee. A model of systemic fungal infection was established in 60 male and female (1:1) C57BL/6 mice (aged 6–8 weeks, weighing 18–22 g). After 1 week of adaptive feeding, Subsequently, the mice were randomly assigned to the following experimental groups: Blank (without cyclophosphamide and *C. albicans*), Control (without *C. albicans*), Model (only *C. albicans*), FLC (2 mg/kg), TA (200 mg/mL), and TA (200 mg/mL) + FLC (2 mg/kg). we intraperitoneally injected the mice with cyclophosphamide (100 mg/kg body weight) for three consecutive days to induce an immunodeficiency model. On the 4th day, we injected the drug-resistant *C. albicans* suspension (3.75×10^6 CFU/mL, 0.1 mL/10 g) through the tail vein to cause systemic infection in the mice. Two hours after model establishment, the experimental mice were dosed intragastrically by weight. Notably, the blank, control, and model mice groups were prepared using a carboxymethylcellulose sodium (CMC-Na) gelling agent.

Mice Weight and Survival Assay

The general state of the experimental animals, including activity status, hair status, weight, and survival rate changes, was observed after successful treatment with *C. albicans*. In addition, the survival status of mice in each group was monitored and recorded for 14 days.

Determination of Fungal Burden

The mice were sacrificed via cervical dislocation under complete anesthesia on the 14th day, and kidneys were collected and weighed. Next, an appropriate amount of PBS (10 μL sterile PBS was needed for 1 mg of internal organs) was added and ground with a homogenizer. Finally, 10 μL of the tissue homogenate was placed on the SDA plate and incubated at 37°C for 48 h to determine the fungal burden in the kidneys. The experiments were performed thrice (independently). The results were expressed as $\log 10^{CFU/g}$, CFU/g = (Number of CFU × dilution times)/weight of tissue.

Histopathological Study of Mouse Kidney

The kidney was dissected and placed in 10% buffered neutral formalin for 24 h. The fixed and shaped tissue was embedded in paraffin, sectioned at a thickness of 5 μm, deparaffinized, and dehydrated using standard techniques. The sections were stained with hematoxylin and eosin (HE) and periodic acid methylamine silver (PASM) to detect inflammatory cells and hyphae. The field of view was randomly selected to observe histopathological changes using an optical microscope at a certain magnification.

Filamentation Assay in a Liquid Medium

To evaluate the effect of TA on the filamentous growth of *C. albicans*, we used Spider medium (1% mannitol, 1% nutrient broth, 0.2% K_2HPO_4, pH 7.2), and Sabouraud Dextrose medium (10 g peptone and 40 g dextrose in 1000 mL ddH2O) supplemented with 10% FBS for hyphae induction experiment (Yang et al., 2018). Four groups were set for this assay: TA (128 μg/mL), FLC (16 μg/mL), a combination of TA (128 μg/mL) with FLC (16 μg/mL), and control group (no drug added). Drugs and *C. albicans* cells (1×10^5 CFU/mL) were added to the hyphae induction medium and incubate at 37°C for 4 h. An inverted microscope (Carl Zeiss) with a camera was used to visualize and take images. The experiment was performed thrice (independently), and each sample was evaluated in three replicates.

Quantitative Real-Time PCR Assays

Four groups were set for this assay: Control, TA (128 μg/mL), FLC (16 μg/mL), and a combination of TA (128 μg/mL) with FLC (16 μg/mL). Planktonic cells of *C. albicans* treated with the

drug and grown in RPMI-1640 (+10% FBS) medium at 37°C for 16 h were diluted to 1×10^5 CFU/mL cell density. The fungal cells were washed three times with sterile PBS and harvested by centrifugation at 3900 rpm for 5 min. Then, the fungal cells were ground into a powder with liquid nitrogen. TRIzol (Invitrogen, United States) was used to extract total RNA according to the instructions. The quality and quantity of the extracted RNA were determined spectrophotometrically (NanoDrop Lite, United States). The Reverse Transcription System kit (Promega, United States) was used to convert the total RNA (1 μg) into cDNA with random primers in a 20 μL reaction volume following the manufacturer's instructions. The primer sequences used for amplification of specific genes are shown in **Table 1**. RT-PCR mixtures contained; 2 μL cDNA, 10 μL GoTaq® qPCR master mix (Promega, United States), 0.5 μL of each primer at a concentration of 10P, and sterile Nuclease-Free water to a final volume of 20 μL. The lightcycler 96 fluorescent quantitative PCR system was used for qRT-PCR analysis. The cycles were as follows: pre-denaturation at 95°C for 10 min, then 95°C for 15 s, 55°C for 30 s, and 72°C for 30 s (40 cycles). Actin (ACT1) was used as the internal control. The transcription level of the selected genes was calculated using the $2^{-\Delta\Delta Ct}$ method. Three independent experiments were performed, each in triplicate.

cAMP Rescue Assay

We prepared *C. albicans* cells in RPMI-1640 (1×10^5 CFU/mL) supplemented with 10% FBS to verify the role of TA combined with FLC in inhibiting the Ras1-cAMP-Efg1 pathway. We added dibutyryl-cAMP (db-cAMP) (MCE, China) immediately after adding the drug to make the final concentration to 128 μM. Cells not treated with db-cAMP were used as controls. An inverted microscope (Carl Zeiss) with a camera was used to observe and take images after incubation at 37°C for 4 h. Each sample was assessed in three replicates.

Statistical Analysis

GraphPad Prism 8 was used for all statistical analyses. The data are expressed as the average of three repeated experiments ± standard deviation (SD). The differences among the groups were evaluated using analysis of variance (ANOVA). $P < 0.05$ was considered statistically significant ($^*p < 0.05$, $^{**}p < 0.01$, $^{***}p < 0.001$, $^{****}p < 0.0001$).

TABLE 1 | Primers used in this study.

Oligo name	Sequence (5′ to 3′)	Product length (bp)
ACT1-F	ACGGTGAAGAAGTTGCTGCT	180
ACT1-R	TGGATTGGGCTTCATCACCA	
RAS1-F	GTGGTGGTGTTGGTAAATCCG	178
RAS1-R	TGTTCTCTCATGGCCAGATATTC	
EFG1-F	AATGTGGCCCAAATGACACG	131
EFG1-R	TTGGCAACAGTGCTAGCTGA	
ECE1-F	TGCCTGTGCTACTGTTTTTGC	123
ECE1-R	ACAGTAGGTGCTTGGTCAGC	
HWP1-F	ACTGAACCTTCCCCAGTTGC	185
HWP1-R	GTCGTAGAGACGACAGCACT	

RESULTS

Antifungal Susceptibility Testing

TA or SL alone had no antifungal effect on sensitive and resistant *C. albicans* (MIC > 1000 μg/mL) (**Table 2**). However, SL combined with FLC showed antagonistic and additive effects on sensitive and resistant strains (FICI, 14.55 and 1.00, respectively). In contrast, TA combined *with* FLC showed an indifference effect and a strong synergistic effect on sensitive and resistant strains (FICI, 2.27 and 0.18, respectively). We used ten clinically drug-resistant *C. albicans* for further antifungal activity experiments to verify whether TA has the same antibacterial effect on all drug-resistant *C. albicans*. TA had no antifungal effect on all drug-resistant *C. albicans* when used alone (MIC > 1000 μg/mL) but had strong synergy on all drug-resistant *C. albicans* when combined with FLC (FICI < 0.5) (**Table 3**).

Time-Kill Curve

TA and FLC showed no antifungal effect on drug-resistant *C. albicans* CA23 when used alone (**Figure 2**). In contrast, combined TA and FLC showed strong synergistic antifungal

TABLE 2 | Antifungal activity of TA and SL against *C. albicans* (*n* = 3).

Drugs	MIC (μg/ml)		FICI		Interaction	
	SC5314	CA3511	SC5314	CA3511	SC5314	CA3511
FLC	6.50	>1000	–	–	–	–
SL	>1000	>1000	–	–	–	–
FLC + SL	94.30	>1000	14.55	1.00	ANT	ADD
TA	>1000	>1000	–	–	–	–
FLC + TA	14.70	180.06	2.27	0.18	IND	SYN

CA, C. albicans; SL, scutellarin; TA, 6,7,4′-O-triacetylscutellarein; FLC, fluconazole; MIC denotes the minimum inhibitory concentration of drug that inhibited fungal growth by 80% compared with the growth control; FICI, fractional inhibitory concentration index; ANT, antagonistic; ADD, additive; IND, indifferent; SYN, synergism. MIC values and FICIs are shown as the median of three independent experiments.

TABLE 3 | The effect of FLC combined with TA against *C. albicans in vitro* (*n* = 3).

Strains	MIC (μg/ml)				FICI	Interaction
	Alone		Combined			
	FLC	TA	FLC	TA		
CA602	105.11	>1000	2.61	13.04	0.0313	SYN
CA550	127.56	>1000	5.89	29.45	0.0609	SYN
CA4508	870.45	>1000	20.24	101.21	0.0738	SYN
CA381	>1000	>1000	10.05	50.28	0.0301	SYN
CA187	>1000	>1000	6.27	31.36	0.0188	SYN
CA800	>1000	>1000	12.15	60.75	0.0364	SYN
CA799	>1000	>1000	14.91	74.59	0.0447	SYN
CA3816	>1000	>1000	13.19	65.96	0.0395	SYN
CA808	>1000	>1000	7.81	39.06	0.0234	SYN
CA23	>1000	>1000	24.61	123.06	0.0738	SYN

CA, C. albicans; TA, 6,7,4′-O-triacetylscutellarein; FLC, fluconazole; MIC denotes the minimum inhibitory concentration of drug that inhibited fungal growth by 80% compared with the growth control; FICI, fractional inhibitory concentration index; SYN, synergism. MIC values and FICIs are shown as the median of three independent experiments.

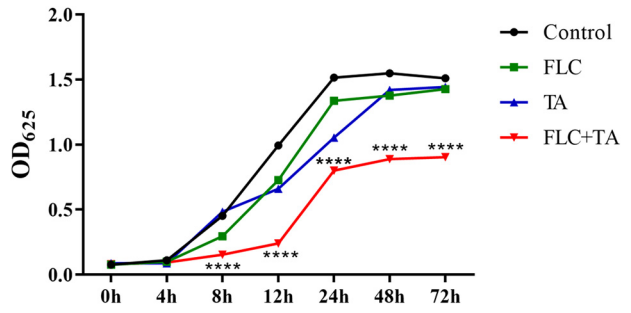

FIGURE 2 | Time-killing curves of *C. albicans* CA23 treated with TA and TA combined with FLC. The combination group was compared with the FLC group. $^{****}P < 0.0001$.

activity after 8 h of treatment, which was very significant even at 72 h ($^{****}P < 0.0001$).

The Effect of FLC Combined With TA on *C. albicans* Biofilm Pre-formation and Formation

The *C. albicans* in the control group formed mature biofilms after 24 h of culture (**Figure 3**). The biofilm formation of the FLC and TA groups was not significantly inhibited compared with that of the control group, forming a nearly mature biofilm with yeast, hyphae, and pseudohyphae. However, biofilm formation in the TA and FLC combined group was strongly inhibited. The fungal cells were sparsely distributed in the FLC + TA group, with most being in the yeast state. For pre-formed biofilm analysis, we first cultivated *C. albicans* for 24 h to form a mature biofilm, then added drugs for further cultivation for 24 h. The FLC and TA groups did not significantly prevent the further growth and development of mature biofilms compared with the control group. However, TA combined with FLC destroyed the structure of mature biofilms, inhibiting further development of mature biofilms.

Evaluation of Antifungal Activity *in vivo* Using Mouse Systemic Fungal Infection Model

Mice Weight and Survival Assay

We first performed weight changes and survival analyses on mice infected with drug-resistant *C. albicans* (CA23) to preliminarily evaluate the antibacterial efficacy of different drug groups *in vivo*. The body weight of mice in the model group, FLC group, and TA group significantly decreased compared with the body weight at first and last days of administration (**Figure 4A**). However, the weight of the mice in the TA combined with the FLC group was not significantly altered ($P > 0.05$). Similarly, there was no significant difference in the survival rate of the model group, FLC group, and TA group ($P > 0.05$) after 14 days of the administration (the survival rates; 25, 40, and 40%, respectively) (**Figure 4B**). However, TA combined with FLC significantly increased the survival rate of mice to 85% ($P < 0.05$). Collectively, these findings indicate that the combination of TA and FLC can significantly improve the survival rate of mice infected with drug-resistant *C. albicans* compared with FLC monotherapy, confirming their antifungal activity in the body.

Determination of Fungal Burden

We conducted a fungal burden analysis to assess the effect of TA combined with FLC on the amount of fungal colonization in the kidney of mice infected with drug-resistant *C. albicans* systemic infection. The fungal burden both the FLC and TA groups was not significantly different compared with the model group ($P > 0.05$) (**Figure 4C**). However, the fungal kidney burden in the TA + FLC group was significantly reduced compared with the control, FLC, and TA groups ($P < 0.01$).

Histopathological Study of Mouse Kidney

The mouse kidney sections were stained with HE and PASM to further assess the fungal burden of mouse kidneys. The HE staining results (**Figure 5**) showed that the kidneys of the Blank and Control group mice did not have inflammatory cell infiltration. However, there was a significant inflammatory cell infiltration in the kidneys of mice in the model and TA and FLC group. In contrast, the infiltration of inflammatory cells in the kidney of mice in TA combined with the FLC group was greatly reduced and was close to that of normal mice. Furthermore, the fungi were stained black or gray-brown in the PASM-stained kidneys (**Figure 6**). Fungi did not invade the kidneys of the mice in the blank and the control groups. However, several fungi invaded the kidneys of mice in model, TA, and FLC groups. Besides, most of these fungi were hyphae. In contrast, there were very few yeast-like fungi in the kidneys of mice in the TA combined with the FLC group.

Filamentation Assay in a Liquid Medium

The pathogenic state of *C. albicans,* hyphae, plays a vital role in the pathogenesis of *C. albicans* (Chen et al., 2020; Li Y. et al., 2020). Spiders and Synthetic Dropout (SD) media were used to induce hyphae formation. *C. albicans* CA23 formed dense and long hyphae in the Spider and SD of the control group (**Figure 7**). In addition, there was no significant difference in the mycelial growth state between the TA and FLC disposable groups and the control group. On the contrary, the length of the hyphae was shorter in the TA combined FLC group than in the other groups. The number of hyphae was also significantly reduced in the TA combined FLC group than in the other groups.

Quantitative Real-Time PCR Assays

We also conducted RT-PCR experiments on the RAS-cAMP-PKA pathway-related genes RAS1 and EFG1 and the hypha-related genes (HWP1 and ECE1) to further assess the antifungal mechanism of TA combined with FLC. RAS1, EFG1, HWP1, and ECE1 expressions were significantly down-regulated in the FLC group and up-regulated in the TA group compared with the control group (**Figure 8**). Interestingly, the following genes were significantly downregulated in the TA combined FLC group compared with the FLC group: RAS1 > 2 times, EGF1 > 2.3 times, HWP1 > 2.25 times, and ECE1 > 2.20 times.

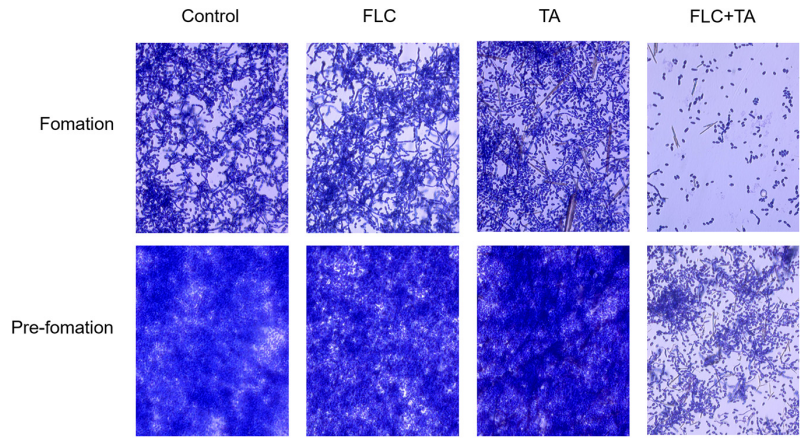

FIGURE 3 | The effect of TA combined with FLC on *C. albicans* biofilm. The morphology of biofilm and hyphae were observed using a microscope (magnification 400×) after incubation at 37°C for 24 h and staining with 0.4% crystal violet. FLC combined with TA effectively inhibited *C. albicans* biofilm formation and positively affected the pre-formed *C. albicans* biofilm.

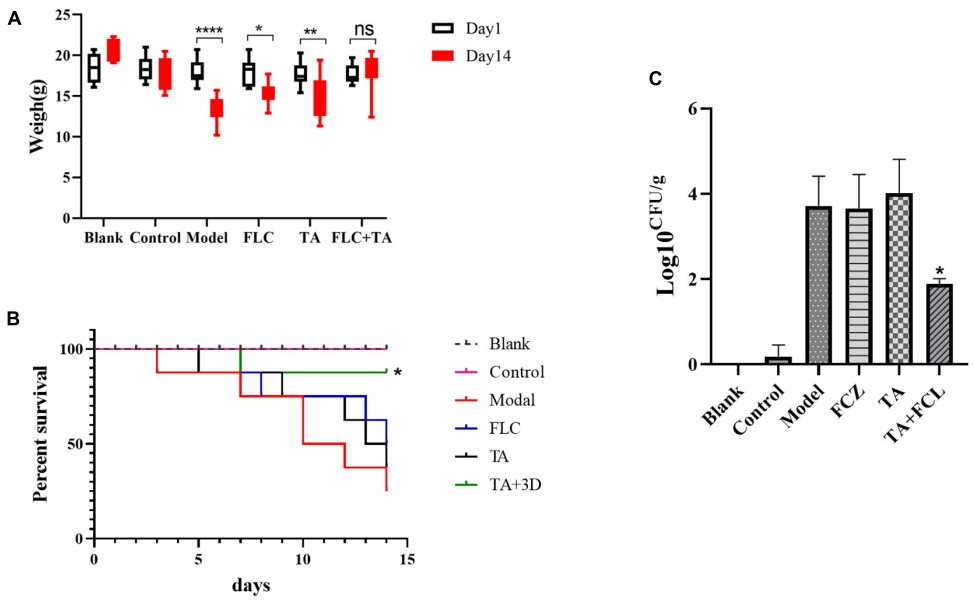

FIGURE 4 | The effect of FLC combined with TA on the infection of drug-resistant *C. albicans in vivo*. **(A)** The effect of FLC combined with TA on the mice body weight. The mice in the model group, TA, and FLC groups significantly lost weight compared with the weight at the first and last days of administration. In contrast, the body weight of the mice in the FLC and TA combination group was not significantly changed. **(B)** The effect of FLC combined with TA on the survival rate of mice. The survival rate of mice was higher in the combined administration group than in the model group. **(C)** Kidney fungal burden. The number of kidney fungi in mice significantly reduced in the TA combined with the FLC group after 14 days of treatment compared with the model group. *$P < 0.05$, **$P < 0.01$, ****$P < 0.0001$.

cAMP Rescue Assay

Cyclic adenosine monophosphate (cAMP) level is essential for activating the RAS-cAMP-PKA signaling pathway (Huang et al., 2019). We confirmed that cAMP is involved in the transition from yeast to hyphae by adding db-cAMP to the medium. The db-cAMP addition successfully rescued the inhibitory effect of TA combined with FLC on the formation of hyphae, partially restoring the ability of *C. albicans* to form hyphae (**Figure 9**). Therefore, the combination of TA and FLC can reduce the cAMP level in fungal cells.

DISCUSSION

Several studies have focused on discovering new antifungal drugs and finding new treatment strategies to solve the increasing fungal drug resistance. Herein, TA combined with FLC showed a better synergistic effect against drug-resistant *C. albicans* than SL. A previous experiment showed that TA combined with FLC has an indifference and a strong synergistic effect on sensitive and resistant *C. albicans* (FICI; 2.27 and 0.18, respectively). Therefore, we used ten clinically drug-resistant *C. albicans* for

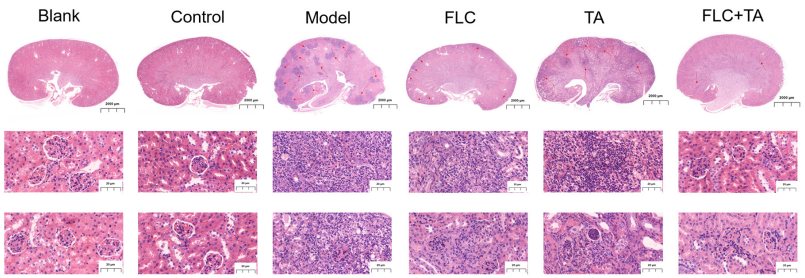

FIGURE 5 | A representative H&E stained section of the kidney. The infiltration of inflammatory cells in the kidney of mice in the combined administration group was significantly reduced. The picture of the whole kidney field is enlarged by 80×, and the other images are enlarged by 400×. The red arrow refers to the characteristic area of inflammatory cell infiltration in mouse kidney tissue.

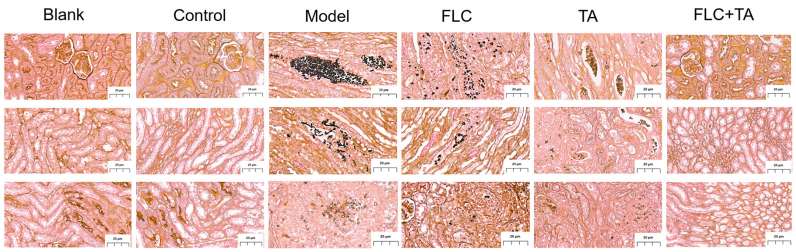

FIGURE 6 | Representative PASM stained section of the kidney. The fungal burden in the kidneys of mice in the combined administration group was significantly reduced (magnification of 400×).

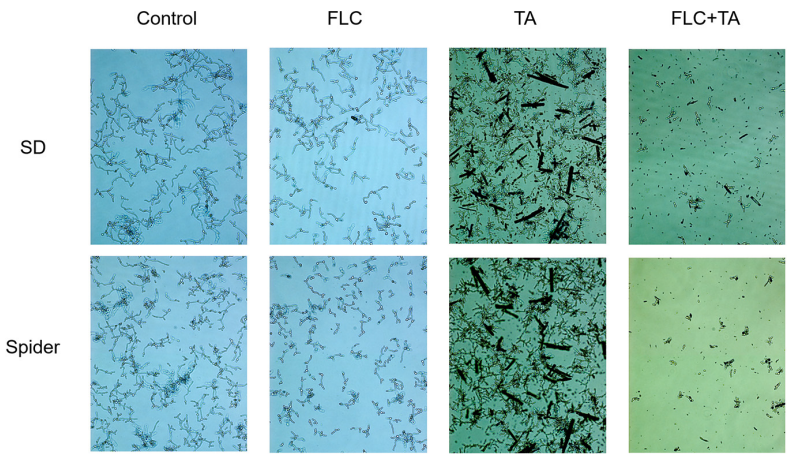

FIGURE 7 | Filamentation assay in a liquid medium. The SD and Spider mycelium induction medium significantly inhibited the growth of drug-resistant *C. albicans* CA23 hyphae in the combined administration group than in the control group (magnification; 400×).

further antifungal activity experiments to verify whether TA has the same antifungal effect on all drug-resistant *C. albicans*. TA combined with FLC showed a strong synergistic effect on all drug-resistant *C. albicans* (FICI < 0.5). Besides, the MIC of FLC decreased from 105.11–1000 μg/mL to 2.61–24.61 μg/mL. We also used the time-kill curve to confirm the synergistic effect of TA combined with FLC.

Persistent *C. albicans* infections in the hospital are often closely related to biofilm formation (Cavalheiro and Teixeira, 2018). Biofilms can reduce the permeability of antifungal drugs and are inherently resistant to antibacterial drugs. Reports have shown that the resistance of *C. albicans* biofilms can reach 1000 times that of planktonic *C. albicans* (Tsui et al., 2016). Therefore, inhibiting biofilm formation can clinically inhibit resistant *C. albicans* infection. Herein, the drug-resistant *C. albicans* CA23 formed a mature biofilm after 24 h of culture (Gulati and Nobile, 2016). These results show that the combination of TA + FLC interacts with fungi for 24 h, making most fungi remain in the yeast state, thus significantly inhibiting the CA23 biofilm formation. The

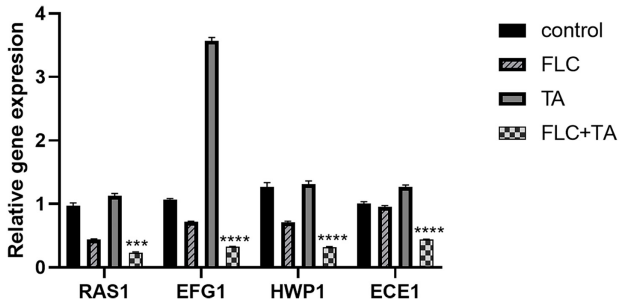

FIGURE 8 | The mRNA transcription levels of the Ras-cAMP-PKA pathway and hyphae-related genes. The mRNA transcripts were significantly down-regulated in the TA combined with the FLC group. ACT1 was used as an internal reference gene and quantified using the $2^{-\Delta\Delta CT}$ method. ***$p < 0.001$, ****$p < 0.0001$.

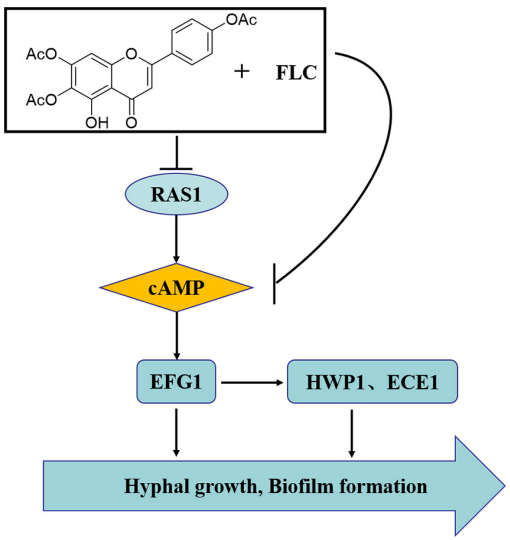

FIGURE 10 | The synergistic mechanism of TA combined with FLC against *C. albicans*. The synergistic mechanism may be related to the changes of downstream hyphae-related genes caused by the RAS-cAMP-PKA pathway inhibition.

combination of TA + FLC also destroyed the structure of the pre-formed biofilm, inhibiting its further development. Therefore, TA combined with FLC could be a promising strategy for treating biofilm-related infections caused by drug-resistant *C. albicans*.

However, *in vivo* experiments were needed to prove the safety and effectiveness of the drug. Herein, we established a mouse model of systemic infection using drug-resistant *C. albicans*. The study showed that the weight of the mice in the TA combined with the FLC treatment group recovered, and the survival rate was significantly improved compared with the weight and survival rate of mice in the FLC group ($P < 0.05$). In addition, a comprehensive analysis of the kidney, the main target organ of invasive *C. albicans, i*nfection was also conducted (Chen et al., 2018). The results showed that the TA combined with the FLC treatment group had a significantly lower kidney fungal burden ($P < 0.05$), reduced number of lesions, and inflammatory cell infiltration. Besides, they compared with the TA and FLC groups, the fungal cells were significantly reduced, especially the hyphae cells. In summary, the synergistic antibacterial effect of TA combined with FLC could be due to the inhibition of *C. albicans* yeast-hyphae transformation.

Candida albicans has a distinct biological feature since it can grow as yeast, pseudohyphae, and hyphae (Sudbery, 2011). However, the hyphae form has been described as a potential virulence factor of *C. albicans*, which induces pathogenicity by invading epithelial cells, causing tissue damage (Meng et al., 2019). In addition, as an important member of biofilm, hyphae is essential for the formation and stability of biofilm (Desai and Mitchell, 2015). Therefore, it is necessary to explore whether

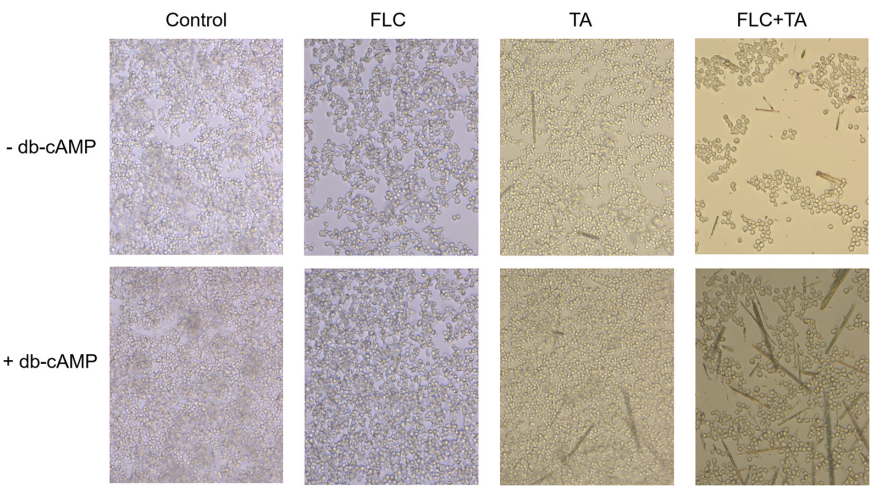

FIGURE 9 | cAMP is related to the formation of hyphae and biofilm of *C. albicans*. The exogenous cAMP restored the mycelium formation of *C. albicans* inhibited by TA combined with FLC (magnification of 400×).

drugs inhibit morphological transformation. Herein, the hyphae of the TA and FLC groups were long and dense after 4 h of incubation in hyphae induction medium, while the hyphae of the TA combined with the FLC group were short and sparse, and most of the remaining bacterial cells remained Yeast form, consistent with the above *in vivo* and *in vitro* results. Therefore, the synergistic effect of TA combined with FLC on drug-resistant *C. albicans* and its biofilm could be due to the inhibitory activity on hyphae.

The EFG1 acts as a positive regulator of yeast-hyphae morphogenesis and mainly depends on the RAS-cAMP-PAK signaling pathway (Sun et al., 2019). The RAS-cAMP-PAK signaling pathway produces the required cAMP-activated protein kinase (PKA). Real-time RT-PCR analysis was used to assess further the antifungal mechanism of TA combined with FLC. We analyzed the expression of Ras/cAMP/PKA signaling pathway-related genes (RAS1 and EFG1) (Lee et al., 2013) and hypha-related genes (HWP1 and ECE1) (Sharkey et al., 1999). Ras1 is a signal transduction GTPase that activates the Ras/cAMP/PKA pathway in *C. albicans* (Li et al., 2014). On the other hand, ECE1 induces cell adhesion and hypha formation by regulating the degree of cell elongation (Engku Nasrullah Satiman et al., 2020). HWP1 is a unique adhesion gene expressed on the surface of mycelium, encoding the cell wall protein of *C. albicans.* Biofilms without the HWP1 gene have weak adhesion to objects (Yan et al., 2019). RAS1, EFG1, HWP1, and ECE1 expressions were significantly down-regulated in the TA combined with the FLC group (RAS1 $>$ 2 times, EGF1 $>$ 2.3 times, HWP1 $>$ 2.25 times, and ECE1 $>$ 2.20 times).

We also added db-cAMP, a functional analog of cAMP, to evaluate whether *C. albicans* treated with TA combined with FLC can restore mycelial growth function in culture for further verification. db-cAMP partially restored the mycelium-forming ability o*f C. albicans,* consistent with previous studies, which showed that TA combined with FLC mainly exerts a synergistic anti-*C. albicans* effect by inhibiting the Ras1-cAMP-PKA pathway (**Figure 10**).

CONCLUSION

In conclusion, we report for the first time that TA combined with FLC has a good synergistic antifungal effect on azole-resistant *C. albicans* both *in vitro* and *in vivo*. Furthermore, our mechanism studies have shown that the morphological transformation inhibition causes the synergy via the RAS-cAMP-PKA signaling pathway. Therefore, there is a need to explore more synergy mechanisms in the future.

DATA AVAILABILITY STATEMENT

The original contributions presented in the study are included in the article/**Supplementary Material**, further inquiries can be directed to the corresponding authors.

ETHICS STATEMENT

All animals were maintained and treated per the guidelines approved by the Animal Care and Use Committee of China. This study was approved by the Animal Care and Welfare Committee of Yunnan University of Traditional Chinese Medicine (R-0620160027).

AUTHOR CONTRIBUTIONS

G-XR and R-RW: providing an overall idea of the experiment. L-YS and G-HN: experimental design and article writing. Y-CL and L-QS: data collation and analysis. JL and J-SL: animal experiment. All authors contributed to the article and approved the submitted version.

FUNDING

This work was financially supported by the National Natural Science Foundation of China (81660737) and Applied Basic Research Foundation of Yunnan Province (2017FF117-003).

ACKNOWLEDGMENTS

We are especially grateful to Li Yu-ye of The First Affiliated Hospital of Kunming Medical University for sharing *C. albicans* strains with us.

SUPPLEMENTARY MATERIAL

The Supplementary Material for this article can be found online at: https://www.frontiersin.org/articles/10.3389/fmicb.2021.692693/full#supplementary-material

REFERENCES

Cavalheiro, M., and Teixeira, M. C. (2018). *Candida* biofilms: threats, challenges, and promising strategies. *Front. Med.* 5:28. doi: 10.3389/fmed.2018.00028

Chen, H., Zhou, X., Ren, B., and Cheng, L. (2020). The regulation of hyphae growth in *C. albicans*. *Virulence* 11, 337–348. doi: 10.1080/21505594.2020.1748930

Chen, X. P., Zheng, H., Li, W. G., Chen, G. D., and Lu, J. X. (2018). Bacteria-induced susceptibility to *C. albicans* super-infection in mice via monocyte methyltransferase Setdb2. *Cell. Microbiol.* 20:e12860. doi: 10.1111/cmi.12860

Desai, J. V., and Mitchell, A. P. (2015). *C. albicans* biofilm development and its genetic control. *Microbiol. Spectr.* 3, 1–3. doi: 10.1128/microbiolspec.MB-0005-2014

Engku Nasrullah Satiman, E., Ahmad, H., Ramzi, A., Abdul Wahab, R., Kaderi, M., Wan Harun, W., et al. (2020). The role of *C. albicans* candidalysin ECE1 gene in oral carcinogenesis. *J. Oral Pathol. Med.* 49, 835–841. doi: 10.1111/jop.13014

Gao, M., Wang, H., and Zhu, L. (2016). Quercetin assists fluconazole to inhibit biofilm formations of fluconazole-resistant *C. albicans* in in vitro and in vivo antifungal managements of vulvovaginal candidiasis. *Cell. Physiol. Biochem.* 40, 727–742. doi: 10.1159/000453134

Gong, Y., Liu, W., Huang, X., Hao, L., Li, Y., and Sun, S. (2019). Antifungal activity and potential mechanism of N-butylphthalide alone and in combination with fluconazole against *C. albicans*. *Front. Microbiol.* 10:1461. doi: 10.3389/fmicb.2019.01461

Gulati, M., and Nobile, C. J. (2016). *C. albicans* biofilms: development, regulation, and molecular mechanisms. *Microbes Infect.* 18, 310–321. doi: 10.1016/j.micinf.2016.01.002

Huang, G., Huang, Q., Wei, Y., Wang, Y., and Du, H. (2019). Multiple roles and diverse regulation of the Ras/cAMP/protein kinase A pathway in *C. albicans*. *Mol. Microbiol.* 111, 6–16. doi: 10.1111/mmi.14148

Huang, S., Cao, Y. Y., Dai, B. D., Sun, X. R., Zhu, Z. Y., Cao, Y. B., et al. (2008). In vitro synergism of fluconazole and baicalein against clinical isolates of *C. albicans* resistant to fluconazole. *Biol. Pharm. Bull.* 31, 2234–2236. doi: 10.1248/bpb.31.2234

Khan, S. H., Younus, H., Allemailem, K. S., Almatroudi, A., Alrumaihi, F., Alruwetei, A. M., et al. (2020). Potential of methylglyoxal-conjugated chitosan nanoparticles in treatment of fluconazole-resistant *C. albicans* infection in a murine model. *Int. J. Nanomedicine* 15, 3681–3693. doi: 10.2147/IJN.S249625

Khodavandi, A., Alizadeh, F., Aala, F., Sekawi, Z., and Chong, P. P. (2010). In vitro investigation of antifungal activity of allicin alone and in combination with azoles against *Candida* species. *Mycopathologia* 169, 287–295. doi: 10.1007/s11046-009-9251-3

Kong, X., Leng, D., Liang, G., Zheng, H., Wang, Q., Shen, Y., et al. (2018). Paeoniflorin augments systemic *C. albicans* infection through inhibiting Th1 and Th17 cell expression in a mouse model. *Int. Immunopharmacol.* 60, 76–83. doi: 10.1016/j.intimp.2018.03.001

Lee, S. H., Jeon, J. E., Ahn, C. H., Chung, S. C., Shin, J., and Oh, K. B. (2013). Inhibition of yeast-to-hypha transition in *C. albicans* by phorbasin H isolated from *Phorbas* sp. *Appl. Microbiol. Biotechnol.* 97, 3141–3148. doi: 10.1007/s00253-012-4549-3

Li, D., Zhao, L., Mylonakis, E., Hu, G., Zou, Y., Huang, T., et al. (2014). In vitro and in vivo activities of pterostilbene against *C. albicans* biofilms. *Antimicrob. Agents Chemother.* 58, 2344–2355. doi: 10.1128/aac.01583-13

Li, L., Liu, X., Su, L., Jiang, X., Zhang, Y., and Wang, R-r (2021). The effect and mechanism of *Panax stipuleanatus* extraction combined with fluconazole against *C. albicans* resistant to fluconazole. *Chin. Arch. Tradit. Chin. Med.* 39, 51–57+269–273. doi: 10.13193/j.issn.1673-7717.2021.01.015

Li, X., Zhang, L., Wang, Y., Zhang, Y., Jin, Z., Li, J., et al. (2020). *C. albicans* SWL-1 reverses fluconazole resistance in by regulating the glycolytic pathway. *Front. Microbiol.* 11:572608. doi: 10.3389/fmicb.2020.572608

Li, Y., Yang, J., Li, X., Su, S., Chen, X., Sun, S., et al. (2020). The effect of ginkgolide B combined with fluconazole against drug-resistant *C. albicans* based on common resistance mechanisms. *Int. J. Antimicrob. Agents* 56:106030. doi: 10.1016/j.ijantimicag.2020.106030

Meng, L., Zhao, H., Zhao, S., Sun, X., Zhang, M., and Deng, Y. (2019). Inhibition of yeast-to-hypha transition and virulence of *C. albicans* by 2-alkylaminoquinoline derivatives. *Antimicrob. Agents Chemother.* 63:e01891-18. doi: 10.1128/AAC.01891-18

Ni, G., Tang, Y., Li, M., He, Y., and Rao, G. (2018). Synthesis of scutellarein derivatives with a long aliphatic chain and their biological evaluation against human cancer cells. *Molecules* 23:310. doi: 10.3390/molecules23020310

Noble, S. M., Gianetti, B. A., and Witchley, J. N. (2016). *C. albicans* cell-type switching and functional plasticity in the mammalian host. *Nat. Rev. Microbiol.* 15, 96–108. doi: 10.1038/nrmicro.2016.157

Rajasekharan, S. K., Kamalanathan, C., Ravichandran, V., Ray, A. K., Satish, A. S., and Mohanvel, S. K. (2018). Mannich base limits *C. albicans* virulence by inactivating Ras-cAMP-PKA pathway. *Sci. Rep.* 8:14972. doi: 10.1038/s41598-018-32935-9

Reyes, G., and Ghannoum, M. A. (2000). Antifungal susceptibility testing of yeasts: uses and limitations. *Drug Resist. Updat.* 3, 14–19. doi: 10.1054/drup.2000.0127

Sharkey, L. L., McNemar, M. D., Saporito-Irwin, S. M., Sypherd, P. S., and Fonzi, W. A. (1999). *HWP1* functions in the morphological development of *Candida albicans* downstream of *EFG1*, *TUP1*, and *RBF1*. *J. Bacteriol.* 181, 5273–5279. doi: 10.1128/JB.181.17.5273-5279.1999

Soll, D. R., and Daniels, K. J. (2016). Plasticity of *C. albicans* biofilms. *Microbiol. Mol. Biol. Rev.* 80, 565–595. doi: 10.1128/mmbr.00068-15

Sudbery, P. E. (2011). Growth of *C. albicans* hyphae. *Nat. Rev. Microbiol.* 9, 737–748. doi: 10.1038/nrmicro2636

Sun, W., Zhang, L., Lu, X., Feng, L., and Sun, S. (2019). The synergistic antifungal effects of sodium phenylbutyrate combined with azoles against *C. albicans* via the regulation of the Ras-cAMP-PKA signalling pathway and virulence. *Can. J. Microbiol.* 65, 105–115. doi: 10.1139/cjm-2018-0337

Tsui, C., Kong, E. F., and Jabra-Rizk, M. A. (2016). Pathogenesis of *C. albicans* biofilm. *Pathog. Dis.* 74:ftw018. doi: 10.1093/femspd/ftw018

Wang, Y. H., Dong, H. H., Zhao, F., Wang, J., Yan, F., Jiang, Y. Y., et al. (2016). The synthesis and synergistic antifungal effects of chalcones against drug resistant *C. albicans*. *Bioorg. Med. Chem. Lett.* 26, 3098–3102. doi: 10.1016/j.bmcl.2016.05.013

Weerasekera, M. M., Wijesinghe, G. K., Jayarathna, T. A., Gunasekara, C. P., Fernando, N., Kottegoda, N., et al. (2016). Culture media profoundly affect *Candida albicans* and *Candida tropicalis* growth, adhesion and biofilm development. *Mem. Inst. Oswaldo Cruz* 111, 697–702. doi: 10.1590/0074-02760160294

Wu, J., Wu, D., Zhao, Y., Si, Y., Mei, L., Shao, J., et al. (2020). Sodium new houttuyfonate inhibits *C. albicans* biofilm formation by inhibiting the Ras1-cAMP-Efg1 pathway revealed by RNA-seq. *Front. Microbiol.* 11:2075. doi: 10.3389/fmicb.2020.02075

Yan, Y., Tan, F., Miao, H., Wang, H., and Cao, Y. (2019). Effect of shikonin against *C. albicans* biofilms. *Front. Microbiol.* 10:1085. doi: 10.3389/fmicb.2019.01085

Yang, L. F., Liu, X., Lv, L. L., Ma, Z. M., Feng, X. C., and Ma, T. H. (2018). Dracorhodin perchlorate inhibits biofilm formation and virulence factors of *C. albicans*. *J. Mycol. Méd.* 28, 36–44. doi: 10.1016/j.mycmed.2017.12.011

Zhang, M., Yan, H., Lu, M., Wang, D., and Sun, S. (2020). Antifungal activity of ribavirin used alone or in combination with fluconazole against *C. albicans* is mediated by reduced virulence. *Int. J. Antimicrob. Agents* 55:105804.

Conflict of Interest: The authors declare that the research was conducted in the absence of any commercial or financial relationships that could be construed as a potential conflict of interest.

Publisher's Note: All claims expressed in this article are solely those of the authors and do not necessarily represent those of their affiliated organizations, or those of the publisher, the editors and the reviewers. Any product that may be evaluated in this article, or claim that may be made by its manufacturer, is not guaranteed or endorsed by the publisher.

frontiers in Microbiology

ORIGINAL RESEARCH
published: 19 August 2021
doi: 10.3389/fmicb.2021.707174

Preliminary Study on Antifungal Mechanism of Aqueous Extract of *Cnidium monnieri* Against *Trichophyton rubrum*

Cao Yanyun[1], Tang Ying[1], Kong Wei[1], Fang Hua[2], Zhu Haijun[3], Zheng Ping[2], Xu Shunming[1]* and Wan Jian[3]**

[1] Department of Dermatology, Pudong New Area People's Hospital, Shanghai, China, [2] Department of Clinical Laboratory, Pudong New Area People's Hospital, Shanghai, China, [3] Department of Emergency and Critical Care Medicine, Pudong New Area People' s Hospital, Shanghai, China

OPEN ACCESS

Edited by:
Keke Huo,
Fudan University, China

Reviewed by:
Min Zhu,
Fudan University, China
Jingjun Zhao,
Tongji University School of Medicine, China

***Correspondence:**
Zheng Ping
jojo_ras@126.com
Xu Shunming
13641930667@163.com
Wan Jian
drjian@yeah.Net

Specialty section:
This article was submitted to Antimicrobials, Resistance and Chemotherapy, a section of the journal Frontiers in Microbiology

Received: *09 May 2021*
Accepted: *21 July 2021*
Published: *19 August 2021*

Citation:
Yanyun C, Ying T, Wei K, Hua F, Haijun Z, Ping Z, Shunming X and Jian W (2021) Preliminary Study on Antifungal Mechanism of Aqueous Extract of Cnidium monnieri Against Trichophyton rubrum. Front. Microbiol. 12:707174. doi: 10.3389/fmicb.2021.707174

Trichoderma rubrum (T. rubrum) is one of the important pathogens because it is the cause of most dermatomycosis. The treatment of *Trichophyton rubrum* infection is time-consuming and very expensive; it is easy for the infections to reoccur, leading to therapeutic failures, persistence, and chronic infection. These issues have inspired researchers to study natural alternative therapies instead. *Cnidium monnieri* (L.), as a kind of traditional Chinese medicine, has a variety of pharmacological activities and a wide range of applications, so it has a high potential for researching and economic value. We detected the effect of aqueous extract of *C. monnieri* (L.) on the activity of *T. rubrum* by Cell Count Kit-8 assay (CCK-8), and we found that 128 and 256 μg/ml of aqueous extracts of *C. monnieri* (L.) co-cultured with *T. rubrum* for 24 h showed the inhibitory effect on *T. rubrum*. The results of scanning electron microscopy (SEM) and transmission electron microscopy (TEM) confirmed that aqueous extract of *C. monnieri* (L.) damaged the *T. rubrum*. At the same time, mass spectrometry screening with *T. rubrum* before and after the treatment of 256 μg/ml of aqueous extracts of *C. monnieri* (L.) showed that 966 differentially expressed proteins were detected, including 524 upregulated differentially expressed genes (DEGs) and 442 downregulated DEGs. The most significantly downregulated protein was chitin synthase (CHS); and the results of qRT-PCR and Western blotting demonstrated that the expression level of CHS was downregulated in the 256 μg/ml group compared with the control group. The study showed that the aqueous extract of *C. monnieri* (L.) could destroy the morphology of mycelia and the internal structure of *T. rubrum*, and it could inhibit the growth of *T. rubrum*. The antifungal effect of aqueous extract of *C. monnieri* (L.) may be related to the downregulation of the expression of CHS in *T. rubrum*, and CHS may be one of the potential targets of its antifungal mechanism. We concluded that aqueous extract from *C. monnieri* (L.) may be a potential candidate for antifungal agents.

Keywords: *Cnidii monnieri*, aqueous extract, *Trichophyton rubrum*, dermatomycosis, chitin synthase

INTRODUCTION

Dermatomycosis is a highly prevalent superficial fungal infection that affects the skin, nails, and hair and is estimated to affect 20–25% of the adult population globally (Seebacher et al., 2008; Zhan and Liu, 2017). It has been observed in different parts of the world. It is an acute and persistent public health problem. *Trichophyton rubrum (T. rubrum)* is the main pathogen of superficial fungal skin infections, accounting for approximately 80–90% of cases (Nenoff et al., 2014). Superficial mycosis generally has mild clinical symptoms and generally affects the quality of life. However, the elderly and those with chronic diseases such as diabetes mellitus (Elewski and Tosti, 2015) and hypoimmune patients have a higher rate of incidence for this disease, and the clinical symptoms may be more serious and even life-threatening (Rouzaud et al., 2015). The treatment of *T. rubrum* infections is time-consuming and very expensive; it is easy for the infections to reoccur. *T. rubrum* may develop drug resistance after a long-term exposure to azole drugs below the inhibitory concentration (Hadrich and Ayadi, 2018), leading to therapeutic failures, persistence, and chronic infection. In addition, several complications, such as bacterial superinfection, may occur (Monod et al., 2019). The causes of unsuccessful treatment also include the susceptibility of the patients, the growth patterns of the drug-resistant fungus, the presence of dormant fungal spores in the affected area, the low bioavailability of drugs, and poor drug penetration (Evans, 2001; Vora et al., 2014; Khamidah and Ervianti, 2018).

These problems have inspired researchers to study natural alternative therapies. Compared with synthetic antibacterial substances, natural plants contain rich biochemical active substances, have broad-spectrum antimicrobial activity, and have a lower toxicity to mammals and less impact on the environment. Drug resistance will not increase with the long-term use of these drugs, which is easy to be widely accepted by the public (Di Vito et al., 2021). On the other hand, the chemical composition of plant extracts determines their medicinal value, and the antibacterial properties largely depend on various factors such as the climatic and geographical conditions, as well as the harvesting, isolation technology, and storage (Helal et al., 2019).

Herbal medicine resources are widely distributed, which plays an important role in a country's healthcare system. The treatment of fungi with herbal medicine has become increasingly popular throughout the world. Schott (*Dryopteris fragrans*) is traditionally used in northern China to treat fungal infections and other skin diseases (Liu et al., 2018). The inhibitory effect predominantly on *T. rubrum* may be related to the synergistic or cumulative effect of the flavanols distributed on the leaf surface (Gomes et al., 2019). Japanese scholars have found that extracts from different solutions of 15 herbal medicines have an inhibitory effect on *T. rubrum* (Xia et al., 2019). Wu et al. (2008) found that plagiochin E (PLE), an antifungal macrocyclic bis(bibenzyl) isolated from *Rehmannia glutinosa*, affected the synthesis of chitin in the cell wall of *Candida albicans*. The extract of *Scutellaria baicalensis* Georgi, Ou-gong, has an obvious antifungal activity (Da et al., 2019). *Scutellaria barbata* has antibacterial and immunomodulatory effects and a low cytotoxic activity in healthy human bodies (Cordeiro et al., 2021). *Cnidium monnieri* (L.) has an inhibitory effect on *T. rubrum*, *Cryptococcus neoformans*, *Fusarium*, *C. albicans*, *Aspergillus*, and other clinically isolated pathogenic fungi (Jun et al., 2007; Lina et al., 2017).

Cnidium monnieri (L.) has a variety of pharmacological activities and a wide range of applications, so it has a high potential for researching and economic value. Coumarins, the main active components of Cnidii Rhizoma, experience a variety of biological activities, including anti-tumor (Shokoohinia et al., 2018), anti-inflammatory (Lee et al., 2014), antispasm (Sadraei et al., 2012), anti-virus (Tamura et al., 2010), and antifungal properties (Matsuda et al., 2002). In order to select effective traditional Chinese medicine preparations based on clinical trial information, Liu et al. (2012) used Chinese e-journal databases to search the relevant Chinese clinical study literature and concluded that *C. monnieri* (L.) should be preferably selected as one of the antifungal plant candidates since they were mostly consistently present in prescriptions or preparations used to treat mycotic vaginitis.

In China, *C. monnieri* (L.) is a compound commonly used with other traditional Chinese medicines such as *Sophora flavescens*, *Phellodendron amurense*, and camphor. Water decoction and tincture are used to treat intractable skin pruritus, eczema, and superficial fungal diseases through fumigation and wet compress. There are few studies on the antifungal mechanism of *C. monnieri* (L.). Previous studies (Wang et al., 2008; Zhao, 2016) showed that the minimum inhibitory concentration (MIC) value of aqueous extract of *C. monnieri* against *Trichophyton rubrum*, *C. albicans*, and *Malassezia* was approximately 5 mg/ml. It is reported that the extract of *C. monnieri* (L.) can enhance the inhibitory effect of macrophages on the *Candida* growth *in vitro* (Matsuda et al., 2002).

In this study, the aqueous extract was obtained directly from the rhizome of *C. monnieri* (L.), *Trichophyton rubrum*, the most common pathogenic fungus, selected for the research. The purpose of this study was to evaluate the inhibitory effect of the aqueous extract of *C. monnieri* (L.) on *T. rubrum*. Scanning electron microscopy (SEM) and transmission electron microscopy (TEM) technologies were used to observe the morphological changes of mycelium. We tried to further explore its antifungal mechanism from proteomics to provide effective targets for the drug research and development involved in treating dermatomycosis.

MATERIALS AND METHODS

Plant Material and Extraction

The aqueous extract of *C. monnieri* (L.) was prepared by decocting 500 g of the dried *C. monnieri* (L.) produced in Shandong Province (purchased from Shanghai Yanghetang Herbal Pieces Co., Ltd., Shanghai, China) with 5 L of boiling distilled water for 2 h, and then it was filtered using filter paper. The aqueous extract was collected in a rotary evaporator and lyophilized, which yielded 75 g of dried powder (yield ratio 15%), and it was stored at −20°C for further use.

TABLE 1 | Primer sequences of qRT-PCR amplification.

Accession number	Target gene primer sequences (5′-3′)	Amplification length (bp)
AB076024	CHS-F GATGACAGTCCGTCCACA CHS-R GATACAGACTTCAGGGTT	133
XM003235298	GAPDH-F ACGGCTTCGGTCGTATTGG GAPDH- R ATGTATTCGGCGATTTGGTCT	112

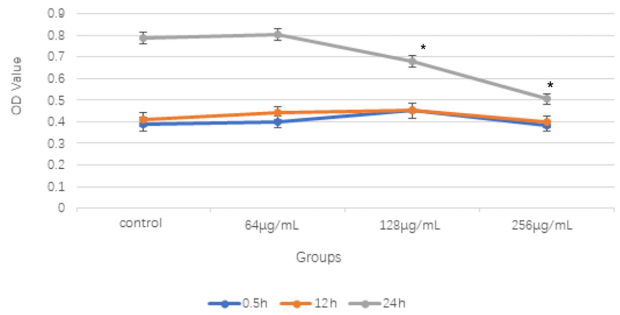

FIGURE 1 | Comparison of OD values of different concentrations of aqueous extract from *Cnidium monnieri* (L.) on *Trichoderma rubrum* in different time periods (x ± s) (*$P < 0.05$). 128 and 256 μg/mL concentrations of aqueous extract from *C. monnieri* (L.) were used to inhibit *T. rubrum* for 24 h, the OD value difference was statistically significant compared with the control group (*$P < 0.05$).

Preparation of Experimental Strains

Twenty strains were isolated from patients with dermatomycosis such as tinea manuum, tinea pedis, and onychomycosis. Then, fungal colonies were identified using a microscope and matrix-assisted laser desorption–time of flight mass spectrometry (MALDI-TOF MS). The isolated *T. rubrum* fungi were inoculated on potato dextrose agar (PDA) plates and cultured at 30°C for 7 days. The fungal suspensions were prepared according to the method of reference (Cao et al., 2020). The fungal suspensions with 0.5 Michaelis concentration were measured by an ultrasonic dispersion counter. The quality control strain was the *T. rubrum* ATCC28188, which was provided by Shanghai Changzheng Hospital.

Cytotoxicity Assays

The cell viability was determined using the Cell Count Kit-8 assay (CCK-8) (Beyotime Institute of Biotechnology, Shanghai, China). The effect of the aqueous extract of *C. monnieri* (L.) on the activity of *T. rubrum* was detected by the CCK-8. The experimental strains were divided into four groups. The dry powder of *C. monnieri* (L.) was adjusted to 64, 128, and 256 μg/ml concentrations, and *C. monnieri* (L.) aqueous extract was added using RPMI-1640 medium; and these were used as the three experimental groups. The fourth group was the control group and did not add any aqueous extract. In a 96-well cell culture plate, 100 μl of fungal suspension was added at the corresponding position, and 100 μl of the three groups with different *C. monnieri* aqueous extract concentrations was added. The control group was treated with 100 μl of fungal suspension and 100 μl of RPMI-1640 medium. Each sample was repeated three times. After incubation at 28°C for 0.5, 12, and 24 h, the samples were treated in strict accordance with the operation instructions of CCK-8 kit. Ten microliters of CCK-8 solution was added to each well and incubated for another 2 h to measure the cell viability. The optical density of the CCK-8 solution was measured at 450 nm in accordance with the kit instructions.

Observation of the Ultrastructural Changes of *Trichoderma rubrum* Affected by the Aqueous Extract of *Cnidium monnieri* (L.) Under Electron Microscope

One microliter of *T. rubrum* suspension with a McFarland turbidity of 0.5 was selected and seeded on two Sabouraud dextrose agar (SDA) plates (Shanghai Komajia Microbiology Technology Co., Ltd., Shanghai, China), and each plate was seeded with four spots. The colonies were grown at 28°C for 5 days. Two points were the control group (inoculated with 1 μl of fungal suspension, without any aqueous extract); the other two points will be 1 μl of fungal suspension and 256 μg/ml of aqueous extract of 10 μl, which were mixed and inoculated on SDA plates for 5 days. One plate was used for the electron microscope observation, and the other plate was used for the protein extraction. We selected the control group and the 256 μg/ml group as the observation objects. A small portion of the colony was placed in a sterile 1.5 ml centrifuge tube and fixed with 2.5% glutaraldehyde for 2 h at 4°C. And then after being rinsed with a phosphate-buffered solution three times for 20 min each time, the sample was soaked in 1% osmic acid solution for approximately 2 h at 4°C; dehydrated with 30, 50, 60, 70, 80, 90, 95, and 100% ethanol for 15 min in turn; and then thoroughly dehydrated with 100% ethanol twice for 10 min each time. The samples were dried at the critical point, vacuum coated, observed, and photographed under a SEM (Tecnai G220, FEI, Bionand, Malaga, Spain). After dehydration, the samples were embedded in an epoxy resin, and then ultrathin sections of the sample were sliced after solidification. The other samples were stained with uranium acetate and lead citrate; and they were observed, photographed, and recorded by TEM (Tecnai G220, FEI, Bionand, United States).

Extraction of the Fungal Protein

After 5 days of culture, the surface of each colony on the SDA plate (Shanghai Komajia Microbiology Technology Co.,

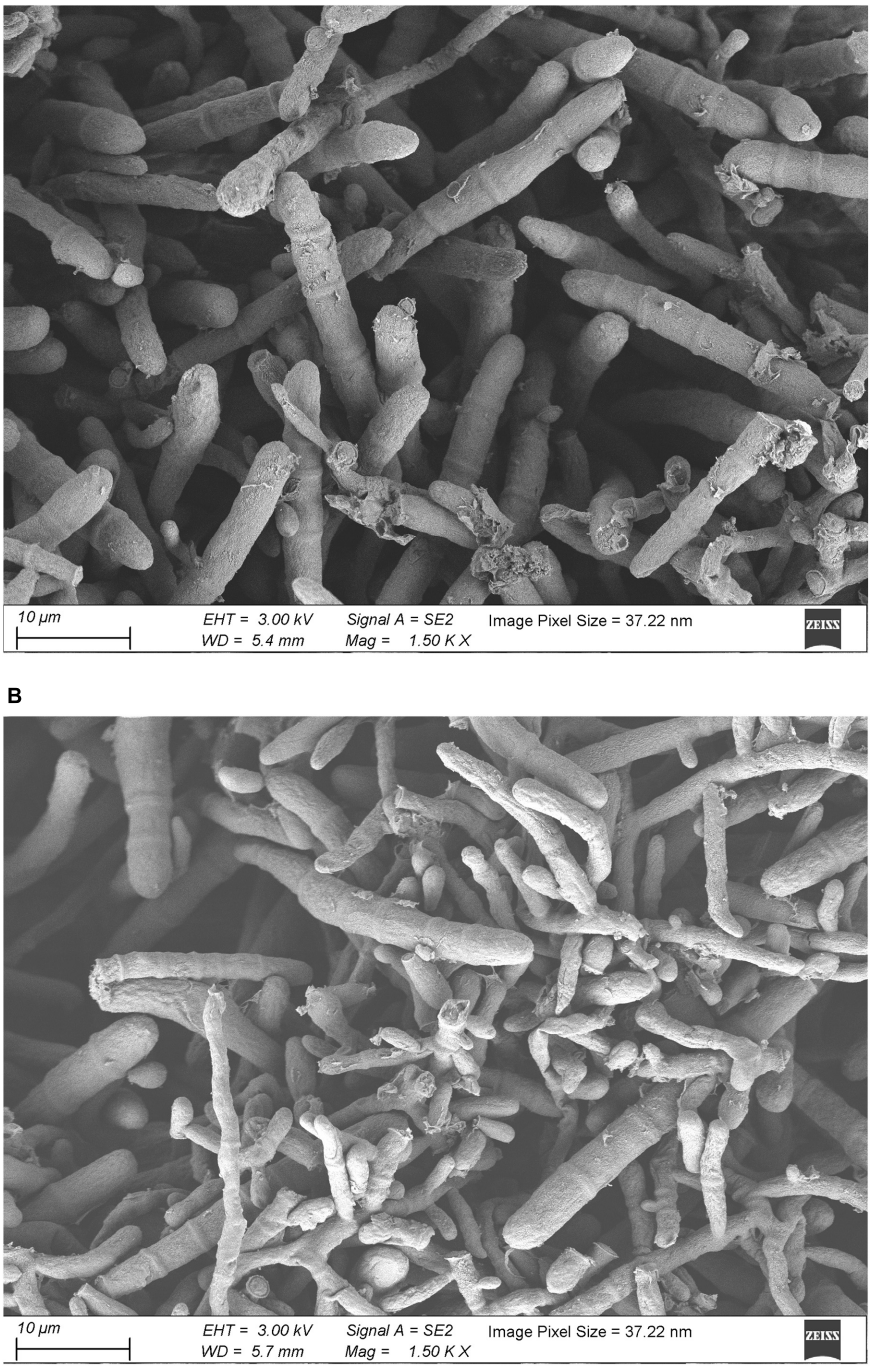

FIGURE 2 | Scanning electron microscopic images of *T. rubrum* of control group and 256 μg/mL group **(A)** control group; **(B)** 256 μg/mL group).

Ltd.) was gently scraped and centrifuged at 4°C and 3,000 rpm for 5–10 min to collect the fungi. The protein was extracted according to the requirements of the kit (BestBio, Shanghai, China; BB-3136). The fungal cells were washed twice with cold PBS, and the supernatant was drained as much as possible after each washing. A 100-mg sample of ground mycelium powder was put into 1 ml of lysate (20 mmol/L of Tris–HCl, pH 7.4, 150 mmol/L of NaCl, 1% NP40, 0.5% sodium hydroxide, 0.1% sodium dodecyl sulfate (SDS), 1 × Protease inhibitor mixture), and it was incubated on ice for 1 h. During this period, it was mixed upside down every 5 min. It was then centrifuged at 4°C for 30 min at 24,000 rpm.

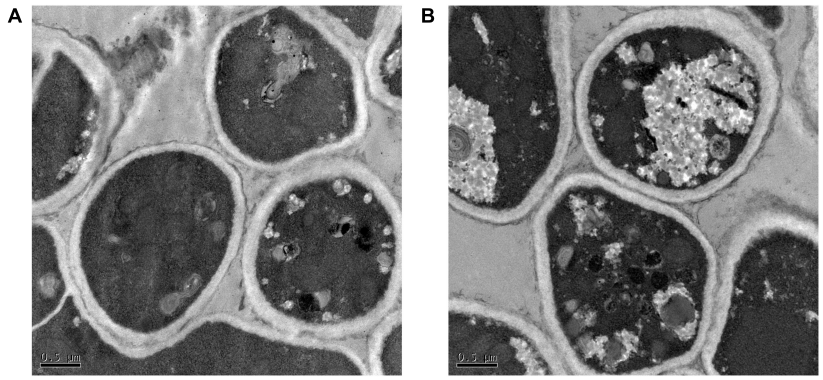

FIGURE 3 | Transmission electron microscopic images of *T. rubrum* of control group and 256 μg/mL group **(A)** control group; **(B)** 256 μg/mL group.

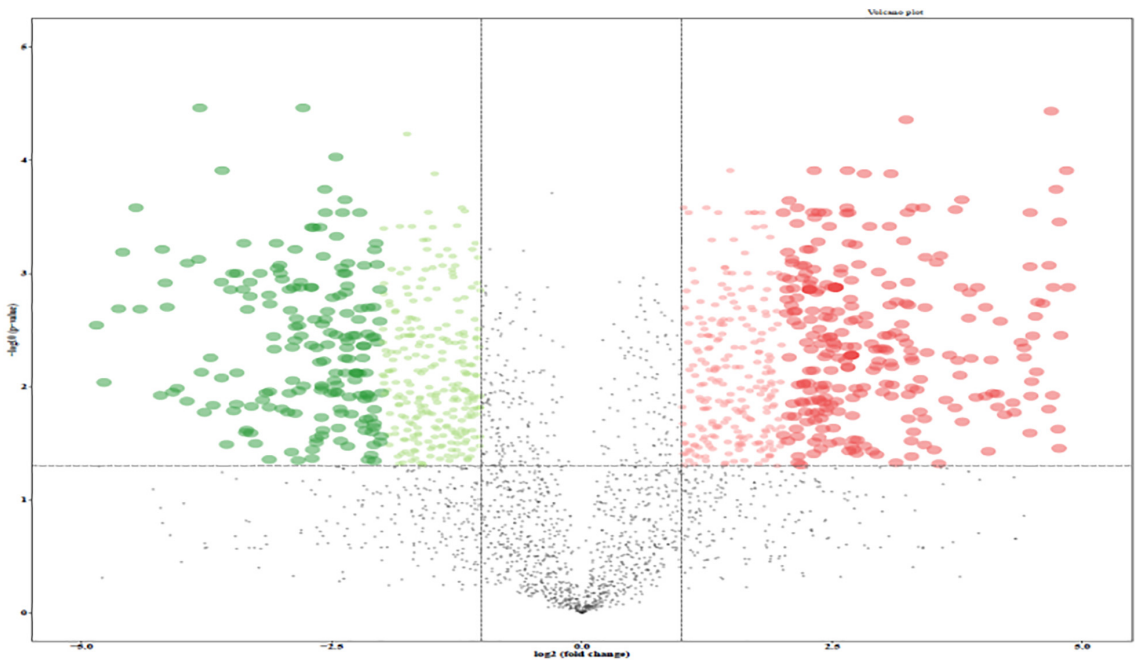

FIGURE 4 | Volcano plot of the differentially expressed genes (DEGs) between control group and 256 μg/mL group. Red dots, green dots, and black dots represent genes with significantly up-regulated expression, significantly down-regulated expression and non-significant difference, respectively.

Proteomics Mass Spectrometry Analysis

A total of 10 fungal protein samples were analyzed on a hybrid trapped ion mobility spectrometry (TIMS) quadrupole TOF MS (TIMS-TOF Pro, Bruker-Daltonics, Billerica, MA, United States) by CaptiveSpray nano spray ion source. The MS was used in the data correlation mode to generate a spectrum library with enhanced ion mobility. We set the cumulative time and the slope time to 100 ms and recorded the mass spectrum in the range of 100 to 1,700 m/z in the positive electrospray mode. The scanning range of the ion mobility was 0.7–1.3 Vs/cm^2. The whole acquisition cycle was 1.17 s, including a complete TIMS-MS scan and 10 parallel accumulation–serial fragmentation (PASEF) MS/MS scans. In the PASEF MS/MS scanning process, the collision energy increased linearly with the increase of mobility from 59 eV at 1/K0 = 1.6 Vs/cm ^{2} to 20 eV at 1/K0 = 0.6 Vs/cm^2.

RNA Isolation and cDNA Synthesis

Total RNA of *T. rubrum* was extracted from five samples of the 256 μg/ml group and five samples of the control group using the Rnaiso plus kit (Takara Bio, Shiga, Japan) according to the manufacturer's instructions. The concentration and purity of total RNA were assessed by ultramicro-spectrophotometers (NanoDrop 2000, Thermo Fisher Scientific, Wilmington, DE, United States) at the absorbance ratios of A260/230 and A260/280. Subsequently, the first strand of cDNA was synthesized from 2 μg of total RNA using the FastQuant RT Kit (with gDNase) (Takara Bio, Shiga, Japan) and was stored at −20°C.

TABLE 2 | The list of top 5 upregulation proteins between 256 μg/mL group and control group.

Accession	Gene symbol
A0A178F5P5_TRIRU	NADH-ubiquinone oxidoreductase
A0A178F853_TRIRU	40S ribosomal protein S6
A0A178F4E8_TRIRU	Cystathionine beta-synthase
A0A178ERV4_TRIRU	Coronin
A0A178EU95_TRIRU	Proteasome subunit alpha type

TABLE 3 | The list of top 5 down-regulation proteins between 256 μg/mL group and control group.

Accession	Gene symbol
O42708_TRIRU	Chitin synthase
A0A178ENR1_TRIRU	DLH domain-containing protein
A0A178EQZ5_TRIRU	Autophagy-related protein17
A0A178F1S3_TRIRU	Uncharacterized protein
A0A178EVQ6_TRIRU	Uncharacterized protein

Quantitative Real-Time PCR Detection

Finally, quantification of cDNA levels was carried out following the instructions of SYBR green fluorescence quantitative detection kit (Takara Bio, Shiga, Japan). The primer sequence and product size are shown in **Table 1**. The reaction process in this study was as follows: pre-denaturation at 94°C for 3 min, 36 repeated cycles for denaturation at 94°C for 30 s and 57°C for 30 s and elongation at 72°C for 1 min, and then maintained at 72°C for 10 min. The whole process of PCR amplification was automatically completed by machine (ABI 7500 Real Time PCR System, ABI, Foster City, CA, United States). The cycle threshold (Ct) value of the target gene (CHS) and internal gene (GAPDH) were obtained, and the relative expression differences for each of the sample were analyzed using the $2^{-\Delta\Delta CT}$ method (Schmittgen and Livak, 2008).

Detection of Chitin Synthase Antibody by Western Blotting

The protein of *T. rubrum* was extracted from the control group and the 256 μg/L experimental group by using the above method. The protein content was determined by a bicinchoninic acid (BCA) assay. The proteins were separated by SDS–polyacrylamide gel electrophoresis (PAGE) and then electro-transferred onto polyvinylidene fluoride membranes (Millipore, Billerica, MA, United States). The blocking solution (WB0161) was closed. Anti-CHS (orb242445, rabbit, 1:1,000 solution; Biorbyt, Cambridge, United Kingdom) was incubated overnight at 4°C, and the TBST solution was washed three times. Horseradish peroxidase (HRP)-conjugated antibody goat anti-rabbit IgG H&L (ab6721, 1:2,000; Abcam, Cambridge, MA, United States) was then incubated for 2 h, and the membrane was washed three times after exposure. The relative intensities of the protein bands were measured by the ImageJ image analysis software.

Statistical Analysis

All data were expressed as the mean ± standard deviation and statistically analyzed by SPSS 21.0 (SPSS Inc., IBM Corp., Armonk, NY, United States). The different groups of data were analyzed using the one-way analysis of variance (ANOVA), and the statistical test level was 0.05. According to the results of the homogeneity test of variance, the least significant difference (LSD) *t*-test was used to test the homogeneity of variance, while Tamhane's T2 test was used to test the heterogeneity of the variance. A $p < 0.05$ was considered statistically significant.

RESULTS

Antibacterial Activity of the Aqueous Extract of *Cnidium monnieri* (L.) With Different Concentrations Against *Trichoderma rubrum*

Three different concentrations at 64, 128, and 256 μg/ml of the aqueous extract of *C. monnieri* (L.) were co-cultured with *T. rubrum* for 0.5 and 12 h, and there was no significant difference compared with the results of the control group. However, when the three concentrations of the *C. monnieri* (L.) aqueous extract were used to inhibit *T. rubrum* for 24 h, the OD value decreased as the concentrations increased, and the difference was statistically significant compared with that of the control group (**Figure 1**).

Electron Microscopic Observations of the Structure of *Trichoderma rubrum* Incubated With Aqueous Extract From *Cnidium monnieri*

The results of SEM revealed that the control group mycelium had normal shape, a smooth surface, and a uniform thickness (**Figure 2A**); however, in the 256 μg/ml group, mycelium surface was rough, atrophied, and wrinkled and had different thickness and many damages, fractures, and holes (**Figure 2B**). Under the TEM, the cell wall of the fungi in the control group was relatively complete, the internal structure was clear, and mitochondria could be seen (**Figure 3A**). In the 256 μg/ml group, the cell wall was relatively complete, the internal structure had changed significantly, and a large number of structures were destroyed and dissolved (**Figure 3B**).

Proteomic Results

A total of 2,634 proteins of *T. rubrum* were identified in all samples. The differentially expressed proteins were screened on the criteria, as follows: fold change > 1.2-fold (upregulated > 1.2-fold or downregulated < 0.83-fold) and *p*-value < 0.05. A total of 966 differentially expressed proteins were detected, including 524 upregulated differentially expressed genes (DEGs) and 442 downregulated DEGs (**Figure 4**). The top five upregulated proteins are listed in **Table 2**, and the downregulated proteins are listed in **Table 3**. Then Gene Ontology (GO) and Kyoto Encyclopedia of Genes and Genomes (KEGG) enrichment

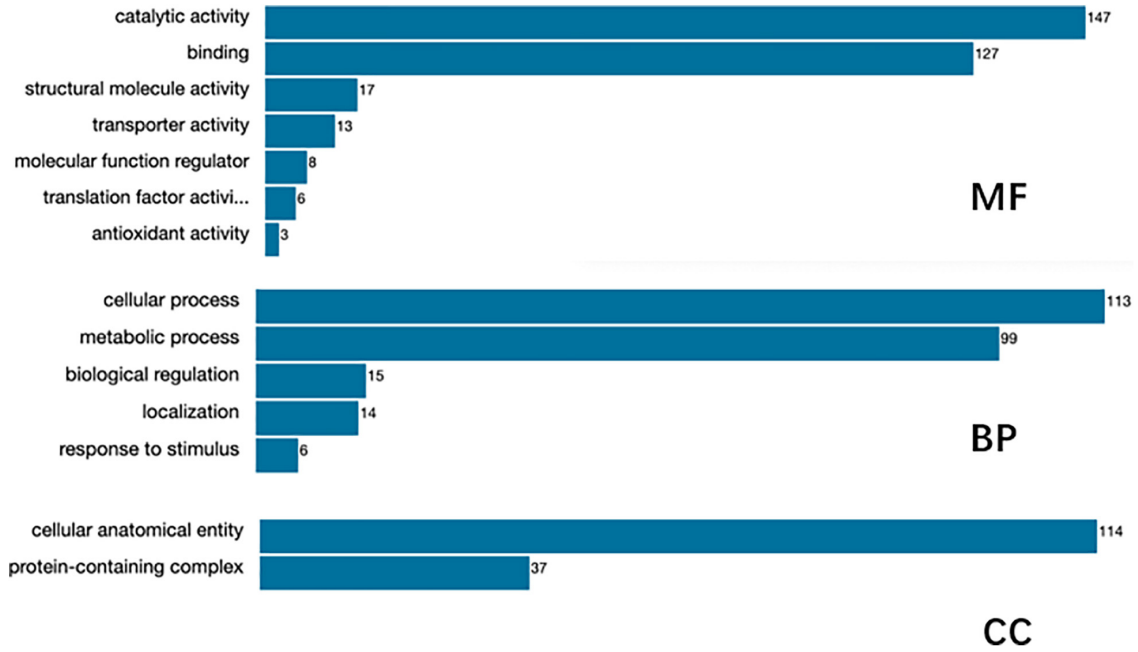

FIGURE 5 | Gene Ontology (GO) function annotation of the identified proteins.

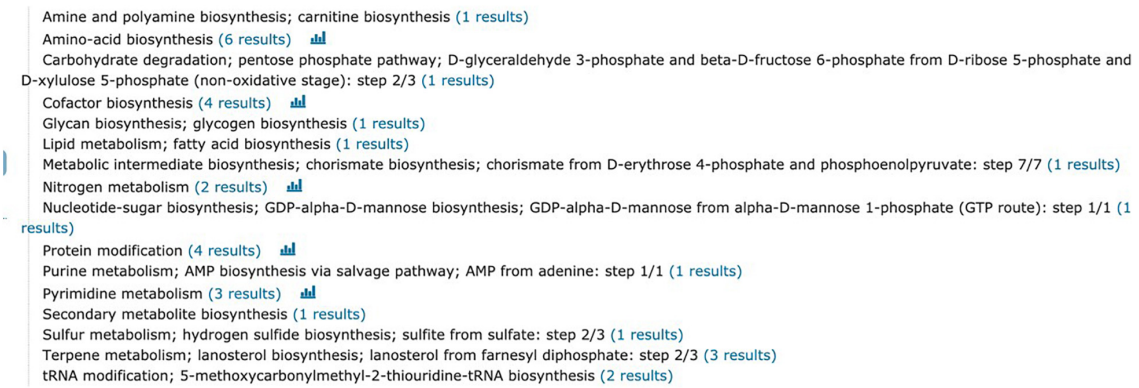

FIGURE 6 | Kyoto Encyclopedia of Genes and Genomes (KEGG) pathway analysis.

analyses were performed on the DEGs with significant difference (**Figures 5**, **6**).

Gene Ontology function annotation of the identified proteins was carried out by BLAST2GO software (**Figure 5**). The annotated candidate proteins are divided into three categories according to their functional characteristics: molecular function (MF), biological process (BP) and cellular component (CC). In the MF, catalytic activity (147 unigenes), binding (127 unigenes), structural molecule activity (17 unigenes), transporter activity (13 unigenes), MF regulator (8 unigenes), and translation factor activity (6 unigenes) were the most abundant groups. Those DEGs were mainly involved in function of the BP, such as cellular process (113 unigenes), metabolic process (99 unigenes), biological regulation (15 unigenes), localization (14 unigenes), and stress response (6 unigenes). The most abundant groups were the cell anatomic bodies and protein-containing complexes in the CC. Another GO category, significant enrichment analysis, was set by Fisher's exact test to visualize the GO functional annotations and enriched KEGG pathways (**Figure 6**), Some important BPs showed obvious changes, such as the amino acid biosynthesis, cofactor biosynthesis, protein modification, and pyrimidine metabolism.

mRNA and Protein Expression Levels of Chitin Synthase

The qRT-PCR results indicated that mRNA expression levels of chitin synthase (CHS) in the 256 μg/ml group were lower than those of the control group ($p < 0.05$; **Figure 7**). As shown in **Figure 8**, compared with that of the control group, the expression level of CHS was significantly downregulated in the 256 μg/ml group as detected by Western blotting ($p < 0.05$).

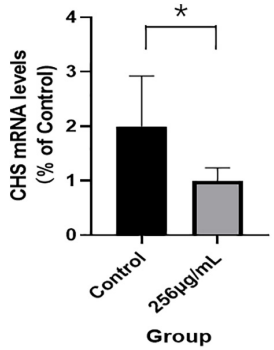

FIGURE 7 | The mRNA expression levels of chitin synthase detected by qRT-PCR (*$P < 0.05$).

DISCUSSION

Trichoderma rubrum is an important pathogen because it causes of most dermatomycosis and is becoming a public health problem, especially when affecting individuals with compromised immune systems (Tullio et al., 2016; Gamage et al., 2020). As an unconditioned pathogen, it is difficult to cure the infection of *T. rubrum*, and it often recurs after drug withdrawal (Kim et al., 2016). Completely removing *T. rubrum* and avoiding its recurrence have always been a difficult problem in treating its infection. At present, topical or oral antifungal drugs are mainly used in the treatment of *T. rubrum*. Existing drugs have their limitations, which include the limited drug types, side effects, and drug resistance. Therefore, there is an urgent need to develop new antifungal drugs with high efficiency, broad spectrum, and selective virulence. Traditional Chinese herbal medicine is rich in compound structure resources, which has become a very important research direction in the search for antifungal drugs with good safety, wide antifungal spectrum, and high efficacy.

Previous studies have shown that the alcohol extract of *C. monnieri* (L.) has a significant inhibitory effect on *T. rubrum*, and the antibacterial rate was enhanced as the drug concentration increased (Lina et al., 2017). In this study, the outcome of the CCK-8 showed that 128 and 256 μg/ml of aqueous extracts of *C. monnieri* (L.) were co-cultured with *T. rubrum* for 24 h, the inhibitory effect on *T. rubrum* was consistent with that of the alcohol extract of *Cnidium ninidium*, and the inhibitory rate was enhanced with the increase of concentration. The results showed that both the water and ethanol extracts of *C. ninidium* had inhibitory effects on *T. rubrum*. However, *Vernonia amygdalina*, *Caulerpa sertularioides*, and *Kappaphycus alvarezii* ethanol extract had an inhibitory effect on *T. rubrum*, and then the aqueous extraction had no obvious inhibition activities (Sit et al., 2018).

To further explore its antifungal mechanism, we selected the aqueous extract of *C. ninidium* with 256 μg/ml concentration and co-incubate it with *T. rubrum* for 5 days. It was observed that the surface of mycelia was rough, atrophied, and uneven in thickness and had multiple damages and fractures with SEM. TEM showed that the cell wall was slightly damaged, and a large number of the internal structures were destroyed and dissolved. This phenomenon indicates that the cell morphology could no longer be maintained and the cell became osmotic and fragile once the continuity of the cell wall was destroyed (Moore et al., 1992). A small damage in the cell wall can result in localized swelling, membrane rupture, and growth inhibition. The results of the SEM and TEM examinations confirmed that the aqueous extract of *C. monnieri* (L.) had a damaging effect on *T. rubrum*. Surprisingly, the results of MS screening of *T. rubrum* before and after the treatment of the drug solution showed that the most significantly downregulated protein was CHS. The mRNA and protein expression levels of CHS were inhibited in the 256 μg/ml group compared with the control group assessed by qRT-PCR and Western blotting.

Chitin synthase is a key enzyme in the chitin synthesis of fungal cell walls, and it is not only involved in the fungi growth and development, host infection, spore formation, and other processes but also closely related to the pathogenicity (Takeshita, 2020). Chitin is indispensable for the construction of the cell wall, and these molecules are usually deeply embedded into the cell wall structure, fixing other components to the cell surface (Brown et al., 2020). The process of *T. rubrum* infection involves the chitin enabling the growth of the fungus and grows hyphae into the toenail. The inhibition of CHS will reduce the proportion of chitin in the cell wall, and the damage to the cell wall and a decrease of electron density can be observed under TEM (Wu et al., 2008). However, our TEM results showed that the cell wall was slightly damaged and that the internal structure of the

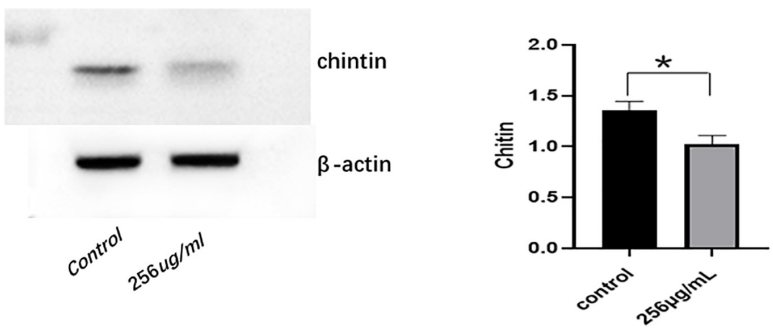

FIGURE 8 | The expression level of chitin synthase (CHS) protein detected by Western blot (*$P < 0.05$).

thallus was obviously damaged. It may be related to many factors such as culture conditions of the fungi, their growth activity, and biological activity of the drugs.

Because chitin is indispensable for the construction of the cell wall of fungi and mammalian cells do not have a cell wall, inhibition of chitin biosynthesis will not cause serious adverse reactions to the human body, which is also a strategy for the research and development of antifungal drugs (Lenardon et al., 2010). The results showed that aqueous extract of *C. monnieri* (L.) inhibited the activity of *T. rubrum*, and the expression of CHS was significantly downregulated. CHS might be one of the potential targets of its antifungal mechanism. The CHS gene affects the fungal growth, cell wall integrity, and toxicity to different extents (Qiu et al., 2021). Therefore, the aqueous extract of *C. monnieri* (L.) may be a potential candidate for safer antifungal agents.

In addition, when combined with common antifungals, natural compounds can minimize the side effects of the dose-related toxicity of these drugs (Zhang et al., 2014) and contribute to the treatment of drug-resistant strains (Ghelardi et al., 2014; Ghannoum, 2016; Danielli et al., 2018; Singh et al., 2018). Coumarin in *C. monnieri* (L.) has recently attracted much attention because it can be used as a common fragment to design new compounds with pharmacological activities (Mladenović et al., 2009; Kurdelas et al., 2010; Ge et al., 2016). For example, researchers have designed novel antifungal CHS inhibitors based on coumarins from *C. monnieri* (L.) that share a side chain with neomycin and polymyxin (Ge et al., 2016). We can also try to modify and transform the chemical structure of the *Cnidium* Cnidii monomer to improve the antimicrobial efficacy of traditional Chinese medicine monomer. In future research, we will continue to expand the sample size of the experiment, to investigate molecular biology technology to conduct more detailed studies on the factors involved in *C. monnieri* (L.) inhibition of *T. rubrum*, and to master the distribution and expression rules of its antimicrobial genes to provide effective targets for the research and development of related drugs.

CONCLUSION

The results showed that the aqueous extract of *C. monnieri* (L.) could destroy the morphology of mycelia and internal structure of *T. rubrum* and could inhibit the growth of *T. rubrum*. The antifungal effect of the aqueous extract of *C. monnieri* (L.) may be related to the downregulation of the expression of CHS in *T. rubrum*, and CHS may be one of the potential targets of its antifungal mechanism. We concluded that the water extract from *C. monnieri* (L.) may be a potential candidate for antifungal agents.

DATA AVAILABILITY STATEMENT

The raw data supporting the conclusions of this article will be made available by the authors, without undue reservation.

AUTHOR CONTRIBUTIONS

CY and WJ conceived and designed this study. CY, TY, KW, and ZH collected the data and wrote the manuscript. FH extracted the protein of fungal samples and detected the protein expression level by Western blot. XS, ZP, and WJ analyzed the data and interpreted the results. All authors read and approved the final manuscript and approved the submitted version.

FUNDING

This work was supported by the Project of Clinical Outstanding Clinical Discipline Construction in Shanghai Pudong New Area (No. PWYgy2018-07), Project of Shanghai Key Laboratory of Molecular Biology of Medical Fungi (No. E19-03), Project of Shanghai Municipality Key Medical Specialties Construction (No. ZK2019C08), and Leading Talent Training in Shanghai Pudong New Area Health System (No. PWRl2018-08).

REFERENCES

Brown, H. E., Esher, S. K., and Alspaugh, J. A. (2020). Chitin: a "Hidden Figure" in the fungal cell wall. *Curr. Top. Microbiol. Immunol.* 425, 83–111. doi: 10.1007/82_2019_184

Cao, Y., Xu, S., Kong, W., Xu, Y., and Fang, H. (2020). Clinical retrospective analysis of long-pulsed 1064-nm Nd:YAG laser in the treatment of onychomycosis and its effect on the ultrastructure of fungus pathogen. *Lasers Med. Sci.* 35, 429–437. doi: 10.1007/s10103-019-02840-2

Cordeiro, M. F., Nunes, T. R. S., Bezerra, F. G., Damasco, P. K. M., Silva, W. A. V., Ferreira, M. R. A., et al. (2021). Phytochemical characterization and biological activities of *Plectranthus barbatus* Andrews. *Braz. J. Biol.* 82:e236297. doi: 10.1590/1519-6984.236297

Da, X., Nishiyama, Y., Tie, D., Hein, K. Z., Yamamoto, O., and Morita, E. (2019). Antifungal activity and mechanism of action of Ougon (*Scutellaria* root extract) components against pathogenic fungi. *Sci. Rep.* 9:1683. doi: 10.1038/s41598-019-38916-w

Danielli, L. J., Pippi, B., Duarte, J. A., Maciel, A. J., Lopes, W., Machado, M. M., et al. (2018). Antifungal mechanism of action of *Schinus lentiscifolius* Marchand essential oil and its synergistic effect in vitro with terbinafine and ciclopirox against dermatophytes. *J. Pharm. Pharmacol.* 70, 1216–1227. doi: 10.1111/jphp.12949

Di Vito, M., Smolka, A., Proto, M. R., Barbanti, L., Gelmini, F., Napoli, E., et al. (2021). Is the antimicrobial activity of hydrolates lower than that of essential oils? *Antibiotics (Basel)* 10:88. doi: 10.3390/antibiotics10010088

Elewski, B. E., and Tosti, A. (2015). Risk factors and comorbidities for onychomycosis: implications for treatment with topical therapy. *J. Clin. Aesthet. Dermatol.* 8, 38–42.

Evans, E. G. (2001). The rationale for combination therapy. *Br J Dermatol.* 145(Suppl. 60), 9–13. doi: 10.1046/j.1365-2133.2001.145s60009.x

Gamage, H., Sivanesan, P., Hipler, U. C., Elsner, P., and Wiegand, C. (2020). Superficial fungal infections in the department of dermatology, University Hospital Jena: a 7-year retrospective study on 4556 samples from 2007 to 2013. *Mycoses* 63, 558–565. doi: 10.1111/myc.13077

Ge, Z., Ji, Q., Chen, C., Liao, Q., Wu, H., Liu, X., et al. (2016). Synthesis and biological evaluation of novel 3-substituted amino-4-hydroxylcoumarin derivatives as chitin synthase inhibitors and antifungal agents. *J. Enzym. Inhib. Med. Chem.* 31, 219–228. doi: 10.3109/14756366.2015.1016511

Ghannoum, M. (2016). Azole resistance in dermatophytes: prevalence and mechanism of action. *J. Am. Podiatr. Med. Assoc.* 106, 79–86. doi: 10.7547/14-109

Ghelardi, E., Celandroni, F., Gueye, S. A., Salvetti, S., Senesi, S., Bulgheroni, A., et al. (2014). Potential of ergos-terol synthesis inhibitors to cause resistance or cross-resistance in Tri-chophyton rubrum. *Antimicrob. Agents Chemother.* 58, 2825–2829. doi: 10.1128/AAC.02382-13

Gomes, N. G. M., Oliveira, A. P., Cunha, D., Pereira, D. M., Valentão, P., Pinto, E., et al. (2019). Flavonoid composition of *Salacia senegalensis* (Lam.) DC. leaves, evaluation of antidermatophytic effects,and potential amelioration of the associated inflammatory response. *Molecules* 24:2530. doi: 10.3390/molecules24142530

Hadrich, I., and Ayadi, A. (2018). Epidemiology of antifungal susceptibility: review of literature. *J. Mycol. Med.* 28, 574–584. doi: 10.1016/j.mycmed.2018.04.011

Helal, I. M., El-Bessoumy, A., Al-Bataineh, E., Joseph, M. R. P., Rajagopalan, P., Chandramoorthy, H. C., et al. (2019). Antimicrobial efficiency of essential oils from traditional medicinal plants of Asir Region, Saudi Arabia, over drug resistant isolates. *Biomed Res. Int.* 2019:8928306. doi: 10.1155/2019/8928306

Jun, Y., Jin, S. X., and Li, W. (2007). Antifungal effects of eight kinds of traditional Chinese medicine in vitro. *Acad. J. PLA Postgrad. Med. Sch.* 28, 299–300.

Khamidah, N., and Ervianti, E. (2018). Combination antifungal therapy for onychomycosis. *Indones. J. Trop. Infect. Dis.* 7, 15–20.

Kim, S. H., Jo, I. H., Kang, J., Joo, S. Y., and Choi, J. H. (2016). Dermatophyte abscesses caused by *Trichophyton rubrum* in a patient without pre-existing superficial dermatophytosis: a case report. *BMC Infect. Dis.* 16:298. doi: 10.1186/s12879-016-1631-y

Kurdelas, R. R., Lima, B., Tapia, A., Feresin, G. E., Gonzalez Sierra, M., Rodríguez, M. V., et al. (2010). Antifungal activity of extracts and prenylated coumarins isolated from *Baccharis darwinii* Hook & Arn. (Asteraceae). *Molecules* 15, 4898–4907. doi: 10.3390/molecules15074898

Lee, T. H., Chen, Y. C., Hwang, T. L., Shu, C. W., Sung, P. J., Lim, Y. P., et al. (2014). New coumarins and anti-inflammatory constituents from the fruits of *Cnidium monnieri*. *Int. J. Mol. Sci.* 15, 9566–9578. doi: 10.3390/ijms15069566

Lenardon, M. D., Munro, C. A., and Gow, N. A. (2010). Chitin synthesis and fungal pathogenesis. *Curr. Opin. Microbiol.* 13, 416–423. doi: 10.1016/j.mib.2010.05.002

Lina, W., Yan, Z., Yongcan, Z., and Honglan, W. (2017). Mechanisms of the inhibition of *Cnidium monnieri* (L.) cuss to *Trichophyton rubrum* based on heat shock protein. *J. Clin. Pathol. Res.* 37, 908–911. doi: 10.3978/j.issn.2095-6959.2017.05.006

Liu, Q., Luyten, W., Pellens, K., Wang, Y., Wang, W., Thevissen, K., et al. (2012). Antifungal activity in plants from Chinese traditional and folk medicine. *J. Ethnopharmacol.* 143, 772–778. doi: 10.1016/j.jep.2012.06.019

Liu, X., Liu, J., Jiang, T., Zhang, L., Huang, Y., Wan, J., et al. (2018). Analysis of chemical composition and in vitro antidermatophyte activity of ethanol extracts of *Dryopteris fragrans* (L.) Schott. *J, Ethnopharmacol.* 226, 36–43. doi: 10.1016/j.jep.2018.07.030

Matsuda, H., Tomohiro, N., Ido, Y., and Kubo, M. (2002). Anti-allergic effects of cnidii monnieri fructus (dried fruits of *Cnidium monnieri*) and its major component, osthol. *Biol. Pharm. Bull.* 25, 809–812. doi: 10.1248/bpb.25.809

Mladenović, M., Vuković, N., Nićiforović, N., Sukdolak, S., and Solujić, S. (2009). Synthesis and molecular descriptor characterization of novel 4-hydroxy-chromene- 2-one derivatives as antimicrobial agents. *Molecules* 14, 1495–1512. doi: 10.3390/molecules14041495

Monod, M., Feuermann, M., Salamin, K., Fratti, M., Makino, M., Alshahni, M. M., et al. (2019). Trichophyton rubrum azole resistance ediated by a new ABC transporter, TruMDR3. *Antimicrob. Agents Chemother.* 63:e00863-19. doi: 10.1128/AAC.00863-19

Moore, C. W., Del Valle, R., McKoy, J., Pramanik, A., and Gordon, R. E. (1992). Lesions and preferential initial localization of [s-methyl-3H] bleomycin A2 on *Saccharomyces cerevisiae* cell walls and membranes. *Antimicrob. Agents Chemother.* 36, 497–505. doi: 10.1128/aac.36.11.2497

Nenoff, P., Kruger, C., Ginter-Hanselmayer, G., and Tietz, H. J. (2014). Mycology-an update. Part 1: dermatomycoses: causative agents, epidemiology and pathogenesis. *J. Dtsch. Dermatol. Ges.* 12, 188–209. doi: 10.1111/ddg.12245

Qiu, L., Zhang, J., Song, J. Z., Hu, S. J., Zhang, T. S., Li, Z., et al. (2021). Involvement of BbTpc1, an important Zn(II)2Cys6transcriptional regulator, in chitin biosynthesis, fungal development and virulence of an insect mycopathogen. *Int. J. Biol. Macromol.* 166, 1162–1172. doi: 10.1016/j.ijbiomac.2020.10.271

Rouzaud, C., Hay, R., Chosidow, O., Dupin, N., Puel, A., Lortholary, O., et al. (2015). Severe dermatophytosis and acquired orinnate immunodeficiency: a review. *J. Fungi (Basel)* 2:4. doi: 10.3390/jof2010004

Sadraei, H., Shokoohinia, Y., Sajjadi, S., and Ghadirian, B. (2012). Antispasmodic effect of osthole and *Prangos ferulacea* extract on rat uterus smooth muscle motility. *Res. Pharm. Sci.* 7, 141–149.

Schmittgen, T. D., and Livak, K. J. (2008). Analyzing real-time PCR data by the comparative CT method. *Nat. Protoc.* 3, 1101–1108. doi: 10.1038/nprot.2008.73

Seebacher, C., Bouchara, J.-P., and Mignon, B. (2008). Updates on the epidemiology of dermatophyte infections. *Mycopathologia* 166, 335–352. doi: 10.1007/s11046-008-9100-9

Shokoohinia, Y., Jafari, F., Mohammadi, Z., Bazvandi, L., Hosseinzadeh, L., Chow, N., et al. (2018). Potential anticancer properties of osthol: a comprehensive mechanistic review. *Nutrients* 10:36. doi: 10.3390/nu10010036

Singh, A., Masih, A., Khurana, A., Singh, P. K., Gupta, M., Hagen, F., et al. (2018). High terbinafine resis-tance in *Trichophyton interdigitale* isolates in Delhi, India harbouring mutations in the squalene epoxidase gene. *Mycoses* 61, 477–484. doi: 10.1111/myc.12772

Sit, N. W., Chan, Y. S., Lai, S. C., Lim, L. N., Looi, G. T., Tay, P. L., et al. (2018). In vitro antidermatophytic activity and cytotoxicity of extracts derived from medicinal plants and marine algae. *J. Mycol. Med.* 28, 561–567. doi: 10.1016/j.mycmed.2018.07.001

Takeshita, N. (2020). Control of actin and calcium for chitin synthase delivery to the hyphal tip of *Aspergillus*. *Curr. Top. Microbiol. Immunol.* 425, 113–129. doi: 10.1007/82_2019_193

Tamura, S., Fujitani, T., Kaneko, M., and Murakami, N. (2010). Prenylcoumarin with rev-export inhibitory activity from cnidii monnieris fructus. *Bioorg. Med. Chem. Lett.* 20, 3717–3720. doi: 10.1016/j.bmcl.2010.04.081

Tullio, V., Cervetti, O., Roana, J., Panzone, M., Scalas, D., Merlino, C., et al. (2016). Advances in microbiology, infectious diseases and public health: refractory *Trichophyton rubrum* infections in Turin, Italy: a problem still present. *Adv. Exp. Med. Biol.* 901, 17–23. doi: 10.1007/5584_2015_5012

Vora, D., Bharti, B., Solanki, P., Kothari, A., and Meher, K. (2014). A study to compare efficacy of various oral antifungals (Fluconazole, Terbinafine, Itraconazole) in treatment of Onychomycosis. *J. Res. Med. Dent. Sci.* 2, 49–52.

Wang, L., Xue-lian, L. V., Sun., L., Shen, Y. N., and Liu, W. D. (2008). Studies on antifungal activity of extracts from six traditional chinese medicine against dermatophy genes. *Chin. J. Derm. Venereol.* 22, 498–500.

Wu, X. Z., Cheng, A. X., Sun, L. M., and Lou, H. X. (2008). Effect of plagiochin E, an antifungal macrocyclic bis(bibenzyl), on cell wall chitin synthesis in *Candida albicans*. *Acta Pharmacol. Sin.* 29, 1478–1485. doi: 10.1111/j.1745-7254.2008.00900.x

Xia, D. A., Duerna, T., Murata, S., and Morita, E. (2019). In vitro antifungal activity of japanese folk herb extracts against *Trichophyton rubrum*. *Biocontrol Sci.* 24, 109–116. doi: 10.4265/bio.24.109

Zhan, P., and Liu, W. (2017). The changing face of dermatophytic infections worldwide. *Mycopathologia* 182, 77–86. doi: 10.1007/s11046-016-0082-8

Zhang, A., Sun, H., and Wang, X. (2014). Potentiating therapeutic effects by enhancing synergism based on active constituents from traditional medicine. *Phytother. Res.* 28, 526–533. doi: 10.1002/ptr.5032

Zhao, H. (2016). Antifungal activity of extracts from Chinese herbal medicines against Yeast. *Chin. J. Trauma Disabil. Med.* 24, 31–32. doi: 10.1016/j.phymed.2019.152884

Conflict of Interest: The authors declare that the research was conducted in the absence of any commercial or financial relationships that could be construed as a potential conflict of interest.

Publisher's Note: All claims expressed in this article are solely those of the authors and do not necessarily represent those of their affiliated organizations, or those of the publisher, the editors and the reviewers. Any product that may be evaluated in this article, or claim that may be made by its manufacturer, is not guaranteed or endorsed by the publisher.

frontiers in Microbiology

ORIGINAL RESEARCH
published: 24 August 2021
doi: 10.3389/fmicb.2021.651221

Transcription Factors of CAT1, EFG1, and BCR1 Are Effective in Persister Cells of *Candida albicans*-Associated HIV-Positive and Chemotherapy Patients

Elham Aboualigalehdari[1†], Maryam Tahmasebi Birgani[2,3†], Mahnaz Fatahinia[4†] and Mehran Hosseinzadeh[5†]*

[1] Department of Medical Mycology, School of Medicine, Ahvaz Jundishapur University of Medical Sciences, Ahvaz, Iran, [2] Department of Medical Genetics, School of Medicine, Ahvaz Jundishapur University of Medical Sciences, Ahvaz, Iran, [3] Cellular and Molecular Research Center, Medical Basic Sciences Research Institute, Ahvaz Jundishapur University of Medical Sciences, Ahvaz, Iran, [4] Infectious and Tropical Diseases Research Center, Health Research Institute and Department of Medical Mycology, School of Medicine, Ahvaz Jundishapur University of Medical Sciences, Ahvaz, Iran, [5] Thalassemia and Hemoglobinopathy Research Center, Health Research Institute, Ahvaz Jundishapur University of Medical Sciences, Ahvaz, Iran

Background: Biofilm is an accumulation of cells, which are formed on mucosal surfaces of the host as well as on medical devices. The inherent resistance of *Candida* strains producing biofilms to antimicrobial agents is an important and key feature for biofilm growth, which can lead to treatment failure. This resistance is due to the regulatory increase of the output pumps, the presence of extracellular matrix, and the existence of persister cells. Persister cells are phenotypic variants that have MICs similar to antibiotic-sensitive populations and are able to tolerate high doses of antibiotics. The current study investigated the possible role of *EFG1, BCR1*, and *CAT1* in the establishment or maintenance of persister cells in *Candida albicans* strains that produce biofilms.

Methods: After identifying *Candida* isolates by molecular methods, *C. albicans* isolates were confirmed by sequencing. Isolation of persister cells and determination of their MIC were performed by microdilution method. Then, RNA extraction and cDNA synthesis were performed from 60 *C. albicans* isolates under promoting and inducing conditions. Afterward, the mean expression of *BCR1, EFG1*, and *CAT1* genes in both persister and non-persister groups was calculated using real-time qPCR. Phylogeny tree of persister and non-persister group isolates was drawn using ITS fragment.

Results: A total of 77 persister isolates were taken from the oral cavity of HIV patients as well as from patients undergoing chemotherapy. Biofilm intensity in persister isolates separated from HIV-infected patients was different from the non-persister group. The mean fold change of *BCR1* (10.73), *CAT1* (15.34), and *EFG1* (2.41) genes in persister isolates was significantly higher than these genes in isolates without persister.

OPEN ACCESS

Edited by:
Miguel Cacho Teixeira, University of Lisbon, Portugal

Reviewed by:
Maryam Roudbary, Iran University of Medical Sciences, Iran
Jing Shao, Anhui University of Chinese Medicine, China

***Correspondence:**
Mahnaz Fatahinia
fatahinia@yahoo.com

†ORCID:
Elham Aboualigalehdari
orcid.org/0000-0002-2517-8847
Maryam Tahmasebi Birgani
orcid.org/0000-0002-9624-1903
Mahnaz Fatahinia
orcid.org/0000-0001-6898-1309
Mehran Hosseinzadeh
orcid.org/0000-0002-9761-3713

Specialty section:
This article was submitted to Antimicrobials, Resistance and Chemotherapy, a section of the journal Frontiers in Microbiology

Received: *08 January 2021*
Accepted: *06 July 2021*
Published: *24 August 2021*

Citation:
Aboualigalehdari E, Tahmasebi Birgani M, Fatahinia M and Hosseinzadeh M (2021) Transcription Factors of CAT1, EFG1, and BCR1 Are Effective in Persister Cells of Candida albicans-Associated HIV-Positive and Chemotherapy Patients. Front. Microbiol. 12:651221. doi: 10.3389/fmicb.2021.651221

Conclusion: It can be concluded that the most important factor in the production of persister cells is biofilm binding and production, not biofilm development or mature biofilm production, which was found in the expression of *BCR1* gene without change in the expression of *EFG1* gene in the persister group. Also, catalase plays an essential role in the production of persister in *C. albicans* biofilm producers with ROS detoxification.

Keywords: oral candidiasis, persister cells, biofilm, HIV patients, patients under chemotherapy, *BCR1, EFG1, CAT1*

INTRODUCTION

Oral candidiasis is known as the most common fungal infection. It is an opportunistic disease among humans, especially in patients undergoing chemotherapy, transplant recipients, and HIV patients. Aging, uncontrolled diabetes mellitus, broad-spectrum antibiotics, corticosteroid, and/or immunosuppressant drug use are predisposing factors for this disease. It acts also as a prognostic marker for systemic diseases such as diabetes mellitus and a common problem in immunocompromised patients such as HIV patients and those undergoing chemotherapy (Aboualigalehdari et al., 2013, 2020; Taff et al., 2013; Cavalheiro and Teixeira, 2018; Putranti et al., 2018).

Studies have indicated that this disease occurs in about 80–90% of HIV-positive patients and also in 7–52% of patients undergoing chemotherapy. This infection is often detected in these patients in chronic and recurrent forms, especially in HIV-positive patients and leads to esophageal candidiasis and subsequent difficulty in digesting and swallowing (Jayachandran et al., 2016; Patil et al., 2018).

Candida albicans is the most important causative agent of oral candidiasis as well as an opportunistic organism that exists as normal microflora on the skin and mucous membranes of the body. This organism causes superficial to systemic infections, and the mortality rate due to infections caused by this organism is reported to be 40%. The prevalence of *C. albicans* isolated orally from patients with leukemia undergoing chemotherapy is about 46.2%, and in AIDS patients, it has been reported to be 37.2–95.2% (Piekarska et al., 2008; Li et al., 2015; Patil et al., 2018; Wuyts et al., 2018).

One of the important features in the pathogenicity of *C. albicans* is its ability to adhere and subsequently form a biofilm on biotic and abiotic surfaces such as mucosal surfaces as well as implanted medical devices. Biofilm formation is among the factors of resistance to antifungal drugs, which leads to treatment failure and disease recurrence. Several phenomena are implicated in biofilm resistance, including increased metabolic activity, production of extracellular biofilm matrix, cell density, upregulation of drug efflux pumps, persister cells, and stress responses (Piekarska et al., 2008; Li et al., 2015; Wuyts et al., 2018; Galdiero et al., 2020).

Another problem is the failure in the treatment of *C. albicans* infection leading to chronic infections. Recently, persister cells have attracted attention as a reason for drug tolerance in *C. albicans*. Persister cells are a special phenotypic type of biofilm population making up a small part of the biofilm population, which are capable of tolerating high doses of anti-fungal therapy. Thus, when a population of persister cells is exposed to a high dose of anti-fungal drugs, a small number of these cells survive, and interestingly, if they are re-cultured and re-exposed to a high dose of anti-fungal drugs, the fungi show a similar reaction. To our knowledge, many studies have indicated failure of anti-fungal drugs in *C. albicans*, which could be due to the presence of persister cells (Clinical and Laboratory Standards Institute [CLSI], 2008; Silva et al., 2012; Maheronnaghsh et al., 2020). For this purpose, this study was performed on fungal pathogens that had MIC associated with amphotericin B-sensitive populations and were exposed to very high doses of amphotericin B. The aim of this study was to better understand fungal persister cells for comparing biofilm intensity and expression of genes involved in biofilm production pathway (*BCR1* and *EFG1*) as well as oxidative stress response pathway (*CAT1*) in persister cells of *C. albicans* isolates taken from patients with HIV who underwent chemotherapy.

MATERIALS AND METHODS

In this study, 201 HIV patients and 200 cancer patients undergoing chemotherapy satisfying baseline criteria were studied with ethical code# IR.AJUMS.REC.1397.894.

Inclusion Criteria

1. Samples were isolated from patients who had one of the following symptoms: Patients who had inflamed lesions in the oral mucosa and on the tongue with red flakes, those who had a false white membrane in their oral cavity or creamy to white plaques, and patients whose sense of taste had changed or had dry mouth.
2. After culturing the oral swab on CHROMagar^{TM} *Candida* media, the number of colonies was counted and the grown samples were entered into the project with $\geq$ 10 colonies as patients colonized with *Candida* (Erköse and Erturan, 2007).
3. Confirmation of *C. albicans* samples was molecular and macroscopic.
4. Insertion of persister *C. albicans* isolates with MIC related to amphotericin B-sensitive population (MIC $<$ 2 μg/ml) as well as non-persister *C. albicans* (Clinical and Laboratory Standards Institute [CLSI], 2008; Maheronnaghsh et al., 2020).

Sample Collection and Phenotypic Identification

The samples taken from the patients were transferred to the Department of Medical Mycology, School of Medicine, Ahvaz Jundishapur University of Medical Sciences, Ahvaz, Iran. Then, the samples were cultured on CHROMagar™ *Candida* media (CHROMagar™, Pioneer, Paris, France) and incubated at 35°C for 48–72 h. In the next step, the grown clinical isolates were compared and identified in terms of colony color based on the desired culture medium brochure and standard samples. Then, the culture medium was examined for colony diversity and the colonies were counted based on colony-forming unit/swab. After that, the isolates were purified on Sabouraud Dextrose Agar + Chloramphenicol (SC) (Liofilchem, Italy). The medium and the isolates were transferred to microtubes containing sterile distilled water for long-term storage (6 months) at two temperatures: 30°C and room temperature.

DNA Extraction

The genomic DNA was directly extracted by boiling method (Yamada et al., 2002; Silva et al., 2012).

PCR-RFLP, Sequencing, and Duplex PCR

To confirm the isolates as *C. albicans*, PCR-RFLP, sequencing, and duplex PCR were performed. The primers for PCR-RFLP are listed in **Table 1**, and the enzyme for PCR-RFLP was *Msp*I. Sequencing was done after PCR of V9g and LS266 area as shown in **Table 1**.

Biofilm Formation Assay

Biofilm production was performed on RPMI 1640 medium. All isolates were cultured in Sabouraud Dextrose Broth and incubated in a shaker incubator at 30°C for 24 h. After 24 h, the grown colonies were washed twice with sterile phosphate buffer solution (1× PBS) (pH 7.4) (Sigma-Aldrich) and centrifuged at 6063 rpm for 3 min at 4°C (SIGMA 1-15PK). Then, a yeast suspension was prepared from colonies with a concentration of 10^6 cfu/ml in RPMI 1640 medium. Subsequently, in each well of flat bottom 96 microplates, 200 μl of suspension was poured in the wells. Culture medium was considered as the negative control and culture medium plus yeast suspension was the positive control. The microplates were placed at 37°C for 48 h. After this period, the culture medium in each well was emptied, and the wells were washed three times with sterile PBS. The microplates were then inverted at room temperature for an hour to dry. One hundred microliters of 0.1% crystal violet solution was added to each well and the microplate was placed at 37°C for 15 min without moving. Then, it was removed from the wells and washed again with sterile PBS, and the microplates were dried at room temperature. In the next step, 100 μl of 96% ethanol was poured into each well and the microplate was gently shaken in a circle by hand to extract the crystal violet color bound to the yeasts forming the biofilm faster. Then, the optical density (OD) of this solution was measured at 595 nm with a microplate reader (BioTek, Elx808). Finally, the biofilms were classified using the following formula (Abraham et al., 2020; El-Baz et al., 2021):

No biofilm: Absorbance $\leq$ Absorbance Control

Weak biofilm: $Ac < A \leq (2 \times Ac)$

Moderate biofilm: $(2 \times Ac) < A \leq (4 \times Ac)$

Strong biofilm: $(4 \times Ac) < A$

The isolates were grouped based on OD value. The isolates with low biofilm formation (LBF) were classified as first quarter (Q1); those with greater OD values were defined in the third quarter, which had high biofilm formation (HBF) (Q3), and the isolates with OD values between the first and third quarters were classified as second quarter and possessed intermediate biofilm formation (IBF) (Q2) (Li et al., 2018).

Persister Cell Assay

All the isolates were cultured on Sabouraud Dextrose Broth and incubated in a shaker incubator at 30°C for 24 h. After this time, the grown colonies were washed twice with sterile PBS and centrifuged at 6063 rpm for 3 min at 4°C. A yeast suspension with a concentration of 10^6 cfu/ml was subsequently prepared from colonies in RPMI 1640 medium. One hundred microliters of the prepared yeast suspension was added to each well of 96-well flat bottom microplate, which was placed at 37°C for 4 h. After this period, the culture medium in each well was discarded and washed with PBS, 100 μl of RPMI1640 culture medium was added to the wells and incubated for 24 h at 37°C. The culture medium in each well was emptied, and 200 μl of amphotericin B (Sigma Aldrich-USA) diluted with RPMI1640 with a concentration of 100 μg/ml (Moazeni et al., 2014; De Brucker et al., 2016; Alonso et al., 2018) was added to the wells and placed at 37°C for 48 h, after which the contents of each well were discarded and washed once with 100 μl of PBS. After washing, 100 μl of PBS was added to each well and

TABLE 1 | Primers for PCR-RFLP, sequencing, and duplex PCR.

Genes	5′ to 3′	Method	References
ITS1	Forward: TCC GTA GGT GAA CCT TGC GG	PCR-RFLP	Abraham et al., 2020
ITS4	Reverse: TCC TCC GCT TAT TGA TAT GC	PCR-RFLP	Abraham et al., 2020
CAL	Forward: TGGTAAGGCGGGATCGCTT	duplex PCR	El-Baz et al., 2021
	Reverse: GGTCAAAGTTTGAAGATATAC		
CDU	Forward: AACTTGTCACGAGATTATTTTT	duplex PCR	El-Baz et al., 2021
	Reverse: AAAGTTTGAAGAATAAAATGGC		
V9g	Forward: TTACGTCCCTGCCCTT TGTA	PCR	Li et al., 2018
LS266	Reverse: GCATT CCCAAACAACTCGACTC	PCR	Li et al., 2018

homogenized using a sterile pipette. Twenty microliters from each well was serially diluted in 1:10 ratio in 10 dilutions of PBS. After dilution, 50 μl of each well was harvested and cultured on yeast peptone dextrose agar or YPD medium (Liofilchem, Italy). The plates were kept in an incubator at 48°C for 48–72 h. The plates were examined for colony count after 48 h and the samples were reported in three categories: high persister, low persister, and non-persister (LaFleur et al., 2006, 2010). Finally, samples containing persister cells were examined for MIC determination of amphotericin B according to CLSI M27-S4 guidelines, and if they were sensitive to the population with MIC < 2 μg/ml, the samples were confirmed as persister isolates (Clinical and Laboratory Standards Institute [CLSI], 2008; Maheronnaghsh et al., 2020).

Evaluation of the Genes Responsible for Biofilm Formation and Oxidative Stress Among Isolates Producing Persister Cells

To determine the maximum and minimum survival rates, the isolates were ranked from highest to lowest based on their survival rates against amphotericin and then the first 15 isolates with the highest survival rates were specified as the persister group and the last 15 isolates not showing survival were chosen as those without persister or non-persister group. There were a total of 30 isolates in these two groups. Evaluation of *BCR1, EFG1,* and *CAT1* gene expression was performed in 30 *C. albicans* isolates by the real-time qPCR method. Real-time qPCR was done on isolates that were under inducing and promoting conditions.

Inducing conditions were applied for isolates in the state of biofilm production while promoting conditions were meant for isolates in the normal condition, and RNA was extracted from these isolates. In other words, the promoting conditions are the conditions before the formation of biofilm, and the inducing conditions are those after the formation of biofilm. Promoting conditions mean the alteration in expression of genes that cause biofilms and inducing conditions are changing the expression of genes causing biofilm formation to give specific properties to cells.

For this purpose, RNA was first extracted (RNX-Plus) and then the purity and integrity of extracted RNA were investigated under both conditions by nanodrop and loading of RNA on agarose gel, after which cDNA was synthesized from RNA (BioFact, South Korea). Finally, real-time qPCR was performed using Real-Time PCR Roche lightcycler®96, BioFACT™ 2X Real-Time PCR Master Mix, and the primers listed in **Table 2**. Real-time qPCR was carried out with the following reaction conditions: 40 cycles of denaturation: 15 s at 95°C; annealing: 60 s at 60°C; and extension: 60 s at 72°C.

Primer efficiency was determined for all the gene expression assays using a standard curve and LinRegPCR software. The absence of dimer primers and contamination was controlled by observing the melting curves and loading products on the agarose gel. The absence of DNA was also checked with no RT control (no reverse transcriptase control). The expression level of *EFG1, BCR1*, and *CAT1* target genes in the isolates relative to that of the reference *ACT1* gene was first calculated manually by Excel and then confirmed by REST2009 software to ensure the accuracy of results. Finally, statistical analysis and plotting with SPSS 22 and GraphPad prism were done.

Sequencing and Comparison of Persister and Non-persister Cells Using ITS Fragment

After sequencing of both groups, a software was used to draw the phylogenetic tree[1], and the phylogenetic tree of *C. albicans* isolates was used using Maximum Likelihood and Boot Strap 100 to ensure the validity and reproducibility of the drawn trees. The table of genetic distances was drawn using MEGA 7 program of Pairwise Distances model. Then, cluster and clade were determined in the phylogenetic tree.

Statistical Analysis

In this study, *t*-test and one-way ANOVA, Fisher's exact test, and Mann–Whitney test with a significance level of <0.05 were used. The normality of data was checked using Shapiro–Wilk test. All tests were analyzed by SPSS software version 22.

RESULTS

A total of 104 *C. albicans* were isolated. Forty-three isolates were taken from patients undergoing chemotherapy and 61 *C. albicans* isolates were identified in HIV patients. All the isolates were confirmed by phenotypic and molecular methods to be *C. albicans*. Afterward, 104 *C. albicans* isolates, including isolates collected from HIV-infected patients and those undergoing chemotherapy, were examined to determine the severity of biofilm formation.

C. albicans Is a Strong Biofilm Producer

Our analysis demonstrated that two isolates had a weak biofilm formation while 102 *C. albicans* isolates showed strong biofilm production. Another classification was also performed based on optical observation of the isolates that were grouped to three quarters as shown in **Figure 1**.

The Prevalence of *C. albicans* Persister Cell Producers Is High Among *C. albicans* Population

In this study, 104 *C. albicans* isolates were tested to separate persister cells from biofilm-forming isolates. This stage of persister cell isolation was done in triplicate and the results of each sample were reported as average. Out of 104 isolates under study that were exposed to 100 μg/ml amphotericin B, 83 had a survival rate in the range of 0.0003–9% and 21 had no survival ability in the face of the drug. Those isolates that were able to survive in the presence of amphotericin B were examined for MIC. To determine the sensitivity of the population, MICs of the isolates were read by microdilution method in the presence

[1]https://www.ebi.ac.uk/goldman-srv/webprank/

TABLE 2 | qPCR primers.

Genes	Primer sequence (5′ → 3′)	Size (bp)	Gene Bank	GC%	TM	References
BCR1	Forward CTTCAGCAGCTTCATTAACACCTA	101	NC_032096.1	41.7	68	LaFleur et al., 2010
	Revers TCTTGGATCAGGTGTACTTTTCAA			37.5	66	
EFG1	Forward TGCCAATAATGTGTCGGTTG	100	XM_709144.2	45	58	Nikoomanesh et al., 2016
	Revers CCCATCTCTTCTACCACGTGTC			54	68	
CAT1	Forward GACTGCTTACATTCAAAC	117	NC_032089.1	38.9	55.1	Moazeni et al., 2014
	Revers AACTTACCAAATCTTCTCA			31.9	55.1	
ACT1	Forward ACTGCTTTGGCTCCATCTTCT	166	XM_019475182.1	48	65	
	Revers TGTGGTGAACAATGGATGGAC			48	62	

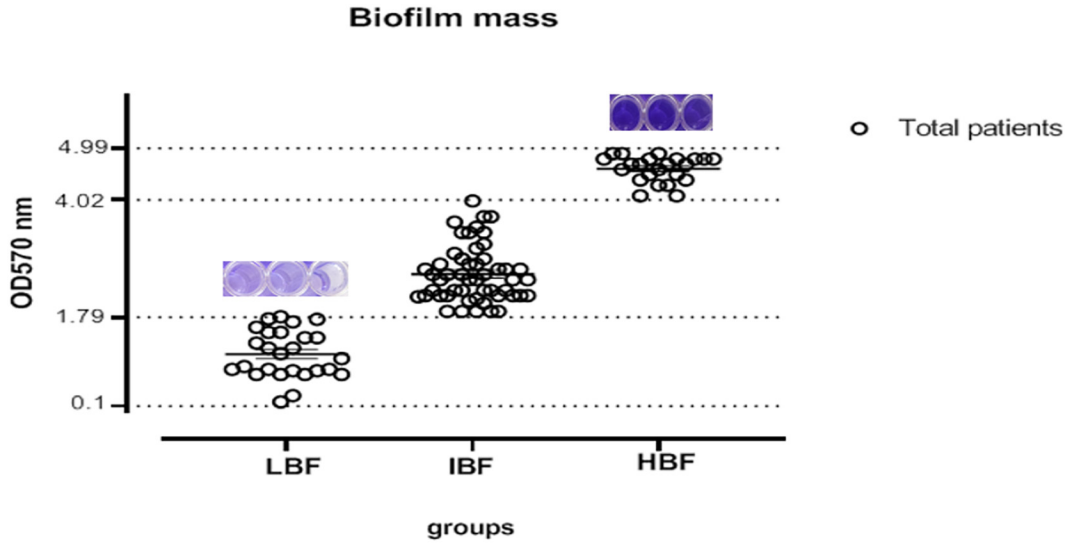

FIGURE 1 | Determination of biofilm production level based on OD quarter; 25% of the isolates had 1.79 ≤ OD (LBF), 50% had 2.5 ≤ OD (IBF), and 75% of the isolates had 4.9 ≤ OD (HBF). LBF, low biofilm formation; IBF, intermediate biofilm formation; HBF, high biofilm formation.

of amphotericin B in the range of 0.3–2 μg/ml. According to available guidelines, namely, CLSI M27-S4, out of 83 isolates, 77 with MIC < 2 μg/ml were sensitive and six isolates with MIC ≥ 2 μg/ml were classified as the resistant population and were excluded from the study. Therefore, 77 *C. albicans* were considered as persister cell isolates (**Table 3** and **Figure 2**).

According to a study by LaFleur et al. (2010), the isolates with a survival rate of >6% were defined as high persister, and those showing survival <6% were classified as low-persister cells. Besides, the isolates that had no survival were defined as non-persistent (Cohen et al., 2013).

TABLE 3 | The persister situation in infected patients with *C. albicans*.

Persister cell (survival rate)			
Patients	**High-persister**	**Low-persister**	**Non-persister**
Cancer patients (39)	1 (8%)	26 (0.0003–0.75%)	12
HIV patients (59)	1 (9%)	49 (0.0003–0.75%)	9
Total patients (98)	2 (8–9%)	75 (0.0003–0.75%)	21
Total patients (100%)	2.04%	76.5%	21.42%

Out of 77 *C. albicans* persister cells, two isolates with 9% and 8% survival were classified in the high-persister cell group, 75 isolates with the ability to survive in 0.75–0.0003% were classified in the low-persister group, and the 21 remaining isolates were classified in the non-persister group. Two high-persister isolates were taken from patients as follows: one was related to a patient undergoing chemotherapy who was hospitalized for approximately 2 months and did not have clear oral candidiasis symptoms. The only symptoms were dry mouth and redness of the tongue. Another isolate was taken from an HIV-infected patient recently discharged from the infectious ward of Razi Hospital who had been hospitalized for approximately 45 days. He had redness, inflammation, dry mouth, change in taste, and burning sensation, and of course, was in the end stage of the disease or so-called AIDS. According to the case file in Razi Hospital, only fluconazole was used for the patient whose disease was chronic and recurrent (**Table 4**).

The mean production of low persister based on survival rate in HIV-infected patients with the ability of 0.04 ± 0.14% (survival rate ± standard deviation) was almost 5.5 times higher than patients undergoing chemotherapy with the ability of 0.008 ± 0.13%. The mean of low persister production in all

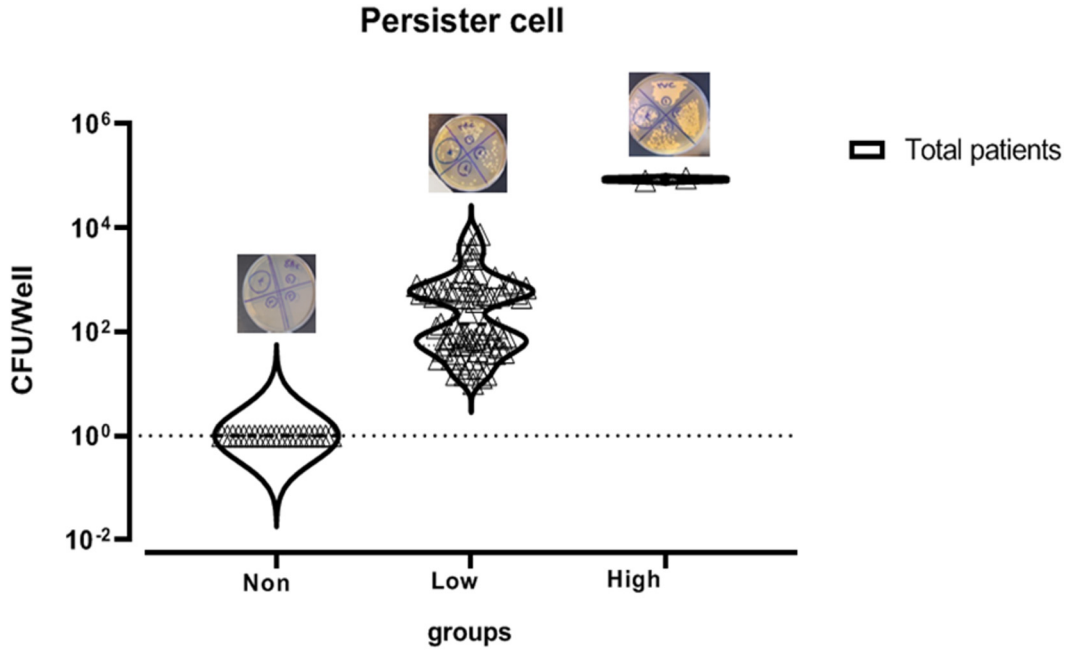

FIGURE 2 | Mean survival rate or persister cell of *Candida albicans* isolates based on logarithmic data.

TABLE 4 | Information from two patients with high persister cells isolated from *Candida albicans*.

	Age	Candida-load	Viral-load	CD4-count cells/mm^3	Type of cancer
High persister (patient under chemotherapy)	75	20 Colonization	–	–	Lung
High persister (HIV patient)	45	10^5 Infection	3,069,499	70	–

patients was 0.01 ± 0.0013%. Since the survival rate and the number of high persisters in patients under study were almost the same, the same mean value was observed for both groups of patients (**Figure 3**).

Comparison of Biofilm Intensity With Persister Cells in *C. albicans*

In this part of the research, we first deal with the relationship between different variables related to HIV patients with those related to patients undergoing chemotherapy with the production of persister cells, and then this variable is examined in all patients.

HIV Patients

In this study, because there was only one isolate from HIV patients with a survival rate of 9%, statistical analysis was performed only in low and non-persister categories. Statistical results showed no significant correlation between qualitative variables of gender, tuberculosis, pneumocystosis, hepatitis B, hepatitis C, receiving antiviral drugs, tuberculosis prophylaxis drugs, HIV transmission from mother to child or through occupational exposure, blood transfusion, CD4 count, homosexuality, common syringe use for injection, and history of drug injection in non- and low-persister cells (**Supplementary Table 1**).

Data related to the age of subjects were normal, and no significant difference was observed between the two groups (low- and non-persister cells). There was no significant difference between viral and *Candida* loads between the two groups of non- and low-persister cells. However, the results of statistical tests showed that the biofilm variable is significantly different in the two groups of non- and low-persister cells (**Supplementary Table 2**) ($p = 0.021$).

Patients Undergoing Chemotherapy

Considering that there was only one isolate in this group with a survival rate of 8% among the high-persister group, the statistical analysis was performed for two groups: low- and non-persister cells. Accordingly, the calculations showed that there was no significant relationship between gender and persister values in the non- and low persister cell groups.

Data related to the age of subjects were normal and no significant difference was observed between the two groups. Statistical results also showed no significant difference in

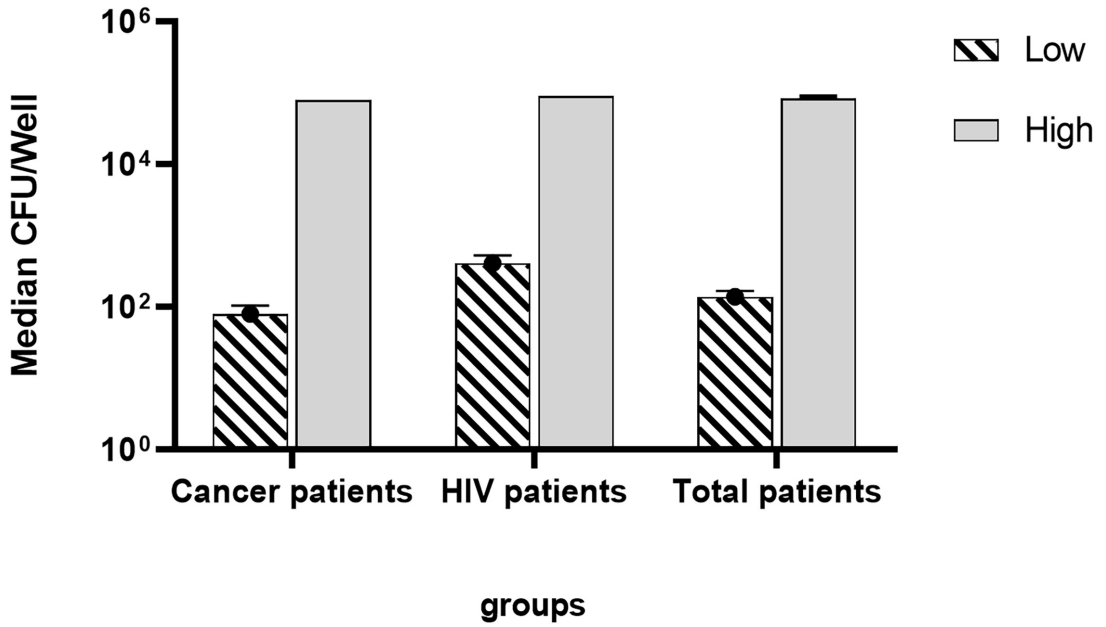

FIGURE 3 | Log mean persister production in patients undergoing chemotherapy and HIV patients.

Candida load and biofilm variables between the two groups (**Supplementary Table 3**).

Statistical analysis was performed using *t*-test in the two groups of non- and low-persister cells, but no significant difference was observed between the two groups (**Figure 4**).

The Higher Expression of *EFG1, BCR1*, and *CAT1* in *C. albicans* Isolates Producing Persister Cells

Real-time qPCR was performed in promoting and inducing conditions. The purity of RNA on the A260/A280 and A260/A230 ratios was 1.8–2.0 and 1.9–2.0, respectively. Then, for the synthesis of cDNA, 500 ng of RNA entered the reaction.

Promoting Condition

After normalizing the data with reference or control gene (*ACT1*), our findings showed an increase in the expression of *EFG1, BCR1*, and *CAT1* genes in persister isolates, among which the highest expression was related to *CAT1* gene, followed by *EFG1* and *BCR1*, respectively.

The mean expression of *EFG1, BCR1*, and *CAT1* genes was statistically evaluated using logarithmic data between the two groups of persister and non-persister isolates using *t*-test. Among the genes, only the expression of the *CAT1* gene was significant between persister and non-persister isolates (**Supplementary Figure 1**).

Inducing Condition

In inducing conditions, the expression of *EFG1, BCR1*, and *CAT1* genes was evident in all isolates of both persister and non-persister groups. After normalizing the data with reference or control gene of *ACT1*, our results showed an increase in the expression of *EFG1, BCR1*, and *CAT1* genes in persister isolates under inducing conditions, among which the highest expression was related to *CAT1* gene, then *BCR1* and *EFG1*, respectively. The mean expression of *EFG1, BCR1*, and *CAT1* genes was statistically evaluated through logarithmic data between the two groups of persister and non-persister using *t*-test. The increasing expression of *BCR1* and *CAT1* was significant between the persister and non-persister groups ($p < 0.05$) (**Supplementary Figure 1**).

The mean increase in gene expression under promoting and inducing conditions is described as fold change (i.e., $2^{-\Delta\Delta CT}$). The highest amount of fold change in both promoting and inducing conditions was related to the *CAT1* gene with 15.34 and 5.54, respectively. The lowest fold change in promoting and inducing conditions was related to *EFG1* gene and its amount was 2.18 and 1.14, respectively (**Table 5** and **Figure 5**).

Phylogenetic Tree in Persister and Non-persister Groups by ITS Component

The DNA sequencing analysis of 20 isolates confirmed the presence of *C. albicans* and was recorded on DNA Data Bank of Japan (Accession No. LC612887-612906). After blasting, the similarity of sequences was reported to be 94–99.88%.

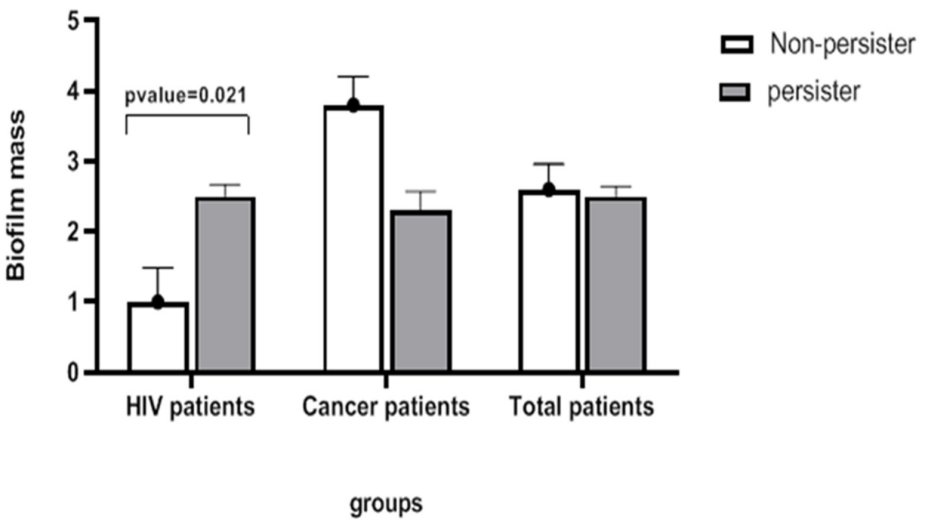

FIGURE 4 | The mean severity of biofilm in the groups of persister and non-persister cells in patients with HIV and those undergoing chemotherapy. A significant relationship between persister cells and biofilm intensity is seen only in HIV-infected patients (*t*-test, *p*-value < 0.05).

TABLE 5 | Comparison of mean fold change ($2^{-\Delta\Delta CT}$) in *EFG1*, *BCR*, and *CAT1* genes under two conditions: promoting and inducing.

	BCR-P	***BCR-I***	***EFG-P***	***EFG-I***	***CAT-P***	***CAT-I***
Persister	3.58 ± 0.25	10.73 ± 0.4	1.14 ± 0.15	2.41 ± 0.49	5.54 ± 0.53	15.34 ± 0.69
Normal	1	1	1	1	1	1
P-value (<0.05)	0.08	0.008*	0.1	0.1	0.03*	0.016*

*SD, standard deviation; P, promoting; I, inducing (t-test,*P-value < 0.05).*

The bootstrapping value was repeated 100 times to draw the phylogenetic tree to ensure the accuracy of drawing the phylogenetic tree. In our study, bootstrapping equal to 100 was reported, indicating that the phylogenetic tree of the desired nucleotides had a high degree of reliability. The similarity and intra-species difference of the sequences is calculated through pairwise distance. The average pairwise distance in sequences with a distance scale of 0.01 was 0.029. In these isolates, the biggest difference was related to 1A–low persister and 5A-normal isolates, which was equal to 8%. Then, the difference was related to 1A–low persister with normal 3A, 7A, and 8A isolates with a value of 7.8%. The isolate 6A–high persister, 5A-normal, and then 7A, 8A, and 3A had the highest difference (approximately 7%). The 6A–high-persister isolate had a genetic distance of 5.7% with the 7C–high-persister isolate.

Based on the mean pairwise distance of 0.029, the sequences were divided into four clusters that were more genetically similar. The largest cluster belongs to cluster IV, which contains persister cell isolates and non-persister ones. Both high-persistent isolates were genetically separated by 5.7% in two separate clusters, and their offspring were completely different. 7c–high persister had no significant difference from the normal population, including 8A, 7A, 5A, 3A, 4A, 2A, and 6C by about 1–2% and was probably derived from the normal population. Most low-persister isolates differ by about 1% from the population of normal isolates, indicating that the nucleotide changes were negligible (**Figure 6**).

DISCUSSION

Over the past 30 years, advances in medical science have caused a significant increase in life-threatening candidiasis, which has a high prevalence and mortality associated with invasive candidiasis infections, despite progress in fungal drugs (Costa-de-Oliveira and Rodrigues, 2020). Today, despite drug susceptibility tests and appropriate treatments, comprehensive medicine has faced the phenomena of treatment failure and recurrence of the disease in patients. It is a concern in medical science to treat a patient with appropriate antifungal medication without failure in antifungal therapy. In fungi and bacteria, this likelihood increases such that populations of drug tolerance and persister cells may be overlooked, leading to treatment failure (Lewis, 2005).

The present study suggests that persister cells are present in *C. albicans* clinical isolates. Populations with high persister (above 6% survival) and low persister (0.0003–0.75%) were observed in the two groups of patients (i.e., HIV patients and those under chemotherapy). High-persister isolates were taken

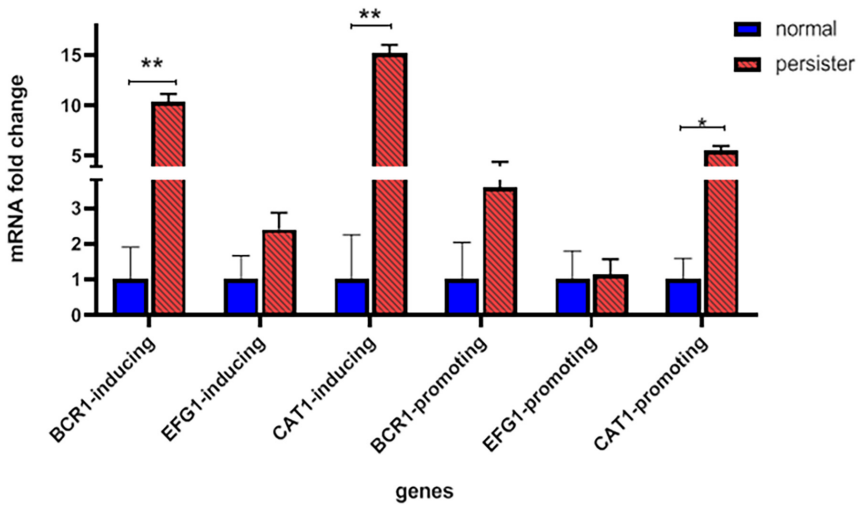

FIGURE 5 | Fold change of $2^{-\Delta\Delta CT}$ related to *CAT1*, *BCR1*, and *EFG1* genes in persister and non-persister isolates in inducing and promoting conditions (*t*-test, **p*-value <0.05, ***p*-value <0.01).

exclusively from patients who had been suffering from oral candidiasis for a long time and shared receiving antifungal drugs and long hospital stays. Also, based on statistical analysis, the total information of patients from whom a high persister cell was isolated proved that the persister cell isolate has no connection with *Candida* load of patients at the time of sampling; in other words, it is likely not related to the presence or absence of obvious oral candidiasis symptoms in the patient (Wuyts et al., 2018). Similar to LaFleur results, our research showed that persister cells were present based on complete removal of isolates using amphotericin B 100 μg/ml, which was not observed in all *C. albicans* isolates (LaFleur et al., 2010). The reason for this difference in the presence and level of persister cells in some isolates and their absence in others is widely discussed and challenged among microbiological researchers (Bink et al., 2011; Stewart and Rozen, 2012). Some researchers have suggested that this difference may be due to the high prevalence of persister, its evolution, and resistance to adverse and stressful conditions (Balaban et al., 2004; Levin et al., 2014). According to a study on persister cells of microorganisms, this group of patients is prone to infections, immune system factors, and antibiotics due to low CD4 counts and receiving immunosuppressive drugs, and they are not able to completely eliminate the pathogen. As a result, these factors can cause relapse and recurrence of the disease (Cohen et al., 2013; Patra and Klumpp, 2013; Van den Bergh et al., 2017). It is argued that persister cells are a type of population-based defense tactic counteracting environmental change and stress (Kussell et al., 2005; Veening et al., 2008). Our findings showed that there is a high rate of persister in patients undergoing chemotherapy as well as HIV patients, which is consistent with the study by LaFleur et al. (2010). The results showed that the expression of BCR1 in the persister group in inducing conditions has an increase of about 10 times compared to the non-persister group. Promoting conditions fully confirmed the results of inducing conditions in that persister isolates have the potential to further increase the expression of *BCR1* and biofilm formation. These data suggested that higher biofilm formation is due to persister cells causing survival against drug treatment in *C. albicans* isolates. Our findings were consistent with the study by Li et al. (2018) on patients with persister and non-persister candidiasis, and *C. albicans* isolates with persister cells had a higher biofilm intensity. *BCR1* gene is essential for biofilm formation in the laboratory as well as in animal models with catheter-based candidiasis. BCR1 proteins express major surface adhesins such as HWP1 and ALS3,1, and *ALS3,1* genes are BCR1-dependent (Nobile and Mitchell, 2005; Dwivedi et al., 2011; Finkel et al., 2012). These reports and our results show that the surface adhesion step in the biofilm, which is controlled by BCR1 gene, plays a critical role in the production of persister and that the formation of the persister depends on the surface adhesion. The study by Sun et al. (2016) examined the production of biofilm in different phases and showed that persister are mainly produced in adhesion and biofilm formation phases. In a 2020 study, vaginal candidiasis was detected in a mouse model using *C. albicans* wild-type isolate and *bcr1*ΔΔ mutant, which reported the *BCR1* gene as a recurrence of the disease, and our data are consistent with this study (Wu et al., 2020).

In our research, the results of *EFG1* expression in the two groups of persister and non-persister showed that there was no significant difference between the two groups in inducing and promoting conditions. *EFG1* regulates morphology (yeast transformation to hyphae) and biofilm development in *C. albicans* (Lassak et al., 2011). Our results showed that biofilm expansion has no role in the production of persister cells and that persister cell production does not require the formation of a complex biofilm structure. LaFleur et al. (2006) reported that *efg*Δ/*cph1*Δ mutants were able to produce persister, which is consistent with our results. Therefore, according to the gene expression reports of *EFG1* and *BCR1* biofilm production

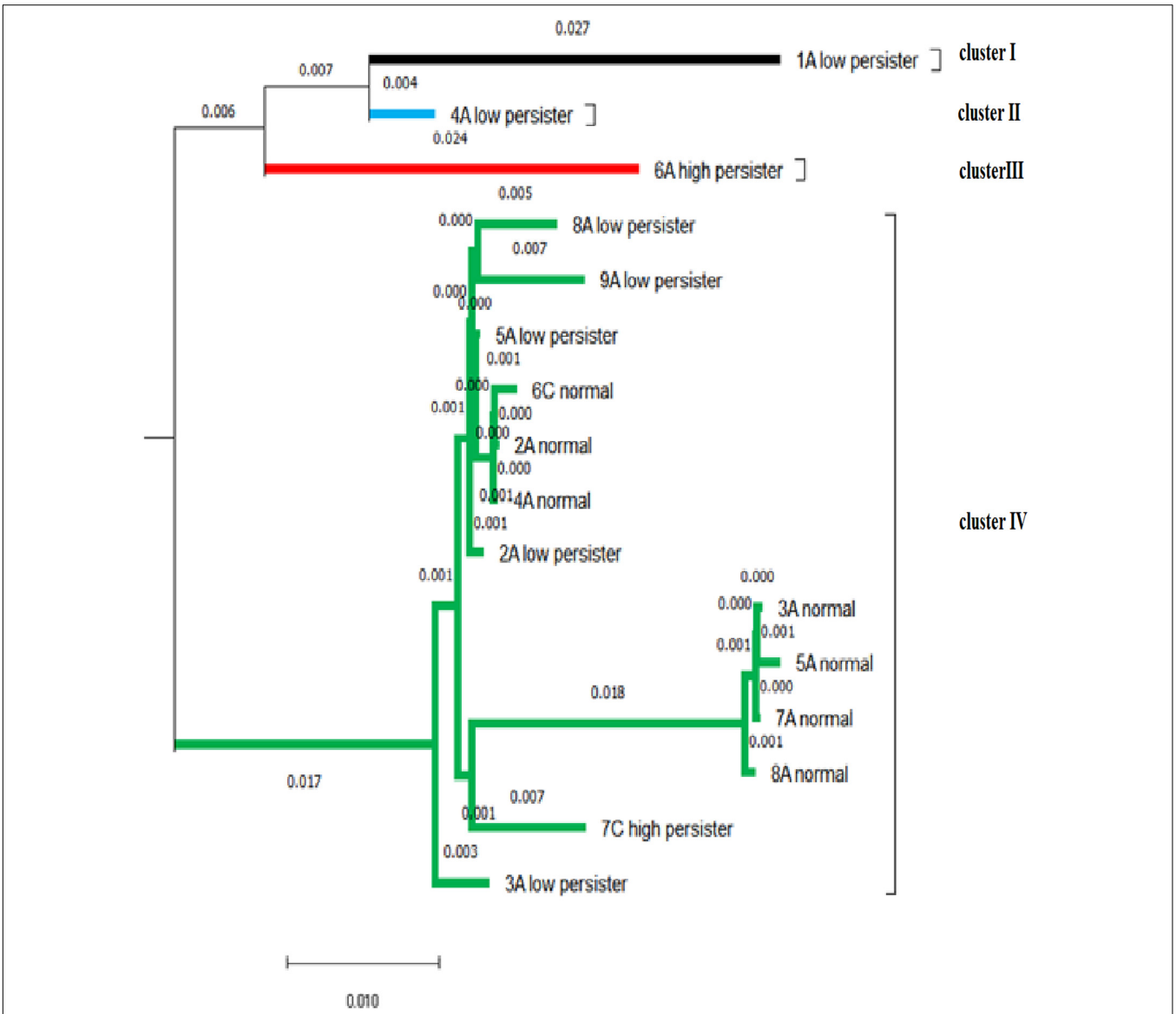

FIGURE 6 | Based on the mean pairwise distance of 0.029, the phylogenetic tree of the isolates shows four clusters.

pathways in this study, it can be concluded that the most important factor in the formation of persister is surface adhesion and biofilm formation, not biofilm development or mature biofilm production. This study suggests that the design of an anti-biofilm drug targeting the *BCR1* can eliminate biofilms and prevent the formation of persister cells in people with mucosal candidiasis or those with candidiasis from venous catheters, dentures, and implants.

The results of *CAT1* in inducing and promoting conditions in two groups of persister and non-persister cells showed that increasing expression of catalase enzyme has a significant role in the production of persister. Our results are consistent with other studies on oxidative stress response pathways on *SOD* and *AHP1*, both of which play a role in the production of persister in *C. albicans* isolates (Bink et al., 2011; Truong et al., 2016). The mRNA level of catalase strongly increases against the oxidative stress response in *C. albicans*. Catalase is among the limited antioxidants secreted outside and inside the cell, and in this respect, it acts differently from other antioxidants of oxidative stress response, except for the rapid response and immediate detoxification of H_2O_2, and over time, its amount in the cell regulates and reduces the ROS signal. Thus, catalase plays a major role in the rapid regulation of the response to oxidative stress after exposure to H_2O_2 (Nakagawa, 2008; Komalapriya et al., 2015; Pradhan et al., 2017). These results highlighted the key role of catalase in this pathway, and recent reports and studies highlight the importance of the oxidative stress response and the role of catalase in the production of persister cells. This relationship can be effective and practical for controlling persister formation in fungal biofilms.

Our findings regarding the phylogenetic tree in persister and non-persister cells showed that there is little difference between them and that the affinity between persister and non-persister cells is high. Consequently, it is suggested that the changes in nucleotides may be the root cause of persister cells. Therefore, according to the results of the evolutionary process in other microorganisms as well as our study, persister cells are phenotypic wild-type variants. Presumably, long-term and high-dose treatment with lethal antibiotics can determine the progression of persister cell formation (Mulcahy et al., 2010; Van den Bergh et al., 2017).

CONCLUSION

Our findings show that there are small subsets of cells tolerating high doses of fungicidal compounds among *C. albicans* biofilm-forming isolates from chemotherapy and HIV patients, which are called persister cells. The high presence of persister cells in this group of patients may be due to prophylaxis, frequent exposure to antibiotics, and a defective immune system. Molecular analysis of two important genes in the biofilm production pathway showed that biofilm production and binding play an important role in the production of persister cells and that the catalase gene of the oxidative stress response pathway can be mentioned as a therapeutic target for the removal of persister cells. However, the conversion of yeast to hyphae and the maturation of biofilm do not affect the formation of persister.

DATA AVAILABILITY STATEMENT

The datasets presented in this study can be found in online repositories. The names of the repository/repositories and accession number(s) can be found below: DDBJ, access number: LC612887-612906.

ETHICS STATEMENT

The studies involving human participants were reviewed and approved by the ethical code# IR.AJUMS.REC.1397.894. Written informed consent to participate in this study was provided by the participants' legal guardian/next of kin.

AUTHOR CONTRIBUTIONS

MF was involved in the study design and interpretation of the data of the study, and the final editing of the manuscript. EA contributed to all the steps of experimental work, data analysis, and preparation of the manuscript draft. MT contributed to the interpretation and analysis of the data. MH contributed to the collection and preparation of clinical samples. All authors contributed to the article and approved the submitted version.

FUNDING

This work was supported by the grant no. OG-9743 from Ahvaz Jundishapur University of Medical Sciences, Ahvaz, Iran.

ACKNOWLEDGMENTS

We are thankful to the Infectious and Tropical Diseases Research Center, Health Research Institute, Ahvaz Jundishapur University of Medical Sciences, Ahvaz, Iran, for cooperation in this study.

SUPPLEMENTARY MATERIAL

The Supplementary Material for this article can be found online at: https://www.frontiersin.org/articles/10.3389/fmicb.2021.651221/full#supplementary-material

Supplementary Figure 1 | The Mean of $2^{-\Delta ct-}$of *CAT1, BCR1,* and *EFG1* genes in persister and non-persister isolates in inducing and promoting conditions (*t*-test, **P*-value < 0.05, ***P*-value < 0.01).

Supplementary Table 1 | Demographic information of HIV patients with and without persister cells. [a]The test was performed after pooling the last two groups (Elementary education, Higher education) in order to eliminate small expected frequencies (Fisher's exact test, *P*-value < 0.05).

Supplementary Table 2 | Quantitative information about HIV patients in the two groups of persister and non-persister cell. Data are median (IQR) or Mean ± SD. **P*-value < 0.05, (*t*-test and Mann–Whitney test).

Supplementary Table 3 | Information about patients undergoing chemotherapy in the two groups of persister and non-persister cells. Data are median (IQR) or Mean ± SD (*t*-test and Mann–Whitney test), *P*-value < 0.05.

REFERENCES

Aboualigalehdari, E., Birgani, M. T., Fatahinia, M., and Hosseinzadeh, M. (2020). Oral colonization by Candida species and associated factors in HIV-infected patients in Ahvaz, southwest Iran. *Epidemiol. Health* 42:e2020033. doi: 10.4178/epih.e2020033

Aboualigalehdari, E., Ghafourian, S., Sadeghifard, N., and Sekawi, Z. (2013). Is Candida albicans a cause of nosocomial infection in Iran? *Rev. Med. Microbiol.* 24, 85–88. doi: 10.1097/mrm.0b013e3283642433

Abraham, S. B., Al Marzooq, F., Himratul-Aznita, W. H., Ahmed, H. M. A., and Samaranayake, L. P. (2020). Prevalence, virulence and antifungal activity of C. albicans isolated from infected root canals. *BMC Oral Health* 20:347. doi: 10.1186/s12903-020-01347-5

Ahmad, S., Khan, Z., Asadzadeh, M., Theyyathel, A., and Chandy, R. (2012). Performance comparison of phenotypic and molecular methods for detection and differentiation of Candida albicans and Candida dubliniensis. *BMC Infect. Dis.* 12:230. doi: 10.1186/1471-2334-12-230

Alonso, G. C., Pavarina, A. C., Sousa, T. V., and Klein, M. I. (2018). A quest to find good primers for gene expression analysis of Candida albicans from clinical samples. *J. Microbiol. Methods* 147, 1–13. doi: 10.1016/j.mimet.2018.02.010

Balaban, N. Q., Merrin, J., Chait, R., Kowalik, L., and Leibler, S. (2004). Bacterial persistence as a phenotypic switch. *Science* 305, 1622–1625. doi: 10.1126/science.1099390

Bink, A., Vandenbosch, D., Coenye, T., Nelis, H., Cammue, B. P., and Thevissen, K. (2011). Superoxide dismutases are involved in Candida albicans biofilm

persistence against miconazole. *Antimicrob. Agents Chemother.* 55, 4033–4037. doi: 10.1128/aac.00280-11

Cavalheiro, M., and Teixeira, M. C. (2018). Candida biofilms: threats, challenges, and promising strategies. *Front. Med.* 5:28. doi: 10.3389/fmed.2018.00028

Clinical and Laboratory Standards Institute [CLSI] (2008). *Reference Method for Broth Dilution Antifungal Susceptibility Testing of Yeasts*. Wayne, PA: Clinical and Laboratory Standards Institute.

Cohen, N. R., Lobritz, M. A., and Collins, J. J. (2013). Microbial persistence and the road to drug resistance. *Cell Host Microbe* 13, 632–642. doi: 10.1016/j.chom.2013.05.009

Costa-de-Oliveira, S., and Rodrigues, A. G. (2020). Candida albicans antifungal resistance and tolerance in bloodstream infections: the triad yeast-host-antifungal. *Microorganisms* 8:154. doi: 10.3390/microorganisms8020154

De Brucker, K., De Cremer, K., Cammue, B. P., and Thevissen, K. (2016). Protocol for determination of the persister subpopulation in Candida albicans biofilms. *Methods Mol. Biol.* 1333, 67–72. doi: 10.1007/978-1-4939-2854-5_6

Dwivedi, P., Thompson, A., Xie, Z., Kashleva, H., Ganguly, S., Mitchell, A. P., et al. (2011). Role of Bcr1-activated genes Hwp1 and Hyr1 in Candida albicans oral mucosal biofilms and neutrophil evasion. *PLoS One* 6:e16218. doi: 10.1371/journal.pone.0016218

El-Baz, A. M., Mosbah, R. A., Goda, R. M., Mansour, B., Sultana, T., Dahms, T. E., et al. (2021). Back to nature: combating candida albicans biofilm, phospholipase and hemolysin using plant essential oils. *Antibiotics* 10:81. doi: 10.3390/antibiotics10010081

Erköse, G., and Erturan, Z. (2007). Oral Candida colonization of human immunodeficiency virus infected subjects in Turkey and its relation with viral load and CD4+ T-lymphocyte count. *Mycoses* 50, 485–490. doi: 10.1111/j.1439-0507.2007.01393.x

Finkel, J. S., Xu, W., Huang, D., Hill, E. M., Desai, J. V., Woolford, C. A., et al. (2012). Portrait of Candida albicans adherence regulators. *PLoS Pathog.* 8:e1002525. doi: 10.1371/journal.ppat.1002525

Galdiero, E., de Alteriis, E., De Natale, A., D'Alterio, A., Siciliano, A., Guida, M., et al. (2020). Eradication of Candida albicans persister cell biofilm by the membranotropic peptide gH625. *Sci. Rep.* 10:5780. doi: 10.1038/s41598-020-62746-w

Jayachandran, A. L., Katragadda, R., Thyagarajan, R., Vajravelu, L., Manikesi, S., Kaliappan, S., et al. (2016). Oral Candidiasis among cancer patients attending a tertiary Care Hospital in Chennai, South India: an evaluation of Clinicomycological association and antifungal susceptibility pattern. *Can. J. Infect. Dis. Med. Microbiol.* 2016:8758461.

Komalapriya, C., Kaloriti, D., Tillmann, A. T., Yin, Z., Herrero-de-Dios, C., Jacobsen, M. D., et al. (2015). Integrative model of oxidative stress adaptation in the fungal pathogen Candida albicans. *PLoS One* 10:e0137750. doi: 10.1371/journal.pone.0137750

Kussell, E., Kishony, R., Balaban, N. Q., and Leibler, S. (2005). Bacterial persistence: a model of survival in changing environments. *Genetics* 169, 1807–1814.

LaFleur, M. D., Kumamoto, C. A., and Lewis, K. (2006). Candida albicans biofilms produce antifungal-tolerant persister cells. *Antimicrob. Agents Chemother.* 50, 3839–3846. doi: 10.1128/aac.00684-06

LaFleur, M. D., Qi, Q., and Lewis, K. (2010). Patients with long-term oral carriage harbor high-persister mutants of Candida albicans. *Antimicrob. Agents chemother.* 54, 39–44. doi: 10.1128/aac.00860-09

Lassak, T., Schneider, E., Bussmann, M., Kurtz, D., Manak, J. R., Srikantha, T., et al. (2011). Target specificity of the Candida albicans Efg1 regulator. *Mol. Microbiol.* 82, 602–618. doi: 10.1111/j.1365-2958.2011.07837.x

Levin, B. R., Concepción-Acevedo, J., and Udekwu, K. I. (2014). Persistence: a copacetic and parsimonious hypothesis for the existence of non-inherited resistance to antibiotics. *Curr. Opin. Microbiol.* 21, 18–21. doi: 10.1016/j.mib.2014.06.016

Lewis, K. (2005). Persister cells and the riddle of biofilm survival. *Biochemistry* 70, 267–274. doi: 10.1007/s10541-005-0111-6

Li, P., Seneviratne, C. J., Alpi, E., Vizcaino, J. A., and Jin, L. (2015). Delicate metabolic control and coordinated stress response critically determine antifungal tolerance of Candida albicans biofilm persisters. *Antimicrob. Agents Chemother.* 59, 6101–6112. doi: 10.1128/aac.00543-15

Li, W.-S., Chen, Y.-C., Kuo, S.-F., Chen, F.-J., and Lee, C.-H. (2018). The impact of biofilm formation on the persistence of candidemia. *Front. Microbiol.* 9:1196. doi: 10.3389/fmicb.2018.01196

Maheronnaghsh, M., Fatahinia, M., Dehghan, P., and Teimoori, A. (2020). Identification of Candida species and antifungal susceptibility in cancer patients with oral lesions in ahvaz, Southern West of Iran. *Adv. Biomed. Res.* 9:50. doi: 10.4103/abr.abr_214_19

Merseguel, K. B., Nishikaku, A. S., Rodrigues, A. M., Padovan, A. C., Ferreira, R. C., de Azevedo Melo, A. S., et al. (2015). Genetic diversity of medically important and emerging Candida species causing invasive infection. *BMC Infect. Dis.* 15:57. doi: 10.1186/s12879-015-0793-3

Mirhendi, H., Makimura, K., Khoramizadeh, M., and Yamaguchi, H. (2006). A one-enzyme PCR-RFLP assay for identification of six medically important Candida species. *Nihon Ishinkin Gakkai Zasshi* 47, 225–229. doi: 10.3314/jjmm.47.225

Moazeni, M., Khoramizadeh, M. R., Teimoori-Toolabi, L., Noorbakhsh, F., and Rezaie, S. (2014). The effect of EFG1 gene silencing on down-regulation of SAP5 gene, by use of RNAi technology. *Acta Med. Iran.* 52, 9–14.

Mulcahy, L. R., Burns, J. L., Lory, S., and Lewis, K. (2010). Emergence of *Pseudomonas aeruginosa* strains producing high levels of persister cells in patients with cystic fibrosis. *J. Bacteriol.* 192, 6191–6199. doi: 10.1128/jb.01651-09

Nakagawa, Y. (2008). Catalase gene disruptant of the human pathogenic yeast Candida albicans is defective in hyphal growth, and a catalase-specific inhibitor can suppress hyphal growth of wild-type cells. *Microbiol. Immunol.* 52, 16–24. doi: 10.1111/j.1348-0421.2008.00006.x

Nikoomanesh, F., Roudbarmohammadi, S., Roudbary, M., Bayat, M., and Heidari, G. (2016). Investigation of bcr1 gene expression in Candida albicans isolates by RTPCR technique and its impact on biofilm formation. *Infect. Epidemiol. Microbiol.* 2, 22–24.

Nobile, C. J., and Mitchell, A. P. (2005). Regulation of cell-surface genes and biofilm formation by the C. albicans transcription factor Bcr1p. *Curr. Biol.* 15, 1150–1155. doi: 10.1016/j.cub.2005.05.047

Patil, S., Majumdar, B., Sarode, S. C., Sarode, G. S., and Awan, K. H. (2018). Oropharyngeal candidosis in HIV-infected patients—an update. *Front. Microbiol.* 9:980. doi: 10.3389/fmicb.2018.00980

Patra, P., and Klumpp, S. (2013). Population dynamics of bacterial persistence. *PLoS One* 8:e62814. doi: 10.1371/journal.pone.0062814

Piekarska, K., Hardy, G., Mol, E., van den Burg, J., Strijbis, K., van Roermund, C., et al. (2008). The activity of the glyoxylate cycle in peroxisomes of Candida albicans depends on a functional β-oxidation pathway: evidence for reduced metabolite transport across the peroxisomal membrane. *Microbiology* 154, 3061–3072. doi: 10.1099/mic.0.2008/020289-0

Pradhan, A., Herrero-de-Dios, C., Belmonte, R., Budge, S., Garcia, A. L., Kolmogorova, A., et al. (2017). Elevated catalase expression in a fungal pathogen is a double-edged sword of iron. *PLoS Pathog.* 13:e1006405. doi: 10.1371/journal.ppat.1006405

Putranti, A., Asmarawati, T., Rachman, B., and Hadi, U. (2018). Oral candidiasis as clinical manifestation of HIV/AIDS infection in Airlangga University hospital patients. *IOP Conf. Ser. Earth Environ. Sci.* 125:012063. doi: 10.1088/1755-1315/125/1/012063

Silva, G., Bernardi, T. L., Schaker, P. D. C., Menegotto, M., and Valente, P. (2012). Rapid yeast DNA extraction by boiling and freeze-thawing without using chemical reagents and DNA purification. *Braz. Arch. Biol. Technol.* 55, 319–327. doi: 10.1590/s1516-89132012000200020

Stewart, B., and Rozen, D. E. (2012). Genetic variation for antibiotic persistence in *Escherichia coli*. *Evolution* 66, 933–939. doi: 10.1111/j.1558-5646.2011.01467.x

Sun, J., Li, Z., Chu, H., Guo, J., Jiang, G., and Qi, Q. (2016). Candida albicans amphotericin B-tolerant persister formation is closely related to surface adhesion. *Mycopathologia* 181, 41–49. doi: 10.1007/s11046-015-9894-1

Taff, H. T., Mitchell, K. F., Edward, J. A., and Andes, D. R. (2013). Mechanisms of Candida biofilm drug resistance. *Future Microbiol.* 8, 1325–1337.

Truong, T., Zeng, G., Qingsong, L., Kwang, L. T., Tong, C., Chan, F. Y., et al. (2016). Comparative ploidy proteomics of Candida albicans biofilms unraveled the role of the AHP1 gene in the biofilm persistence against amphotericin B. *Mol. Cell. Proteom.* 15, 3488–3500. doi: 10.1074/mcp.m116.061523

Van den Bergh, B., Fauvart, M., and Michiels, J. (2017). Formation, physiology, ecology, evolution and clinical importance of bacterial persisters. *FEMS Microbiol. Rev.* 41, 219–251. doi: 10.1093/femsre/fux001

Veening, J.-W., Smits, W. K., and Kuipers, O. P. (2008). Bistability, epigenetics, and bet-hedging in bacteria. *Annu. Rev. Microbiol.* 62, 193–210. doi: 10.1146/annurev.micro.62.081307.163002

Wu, X., Zhang, S., Li, H., Shen, L., Dong, C., Sun, Y., et al. (2020). Biofilm formation of Candida albicans facilitates fungal infiltration and persister cell formation in vaginal candidiasis. *Front. Microbiol.* 11:1117. doi: 10.3389/fmicb.2020.01117

Wuyts, J., Van Dijck, P., and Holtappels, M. (2018). Fungal persister cells: the basis for recalcitrant infections? *PLoS Pathog.* 14:e1007301. doi: 10.1371/journal.ppat.1007301

Yamada, Y., Makimura, K., Merhendi, H., Ueda, K., Nishiyama, Y., Yamaguchi, H., et al. (2002). Comparison of different methods for extraction of mitochondrial DNA from human pathogenic yeasts. *Jpn. J. infect. Dis.* 55:122.

Conflict of Interest: The authors declare that the research was conducted in the absence of any commercial or financial relationships that could be construed as a potential conflict of interest.

Publisher's Note: All claims expressed in this article are solely those of the authors and do not necessarily represent those of their affiliated organizations, or those of the publisher, the editors and the reviewers. Any product that may be evaluated in this article, or claim that may be made by its manufacturer, is not guaranteed or endorsed by the publisher.

frontiers in Microbiology

ORIGINAL RESEARCH
published: 03 September 2021
doi: 10.3389/fmicb.2021.700008

Evaluation of Droplet Digital PCR Assay for the Diagnosis of Candidemia in Blood Samples

Biao Chen[1,2†], Yingguang Xie[3†], Ning Zhang[1], Wenqiang Li[3], Chen Liu[1], Dongmei Li[4], Shaodong Bian[1], Yufeng Jiang[2,5], Zhiya Yang[1], Renzhe Li[5], Yahui Feng[6], Xiaojie Zhang[2] and Dongmei Shi[1,7]**

[1]The Laboratory of Medical Mycology, Jining No. 1 People's Hospital, Jining, China, [2]Postdoctoral Mobile Station of Shandong University of Traditional Chinese Medicine, Jinan, China, [3]Intensive Care Unit, Jining No. 1 People's Hospital, Jining, China, [4]Department of Microbiology and Immunology, Georgetown University Medical Center, Washington, DC, United States, [5]Clinical Laboratory, Jining No. 1 People's Hospital, Jining, China, [6]Clinical Medicine College, Jining Medical College, Jining, China, [7]Department of Dermatology, Jining No. 1 People's Hospital, Jining, China

OPEN ACCESS

Edited by:
Ying-Chun Xu,
Peking Union Medical College Hospital (CAMS), China

Reviewed by:
Ott Scheler,
Tallinn University of Technology, Estonia
Weida Liu,
Chinese Academy of Medical Sciences and Peking Union Medical College, China

***Correspondence:**
Dongmei Shi
shidongmei28@163.com
Xiaojie Zhang
qlzxj@126.com

†These authors share first authorship

Specialty section:
This article was submitted to Antimicrobials, Resistance and Chemotherapy, a section of the journal Frontiers in Microbiology

Received: 25 April 2021
Accepted: 26 July 2021
Published: 03 September 2021

Citation:
Chen B, Xie Y, Zhang N, Li W, Liu C, Li D, Bian S, Jiang Y, Yang Z, Li R, Feng Y, Zhang X and Shi D (2021) Evaluation of Droplet Digital PCR Assay for the Diagnosis of Candidemia in Blood Samples. Front. Microbiol. 12:700008. doi: 10.3389/fmicb.2021.700008

Numerous studies have shown that droplet digital PCR (ddPCR) is a promising tool for the diagnosis of pathogens, especially in samples with low concentrations of pathogenic DNA. An early diagnosis of candidemia is critical for the effective treatment of patients. In this study, we evaluated the sensitivity and specificity of ddPCR assay for *Candida* DNA detection both *in vitro* by mixing fungal cells with human blood and *in vivo* by analyzing blood samples from infected mice and patients with suspected candidemia. The results showed that ddPCR assay could detect a minimum of 4.5 DNA copies per reaction in blood samples. ddPCR showed higher sensitivity and specificity for *Candida* DNA detection than traditional culture and quantitative PCR (qPCR) methods and also exhibited significantly better positive and negative predictive values than the culture and qPCR methods that were commonly used in clinical practice. Hence, our study demonstrates that ddPCR assay is a promising method for the timely diagnosis of candidemia and could be useful for monitoring the treatment of candidemia.

Keywords: droplet digital PCR, diagnosis, candidemia, blood samples, sensitivity, specificity

INTRODUCTION

Candidemia is a leading cause of fungal infections among neonates and infants, and it also affects immunocompromised adults (Golan et al., 2005; Mantadakis et al., 2018). The incidence of candidemia is 13.3 per 100,000 people, and the mortality ranges from 36 to 50% (Ngamchokwathana et al., 2021). Given the rapid and fatal course of candidemia, timely and effective treatment depends on rapid and accurate diagnosis of this invasive fungal infection (Pfaller and Diekema, 2007; Schroeder et al., 2020).

The traditional procedure for diagnosing candidemia relies on blood cultures for the isolation of *Candida* spp. However, this method has low sensitivity and requires large volumes of blood (Clancy and Nguyen, 2013; Pappas et al., 2018). The growth, isolation, and identification of *Candida* spp. routinely take 24–48 h. This time-consuming approach takes even longer time when dealing with slower-growing fungal species, which will prevent the timely diagnosis and

the initiation of appropriate anti-fungal treatment. The first 12–48 h post-infection is a critical period since delaying treatment significantly increases the mortality of candidemia (Tumbarello et al., 2007; Tulasidas et al., 2018). Hence, the broad-spectrum empirical anti-fungal treatment is frequently used for high-risk patients. However, this will unnecessarily increase costs and risk of adverse reactions in these patients (Tumbarello et al., 2007; de Pauw et al., 2008).

Recent efforts in the development of early diagnostic methods have focused on the identification of molecular markers of pathogens. Also, quantitative PCR (qPCR)-based methods for DNA detection have become more popular than other non-culture methods. They facilitate the rapid diagnosis of bloodstream fungal infections, allowing for the initiation of species-oriented therapy as soon as 6 h after the onset of sepsis (Mcmullan et al., 2008). However, the sensitivity, accuracy, and replicability of these techniques do not fulfill the requirements of clinical practice, especially in the cases of samples with low abundance of pathogen DNA or with insufficient volumes of blood, as is common in premature or young infants (Nyaruaba et al., 2019).

Droplet digital PCR (ddPCR), based on water–oil emulsion droplet technology, is a new PCR method for nucleic acid detection that allows more accurate quantification of DNA templates (Schell et al., 2012). Each sample is partitioned into approximately 20,000 droplets before being subjected to the procedure. Ideally, each droplet contains one target molecule or none. Unlike qPCR, there is no need to establish a standard curve. The number of droplets with their amplification products is counted at the end of amplification, allowing for an estimate of template concentration based on Poisson's Law of Small Numbers. With a high sensitivity to detect low copies of DNA, ddPCR assay has been applied in several viral infections such as *human papilloma virus* (Schiavetto et al., 2021), *hepatitis B virus* (Lillsunde), chromosomally integrated *human herpes virus* 6 (Sedlak et al., 2014), and *Mycobacterium* spp. detection for tuberculosis (Yang et al., 2017) and leprosy (Cheng et al., 2019). However, the clinical utility of ddPCR assay for fungal detection remains unclear. To further optimize the ddPCR assay for the detection of *Candida* spp., the diagnostic performance of ddPCR assay was compared with conventional culture and qPCR assays using blood samples from mice with experimental candidemia and patients with suspected candidemia. The specificity of ddPCR for *Candida* spp. was also estimated using non-*Candida* fungal templates *in vitro*.

MATERIALS AND METHODS

Fungal and Bacterial Strains and Culture Conditions

Several typical fungal and bacterial strains, including *Candida albicans* (SC 5314), *C. tropicalis* (CBS 8072), *C. parapsilosis* (ATCC 22019), *C. krusei* (CBS 6451), *Trichophyton rubrum* (ATCC 4438), *Aspergillus fumigatus* (MAY 3626), *Staphylococcus aureus* (ATCC 25923), *Escherichia coli* (ATCC 35218), *Pseudomonas aeruginosa* (ATCC 27853), and *Streptococcus pneumoniae* (ATCC 49619), were obtained from the Laboratory of Medical Mycology, Jining No. 1 People's Hospital, Shandong, China. Fungal cells were inoculated on Sabouraud-glucose-agar (SDA) plates for 72 h at 30°C, and bacterial strains were cultured on blood agar plates (Jinan Baibo Biotechnology Co., Ltd.) for 24 h at 37°C.

DNA Extraction

Fungal DNA extraction was performed according to the manufacturer's (OMEGA) instructions. Each blood sample (0.25 ml) was transferred into sterile micro-centrifuge tubes containing 25 µl OB protease solution and 250 µl BL buffer. After incubation at 65°C for 10 min, 260 µl ethanol was added to each blood sample, which was then vortexed at the maximum speed for 20 s and transferred into HiBind® DNA mini-columns and centrifuged at 10,000 *g* for 1 min. In a new collection tube, 500 µl HBC buffer was added to a DNA mini-column. After centrifuging again at 1,000 *g* for 1 min, DNA was washed with 700 µl wash buffer and finally collected in a nuclease-free 2-ml micro-centrifuge tube with 200 µl elution buffer at 65°C at 13,000 *g* for 1 min. The DNA samples were immediately stored at −20°C until use. All laboratory equipment was disinfected and decontaminated using UV-treatment prior to DNA preparation. Laboratory equipment and surfaces were also regularly disinfected using 10% bleach and 70% ethanol before conducting any analysis.

Quantitative PCR

Candida albicans in blood samples was detected by a qPCR assay using the primers (forward: 5'-TCAAAACTT TCAACAACGGATCTC-3'; and reverse: 5'-CGCATTTCGCTG CGTTCT-3') synthesized by China Electronics Huada Technology Co. Ltd. In a total volume of 25 µl qPCR reaction, 12.5 µl TB Green Premix Ex Taq II was mixed with 4.84 µl of DNA (66 ng), 1 µl (25 pmol) each of forward primer and reverse primer, and 5.66 µl H_2O. The amplification was performed under the following conditions: the initial denaturation at 95°C for 30 s and 40 cycles of amplification at 95°C for 5 s and 57°C for 30 s. Bio-Rad CFX Maestro detection system was used for amplification, detection, and data analysis. Internal, positive, and negative controls were included in each experiment. To avoid the risk of false positive results due to laboratory contamination, all the experimental setups were performed in a biosafety cabinet.

Droplet Digital PCR

All ddPCR assays were conducted using QX200 Droplet Digital PCR system (Bio-Rad, United States) in a 22-µl volume system. The primers and probe for *C. albicans* were as follows: forward primer 5'-TCAAAACTTTCAACAACGGATCTC-3'; reverse primer 5'-CGCATTTCGCTGCGTTCT-3', and the probe: 5'-TGGTTCTCGCATCGAT-3'. The probe was labeled with FAM. The probe and two primers were synthesized by China Electronics Huada Technology Co. Ltd. Internal, positive, and negative controls were included in each ddPCR run. Each reaction contained 11 µl Bio-Rad 2 × ddPCR Supermix, 1.1 µl forward primer (18 µM) and 1.1 µl reverse primer (18 µM),

1.1 µl probe (5 µM), 4.84 µl template DNA (66 ng), and 2.86 µl H_2O. The PCR mix and sample DNA were thoroughly mixed before loading to a droplet generator cartridge. After droplet generation oil was added, the DNA mixtures were placed into a droplet generator (Bio-Rad, United States). Droplet-partitioned samples were transferred to a ddPCR 96-well plate, which was then sealed at 180°C using a PX1TM PCR plate sealer (Bio-Rad) before being amplified in a thermal cycler. The PCR annealing temperature was optimized at 57°C, as this temperature provided a clear separation between DNA-positive and negative droplets in the preliminary analysis. PCR was performed in a T100TM thermal cycler under the following conditions: 95°C for 10 min, followed by 40 cycles of 94°C for 30 s and 57°C for 60 s, and the final extension at 98°C for 10 min. Moreover, a ramp rate was set up at 2°C/s in the PCR program for every amplification step. After amplification, droplets remained at 4°C for at least 30 s. DNA targets in each droplet were quantized by thermal cycling and analyzed by the Bio-Rad QX200TM droplet reader. To limit laboratory contamination, all the setup procedures before thermal cycler use were performed in a biosafety cabinet.

Estimation of the Limit of Detection and Specificity

To calculate the limit of detection (LOD) of *C. albicans* DNA in blood samples, 10-fold dilutions of 1×10^{-1} ng/µl stock of *C. albicans* DNA were prepared with PBS. The final range of DNA dilution was 10^{-1}–10^{-7} from the *C. albicans* stock concentration (1 ng/µl) in ddPCR analysis. The specificity of ddPCR for *C. albicans* DNA detection was evaluated with the DNA extractions from *C. tropicalis*, *C. parapsilosis*, *C. krusei*, *Staphylococcus aureus*, *Escherichia coli*, *Pseudomonas aeruginosa*, *Streptococcus pneumoniae*, and *Klebsiella pneumoniae* using the same primer set for *C. albicans* assay. DNA stock used in this experiment was quantified using NanoDrop One/OneC (Thermo, USA).

Experimental Candidemia in Mice With *C. albicans*

Experimental candidemia was established in mice by intravenous challenge with cultured cells of *C. albicans*. In each experiment, BALB/c female mice (aged 4–8 weeks) were infected by the tail vein injection of *C. albicans* cells in 500 µl sterile PBS at 2×10^6 CFU, 2×10^5 CFU, or 2×10^4 CFU, respectively. Each concentration of *C. albicans* was injected into 15 female mice. Animals were randomly assigned to different groups. At subsequent time points (days 1, 3, and 7 post-infection), the mice were euthanized by carbon dioxide. The blood samples were obtained by orbital puncture, collected in EDTA tubes, and divided into three parts for quantitative culturing on SDA agar plates, conventional qPCR and ddPCR testing.

Blood Sampling From Patients With Suspected Candidemia

Forty-five blood samples of hospitalized patients with suspected candidemia were collected between January 2019 and April 2020 at Jining No. 1 People's Hospital (Jining, China). The blood samples were collected into EDTA tubes for immediate detection or storage at −80°C for further use. All samples were ultimately used for culture, and the extracted DNA samples were used for qPCR and ddPCR analyses.

Ethics Statement

The study was approved by Jining Medical College and Jining No. 1 People's Hospital, Shandong, China (Approval No. 2020–028). The guidelines given by the Genetic Risk Prediction Studies were followed. Written informed consent was obtained from each participant or from legal guardians of any minors. Meanwhile, all the animal experiments were conducted as per the guidelines of the Animal Ethics Committee of Jining No. 1 People's Hospital. The animal study was reviewed and approved by the Jining Medical College, Shandong.

Statistical Analysis

We considered the qPCR or culture assay as "gold standard" for fungal identification (Momin et al., 2020). Then, we used these techniques to estimate positive detection rates, sensitivities, specificities, and positive predictive and negative predictive values of ddPCR in suspected candidemia. IBM SPSS Statistics for Windows, Version 24.0 (IBM Corp., Armonk, NY) was used for all statistical analyses.

RESULTS

Designed ddPCR Assay Is Specific to *C. albicans*

The primers and probe designed in this study for both qPCR and ddPCR were genus-specific for *C. albicans*. To analyze the general specificity of the ddPCR method, we used the same primers, probe, and amplification procedure against genomic DNA preparations from other fungal and bacterial species. These other pathogens are also commonly found in bacteremia or candidemia blood samples. The ddPCR results showed that *C. tropicalis*, *C. parapsilosis*, and *C. krusei* could be amplified; however, all the bacterial samples were negative with *C. albicans*-specific primers, even though the concentrations of DNA template were 66 ng per ddPCR reaction. Meanwhile, the negative controls showed no amplified product. Since all the bacterial samples with non-target DNA were negative, ddPCR assay showed good specificity in detecting *Candida* spp. (**Figure 1**).

ddPCR Has Improved Quantitative Range in Comparison to qPCR

The minimum concentration necessary for DNA in the blood samples for ddPCR detection was first determined *in vitro* by 10-fold serial dilution from an initial concentration of 1×10^{-1} ng/µL DNA from *C. albicans* strain (SC 5314). The DNA copies per reaction ranged from 142,600 to 0. The fraction of positive droplets ranged from 0.9977 to 0. The target copies/droplet ranged from 15.8058 to 0. And, the results showed that the LOD for ddPCR detection for *C. albicans* was 4.5 copies per

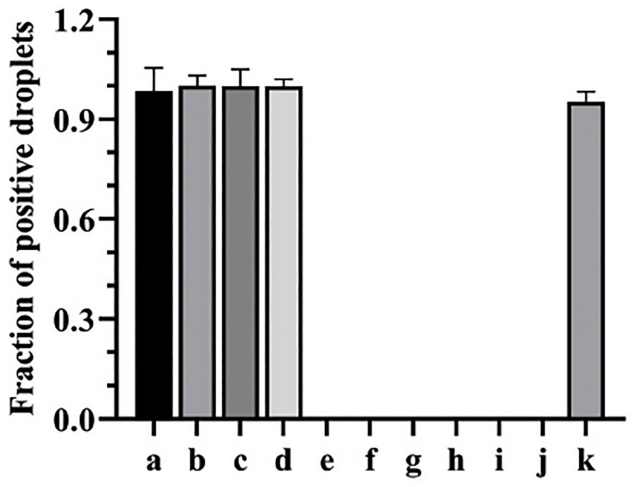

FIGURE 1 | The specificity of ddPCR assay for the detection of *Candida albicans*. a, b, c, d, e, f, g, h, i, and g represent the fraction of positive droplets of *Candida tropicalis*, *C. parapsilosis*, *C. krusei*, *C. albicans*, *Trichophyton rubrum*, *Aspergillus fumigatus*, *Staphylococcus aureus*, *Escherichia coli*, *Pseudomonas aeruginosa*, and *Streptococcus pneumoniae*, respectively. k represents positive control (*C. albicans*).

reaction, provided by 2×10^{-7}-fold dilution sample. When compared with ddPCR, the minimum number of DNA concentration for qPCR must be greater than the number of DNA concentration in 1×10^{-6}-fold dilution sample, since the qPCR method requires a 34.3 Cq value (1/Cq value with 0.029) for *C. albicans* detection at the 1×10^{-6}-fold dilution point. This Cq value was almost indistinguishable from the 36.7 Cq value (1/Cq value with 0.027) obtained from the negative control (**Figure 2** and **Supplementary Table 1**). Therefore, the results indicated that the ddPCR method had at least 5-fold higher sensitivity than the qPCR method for *C. albicans* DNA detection in blood samples.

ddPCR Detected Candidemia *in vivo*

To further evaluate the performance of ddPCR in the detection of *C. albicans* infection *in vivo*, we used infected mice to mimic candidemia in humans. Blood samples from infected mice were collected at day 1, 3, and 7 post-infection with different concentrations of *C. albicans* cells. As expected, the detection capacity of fraction of positive droplets by ddPCR method increased with higher dosages of *C. albicans*. For example, at day 1, the fraction of positive droplets were found to be 0.00055, 0.00114, and 0.00085 for inoculations of 1×10^4 CFU, 1×10^5 CFU, and 1×10^6 CFU, respectively (**Figure 3**). The fractions of positive droplets were 0.00161, 0.00531, and 0.01584 at day 3, and then dropped slightly to 0.00146, 0.00132, and 0.00488 at day 7 post-infection. Indeed, this peak at day 3 was consistent with the peak infection course in the mouse infection model. These mice often died or became seriously ill during the 3–5 days post-infection. These results suggested that the ddPCR assay was not only useful for an early diagnosis but also provided prognostic value for candidemia management.

ddPCR Showed Higher Sensitivity in Detecting *Candida* Among Suspected Candidemia Samples

A total of 45 blood samples from hospitalized patients with suspected candidemia were used to further evaluate the effectiveness of ddPCR in detecting *Candida* in clinical samples. The detection rates of the ddPCR method were also compared with those obtained from culture and qPCR methods. The results showed that the positive detection rates were 44% for culture method ($n=20$), 51% for qPCR ($n=23$), and 73% for ddPCR ($n=32$), respectively, of which 29 patients (64%) were positive either by culture or qPCR method alone, or by both methods, which was inferior to the positive rate of the ddPCR method. When compared with the two other methods, the sensitivity of ddPCR was much higher, with 94 *vs.* 69% for culture and 79% for qPCR method (**Table 1**). With 91% positive predictive value and 85% negative predictive value, the ddPCR method was more sensitive and efficient than either culture or qPCR method for candidemia diagnosis.

DISCUSSION

This study demonstrated that ddPCR assay facilitated accurate quantification of *Candida* DNA in human blood. As no standard curve is needed, ddPCR also allows for the direct comparison of *Candida* concentrations measured by different laboratories. Previous studies found that variation in quantification between technical replicates was considerably lower for ddPCR than for qPCR (Sedlak et al., 2014; Wu et al., 2018). Hence, ddPCR has advantages over other qPCR methods for pathogen DNA detection in clinical samples. Despite the popularity of qPCR, differences between testing instruments, different agents or suppliers, or variations in the standard curves can confound the interpretation and the portability of results (Chindamporn et al., 2018; Cutarelli et al., 2021).

The ddPCR method showed good reproducibility and high specificity in this study. As expected, the sensitivity of ddPCR assay for *Candida* spp. detection in blood samples was significantly higher than that of culture or qPCR methods. The sensitivity of ddPCR (94%) was higher than the 86% observed in neonates in a previous study (Li et al., 2019). Given that our patients were mainly adults, this difference could be due to quantitative differences of fungal cells in the blood between adults and neonates after the onset of disease (sampling time). The ddPCR method also has other diagnostic advantages over conventional qPCR, including lower sample volume requirements and faster execution times, because the thermocycling times are shorter (De falco et al., 2021).

The specificity of the probe sets used in ddPCR assays for specific microbes is often established using closely related species and unrelated species such as human DNA. The probe in the present study was 100% specific for *Candida* genus and did not hybridize with human DNA. The probe was designed based on two observations. First, about 80% of current systemic fungal infections are caused by *Candida* species; second,

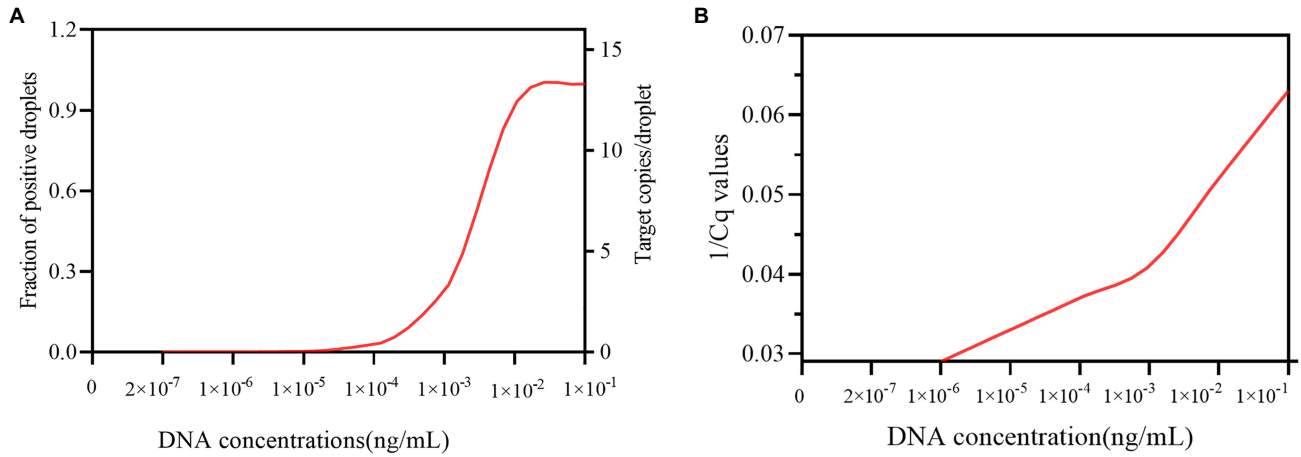

FIGURE 2 | The sensitivity of the ddPCR and qPCR assays in detecting candidemia. **(A)** Shows the sensitivity of ddPCR in detecting candidemia. X-axis represents the theoretical dynamic range of DNA concentration (2×10^{-7}–1×10^{-5} ng/ml). Y-axis on the left represents the fraction of positive droplets detected by ddPCR. Y-axis on the right represents target copies/droplet detected by ddPCR. **(B)** Shows the sensitivity of qPCR in detecting candidemia. X-axis indicates the DNA concentration, ranging from 2×10^{-7}–1×10^{-1} ng/ml Y-axis indicates the 1/Cq value detected by qPCR.

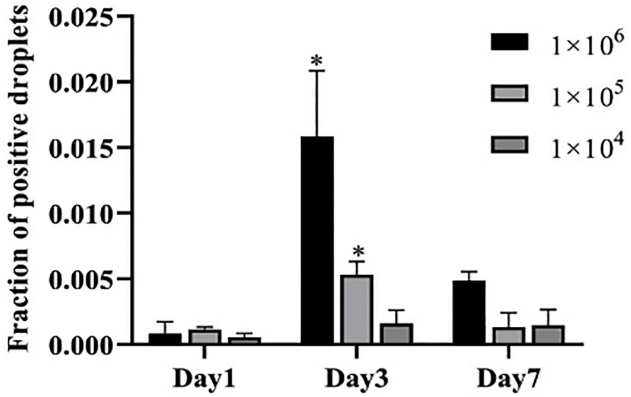

FIGURE 3 | Determination of fraction of positive droplets by ddPCR assay in infected mice. Three concentrations of *Candida* cells were injected into three groups of mice ($n = 5$ for each group) *via* tail vein. The copies of *C. albicans* DNA in blood samples are determined at days 1, 3, and 7 post-infection. Y-axis represents fraction of positive droplets. The fraction of positive droplets is significantly higher at day 3 post infection with 1×10^6 and 1×10^5 inoculations than at the time points of days 1 and 7. *Present the p value <0.05.

TABLE 1 | Positive and negative predictive values, sensitivity and specificity of different diagnostic assays in patients with suspected candidemia ($n = 45$, including two neonates).

Diagnostic method	Detection rate (%)	Sensitivity (%)	Specificity (%)	Positive predictive value (%)	Negative predictive value (%)
Culture	44	69	100	100	64
RT-PCR	64	89	76	86	81
ddPCR	73	94	79	91	85

RT-PCR, Real Time-PCR; and ddPCR, droplet digital PCR.

approximately 60% of fungal isolates are *C. albicans* (Kim et al., 2020). However, non-*albicans* species, such as *C. tropicalis*, *C. parapsilosis*, *C. glabrata*, and *C. krusei*, are also prevalent (Krcmery and Barnes, 2002; Wisplinghoff et al., 2014). The probe and primer set used in this study could detect DNA from non-*albicans* species, such as *C. tropicalis*, *C. parapsilosis* and *C. glabrata*, which would reduce the likelihood of overlooking the presence of non-*albicans* species in clinical practice. Meanwhile, this probe and primer set based on the *Candida* genus could not detect other fungal pathogens, such as *Aspergillus* spp. and *T. rubrum*, and bacteria such as *S. aureus*, *E. coli*, *P. aeruginosa*, and *S. pneumoniae*, which are commonly found in patients with bacteremia.

Both high sensitivity and specificity in ddPCR could facilitate the studies on other fungal detections in future. For example, an assay to identify fungal species in a single run of ddPCR assay could be developed using two probes, of which one probe could be based on the genus and the second probe could be based on the particular species. We will continue to evaluate the sensitivity and specificity of ddPCR in larger candidemia cohorts, and in other types of clinical samples (*e.g.*, urine or BAL). Given its higher sensitivity, a prospective clinical study using the ddPCR assay for the identification of patients at high risk for invasive fungal infections is underway.

The high specificity and sensitivity of ddPCR facilitates its application in the early diagnosis of candidemia. In this study, two blood samples were obtained from infants suspected with candidemia. Both infants were detected positive by ddPCR assay but negative by culture and qPCR assays. Following the diagnosis of candidemia based on the ddPCR assay, these two infant patients were immediately given anti-fungal treatment and quickly cured. In order to avoid false negative result, a series of diluted samples need to be prepared and detected by ddPCR assay in the early diagnosis of candidemia.

DATA AVAILABILITY STATEMENT

The raw data supporting the conclusions of this article will be made available by the authors, without undue reservation.

ETHICS STATEMENT

The studies involving human participants were reviewed and approved by the Jining Medical College and Jining No. 1 People's Hospital, Shandong, China (2020–028). Written informed consent to participate in this study was provided by the participants' legal guardian/next of kin. The animal study was reviewed and approved by the Jining Medical College, Shandong, China (2020–028).

AUTHOR CONTRIBUTIONS

BC was mainly for investigation, formal analysis, and writing-original draft. NZ was mainly for investigation and formal analysis. WL, DL, CL, SB, YJ, ZY, RL, and YF were mainly for collecting samples. YX, XZ, and DS were mainly for designing the study, funding acquisition, investigation, and review and editing. All authors contributed to the article and approved the submitted version.

FUNDING

This work was supported in part by grants from the National Natural Science Foundation of China (NM 81773337), the Key Research and Development Plan of Shandong Province (NM 2019GSF108191), the Key Research and Development Plan of Jining (NM2019SMNS008), the Doctoral Fund of Jining No.1 People's Hospital (2019004), the Technology Development Program of Shandong Province (2018WS469 and 2018WS477), the China Postdoctoral Science Foundation (2020T130073ZX), and the Natural Science Foundation of Shandong Province (NM ZR2020QH272), China.

SUPPLEMENTARY MATERIAL

The Supplementary Material for this article can be found online at: https://www.frontiersin.org/articles/10.3389/fmicb.2021.700008/full#supplementary-material

REFERENCES

Cheng, X., Sun, L., Zhao, Q., Mi, Z., Yu, G., Wang, Z., et al. (2019). Development and evaluation of a droplet digital PCR assay for the diagnosis of paucibacillary leprosy in skin biopsy specimens. *PLoS Negl. Trop. Dis.* 13:e0007284. doi: 10.1371/journal.pntd.0007284

Chindamporn, A., Chakrabarti, A., Li, R., Sun, P. L., Tan, B. H., Chua, M., et al. (2018). Survey of laboratory practices for diagnosis of fungal infection in seven Asian countries: An Asia fungal working group (AFWG) initiative. *Med. Mycol.* 56, 416–425. doi: 10.1093/mmy/myx066

Clancy, C. J., and Nguyen, M. H. (2013). Finding the "missing 50%" of invasive candidiasis: how nonculture diagnostics will improve understanding of disease spectrum and transform patient care. *Clin. Infect. Dis.* 56, 1284–1292. doi: 10.1093/cid/cit006

Cutarelli, A., De Falco, F., Uleri, V., Buonavoglia, C., and Roperto, S. (2021). The diagnostic value of the droplet digital PCR for the detection of bovine deltapapillomavirus in goats by liquid biopsy. *Transbound. Emerg. Dis.* doi: 10.1111/tbed.13971 [Epub ahead of print].

De Falco, F., Corrado, F., Cutarelli, A., Leonardi, L., and Roperto, S. (2021). Digital droplet PCR for the detection and quantification of circulating bovine deltapapillomavirus. *Transbound. Emerg. Dis.* 68, 1345–1352. doi: 10.1111/tbed.13795

de Pauw, B., Walsh, T. J., Donnelly, J. P., Stevens, D. A., Edwards, J. E., Calandra, T., et al. (2008). Revised definitions of invasive fungal disease from the European Organization for Research and Treatment of cancer/invasive fungal infections cooperative group and the National Institute of Allergy and Infectious Diseases mycoses study group (EORTC/MSG) consensus group. *Clin. Infect. Dis.* 46, 1813–1821. doi: 10.1086/588660

Golan, Y., Wolf, M. P., Pauker, S. G., Wong, J. B., and Hadley, S. (2005). Empirical anti-Candida therapy among selected patients in the intensive care unit: a cost-effectiveness analysis. *Ann. Intern. Med.* 143, 857–869. doi: 10.7326/0003-4819-143-12-200512200-00004

Momin, K. M., Milton, A. A. P., Ghatak, S., Thomas, S. C., Priya, G. B., Das, S., et al. (2020). Development of a novel and rapid polymerase spiral reaction (PSR) assay to detected *Salmonella* in pork and pork products. *Mol. Cell. Probes.* 50:101510. doi: 10.1016/j.mcp.2020.101510

Kim, E. J., Lee, E., Kwak, Y. G., Yoo, H. M., Choi, J. Y., Kim, S. R., et al. (2020). Trends in the epidemiology of candidemia in intensive care units from 2006 to 2017: results from the Korean National Healthcare-Associated Infections Surveillance System. *Front. Med.* 7:606976. doi: 10.3389/fmed.2020.606976

Krcmery, V., and Barnes, A. J. (2002). Non-albicans *Candida* spp. causing fungaemia: pathogenicity and antifungal resistance. *J. Hosp. Infect.* 50, 243–260. doi: 10.1053/jhin.2001.1151

Li, H. T., Lin, B. C., Huang, Z. F., Yang, C.-Z., and Huang, W.-M. (2019). Clinical value of droplet digital PCR in rapid diagnosis of invasive fungal infection in neonates. *Zhongguo Dang Dai ErKe Za Zhi* 21, 45–51. doi: 10.7499/j.issn.1008-8830.2019.01.009

Mantadakis, E., Pana, Z. D., and Zaoutis, T. (2018). Candidemia in children: epidemiology, prevention and management. *Mycoses* 61, 614–622. doi: 10.1111/myc.12792

McMullan, R., Metwally, L., Coyle, P. V., Hedderwick, S., McCloskey, B., O'Neill, H. J., et al. (2008). A prospective clinical trial of a real-time polymerase chain reaction assay for the diagnosis of candidemia in nonneutropenic, critically ill adults. *Clin. Infect. Dis.* 46, 890–896. doi: 10.1086/528690

Ngamchokwathana, C., Chongtrakool, P., Waesamaae, A., and Chayakulkeeree, M. (2021). Risk factors and outcomes of non-*albicans candida* bloodstream infection in patients with candidemia at siriraj hospital-thailand largest national tertiary referral hospital. *J. Fungi.* 7:269. doi: 10.3390/jof7040269

Nyaruaba, R., Mwaliko, C., Kering, K. K., and Wei, H. (2019). Droplet digital PCR applications in the tuberculosis world. *Tuberculosis* 117, 85–92. doi: 10.1016/j.tube.2019.07.001

Pappas, P. G., Lionakis, M. S., Arendrup, M. C., Ostrosky-Zeichner, L., and Kullberg, B. J. (2018). Invasive candidiasis. *Nat. Rev. Dis. Primers.* 4:18026. doi: 10.1038/nrdp.2018.26

Pfaller, M. A., and Diekema, D. J. (2007). Epidemiology of invasive candidiasis: a persistent public health problem. *Clin. Microbiol. Rev.* 20, 133–163. doi: 10.1128/CMR.00029-06

Schell, W. A., Benton, J. L., Smith, P. B., Poore, M., Rouse, J. L., Boles, D. J., et al. (2012). Evaluation of a digital microfluidic real-time PCR platform to detect DNA of Candida albicans in blood. *Eur. J. Clin. Microbiol. Infect. Dis.* 31, 2237–2245. doi: 10.1007/s10096-012-1561-6

Schiavetto, C. M., de Abreu, P. M., von Zeidler, S. V., de Jesus, L. M., Carvalho, R. S., Cirino, M. T., et al. (2021). Human papillomavirus DNA detection by droplet digital PCR in formalin-fixed paraffin-embedded tumor tissue from oropharyngeal squamous cell carcinoma patients. *Mol. Diagn. Ther.* 25, 59–70. doi: 10.1007/s40291-020-00502-6

Schroeder, M., Weber, T., Denker, T., Winterland, S., Wichmann, D., Rohde, H., et al. (2020). Epidemiology, clinical characteristics, and outcome of candidemia in critically ill patients in Germany: a single-center retrospective 10-year analysis. *Ann. Intensive Care* 10:142. doi: 10.1186/s13613-020-00755-8

Sedlak, R. H., Kuypers, J., and Jerome, K. R. (2014). A multiplexed droplet digital PCR assay performs better than qPCR on inhibition prone samples. *Diagn. Microbiol. Infect. Dis.* 80, 285–286. doi: 10.1016/j.diagmicrobio.2014.09.004

Tulasidas, S., Rao, P., Bhat, S., and Manipura, R. (2018). A study on biofilm production and antifungal drug resistance among Candida species from vulvovaginal and bloodstream infections. *Infect Drug Resist.* 11, 2443–2448. doi: 10.2147/IDR.S179462

Tumbarello, M., Posteraro, B., Trecarichi, E. M., Fiori, B., Rossi, M., Porta, R., et al. (2007). Biofilm production by *Candida* species and inadequate antifungal therapy as predictors of mortality for patients with candidemia. *J. Clin. Microbiol.* 45, 1843–1850. doi: 10.1128/JCM.00131-07

Wisplinghoff, H., Ebbers, J., Geurtz, L., Stefanik, D., Major, Y., Edmond, M. B., et al. (2014). Nosocomial bloodstream infections due to Candida spp. in the USA: species distribution, clinical features and antifungal susceptibilities. *Int. J. Antimicrob. Agents* 43, 78–81. doi: 10.1016/j.ijantimicag.2013.09.005

Wu, X., Xiao, L., Lin, H., Chen, S., Yang, M., An, W., et al. (2018). Development and application of a droplet digital polymerase chain reaction (ddPCR) for detection and investigation of African swine fever virus. *Can. J. Vet. Res.* 82, 70–74.

Yang, J., Han, X., Liu, A., Bai, X., Xu, C., Bao, F., et al. (2017). Use of digital droplet PCR to detect *mycobacterium tuberculosis* DNA in whole blood-derived DNA samples from patients with pulmonary and extrapulmonary tuberculosis. *Front. Cell. Infect. Microbiol.* 7:369. doi: 10.3389/fcimb.2017.00369

Conflict of Interest: The authors declare that the research was conducted in the absence of any commercial or financial relationships that could be construed as a potential conflict of interest.

Publisher's Note: All claims expressed in this article are solely those of the authors and do not necessarily represent those of their affiliated organizations, or those of the publisher, the editors and the reviewers. Any product that may be evaluated in this article, or claim that may be made by its manufacturer, is not guaranteed or endorsed by the publisher.

frontiers in Microbiology

ORIGINAL RESEARCH
published: 07 September 2021
doi: 10.3389/fmicb.2021.709880

Effects of 3% Boric Acid Solution on Cutaneous *Candida albicans* Infection and Microecological Flora Mice

Qing Liu[1], Zhao Liu[2], Changlin Zhang[1], Yanyan Xu[2], Xiaojing Li[2] and Hongqi Gao[2]**

[1] Department of Clinical Medicine, Hebei University of Engineering, Handan, China, [2] Department of Dermatology, Affiliated Hospital of Hebei University of Engineering, Handan, China

OPEN ACCESS

Edited by:
Keke Huo,
Fudan University, China

Reviewed by:
Xuhua Tang,
The First Affiliated Hospital of Sun Yat-sen University, China
Ping Zhan,
Jiangxi Provincial People's Hospital, China

***Correspondence:**
Xiaojing Li
zlmdsh@126.com
Hongqi Gao
710677661@qq.com

Specialty section:
This article was submitted to Antimicrobials, Resistance and Chemotherapy, a section of the journal Frontiers in Microbiology

Received: *14 May 2021*
Accepted: *25 June 2021*
Published: *07 September 2021*

Citation:
Liu Q, Liu Z, Zhang C, Xu Y, Li X and Gao H (2021) Effects of 3% Boric Acid Solution on Cutaneous Candida albicans Infection and Microecological Flora Mice. Front. Microbiol. 12:709880. doi: 10.3389/fmicb.2021.709880

To determine the effect of 3% boric acid solution on cutaneous infections with *Candida albicans* (CA) in mice and its effect on skin microflora. Female mice were divided into three groups, with 18 mice in each group. Two injection sites were randomly selected, and 0.1 mL of CA mycelium suspension was injected into the epidermis and dermis of the back of mice. Group N was treated with sterile water for injection (SWFI). We observed the clinical manifestations, fungal fluorescence microscopic examination and colony count. Group B were hydropathically compressed with 3% boric acid solution for 30 min every 12 h. Group M was treated with SWFI, and group N was not treated. One week later, each group was observed with naked eyes, and skin samples were collected. The effect of boric acid on skin microflora was measured using Internal Transcribed Spacer Identification (ITS) and 16S rRNA genes. There were no significant changes in group M. In group B, the degree of skin injury was alleviated, the wounds healed markedly, and the exudate amount decreased. The effective rate of group B (83%) was significantly higher than that of group M (25%) ($P < 0.05$). The relative average abundance of *Candida* ($P < 0.0001$) and CA ($P < 0.05$) in group B was significantly lower than that in group M. Compared with group M, the microbial richness of group B changed little, but the diversity decreased. The flora structure of group B was significantly different from that of group M, but like that of group N. In group B, the abundance of *Proteobacteria* ($P < 0.001$), *Enterobacteriaceae* ($P < 0.001$), and *Escherichia-Shigella* ($P < 0.001$) was significantly greater, and the abundance of *Firmicutes* ($P < 0.001$), *Staphylococcaceae* ($P < 0.001$), and *Staphylococcus* ($P < 0.001$) were significantly lower. The 3% boric acid solution significantly reduced the symptoms of skin infection with *Candida albicans*. It inhibited the growth of *Candida albicans* and CA, reduced the diversity of skin microorganisms, increased the abundance of *Proteobacteria, Enterobacteriaceae, Escherichia-Shigella,* and reduced the abundance of *Firmicutes, Staphylococcaceae, Staphylococcus*.

Keywords: boric acid, *Candida albicans*, mice, ITS, 16S rRNA, skin microecology

INTRODUCTION

There are more than 200 species of *Candida*, dozens of which have been proved to cause human candidiasis. Cutaneous candidiasis is the most common and most pathogenic (Sardi et al., 2013; Dardas et al., 2014).*Candida albicans* (CA) typically colonizes the surface of normal human skin and mucous membranes. The carriage rate of CA in normal people is as high as 14–45% (Perlorth et al., 2007). When immunological resistance is low or flora imbalances, CA often invades skin folds and causes cutaneous candidiasis, with a high incidence in summer and autumn. It is more common in infants, diabetics, obese, hyperhidrotic individuals, and those working in humid environments (Wang et al., 2012). In severe cases, *Candida* can cause deep infections. For immunosuppressed individuals, systemic infection is often life-threatening and difficult to treat, with mortality rates between 46 and 75% (Brown et al., 2012).

The treatment of superficial skin CA infection is mainly external use of drugs, once or twice a day. The course of treatment is 2–4 weeks. Imidazoles and acrylamines are preferred, and imidazoles include miconazole, bifonazole, ketoconazole and so on. Allylamines include terbinafine, butenafine, and naftifine. Others include morpholine, lira naphthyl ester (thiocarbamate), cyclopamine (cyclopyrone), imidazoles, and acrylamines (Katoh, 2009; Riachi, 2013). Patients with severe infections should be treated with combinations of oral medications. The partial effect of local treatment alone is unsatisfactory. The tissue selectivity of drugs is low. There are relatively many toxic side effects and adverse reactions, and drug resistance is possible. Therefore, there is an urgent need for alternative therapies.

As a common topical drug in dermatology, boric acid is less expensive, widely available, easy to use, and causes little irritation. *In vitro* tests showed that boric acid and boron-containing compounds inhibited *Candida*, *Trichophyton*, gram-positive bacteria, and gram-negative bacteria (Gerdon and Flynm, 2014). Its antibacterial activity is time-dependent and concentration-dependent (Iavazzo et al., 2011). A low concentration of boric acid inhibits pathogenic bacteria, while high concentrations of boric acid kill pathogenic bacteria (Brittingham and Wilson, 2014). Boric acid at 10–20 mg/mL inhibits almost all common bacteria or fungi (Hui et al., 2016). Boric acid has been used to treat cutaneous CA infections for more than one hundred years (Javad et al., 2015; Gao and Pan, 2016); nevertheless, its specific mechanisms are not clear but may involve the inhibition of mitochondrial enzyme activity and energy metabolism (Schmidt et al., 2018). Studies showed that boric acid increases the permeability of the pathogen cell wall, destroys cell membranes, and inhibits cell membrane formation (Brittingham and Wilson, 2014; Marrazzo et al., 2019). Nevertheless, the effect of boric acid on microflora has been rarely reported.

Therefore, in the present study, a mouse cutaneous CA infection model was established. ITS and 16S rRNA high-throughput sequencing were used to measure the improvement of clinical symptoms and skin microflora before and after treatment.

Laboratory Animals and Strains

Healthy female ICR mice aged 6–8 weeks, weighing 22–24 g, were purchased from Beijing Weitong Lihua Experimental Animal Technology Co., Ltd. *Candida albicans* standard strain SC 5314 was purchased from the American Type Culture Collection.

Reagents and Instruments

The 3% boric acid solution was provided by the Affiliated Hospital of Hebei Engineering University. The DNA extraction kit was purchased from MP Biomedicals (US). The library-building kit was provided by Bioo Scientific Corp. (US).

Preparation of *Candida albicans* Liquid

The standard strain of CA (SC5314) stored at –4°C was thawed at room temperature. The concentration of bacteria was adjusted to 1.5×10^9 colony-forming units CFU/mL through purification and activation of bacteria.

Model Construction and Group Intervention

Mice were randomly divided into N (n = 18), M (n = 18), and B groups (n = 18). Chlorpromazine solution 0.2 mL was injected intramuscularly for anesthesia, hair on the back was shaved, and two injection sites were randomly selected. The mycelium suspension 1.5×10^9 cells/0.1 mL was injected into the M and B groups, and the control group was treated with SWIF. Six mice were randomly selected to observe the clinical manifestations. Fungal fluorescence microscopy and colony count were used to determine whether the mouse skin CA infection model was successfully constructed.

On the fifth day after inoculation, 12 mice in each group were anesthetized by the above methods. Each mouse in group B was hydropathic compressed with six layers of sterile gauze and 3% boric acid solution for 30 min, once every 12 h. Group M was treated with SWIF, while the blank group was fed normally without treatment.

Sample Collection

On the 7th day of treatment, an aseptic flocking cotton swab infiltrated with saline was repeatedly wiped at each mouse's back in each group for 30 s to remove the microorganisms on the skin surface. We cut the cotton swab head into 2.0 mL aseptic frozen tubes, quick-frozen in liquid nitrogen, and stored at –80°C.

TABLE 1 | PCR Sequencing regions and primer sequences.

Sequencing area	Up-primer	Lower-stream primers
Bacteria 16S rDNA 338F_806R District	338F: ACTCCTACG GGAGGCAGCAG	806R: GGACTACH VGGGTWTCTAAT
Fungi ITS1F_ITS1F District	ITS1F: CTTGGTCATTT AGAGGAAGTAA	ITS1F: GCTGCGTTCT TCATCGATGC

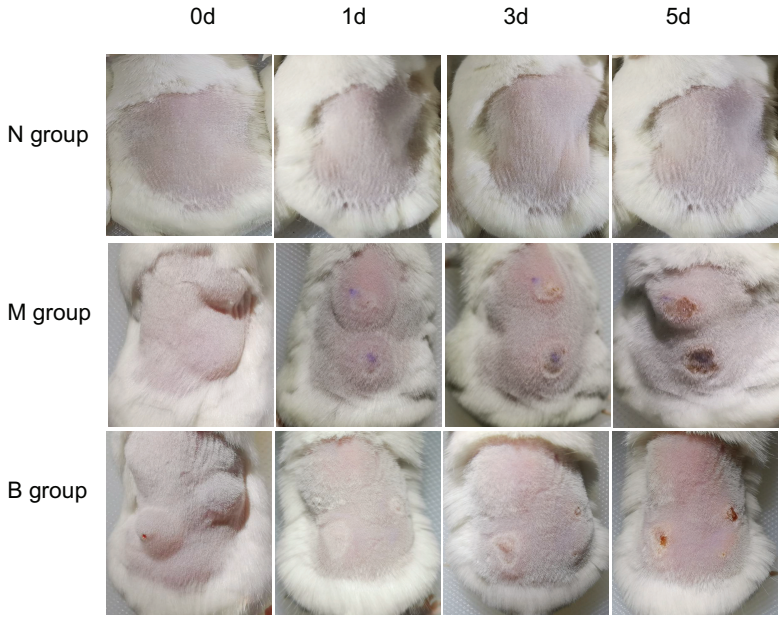

FIGURE 1 | Skin changes from days 0 to 5 in each group.

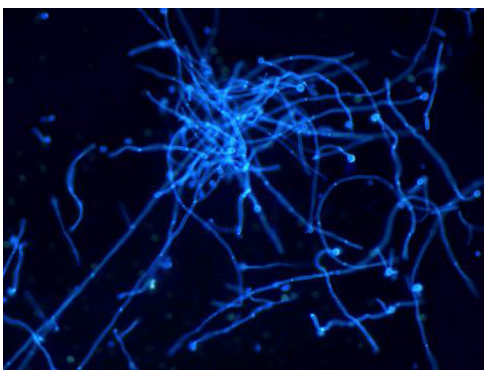

FIGURE 2 | Direct skin microscopic results (×400 magnification).

Fluorescence Microscopic Examination of Fungi

Five days after inoculation, two mice were randomly selected from each group, a total of six mice. An aseptic cotton swab infiltrated with saline was used to wipe and rotate each mouse's back in each group, spread on glass slides, and observed under a light microscope after adding potassium hydroxide solution dropwise.

Colony Counts

Five days after inoculation, two mice were randomly selected from each group, a total of six mice. The infected tissue was quickly cut along the edge of the skin lesion with surgical scissors in the aseptic operating table, and the infected tissue was broken, centrifuged, diluted, and colony counted.

Judgment of Curative Effect

The curative effect was judged by the standard as described (Jie et al., 2019). A markedly effective refers to the original skin lesion healing after 7 days of treatment; effective refers to the decrease of the original purulent exudate and improvement of skin lesion healing after 7 days of treatment. Ineffective means that the clinical symptoms are not significantly improved or even aggravated.

Detection of Microflora Diversity

Skin samples frozen at −80°C were removed and treated with FastDNA SpinKitforSoil® to extract the total DNA of skin microorganisms. The library was prepared by DNA purity and concentration detection, and PCR amplification. The corresponding regions of bacterial 16srRNA and fungal ITS primers for high-throughput sequencing PCR amplification were shown in **Table 1**. Finally, the Miseq PE300/NovaSeqPE250 platform of Illumina Company was used for sequencing, reads-splicing and filtering, OTUs clustering, bioinformatics analysis, and data processing.

Statistical Analysis

SPSS23.0 software was used for statistical analysis. The measurement data were expressed as mean ± standard deviation ($\chi \pm s$). Analysis of variance or the Kruskal–Wallis test was used for comparisons among groups. The least-squares difference test was used to analyze the differences between the two groups further. The independent sample *t*-test was used for comparisons between the two groups. Differences were statistically significant when $P < 0.05$. We use mothur software to calculate alpha diversity indexes (Chao1, ACE, Shannon, and Simpson) and R language tools to create drawings.

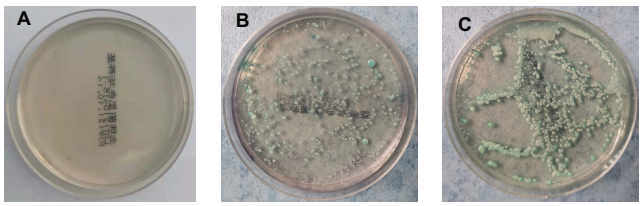

FIGURE 3 | Color culture of *Candida albicans*. **(A)** Refers to group N, **(B)** refers to group M, and **(C)** refers to group B.

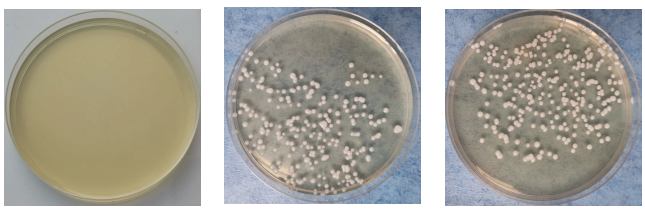

FIGURE 4 | Growth of *Candida albicans* coated plate. **(A)** Refers to group N, **(B)** refers to group M, and **(C)** refers to group B.

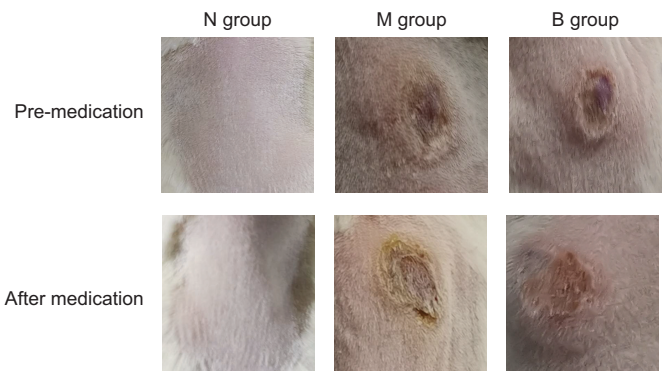

FIGURE 5 | Skin conditions before and after treatment.

TABLE 2 | Comparison of therapeutic effects among groups.

Group	Markedly effective	Effective	Ineffective	Total	*P*
M	0	3	9	12	0.012
B	0	10	2	12	

TABLE 3 | Comparison of abundance of *Candida* in each group.

Group	Candida	CA	*P*
M (*n* = 20)	99.83 ± 0.31	99.70 ± 0.33	0.00
B (*n* = 24)	91.15 ± 19.07	90.99 ± 19.05	0.04

Clinical Manifestations

After inoculating CA SC5314 (**Figure 1**), subcutaneous masses formed in M and B groups. Over time, the subcutaneous masses were gradually absorbed, white filmS appeared on the first day, and mild necrosis appeared on the third day, which was most apparent on the 5th day. Erosions and ulcers could be seen in the model. There were no changes in group N.

Fluorescence Microscopic Examination of Fungi

On the 5th day after inoculation of CA SC5314 (**Figure 2**), evident agglomerated hyphae were found in both M and B groups. The microscopic examination of fungi in group N was negative.

Colony Counts

On the 5th day after inoculation of CA SC5314 (**Figure 3**), CA was cultured in a chromogenic screening medium. CA appeared emerald-green with smooth colonies in M and B groups, while CA was negative in group N. Microscopic observation and counting showed that both M and B groups had higher fungal loads, about 10^5–10^6 CFU/g (**Figure 4**). We observed that the cutaneous infection model was successfully established from the three indicators of

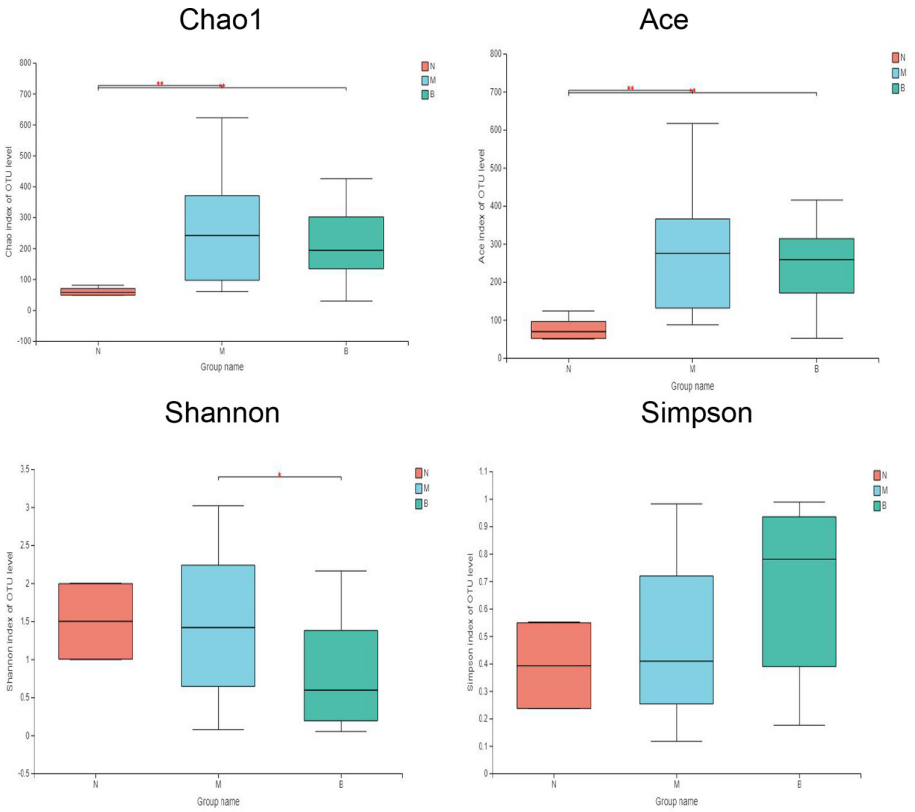

FIGURE 6 | Comparative analysis of diversity indices of different treatment groups. *$P \leq 0.05$; **$P \leq 0.01$.

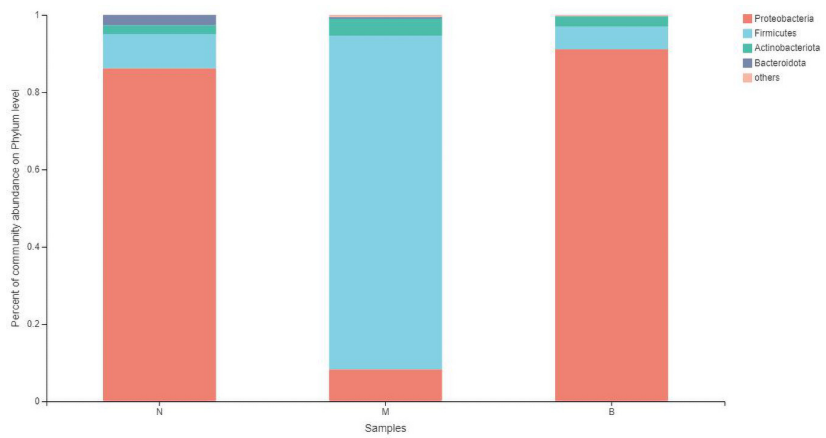

FIGURE 7 | The abundance of phylum level.

clinical manifestations, microscopic examination of fungi, and colony counts.

Therapeutic Effect

There was no irritation after treatment, and the skin lesions at the modeling site were observed with naked eyes on the 7th day (**Figure 5**). There was no apparent change in group N; however, erosions could be seen in group M, which was not significantly better than before treatment. The degree of injury was reduced in group B, suggesting that the wound underwent apparent healing without exudate. Treatment results are shown in **Table 2**. The number of markedly effective cases was 0; however, after 3% boric acid solution treatment, ten cases were effective, two cases were ineffective, and the effective rate was 83%. After SWFI, three cases were effective, nine were ineffective, and the effective rate was 25%. By comparison, the effective rate of group

B was significantly higher than that of group M ($P < 0.05$), suggesting that 3% boric acid solution had a therapeutic effect on cutaneous CA infections.

The Average Relative Abundance

A total of 72 skin samples were collected from 24 skin samples in each group, of which 44 skin samples were qualified and were sequenced using ITS. The bands of PCR amplification products of all skin samples in the blank group were too weak or were not detected, and no follow-up experiments were carried out. Considering that this phenomenon may have been related to fungi's low content in mouse skin, it was challenging to obtain sufficient samples. Referring to the Unite database of ITS, the dominant fungus of genus level was *Candida* (95.40%), and the dominant fungus on the species level was CA (95.26%), consistent with the results of our fungal microscopic examination, further demonstrating that the mouse skin was infected with CA successfully. The average relative abundance of *Candida and* CA in each group was compared (**Table 3**). The *Candida* ($P < 0.01$) and CA ($P < 0.05$) of group B were significantly lower than those of group M, suggesting that boric acid had a therapeutic effect. The therapeutic effect was consistent with that of naked-eye observation.

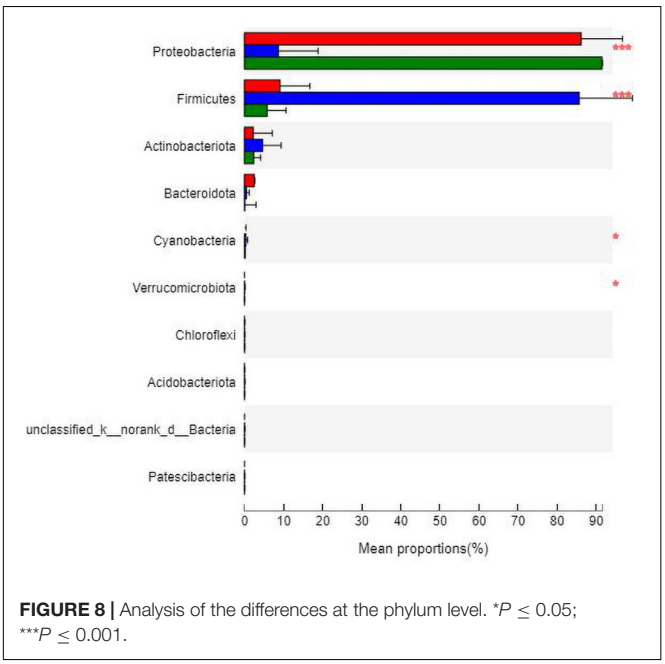

FIGURE 8 | Analysis of the differences at the phylum level. *$P \leq 0.05$; ***$P \leq 0.001$.

Alpha Diversity of Bacterial Flora

The diversity indices of the three groups are shown in **Figure 6** (Li et al., 2013). Compared with group N, the Ace and Chao1 indexes of group M ($P < 0.01$) and group B ($P < 0.01$) were significantly increased, while there was no significant difference between group M and group B, suggesting that the flora richness of group M and group B was higher. This finding suggests that the microflora richness of the model and boric acid groups were higher. This may be related to skin infection with CA in both groups of mice. In comparing the diversity index, we found that the Shannon index of group B was significantly lower than that of group M ($P < 0.05$), and the Shannon index of group B was lower than that of group N ($P = 0.126$); however, the difference was not significant. The Simpson index in group B was higher than those of groups N ($P = 0.094$) and M ($P = 0.054$); however, the differences were not significant. These findings suggest that the skin microflora diversity of group B was decreased than that of the other two groups, and boric acid may reduce the bacterial flora diversity on the skin surface.

Analysis at the Phylum Level

At the phylum level (**Figure 7**), the community bar diagram showed that *Proteobacteria*, *Firmicutes*, *Actinobacteria*, *Bacteroidota* were dominant colonies in mouse skin. However, the abundance of these four bacteria in the three groups were significantly different, 86.19, 8.87, 2.31 and 2.63% in group N,

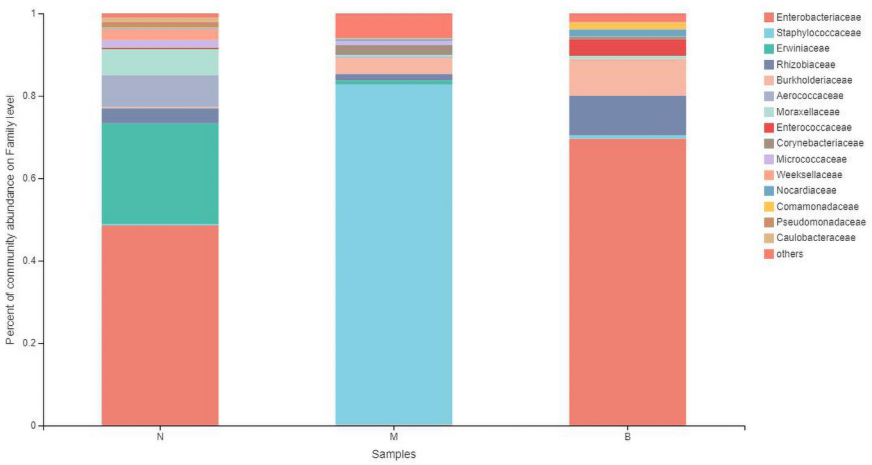

FIGURE 9 | The abundance of the family level.

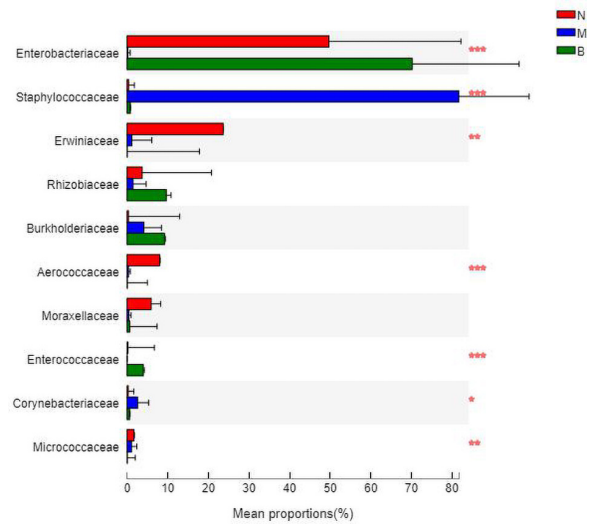

FIGURE 10 | Analysis of the differences at the level of the family level. $^{*}P \leq 0.05$; $^{**}P \leq 0.01$; $^{***}P \leq 0.001$.

8.26, 86.40, 4.34 and 0.46% in group M, and 91.07, 5.86, 2.67, and 0.09% in group B, respectively.

The analysis of species differences is shown in **Figure 8**. Compared with group N, the *Cyanobacteria* and *Verrucomicrobiota* in groups M ($P < 0.05$) and B ($P < 0.05$) were significantly higher. Compared with group M, the *Proteobacteria* in groups N ($P < 0.001$) and B ($P < 0.001$) were significantly higher. At the same time, the *Firmicutes* were significantly lower in groups N ($P < 0.001$) and B ($P < 0.001$).

Analysis at the Family Level

At the family level (**Figure 9**), *Enterobacteriaceae* was the most abundant species in groups N and B, with proportions of 48.52 and 69.58%, respectively. *Enterobacteriaceae* only accounted for 0.14% in group M. *Staphylococcaceae* was the most abundant species in group M, with a proportion of 82.61%, and *Staphylococcaceae* abundances were 0.35 and 0.77% in groups N and B, respectively.

The analysis of species differences is shown in **Figure 10**. *Erwiniaceae* and *Aerococcaceae* in group N were significantly increased ($P < 0.01$). In group M, *Enterobacteriaceae* was significantly decreased, while *Staphylococcaceae* and *Corynebacteriaceae* were significantly increased ($P < 0.01$). In group B, Enterococcaceae was significantly increased, and Micrococcaceae was significantly decreased ($P < 0.01$).

Analysis at the Genus Level

At the genus level (**Figure 11**), *Enterobacter* was the most abundant species in group N, accounting for 48.49%, while only 0.12 and 0% in groups M and B, respectively. The dominant species in group M was *Staphylococcus*, accounting for 79.05% and only 0.34 and 0.70% in groups N and B, respectively. The most abundant strain in group B was *Escherichia*, followed by *Shigella*, with a proportion of 69.58%, while in groups B and M, both were close to 0%.

The analysis of species differences is shown in **Figure 12**. In group B, *Enterobacter*, *Pantoea,* and *Aerococcus* were significantly increased ($P < 0.01$), and *Ralstonia* was significantly decreased ($P < 0.05$). *Staphylococcus* in group M was significantly increased ($P < 0.01$). *Escherichia-Shigella* and *Enterobacter* in group B were significantly increased ($P < 0.01$).

Community Heatmap Map

At the family and genus level, a heatmap of species clustering was drawn (**Figure 13**). We found that the dominant bacteria genera of the microorganisms in the three groups were different. Most of groups N and B were from *Proteobacteria*, and most of group M were from *Firmicutes*. At the family level, the cross-clustering between group N and group B indicated that the dominant bacteria family composition of the two groups was more similar but different from that of group M. However, at the genus level, the cross-clustering between groups M and B suggested that the dominant bacteria genus composition of the two groups was more similar. However, the dominant bacterial genus of group B showed a changing trend of transformation to group N, suggesting that boric acid may improve the structure of the skin bacteria community and develop toward a healthy and beneficial trend.

DISCUSSION

With the widespread use of antibiotics, the prevalence of diabetes and obesity, dentures, and other factors, the risk of cutaneous CA infection has become significant. These infections include chronic skin candidiasis, *Candida* intertriginous rash, angular stomatitis, oral candidiasis, candidal onychomycosis and onychomycosis, vaginitis, and balanitis, and others (Spampinato and Leonardi, 2013).

Animal models play essential roles in the study of CA pathogenicity, immunity, drug screening, and new drug research and development. In recent years, there have been several established models, including a systemic *Candida* infection model (Fouts et al., 2012), an oral candidiasis infection model (Solis and Filler, 2011), a vaginal candidiasis infection model (Liu and Wu, 2019), a *Candida* keratitis infection model (Iliev et al., 2012), a lower respiratory tract infection model (Xie, 2011), and a non-mammalian infection model (Sampaio et al., 2018). Nevertheless, there are only a few reports of a cutaneous Candida infection model, including two specific methods. The first method is the classical method of directly applying CA solution to the exfoliated epidermis, described by Gaspari (Santus et al., 2018). In this study, we selected the second method of direct intradermal injection discovered by Fang (Fang et al., 2020) to induce the formation of a CA infection model. Five days after inoculation, white membranes, necrosis, erosions, and ulcers appeared on the back of mice. Fungal hyphae could be seen under a fluorescence microscope, smooth emerald green colonies were shown on the CA screening medium, and the colony culture count reached 10^5–10^6 CFU/g.

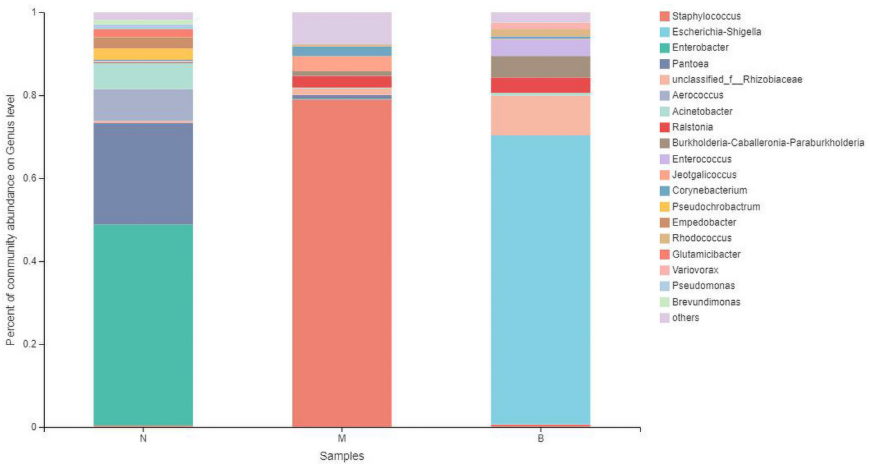

FIGURE 11 | The abundance of the genus level.

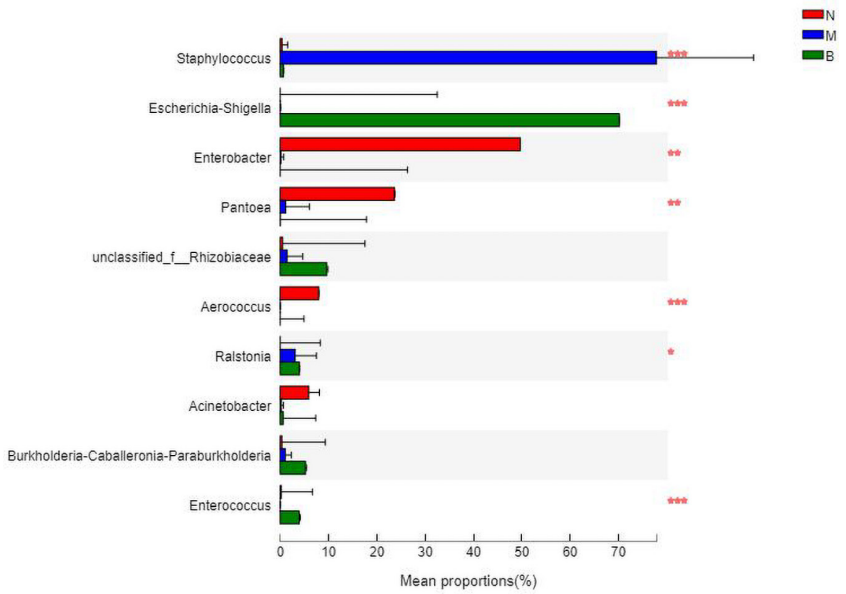

FIGURE 12 | Analysis of the differences at the level of the genus level. *$P \leq 0.05$; **$P \leq 0.01$; ***$P \leq 0.001$.

Boron exists in the form of boric acid at physiological pH (Larsen et al., 2018). Boric acid, a common antibacterial agent (Schmidt et al., 2010), is widely used to treat fungal infections. In recent years, boric acid has been found to have therapeutic effects on cutaneous CA infections, and relevant research has been incorporated into clinical guidelines (Pointer and Schmidt, 2016). Compared with traditional antifungal drugs, adverse reactions associated with boric acid are rare (Powell et al., 2019), there are no interactions with other drugs, and it does not cause microbial drug resistance. Boric acid has antibacterial activity against various yeasts, limiting the growth of CA and inhibiting smooth *Candida albicans* (Pointer et al., 2015).

Nevertheless, its mechanisms of action are not clear. They may involve destroying the cytoskeleton and preventing actin recombination, resulting in abnormal mycelium development, thereby inhibiting mycelium growth (Larsen et al., 2018). Some investigators found that boric acid inhibits glyceraldehyde 3-phosphate dehydrogenase (an NAD glycolysis-dependent enzyme) and ethanol dehydrogenase (an NADH-dependent fermentation enzyme) in CA, thereby inhibiting NAD/NADH-dependent reactions in carbohydrate metabolism, affecting energy metabolism, promoting ethanol production, and increasing the sensitivity of CA to ethanol toxicity (Pointer and Schmidt, 2016). In the present study, we found that, after boric acid treatment, the skin showed no irritation, and the degree of injury was alleviated, suggesting wound healing. ITS sequencing analysis showed that the abundance of *Candida* and CA in group B was significantly lower, further suggesting that boric acid

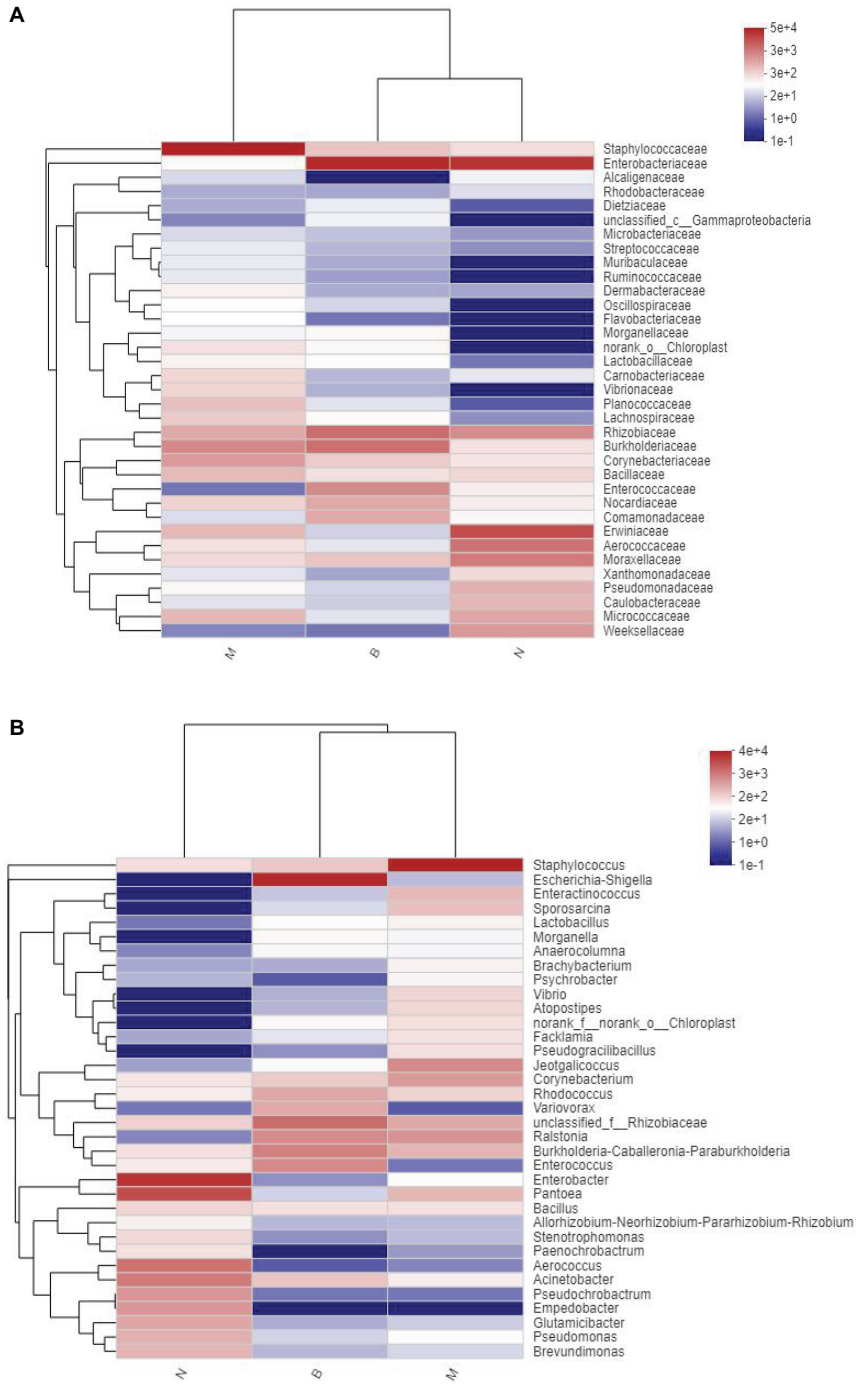

FIGURE 13 | Distribution Heatmap of microbial communities in each group. **(A)** Refers to the family level; **(B)** refers to the genus level.

inhibited *Candida* and CA growth. The effects of boric acid on the microbial richness, diversity, and composition of microflora in the skin of mice infected with CA were analyzed using the 16S rRNA sequencing technique. We found that boric acid improves the skin microecology and reduced skin microbial diversity but had little effect on richness. Boric acid increased the abundance of *Proteobacteria*, *Enterobacteriaceae,* and *Escherichia-Shigella and* reduced *Firmicutes*, *Staphylococcaceae,* and *Staphylococcus*.

There are large and complex microbial populations on the skin's surface, up to more than 10,000 (Arnold et al., 2019), all of which are important for maintaining the balance of skin

microecology. There is competition or restriction in the normalskin micro-ecosystem. The abnormal increase, decrease, or even disappearance of skin microflora leads to the destruction of skin microecology, called skin microecological imbalance. The microecological imbalance may directly lead to infection reaction, divided into endogenous and exogenous types. The endogenous type comes from proportion imbalances, localized metastases, and double infections with normal microbiota. The exogenous type comes from the invading competition of foreign bacteria, which greatly reduces or even eradicates resident bacteria, resulting in skin damage (Wu et al., 2016; Eisenstein, 2020). The microbial population of adult skin is highly personalized, and the composition of strains is stable. Living with trillions of microbes is not without risk (Oh et al., 2014; Kuhbacher et al., 2017). CA is usually present in human skin; however, it is not a symbiotic bacteria on mouse skin surfaces (Iliev et al., 2012). ITS sequencing showed that boric acid decreased the abundance of *Candida*; however, it did not reach the strain level; therefore, further metagenomic sequencing was needed. *Escherichia-Shigella* belongs to Proteobacteria, Enterobacteriaceae. *Staphylococcus* belongs to Staphylococcaceae, Firmicutes. The 16S rRNA sequencing showed a significant difference in the flora structure between the boric acid and the model groups; however, the former was like the blank group. Boric acid may play a protective role by adjusting the microecological skin flora to achieve dynamic balance.

In summary, by constructing a cutaneous CA infection model in mice and measuring the therapeutic effect of 3% boric acid on skin microflora, we concluded that boric acid inhibited Candida and CA's growth, reduced microbial diversity, and improved the microecological flora in mouse skin. This study will expand the understanding of boric acid as an antifungal and provide a basis for developing new antifungal drugs.

DATA AVAILABILITY STATEMENT

The data presented in the study are deposited in the Sequence Read Archive (SRA) repository, accession number SUB9815704.

ETHICS STATEMENT

The animal study was reviewed and approved by the Biomedical Ethics Committee of Medical School of Hebei University of Engineering.

AUTHOR CONTRIBUTIONS

QL wrote the manuscript. XL and HG revised the manuscript. ZL, CZ, and YX gave some helpful suggestions. All authors contributed to manuscript revision, read, and approved the submitted version.

REFERENCES

Arnold, W. M., Hill, E. S., Na, F., Yee, A. L., and Gilbert, J. A. (2019). The human microbiome in health and disease. *Genomic. Appl. Pathol.* 375, 607–618.

Brittingham, A., and Wilson, W. A. (2014). The antimicrobial effect of boric acid on trichomonas vaginalis. *Sex Transm. Dis.* 41, 718–722. doi: 10.1097/olq.0000000000000203

Brown, G. D., Denning, D. W., Gow, N. A. R., Levitz, S. M., Netea, M. G., White, T. C., et al. (2012). Hidden killers: human fungal infections. *Sci. Transl. Med.* 4:165rv13. doi: 10.1126/scitranslmed.3004404

Dardas, M., Gill, S. R., Grier, A., Pryhuber, G. S., Gill, A. L., Lee, Y. H., et al. (2014). The impact of postnatal antibiotics on the pretermin testinal microbiome. *Pediatr. Res.* 76, 150–158. doi: 10.1038/pr.2014.69

Eisenstein, M. (2020). The skin microbiome and its relationship with the human body explained. *Nature* 588, S210–S211.

Fang, J. Y., Tang, K. W., Yang, S. H., Alalaiwe, A., Yang, Y. C., Tseng, C. H., et al. (2020). Synthetic naphthofuranquinone derivatives are effective in eliminating drug-resistant *Candida albicans* in hyphal, biofilm, and intracellular forms: an application for skin-infection treatment. *Front. Microbiol.* 11:2053. doi: 10.3389/fmicb.2020.02053

Fouts, D. E., Szpakoowski, S., Purushe, J., Torralba, M., Waterman, R. C., MacNeil, M. D., et al. (2012). Next generation sequencing to define prokaryotic and fungal diversity in the bovine rumen. *PLoS One* 7:e48289. doi: 10.1371/journal.pone.0048289

Gao, J., and Pan, L. (2016). Experimental study on the effect of boric acid on *Candida albicans*. *Chin. J. Mycol.* 11, 275–288.

Gerdon, S., and Flynm, D. (2014). *Compositions and Methods for Treating Vaginal infections and Pathogenic Vaginal Biofilms*. China, CN101951868B.

Hui, Y., Yuan, X. D., and Zhang, T. (2016). *Vaginal Retained Boric Acid Preparation and Preparation Method Thereof*. China, CN105362289B.

Iavazzo, C., Gkegkes, I. D., Zarkada, I. M., and Falagas, M. E. (2011). Boric acid for recurrent vulvovaginal candidiasis: the clinical evidence. *J Womens Health* 20, 1245–1255. doi: 10.1089/jwh.2010.2708

Iliev, I. D., Funari, V. A., Taylor, K. D., Nguyen, Q., Reyes, C. N., Strom, S. P., et al. (2012). Interactions between commensal fungi and the C-type lectin receptor Dectin-1 influence colitis. *Science* 336, 1314–1317. doi: 10.1126/science.1221789

Javad, G., Sarvtin, M. T., Hedayati, M. T., Hajheydari, Z., Yazdani, J., Shokohi, T., et al. (2015). Evaluation of *Candida* colonization and specific humoral responses against *Candida albicans* in patientswith atopic dermatitis. *BioMed Res. Int.* 2015:849206.

Jie, M. F., Ou, G. Z., and Zhu, Z. C. (2019). Clinical efficacy of closed drip irrigation combined with negative pressure drainage in treating infectious pressure ulcers or skin ulcers. *Chin. J. Contemp. Med.* 26, 39–41.

Katoh, T. (2009). Guidelines for diagnosis and treatment of mucocutaneous candidiasis. *Nihon Ishinkin Gakkai Zasshi* 50, 207–212. doi: 10.3314/jjmm.50.207

Kuhbacher, A., Burger-kentischer, A., and Rupp, S. (2017). Interaction of *Candida* Species with the Skin. *Microorganisms* 5:E32.

Larsen, B., Petrovic, M., and De Seta, F. (2018). Boric acid and commercial organoboron products as inhibitors of drug-resistant *Candida albicans*. *Mycopathologia* 183, 349–357. doi: 10.1007/s11046-017-0209-6

Li, B., Zhang, X., Guo, F., Wu, W., and Zhang, T. (2013). Characterization of tetracycline resistant bacterial community in saline activated sludge using batch stress incubation with high—throughput sequencing analysis. *Water Res.* 47, 4207–4216. doi: 10.1016/j.watres.2013.04.021

Liu, D. F., and Wu, Q. K. (2019). Observation on the efficacy of Rishuan lotion combined with clotrimazole in the treatment of vulvovaginal candidiasis in mice. *Chin. J. Mycol.* 14, 36–40.

Marrazzo, J. M., Dombrowski, J. C., Wierzbicki, M. R., Perlowski, C., Pontius, A., Dithmer, D., et al. (2019). Safety and efficacy of a novel vaginal anti-infective, TOL-463, in the treatment of bacterial vaginosis and vulvovaginal candidiasis: a

randomized, single-blind, phase 2, controlled trial. *Clin. Infect. Dis.* 68, 803–809. doi: 10.1093/cid/ciy554

Oh, J., Byrd, A. L., Deming, C., Conlan, S., Nisc Comparative Sequencing Program, Kong, H. H., et al. (2014). Biogeography and individuality shape function in the human skin metagenome. *Nature* 514, 59–64. doi: 10.1038/nature13786

Perlorth, J., Choi, B., and Spellberg, B. (2007). Nosocomial fungal infections. epidemiology, diagnosis, and treatment. *Med. Mycol.* 45, 321–346. doi: 10.1080/13693780701218689

Pointer, B. R., Boyer, M. P., and Schmidt, M. (2015). Boric acid destabilizes thehyphal cytoskeleton and inhibits invasive growth of *Candida albicans*. *Yeast* 32, 389–398. doi: 10.1002/yea.3066

Pointer, B. R., and Schmidt, M. (2016). Boric acid-dependent decrease in regulatory histone H3 acetylation is not mutagenic in yeast. *FEMS Microbiol. Lett.* 363, 1–6.

Powell, A., Ghanem, K. G., Rogers, L., Zinalabedini, A., Brotman, R. M., Zenilman, J., et al. (2019). Clinicians' use of intravaginal boric acid maintenance therapy for recurrent vulvovaginal candidiasis and bacterial vaginosis. *Sex Transm. Dis.* 46, 810–812. doi: 10.1097/olq.0000000000001063

Riachi, M. (2013). Treatment of oral candidiasis. *Northwest Dent.* 92:4.

Sampaio, A. D. G., Gontido, A. V. L., and Ito, C. Y. K. (2018). In Vivo Efficacy of Ellagic Acid against *Candida albicans* in a *Drosophila* melanogaster Infection Model. *Antimicrob. Agents Chemother.* 62, 1716–1718.

Santus, W., Mingozzi, F., Vai, M., Granucci, F., and Zanoni, I. (2018). Deep dermal injection as a model of *Candida albicans* skin infection for histological analyses. *Vis. Exp.* 136:e57574.

Sardi, J. C., Scorzoni, L., Bernardi, T., Fusco-Almeida, A. M., and Mendes Giannini, M. J. S. (2013). *Candida* species: current epidemiology, pathogenicity, biofilm formation, natural antifungal products and new therapeutic options. *J. Med. Microbiol.* 62(pt1), 10–24. doi: 10.1099/jmm.0.045054-0

Schmidt, M., Schaumberg, J. Z., Steen, C. M., and Boyer, M. P. (2010). Boric acid disturbs cell wall synthesis in saccharomyces cerevisiae. *Int. J. Microbiol.* 2010:930465.

Schmidt, M., Tran-Nguyen, D., and Chizek, P. (2018). Influence of boric acid on energy metabolism and stress tolerance of *Candida albicans*. *J. Trace Elem Med. Biol.* 49, 140–145. doi: 10.1016/j.jtemb.2018.05.011

Solis, N. V., and Filler, S. G. (2011). Mouse model of oropharyngeal candidiasis. *Nat. Protoc.* 7, 637–642. doi: 10.1038/nprot.2012.011

Spampinato, C., and Leonardi, D. (2013). *Candida* infections, causes, targets, and resistance mechanisms: traditional and alternative antifungal agents. *Biomed. Res. Int.* 2013:204237.

Wang, A. P., Yu, J., and Li, R. (2012). Progress in diagnosis and treatment of cutaneous candidiasis. *Chin. J. Mycol.* 7, 372–374.

Wu, X., Dou, X., and Yu, B. (2016). Research progress of atopic dermatitis and skin microecology. *Int. J. Dermatol.* 442, 424–426.

Xie, L. X. (2011). *Clinical and Animal Experimental Study on Imaging Features of Invasive Pulmonary Fungal Infection*. Shanghai: Second military Medical University.

Conflict of Interest: The authors declare that the research was conducted in the absence of any commercial or financial relationships that could be construed as a potential conflict of interest.

frontiers in Microbiology

ORIGINAL RESEARCH
published: 14 September 2021
doi: 10.3389/fmicb.2021.709942

Contribution of NADPH-cytochrome P450 Reductase to Azole Resistance in *Fusarium oxysporum*

*Dan He[1], Zeqing Feng[1], Song Gao[1,2], Yunyun Wei[1], Shuaishuai Han[1,2] and Li Wang[1]**

[1] Department of Pathogenobiology, Jilin University Mycology Research Center, Key Laboratory of Zoonosis Research, Ministry of Education, College of Basic Medical Sciences, Jilin University, Changchun, China, [2] Beijing ZhongKaiTianCheng Bio-technonogy Co. Ltd., Beijing, China

Fusarium species exhibit significant intrinsic resistance to most antifungal agents and fungicides, resulting in high mortality rates among immunocompromised patients. Consequently, a thorough characterization of the antifungal resistance mechanism is required for effective treatments and for preventing fungal infections and reducing antifungal resistance. In this study, an isolate of *Fusarium oxysporum* (wild-type) with broadly resistant to commonly antifungal agents was used to generate 1,450 T-DNA random insertion mutants *via Agrobacterium tumefaciens*-mediated transformation. Antifungal susceptibility test results revealed one mutant with increased sensitivity to azoles. Compared with the resistant wild-type, the mutant exhibited low MICs to KTZ, ITC, VRC, POS, and PCZ (0.125, 1, 0.06, 0.5, and 0.125 μg/ml, respectively). The T-DNA insertion site of this mutant was characterized as involving two adjacent genes, one encoding a hypothetical protein with unknown function and the other encoding the NADPH-cytochrome P450 reductase, referred as CPR1. To confirm the involvement of these genes in the altered azole susceptibility, the independent deletion mutants were generated and the *Cpr1* deletion mutant displayed the same phenotypes as the T-DNA random mutant. The deletion of *Cpr1* significantly decreased ergosterol levels. Additionally, the expression of the downstream *Cyp51* gene was affected, which likely contributed to the observed increased susceptibility to azoles. These findings verified the association between *Cpr1* and azole susceptibility in *F. oxysporum*. Furthermore, this gene may be targeted to improve antifungal treatments.

Keywords: *Fusarium oxysporum*, NADPH-cytochrome P450 reductase, azole resistance, *Agrobacterium tumefaciens*-mediated transformation, ergosterol biosynthesis, antifungal susceptibility

OPEN ACCESS

Edited by:
Weihua Pan,
Shanghai Changzheng Hospital, China

Reviewed by:
Ling Lu,
Nanjing Normal University, China
Giuseppe Ianiri,
University of Molise, Italy

***Correspondence:**
Li Wang
wli99@jlu.edu.cn

Specialty section:
This article was submitted to Antimicrobials, Resistance and Chemotherapy, a section of the journal Frontiers in Microbiology

Received: *14 May 2021*
Accepted: *18 August 2021*
Published: *14 September 2021*

Citation:
He D, Feng Z, Gao S, Wei Y, Han S and Wang L (2021) Contribution of NADPH-cytochrome P450 Reductase to Azole Resistance in Fusarium oxysporum. Front. Microbiol. 12:709942. doi: 10.3389/fmicb.2021.709942

INTRODUCTION

Fusarium species, which are well-known filamentous ascomycetous fungi, include many agriculturally important plant pathogens and opportunistic pathogens of humans and other animals (Ma et al., 2013; Al-Hatmi et al., 2016; Tupaki-Sreepurna and Kindo, 2018; Zhao et al., 2021). *Fusarium* species usually cause local infections, including fungal keratitis, which often leads to blindness. However, over the last few decades, the number of dangerously invasive infections has increased in immunocompromised individuals, especially cancer patients with prolonged

neutropenia and patients with hematological disorders. These infections can spread to the lungs, heart, liver, kidneys, and central nervous system (Tupaki-Sreepurna and Kindo, 2018; Lockhart and Guarner, 2019; Batista et al., 2020; Hof, 2020). As emerging fungal pathogens, some *Fusarium* species, such as *Fusarium oxysporum* and *Fusarium solani*, are now among the most common pathogenic molds associated with significant morbidity and mortality, behind only *Aspergillus* and Mucorales molds (Miceli and Lee, 2011; Guarro, 2013; Tortorano et al., 2014; Al-Hatmi et al., 2016; Lockhart and Guarner, 2019; Hof, 2020).

Antifungal therapy is necessary for successful disease management. However, because of intrinsic resistance and selection pressure, infections caused by *Fusarium* species are relatively difficult to treat. Most species of this genus are typically resistant to a broad range of antifungal agents developed for clinical use, including azoles, polyenes, and echinocandin. They are also minimally susceptible to agricultural fungicides (Azor et al., 2007; Miceli and Lee, 2011; Ma et al., 2013; Ribas et al., 2016; Sharma and Chowdhary, 2017; Batista et al., 2020; Hof, 2020). *In vitro* studies have indicated amphotericin B and echinocandin are relatively ineffective for controlling *Fusarium* species, whereas triazoles, such as voriconazole and posaconazole, are effective against almost 50% of isolates (Azor et al., 2007; Miceli and Lee, 2011; Tortorano et al., 2014). Therefore, the mechanisms underlying the antifungal resistance of *Fusarium* species must be characterized.

Most of the studies on the antifungal resistance of pathogenic fungi conducted to date have focused on the genera *Candida* and *Aspergillus*. There has been relatively little related research regarding *Fusarium* species, with most studies examining the susceptibility of the species to antifungal agents. The few studies analyzing resistance mechanisms have mostly involved plant pathogens and investigations of the changes in the amino acid sequence encoded by the *Fks1* gene or the effects of overexpressing the *Cyp51* gene or the genes encoding ABC efflux pumps (Katiyar and Edlind, 2009; Abou Ammar et al., 2013; Zhang et al., 2021; Zhao et al., 2021).

To identify genes related to the antifungal resistance of *Fusarium* species, *Agrobacterium tumefaciens*-mediated transformation (ATMT) was used to construct T-DNA random insertion mutants. The 1,450 generated mutants from a broadly resistant isolate of *F. oxysporum* included FOM1123, which exhibited altered susceptibility to azoles. We functionally characterized the genes interrupted by the T-DNA insertion and clarified their regulatory roles related to antifungal resistance.

MATERIALS AND METHODS

Strains and Plasmids

Wild-type *F. oxysporum* JLCC31768, which was originally isolated from a patient with fungal keratitis in Jilin province, China, was used to construct T-DNA random insertion mutants. The antifungal susceptibility test (AFST) results revealed it is broadly resistant to different azoles, amphotericin B, and caspofungin commonly used in clinical settings (**Table 1**).

Plasmids pXEH and pXEN (containing neomycin and kanamycin resistance tags) as well as *A. tumefaciens* Agr0 and AgrN (containing pXEN) were used to generate *F. oxysporum* mutants. All strains and plasmids were preserved at the Jilin University Mycology Research Center (Jilin, China).

Construction of Random Insertion Mutants

Antifungal resistance tests indicated that wild-type *F. oxysporum* is sensitive to geneticin (G418). Accordingly, geneticin was selected as a resistance tag. The geneticin phosphotransferase II gene (*Neo*) mediating G418 resistance was ligated to pXEH to construct the pXEN recombinant plasmid. *A. tumefaciens* Agr0 cells were transformed with pXEN to obtain the AgrN strain, which was used for ATMT.

The *F. oxysporum* T-DNA insertion mutants were generated as previously described (Fan et al., 2016). Briefly, fungal spores (1×10^4 CFU/ml) were mixed with an equal volume (1 ml) of AgrN cells ($OD_{600nm} = 0.8$). A Millipore filter was placed on the surface of solid induction medium containing 200 μm acetosyringone. A 200 μl aliquot of the spore–AgrN mixture was spread evenly on the filter. After incubating for 48 h at 25°C in darkness, the filter was transferred to selection medium (PDA containing 200 μm cefotaxime sodium and 100 μg/ml G418) and incubated at 25°C. The mutants were used to inoculate PDA slants in tubes.

Genomic DNA was extracted from randomly selected mutants using the TIANgel Rapid Mini Plasmid Kit (Tiangen Biotech, Beijing, China) for a PCR amplification using the neoF and neoR primers specific for the *Neo* gene (**Table 2**). The amplified products were sequenced by Comate Bioscience Co., Ltd (Jilin, China), after which the sequences were analyzed to determine whether the T-DNA was inserted into the *F. oxysporum* genome. After multiple transformations, many T-DNA insertion mutants were preserved for further research.

Antifungal Susceptibility Testing

The AFST was performed using the CLSI broth microdilution method as described in M38-Ed3 (Clinical and Laboratory Standards Institute, 2017). The following antifungal agents, including azole fungicides, were tested: fluconazole (FLU; NICPBP, Beijing, China), itraconazole (ITC; Sigma, St. Louis, MO, United States), voriconazole (VRC; Sigma), posaconazole (POS; Sigma), amphotericin B (AMB; Sigma), caspofungin (CFG; Meilunbio, Dalian, China), ketoconazole (KTZ; NICPBP), and propiconazole (PCZ; NICPBP). The antifungal agents were diluted 10 times (2-fold dilutions) for the following concentration ranges: FLU, 0.125–64 μg/ml; ITC, VRC, POS, AMB, CFG, KTZ, and PCZ, 0.03–16 μg/ml. As recommended by CLSI, *Candida krusei* ATCC6258 and *Candida parapsilosis* ATCC22019 were used as quality control strains. The MIC endpoint for AMB was defined as the lowest concentration with 100% growth inhibition relative to the antifungal-free control. For the other antifungal agents, the MICs were defined as the lowest concentration with a prominent decrease in growth (almost

TABLE 1 | Antifungal susceptibility test results for the wild-type *Fusarium oxysporum* and the mutants (MIC, μg/ml).

	KTZ	FLU	ITC	VRC	POS	PCZ	AMB	CFG
Wild-type	8	>64	>16	4	4	8	1	>16
FOM1123	0.125	>64	1	0.06	0.5	0.125	1	>16
ΔHPG	8	>64	>16	4	4	8	1	>16
ΔCPR1	0.125	>64	1	0.06	0.5	0.125	1	>16
ΔCPR2	8	>64	>16	4	4	8	1	>16
ΔCPR3	8	>64	>16	4	4	8	1	>16
ΔCPR4	8	>64	>16	4	4	8	1	>16

50%) relative to the control. After a comparison with the wild-type *F. oxysporum*, the mutants with altered antifungal susceptibility were selected.

Bioinformatics Analysis of Related Genes in Mutants With Altered Antifungal Susceptibility

The sequences flanking the inserted T-DNA were amplified by touchdown-TAIL-PCR using previously described primers (**Table 2**; Gao et al., 2016). To determine the insertion sites, the flanking sequences were aligned with the *F. oxysporum* f. sp. *lycopersici* genome (taxid: 426428) using the Basic Local Alignment Search Tool (BLAST).[1] Relevant information regarding the interrupted genes was obtained from the NCBI, KEGG, and UniProtKB databases.

Construction of Deletion Mutants

By exploiting homologous genetic recombination, the genes interrupted by the T-DNA insertion, including *Hpg* as well as *Cpr1* and its homologs (*Cpr2*, *Cpr3*, and *Cpr4*), were targeted using specific primers (**Table 2**) to produce *F. oxysporum* deletion mutants. The *Hpg*, *Cpr1*, *Cpr2*, *Cpr3*, and *Cpr4* genes were replaced by *Neo* in pXEN, which was then inserted into Agr0 cells. The ΔHPG, ΔCPR1, ΔCPR2, ΔCPR3, and ΔCPR4 deletion mutants were generated by ATMT.

Analysis of the Biological Characteristics of the Deletion Mutants

To compare colony morphologies, PDA medium was inoculated with the wild-type *F. oxysporum* and the deletion mutants and then incubated at 25°C for 5 days. Slide cultures were prepared for these strains and then examined using a microscope after lactophenol cotton blue staining. Additionally, the susceptibility of the deletion mutants to antifungal agents was tested as described in M38-Ed3 (Clinical and Laboratory Standards Institute, 2017).

Determination of Ergosterol Content

Fungal spores (1×10^6 CFU) were used to inoculate 100 ml PDB medium, which was then incubated at 25°C for 48 h with shaking (180 rpm). In the antifungal treatment group, VRC (amount corresponding to the 0.5 MIC) was added after 24 h. Next, 100 mg mycelia were collected and resuspended in 5 ml deionized water before being disrupted for 20 min using the Scientz-IID ultrasonic cell disrupter (SCIENTZ, Ningbo, China). A 5 ml aliquot of the solution was mixed with 20 ml ether. The absorbance of the resulting extract was measured at 281.5 nm. The ergosterol content was calculated using a standard curve.

Expression Analysis of Genes Involved in Ergosterol Biosynthesis

Mycelia were disrupted by grinding in liquid nitrogen. Total RNA was extracted from the ground material using the RNAiso Plus kit (Takara, Shiga, Japan). The RNA concentration was determined using the NanoDrop One spectrophotometer (Thermo Fisher, San Jose, CA, United States). The RNA served as the template for synthesizing cDNA using the HiScript II Q RT SuperMix for qPCR (Vazyme, Nanjing, China). Quantitative real-time PCR was performed using the AceQ qPCR SYBR Green Master Mix (Vazyme), gene-specific primers (**Table 3**), and the 7500 Fast Real-Time PCR System (Applied Biosystems, Foster City, CA, United States). The expression levels of genes related to ergosterol synthesis (e.g., *Cpr*, *Cytb5*, and *Cyp51*) were normalized against the expression of the 18S rRNA housekeeping gene. Relative gene expression levels were calculated according to the $2^{-\Delta\Delta CT}$ method (Livak and Schmittgen, 2001).

Statistical Analysis

Data are presented as the mean ± standard deviation of at least three replicated measurements. Differences between the VRC-treated and untreated samples were evaluated by a one-way ANOVA followed by the *T* test using SPSS 2.0 ($p < 0.05$ was set as the threshold for significance).

RESULTS

Construction of T-DNA Random Insertion Mutants

Using an established ATMT system, wild-type *F. oxysporum* was transformed, with an efficiency of 250 mutants per 10^4 CFU. The PCR amplification of the *Neo* gene resulted in a single specific amplicon (approximately 700 ~ 750 bp) for all T-DNA random mutants generated in this study (**Figure 1**). The sequenced fragment was 99% similar to the *Neo* gene, indicating

[1]http://blast.ncbi.nlm.nih.gov/

TABLE 2 | Primers used to generate the T-DNA insertion mutants and deletion mutants.

Primer name	Nucleotide sequence (5′ to 3′)
neoF	ATCTCCTGTCATCTCACCTTGCTC
neoR	GTCTCCTTCCGTGTTTCAGTTAGC
LB1	GGGTTCCTATAGGGTTTCGCTCATG
LB2	CATGTGTTGAGCATATAAGAAACCCT
LB3	GAATTAATTCGGCGTTAATTCAGT
RB1	GGCACTGGCCGTCGTTTTACAAC
RB2	AACGTCGTGACTGGGAAAACCCT
RB3	CCCTTCCCAACAGTTGCGCA
AD1	TGAGNAGTANCAGAGA
AD2	AGTGNAGAANCAAAGG
AD3	CATCGNCNGANACGAA
AD4	CAAGCAAGCA
4LTf	CCCAAGCTTCATGTCGTTCAGTATCTCGCTATAAGCAT
4LTr	CGCGGATCCGTGTCCAATTCACTTTCGGGTTT
4RTf	CGGGGTACCCATTAACGAACGCGACGACCT
4RTr	CGGACTAGTCAGACATAGAAATAAGCCTTCTG
3LTf	CCGGAATTCGCCTGAACAGCAACATGTAAGAGTT
3LTr	CGGGGTACCGAAACTTGCCAATTGGAACCT
3RTf	TGCTCTAGAGTATTCCCGCGATACAGCCCAGAT
3RTr	CGCGTCGACCCCCTCAAATTATAGAAAACTTGTGC

TABLE 3 | Primers used for the quantitative real-time PCR analysis.

Primer Name	Nucleotide Sequence (5′ to 3′)	Purpose
18Sqf	CGCCAGAGGACCCCTAAAC	normalization
18Sqr	ATCGATGCCAGAACCAAGAGA	
CPR1qf	TGCAATCCCGCAATTGAGCC	FOXG 08274
CPR1qr	TCAGAACAGCTACGGAATGCCA	
CPR2qf	TGAGTTGACATCCCGAGCCA	FOXG_07461
CPR2qr	TCTCCAGAGAGGCCAAGCAA	
CPR3qf	GGTATTGATAACTCGCCTCTTC	FOXG_03206
CPR3qr	GTTGCTTGCTGTCACCATTA	
CPR4qf	GCAGCCGATAACCTACAC	FOXG_04834
CPR4qr	CCAGGACCAACCATAAGAATAG	
Cytb5qf	GACGGCAAGACAGTGAATCGC	FOXG_03180
Cytb5qr	CCGAGGGAGAGATTGGCAAGG	
CYP51Aqf	TCACCCTTCTCATGGCTGGAC	FOXG_11545
CYP51Aqr	GGGAGAACACCATCAGCACTCA	
CYP51Bqf	ATTGCTCTCCTCATGGCTGGC	FOXG_00394
CYP51Bqr	GGGAGGCAAATCAGCACCGA	
CYP51Cqf	GAATGGACAGGTTATCAAGGAG	FOXG_13138
CYP51Cqr	GGAGAAGCGAGGAGTGTAT	

the T-DNA containing the G418 resistance tag was inserted into the *F. oxysporum* genome. After multiple transformations, 1,450 mutants were obtained.

Identification of Mutants With Altered Antifungal Susceptibility

The AFST results for the 1,450 confirmed mutants revealed one mutant (FOM1123) with altered antifungal susceptibility. More specifically, this mutant exhibited significantly increased susceptibility to azoles (except for FLU) with low MICs to KTZ, ITC, VRC, POS, and PCZ (0.125, 1, 0.06, 0.5, and 0.125 μg/ml, respectively), compared with the resistant wild-type with high MICs (8,>16, 4, 4, and 8 μg/ml, respectively). In contrast, its susceptibility to the polyene AMB and the echinocandin CFG was unchanged (**Table 1**). These observations suggested that the gene interrupted by T-DNA insertion in this mutant might be related to azole resistance in the wild-type *F. oxysporum*.

Bioinformatics Analysis of Related Genes in the Mutant FOM1123

The sequences flanking the inserted T-DNA in the mutant FOM1123 were amplified by touchdown-TAIL-PCR and sequenced. The subsequent BLAST analysis of the *F. oxysporum* genome indicated the T-DNA fragment replaced a 5,312 bp sequence from 2,932,119 bp to 2,937,431 bp on chromosome 2 between the initiation regions of genes FOXG_08273 and FOXG_08274 (**Figure 2**). The FOXG_08273 gene encodes a hypothetical protein (HPG) comprising 2,548 amino acids. Its function is unknown, and no homologs were identified. The FOXG_08274 gene encodes an NADPH-cytochrome P450 reductase (CPR1) consisting of 692 amino acids. This gene, which is related to ergosterol biosynthesis, contributes to the delivery of electrons to P450 enzymes, similar to *Cytb5* (cytochrome *b5*). It has three homologs, namely, FOXG_07461 (*Cpr2* on chromosome 4), FOXG_03206 (*Cpr3* on chromosome 8), and FOXG_04834 (*Cpr4* on chromosome 7).

Biological Characteristics of Deletion Mutants

Compared with the wild-type *F. oxysporum*, the T-DNA insertion mutant FOM1123 and the deletion mutants ΔHPG, ΔCPR1, ΔCPR2, ΔCPR3, and ΔCPR4 had no obvious differences regarding colony and microscopic morphological characteristics, including mycelial growth, pigment production, spore germination, and spore structure (**Figure 3**).

On the basis of the AFST results, ΔCPR1 had the same phenotypes as that of T-DNA mutant FOM1123 displaying low MICs to azoles (except for FLU). In contrast, the other deletion mutants (ΔHPG, ΔCPR2, ΔCPR3, and ΔCPR4) had the same phenotypes as that of the wild-type *F. oxysporum*, implying the corresponding genes were unrelated to antifungal resistance (**Table 1**). Accordingly, of the examined genes, only *CPR1* appears to be associated with azole resistance.

Ergosterol Content Analysis

To clarify the regulatory effects of CPR1 on ergosterol synthesis in cell membranes, we measured the ergosterol content. Without any treatment, the ergosterol content was lower in ΔCPR1 than in the wild-type control. In response to the VRC treatment, the ergosterol contents of the examined strains decreased, and the ergosterol content in ΔCPR1 remained low (**Table 4**).

Expression Analysis of Genes Involved in Ergosterol Biosynthesis

To analyze the expression-level changes to the genes involved in the ergosterol biosynthesis pathway, we analyzed the relative

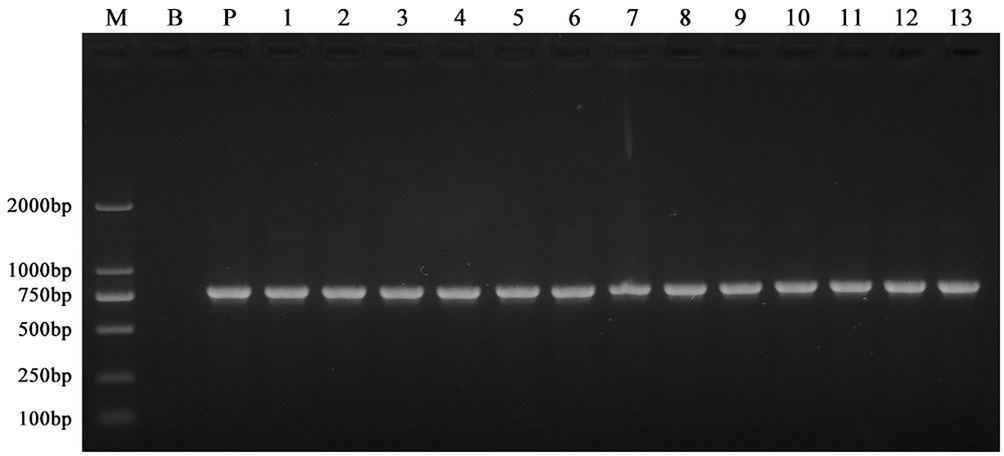

FIGURE 1 | PCR amplification of the *Neo* gene in the wild-type *F. oxysporum* and the T-DNA insertion mutants. Genomic DNA of the mutants grown on the selection medium containing G418 was amplified using the neoF and neoR primers. All the mutants generated in this study produced a specific amplicon (approximately 700 ~ 750 bp). Here, only showed the results of 13 different mutants selected randomly. These indicated the T-DNA containing the G418 resistance tag was inserted into the *F. oxysporum* genome. M: Trans 2 K marker; B: wild-type; P: pXEN; and lanes 1–13: 13 mutants with different T-DNA insertion.

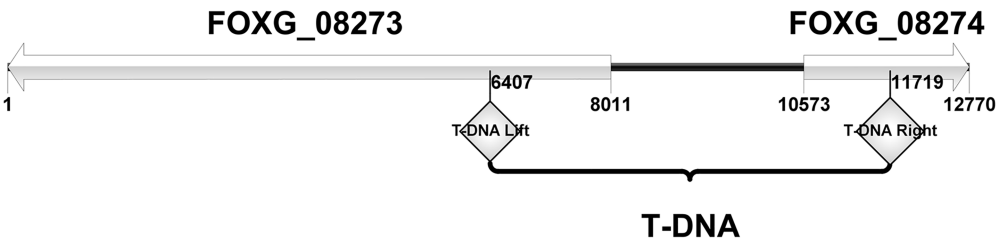

FIGURE 2 | The site of T-DNA insertion of mutant FOM1123. It was characterized as involving 2 adjacent genes, FOXG_08273 and FOXG_08274. The inserted T-DNA replaced a 5,312 bp sequence between the initiation regions of these two genes, from 2,932,119 bp to 2,937,431 bp on *F. oxysporum* chromosome 2.

expression of *Cpr*, *Cytb5*, and *Cyp51*. Following the VRC treatment, the *Cpr1* and *Cpr2* expression levels increased by about 7-fold, whereas *Cpr3* was almost unexpressed and *Cpr4* was unaffected in the wild-type *F. oxysporum*. In the deletion mutant ΔCPR1, the *Cpr2* expression level was about 2-fold higher than the corresponding level in the wild-type control, whereas *Cpr3* and *Cpr4* were almost unexpressed. When ΔCPR1 was treated with VRC, the expression of *Cpr2* increased by about 8.5-fold, whereas *Cpr3* and *Cpr4* expression levels were unaffected (**Figure 4A**).

The *Cytb5* expression level was about 5-fold higher in ΔCPR1 than in the wild-type *F. oxysporum*. The VRC treatment upregulated *Cytb5* expression by about 7.5-fold and 8-fold in the wild-type control and ΔCPR1, respectively (**Figure 4B**). Three homologous genes (*Cyp51A*, *Cyp51B*, and *Cyp51C*) encode proteins targeted by azole antifungal agents. These proteins may receive electrons from CPR and Cytb5. The *Cyp51A* and *Cyp51B* expression levels were about 30-fold higher in ΔCPR1 than in the wild-type control. The exposure to VRC increased the *Cyp51A* expression level by about 67-fold in the wild-type *F. oxysporum*. In contrast, *Cyp51A* and *Cyp51B* expression levels were downregulated by about 33 and 57%, respectively, in ΔCPR1. There were no significant changes to *Cyp51C* expression in any sample (**Figure 4C**).

DISCUSSION

Fusarium species are resistant to multiple common antifungal agents (Azor et al., 2007; Al-Hatmi et al., 2016; Tupaki-Sreepurna and Kindo, 2018; Zhao et al., 2021). Analyses of their resistance mechanisms are critical for improving clinical treatments and for preventing or mitigating antifungal resistance. Previous research confirmed *F. solani* exhibits intrinsic resistance to echinocandin, likely because of a mutation to the gene (*Fks1*) encoding the catalytic subunit of β-1,3-glucan synthase (Katiyar and Edlind, 2009; Al-Hatmi et al., 2016).

The histidine kinase III gene (*Fhk1*) in *F. oxysporum* helps regulate the Hog1-MAPK signaling pathway during stress responses. Deleting this gene leads to increased resistance to phenylpyrrole and dicarboximide fungicides (Rispail and Di Pietro, 2010). Mutations in the genes encoding β1-tubulin and β2-tubulin, which are targeted by benzimidazole fungicides, can lead to increased resistance to carbendazim in various *Fusarium* species, including *Fusarium graminearum*, *Fusarium fujikuroi*, and *Fusarium asiaticum* (Suga et al., 2011; Chen et al., 2014; Zhou et al., 2016). Hence, the antifungal resistance of *Fusarium* species is complex and regulated by multiple genes.

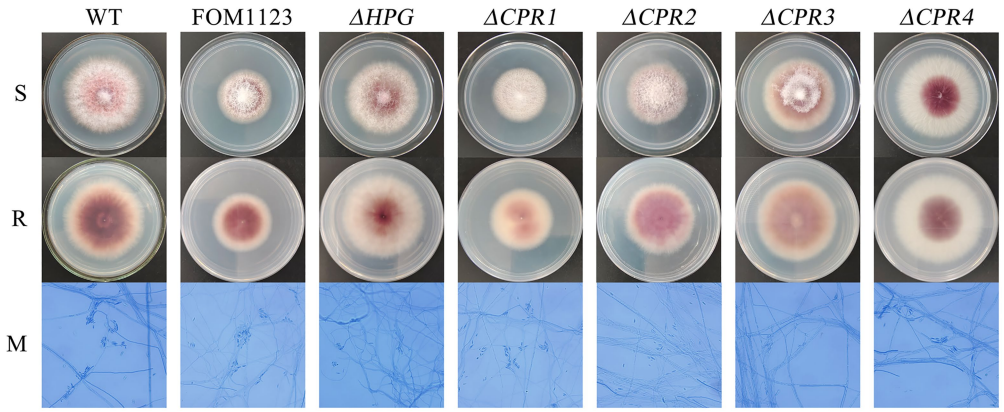

FIGURE 3 | Colony and microscopic morphology of the wild-type *F. oxysporum* and the mutants. Strains cultured on PDA medium were incubated at 25°C for 5 days. Slide cultures were examined after lactophenol cotton blue staining (PDA, 25°C, 3 days, 400 × magnification). S: surface of colony, R: reverse of colony, and M: micromorphology.

TABLE 4 | Ergosterol content of the wild-type *F. oxysporum* and the mutant.

Strain	Ergosterol content(mg/g)	
	VRC-treated samples	Untreated samples
Wild-type	1.62 ± 0.1007*	3.78 ± 0.157
ΔCPR1	1.08 ± 0.1058*	2.65 ± 0.08*

*Data were analyzed according to ANOVA ($p < 0.005$, T test).

The precise mechanisms mediating this antifungal resistance remain to be investigated.

In this study, an isolate of *F. oxysporum* with broadly resistant to commonly antifungal agents and an ATMT-based random insertional mutagenesis method was used to construct T-DNA insertion mutants. And a total of 1,450 T-DNA insertion mutants were obtained. According to the AFST results, compared with the resistant wild-type, one mutant (FOM1123) exhibited significantly increased susceptibility to azoles other than FLU (**Table 1**). It indicated that the gene interrupted by T-DNA insertion in this mutant might be related to the resistance of wild-type.

Bioinformatics analyses indicated that the T-DNA insertion might have affected two genes (*Hpg* and *Cpr1*; **Figure 2**). To confirm the involvement of these genes to the changes with azole susceptibility, the independent mutants (ΔHPG and ΔCPR1) were generated. And the AFST results revealed that only ΔCPR1 mutant had the same phenotypes with MICs as the T-DNA mutants (**Table 1**). It suggested that the *Cpr1* gene might be related to the resistance of *F. oxysporum*.

The *Cpr1* gene encodes NADPH-cytochrome P450 reductase, which is important for electron transport in various organisms. In fungi, it also participates in ergosterol biosynthesis. In an earlier study by Sutter and Loper (1989), the deletion of the CPR-encoding gene in *Saccharomyces cerevisiae* resulted in increased susceptibility to KTZ. The *F. oxysporum* genome includes four *Cpr* homologs. The independent mutants (ΔCPR2, ΔCPR3, and ΔCPR4) were generated in this study, and the AFST results implied these three genes do not influence antifungal resistance (**Table 1**). Accordingly, only *Cpr1* is associated with azole resistance in *F. oxysporum*.

Because of its function related to electron transport, CPR1 can affect the function of CYP51, which is targeted by azole antifungal agents, in the ergosterol biosynthesis pathway. Previous studies proved that deleting *CYP51A* can lead to increased susceptibility to azoles in *Magnaporthe oryzae*, *Aspergillus fumigatus*, and *F. graminearum* (Mellado et al., 2007; Yan et al., 2011). Unlike other fungi, the genomes of *Fusarium* species contain three *Cyp51* genes (*Cyp51A*, *Cyp51B*, and *Cyp51C*). Fan et al. (2013) heterologously expressed three *F. graminearum Cyp51* genes in *S. cerevisiae*. They revealed that *Cyp51A* is associated with azole susceptibility, whereas *Cyp51B* and *Cyp51C* are not. Additionally, *Cyp51A* expression is reportedly induced by ergosterol depletion. Moreover, it is responsible for the intrinsic variation in azole susceptibility. These findings imply CYP51A might be the main target regulated by CPR1.

Because both CPRs and Cytb5 can deliver electrons to CYP51s, we analyzed the expression of the corresponding genes. In this study, when the wild-type *F. oxysporum* was treated with VRC, the *Cpr1*, *Cpr2*, and *Cytb5* expression level increased (**Figures 4A,B**). Subsequently, the expression of *Cyp51A* and *Cyp51B* was upgraduated (**Figure 4C**). In response to the VRC treatment, *Cytb5* expression in ΔCPR1 was not significantly different from that in the wild-type control (**Figure 4B**), indicating *Cyp51* was unaffected by *Cytb5*. At the same time, though the expression of *Cpr2* increased (**Figure 4A**), the electron supply to CYP51 was insufficient owing to *Cpr1* deletion, lead to the expression of *Cyp51A* and *Cyp51B* was downgraduated than that in the wild-type (**Figure 4C**). Consequently, ergosterol biosynthesis was restricted, the ergosterol levels decreased significantly in *Cpr1* deletion mutant than the wild-type (**Table 4**), which contributed to the increase in azole susceptibility.

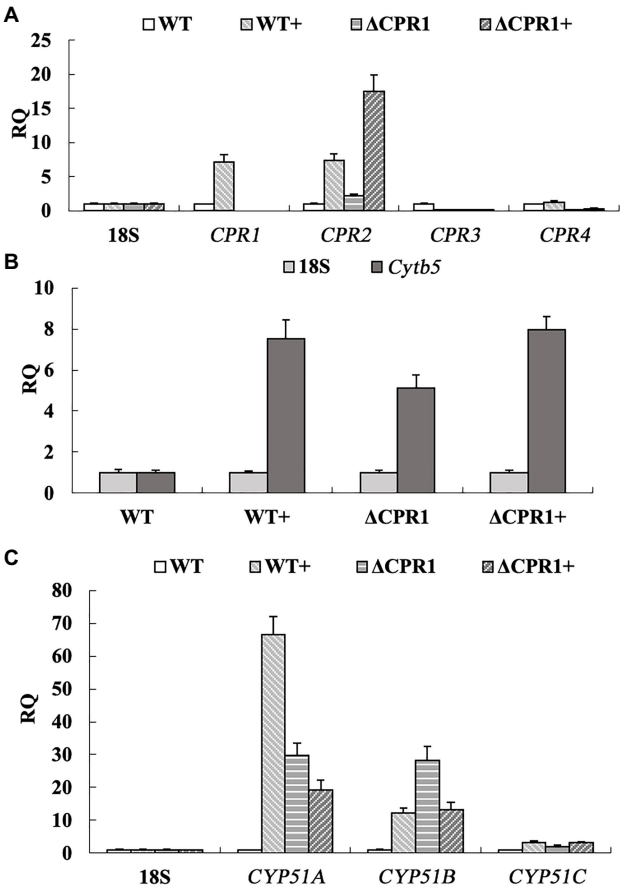

FIGURE 4 | Relative expression levels of genes involved in ergosterol biosynthesis were calculated, using the 18S rRNA gene as the internal reference. **(A)** Expression of *Cpr1* and its homologs. **(B)** Expression of *Cytb5*. **(C)** Expression of *Cyp51*. "+" represents strains were treated with VRC.

In conclusion, our results indicate that CPR1 plays an important role in the ergosterol biosynthesis pathway. Furthermore, it is the only NADPH-cytochrome P450 reductase related to azole resistance in *F. oxysporum*. The increased expression in the CPR1 content may ensure sufficient electrons are supplied to CYP51s for the biosynthesis of ergosterol. This may help to explain why the wild-type fungus was resistant to all tested azoles. Thus, it represents a novel therapeutic target for fungal infections.

DATA AVAILABILITY STATEMENT

The original contributions presented in the study are included in the article/supplementary material, further inquiries can be directed to the corresponding author.

AUTHOR CONTRIBUTIONS

DH and LW: conceptualization and design. ZF, SG, and SH: methodology and experiments. YW: data analysis. DH: original manuscript. LW: review and editing. All authors have read and approved the manuscript for publication.

FUNDING

This study was supported by grants from the National Natural Science Foundation of China (81772162 and U1704283) and the Foundation of Jilin Education Committee (JJKH20211150KJ).

ACKNOWLEDGMENTS

We thank all members of our research center for helpful discussions. We also thank Liwen Bianji (Edanz) (www.liwenbianji.cn/) for editing the English text of a draft of this manuscript.

REFERENCES

Abou Ammar, G., Tryono, R., Doll, K., Karlovsky, P., Deising, H. B., and Wirsel, S. G. (2013). Identification of ABC transporter genes of *Fusarium graminearum* with roles in azole tolerance and/or virulence. *PLoS One* 8:e79042. doi: 10.1371/journal.pone.0079042

Al-Hatmi, A. M., Meis, J. F., and de Hoog, G. S. (2016). *Fusarium*: molecular diversity and intrinsic drug resistance. *PLoS Pathog.* 12:e1005464. doi: 10.1371/journal.ppat.1005464

Azor, M., Gene, J., Cano, J., and Guarro, J. (2007). Universal in vitro antifungal resistance of genetic clades of the *Fusarium solani* species complex. *Antimicrob. Agents Chemother.* 51, 1500–1503. doi: 10.1128/AAC.01618-06

Batista, B. G., Chaves, M. A., Reginatto, P., Saraiva, O. J., and Fuentefria, A. M. (2020). Human fusariosis: An emerging infection that is difficult to treat. *Rev. Soc. Bras. Med. Trop.* 53:e20200013. doi: 10.1590/0037-8682-0013-2020

Chen, Z., Gao, T., Liang, S., Liu, K., Zhou, M., and Chen, C. (2014). Molecular mechanism of resistance of *Fusarium fujikuroi* to benzimidazole fungicides. *FEMS Microbiol. Lett.* 357, 77–84. doi: 10.1111/1574-6968.12504

Clinical and Laboratory Standards Institute (2017). *Reference Method for Broth Dilution Antifungal Susceptibility Testing of Filamentous Fungi—Approved Standard CLSI Document M38-Ed3*. Wayne, PA, USA: Clinical and Laboratory Standards Institute.

Fan, J., Urban, M., Parker, J. E., Brewer, H. C., Kelly, S. L., Hammond-Kosack, K. E., et al. (2013). Characterization of the sterol 14alpha-demethylases of *Fusarium graminearum* identifies a novel genus-specific CYP51 function. *New Phytol.* 198, 821–835. doi: 10.1111/nph.12193

Fan, Z., Yu, H., Guo, Q., He, D., Xue, B., Xie, X., et al. (2016). Identification and characterization of an anti-oxidative stress-associated mutant of *Aspergillus fumigatus* transformed by *Agrobacterium tumefaciens*. *Mol. Med. Rep.* 13, 2367–2376. doi: 10.3892/mmr.2016.4839

Gao, S., He, D., Li, G., Zhang, Y., Lv, H., and Wang, L. (2016). A method for amplification of unknown flanking sequences based on touchdown PCR and suppression-PCR. *Anal. Biochem.* 509, 79–81. doi: 10.1016/j.ab.2016.07.001

Guarro, J. (2013). Fusariosis, a complex infection caused by a high diversity of fungal species refractory to treatment. *Eur. J. Clin. Microbiol. Infect. Dis.* 32, 1491–1500. doi: 10.1007/s10096-013-1924-7

Hof, H. (2020). The medical relevance of *Fusarium* spp. *J. Fungi* 6:117. doi: 10.3390/jof6030117

Katiyar, S. K., and Edlind, T. D. (2009). Role for Fks1 in the intrinsic echinocandin resistance of *Fusarium solani* as evidenced by hybrid expression in *Saccharomyces*

cerevisiae. *Antimicrob. Agents Chemother.* 53, 1772–1778. doi: 10.1128/AAC.00020-09

Livak, K. J., and Schmittgen, T. D. (2001). Analysis of relative gene expression data using real-time quantitative PCR and the $2^{-\Delta\Delta CT}$ method. *Methods* 25, 402–408. doi: 10.1006/meth.2001.1262

Lockhart, S. R., and Guarner, J. (2019). Emerging and reemerging fungal infections. *Semin. Diagn. Pathol.* 36, 177–181. doi: 10.1053/j.semdp.2019.04.010

Ma, L. J., Geiser, D. M., Proctor, R. H., Rooney, A. P., O'Donnell, K., Trail, F., et al. (2013). *Fusarium* pathogenomics. *Annu. Rev. Microbiol.* 67, 399–416. doi: 10.1146/annurev-micro-092412-155650

Mellado, E., Garcia-Effron, G., Alcazar-Fuoli, L., Melchers, W. J., Verweij, P. E., Cuenca-Estrella, M., et al. (2007). A new *Aspergillus fumigatus* resistance mechanism conferring in vitro cross-resistance to azole antifungals involves a combination of *cyp51A* alterations. *Antimicrob. Agents Chemother.* 51, 1897–1904. doi: 10.1128/AAC.01092-06

Miceli, M. H., and Lee, S. A. (2011). Emerging moulds: epidemiological trends and antifungal resistance. *Mycoses* 54, e666–e678. doi: 10.1111/j.1439-0507.2011.02032.x

Ribas, E. R. A. D., Spolti, P., Del Ponte, E. M., Donato, K. Z., Schrekker, H., and Fuentefria, A. M. (2016). Is the emergence of fungal resistance to medical triazoles related to their use in the agroecosystems? A mini review. *Braz. J. Microbiol.* 47, 793–799. doi: 10.1016/j.bjm.2016.06.006

Rispail, N., and Di Pietro, A. (2010). The two-component histidine kinase Fhk1 controls stress adaptation and virulence of *Fusarium oxysporum*. *Mol. Plant Pathol.* 11, 395–407. doi: 10.1111/j.1364-3703.2010.00612.x

Sharma, C., and Chowdhary, A. (2017). Molecular bases of antifungal resistance in filamentous fungi. *Int. J. Antimicrob. Agents* 50, 607–616. doi: 10.1016/j.ijantimicag.2017.06.018

Suga, H., Nakajima, T., Kageyama, K., and Hyakumachi, M. (2011). The genetic profile and molecular diagnosis of thiophanate-methyl resistant strains of *Fusarium asiaticum* in Japan. *Fungal Biol.* 115, 1244–1250. doi: 10.1016/j.funbio.2011.08.009

Sutter, T. R., and Loper, J. C. (1989). Disruption of the *Saccharomyces cerevisiae* gene for NADPH-cytochrome P450 reductase causes increased sensitivity to ketoconazole. *Biochem. Biophys. Res. Commun.* 160, 1257–1266. doi: 10.1016/S0006-291X(89)80139-1

Tortorano, A. M., Prigitano, A., Esposto, M. C., Arsic Arsenijevic, V., Kolarovic, J., Ivanovic, D., et al. (2014). European Confederation of Medical Mycology (ECMM) epidemiological survey on invasive infections due to *Fusarium* species in Europe. *Eur. J. Clin. Microbiol. Infect. Dis.* 33, 1623–1630. doi: 10.1007/s10096-014-2111-1

Tupaki-Sreepurna, A., and Kindo, A. J. (2018). *Fusarium*: The versatile pathogen. *Indian J. Med. Microbiol.* 36, 8–17. doi: 10.4103/ijmm.IJMM_16_24

Yan, X., Ma, W. B., Li, Y., Wang, H., Que, Y. W., Ma, Z. H., et al. (2011). A sterol 14alpha-demethylase is required for conidiation, virulence and for mediating sensitivity to sterol demethylation inhibitors by the rice blast fungus *Magnaporthe oryzae*. *Fungal Genet. Biol.* 48, 144–153. doi: 10.1016/j.fgb.2010.09.005

Zhang, Y., Mao, C. X., Zhai, X. Y., Jamieson, P. A., and Zhang, C. Q. (2021). Mutation in *cyp51b* and overexpression of *cyp51a* and *cyp51b* confer multiple resistant to DMIs fungicide prochloraz in *Fusarium fujikuroi*. *Pest Manag. Sci.* 77, 824–833. doi: 10.1002/ps.6085

Zhao, B., He, D., and Wang, L. (2021). Advances in *Fusarium* drug resistance research. *J. Glob. Antimicrob. Resist.* 24, 215–219. doi: 10.1016/j.jgar.2020.12.016

Zhou, Y., Zhu, Y., Li, Y., Duan, Y., Zhang, R., and Zhou, M. (2016). β1 Tubulin Rather Than β2 Tubulin Is the Preferred Binding Target for Carbendazim in *Fusarium graminearum*. *Phytopathology* 106, 978–985. doi: 10.1094/PHYTO-09-15-0235-R

Conflict of Interest: Authors SG and SH were employed by Beijing ZhongKai TianCheng Bio-technology Co. Ltd., (Beijing, China).

The remaining authors declare that the research was conducted in the absence of any commercial or financial relationships that could be construed as a potential conflict of interest.

Publisher's Note: All claims expressed in this article are solely those of the authors and do not necessarily represent those of their affiliated organizations, or those of the publisher, the editors and the reviewers. Any product that may be evaluated in this article, or claim that may be made by its manufacturer, is not guaranteed or endorsed by the publisher.

Advantages of publishing in Frontiers

OPEN ACCESS
Articles are free to read for greatest visibility and readership

FAST PUBLICATION
Around 90 days from submission to decision

HIGH QUALITY PEER-REVIEW
Rigorous, collaborative, and constructive peer-review

TRANSPARENT PEER-REVIEW
Editors and reviewers acknowledged by name on published articles

Frontiers
Avenue du Tribunal-Fédéral 34
1005 Lausanne | Switzerland

Visit us: www.frontiersin.org
Contact us: frontiersin.org/about/contact

REPRODUCIBILITY OF RESEARCH
Support open data and methods to enhance research reproducibility

DIGITAL PUBLISHING
Articles designed for optimal readership across devices

FOLLOW US
@frontiersin

IMPACT METRICS
Advanced article metrics track visibility across digital media

EXTENSIVE PROMOTION
Marketing and promotion of impactful research

LOOP RESEARCH NETWORK
Our network increases your article's readership